LEABHARLANN CHOLÁISTE NA TRÍONÓIDE, BAILE ÁTHA CLIATH | TRINITY COLLEGE LIBRARY DUBLIN
Ollscoil Átha Cliath | The University of Dublin

Terms and Conditions of Use of Digitised Theses from Trinity College Library Dublin

Copyright statement

All material supplied by Trinity College Library is protected by copyright (under the Copyright and Related Rights Act, 2000 as amended) and other relevant Intellectual Property Rights. By accessing and using a Digitised Thesis from Trinity College Library you acknowledge that all Intellectual Property Rights in any Works supplied are the sole and exclusive property of the copyright and/or other IPR holder. Specific copyright holders may not be explicitly identified. Use of materials from other sources within a thesis should not be construed as a claim over them.

A non-exclusive, non-transferable licence is hereby granted to those using or reproducing, in whole or in part, the material for valid purposes, providing the copyright owners are acknowledged using the normal conventions. Where specific permission to use material is required, this is identified and such permission must be sought from the copyright holder or agency cited.

Liability statement

By using a Digitised Thesis, I accept that Trinity College Dublin bears no legal responsibility for the accuracy, legality or comprehensiveness of materials contained within the thesis, and that Trinity College Dublin accepts no liability for indirect, consequential, or incidental, damages or losses arising from use of the thesis for whatever reason. Information located in a thesis may be subject to specific use constraints, details of which may not be explicitly described. It is the responsibility of potential and actual users to be aware of such constraints and to abide by them. By making use of material from a digitised thesis, you accept these copyright and disclaimer provisions. Where it is brought to the attention of Trinity College Library that there may be a breach of copyright or other restraint, it is the policy to withdraw or take down access to a thesis while the issue is being resolved.

Access Agreement

By using a Digitised Thesis from Trinity College Library you are bound by the following Terms & Conditions. Please read them carefully.

I have read and I understand the following statement: All material supplied via a Digitised Thesis from Trinity College Library is protected by copyright and other intellectual property rights, and duplication or sale of all or part of any of a thesis is not permitted, except that material may be duplicated by you for your research use or for educational purposes in electronic or print form providing the copyright owners are acknowledged using the normal conventions. You must obtain permission for any other use. Electronic or print copies may not be offered, whether for sale or otherwise to anyone. This copy has been supplied on the understanding that it is copyright material and that no quotation from the thesis may be published without proper acknowledgement.

ON THE DEVELOPMENT OF MOLECULAR APPROACHES TO THERAPY FOR RETINITIS PIGMENTOSA

A Thesis Submitted to the University of Dublin
for the Degree of Doctor of Philosophy

By

Anh Thi Hong Nguyen
(Thi Hong Anh Nguyen)

Department of Genetics
University of Dublin
Trinity College

October 2013

TRINITY COLLEGE
- 4 MAR 2014
LIBRARY DUBLIN

Declaration

I declare that this thesis has not been submitted as an exercise for a degree at this or any other university and it is entirely my own work.

I agree to deposit this thesis in the University's open access institutional repository or allow the library to do so on my behalf, subject to Irish Copyright Legislation and Trinity College Library conditions of use and acknowledgement.

Signed:

Anh Thi Hong Nguyen (Thi Hong Anh Nguyen)

14th October 2013

Acknowledgements

I would like to take this opportunity to thank all those who have helped, inspired, and motivated me during the course of my PhD. Firstly, a big thank you to Prof. Pete Humphries who has given me this wonderful opportunity to embark on such an interesting project. I would also like to thank Dr. Sophie Kiang, Dr. Matthew Campbell, and Dr. Lawrence Tam for your guidance and support throughout the years. In particular, thanks Sophie for correcting and proofreading my thesis, and for being such a great friend with whom I could discuss about every aspect of life in addition to scientific research. I would also like to thank Dr. Marian Humphries, the cloning expert, for helping me with general molecular work and patiently listening to my different stories. I would also like to thank Dr. Paul Kenna for all the animal work, and also those who work in the animal unit including Rebecca, David and Caroline for taking care of my animals. To all my past and present friends in the Ocular Genetics Unit Claire, Clare, Elif, Finn, James, Mayu, Ema, and everyone else; thank you for making the lab such a cheerful place to work in; especially Claire and Clare for everything that we have been through together.

To all my Vietnamese friends in Ireland, thank you so much for your continuous support and for always being there for me, especially a. Tuấn, Thúy, Bình, Tâm and many more that I have known and been friends with throughout the years of this PhD. Con cũng xin cám ơn tình yêu thương con vô bờ bến của bố mẹ, bố mẹ luôn là nguồn động viên, điểm tựa bình yên cho con. To my lovely brother Cường, thank you for always cheering me up and listening to my thoughts. Lastly, David, I couldn't have done it without you and your patience! Thank you for always being by my side no matter what happens. THANK YOU ALL!

Summary

Endothelial cells lining the microvasculature of the retina have highly evolved "tight junctions" reducing the space between adjacent cells to form a selective and highly regulatable barrier called the inner blood-retina barrier (iBRB). While many degenerative retinopathies are potentially treatable using available low molecular weight drugs, an estimated 98% of these cannot diffuse passively across the iBRB (Pardridge, 2007). In addition, intra-ocular injection of therapeutic agents is widely used experimentally in rodent models of retinal degeneration, however regular intravitreal injections in humans poses a low, but significant risk of severe endophthalmitis, haemorrhage, or detachment of the retina and is not a realistic option for repeated administration. Using an RNAi approach, hydrodynamic injection in mice of siRNA targeting the tight junction protein claudin-5 results in a transient opening of the iBRB to molecules of up to 1 kDa for a period of between 24 and 72 hours post injection (Campbell *et al.*, 2009, Campbell *et al.*, 2010). Subretinal inoculation of AAV2/9 expressing a doxycycline-inducible shRNA targeting claudin-5 (CLDN5 AAV2/9) results in a similar barrier modulation for the period of time during which the inducing agent doxycycline is administered, providing a means of systemic drug delivery specifically to the retina and avoiding systemic access to the brain (Campbell *et al.*, 2011). In addition, this process has no negative impact on neuronal transcription or visual function and does not induce neuronal or retinal oedema.

The overall objective of the research described in this PhD was to use this iBRB modulatory system to systemically deliver low molecular weight drugs to the retinas of animal models of retinal degeneration in order to retard disease progression. Three types of models were used: 1) the murine Balb/c light-induced retinal degeneration model; 2) IMPDH1 mouse models of the RP10 form of autosomal dominant retinitis pigmentosa (adRP) and 3) rat and mouse models of P23H rhodopsin-linked adRP. These animal models have been widely used to investigate photoreceptor cell death (model 1) and retinal

degeneration due to protein misfolding (models 2 and 3). For studies involving the Balb/c light-induced degeneration model in which calpain-linked apoptosis has been highly implicated, two low molecular weight calpain inhibitors ALLM and ALLN which exhibit poor penetration across the iBRB, were selected as potential protective agents against cell death in this model (Donovan and Cotter, 2002). Following iBRB modulation using claudin-5 siRNA, systemic administration of these inhibitors did indeed offer protection against photoreceptor cell death post light-induced ablation; ALLM being more effective when compared to ALLN (Campbell *et al.*, 2009, Nguyen *et al.*, 2012). Furthermore, intra-peritoneal injection of ALLM into mice which had previously been subretinally injected with CLDN5 AAV2/9 and administered doxycycline resulted in up to 70% protection from photoreceptor cell death compared to controls.

Protein aggregation has been implicated in many retinopathies and is directly linked to earlier events triggered by misfolded mutant proteins which stimulate activation of the heat shock protein 90 superchaperone complex in the cytosol and/or the unfolded protein response (UPR) in the endoplasmic reticulum (Aherne *et al.*, 2004, Kosmaoglou *et al.*, 2008, Tam *et al.*, 2010). Earlier work in this laboratory by Tam *et al.*, (2010) using AAV2/5 expressing mutant IMPDH1 to induce the RP10 form of adRP in mice, demonstrated that following iBRB modulation with claudin-5 siRNA, enhanced delivery of an inhibitor of Hsp90 derived from geldanamycin, 17-AAG, could reduce retinal degeneration although this required delivery of repeated doses of siRNA to prolong iBRB modulation. In studies for this PhD, similar experiments were carried out except that claudin-5 siRNA was endogenously produced in the retina following subretinal injection of the doxycyline-inducible CLDN5 AAV2/9 system. However, due to complications mainly arising from the requirement to introduce two different AAVs (CLDN5 AAV2/9 and IMP224 AAV2/5) conclusive results were not obtained although clear positive trends were noted. These problems arising from the use of an AAV-induced model highlighted the

need to generate a transgenic model of RP10. The design and partial characterization of such a novel model expressing a mutant human IMPDH1 transgene forms the subject of another chapter in this thesis.

Although 17-AAG has been used in various clinical trials for treatment of cancer, it is rapidly metabolised, forms toxic metabolites and exhibits limited aqueous solubility (Egorin *et al.*, 1998) while 17-DMAG a newer derivative of geldanamycin also under clinical trials for various types of cancer, is water soluble, undergoes limited metabolism, has high oral bioavailability and shows increased efficacy compared to 17-AAG (Egorin *et al.*, 2001, Egorin *et al.*, 2002). Many studies done in the 90s reported that the vast majority of adRP-linked rhodopsin mutations including the most studied mutation P23H (P23H RHO), lead to misfolding of the rhodopsin protein (Lin and Lavail, 2010). In addition, 17-AAG has been shown previously to have a positive effect in reducing insoluble P23H RHO *in vitro* (Mendes and Cheetham, 2008). Hence, the effect of 17-DMAG on the rate of degeneration of photoreceptors in P23H RHO mouse and rat models were further subjects of investigation in this thesis. Using the CLDN5 AAV2/9 system together with systemic administration of 17-DMAG, significant preservation of the outer nuclear layer (~ 48%) and rescue of visual function (~ 36%) were observed in treated retinas compared to controls in P23H-line 3 rats, a model involving slow retinal degeneration. In order to examine the potential versatility of this therapeutic, the effect of 17-DMAG was also tested in a rapidly degenerating P23H mouse model and in an AAV2/5 P23H-induced mouse model. However, these P23H murine models proved less useful than the more robust rat model.

To summarize, data presented here provide proof of principle for transient, localized and inducible delivery of small molecular weight drugs via modulation of the iBRB following a once-off subretinal injection of CLDN5 AAV2/9. Furthermore, since 17-DMAG is already in clinical trial for various types of cancer, administration of this drug in

combination with modulation of the iBRB could be used to develop a common therapy for the treatment of all retinopathies associated with ER stress. In this regard, this therapeutic approach has recently been designated with orphan medicinal product status by the European Medicines Agency which should expedite translation to clinical use in the near future.

Table of Contents

Chapter 1: General Introduction

1.1 General Introduction 2

1.2 The blood-brain barrier 3

1.3 The Blood-retina Barrier 5

1.3.1 The inner blood-retina barrier 5

1.3.2 The outer blood-retina barrier 6

1.4 Tight junction proteins 7

1.4.1 Claudin-5 in the blood-retina barrier 10

1.5 Transport systems across the BRB 12

1.6 Structure of the eye 15

1.6.1 The retina 16

1.6.2 Photoreceptors 16

1.7 Drug delivery in the retina 17

1.7.1 Systemic administration 18

1.7.2 Topical administration 19

1.7.3 Intravitreal and sub-conjunctival injections 20

1.7.4 Intravitreal implants 21

1.8 Retinitis pigmentosa 22

1.9 Protein aggregation and diseases 24

1.10 Apoptosis in neurodegenerative diseases 25

1.11 RNA interference (RNAi) 26

1.12 The potential of RNAi 30

1.12.1 Non-viral delivery of RNAi ____ 32

1.12.2 Viral-mediated delivery of RNAi ____ 33

1.13 Potential 'off-target' effect of RNAi ____ *37*

1.13.1 Cross reactions with miRNA pathway ____ 37

1.13.2 Off-target effects ____ 38

1.13.3 Innate immune response ____ 38

1.14 AAV vectors in the retina ____ *40*

1.15 BBB/iBRB modulation as a potential drug delivery method ____ *43*

1.16 Objectives ____ *45*

Chapter 2: Materials and Methods

2.1 Materials ____ *62*

2.1.1 Buffers and reagents for general procedures ____ 62

2.1.2 Buffers and reagents for bacterial culturing ____ 62

2.1.3 Cell culturing materials and reagents ____ 63

2.1.4 RNA materials and reagents ____ 63

2.1.5 Protein materials and reagents ____ 64

2.1.6 Materials and reagents used for western blotting ____ 64

2.1.7 Anaesthetic and reagents used for animal procedures (mouse) ____ 65

2.1.8 Materials and reagents used for histology and immunohistochemistry ____ 66

2.2 General cloning techniques ____ *66*

2.2.1 DNA/RNA spectrophotometry ____ 66

2.2.2 Agarose gel electrophoresis ____ 67

2.2.3 Restriction enzyme digestion ____ 67

2.2.4 Enzyme reaction clean up (Qiagen) ____ 67

2.2.5 Agarose gel extraction (Qiagen) 68

2.2.6 Phenol-chloroform extraction 68

2.2.7 XL1-blue competent cells 68

2.2.8 Transformation using XL1-Blue competent cells 69

2.2.9 DNA mini-preparation (Qiagen kit) 69

2.2.10 DNA maxi-preparation (Qiagen kit) 70

2.2.11 Sequencing (GATC or Source Bioscience LifeSciences) 70

2.3 Cell culturing procedures *70*

2.3.1 Cell growth 70

2.3.2 Cell passaging 71

2.3.3 Cell counting using a Haemocytometer 71

2.3.4 Freezing cells 71

2.4 RNA Methods *72*

2.4.1 Ribonuclease (RNase) free conditions 72

2.4.2 RNA isolation from HeLa cells (Using Tri-reagent) 72

2.4.3 RNA isolation from HeLa cells (RNeasy® Plus mini kit) 72

2.4.4 DNase treatment of HeLa cell RNA 73

2.4.5 RNA isolation from mouse retina (RNeasy mini kit) 73

2.4.6 DNase treatment of mouse retinal RNA (on column digestion) 73

2.4.7 General One Step Real- Time RT-PCR protocol 74

2.5 Protein techniques *76*

2.5.1 Protein extraction from HeLa cells 76

2.5.2 Protein extraction from mouse retina 76

2.5.3 Determination of protein concentrations 76

2.5.3.1 Bicinchoninic acid (BCA) protein assay 76

2.5.3.2 Qubit™ Protein Assay Kits 77

2.6 Western Blot Protocol 78

2.6.1 Preparation of SDS PAGE gels 78

2.6.2 Loading samples and electrophoresis 78

2.6.3 Transfer of proteins 79

2.6.4 Ponceau S Staining 79

2.6.5 Blocking of immunoblots 79

2.6.6 Incubation with antibodies 79

2.6.7 Chemiluminescent detection of proteins 80

2.6.8 Stripping of immunoblots 80

2.6.9 Quantification of Western blots 81

2.7 Animal procedures 81

2.7.1 Housing of animals 81

2.7.2 DNA isolation from mouse tails 81

2.7.3 Subretinal AAV injection 82

2.7.4 Electroretinograms (ERG) 82

2.7.5 Fixation of eyes 83

2.7.6 Preparation of the eyes for cryosectioning 84

2.7.8 Immunohistochemistry 84

2.7.9 Magnetic Resonance Imaging (MRI) 85

2.8 Statistical analysis 85

Chapter 3: Enhanced systemic delivery of calpain inhibitors prevents photoreceptor cell death in a murine model of light-induced retinal degeneration

3.1 Introduction 88

3.1.1 Apoptosis in neurodegenerative diseases 89

3.1.1.1 Caspase-dependent apoptosis 89

3.1.1.2 Caspase-independent apoptosis 91

3.1.2 Calpain activation and retinopathies 92

3.1.3 Light ablation model 95

3.1.4 Objectives 97

3.2 Methods *98*

3.2.1 siRNA and AAV production 98

3.2.2 *In vivo* delivery of siRNA to retinal capillary endothelial cells 99

3.2.3 Light ablation methodology 99

3.2.4 TdT-mediated dUTP nick end labeling (TUNEL) staining 100

3.2.5 Western Blot Analysis 100

3.2.6 Statistical Analysis 101

3.3 Results *102*

3.3.1 Safety of systemic administration of CLDN5 siRNA 102

3.3.2 Effect of ALLM and CLDN5 siRNA on light-induced photoreceptor cell death 103

3.3.3 Effect of ALLN and CLDN5 siRNA on light-induced photoreceptor cell death 104

3.3.4 Effect of subretinal delivery of CLDN5 AAV2/9 and systemic administration of ALLM105

3.4 Discussion *107*

Chapter 4: Effects of 17-AAG on retinal degeneration in a mouse model of RP10 and Partial characterization of a new RP10 model

4.1 Introduction *122*

4.1.1 Mutations in *IMPDH1* gene cause the RP10 form of autosomal dominant RP 122

4.1.2 Molecular chaperones 127

4.1.2.1 Hsp70 128

4.1.2.2 Hsp90 129

4.1.2.3 Hsp70/Hsp90 complex and misfolded protein 130

4.1.3 Protein aggregation and diseases 131

4.1.4 Hsp90 inhibitors 132

4.1.5 Objectives 134

4.2 Materials and Methods *135*

4.2.1 17-AAG treatment 135

4.2.2 Doxycycline intake measurements 135

4.2.3 Measurements of transduced ONL area per unit length 135

4.2.4 Immunohistochemistry 136

4.2.5 Genotyping for transgenic animals (PCR) 136

4.2.6 Quantitative PCR on genomic DNA from transgenic animals 137

4.2.7 Statistical Analysis 138

4.3 Results *139*

4.3.1 Delivery of hsp90 inhibitor in a murine model of RP10 retinitis pigmentosa 139

4.3.2 RP10 transgenic model 141

4.4 Discussion *144*

Chapter 5: Prevention of Retinal Degeneration in a P23H rat model of Retinitis Pigmentosa by Systemic Administration of 17-DMAG

5.1 Introduction *170*

5.1.1 Endoplasmic reticulum stress and protein folding 171

5.1.1.1 Chaperones in the ER 171

5.1.1.2 Unfolded protein response 175

5.1.1.3 ER stress signaling and ER chaperones 177

5.1.1.4 ER chaperones facilitate ER-associated protein degradation 180

5.1.1.5 ER stress and Apoptosis 181

5.1.2 Rhodopsin and adRP 184

5.1.2.1 Current therapeutic strategies for P23H RHO linked RP 189

5.1.3 Objectives 192

5.2 Materials and Methods 194

5.2.1 Animal and Experimental Groups 194

5.2.2 Subretinal and intravitreal AAV injection 194

5.2.3 Generation of P23H pcDNA3 construct 194

5.2.4 QuikChange Site-Directed Mutagenesis 195

5.2.5 Cell culture and cell transfection 195

5.2.6 Western blot analyses 196

5.2.7 Xbp1 PCR analysis 196

5.2.8 SuperScript® Reverse Transcriptase system (Invitrogen) 197

5.2.9 RT-PCR analysis 197

5.2.10 MRI 198

5.2.11 Therapeutic agent 198

5.2.12 Immunohistochemistry 199

5.2.13 Determination of the outer nuclear layer thickness 199

5.2.14 ERG analysis 200

5.2.15 Dose calculation from animal to human 200

5.2.16 Statistical analysis 201

5.3 Results 202

5.3.1. P23H point mutation and RHO structure 202

5.3.2 Effect of 17-DMAG *in vitro* 202

5.3.2.1 Effect of 17-DMAG in untransfected cells 202

5.3.2.2 Effect of P23H RHO on the UPR 203

5.3.2.3 17-DMAG alleviates ER stress at mRNA levels 204

5.3.2.4 17-DMAG reduces ER stress at protein levels 206

5.3.2.5 17-DMAG reduces aggregation of P23H RHO 207

5.3.2.6 Effect of 17-DMAG on expression levels of Hsp protein in the cytoplasm 208

5.3.3 Effect of 17-DMAG *in vivo* 208

5.3.3.1 Intra-vitreal delivery of 17-DMAG leads to reduction in ER tress in P23H-3 rats 208

5.3.3.2 Systemic delivery of 17-DMAG leads to rescue of visual function 210

5.3.3.3 Systemic delivery of 17-DMAG leads to preservation of retina structure 213

5.3.3.4 Minimum dose of 17-DMAG for the systemic approach 214

5.4 Discussion ***215***

Chapter 6: Studies on Murine Models of P23H Rhodopsin

1. Characterisation of models generated by AAV2/5 delivery of WT and P23H rhodopsin

2. Effect of 17-DMAG in a P23H transgenic mouse model exhibiting rapid degeneration

6.1 Introduction ***284***

6.1.1 Objectives 288

6.2 Materials and Methods ***290***

6.2.1 AAV construction 290

6.2.2 Ligation 291

6.2.3 RT-PCR for expression level of human RHO 292

6.2.4 Determination of AAV titer (Rohr *et al.*, 2002) 292

6.2.5 Genotyping ____ 293

6.2.6 TaqMan® gene expression analysis ____ 294

6.2.7 Statistical analysis ____ 294

6.3 Results ____ *295*

6.3.1 Generation of AAV constructs ____ 295

6.3.2 Determination of AAV titres ____ 296

6.3.3 Effect of AAV2/5 – mediated delivery of WT and P23H RHO in 129Sv WT mice ____ 297

6.3.4 Effect of WT RHO and P23H AAV2/5 in Rho+/- mice ____ 298

6.3.5 Effect of 17-DMAG in P23H+/- Rho-/- mice ____ 299

6.4 Discussion ____ *301*

Chapter 7: Concluding remarks and Future Studies ____ *323*

Appendix ____ *329*

References

Figures and Tables

Figure 1. 1: The blood retina barrier. ---- 48

Figure 1. 2: Cross section of the inner and outer BRB. ---- 49

Figure 1. 3: Tight junctions of the retina/brain. ---- 50

Figure 1. 4: Model of the conserved structural and functional features of claudins. ---- 51

Figure 1. 5: Impairment of the blood–brain barrier in the claudin-5 -/- mouse. ---- 52

Figure 1. 6: Cross section of the mammalian eye. ---- 53

Figure 1. 7: Cross section through a mammalian retina. ---- 54

Figure 1. 8: Different routes of drug administration to the posterior eye. ---- 55

Figure 1. 9: Photographs of a normal (left) and RP retina (right). ---- 56

Figure 1. 10: RNAi pathway. ---- 57

Table 1. 1: Different types of RP and estimated percentages of these types. ---- 58

Table 1. 2: Identified genes responsible for RP and functions of their protein products. ---- 60

Figure 3. 1: Overview of the main molecular pathways leading to apoptosis. ---- 110

Figure 3. 2: CLDN5 and NT shRNA vector constructs. ---- 111

Figure 3. 3: Overview of light ablation experiments in Balb/c mice. ---- 112

Figure 3. 4: Safety assessment for CLDN5 siRNA. ---- 113

Figure 3. 5: Suppression of CLDN5 expression. ---- 114

Figure 3. 6: Effects of CLDN5 and ALLM on cell death. ---- 115

Figure 3. 7: Effect of CLDN5 siRNA and ALLM on α-fodrin cleavage. ---- 116

Figure 3. 8: Effect of CLDN5 siRNA and ALLN on cell death. ---- 117

Figure 3. 9: Effect of CLDN5 siRNA and ALLN on α-fodrin cleavage. ---- 118

Figure 3. 10: Effect of CLDN5 AAV2/9 and ALLM on photoreceptor degeneration in Balb/c mice 24 h post light ablation. ---- 119

Figure 3. 11: Effect of CLDN5 AAV2/9 and ALLM on α-fodrin cleavage. ---- 120

Figure 4. 1: Guanine nucleotide biosynthesis. ---- 148

Figure 4. 2: Genomic structure and retinal isoforms of IMPDH1 in mouse and human. -------- 149

Figure 4. 3: Mutations identified in IMPDH1 protein. ---------- 150

Figure 4. 4: Roles of heat shock protein chaperons in protein folding in eukaryotic cells. ----- 151

Figure 4. 5: Rod isolated response in mice treated with 1 and 2 weeks of 17-AAG. ---------- 153

Figure 4. 6: Representative images of IMP224-hrGFP staining. ---------- 155

Figure 4. 7: Transduced outer nuclear thickness per unit length post 7 weeks of 17-AAG treatment. ---------- 156

Figure 4. 8: Rod isolated response post 5 weeks of 17-AAG treatment.---------- 157

Figure 4. 9: Transduced ONL area per unit length of retinal sections 5 weeks post 17-AAG treatment. ---------- 158

Figure 4. 10: Average doxycycline intake by each mouse every 3 days. ---------- 159

Figure 4. 11: ERG measurements post 1 week of 17-AAG treatment.---------- 160

Figure 4. 12: Average intake of doxycycline every 3 days. ---------- 161

Figure 4. 13: Transgene construct for RP10 mouse model.---------- 162

Figure 4. 14: Gel electrophoresis for transgene in founder animals. ---------- 163

Figure 4. 15: ERG measurements of rod photoreceptors in founder animals. ---------- 164

Figure 4. 16: Schematic diagrams of different IMP224 transgenic generations. ---------- 166

Figure 4. 17: Sequencing for presence of rd8 mutation. ---------- 167

Table 4. 1: b-wave amplitudes of rod isolated response (μV). ---------- 168

Figure 5. 1: Unfolded protein response (ER stress response). ---------- 225

Figure 5. 2: The retinal rod photoreceptor cell. ---------- 226

Figure 5. 3: Phototransduction cascade. ---------- 227

Figure 5. 4: Mutations found in the RHO protein. ---------- 228

Figure 5. 5: The BiP/Grp94 chaperone system ---------- 229

Figure 5. 6: Effect of 17-DMAG in ER stress. ---------- 230

Figure 5. 7: pcDNA3 vector ---------- 231

Figure 5. 8: pcDNA3.1 (+/-) vector---------- 232

Figure 5. 9: Aggregation hotspots of human WT RHO and P23H RHO protein sequences.----- 233

Figure 5. 10: Effect of 17-DMAG on untransfected cells. ---------- 235

Figure 5. 11: Sequence analysis of WT RHO pcDNA3 and P23H RHO pcDNA3. ---------- 236

Figure 5. 12: Effect of P23H RHO on ER stress. ---------- 238

Figure 5. 13: Effect of 17-DMAG on ER stress in cells transfected with plasmid DNAs. --------- 240

Figure 5. 14: 17-DMAG treatment in cells transfected with P23H RHO.---------- 243

Figure 5. 15: 17-DMAG treatment and BiP expression levels in cells transfected with control DNA and WT RHO. ---------- 244

Figure 5. 16: 17-DMAG treatment and CHOP expression levels in cells transfected with control DNA and WT RHO. ---------- 246

Figure 5. 17: 17-DMAG treatment and Grp94 expression levels in cells transfected with control DNA and WT RHO. ---------- 248

Figure 5. 18: Gel electrophoresis of PCR products of Xbp1 cDNA obtained from mRNA in cells. ---------- 250

Figure 5. 19: Effect of 17-DMAG on BiP, Grp94 and peIF2α protein levels in cells transfected with P23H RHO.---------- 251

Figure 5. 20: Quantification of BiP, Grp94 and pEIF2α protein levels from figure 5.19. -------- 253

Figure 5. 21: Effect of 17-DMAG on CHOP and cleaved ATF6 protein levels in cells transfected with P23H RHO.---------- 254

Figure 5. 22: Quantification of cleaved ATF6 and CHOP protein levels from figure 5.21. ------ 255

Figure 5. 23: Aggregation of P23H RHO in cells.---------- 257

Figure 5. 24: Effect of 17-DMAG on RHO protein level in the insoluble fractions. ---------- 258

Figure 5. 25: Effect of 17-DMAG on Hsp40, Hsp70 and Hsp90 expression levels.---------- 260

Figure 5. 26: 17-DMAG concentrations and ER stress response in P23H-3 rats. ---------- 262

Figure 5. 27: Effect of 17-DMAG on BiP and CHOP expression levels in P23H-3 rats.---------- 263

Figure 5. 28: Effect of 17-DMAG on Grp94 and Xbp1 expression levels in P23H-3 rats. -------- 264

Figure 5. 29: Xbp1 splicing in P23H rats treated with 17-DMAG.---------- 265

Figure 5. 30: Western blot analyses of BiP in P23H-3 rats treated with 17-DMAG. ---------- 266

Figure 5. 31: Western blot analyses of CHOP in P23H-3 rats treated with 17-DMAG. ---------- 267

Figure 5. 32: Western blot analyses of Grp94, cleaved ATF6, peIF2α in P23H-3 rats treated with 17-DMAG. ---------- 268

Figure 5. 33: Western blot analyses of Grp94, cleaved ATF6, peIF2α in P23H-3 rats treated with 17-DMAG. ---------- 269

Figure 5. 34: Effect of 2 mg/kg/day 17-DMAG on the degenerating P23H-3 rat retina. --------- 270

Figure 5. 35: Effect of 4 mg/kg/day 17-DMAG on the degenerating P23H-3 rat retina. --------- 271

Figure 5. 36: Phenotypic analysis of the modulated iRBR in P23H-3 rats. ---------- 272

Figure 5. 37: Measurements of ONL thickness in P23H-3 rats treated with 17-DMAG. --------- 273

Figure 5. 38: Histological analysis of retinas of P23H-3 rats supplemented with 17-DMAG and doxycycline for 9 weeks. ---------- 274

Figure 5. 39: Rhodopsin staining of retinas of P23H-3 rats supplemented with 17-DMAG and doxycycline for 9 weeks. ---------- 275

Figure 5. 40: CLDN5 staining of retinas of P23H-3 rats supplemented with 17-DMAG and doxycycline for 9 weeks. ---------- 276

Figure 5. 41: ERG measurements of rod isolated response in P23H-3 rats treated with 0.2 mg/kg/day 17-DMAG. ---------- 277

Figure 5. 42: Effect of 0.2 mg/kg/day 17-DMAG on the degenerating P23H-3 rat retina. ------ 279

Figure 5. 43: Measurements of ONL thickness in rats treated with 0.2 mg/kg/day. ---------- 280

Table 5. 1: Weight of P23H-3 rats treated with A) 4 mg/kg/day and B) 0.2 mg/kg/day 17-DMAG. ---------- 281

Figure 6. 1: Schematic presentations of DNA construct. ---------- 305

Figure 6. 2: Gel electrophoresis of DNA fragments important for the generation of P23H and WT RHO pAAV-BB24 constructs. ---------- 306

Figure 6. 3: Sequencing results for WT RHO and P23H constructs. ---------- 307

Figure 6. 4: Expression levels of human RHO in adult 129Sv WT mice injected with WT RHO and P23H AAVs.---------- 308

Figure 6. 5: Titres of WT RHO AAV2/5 and P23H AAV2/5. ---------- 309

Figure 6. 6: ERG readouts in mice injected with P23H AAV2/5. ---------- 310

Figure 6. 7: Expression of RHO protein in 129Sv WT mice injected with WT RHO and P23H AAVs. ---------- 311

Figure 6. 8: ERG of mice treated with Dose 1 or 2 of AAV2/5. ---------- 312

Figure 6. 9: Effect of WT RHO AAV2/5 and P23H AAV2/5 in C57BL/6J and 129Sv Rho+/- mice.314

Figure 6. 10: ERG in C57BL/6J Rho+/- mice injected with AAV2/5. ---------- 316

Figure 6. 11: ERG in C57BL/6J Rho+/- mice injected with AAV2/5. ---------- 317

Figure 6. 12: ERG in C57BL/6J Rho+/- mice injected with AAV2/5 at 14 weeks post injection.318

Figure 6. 13: P23H RHO genotyping of transgenic animals.---------- 319

Figure 6. 14: Relative expression of levels of ER stress markers in P23H+/- Rho-/- mice treated with 17-DMAG. ---------- 320

Appendix Figure 1: IMP224 pAAV sequence ---------- 333

Appendix Figure 2: Standard curve of hrGFP-PolyA primers. ---------- 333

Appendix Table 1: Quantitative PCR results of primers for the IMPDH1 transgene and house-keeping genes. ---------- 335

Abbreviations

17-AAG	17-N-allylamino-17-demethoxygeldanamycin
17-DMAG	17-(dimethylaminoethylamino)-17-demethoxygeldanamycin
AAV	Adeno-associated virus
ABC	ATP-binding cassette
adRP	Autosomal domimant retinitis pigmentosa
AIF	Apoptosis-inducing factor
ALLM	N-Acetyl-Leu-Leu-Met-CHO
ALLN	N-Acetyl-Leu-Leu-Nle-al
AMD	Age related macular degeneration
Amp	Ampicillin
Apaf-1	Apoptotic protease activating factor 1
ASK	Apoptosis signal-regulating kinase
ATF6	Activating transcription factor 6
BAG-1	Bcl-2 associated athanogene-1
BBB	Blood-brain barrier
BCA	Bicinchoninic acid
Bcl-2	B-cell lymphoma 2
BCRP	Breast cancer resistance protein
bEND.3	Brain-derived endothelial
B-glob pA	Beta-globin polyA
BH	Bcl-2 homology
BiP	Immunoglobulin heavy chain binding protein
BRB	Blood-retina barrier
BSA	Bovine serum albumin
CD95	Cluster of differentiation 95
CDD	C-terminal dimerization domain
CHIP	Carboxyl terminus of Hsp70-interacting protein
CLDN	Claudin
CMT	Carrier-mediated transport
CNS	Central nervous system
CNV	Choroidal neovascularisation
CSF	Cerebrospinal fluid
Da	Dalton

DAPI	4', 6-diamidine-2-phenylindoledihydrochloride
DFF	DNA fragmentation factor
DHA	Dehydroascorbic acid
DIABLO	Direct IAP-binding protein with low PI
Dlg	Drosophila discs large protein
DMEM	Dulbecco's modified eagle media
DMSO	Dimethyl Sulfoxide
Dox	Doxycycline
dsRBD	dsRNA binding domain
dsRNA	Double-stranded RNA
DTT	Dithiothreitol
EDEM	ER degradation-enhancing α-mannosidase-like protein
EFEMP1	Epidermal growth factor-containing fibulin-like extracellular matrix protein 1
eIF2α	Eukaryotic translation initiation factor 2
ELOVL4	Elongation of very long chain fatty acids protein 4
endo G	Endonuclease G
ERAD	ER-associated degradation
ERdj	ER resident DnaJ
ERG	Electroretinogram
ERSE	ER stress element
f1 ori	F1 origin of replication
FSCN	Retinal fascin protein
GA	Geldanamycin
GCL	Ganglion cell layer
GCV	Ganciclovir
GLUT1	Glucose transporter 1
Grp	Glucose-related protein
GSL	Golgi localization sequence
GTP	Guanosine-5'-triphosphate
HPRT	Hypoxanthine phosphoribosyl transferase
Hsp	Heat shock protein
HSV-1	Herpes simplex virus type 1
i.p.	Intraperitoneal
iBRB	Inner blood-retina barrier

iBREC	Immortalised bovine retinal endothelial cells
IgG	Immunoglobulin G
IKK	Inhibitor of κB kinase
IMPDH1	Inosine 5'-monophosphate dehydrogenase
INL	Inner nuclear layer
IPL	Inner plexiform layer
IRE1	Inositol requiring kinase 1
ITR	Inverted terminal repeat
JAM	Junctional adhesion molecule
JNK	c-Jun amino-terminal kinase
kDa	Kilodalton
MAGUK	Membrane associated guanylate kinase
MD	Middle domain
miRNA	micro RNA
miRNP	miRNA ribonucleoprotein complex
MRI	Magnetic resonance imaging
MRP	Multi-drug resistance associated protein
NBD	N-terminal nucleotide binding ATPase domain
NGF	Nerve growth factor
NHR	Normal human allele
NMDA	N-methyl-D-aspartate
oBRB	Outer blood-retina barrier
ONL	Outer nuclear layer
OPL	Outer plexiform layer
OS-9	Osteosarcoma amplified 9
PARP-1	Poly (ADP-ribose) polymerase-1
PAZ	Piwi-Argonaute-Zwille
PDE-6	Phosphodiesterase-6
PDI	Protein disulfide isomerase
PEDF	Pigment epithelium derived growth factor
PEI	Polyethylenimine
peIF2α	phosphorylated eukaryotic translation initiation factor 2
PERK	Protein kinase-like endoplasmic reticulum kinase
PFA	Paraformaldehyde
P-gp	Permeability glycoprotein

PPI	Peptidyl prolyl isomerise
PSD	Post-synaptic density 95 kDa
PTGS	Post transcriptional gene silencing
pTRE-U6	Tet-responsive U6 promoter
pUC	pUC origin of replication
Rd	Retinal degeneration
RHO/Rho	Rhodopsin
RIS	Rod inner segment
RISC	RNA-induced silencing complex
RLBP1	Retinaldehyde binding protein
RMT	Receptor-mediated transport
RNAi	RNA interference
ROM	Rod outer segment protein
ROS	Rod outer segment
RP	Retinitis pigmentosa
RPE	Retinal pigment epithelium
RPE65	Retinal pigment epithelium-specific protein 65kDa
RPGR	Retinitis pigmentosa GTPase regulator
RT-PCR	Reverse transcriptase-PCR
S1P	Site-1 protease
SEM	Standard error of the mean
shRNA	Short, hairpin RNA
sHsp	Small heat shock protein
siRNA	Short interfering RNA
SLC	Solute carrier
ssRNA	Single-stranded RNA
Tat	Transactivator
Tet	Tetracycline
TJ	Tight junction
TLR	Toll like receptors
TNF	Tumour necrosis factor
TRAF2	TNF receptor-associated factor 2
tTS	Tetracycline inducible transcriptional suppressor
TUDCA	Tauroursodeoxycholic acid
TUNEL	TdT-mediated dUTP nick end labelling

UPR	Unfolded protein response
UPRE	Unfolded protein response element
USH2A	Usher's syndrome type II A
VEGF	Vascular endothelial growth factor
VEGFA	Vascular endothelial growth factor A
VEGFR	Vascular endothelial growth factor receptor
WBN/Kob	Wistar Bonn/Kobori
Xbp1	X-box binding protein -1
Xbp1s	Spliced Xbp1
ZO	Zonula occluden

Chapter 1

General Introduction

1.1 General Introduction

The endothelial cells lining the microvessels of the brain and the inner retina are joined by so-called tight junctions, comprising of upwards of 30 proteins, which, together form an exceedingly tight seal between these cells, representing the blood-brain and inner blood retina barriers. While allowing an abundant supply of oxygen and nutrients to the central nervous system, these barriers also prevent passive diffusion into the brain or retina of potentially harmful blood-borne agents such as antibodies, pathogens, immune cells and anaphylatoxins (Hawkins and Davis, 2005). While many degenerative retinopathies are potentially treatable using available low molecular weight drugs an estimated 98% of these cannot diffuse passively across these barriers (Pardridge, 2007). Poor penetration of such compounds is a result of the low rates of diffusion across tight junctions, the presence of P-glycoprotein efflux pump activities and a range of specific efflux receptors present in the microvascular endothelium. Many efforts have been made for the treatment of retinopathies by topical or intravitreal drug delivery. However, topical delivery is often ineffecient in producing therapeutic concentrations in posterior segment tissues owing to the long diffusion distance (Christie and Kompella, 2008). Although this problem can be overcome by intravitreal delivery of drugs by means of implants or injections, significant side effects have been linked with this type of delivery, such as postoperative endophthalmitis, haemorrhage and retinal detachment (Jager *et al.*, 2004).

Hence, in this introductory chapter, an outline of the structure of the blood-brain barrier/blood-retina barrier, together with details of tight junction proteins, which make up the seal characteristic of these barriers, will be provided. Different routes of drug delivery to the posterior segment of the eye will be discussed in terms of their advantages and disadvantages. In the developed world, the hereditary retinopathy, retinitis pigmentosa (RP) is the most prevalent cause of registered visual handicap among working-aged populations, the condition having been described as 'possibly the most genetically

heterogeneous of any hereditary condition for which molecular pathologies have been explored' - a major barrier to the development of genetic medicines. Thus, I will provide a brief overview of the structure of the human eye, the retina, and of the major symptoms and genetic etiologies associated with RP. In addition, since RNA interference-mediated suppression of transcript expression has been used extensively in this work, an introduction to this powerful technology will be outlined and how it forms the basis of a new technology, experimentally validated in this thesis, whereby reversible and transient modulation of the inner blood-retina barrier can facilitate systemic delivery of low molecular weight drugs in animal models of retinal degeneration induced by light ablation, or by mutations within the *IMPDH1* and *P23H* genes, which are established causes of adRP.

1.2 The blood-brain barrier

Despite much progress having been made in the pharmaceutical industry in the last few years, the number of products launched to treat diseases of the central nervous system has not met demand. This has been largely due to a shortfall in our understanding both of the underlying biology behind the diseases themselves and many factors contributing to the inefficiency of systemic central nervous system (CNS) drug delivery (Pardridge, 2002). The CNS is highly protected by the blood-brain barrier (BBB), the blood-retina barrier (BRB) and the blood-cerebrospinal-fluid (blood-CSF) barrier. The BBB is located at the endothelial cells of the brain capillaries while the blood-CSF barrier is located at the choroid plexus and meninges. These unique barriers regulate and control the selective transport of both exogenous and endogenous materials between the blood and neuronal tissues, thus maintaining the delicate microenvironment critical to the functions of the CNS machinery.

The BBB was first described by the German microbiologist Paul Ehrlich, in a series of experiments designed to compare oxygen consumptions of different organs (Ehrlich,

1885). Compared with peripheral organs, a lack of coloration in the brain and spinal cord was observed after intravenous injection of aniline dyes. At the time, Ehrlich concluded that this phenomenon was due to the nature of the dye. However, fifteen years after this observation, it was suggested that a mechanical membrane, termed the BBB separating the blood from brain, was involved in pharmacological actions excluding intravenously administered bile acids of ferrocyanide from the CNS (Lewandowski, 1990). In addition, nearly thirty years later, Ehrlich's student, Edwin Goldman, observed that coloration was confined to the CNS but not in other organs after injecting Trypan blue into the cerebrospinal fluid (Goldmann, 1913). Subsequently, the framework of the BBB structure was revealed by electron microscopy studies to be an endothelial barrier located in capillaries throughout the brain (Reese and Karnovsky, 1967, Brightman and Reese, 1969). The BBB is composed of brain microvascular endothelial cells, pericytes, a basement membrane, astrocytes and neurons. Anatomically, the brain microvascular endothelial cells are distinguished from peripheral endothelial cells by the higher mitochondrial content, the absence of fenestrations, low pinocytotic/endosomal transport activity and the presence of tight junction (TJ) proteins (Hawkins and Davis, 2005). These TJs play an important role in reducing paracellular permeability, increasing electrical resistance and controlling the slow rates of fluid phase transcytosis. Breakdown or dysfunction of the BBB has been described in several neurodegenerative and inflammatory diseases of the brain. For example, increased BBB permeability is caused by ischemic stroke and traumatic brain injury while the disruption of BBB is a precipitating event of multiple sclerosis (Klohs *et al.*, 2009, Cunnea *et al.*, 2010). Disturbance of BBB has also been associated with Alzheimer's disease although the relationship between BBB breakdown and pathology is not yet clear (Blennow *et al.*, 1990). In addition to ischemic/hypoxic factors, BBB function can also be compromised by drug abuse. It has been found that nicotine treatment distorts microvascular distribution of some TJ proteins, including zonula occluden-1 (ZO-1) and

claudin-3 and increased BBB permeability to sucrose in rats (Hawkins *et al.*, 2004). TJ abnormalities also appear to be involved in some forms of brain tumor which are characterised by oedema (Papadopoulos *et al.*, 2004). These authors also suggested that incomplete structure of tumor vasculature TJs was caused by the proangiogenic environment of tumor growth.

1.3 The Blood-retina Barrier

Similar to the BBB, the blood-retina barrier plays an important role in maintaining homeostasis of the microenvironment in the retina. It regulates movements of molecules and fluid between the blood flow and the retina through its inner and outer retina barriers (**Figure 1.1**). The inner retina barrier (iBRB) is composed of TJs between retinal capillary endothelial cells, while the outer blood retina barrier (oBRB) is formed by TJs between adjacent retinal pigmented epithelium cells. In addition, Muller cells, pericytes and astrocytes have also been reported to contribute to the proper functioning of the iBRB (Reichenbach *et al.*, 2007, Kaur *et al.*, 2008). The oBRB is important in regulation of nutrient transportation from the blood into the outer retina and also acts as a barrier for macromolecules from entering the retina.

1.3.1 The inner Blood-retina barrier

The retinal capillaries are located in the nerve fibre, ganglion cell and inner plexiform layers and at the junction of the inner nuclear and the outer plexiform layer of the retina (**Figure 1.1**). At the molecular level, the iBRB is extremely similar to the BBB, being made up of TJs of endothelial cells sheathed in pericytes, and glial cells which together constitute the iBRB. The TJs of the retinal epithelium are formed by binding of the outer leaflets of adjacent retinal endothelial cells; thus creating a highly restrictive and selective barrier for molecules in the lumen to cross into the retinal avasculature. In addition to the TJs, Muller cells, pericytes and astrocytes are also thought to contribute to the formation

and maintenance of the iBRB (**Figure 1.2**). Pericytes have been shown to be involved in maintenance of capillary structure and inhibition of endothelial cell proliferation (Hirschi and D'Amore, 1996). They are also known to strengthen the integrity of the iBRB by inducing expression of occludin and ZO-1 under normoxia and by partially reversing the decrease of occludin under hypoxic conditions (Wang *et al.*, 2007). Reduction in pericyte-endothelial cell contact associated with capillary changes during ageing has been shown to cause destabilization of the capillaries and impairment of metabolite exchange required for optimal neuronal function (Hughes *et al.*, 2006).

Muller cells also play an essential role in proper functioning of the iBRB. During hypoxic and inflammatory conditions, vascular endothelial growth factor (VEGF) secretion causes an increase of permeability of the iBRB. Under normal conditions, Muller cells are known to secrete pigment epithelium derived growth factor (PEDF) which is a VEGF antagonist, thus maintaining the integrity of iBRB (Eichler *et al.*, 2004). However, during hypoxic conditions, Muller cells have been shown to enhance secretion of VEGF, leading to destabilization and impairment of the TJs (Eichler *et al.*, 2000, Kaur *et al.*, 2006). Moreover, Muller cell dysfunction has been suggested to be involved in the breakdown of the BRB during diabetes (Tretiach *et al.*, 2005).

The third cell type important for the integrity of the iBRB is astrocytes. Astrocytes are closely associated with the retinal vessels and their contact with the mature brain vasculature has been reported to enhance expression of the TJ proteins ZO-1, occludin and claudin-5 (Willis *et al.*, 2004). Also, dysfunction of astrocytes has been reported to cause breakdown of the iBRB, triggering vasogenic oedema (Rungger-Brandle *et al.*, 2000).

1.3.2 The outer Blood-retina barrier

Unlike the BBB, the BRB also contains the oBRB, which is formed by a single layer of retinal pigmented epithelium (RPE) cells located between the neural retina and the choroid. The apical membrane of the RPE faces the outer segment layer and its basolateral

membrane faces the Bruch's membrane, separating the RPE from the fenestrated capillaries of the choroid (**Figure 1.2**). In addition to being a barrier layer for the retina, functions of the RPE also include absorption of light and protection of the retina from photooxidation, phagocytosis of shed photoreceptors membrane discs, conversion of all-trans retinal to 11-cis retinal in the visual cycle, maintenance of structural integrity of the retina through secretion of various factors (Simo *et al.*, 2010) and regulation of transport between the retina and fenestrated capillaries of the choroid. Moreover, the RPE also contributes to the maintenance of the immune privilege status of the eye by secreting immunosuppressive substances within the eye.

1.4 Tight junction proteins

TJs are contact points between the plasma membrane of adjacent epithelial and endothelial cells and are the major barrier for paracellular transport across these cells. The degree of paracellular transport varies among tissues and is dictated by the tightness of TJs. In contrast to cellular barriers in other parts of the body, the intercellular space between TJs present at the BRB/BBB is completely occluded due to the extremely tight lateral association of each pair of TJ strands. In addition to being the barrier to passive paracellular diffusion of water soluble substances from the circulation to the retina, TJs are also involved in vesicle targeting, cytoskeletal dynamics, signalling during proliferation and transcription, and defining cellular polarity (Campbell *et al.*, 2010b).

TJ proteins include integral transmembrane protein (occludin and claudins), junctional adhesion molecules (JAMs) and cytoplasmic proteins ZO, cingulin, 7H6 antigen, and symplekin) (**Figure 1.3**). Occludins and claudins are intercellular proteins which are linked to cytoplasmic and regulatory proteins ZO 1-3, symplekin, 7H6 and cingulin. JAM-1 (40 kDa) is a member of the IgG superfamily and mediates the primary attachment of adjacent cell membranes by homophilic interactions. JAM-1 contains a single transmembrane chain

with a large extracellular domain. JAM-2 and JAM-3 are also found present in endothelial and lymphatic cells, but not in epithelia (Bauer H-C, 2004).

Occludin, a 60 to 65 kDa protein has four transmembrane domains with the carboxyl and amino terminals oriented to the cytoplasm and two extracellular loops that span the intercellular cleft. Occludin has multiple sites for phosphorylation on serine and threonine residues and phosphorylation of this protein appears to regulate occludin association with the cell membrane (Hawkins and Davis, 2005). Claudins have similar membrane topology to occludin but no sequence homology. It has been suggested that claudins form the primary seal of the TJ and occludin acts as an additional supporting structure. Overexpression of claudins in fibroflasts can induce cell aggregation and formation of TJ strands; whereas this is not the case for occludin which is localised to TJ already formed by transfection with claudins (Kubota *et al.*, 1999). Furthermore, occludin knockout mice exhibit a morphologically and functionally normal phenotype thereby suggesting that occludin is not important for the formation of TJs (Saitou *et al.*, 2000). However, the presence of occludin at the TJs can increase TJ tightness (electrical resistance) which is mediated by the second extracellular loop domain (Wong and Gumbiner, 1997).

Up to 24 claudins (20-24 kDa) have been identified in mammals (Bauer H-C, 2004). All claudins have similar predicted folding and high sequence homology in the first and fourth transmembrane domains and extracullular loops with a very short internal N terminus (2-6 residues) (Heiskala *et al.*, 2001). Claudins are thought to form dimers through their extracellular loops via homophilic and heterophilic interaction between adjacent endothelial or epithelial cells (Furuse *et al.*, 1999). The first extracellular loop has a set of highly conserved amino acids (W-GLW-C-C) and it is highly possible that the two cysteine residues form a disulfide bond. The first loop influences paracellular charge selectivity (Colegio *et al.*, 2002) while the second extracellular loop has a bacterial recognizing site (Fujita *et al.*, 2000). The carboxyl terminus possesses a phosphorylation

site at Threonine 192 and a PDZ domain (except claudin-12) that binds to PDZ domains of other supporting proteins such as ZO 1-3 (Bazzoni, 2006) (**Figure 1.4**). The PDZ domain is a region of sequence homology in diverse signalling proteins. The name PDZ is derived from the first three proteins in which these domains were found: PSD-95 (post-synaptic density 95 kDa), Dlg (Drosophila discs large protein) and ZO-1. The expression pattern of claudins varies immensely among tissues and cell types and during different developmental stages. Consequently, the TJs at these tissues vary in electrical conductance, charge selectivity, solute permeability and size discrimination (Van Itallie *et al.*, 2004, Van Itallie and Anderson, 2006).

In addition to the integral transmembrane components of the TJs, there are several scaffolding proteins that are associated with them in the cytoplasm. These include members of the membrane associated guanylate kinase-like (MAGUK) homolog family. Three MAGUK proteins have been identified are ZO-1, ZO-2, ZO-3 which seem to be involved in the coordination and clustering of protein complexes to the cell membrane and in regulation of gene expression (Gonzalez-Mariscal *et al.*, 2000). ZO-1 (220 kDa) was the first protein positively linked to TJs and expressed in endothelial and epithelial cells as well as many cell types that do not express TJs. ZO-1 and ZO-2 (160 kDa) are phosphoproteins with high sequence homology which link transmembrane TJ proteins to the actin skeleton, bind to signalling molecules to communicate the state of the TJ to the interior of the cell and vice versa, and localize in the nucleus during stress and proliferation. Moreover, ZO-2 seems to have an ability to replace ZO-1 and facilitate normal formation of the TJ in cultured epithelia lacking ZO-1. ZO-3 (130 kDa) has been found to be in a complex with ZO-1 and ZO-2 (Hawkins and Davis, 2005).

Other accessory proteins of the BRB include cingulin and 7H6. Cingulin is about 140-160 kDa in weight and associated with ZOs and myosin (Citic, 1989). It is suggested to mediate the interaction between tight junction and the cytoskeleton via force transduction.

The function of 7H6 is not yet elucidated but this protein has been found to reversibly dissociate from the TJ complex under ATP depletion (Zhong *et al.*, 1994).

In addition, adherence junctions are formed by intracellular cadherin proteins to maintain cell-cell adhesion between neighboring endothelial cells. Similar to occludin and claudins, cadherin proteins are also linked to the cytoplasm by scaffolding proteins, including catenin (Petty and Lo, 2002).

1.4.1 Claudin-5 in the blood-retina barrier

There are reports of at least 24 members of the claudin family (Van Itallie and Anderson, 2006). Claudins-1, -3, -5 have been detected in brain capillary endothelial cells and they are likely to play important roles in creating the characteristic seal which defines the BRB/BBB. In particular, expression of claudin-5 has been reported to be at least 593-fold greater than that of claudin-1, 3, and -12 (Morita *et al.*, 1999) and to play an important role not only in the BBB but also in the iBRB. Indeed, Nitta *et al.* (2003) in their seminal work on claudin-5 knockout mice, highlighted the importance of claudin-5 in maintaining the BBB integrity. The knockout mice were born alive, but died within one day of birth without any morphological abnormalities in the brain. However, tracer perfusion experiments and magnetic resonance imagining (MRI) analyses in these mice revealed that the BBB was impaired in brain endothelial cells (**Figure 1.5**) and allowed diffusion of molecules up to 800 Da in size.

Koto *et al.* (2007) have suggested that down-regulation of claudin-5 under hypoxia disrupts the neural vasculature barrier both *in vivo* and *in vitro*. In this study, changes of claudin-5 protein levels in the plasma membrane of brain-derived endothelial (bEND.3) cells under hypoxia were shown to correlate with changes in the transendothelial electrical resistance. Moreover, claudin-5 is highly expressed in the plasma membrane of retinal microvascular endothelial cells under normal conditions *in vivo* while hypoxia significantly reduces the level of claudin-5 in the membrane of these cells. In addition, inhibition of

claudin-5 expression using RNAi leads to a reduction of transendothelial electrical resistance in bEND.3 cells even under normoxic conditions. These studies imply that claudin-5 has a critical role in maintaining the integrity of the BRB under hypoxic conditions. Other protein members (occludin, claudin-1, claudin-3) of the TJ have also been implicated to be hypoxia-sensitive. Therefore, understanding of hypoxia-induced breakdown of barrier function of neural endothelial cells could potentially identify new therapeutic targets for diseases such as diabetic retinopathy and cerebral ischemic diseases. Interestingly, diabetic retinopathy has been linked with deregulation of vascular endothelial growth factor (VEGF) expression, which is induced under hypoxic conditions. An increase in VEGF expression raises the permeability of vascular surfaces resulting in a breakdown of the BRB both *in vivo* and *in vitro*. Deissler *et al.* (2008) showed that treatment of immortalised bovine retinal endothelial cells (iBREC) with $VEGF_{165}$ had no effect on the expression of claudin-5 while significantly diminishing localisation of claudin-1 in plasma membrane. Moreover, Barber and Antonetti (2003) suggested that VEGF increased permeability of the BRB through redistribution of occludin while localisation of claudin-5 in the plasma membrane of endothelial cells was not affected.

Furthermore, levels of claudin-5 have been shown to correlate with permeability changes during the intermediate stage of chick RPE development (Kojima et al, 2002). In this study, claudin-5 was demonstrated to be transiently expressed during the development of RPE using Northern blotting, semi-quantitative RT-PCR and immunoblotting. On the other hand, claudin-3 was expressed only in the choroid layer of the eye. The expression level of claudin-5 was at peak during the intermediate stage of development (between embryonic days 10 and 14). The study also speculated that an increase in claudin-5 during this developmental stage could lead to an increase in strand number or branching since rudimentary junctions formed by occludin at E7 could be strengthened by the increase in claudin-5.

1.5 Transport systems across the BRB

In general, there are two main routes by which molecules are transported across the iBRB: a paracellular route and a transcellular route. Paracellular transport is passive and driven by a gradient mechanism via TJs between neighboring endothelial cells. The pathway is highly evolved and more selective than in any other region of the body; therefore the majority of molecules circulating in the blood can cross the iBRB only via the transcellular route, which is both an active and passive transport system allowing sets of small and large hydrophilic molecules to enter the brain through cell membranes. The transcellular route can be classified into free diffusion, carrier-mediated transport (CMT), and receptor-mediated transport (RMT). Only molecules which are either less than 400 Da and/or highly lipophilic and are not substrates of efflux transporters can cross the barrier by free diffusion. The essential nutrients, glucose and certain amino acids are transported via CMT by the specific membrane transporting proteins which are present in relatively high concentrations in the BRB (Gaudana *et al.*, 2010). Certain large-molecule peptides or plasma proteins are selectively transported across the barrier via RMT initiated with receptor-mediated endocytosis of the molecules.

There are two types of transporters present at the BRB: influx transporters and efflux transporters. Efflux transporters mainly belong to the ATP binding cassette superfamily whereas influx transporters belong to the solute carrier (SLC) superfamily. Influx transporters facilitate the translocation of essential nutrients and xenobiotics across the barrier membrane. These include carriers for amino acids, peptides, vitamins, glucose, lactate, and nucleoside/nucleobases. For example, Glucose transporter 1 (GLUT1) transports D-glucose the main energy source for the retina and dehydroascorbic acid (DHA) an omega-3 fatty acid essential for visual function from blood to retina (Puchowicz *et al.*, 2004). GLUT1 is present in both the luminal and abluminal membranes of the iBRB and in both the apical and basolateral membranes of the RPE. Although GLUT1 is

expressed in two sides of the membranes, D-glucose and DHA are predominantly transported from the blood to retina rather than the opposite direction. This is due to the fact that GLUT1 is expressed from two to threefold greater at the luminal membrane of the iBRB/basolateral of the oBRB than at the abluminal/apical membrane in humans and rats (Takata *et al.*, 1992). Glycosylated neuropeptides were also shown to be transported from blood to brain via GLUT1 transport at the BBB. This suggests that anologs of GLUT1 substrates can be transported from blood to retina at the BRB (Polt *et al.*, 1994).

Precursors of neurotransmitters and protein synthesis such as L-Leucine and L-phenylalanine are transported from blood to retina via a Na^+ independent neutral amino acid transporter (system L) at the BRB (Tomi *et al.*, 2005). Several other amino acid transporters have been suggested to be involved in blood to retina influx transport of amino acids such as taurine, glycine, L-cystine and D/L serine at the iBRB (Hosoya and Tachikawa, 2009). Creatine is essential for energy homeostasis while biotin is a coenzyme in the metabolism of fatty acids and leucine in the retina. Na^+ dependent creatine transporter and Na^+ dependent multivitamin transporter are expressed in the iBRB and responsible for the transport of creatine and biotin from blood to retina (Nakashima *et al.*, 2004, Ohkura *et al.*, 2010). Creatine and biotin are constantly transported from blood to retina to maintain their concentration in the retina.

Monocarboxylates such as lactate, pyruvate and ketone bodies are vital molecules in cellular physiology of most mammalian cells. L-lactic acid especially appears to be a required energy source in addition to D-glucose in photoreceptors. Therefore, monocarboxylate transporters are expressed in both sides on membranes of the iBRB and RPE (Philp *et al.*, 1998, Martin *et al.*, 2007). In addition, nucleoside transporters transport adenosine which is essential in retinal neurotransmission, blood flow, vascular development and response to ischemia through cell surface adenosine receptors (Nagase *et al.*, 2006). Other types of transporters present at the BRB include folate transporters for

influx of folates which are required for the *de novo* synthesis of purines, pyrimindines, some amino acids and for the conversion of homocysteine and methionine; and organic cation transporters which mediates the transport of cations such as acetyl-L-carnitine from blood to retina.

Although the systems described above are influx transportations from blood to retina, highly active efflux pumps present in relatively high concentrations at the BRB function in the opposite direction, from retina to blood. This offers an additional layer of protection to the retina by expelling harmful molecules back into the blood but also results in limiting the delivery of systematically available substrates to the retina (Bellavance *et al.*, 2008). Efflux of xenobiotics including drugs which are taken up by the circulating blood can be initiated by ATP-binding cassette (ABC) transporters which are expressed at the luminal and basolateral membrane of the inner and outer BRB. Permeability glycoprotein (P-gp), an ATP-dependent efflux pump, is present in relatively high concentrations in the luminal membrane of the iBRB and the basolateral membrane of oBRB. P-gp mediates rapid removal of lipophilic compounds from the retina to blood. In addition, several multi-drug resistance associated proteins (MRP) and the breast cancer resistance protein (BCRP) are expressed at the inner and outer BRB. MRPs efflux organic anions and conjugated compounds such as glucuronic acid conjugates and glutathione conjugates whereas BRCP transporters efflux both drugs and photosensitive toxins (Hosoya and Tachikawa, 2009).

In addition, there is a large volume of water produced in the retina as a consequence of high metabolic turnover in neurons and photoreceptors. Intraocular pressure also leads to the movement of water from the vitreous chamber into the retina. Therefore, water is constantly removed from the inner retina to retinal capillaries via Muller cells and from the subretinal space to choriocapillaries via the RPE. Due to the presence of TJs, the paracellular resistance is 10 times higher than the transcellular resistance. Thus, water

transport occurs predominantly through the transcellular route driven by the transport of K^+ and Cl^- ions and facilitated by aquaporin-1 (Simo *et al.*, 2010).

Overall, the transport systems for essential molecules at the BRB are highly regulated by TJ proteins and different types of efflux and influx transporters. Together, they protect the neural retina from xenobiotics, toxic and blood borne substances; restrict non-specific transports while supplying necessary nutrients for the energy demanding retina. Thus, the presence of the BRB makes it a very challenging task to introduce drugs to the posterior segment of the eye for the treatment of neurodegenerative diseases. It has been shown that molecules with size less than 400 Da and high liposolubility have potential to cross the BRB in pharmacologically significant amounts (Pardridge, 2003). Therefore, increasing lipophilicity of such molecules is an efficient strategy to increase BRB permeability of compounds, and has been applied to drug development in the pharmaceutical industry for a long time (Li and Cha, 2007). However it seems to have reached the limitation as those drugs treat only a handful of CNS conditions, generally restricted to affective disorders such as epilepsy and insomnia (Krause *et al.*, 2008). In addition, modifying drugs to allow targeting of various influx transporters while simultaneously avoiding efflux transporters has had some success; however, this method is costly and time consuming due to the specificity of these transporters (Mannermaa *et al.*, 2006, Hosoya and Tachikawa, 2009).

1.6 Structure of the eye

The eye is a unique and delicate sensory organ that carries out one of the most energy demanding process of any organ or tissue in the body. The eye can be divided into three distinct layers: 1) the external layer forming the sclera and cornea, 2) the intermediate layer consisting of two parts: anterior (iris and ciliary body) and posterior (choroid), and 3) the internal sensory part of the eye, the retina. To add to the complexity, there are three chambers of fluid within the eye including the anterior chamber (between the cornea and the iris), the posterior chamber (between the iris, suspensory ligaments and transparent

lens), the vitreous chamber (between the lens and the retina). The first two chambers contain aqueous humour whereas the vitreous chamber is filled with a more viscous fluid, the vitreous humour (**Figure 1.6**).

1.6.1 The retina

Light entering the eye is focused on the retina by the transparent cornea and lens. The focus point for image in the retina is the fovea. **Figure 1.7** shows a cross section of the mammalian retina. Light hits the ganglion cell layer first and then passes through the inner plexiform layer, the inner nuclear layer, the outer plexiform layer before reaching the outer nuclear layer containing nuclei of photoreceptors. The heavily pigmented layer, the RPE absorbs light not absorbed by the photoreceptors. Humans possess five types of photo-sensitive neuron in their retina: rod photoreceptors containing the photoreactive pigment rhodopsin; three types of cone photoreceptors containing either red, blue or green opsins which have peak absorption spectra in the red, blue, green wavelengths, respectively; and melanopsin containing ganglion cells. Photoreceptors are responsible for initiation of vision while photo-sensitive ganglion cells are involved in maintenance of circadian rhythms. In addition to these neurons, the retina also contains amacrine cell, bipolar cell and horizontal cell neurons in the inner nuclear layer. Hence, the retina is a very complex tissue with different types of neurons forming a dynamic network to convert light energy into electrical pulses for image processing in the brain.

1.6.2 Photoreceptors

Rod and cone photoreceptors are generated in precise patterns over the retina during development. In particular, rod photoreceptors are highly sensitive and mediate vision at night or in dim light while cone photoreceptors are less sensitive and mediate colour vision and fine acuity in daylight. The vertebrate retina has only one type of rod but several types of cones containing different opsins. However, rods are the most abundant photoreceptor

cell in the eye, consisting of approximately 95% of all photoreceptor cells (Rattner *et al.*, 1999). Most mammalian species have dichromatic color vision mediated by two cone opsins that respond to blue and green wavelengths of light. On the other hand, humans generally possess trichromatic color vision due to the presence of red light-sensitive opsin. Rod and cone photoreceptors are also distributed in distinct patterns over the entire retina. These patterns are different among species. For example, in the human retina, the three types of cone photoreceptors occur in a mosaic pattern and are greatly concentrated in and around the fovea where there are no rod photoreceptors (Xiao and Hendrickson, 2000), while approximately 125 million rods are located mainly around the peripheral retina. In contrast, blue and green opsins are distributed in opposing gradients in cones over the superior-inferior plane of the mouse retina, and cones are interspersed throughout with greater number of rods (Xiao and Hendrickson, 2000).

1.7 Drug delivery in the retina

Currently, there are still no available treatments for various common retinopathies and neurodegenerative diseases. Local drug delivery to the retina is particularly challenging because of the presence of the BRB. Various strategies have been attempted to deliver drugs to the retina. One such method is by the transient modification of the barrier properties of the RPE and endothelial cells of the iBRB by intracarotid infusion of a hyper-osmotic solution such as mannitol or arabinose; however, this results in a non-specific opening of the BRB and is associated with retinal and nervous system toxicity (Frank *et al.*, 1986, Millay *et al.*, 1986). Another common method to bypass the BRB is the chemical modification of drug molecules to lipophilic prodrugs, a process which increases transcellular diffusion into the neural retina (Macha and Mitra, 2002). The amount of drug retained in the retina after administration depends on the delivery method. Common delivery techniques include systemic administration, topical application, intravitreal injection, local injection and the use of ocular implants (**Figure 1.8**).

1.7.1 Systemic administration

Following systemic administration, the blood-aqueous barrier and the BRB are the major barriers for anterior chamber and posterior chamber drug delivery, respectively. The blood aqueous layer consists of two cell layers located in the anterior segment of the eye which are the endothelium of the iris/ciliary blood vessels and the non-pigmented ciliary epithelium. TJ complexes present in these two layers prevent the entry of solutes into the intraocular environment of the aqueous humor (Barar *et al.*, 2008). A number of hydrophilic and many lipophilic substances such as chloramphenicol and tetracycline can penetrate the blood aqueous barrier. However, typically only 1-2% of plasma drug concentration reaches the vitreous humor. Thus, this method requires repeated administration and high dosage of drugs in order to maintain minimum working concentrations in the ocular tissue, which can potentially lead to complications including non-specific absorption by other tissues. This in turn could cause serious toxicities thus outweighing the advantages of this method (Duvvuri *et al.*, 2003). For example, in glaucoma therapy, oral carbonic anhydrase inhibitors such as acetazolamide and ethoxzolamide have been discontinued in most cases owing to their systemic toxicity (Kaur *et al.*, 2002).

On the other hand, the BRB restricts penetration of drugs from blood into the posterior segment of the eye. Following oral or intravenous dosing, drugs can easily enter the choroid owing to the high degree of vascularisation and high fenestration of the choriocapillaries compared to retinal capillaries. However, the RPE constituting the oBRB restricts further entry of drugs from the choroid into the retina. Permeability of most therapeutic compounds across the BRB is very low or non-existant, except for extremely lipophilic compounds such as chloramphenicol and benzyl penicillin (Hughes *et al.*, 2005). Therefore, highly specific drug delivery systems are needed to overcome the strict

regulation of the BRB and facilitate drug absorption from the choroid or retinal capillaries into deeper layers of the retina.

1.7.2 Topical administration

Topical administration is the preferred method of drug delivery due to better patient compliance and cost affordability. Topical applications, including ophthalmic solutions and ointments are efficient delivery methods for the anterior segment comprising of the cornea, conjunctiva, sclera, iris-ciliary body and lens. However, topical delivery of drugs is ineffective in producing therapeutically relevant concentrations in the posterior segment due to the long diffusion distance (Christie and Kompella, 2008). Drug absorption from topical delivery has been suggested to occur through two routes: the corneal and non-corneal (conjunctival/scleral) pathways. In the corneal pathway, constraints to drug absorption include solution drainage, lacrimation and tear dilution, tear turnover, conjunctival absorption and the corneal epithelium barrier. On average, application of an aqueous dose leaves the pre-corneal area within 5 minutes in humans (Chrai *et al.*, 1974, Makoid *et al.*, 1976) and typically, less than 1-3% of the topically applied dose gets absorbed into the aqueous humor (Bird *et al.*, 1986, Duvvuri *et al.*, 2003). This low fraction of applied drug reaching the aqueous humor undergoes further elimination from the intraocular tissues and fluids by distribution into non-target tissues and as a consequence of aqueous humor flow. Enzymatic metabolism also takes place resulting in further loss of drug in the anterior chamber before it reaches the posterior segment. Clearly, barriers towards drug absorption through the pre-corneal pathway are not easy to overcome.

The non-corneal route of absorption involves penetration across the conjunctiva and sclera and then into the intraocular tissues. This mechanism of absorption has been shown to be significant for compounds with poor corneal penetration properties such as insulin, timolol maleate and prostaglandin PGF2-ALPHA (Bito and Baroody, 1981, Schoenwald *et al.*,

1997). However, this route tends to be considered non-productive with respect to drug availability in the anterior chamber of the eye and also causes significant uptake into systemic circulation due to the presence of conjunctival blood capillaries and lymphatics. Many efforts have been made to increase drug absorption through the corneal pathway by using high concentrations of penetration enhancers to increase bioavailability; however, this can lead to toxicological complications (Janoria *et al.*, 2007).

1.7.3 Intravitreal and sub-conjunctival injections

Intravitreal injection requires direct injection of drug into the posterior segment, thus bypassing all the barriers. Many studies have been carried out to evaluate the pharmacokinetic parameters of antiviral agents, antibiotics, steroids and monoclonal antibodies following intravitreal injection so that proper dose and dosing frequency could be developed. This route of administration is more suitable for drugs with high molecular weight (>500 Da) and longer half-life. Although this method can increase drug concentration in the neural retina and lower the required dose, thus offering advantages over systemic and topical routes for drug delivery, it suffers from many drawbacks due to the requirement for repeated injections, including retinal detachment, retinal haemorrhage, endophthalmitis and patient non-compliance (Jager *et al.*, 2004). For example, intravitreal injections of ganciclovir (GCV) to control cytomegalovirus retinitis have been shown to cause retinal detachment in 6%; intravitreal haemorrhages in 1% and endophthlamitis in 1% of treated eyes (Ausayakhun *et al.*, 2005). Thus, intravitreal injection is not necessarily the ultimate strategy for drug delivery to the posterior segment.

As an alternative method, peri-ocular injections have also been developed. This type of drug delivery includes subconjunctival, subtenon, retrobulbar and peribulbar administration and is considered less invasive than intravitreal injection. In particular, sub-conjunctival injection avoids the conjunctival epithelial barrier, which regulates permeation of water soluble drugs. Nevertheless, there are many other factors limiting drug

access to the posterior segment of the eye. These include dynamic barriers such as conjunctival blood and lymphatic circulation leading to rapid drug elimination after sub-conjunctival injections (Kim *et al.*, 2008). The molecules that escape this elimination permeate through sclera and choroid to reach the retina. The sclera is a highly permeable barrier and permeability across this barrier depends on the molecular size rather than lipophilicity of the molecule (Unlu and Robinson, 1998). However, the high blood flow of the choroid and BRB are the significant barriers to the drug access into the retina.

1.7.4 Intravitreal implants

Intravitreal implants have been developed as an alternative method to intravitreal injections. Vitrasert is a non biodegradable intraocular GCV implant to treat cytomegalovirus retinitis. It is surgically placed in the posterior segment of the eye and replaced every 5-8 months after locally delivering all of its GCV content. Phase III clinical trial data showed that disease progression was significantly delayed in patients implanted with Vitrasert compared to patients intravenously injected with GCV. However, the risks encountered with GCV intravitreal injection were not fully eliminated. Adverse reactions reported for Vitrasert include vitreous haemorrhage, retinal detachment, lens opacities, cataract formation, macular abnormalities, intraocular pressure spikes, optic disk/nerve changes, hyphemas, uveitis, acute or delayed onset endophthalmitis and loss of visual acuity (Sakurai *et al.*, 2001). In addition, repeated surgeries are required for implantation and removal of the implant.

Scleral implants are also employed to avoid the risks associated with injection method. Different biodegradable devices have been recently developed to lower the surgery related risk (Sakurai *et al.*, 2001). Similar to intravitreal implants, the main disadvantages to these sclera implants are repeated surgeries and patient discomfort.

1.8 Retinitis pigmentosa

Retinitis pigmentosa is a group of inherited retinopathies that affect 1 in 3500 people worldwide (Haim, 2002, Daiger *et al.*, 2007). RP encompasses many hereditary conditions with many distinct causes and diverse biological pathways but with overlapping symptoms and similar consequences (Daiger *et al.*, 2007). The early symptoms of RP include night blindness followed by loss of visual field from mid-periphery to far-periphery, leading to tunnel vision and eventually legal blindness or complete blindness (Daiger *et al.*, 2007). As the disease progresses, retinal vessels are attenuated and pigmented deposits in a bone-spicule configuration can be observed on the surface of the retina (Farrar *et al.*, 2002) (**Figure 1.9**). The symptoms of RP may start in early teenage years and severe visual impairment normally occurs around 40-50 years of age. However, some patients remain asymptomatic until mid-adulthood. On the other hand, there are early onset forms of RP that are often diagnosed as recessive Leber congenital amaurosis; and even non-penetrant forms (Hartong *et al.*, 2006, Daiger *et al.*, 2007). Electroretinograms (ERGs) which measure the electrical response of the retina to flashes of light and other tests for visions show that retinal degeneration already persists at the age of 6 years even in patients who remain asymptomatic until young adulthood (Berson *et al.*, 1985).

At the cellular level, the characteristics of RP include progressive degeneration of the retinal photoreceptors including rods and cones; typically starting in the mid-periphery and advancing towards the macula and fovea (Heckenlively *et al.*, 1988). RP is caused by death of rod photoreceptors leading to loss of cone photoreceptors and eventually complete loss of vision. In most forms of RP, loss of rod photoreceptors is much greater than that of cone photoreceptors. On the other hand, rod and cone functions decline are at similar rates in some forms of RP. Interestingly, in cone-rod degeneration type RP, early symptoms involve loss of visual acuity during daytime and defective colour vision due to greater loss

of cones compared to rods (Hartong *et al.*, 2006). Collectively, all of these studies show that RP is a very complex and highly variable disorder.

Moreover, there are different inherited forms of RP including autosomal recessive (13% of cases), autosomal dominant (20% of cases), X-linked (8% of cases) (Daiger *et al.*, 2007) (**Table 1.1**). In addition, non-Mendelian inheritance patterns of RP have also been reported such as rare mitochondrial and digenic forms which occur in very small proportion of cases (Zeviani *et al.*, 1988, Kajiwara *et al.*, 1994). Although RP is often confined to retinal degeneration, about 20-30% patients have RP as a part of more complex syndromes such as Usher's syndrome and Bardet-Biedl syndrome (Hartong *et al.*, 2006). In Usher's syndrome – one of the most common syndromic forms of RP, patient suffer from hearing impairment from as early as birth and later from RP by early teenage years (Kimberling *et al.*, 2000, Keats and Savas, 2004). Pennings *et al.* (2003) have shown that Usher's syndrome can be caused by mutations in at least 11 genes. Interestingly, mutations in some of these genes can cause either RP without hearing loss (Rivolta *et al.*, 2002, Aller *et al.*, 2004) or deafness without RP (Astuto *et al.*, 2002). Another frequent syndromic form of RP is Bardet-Biedl syndrome (5-6% of cases) which is associated with obesity, mental retardation, polydactyly, renal abnormalities, hypogenitalism (Beales *et al.*, 1999, Katsanis, 2004). To date, ten genes responsible for this syndrome have been identified and known to cause about 70% of cases (Stoetzel *et al.*, 2006). Moreover, there are also many rare syndromic forms of retinitis pigmentosa including Bassen-Kornzweig syndrome (abetalipoproteinaemia) and Refsum's disease (phytanic acid oxidase deficiency) (Hartong *et al.*, 2006).

During the past few decades, knowledge of genes and mutations causing inherited retinal diseases especially RP has greatly advanced. The first dominant RP gene was found to be tightly linked to the region encoding the photoreceptor pigment rhodopsin (McWilliam *et al.*, 1989, Farrar *et al.*, 1990). Later, Dryja *et al.* (1991) confirmed that mutations within

the rhodopsin (*RHO*) gene result in adRP. In addition to *RHO*, mutations in many genes with many diverse functions have been associated with RP. For example, some encodes proteins of phototransduction cascade (Dryja *et al.*, 2000) and rod cGMP gated cation channel α, β subunits (Dhallan *et al.*, 1992, Korschen *et al.*, 1999, Poetsch *et al.*, 2001). Mutations in genes essential for vitamin A metabolism that are associated with photoreceptor degeneration include retinal pigment epithelium-specific protein 65kDa (RPE65) (Moiseyev *et al.*, 2005) and retinaldehyde binding protein (RLBP1) (Saari *et al.*, 2001). In addition, genes with important functions in cell signalling, protein trafficking, pH regulation, phagocytosis have also been found to be associated with RP (**Table 1.2**).

To date, 17 autosomal dominant, 16 autosomal recessive and 6 X linked genes have been identified by linkage studies and candidate gene screening; in addition to many other genes involved in syndromic and systemic disorders (http//:www.sph.uth.tmc.edu/RetNet/ provided in the public domain by the University of Texas Houston Health Science Center, Houston, TX). Most genes for RP cause only a small proportion of cases while the *RHO* gene accounts for approximately 30-40% of adRP, the Usher's syndrome type II A (*USH2A*) gene is potentially linked to approximately 20% of recessive disease and the retinitis pigmentosa GTPase regulator (*RPGR)* gene is involved in approximately 70% of X linked RP (Hartong *et al.*, 2006).

1.9 Protein aggregation and diseases

It is widely accepted that aggregation of misfolded proteins causes many neurodegenerative diseases and retinopathies. In the case of retinopathies, a missense at amino acid position 23 (P23H) is the most common RHO mutation leading to autosomal dominant RP in North America (Dryja *et al.*, 1991). Various studies have suggested that the P23H protein is misfolded in the ER, extremely prone to aggregation, recruits cellular chaperones and targets wild type rhodopsin for degradation by the ubiquitin proteasome degradation (Saliba *et al.*, 2002). Thus, ER stress caused by overloading of mutant opsins

could initiate a detrimental cascade leading to photoreceptor apoptosis. In addition, some mutations in the *RDS-peripherin* gene (e.g missense mutation N244K) have been implicated in protein misfolding (Conley *et al.*, 2010). Marmorstein *et al.* (2002) demonstrated that inefficient secretion and accumulation of epidermal growth factor-containing fibulin-like extracellular matrix protein 1 (EFEMP1) in RPE cells could lead to EFEMP1 aggregation resulting in apoptosis cell death in age related macular degeneration. Additionally, it has been previously reported that the missense mutation Arg224Pro in the inosine 5'-monophosphate dehydrogenase (*IMPDH1)* gene responsible for the RP10 form of RP results in misfolded and insoluble aggregation of mutated proteins in the cell cytosol (Aherne *et al.*, 2004). Protein aggregation has been also observed in many common neurodegenerative disorders such as Alzheimer's disease, Parkinson's disease as well as Huntington's disease, amyotrophic lateral sclerosis, prion diseases and others (Sherman and Goldberg, 2001, Bucciantini *et al.*, 2002, George, 2002).

1.10 Apoptosis in neurodegenerative diseases

Apoptosis has been proposed to be the mode of cell death in various neurodegenerative conditions such as Huntington's disease, Alzheimer's diseases, age related macular degeneration, glaucoma and retinitis pigmentosa. However, the precise mechanism of this process is not fully understood. In the classical sense, apoptosis involves activation of various caspases which in turn cleave different intracellular proteins leading to cytoskeletal destruction, DNA fragmentation and autophagocytosis. There are two major apoptotic pathways. The extrinsic pathway occurs upon ligands binding to cell surface receptors resulting in activation of pro-caspase 8 which then cleaves downstream caspases. On the other hand, cellular stress such as oxidative stress triggers release of cytochrome c from the mitochondria into the cytosol in the intrinsic pathway. Cytochrome c then forms a complex with apoptotic protease activating factor 1 (Apaf-1) that turns pro-caspase 9 into its active form initiating a caspase cascade. However, the two apoptosis pathways are not mutually

exclusive. Caspase 8 can interact with BH3 interacting-domain protein (Bid), a pro-apoptotic protein of the B-cell lymphoma 2 (Bcl-2) family which then leads to release of mitochondrial cytochrome c into the cytoplasm. Recently, the mechanism of apoptosis has been questioned since studies in which caspases were inhibited by pharmacological inhibition or genetic manipulation did not necessarily increase cellular survival. Furthermore, accumulating evidence showing calpain activation during apoptosis (Nath *et al.*, 1996) suggests that apoptosis could occur in a caspase independent fashion.

Calpain activation has been implicated in various neuronal pathological conditions such as Alzheimer's disease, Parkinson's disease and Huntington's disease (Nixon, 2003, Bizat *et al.*, 2005). In addition, calpain mediated proteolysis has been observed in retinal degeneration in several animal models of RP and glaucoma (Donovan and Cotter, 2002, Doonan *et al.*, 2003, Huang *et al.*, 2010). Intravitreal injection of calpastatin, an endogenous calpain inhibitor, into the *rd1* mouse model for RP reduced photoreceptor cell death (Paquet-Durand *et al.*, 2010). However, treatment of rd mouse retinal explants with the calpain inhibitor N-Acetyl-Leu-Leu-Nle-al (ALLN) effectively reduced cleavage of alpha fodrin but did not protect photoreceptor survival (Doonan *et al.*, 2005). Moreover, many other calpain inhibitors cross inhibit other cysteine proteases such as caspases and cathepsins. The same is true for so called caspase specific inhibitors such as zVAD-fmk and z-DEVD-fmk which also potently inhibit calpains (Paquet-Durand *et al.*, 2007). In addition, SNJ-1945, a novel oral calpain inhibitor, significantly reduces cell loss in the ganglion cell layer and thinning of the inner plexiform layer induced by NMDA (N-methyl-D-aspartate) (Shimazawa *et al.*, 2010).

1.11 RNA interference (RNAi)

The recently discovered phenomenon of RNAi has not only given insight into complex cellular regulation of gene expression but also created a powerful tool for the study of gene function. RNAi was first reported in studies of petunia plants by two independent groups

23 years ago (Napoli *et al.*, 1990, van der Krol *et al.*, 1990). The original experiments were set out to increase the colour intensity of petunia petals by introducing extra copies of chalcone synthase gene, which is responsible for the synthesis of red pigment. In contrast to their expectation, many of the genetically engineered flowers lost their natural pigmentation while patterned flowers with white non-clonal sectors on wild-type pigmented background were produced. This ambiguous effect was later termed as co-suppression. At this time, it was thought that single-stranded RNAs (ssRNAs) were capable of inducing gene silencing through studies in *C. elegans* (Seydoux and Fire, 1994, Guo and Kemphues, 1995). However, Fire *et al.* (1998) surprisingly demonstrated that double-stranded RNAs (dsRNAs) were over 100-fold effective in silencing the *unc-22* gene than antisense ssRNA in *C.elegans*. It turned out to be that both sense and antisense ssRNA samples in previous studies were contaminated with dsRNA. Subsequently, this dsRNA mediated silencing now known as RNAi has been found to be a common process encountered in unicellular protozoans, insects, fungi, invertebrates, vertebrates and plants (Prawitt *et al.*, 2004, Drinnenberg *et al.*, 2009).

RNAi is a process in which dsRNA can trigger transcriptional or translational repression of a gene homologous to the dsRNA sequence. dsRNAs (the trigger) are processed *in vivo* into small dsRNAs of ~21-25 bp in length that guide target recognition (Elbashir *et al.*, 2001a, Elbashir *et al.*, 2001b). There are two types of naturally occurring small RNAs that can act as gene silencers: short interfering RNA (siRNA) and micro RNA (miRNA) (Rao and Sockanathan, 2005) (**Figure 1.10**). Each of these small RNAs is derived from different triggers of the RNAi process. siRNAs arise from long dsRNA duplexes. These dsRNA duxplexes are often produced during viral production within cells (foreign dsRNAs); or from bi-directionally transcribed endogenous RNAs that can anneal to form dsRNA. In addition, these dsRNA can also be introduced into the cell exogenously (Hannon, 2002). On the other hand, miRNAs are produced from a specific precursor that is encoded in the

genome. In most metazoan cells, the transcripts of these specific miRNA precursors contain 20-50 bp inverted repeats of complementary sequences (Bartel and Chen, 2004). These transcripts fold back on themselves and base pair along complementary sequences to form dsRNA hairpins (pri-miRNA). Hairpin precursors are first cleaved to shorter, pre-miRNAs (~70 bp) by an RNase III enzyme called Drosha in the nucleus (Lee *et al.*, 2003). These pre-miRNAs are then exported to the cytoplasm by Exportin-5 and undergo another cleavage into ~21-25 mature miRNAs by Dicer, an RNA III enzyme (Lee *et al.*, 2002). These mature, imperfect miRNA duplexes (miRNA:miRNA*) contain both the mature miRNA strand and its complementary strand (miRNA*). Drosha and Dicer are dsRNA specific endonucleases that generate 2 nucleotide long 3' overhangs at the cleavage site (He and Hannon, 2004).

In contrast to miRNAs, precursors of siRNAs are present in the cytoplasm and processed into 21-22 bp siRNA duplexes by Dicer enzyme (Bernstein *et al.*, 2001). Dicer is a large protein (~220 kD) containing a putative helicase domain, a DUF283 domain, a PAZ (Piwi-Argonaute-Zwille) domain, two tandem RNase III domains and a dsRNA binding domain (dsRBD) (Bernstein *et al.*, 2003). Hence, Dicer can unwind dsRNA duplexes using its helicase domain and cleave these into smaller duplexes. Some organisms such as mammals and *C.elegans* have only one copy of *Dicer* gene (Rao and Sockanathan, 2005). In contrast, other organisms have several paralogs of this gene that are each responsible for cleaving dsRNAs from different sources. One such organism is *D. melanogaster* which has two paralogs DCR-1 and DCR-2. DCR-1 processes long dsRNA duplexes whereas DCR-2 processes pre-miRNAs (Lee *et al.*, 2004). In addition, there are also different requirements for Dicer activity in different organisms. For example, human Dicer does not use ATP while Drosophila DCR-2 activity requires ATP hydrolysis (Nykanen *et al.*, 2001, Zhang *et al.*, 2002). Similar to Dicer, Drosha also contains two tandem RNase III domains and carries out a single cleavage to generate pre-miRNA (He and Hannon, 2004). Although

current knowledge of these enzymes and their roles in RNAi has been increased significantly in the last few years, their exact biochemical mechanisms and the structural elements required for their role in dsRNA cleavage are not fully understood.

RNA-mediated gene silencing can affect expression of homologous genes post transcriptionally in two different ways: translational repression and mRNA cleavage. Upon cleavage by Dicer in the cytoplasm, mature miRNA duplexes and siRNAs are unwound. The mature miRNA* strand or one strand (antisense) of the siRNA duplexes are then incorporated into either miRNA ribonucleoprotein complex (miRNP) or an effector complex (the RNA-induced silencing complex, RISC), respectively (Hammond *et al.*, 2000, Mourelatos *et al.*, 2002). However, many studies have shown that miRNA and siRNA are associated with similar RISC complexes (Hammond *et al.*, 2001). Once bound to a RISC complex, a given single stranded siRNA forms a perfect duplex with its target transcript directing cleavage to this duplex in a process which is also known as post transcriptional gene silencing (PTGS) as well as RNA interference (Zamore *et al.*, 2000). On the other hand, most animal miRNAs bind to the target 3'UTR through imperfect complementarity at multiple sites and thus repress translation of the target (Bartel, 2004). However, many other studies have reported that the mechanisms of gene silencing mediated by siRNA and miRNA are not always the same as previously described but rather a much more complex process which is not fully understood. For example, with the exception of *miR-172,* which acts as a translationational repressor, all identified plant miRNAs form a near perfect duplex with its target mRNA at one site either in the coding region or in the UTR and thus direct mRNA cleavage (Llave *et al.*, 2002, Chen, 2004). Similarly, siRNAs which are not perfectly complementary to targets can repress translation rather than direct mRNA degradation (Doench *et al.*, 2003, Saxena *et al.*, 2003).

In addition to playing a crucial role in endogeneous defense mechanism against virus infection or parasitic nucleic acids (Hannon, 2002), siRNAs can also induce sequence

specific promoter methylation in plants (Aufsatz *et al.*, 2002), are essential for heterochromatin formation in fission yeasts (Grewal and Moazed, 2003) and transposon silencing in worms (Tabara *et al.*, 1999). On the other hand, miRNAs have been found to regulate gene expression in diverse developmental and physiological processes. For example, *lin-4*, the first miRNA discovered, regulates developmental transition between the first two larval stages (L1 and L2) by targeting *lin-14* and *lin-28* in *C.elegans* (Lee *et al.*, 1993, Wightman *et al.*, 1993, Moss *et al.*, 1997). Moreover, misregulation of miRNAs can lead to human diseases. Expression levels of *miR-15* and *miR-16* are reduced in chronic lymphocytic leukaemias (Calin *et al.*, 2002). In contrast, *miR-155* level is upregulated in Burkitt lymphoma tissues and the location of this miRNA correlates with a specific chromosomal translocation (Metzler *et al.*, 2004).

1.12 The potential of RNAi

RNAi not only is an important process for regulation of gene expression but also has proven to be a great technical advance in biomedical research. Traditional methods for loss of function experiments which used antisense DNA, morpholinos, chemically modified nucleic acids, or ribozymes were often plagued with non-specific side effects, inconsistent results, short lived silencing effects and limited systems of choice (Heasman, 2002, Kos *et al.*, 2003). Since its discovery, knowledge of RNAi processes has been widely used to study embryonic development in different organisms including *C. elegans* and *D. melanogaster* by simply introducing dsRNAs into embryos through injection or feeding (Kennerdell and Carthew, 1998, Timmons and Fire, 1998). However, many studies reported that the introduction of long dsRNA duplexes could trigger a non-specific interferon response in mammalian cells (Stark *et al.*, 1998). Subsequently, Elbashir *et al.* (2001a) demonstrated that shorter dsRNAs duplexes (<30 bp) can elude this interferon response. In addition, transfection of mammalian cells with commercially synthesised siRNAs has been shown to lead to dramatic, sequence specific silencing of the target

transcript (Elbashir *et al.*, 2002). Moreover, there is also another type of dsRNAs called esiRNAs which are generated by endonuclease digestion of long dsRNAs into 15-40 bp fragments (Yang *et al.*, 2002a). All of these three types of dsRNA duplexes have been shown to be effective in gene silencing in various systems except the long dsRNAs which can trigger immune responses in mammalian systems. So far, siRNAs have been proven to be most efficient in gene silencing and least toxic for cells (Rao *et al.*, 2004). In addition, siRNAs are favoured over esiRNAs in the mammalian systems because they are less likely to have non-specific effects (Rao and Sockanathan, 2005). esiRNAs are a mixture of different dsRNA duplexes which can target genes other than those of interest. In contrast, care in sequence design of siRNAs can help to reduce this non-specific effect.

Another method of current interest is the plasmid-based system which has been developed to express short, hairpin RNA (shRNA) that can be processed by Dicer and serve as a template for sequence-specific gene silencing (Paddison *et al.*, 2004). shRNAs are single stranded RNA molecules containing inverted repeats which therefore fold to form hairpin structures compromising a single stranded loop with two arms which form dsRNA duplexes. An advantage of this method is that it ensures a stable expression level of shRNAs and thus lengthens the effect of gene silencing compared to other types of dsRNA which only have transient effects due to the limited half-life of RNA in the cell. Moreover, shRNA expression plasmids can be engineered to contain selectable markers to generate stable transfectants or reporter genes such as GFP to aid identification of transfected cells (Hannon and Conklin, 2004). For *in vitro* studies, dsRNAs of all lengths and shRNA expressing vectors can be introduced into cells by standard methods of transfection. One additional advantage of an shRNA-based approach is that cells which are difficult to transfect such as some primary cultures can be infected with viruses engineered to express shRNAs (Hannon and Conklin, 2004).

1.12.1 Non-viral delivery of RNAi

Non-viral delivery of an RNAi-inducing agent typically involves delivery of either naked or plasmid based nucleic acids directly into cells. This process can involve transfection of these molecules into cells using various particles such as liposomes, nanoparticles, aptamers, etc. Liposomes are vesicles consisting of a phopholipid bilayer that are capable of carrying nucleic acids across the cell membrane by endocytosis (Yuan *et al.*, 2011). Lipid encapsulation is an attractive approach because it simply involves mixing and incubating components to form complexes. In addition, these complexes can be modified for specific delivery through conjugation of targeting moieties directly to the lipid molecules before liposome production. For example, Lipofectamine™ (Invitrogen) is a commercially available and wildly used RNAi transfecting reagent in tissue culture. It is a cationic liposome based reagent, which encloses DNA/RNA in a cationic lipid bilayer thus providing enhanced cell entry and increase protection against serum enzymes. In addition, SNALP (stable nucleic acid lipid particle) is a recently developed approach for delivering liposome mediated RNAi *in vivo*. These nucleic acid containing particles have a long blood circulation time leading to increased accumulation in areas of vascular leakage that are often found at the disease target sites of tumour growth, infection or inflammation (Judge *et al.*, 2005).

Polymeric nanoparticles are promising gene delivery systems because they offer stability and control, encapsulate large amount of genetic materials, allow for co-delivery and can be modified to enhance stability, transport properties, targeting or uptake (Gavrilov and Saltzman, 2012). In addition, these polymers are biodegradable, biocompatible and non toxic making them promising candidates for siRNA delivery *in vivo*. One such popular delivery system is Polyethylenimine (PEI) which is a water soluble polymer with high cationic charge. PEI is one of the promising candidates for transfection *in vivo* due to high gene transfer efficiency via endocytosis and intracellular release through the proton sponge

effect (two-third of the amino groups of PEI are unprotonated), capability of condensing and compacting the carried DNA/RNA into small colloidal particle complexes and protection of the carried DNA/RNA from degradation (Gunther *et al.*, 2011).

Another common method for DNA/RNA delivery is selective targeting to diseased cells or tissues by conjugating the genetic material to ligands such as antibodies, aptamers, small molecules and peptides that specifically interact with corresponding surface moieties of target cells (Allen, 2002). Antibodies have been used in a number of drug delivery methods due to their specificity, diversity and ability to modulate biodistribution. However, their large size makes them difficult to conjugate to particle surfaces at high concentrations. In addition, long term administration of treatment might be limited by immune response to the targeting reagent (Gavrilov and Saltzman, 2012). Aptamers have been explored for targeted siRNA delivery. Aptamers are able to bind their ligand molecules with similar affinity and specificity as antigen-antibody partners but unlike antibodies, they are not recognized by native antibodies. These properties make aptamers highly suitable for long term treatment plans. However, the number of aptamers known to bind specific markers for diseases is extremely small and cargo internalization does not always happen after the binding of aptamers to targets (Guo *et al.*, 2010). An additional targeting method is using siRNA loaded particles conjugated with moieties that are recognized by surface receptors such as folate and transferrin receptors. These receptors are highly overexpressed in certain cancers and matastasized tumors; thus, they have become a common strategy in cancer drug therapy (Heidel *et al.*, 2007, Yoshizawa *et al.*, 2008).

1.12.2 Viral-mediated delivery of RNAi

So far, a number of viruses including retroviruses, lentiviruses, adenoviruses, adeno-associated virus (AAV) and herpes simplex virus type 1 (HSV-1) have been used extensively to deliver stable knockdown *in vivo* by integration into the genome or by extrachromosomal existence. Of all these viruses, AAVs have proven to be the most

effective delivery systems for siRNA because of their unique features that distinguish them from other therapeutic vectors (Stilwell and Samulski, 2003). Firstly, AAVs are capable of infecting a broad range of host cells including dividing and non-dividing cells *in vitro* and *in vivo* with very high efficiency. Secondly, AAVs have never been implicated with any disease pathology such as immune responses caused by retroviral vectors (Ghazizadeh *et al.*, 1997). Thirdly, AAVs can persist episomally without intergration into the host genome which might disrupt gene regulation and expression. Although the wild-type AAV shows site-specific integration to the human chromosome 19q13.3-qter (*AAVS1*), recombinant AAVs can be engineered to have a low rate of integration (Surosky *et al.*, 1997, McCarty *et al.*, 2004). Fourthly, microarray analysis also has shown that the introduction of AAV vectors has no impact on the overall pattern of cellular gene expression (Stilwell and Samulski, 2003). Finally, AAV vectors maintain persistent expression of shRNA *in vivo* and the vector genomes can be modified to aid in tissue specific delivery or to allow inducible expression of shRNAs (Srivastava, 1994).

AAVs which belong to the class Paroviridae have small (4681 nucleotides) single stranded DNA genomes, which are contained inside icosahedral and non-enveloped viral capsids. AAV relies on other viruses such as adenovirus or herpes simplex virus to facilitate productive infection and replication. The AAV genome consists of two open reading frames which are *rep* required for viral genome replication and *cap* encoding AAV structural proteins. These two genes can be provided in *trans* for viral replication between the 5' and 3' inverted terminal repeats (ITRs) of the viral genome. In laboratories, recombinant AAV vectors are produced by removing the rep and cap sequences, leaving ITRs which are important for viral replication and integration. Commonly, a DNA sequence of up to 4.7 kb driven by promoters such as pol-II and pol-III can be cloned into this vector. These promoters can be modified to facilitate expression of a transgene of interest in specific tissues and organs.

Since the establishment of the first and most characterized AAV serotype 2 (AAV2) in 1982, new AAV serotypes have been discovered to target nearly every organ or tissue. One strategy for recombinant AAV production is based on co-transfection into permissive cells (usually human embryonic kidney 293 cells) of three separate plasmids. One plasmid contains the viral ITRs flanking the therapeutic gene cassette; a packaging plasmid encodes for the rep and cap proteins; the helper plasmid for the essential adenoviral helper gene (Rabinowitz and Samulski, 1998, Zolotukhin, 2005). Recombinant AAV vectors can be generated using both capsid proteins and genomes from the same serotype or the vector genome can be derived from AAV2, and the cap protein from an alternative AAV serotype. As a result, these hybrid vectors are created and named AAV2/1-n, where the first number indicates the serotypes of genome origin and the second the capsid. So far, up to 108 novel capsid sequences have been isolated from 55 human and 53 non human primates (Surace and Auricchio, 2008). Thus, this leads to a great pool of recombinant AAV vectors with high efficiency, specific cellular tropism and intensity as well as various onsets of gene expression. For example, AAV 2/1, 2/7, and 2/9 efficiently transduce muscle and heart by either direct or systemic vector administration. In addition, AAV 2/1, 2/4, 2/5 and 2/9 can transduce different cells of the central nervous system (Surace and Auricchio, 2008). Onset of gene expression also depends on the capsid proteins. Transgene expression can be detected within days after sub-retinal administration of AAV2/5 and AAV2/1, however, it takes several weeks for the same level of transgene expression using AAV2/2 (Auricchio *et al.*, 2001).

Systems to regulate the timing and levels of transgene expression have been developed to obtain therapeutic efficacy and avoid toxicity. Transcription factors have been engineered and incorporated into the vector genome and can be positively or negatively regulated by small molecule drugs. Two inducible systems have been developed and tested in the murine and non-human primate retina. The first system is based on the ability of

rapamycin to reconstitute a functional transcription factor that binds to a promoter element upstream of the target gene (Rivera *et al.*, 1996, Pollock *et al.*, 2000). The second system uses the tetracycline (tet)-inducible system involving an activator or silencer (tetON or tetOFF, respectively) and an inducible doxycycline vector (Dejneka *et al.*, 2001, Smith and Leyden, 2005, Stieger *et al.*, 2006). Sub-retinal administration of AAV containing the regulated system followed by systemic administration of rapamycin or doxycycline results in expression of the target gene that is drug dependent in timing and levels.

However, there are a few drawbacks in using AAV vectors for gene therapy, the principle one being the small 4.7 kb size limit of the DNA to be inserted. Although recent findings show that AAV is capable of packaging and protecting an insert of up to 6 kb, these larger AAV tend to be degraded by the proteosome, unless proteosome inhibitors are added (Grieger and Samulski, 2005). Other strategies have been developed to overcome this packaging capacity such as splitting a gene and its regulatory elements into two separate AAV vectors which can be co-delivered into target cells. This results in the formation of head to tail heterodimers of the two AAV genomes. In addition, the use of trans splicing signal sequences and overlapping fragments allow expression of a large gene following post transcriptional processing such as splicing and recombination events (Allocca *et al.*, 2006).

A second disadvantage is that the onset of gene expression is generally slow due to the requirement of conversion of single stranded AAV DNA into double stranded DNA before initiation of gene expression. This can be overcome by inserting double stranded DNA in the form of sense and anti sense into the vector; however, this method further reduces the size of transgene inserted. In spite of these existing limitations, AAV vectors have become the vector of choice in a wide range of gene therapy clinical trials to treat diseases such as cancer, cystic fibrosis, heart failure, Parkinson's and Alzheimer's diseases, haemophilia, muscular dystrophies and some ocular diseases (Coura Rdos and Nardi, 2007).

1.13 Potential 'off-target' effect of RNAi

1.13.1 Cross reactions with miRNA pathway

Recent studies have shown that combinations of siRNAs targeting different sites on the same mRNA enhance gene silencing compared with each single siRNA (Ji *et al.*, 2003). In addition, single vectors expressing multiple shRNAs have been shown to improve the silencing efficiency (Gonzalez *et al.*, 2005, Chung *et al.*, 2006). On the other hand, combinatorial delivery of siRNAs or shRNAs appears to hold the inherent risk of competition for critical RNAi components, thus altering the regulatory functions of some cellular miRNAs which can lead to severe toxicity (Grimm *et al.*, 2006, Castanotto *et al.*, 2007). As mentioned above, Exportin 5 exports pre-miRNAs from the nucleus into the cytoplasm and this process is a saturable transport pathway which is also required by expressed shRNAs. Excessive production of shRNAs could result in a decrease of miRNA function due to the competition for Exportin 5 between endogenous miRNAs and shRNAs (Yi *et al.*, 2005). Although siRNAs do not depend on Exportin 5 for their transport to the cytoplasm, it has been shown that the competition between shRNAs with cellular miRNAs is a general phenomenon that also takes place with siRNAs (Castanotto *et al.*, 2007). Interestingly, this group also showed that ectopically expressed shRNAs and siRNAs but not ectopically expressed miRNAs are able to interfere with each other and with the endogenous miRNA pathway through their ability to be incorporated into the RISC complex. One possible way to address this problem is by incorporating the sequence encoded for shRNAs/siRNAs into a pre-miRNA backbone. For example, Boden *et al.* (2004) have reported that when the sequences encoding for siRNA directed against HIV-1 transactivator protein (*tat*) were incorporated into a human miR-30 pre-miRNA backbone, the *tat* siRNA delivered as pre-miRNA precursor into cells showed significantly higher reduction of HIV-1 p24 antigen production than *tat* siRNA expressed from conventional shRNA backbone.

1.13.2 Off-target effects

Jackson and co-workers (2003, 2006) first discovered that ectopically applied siRNAs could alter the expression levels of dozens of non-target transcripts using gene array profiling. Indeed, siRNAs could target transcripts that have as few as 11 contiguous nucleotides of identity to the siRNA. It was later suggested that this off-target effect is due to inhibition of the miRNA pathway and that this can be reduced by a single 2'-OMe substitution on the ribose of the second nucleotide of the guide siRNA strand (Jackson *et al.*, 2006).

1.13.3 Innate immune response

The ability of the host to defend against invading pathogens is largely mediated by a group of pattern recognition receptors such as Toll like receptors (TLR) which recognize a large number of molecular patterns in bacteria and viruses. TLRs are expressed either on the cell surface or in intracellular endocytic vesicles or organelles. Upon TLR recognition of pathogens, the antigen presenting capacity of dendritic cells is increased and production of type I interferons is upregulated. In immune cells, TLRs that recognise nucleic acids are expressed exclusively in endosomes. These include TLR3, TLR7/8, and TLR9, which sense dsRNAs, ssRNA and ssDNA, respectively, whereas other TLRs on the cell surface recognise lipopeptides, lipopolysaccharide, flagellin, and propelin (Sioud, 2010). In immune cells, the response towards siRNAs is mainly mediated through TLR7 in mice and TLR7/8 in humans. In fact, TLR7 knockout mice lack the immune activation in response to siRNAs (Sioud, 2005). Microarray studies demonstrated that expression levels of about 400 genes were affected by the activation of TLR upon treatment with either ds siRNAs or ss siRNAs in blood cells (Cekaite *et al.*, 2007).

Initial data from human monocytes indicate that some types of secondary structures and/or specific nucleotides are responsible for the activation of NF-κβ (nuclear factor kappa-light-chain-enhancer of activated B cells) signalling pathway by siRNAs. Some studies

suggested that specific nucleotides need to be present within the siRNA for TLR7 recognition. In one study, a GU based 'UGUGU' immunostimulatory sequence triggered the activation of TLR7 leading to interferon induction (Hornung *et al.*, 2005). However, a RNA motif (5'-GUCCUUCAA-3') within siRNA duplexes was also found to be recognised by TLR7 and some siRNA sequences that stimulate monocytes to secret TNF-α do not contain GU motifs (Judge *et al.*, 2005). Furthermore, uridines have been shown to trigger TLR7/8 dependent cytokine production and replacement of uridines with adenosines abrogated immune activation (Sioud, 2006).

Thus, these studies have raised concerns about the safety of RNAi use in therapeutics. Instead of using naked siRNAs, chemical modifications seem to be an effective method to overcome the immune response. The inclusion of various 2'-modified nucleotides that included DNA bases, 2'-O-methyl purines, 2'-flouro pyrimidines, terminal inverted-dt bases, and PS-linkage modification at selected positions can abolish siRNA immune activation (Morrissey *et al.*, 2005). However, the chemical modifications need to be considered carefully in order to maintain silencing activity of these siRNAs.

Furthermore, siRNAs also activate TLR3 on the surface of vascular endothelial cells, inducing interferon- γ (IFN-γ) and interleukin-12 (IL-12) release, which subsequently facilitates nonspecific anti-angiogenic effects (Kleinman *et al.*, 2008). In the context of retinal degeneration, angiogenesis occurs in the choroidal neovascularisation (CNV) associated with the wet form of age related macular degeneration (AMD). siRNAs targeting vascular endothelial growth factor A (VEGFA) or its receptors (VEGFR-1 and VGFR-2) have been used in clinical trials for AMD (clinicaltrials.gov). However, CNV inhibition can be induced by any 21 nucleotide or longer siRNAs targeting non-mammalian genes, non-expressed genes, and RNAi incompetent siRNAs in mice through interaction with cell surface TLR3. The same effect was not observed in TLR3 knockout mice. A minimum of 21 nucleotides was required for CNV inhibition; however, shorter

siRNAs can also interact with TLR3 but with a free energy of binding lower than the threshold required for dimer stabilisation and receptor activation (Kleinman *et al.*, 2008). RNAi technology has great potential in therapeutics and been used in numerous studies and clinical trials. However, the potential 'off target' effect of siRNAs should be thoroughly considered during the process of siRNAs design and data analyses.

1.14 AAV vectors in the retina

The structure and accessibility of the retina make it an ideal target organ for gene therapies. In addition, the immune privileged properties of the eye limit the immune response towards the transgene and the vector. The presence of the BRB also helps to avoid unintentional spread of vector into the systemic circulation. The efficiency of the therapy can be monitored by non-invasive and quantitative methods such as electroretinography, ophthalmoscopy, optical coherence tomography, etc.

Two main routes of vector administration in the retina are sub-retinal and intravitreal injection. Intravitreal injection involves introducing the vector into the vitreous and is a very routine clinical ophthalmologic procedure. Among vectors with unmodified capsids (AAV2/1, AAV2/2, AAV2/5, AAV2/6, AAV2/8, AAV2/9), AAV2/2 and AAV2/6 serotypes have the ability to transduce the retina post intravitreal injection (Vandenberghe and Auricchio, 2012). AAV2/2 can efficiently transduce the ganglion cells, the trabecular meshwork and occasionally Muller cells. Compared to AAV2/2, AAV2/6 appears to penetrate deeper in the retina where it can transduce amacrine, bipolar and Muller cells. The inability of other vectors to transduce the retina following intravitreal administration is perhaps due to the abundance of AAV serotype receptors on the inner limiting membrane which limits the diffusion across this barrier (Petrs-Silva *et al.*, 2009) (Dalkara *et al.*, 2009). Novel vectors such as those with multiple tyrosine mutations have been developed to overcome this hurdle and seem unaffected by the inner limiting membrane showing significant potential to transduce the RPE and photoreceptors following intravitreal

injection in small animals (Petrs-Silva *et al.*, 2011). However, recent studies indicate an increased risk of systemic vector distribution and immune activation following intravitreal administration of vectors (Bainbridge *et al.*, 2008, Lukason *et al.*, 2011). This questions the safety of this approach for gene therapy.

Subretinal administration in humans and large animals is usually performed with a (partial) vitrectomy to provide more volume for the vector containing solution and to relieve ocular pressure (**Figure 1.6**). This type of injection induces a regional retinal detachment which flattens within hours or days after vector uptake and diffusion of the diluents (Liang *et al.*, 2001). Although the sub-retinal method is more technically challenging than the intravitreal method due to its higher potential for surgical error, it is still the most efficient method for targeting photoreceptors and retinal pigment epithelium which are the most relevant cell types for many inherited blindness disorders. Subretinal injection of any AAV serotypes tested to date can efficiently transduce the RPE and also to a variable extent the photoreceptors depending on the serotypes and viral titre used. The first serotype tested using subretinal injection was AAV2/2 which resulted in the transduction of both photoreceptors and RPE cells (Ali *et al.*, 1996). AAV2/5 was subsequently identified as outperforming AAV2/2 in terms of photoreceptor transduction efficiency and the onset of transgene expression. The onset of transgene expression mediated by AAV2/5 peaks at 5 weeks post treatment, at a time which AAV2/2 only begins to express its transgene (Auricchio *et al.*, 2001). In addition, AAV2/5 transduces a significantly higher number of photoreceptors than AAV2/2 at 5 and 15 weeks post injection (1000 times and up to 400 times more; respectively) (Yang *et al.*, 2002b). Recently, AAV2/8 has been found to be more efficient than AAV2/5 at targeting photoreceptors in mice, dogs, pigs and non-human primates studies (Vandenberghe and Auricchio, 2012). In terms of RPE transduction, AAV2/1 and AAV2/6 exhibit higher efficiency, specificity and faster onset of transgene expression following sub-retinal injection compared to AAV2/2 (Yang *et al.*, 2002b).

Moreover, the AAV2/9 vector has been reported to transduce endothelial cells of the neuronal microvasculature with high efficiency (Foust *et al.*, 2009, Foust *et al.*, 2010).

Inherited retinal degenerations with an overall prevalence of 1/2000 worldwide are a major cause of blindness and affect over 200,000 people in the EU (Vandenberghe and Auricchio, 2012). Among the most prevalent and severe forms of these inherited blindness are RP, Leber congenital amaurosis (LCA) and Stargardt diseases (SD). In recessively inherited retinal degeneration such as LCA which are caused by loss of function mutations, gene replacement therapy represents the most effective approach. One form of LCA is caused by mutations in the *RPE65* gene which is primarily expressed in the RPE and accounts for 10% of LCA cases (Morimura *et al.*, 1998). RPE65 AAV2/5 administration in the naturally occurring rd12 murine model of LCA restores its retinal structure and function (Pang *et al.*, 2006). Sub-retinal injection of RPE65 AAV2/2 in the Swedish Briard dog results in structural and biochemical recovery of the retina and visual cycle that induces long term restoration of visual function (Narfstrom *et al.*, 2003). Indeed, the gene replacement approach in Briard dogs represents the first long term success for the treatment of an inherited retinal disease. Following this success, three different clinical trials using sub-retinal injection of RPE65 AAV2/2 were set up for the treatment of this form of LCA (Bainbridge *et al.*, 2008, Hauswirth *et al.*, 2008, Maguire *et al.*, 2008). All studies reported no vector dissemination and no adverse immune response to either the vector or the *RPE65* transgene.

In autosomal recessive and X-linked RP, the principal of the therapy is to introduce a wild type version of a mutated gene into cells where normal function of this gene is required. However, in adRP, suppression of expression of mutated alleles is also required. Gene silencing can be achieved through the use of antisense oligonucleotides, ribozymes and siRNAs (Millington-Ward *et al.*, 1997, Kiang *et al.*, 2005, Evans *et al.*, 2007). As mentioned before, RP is a highly heterogeneous disease caused by many different

mutations in different genes. A promising strategy employed to address this heterogeneity is mutation independent suppression and gene replacement which involves silencing both mutant and wild type genes using a suppressor (siRNA/shRNA) which targets a commonly accessible site independent of mutations, together with delivering suppressor resistant replacement genes (based on 3rd base wobble substitution or non-coding 5' or 3' UTR sequences) that encode wild type protein (Farrar *et al.*, 2002). For example, subretinal delivery of recombinant AAV2/5 vectors expressing a codon modified rhodopsin replacement gene in the presence of shRNA targeting rhodopsin transcripts significantly protected the outer nuclear layer of the retina in mouse with retinal degeneration (Palfi *et al.*, 2006, O'Reilly *et al.*, 2007, Millington-Ward *et al.*, 2011). For treatment of the RP10 form of RP caused by mutations in the *IMPDH1* gene, Tam *et al.* (2008) have shown that delivery of AAV co-expressing a mutant human *IMPDH1* gene together with shRNA targeting both human and mouse *IMPDH1* transcripts significantly inhibited the negative pathological effects of mutant *IMPDH1 in vivo.*

1.15 BBB/iBRB modulation as a potential drug delivery method

As mentioned above, the iBRB is the main element preventing systemic delivery of low molecular weight therapeutic drugs for treatment of retinal diseases. Claudin-5 is present in abundance at the TJs of the iBRB. Although the BBB in claudin-5 knockout mice becomes permeable to molecules of up to 800 Da, the barrier remains intact and resistant to larger molecules with no evidence of bleeding or oedema (Yoshida *et al.*, 2002, Nitta *et al.*, 2003). However, these mice die shortly after birth probably due to the important role of claudin-5 during development. Similarly, hypoxic conditions greatly affect the expression of claudin-5 in the BRB and mice experiencing hypoxia show similar phenotypes as seen in claudin-5 deficient mice (Koto *et al.*, 2007). Hydrodynamic tail vein delivery of siRNA targeting transcripts encoding claudin-5 significantly suppresses the expression of claudin-5 at 24 and 48 hours with levels of expression returning 72 hours post-injection in mice

(Campbell *et al.*, 2008, Campbell *et al.*, 2009). The group also showed an increase in permeability at the BBB to small molecules of up to 1 kDa but not 4400 Da. This was the first report of reversible, transient, controlled RNAi mediated size selective opening of the BBB, representing a novel approach for delivery of small molecular drugs that cannot passively diffuse across this barrier. In a subsequent study the authors repeated the same approach for modulation of the iBRB and reported a similar increase in the permeability of the iBRB. In addition, this process has no negative impact on neuronal transcription or visual function as measured by microarray analysis and ERG respectively nor does it induce neuronal or retinal oedema as evidenced by MRI analysis. To test the potential of this method in drug delivery, a mouse model of IMPDH1 retinitis pigmentosa was used. These IMPDH1-/- mice lack the rate limiting enzyme for the *de novo* synthesis of guanosine triphosphate (GTP) which is a central mediator of visual phototransduction. GTP has a molecular weight of 523 Da and cannot diffuse passively across the iBRB following systemic administration. Thus, GTP was systemically injected into these mice 48 hours post claudin-5 (CLDN5) siRNA injection when the suppression of claudin-5 is maximal, and these mice showed an improvement of visual function. Moreover, iBRB modulation was furthered improved by conjugating CLDN5 siRNA with the polymer carrier, *in vivo-JetPEI®,* thus allowing the siRNA to be administered in a much lower volume. Indeed, siRNA/*in vivo-JetPEI®* complexes are currently being used in clinical trial Phase I and have been approved for systemic use by the US Food and Drug Aministration (http://www.popylus-transfection.com/).

Protein aggregation has been implicated in many retinopathies such as RP thus upstream processes of this endpoint, including the heat shock protein chaperone complex and the ER stress response, have been identified as therapeutic targets in disease models. For example, systemic administration of conjugated CLDN5 siRNA/*in vivo-JetPEI* complexes together with the therapeutic Hsp90 inhibitor, 17-N-allylamino-17-demethoxygeldanamycin (17-

AAG), has been reported to offer protection against the dominant negative effect of aggregation of mutant IMPDH1 in the RP10 mouse model (Tam *et al.*, 2010). In addition, administration of CLDN5 siRNA/*in vivo-JetPEI* targeting the BBB has showed an enhanced exchange of water in the brains of mice with a focal cerebal oedema, a model of traumatic brain injury, for a period of between 24 and 72 hours resulting in smaller lesion size at the site of injury and cognitive improvement (Campbell *et al.*, 2012). All these data indicate that barrier modulation method is safe and also provides an efficient method for drug delivery to the retina and brain.

To increase the safety and practicality for long term treatments, a localized and controllable barrier modulation method is preferable. Thus, a doxycycline-inducible AAV2/9 system was developed. Indeed, subretinal inoculation of AAV2/9 expressing a doxycycline-inducible shRNA targeting claudin-5 results in iBRB modulation for the period of time during which the inducing agent doxycycline is administered, providing a means of systemic drug delivery specifically to the retina, avoiding systemic access to the brain (Campbell *et al.*, 2011). Again, the process was shown to have no negative impact on neuronal function and no neuronal oedema was observed. Furthermore, using the same inducible system, CNV, a hallmark of pathology in AMD, was suppressed by systemic administration of low molecular weight compounds, subtinib malate and 17-AAG in mice subjected to laser-induced CNV.

1.16 Objectives

The overall objective of the research described in this PhD was to use the iBRB modulation system to systemically deliver low molecular weight drugs to the retinas of animal models of retinal degeneration in order to reduce disease progression. Three types of models were used: 1) the Balb/c light induced retinal degeneration model; 2) IMPDH1 mouse models of the RP10 form of adRP and 3) the P23H rat and mouse models of adRP.

These animal models have been widely used to investigate photoreceptor cell death (model 1) and retinal degeneration due to protein misfolding (models 2 and 3).

For studies involving the Balb/c light induced generation model where calpain linked apoptosis has been highly implicated, two calpain inhibitors ALLM and ALLN were selected as the potential protective agents of this form of cell death (Donovan and Cotter, 2002). These two compounds do not normally cross the inner BRB thus they are good candidates to access the efficacy of the BRB modulation approach using both CLDN5 siRNAs and CLDN5 AAV2/9 system.

Protein aggregation has been implicated in many retinopathies and is directly linked to earlier events triggered by misfolded mutant proteins involving the heat shock protein 90 superchaperone complex in the cytosol and/or the unfolded protein response (UPR) in the endoplasmic reticulum (Aherne *et al.*, 2004, Kosmaoglou *et al.*, 2008, Tam *et al.*, 2010). Earlier work in this lab by Tam *et al.*, (2010) using an AAV-mediated induced model of the RP10 form of adRP, demonstrated proof of principle that enhanced delivery, following iBRB modulation with CLDN5 siRNA, of a small molecule drug could reduce retinal degeneration. The drug used in this study was 17-AAG, an inhibitor of Hsp90, the effect of which paradoxically increases the rate of protein folding by upregulating components of the superchaperone complex. In this PhD, similar experiments were carried out except that the iBRB was modulated via subretinal injection of CLDN5 AAV2/9 in order to investigate where this method would offer even better protection against photoreceptor cell death in this RP10-induced model. In addition, since there are currently no IMPDH1 animal models which show similar progression of this form of RP as that observed in humans, another part of this PhD involved design and characterization of a new transgenic model which expresses the mutant human IMPDH1 transgene. It is likely that this animal model may prove suitable for studying disease progression and exhibit less variation in terms of gene expression level compared to the AAV-induced model.

As regards the mechanism of and treatment for adRP it is noteworthy that many adRP-linked rhodopsin mutations lead to misfolding of the rhodopsin protein (Lin and Lavail, 2010), the most common being P23H (Dryja *et al.*, 1990) and that geldanamycin (GA) and derivatives have been observed to ameliorate effects of misfolded rhodopsin. In particular, GA and 17-AAG have been shown to have a positive effect in reducing insoluble P23H RHO *in vitro* although they did not seem to promote P23H RHO trafficking to the cell membrane or increase the levels of soluble P23H (Mendes and Cheetham, 2008). However, 17-AAG is rapidly metabolised, forms toxic metabolites and exhibits limited aqueous solubility (Egorin *et al.*, 1998) while 17-(dimethylaminoethylamino)-17-demethoxygeldanamycin (17-DMAG) a newer derivative of GA also under clinical trials for various types of cancer, is water soluble, undergoes limited metabolism, has high oral bioavailability and shows increased efficacy compared to 17-AAG (Egorin *et al.*, 2001, Egorin *et al.*, 2002). Increased levels of the ER chaperone BiP was also shown to be protective against ER stress induced apoptosis in the same rat model (Gorbatyuk *et al.*, 2010). Thus, in this body of work there was a large emphasis on the effect of 17-DMAG on the rate of degeneration of photoreceptors in P23H mouse and rat models of adRP. Furthermore, the method of inducible barrier modulation together with systemic administration of 17-DMAG was also employed to determine if this would provide improved protection from retinal degeneration in these models. Finally, since retinal degeneration in the P23H rat and mouse models used in this study occur over a long and very short periods of time respectively, an AAV P23H-mediated induced model of P23H adRP was also developed in an attempt to provide a model with an intermediate rate of retinal degeneration.

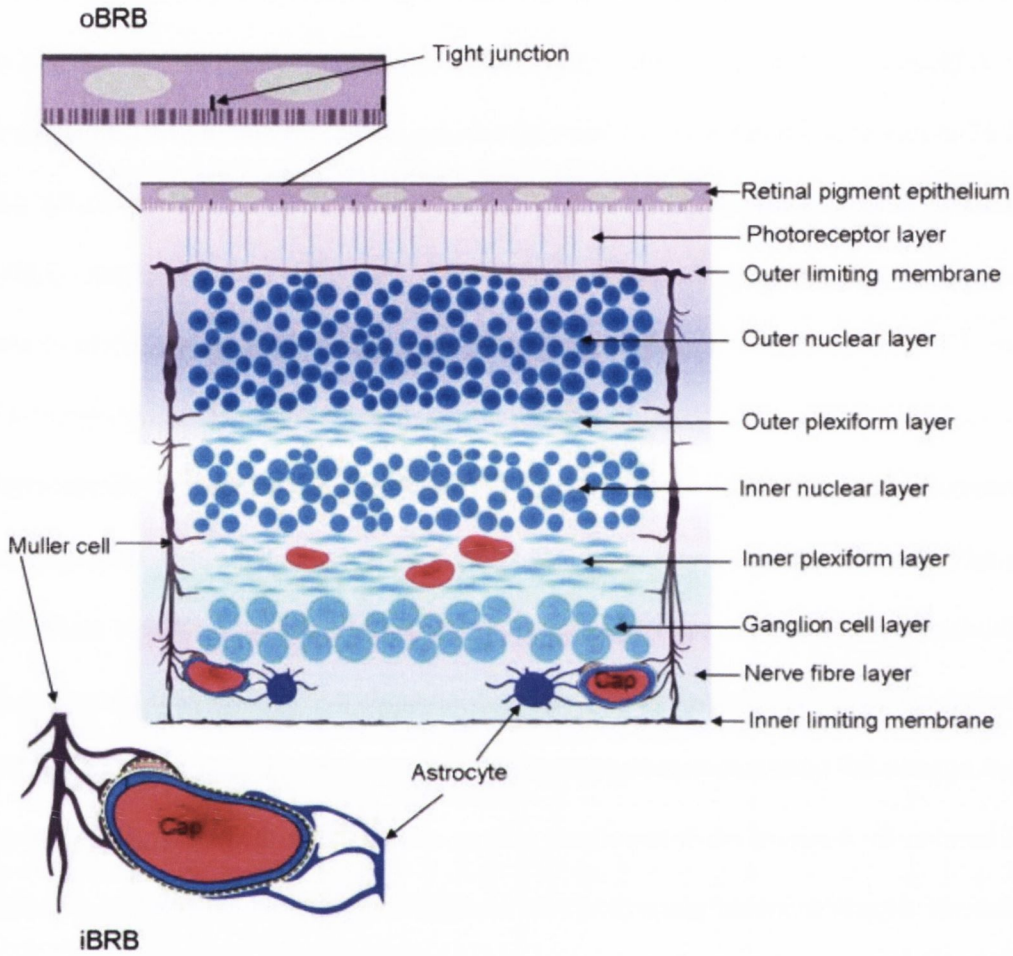

Figure 1. 1: The blood retina barrier.

The BRB consists of the outer and inner blood retina barriers. The iBRB is composed of tight junctions between retinal capillary endothelial cells located in the nerve fiber, ganglion cell layers, inner plexiform layer; and at the junction of the inner nuclear and the outer plexiform layer of the retina; while the oBRB is formed by tight junctions between adjacent retinal pigment epithelium cells. The figure was obtained from Kaur *et al.* (2008).

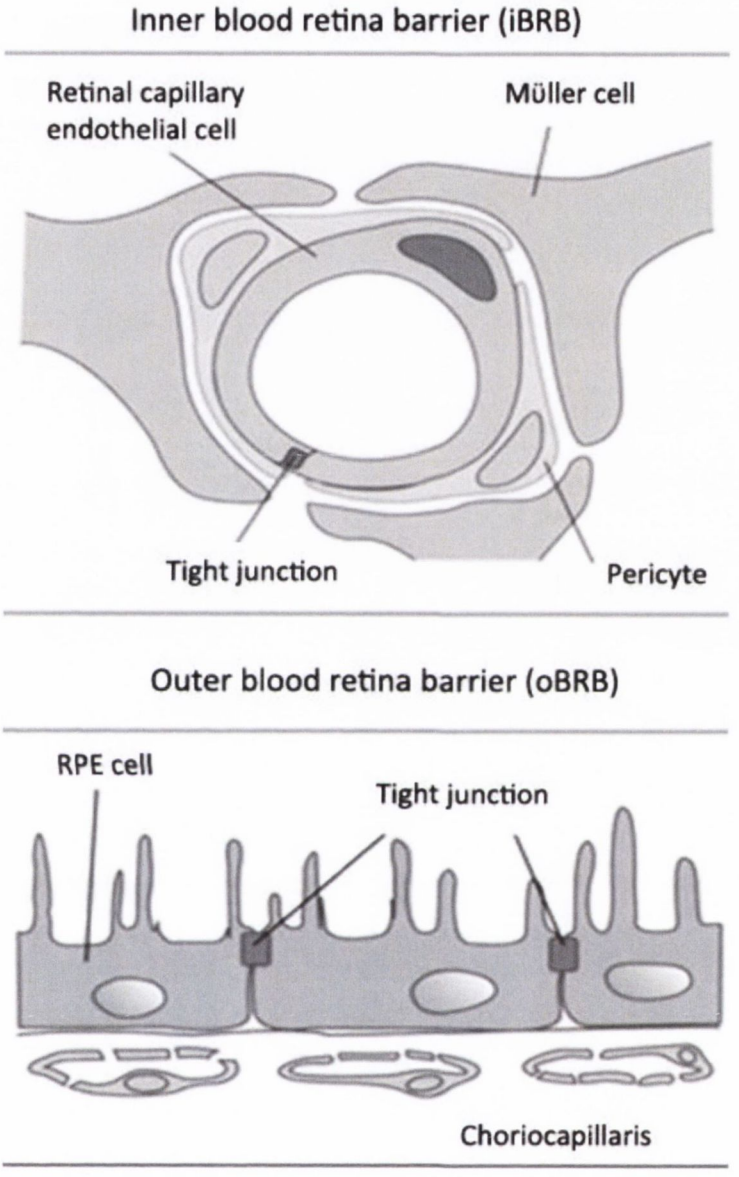

Figure 1. 2: Cross section of the inner and outer BRB.

Retinal capillary endothelial cells of the iBRB are surrounded by pericyte and Muller cell foot process. The apical membrane of the RPE faces the outer segment layer and its basolateral membrane faces the Bruch's membrane separating the RPE from the fenestrated capillaries of the choroid. The figure was adapted from Hosoya *et al.* (2011).

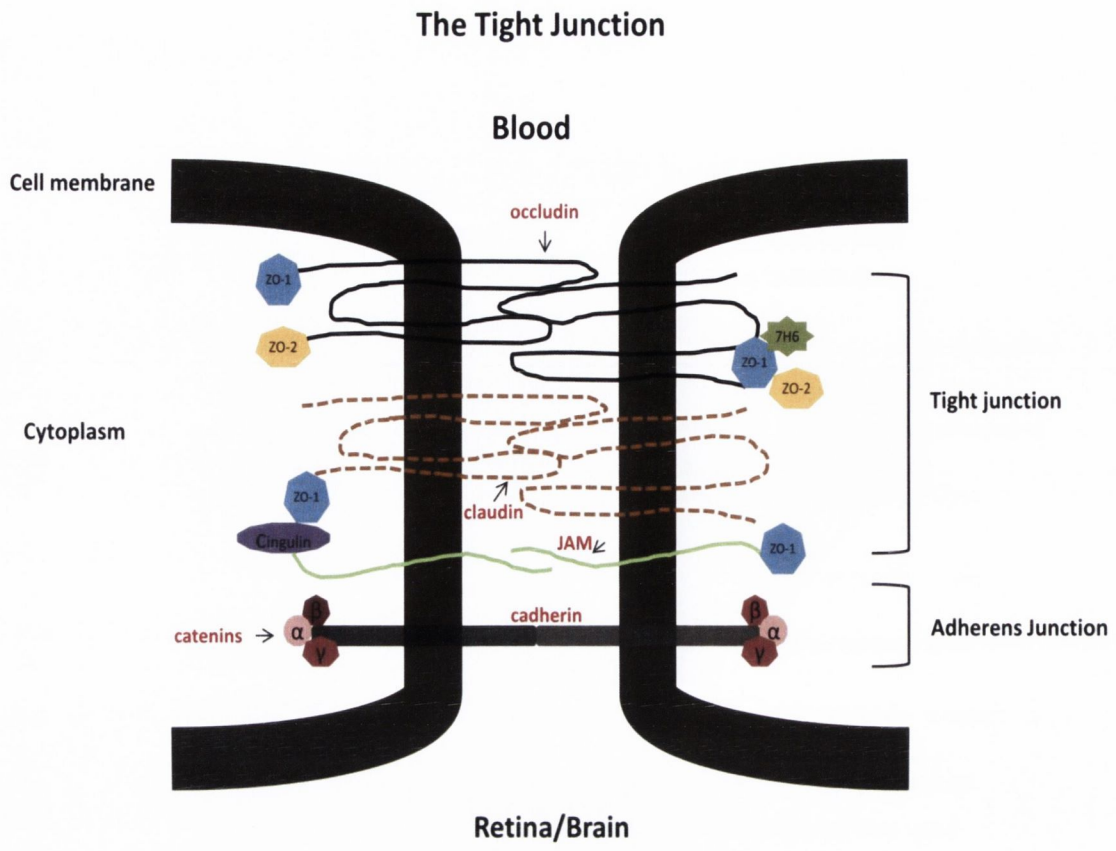

Figure 1. 3: Tight junctions of the retina/brain.

TJs are localised at the apical periphery of endothelial cells lining the fine capillaries of the brain and retina. TJs are composed of a complex of interacting transmembrane proteins and scaffolding proteins linking to the cytoskeleton. Tight junction proteins include integral transmembrane protein (occludin and claudins), junctional adhesion molecules (JAMs) and cytoplasmic proteins (zonula occludens, cingulin, 7H6 antigen). Occludins and claudins are intercellular proteins which are linked to cytoplasmic and regulatory proteins ZO 1-3, symplekin, 7H6 and cingulin. In addition to the TJs, adherens junction is important in maintaining cell-cell adhesion between adjacent endothelial cells. Adherens junction consists of trasmembrane cadherin which are linked to the cytoplasm by scaffolding proteins such as catenins.

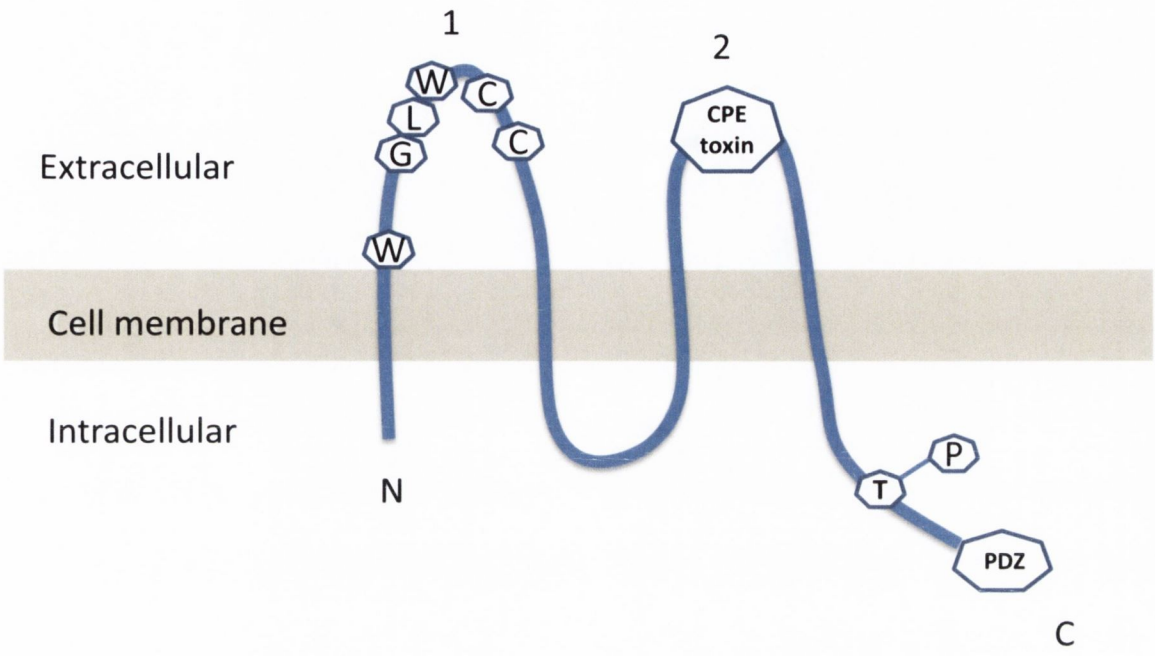

Figure 1. 4: Model of the conserved structural and functional features of claudins.
The first extracellular contains the conserved residues W-GLW-C-C and influences charge selectivity. The second extracellular loop has a bacterial recognizing site. The C terminus of claudins contains a phosphorylation site at Threonine 192 and a PDZ binding motif which binds to PDZ containing cytoplasmic proteins such as ZO-1, ZO-2 and ZO-3.

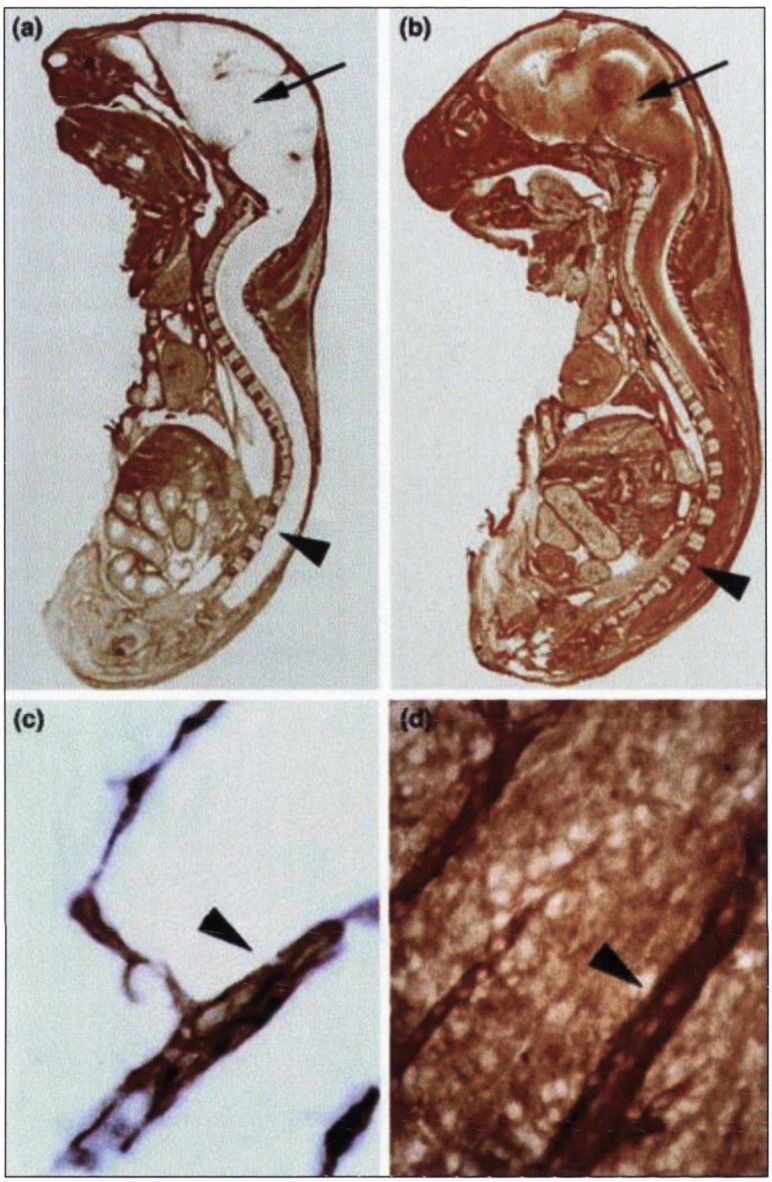

Figure 1. 5: Impairment of the blood–brain barrier in the claudin-5 -/- mouse.

'A 443-Da tracer (a primary amine-reactive biotinylation reagent) perfused via the heart of an 18.5-day-old mouse embryo is detected in sagittal sections throughout the whole body. At low magnification, the tracer is excluded from the brain (arrow) and spinal cord (arrowhead) of a wild-type mouse **(a)** and, by contrast, intense and diffuse tracer signals are present in the central nervous system of a claudin-5-deficient mouse **(b)**. At higher magnification, the brain of the claudin-5-deficient mouse **(d)**, but not that of the wild-type mouse **(c)**, shows abundant infiltration of the tracer into the parenchyma from blood vessels (arrowheads)'. The figure was obtained from Nitta *et al.* (2003), Furuse and Tsukita (2006).

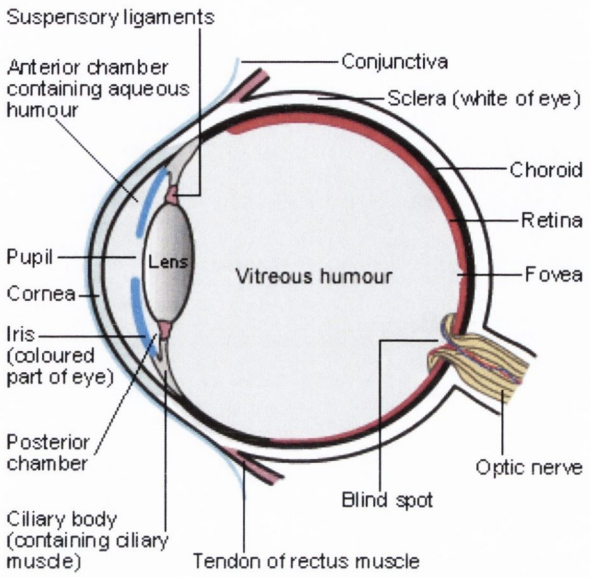

Figure 1. 6: Cross section of the mammalian eye.

The eye can be divided into three distinct layers: 1) the external layer formed the sclera and cornea, 2) the intermediate layer consisting of two parts: anterior (iris and ciliary body) and posterior (choroid), and 3) the internal sensory part of the eye, the retina. There are three chambers of fluid within the eye including the anterior chamber (between the cornea and the iris), the posterior chamber (between the iris, suspensory ligaments and transparent lens), the vitreous chamber (between the lens and the retina). The first two chambers contain aqueous humour whereas the vitreous chamber is filled with a more viscous fluid, vitreous humour. The figure was obtained from http://www.mydr.com.au.

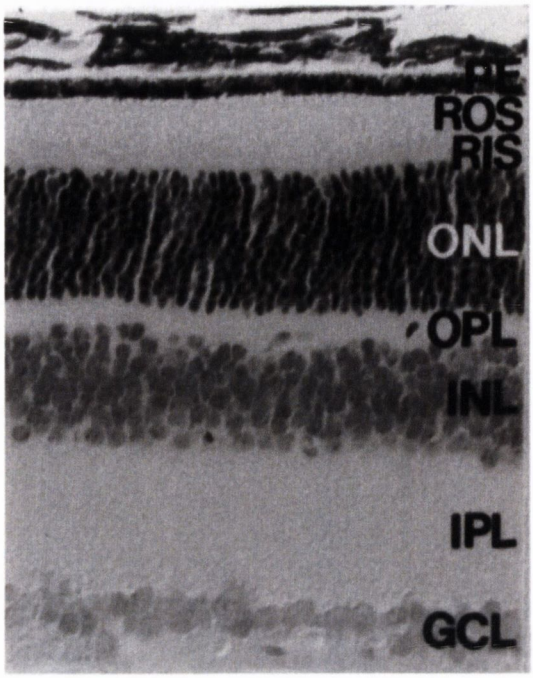

Figure 1. 7: Cross section through a mammalian retina.

Different layers of the retina are identified: retinal pigment epithelium (RPE), rod outer segments (ROS), rod inner segments (RIS), outer nuclear layer (ONL), outer plexiform layer (OPL), inner nuclear layer (INL), inner plexiform layer (IPL) and ganglion cell layer (GCL). The figure was obtained from Farrar *et al.* (2002).

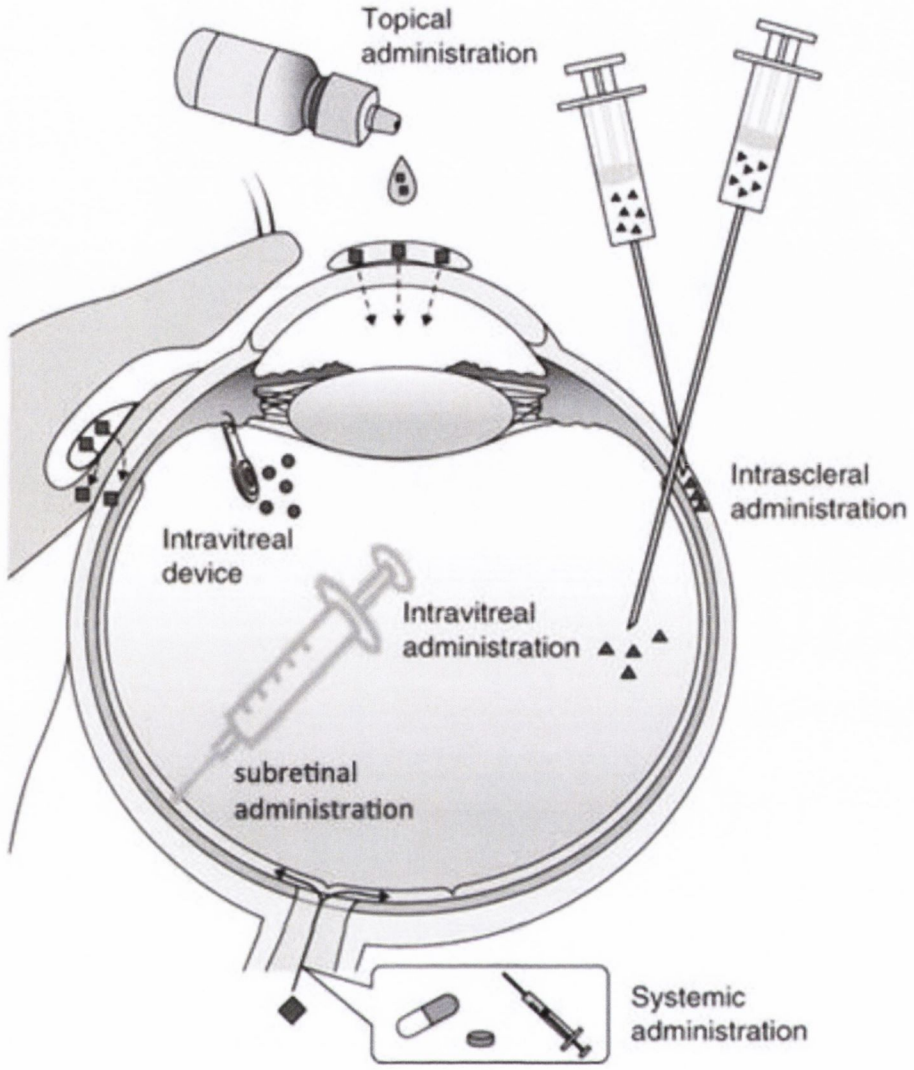

Figure 1. 8: Different routes of drug administration to the posterior eye.

Common drug delivery techniques to the retina include systemic administration, topical application, intravitreal injection, local injection and ocular implants. In addition, subretinal administration of viral vectors is commonly used to increase transduction efficiency and specificity in the retina. The figure was adapted from Hosoya *et al.* (2011).

Figure 1. 9: Photographs of a normal (left) and RP retina (right).

In the RP retina, typical features of RP are present including attenuated retinal vessels, bone-spicule intraretinal pigmentary deposits, optic disc pallor and epithelial thinning. The figure was obtained from Farrar *et al.* (2002).

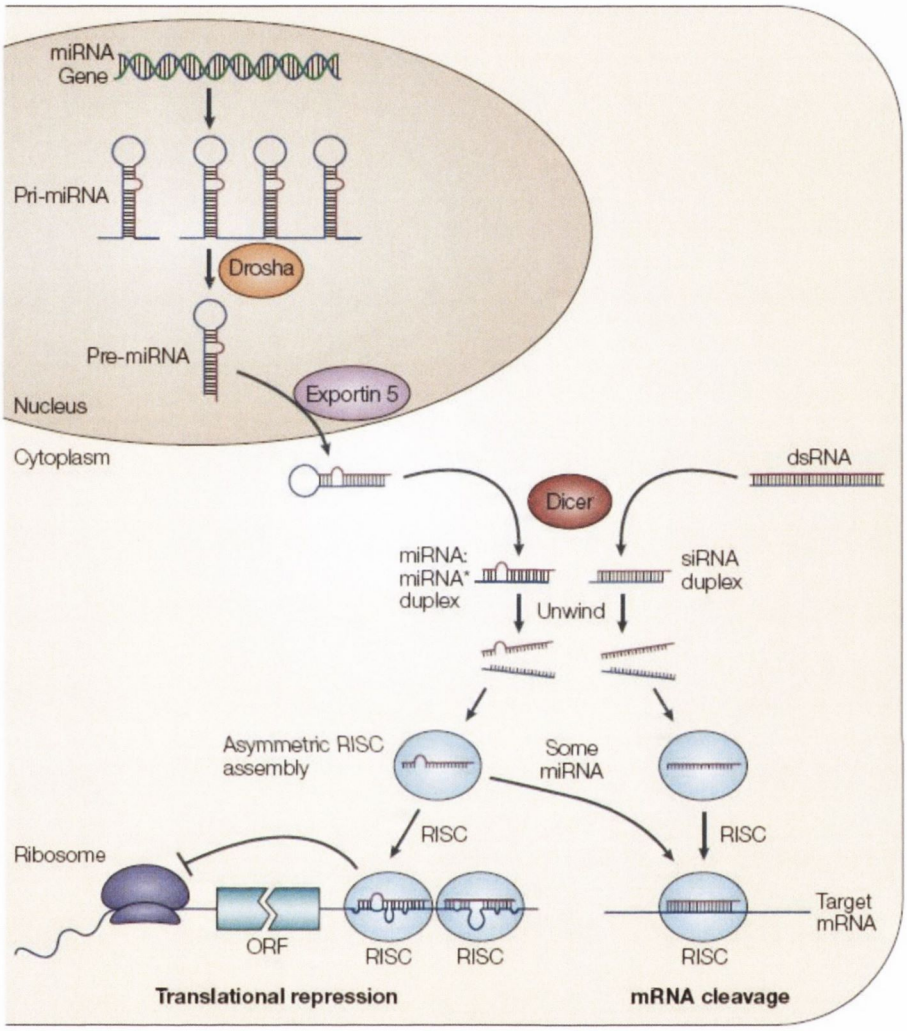

Figure 1. 10: RNAi pathway.

Pri-miRNA is processed into a ~70 bp pre-miRNA by Drosha in the nucleus. Pre-miRNA is then transported to the cytoplasm where it is further processed to a miRNA duplex (miRNA: mature miRNA*) by Dicer which also cleaves dsRNA into siRNA duplex. The mature single stranded miRNA* or siRNA is then incorporated into RISC complex which directs translational suppression or mRNA cleavage of their target. The figure was obtained from He and Hannon (2004).

Category	Type	% of Total
Nonsyndromic RP	Autosomal dominant RP	20
	Autosomal recessive RP	13
	X-linked RP	8
	Isolated or unknown RP	20
	Leber congenital amaurosis	4
	Subtotal	65
Syndromic and Systemic RP	Usher's syndrome	10
	Bardet-Biedl syndrome	5
	Other	10
	Subtotal	25
Other or unknown types of RP		10
Total		**100**

Table 1. 1: Different types of RP and estimated percentages of these types.

The total prevalence is 1 case per 3100 persons (adapted from Daiger *et al.*, 2007).

	Inheritance
Phototransduction cascade	
RHO, rhodopsin (G-protein coupled photon receptor)	Dominant, recessive
PDE6A, rod cGMP-phosphodiesterase α subunit (G-protein effector enzyme)	Recessive
PDE6B, rod cGMP-phosphodiesterase β subunit (G-protein effector enzyme)	Recessive
CNGA1, rod cGMP-gated cation channel α subunit	Recessive
CNGB1, rod cGMP-gated cation channel β subunit	Recessive
SAG, arrestin (rhodopsin deactivation)	Recessive
Vitamin A metabolism	
ABCA4, ATP-binding cassette protein A4 (photoreceptor disc membrane flippase for vitamin A)	Recessive
RLBP1, retinaldehyde binding protein (11-cis-retinaldehyde carrier)	Recessive
RPE65, (vitamin A trans-cis isomerase)	Recessive
LRAT, lecithin retinol acetyltransferase (synthesises vitamin A esters)	Recessive
RGR, RPE-vitamin A G-protein coupled receptor (photon receptor in RPE)	Recessive
Structural or cytoskeletal	
RDS, peripherin (outer disc segment membrane protein)	Dominant, digenic
ROM1, rod outer segment protein	Digenic
FSCN2, fascin (actin bundling protein)	Dominant
TULP1, tubby-like protein 1	Recessive
CRB1, crumbs homologue (transmembrane protein, adherent junctions)	Recessive
RP1, microtubule-associated protein (microtubule formation and stabilisation)	Dominant, recessive
Signalling, cell-cell interaction, or synaptic interaction	
SEMA4A, semaphorin B, transmembrane immune system protein	Dominant
CDH23, cadherin 23 (adhesion receptor)	Recessive
PCDH15, protocadherin 15 (adhesion receptor)	Recessive
USH1C, Usher's syndrome type 1C (integrating scaffold protein harmonin)	Recessive
USH2A, Usher's syndrome type IIA (Usher's network protein)	Recessive
MASS1, monogenic audiogenic seizure susceptibility 1 (Usher's network protein)	Recessive
USH3A, Usher's syndrome type IIIA (transmembrane protein clarin 1)	Recessive
RP2, plasma membrane associated protein	X-linked
RNA intron-splicing factors	
PRPF31, precursor mRNA-processing factor 31 (spliceosome component)	Dominant
PRPF8, precursor mRNA-processing factor 8 (spliceosome component)	Dominant

PRPF3, precursor mRNA-processing factor 3 (spliceosome component)	Dominant
RP9, PIM1-associated protein (RNA splicing factor)	Dominant
Trafficking of intracellular proteins	
MYO7A, myosin 7A (melanosome motility protein)	Recessive
USH1G, scaffold protein containing ankyrin repeats and SAM domain (Usher's type I protein traffic regulator)	Recessive
Maintenance of cilia/ciliated cells (possible role in intracellular trafficking)	
BBS1, Bardet-Biedl syndrome 1	Recessive
BBS2, Bardet-Biedl syndrome 2	Recessive
ARL6, ADP-ribosylation factor like 6	Recessive
BBS4, Bardet-Biedl syndrome 4	Recessive
BBS5, Bardet-Biedl syndrome 5	Recessive
MKKS, McKusick-Kaufman syndrome	Recessive
BBS7, Bardet-Biedl syndrome 7	Recessive
TTC8, tetratricopeptide repeat domain 8	Recessive
PTHB1, parathyroid hormone-responsive B1 gene	Recessive
RPGR, trafficking of proteins in the cilia	X-linked
pH regulation (choriocapillaris)	
CA4, carbonic anhydrase IV (carbon dioxide/bicarbonate balance)	Dominant
Phagocytosis	
MERTK, mer tyrosine kinase proto-oncogene (RPE receptor involved in outer segment phagocytosis)	Recessive
Other	
CERKL, ceramide kinase-like (ceramide converting enzyme)	Recessive
IMPDH1, inosine-5′ monophosphate dehydrogenase type I (guanine nucleotide synthesis)	Dominant
BBS10, vertebrate-specific chaperonin-like protein	Recessive

RPE=retinal pigment epithelium.

Table 1. 2: Identified genes responsible for RP and functions of their protein products.

The table was obtained from Hartong *et al.* (2006). Recently, a dominant mutation in the RPE65 gene has been found to cause adRP with choroidal involvement (Bowne *et al.*, 2011).

Chapter 2

Materials and Methods

2.1 Materials

2.1.1 Buffers and reagents for general procedures

• Tris-acetate-EDTA electrophoresis buffer 10x (TAE, pH 8.3): 400 mM Tris-Acetate and 10 mM EDTA (Diluted 1/10 in ddH2O for a 1x working solution)

• Agarose gel: Agarose powder (Sigma-Aldrich) diluted in the appropriate volume of 1x TAE to make 1, 2 or 2.5% gels.

• Ethidium Bromide: 10 mg/ml

• Agarose gel loading dyes (Sigma-Aldrich):

1. Xylene Cyanol (6x)
2. Bromophenol blue (6x)

• Molecular weight markers: 100 bp ladder (New England Biolabs) and 1 kb ladder (New England Biolabs) were used as size markers on agarose gels 1 µl of marker was diluted in 4 µl of ddH_2O with 1 µl of loading dye.

2.1.2 Buffers and reagents for bacterial culturing

• LB/Agar: tryptone (1%), 5 g yeast extract (0.5%), 10 g NaCl (1%) and BBL™Agar Grade A (1.5%) was added to 1 litre of ddH2O and the LB/agar autoclaved

• LB/Agar plates: 400 ml of LB/Agar was melted and cooled to a temperature of approximately 60°C, the appropriate antibody was added and the LB/Agar was subsequently poured immediately into sterile plastic petri dishes and allowed to set

• XL1-Blue Supercompetent Competent Cells (Stratagene)

• Antibiotics (Sigma-Aldrich):

Antibiotic	**Stock Solution** (mg/ml)	**Working solution** (µg/ml)
Ampicillin	20	50

Tetracycline	10	25
Spectinomycin	10	50

• E. Coli Lysis Solution 1: 50 mM Tris pH 8 (50 mM), 25% sucrose (Sigma-Aldrich) and 2 mM EDTA pH8

• Lysozyme (40 mg/ml): 40 mg Lysozyme (Fluka Biochemika), 250 mM Tris pH8

• M-STET: 5% trition X-100 (Sigma-Aldrich), 50 mM EDTA pH8. 5% sucrose and 50 mM Tris pH8 and was sterilised by autoclaving

• RNase A (1 mg/ml, Sigma-Aldrich)

2.1.3 Cell culturing materials and reagents

• Complete DMEM: 10% fetal calf serum (FCS, PAA Laboratories), 2 mM L-Glutamine (Gibco) & 2 mM Sodium Pyruvate (Gibco) in Dulbecco's modified eagle media (DMEM, Gibco). FCS was first heat inactivated at 50°C for 30 min. Complete DMEM was stored at 4°C for up to 1 month.

• 1x Sterile Phosphate Buffer Saline (PBS, Gibco)

• Trypsin-EDTA (Gibco)

• 2x Freezing Media: 25% Dimethyl Sulfoxide (DMSO, Sigma-Aldrich), 25% FCS and 50% complete DMEM

• Lipofectamine® 2000 reagent (Invitrogen)

• Opti-MEM (Invitrogen)

2.1.4 RNA materials and reagents

• Nuclease free (NF) water (Ambion)

• RNase Away® (Invitrogen)

• Tri-Reagent (Molecular Research Centre)

• β-mercaptoethanol (BDH chemicals LTD)

• RQ1 DNase (Promega)

• RQ1 DNase 10x Buffer (Promega): 400mM Tris-HCl (pH8), 100mM MgSO4 and 10mM

• CaCl2

• RQ1 Stop solution (Promega): 20mM EGTA (pH8)

• Hanks Balanced Salt Solution without Ca, Mg and Phenol red (HBSS [Lonza BioWhittaker®])

• DNase I, RNase-Free (lyophilised, Qiagen)

• Buffer RDD (Qiagen)

•QuantiTect SYBR Green reverse transcriptase (RT)-PCR Master Mix (Qiagen): HotStarTaq® DNA Polymerase, QuantiTect SYBR Green RT-PCR Buffer, dNTP mix, including dUTP, SYBR Green 1, ROX passive reference dye, 5 mM $MgCl_2$

2.1.5 Protein materials and reagents

• 1% Triton X-100

• 0.5 M EDTA (pH 8)

• 10x TBS (pH7.5): 30.3 g Tris (Sigma-Aldrich), 80 g NaCl (Sigma-Aldrich) and 2 g KCl (Sigma-Aldrich)

• Roche protease inhibitor mix: 1 complete mini-protease inhibitor cocktail tablet (Roche) in 10 ml of protein lysis buffer

• Protein lysis buffer: 1% triton X-100, 1 mM EDTA (pH 8), 10x TBS (pH 7.5)

• 10x PBS (Sigma-Aldrich)

• Bicinchoninic acid (BCA) protein assay reagent (Thermo Scientific)

• Qubit™ Protein Assay Kits (Invitrogen)

2.1.6 Materials and reagents used for western blotting

• 10% Sodium Dodecyl Sulphate pH 7.2 (SDS) (Sigma-Aldrich)

• 1.5 M Tris-HCl pH 8.8

• 0.5 M Tris-HCl pH 6.8

• 10% Ammonium Persulphate (APS) (Sigma-Aldrich)

• 5x Lane Marker Reducing Sample Buffer (Thermo Scientific): 0.3M Tris-HCL, 5% SDS, 50% glycerol, 100 mM Dithiothreitol (DTT) and proprietary pink tracing dye

• Prestained protein loading marker-broad range (7-175 kDa) (New England Biolabs)

• Resolving gel for SDS-PAGE electrophoresis:

1. 12% gel: 5 ml of 1.5 M Tris-HCl pH 8.8, 6.6 ml of ddH2O, 8 ml of bis-acrylamide (30%, Sigma-Aldrich), 200 µl of 10% SDS, 200 µl of APS and 20µl of TEMED (Sigma Aldrich).
2. 10% gel: 7.9 ml of 1.5 M Tris-HCl pH 8.8, 6.7 ml of ddH2O, 5 ml of bis-acrylamide, 200 µl of 10% SDS, 200 µl of APS and 20µl of TEMED

• Stacking gel for SDS-PAGE electrophoresis (4%): 2.5 ml of 0.5 M Tris-HCl pH 6.8, 6.8 ml of ddH2O, 1.33 ml of bis-acrylamide, 100 µl of 10% SDS, 100 µl of APS and 10 µl of TEMED.

• 10x Running buffer (pH 8.6): 30.3 g Tris, 144.2 g Glycine (Sigma-Aldrich) and 1% SDS

• Transfer buffer: 3.03 g Tris, 14.42 g Glycine and 20% methanol (Sigma Aldrich)

• Ponceau S (Sigma-Aldrich): 0.1% PonceauS (w/v) in 5% (v/v) acetic acid.

• 5% blocking solution: 5% Marvel original dries skimmed milk in 1x TBS

• Amersham™ ECL™ Western Blotting Detection Reagents (GE Healthcare)

• Developer (Kodak GBx developer and replenisher (Sigma-Aldrich)

• Fixer (Kodak GBx fixer and replenisher (Sigma-Aldrich)

• Restore™ Western Blotting Stripping Buffer (Thermo Scientific)

2.1.7 Anaesthetic and reagents used for animal procedures (mouse)

• Anaesthetic for subretinal injections: Medetomidine (10 mg/10 g body weight) and Ketamine (750 mg/10 g body weight) was administered via i.p. injection

• Anaesthetic for ERGs: Ketamine (16mg/10g body weight) xylazine (1.6mg/10g body weight)

• For dilating eyes: 1% Cyclopentolate and 2.5% Phenylephrine was administered

• Analgesia: 1% Amethocaine and Vidisic gel

• Reversal agent: Atipamezole Hydrochloride was administered at a dose of 100 mg/10 g body weight via i.p. injection

2.1.8 Materials and reagents used for histology and immunohistochemistry

• 4% Paraformaldehyde (PFA) (Sigma-Aldrich): 4% PFA was dissolved in 1L 1x PBS by heating at 64°C on a hot stir plate. The pH 7.4 was obtained using NaOH and HCl.

• 10, 20, 30% sucrose (Sigma-Aldrich) was made in 1x PBS

• Optimal cutting temperature compound (OCT compound, Lennox Laboratory Supplies)

• Polysine adhesion slides (Thermo Scientific)

• Goat Serum (Sigma-Aldrich)

• 10% Triton-PBS solution: 10% Triton x 100 in 1x PBS

• Blocking solution: 10% goat serum, 0.3% Triton-PBS in 1x PBS

• Antibody solution: 2% donkey serum, 0.1% Triton-PBS in 1x PBS

• 4',6-diamidine-2-phenylindole-dihydrochloride (DAPI) (Sigma-Aldrich): 1/10,000 dilution in 1x PBS

• Aqueous mounting media (Aqua PolyMount, Polysciences)

2.2 General cloning techniques

2.2.1 DNA/RNA spectrophotometry

DNA and RNA concentrations were calculated from absorbance at a wavelength (λ) of 260 nm (A260) using the NanoDropTM1000 spectrophotometer (Thermo Scientific). 2 µl of NF water was added to the optical surface of the nanodrop in order to obtain a blank measurement. The software was either set to DNA50 or RNA40 depending on the nucleic

acid being measured. 2 µl of each sample was loaded onto the optical surface and a concentration for each was calculated. Purity of nucleic acids was measured by examining A260/A280 ratios measured on the nanodrop.

2.2.2 Agorose gel electrophoresis

Agarose gels were made by adding the appropriate amount of agarose extract to 1x TAE buffer and heating in a microwave oven until all the agarose had melted. 1 µl Ethidium Bromide was added to 30 ml of melted agarose. This was poured into a gel cast (Bio-Rad) with a comb and the gel was left to set for at least twenty min. Loading dye was added to each DNA sample at a dilution of 1 in 6 and each sample was loaded onto the gel along with a DNA ladder. The gel was electrophoresed at a constant voltage of 100 mV and DNA was visualised on a UV transilluminator (Vilber Lourmat). Photographs were taken using a Mini Bis PRO (DNR, Bio-Imaging Systems) with Gel capture software (DNR, Bio-Imaging Systems).

2.2.3 Restriction enzyme digestion

Restriction enzyme digestion of DNA was performed as follows: A 1x concentration of the recommended enzyme buffer and bovine serum albumin (BSA) was added to each reaction. The amount of units of restriction enzyme was recommended by the manufactures. Reactions were typically performed in a 50 µl volume in ddH_2O. Unless otherwise stated all reactions were carried out for 2 hours at 37°C. The enzyme activity was inactivated by heating to 65°C for 20 min, by a reaction enzyme clean up kit or agarose gel extraction.

2.2.4 Enzyme reaction clean up (Qiagen)

Purification of PCR products and restriction digests was carried out using the QIAquick PCR purification kit (Qiagen). A 5:1 volume of buffer PB to DNA was added and this was

transferred to a QIAquick spin column. The remainder of the protocol was carried out according to the manufacturer's instructions. DNA was eluted in 50 µl of NF H_2O.

2.2.5 Agarose gel extraction (Qiagen)

DNA was extracted from 1% agarose gels using the QIAquick gel extraction kit (Qiagen). DNA on agarose gels were visualised under the UV transilluminator (Vilber Lourmat) and using a sterile blade, gel sections containing DNA of interest was excised. The gel slice was weighed and 3 volumes of Buffer QG was added per 100 mg of gel. The remainder of the protocol was carried out according to the manufacturer's instructions. DNA was eluted in 50µl of NF H_2O.

2.2.6 Phenol-chloroform extraction

Buffer-saturated phenol was added to an equal volume of DNA solution, the sample was vortexed and centrifuged at 13,000 rpm (IEC Micromax Microcentrifuge, Thermo-Electron) for 1 min. The top aqueous layer (containing the DNA) was taken and again an equal amount of phenol was added, vortexed and centrifuged at 13,000 rpm for 1 min. The upper aqueous layer was removed and mixed with a 1:1 mixture of phenol chloroform, was vortexed and centrifuged as above. Again the top phase was taken, mixed with an equal volume of chloroform, vortexed and centrifuged at 13,000 rpm. The upper aqueous phase containing the DNA was removed and the DNA was precipitated with by ethanol precipitation.

2.2.7 XL1-blue competent cells

A colony of XL1- blue *E.coli* was streaked onto an LB/agar plate containing tetracycline. This was incubated overnight at 37°C. Using a toothpick a single colony from this plate was used to inoculate 10 ml LB broth with tetracycline, which was and incubated overnight in an orbital incubator, shaking at 220 rpm (Innova 4300) at 37°C. 250 µl of the overnight culture was added to a conical flask containing 25 ml of LB broth and

tetracycline which was grown in an orbital incubator for approximately 2 hours until the bacterial cells were in their early exponential growth phase (OD600 of 0.3 to 0.5). Cells were centrifuged at 3,000 rpm (Centrifuge 5810, Eppendorf) for 5 min and the supernatant was removed. 25 ml of ice cold, sterile 50 mM $CaCl_2$ was added to the cells and the pellet was gently resuspended. The cell suspension was left on ice for 15 min and centrifuged at 3,000 rpm for 5 min. The supernatant was removed and the cell pellet was resuspended in 5 ml ice cold, sterile 50 mM $CaCl_2$. The competent cells were stored on ice and were used within 2 days.

2.2.8 Transformation using XL1-Blue competent cells

5 µl of ligated DNA was added to 200 µl of XL1-Blue competent cells and placed on ice for 20 min. Cells were heat shocked at 42°C for 5 min in a water bath. 1 ml of LB was added to each tube and this was incubated at 37°C for 1 hour. 200 µl of each sample was spread on an LB/agar plate and left to dry. Each LB/Agar plate contained the appropriate antibiotic for selecting transformed bacterial colonies (unless otherwise stated the antibiotics used were Ampicillin and Tetracycline). Each plate was incubated at 37°C overnight. Transformation controls were also included in this experiment. A circular plasmid was transformed to confirm the transformation process was efficient. In addition non-transformed competent cells were plated, to ensure the competent cells and the LB/agar plates were not contaminated.

2.2.9 DNA mini-preparation (Qiagen kit)

DNA mini-preparation was carried out using the QiAprep® miniprep kit (Qiagen). Cells from single colonies were grown in 5 ml of LB supplemented with appropriate antibiotics overnight at 37°C in an orbital incubator (Innova 4300). The overnight culture was centrifuged at 3,000 rpm (Centrifuge 5810, Eppendorf) for 10 min and the supernatant was removed. A mini-preparation was carried out on the pellet according to the QIAprep®

miniprep handbook (Qiagen). DNA was resuspended in 50 µl of NF H_2O and stored at -20° C.

2.2.10 DNA maxi-preparation (Qiagen kit)

DNA maxi-preparation (to get high quality DNA of up to 1 mg) was carried out using the HiSpeed® Plasmid Midi and Maxi kit (Qiagen). 5 ml of LB broth with the appropriate antibiotic was inoculated with the colony to be prepared. This starter culture was grown for 8 hours at 37°C in an orbital incubator, shaking at 220 rpm (Innova 4300). Following this, 250 µl (1/1000 dilution) of this starter culture was used to inoculate 250 ml LB broth containing the appropriate antibiotic. Cultures were grown at 37°C overnight, shaking at 220 rpm in an orbital incubator. The next day the cultures were centrifuged at 3000rpm for 15 min (Centrifuge 5810, Eppendorf) and the supernatant was removed. The maxi-preparation was carried out on bacterial pellets according to the HiSpeed® Plasmid Purification handbook. Pellets were re-suspended in 1 ml NF H_2O and stored at -20°C.

2.2.11 Sequencing (GATC or Source Bioscience LifeSciences)

Sequencing reactions were outsourced to Source Bioscience LifeSciences. Plasmid DNA samples were sent at a concentration of approximately 30-100 ng/µl along with 3.2 pmoles/µl of the sequencing primer. Sequencing was performed on a 7x ABI 3730xl sequencer. Results were viewed using Finch TV.

2.3 Cell culturing procedures

2.3.1 Cell growth

HeLa cells (America type culture collection [ATCC] no. CCL-2) were maintained in complete DMEM and grown at 37°C in a humidified Sterile Cycle CO2 incubator (Hepa Class 100, Thermo Scientific) in the presence of 5% CO_2. All cell culture procedures were

carried out in a laminar flow cabinet (Holten LaminAir Model 1.2, Thermo Electron Corporation). Cells were visualised using a microscope (Olympus CK30).

2.3.2 Cell passaging

Cells were passaged routinely on average every 2-3 days. Complete DMEM was removed from cells. Cells were then washed with PBS and removed from tissue culture dishes by incubation with 1-2 ml of Trypsin-EDTA at 37°C for 5 min. Once the cells had been removed from the tissue culture plates a 5-fold excess of complete DMEM was added to the cell suspension in order to inactivate the Trypsin. 1/6 of the total cell suspension was then added to new 10 cm tissue culture dishes and grown in complete DMEM.

2.3.3 Cell counting using a Haemocytometer

Cells were prepared for counting by trypsinising, adding a 5-fold excess of complete DMEM and centrifuging at 1000 rpm for 10 min (IEC-Centra-3C centrifuge). The resulting cell pellet was resuspended in 10 ml complete DMEM. A 1:10 dilution of cell suspension was counted using a Haemocytometer. The Haemocytometer was washed with 70% ethanol and dried. A clean coverslip was placed over the counting area and the cell suspension was applied beneath the coverslip by capillary action. The number of cells per grid of 16 squares was counted. Cells were counted in 8 different grids and the average was taken. In order to obtain the number of cells per ml this average was multiplied by 10^4.

2.3.4 Freezing cells

Cells were frozen at low passage numbers in order to maintain stocks. 500 µl of cells were placed in a Nunc Cryo TubeTM (Nunc) along with 500 µl of 2x freezing media. These were placed in a prechilled cryo freezing container (Nalgene) and frozen at -80°C.

2.4 RNA Methods

2.4.1 Ribonuclease (RNase) free conditions

In order to prevent RNA degradation by RNases certain precautions were taken. Nuclease-free eppendorf tubes (Axygen Scientific Inc.), nuclease-free filtered pipette tips (Axygen Scientific Inc.) and nuclease-free water (Ambion) were used at all times. RNA samples were kept on ice during experiments. The benches were wiped with 70% ethanol and RNase AWAY® (Invitrogen).

2.4.2 RNA isolation from HeLa cells (Using Tri-reagent)

RNA was extracted from cells at a required timepoint post-transfection. The medium was removed from each well and the cells were washed gently with 500 µl PBS. Cells were lysed by pipetting 250 µl of Tri-reagent into each well and mixing gently. The plate was incubated at room temperature (RT) for 5 min. Triplicate transfection samples were pooled and 200 µl of chloroform was added. Each tube was shaken vigorously for 2 min and left for 2-3 min at RT. The samples were centrifuged at 12,000 rpm for 15 min at 4°C (Beckman GS-6 centrifuge). 300 µl of the upper phase of each sample was transferred to a new eppendorf tube. RNA was precipitated with 200 µl of isopropanol at RT for 10 min. Tubes were subsequently centrifuged at 4°C for 10 min at 12,000rpm. The supernatant was removed and RNA pellets were washed with 75% ethanol. Tubes were centrifuged for 5 min at 12,000rpm at 4°C. RNA pellets were first air dried then resuspended in 50 µl NF H_2O. RNA samples were stored at -80°C.

2.4.3 RNA isolation from HeLa cells (RNeasy® Plus mini kit)

RNA was isolated using the RNeasy® Plus mini-kit (Qiagen). 87.5µl of Buffer RLT plus (0.88µl β-mercaptoethanol) was added to each well and quadruplicate transfection samples were pooled. The pooled cell lysates were then homogenised by placing them onto a QIAshredder spin column placed in a 2 ml collection tube. Samples were centrifuged at

13,000 rpm (IEC Micromax Microcentrifuge, Thermo-Electron) for 2 min. The remainder of the isolation was carried out according to the manufacturer's instructions. Samples were resuspended in 50 µl NF water.

2.4.4 DNase treatment of HeLa cell RNA

In order to remove contaminating DNA from HeLa cell RNA samples, 5 µl of RQ1 DNase and 6 µl RQ1 DNase Buffer was added to each sample. Samples were incubated at 37°C for 1 hour and the DNase was deactivated by adding 6.5 µl of RQ1 stop solution and by heating samples to 80°C for 10 min. Each RNA sample was frozen and stored at -80°C.

2.4.5 RNA isolation from mouse retina (RNeasy mini kit)

Unless otherwise stated all *in vivo* RNA isolations were carried out using the RNeasy mini kit

(Qiagen). Retinas were extracted from mice and immediately washed in 1 ml ice cold 1x SBS. The lens was removed from the retina, and each retina was placed into 350 µl buffer RLT (containing 3.5 µl of β-mercaptoethanol). The retina was homogenised by pipetting the sample up and down a number of times. Retinal RNA extraction following addition of buffer RLT was carried according to the manufacturer's protocol. RNA was eluted in 50 µl NF water.

2.4.6 DNase treatment of mouse retinal RNA (on column digestion)

During the above protocol (using the RNeasy mini kit), an on column DNase digestion step was performed. The RNeasy spin column was washed with 350 µl Buffer RW1 and centrifuged for 15 s at 10000 rpm (IEC Micromax Microcentrifuge, Thermo-Electron), the flow through was discarded. Following this, 80 µl of DNase 1 in Buffer RDD (10 µl DNase 1 + 70 µl Buffer RDD) was added to the centre of each column and incubated for 2 h at 37°C. The column was then briefly centrifuged to remove the DNase in RDD Buffer

mixture and subsequently washed with 350 µl of Buffer RW1. The sample was centrifuged at 10,000 rpm for 15 s and the flow through discarded.

2.4.7 General One Step Real- Time RT-PCR protocol

Real-time reverse transcriptase-PCR (RT-PCR) was used to measured levels of RNA. In all one-step real-time RT-PCR experiments in this thesis, a relative standard curve method for quantification was used. This method determines the ratio between the amount of RNA of interest and an internal control housekeeping gene (Applied Biosystems Real-Time PCR systems chemistry guide, 2005). The mRNA transcript of a housekeeping gene is ubiquitously expressed, therefore by comparing the ratio of expression of RNA of interest and the housekeeper RNA levels, expression of RNA of interest across different samples can accurately be compared. A one step real-time RT-PCR kit, the QuantiTect®SYBR® Green RT-PCR kit (Qiagen) was used in all one-step RT-PCR reactions which were carried out on an Applied Biosystems 7300 Real-Time PCR system. This system uses the SYBR Green 1 fluorescent dye. SYBR Green 1 binds to double stranded DNA and fluoresces. During the PCR reaction the more DNA that has been amplified, the more SYBR Green 1 will bind to it and the higher the fluorescent intensity (Applied Biosystems Real-Time PCR systems chemistry guide, 2005). The 7300 real-time RT-PCR machine measures the fluorescence after each PCR cycle and records this. Each reaction was carried out in a final volume of 20 µl containing 10 µl of the supplied SYBR Green master mix, 0.147µl of the RT Mix (containing reverse transcriptase enzymes), 10 pmoles of the forward and reverse primer, 4.35 µl NF H2O and 4.5µl of each RNA sample. These solutions were kept on ice at all times. Each reaction was performed in triplicate in a MicroAMP™optical 96-58 well reaction plate (Applied Biosystems). A negative control (water blank) to which no RNA was added was included. The real-time RT-PCR program was as follows:

• **Reverse transcription:** 50°C for 20 min

• **Activation of DNA polymerase:** 95°C for 15 min.

• **cDNA amplification:** 37 cycles at 95°C for 15 seconds, 60°C for 1 min.

• **Dissociation:** 95°C for 15 seconds, 60°C for 30 seconds and 95°C for 15 seconds.

Analysis was carried out using sequence detection software v1.4 (Applied Biosystems). Initially in order to verify the presence of each RT-PCR product a dissociation curve analysis was performed. Each product has a particular melting temperature (Tm); therefore examining the temperature at which the PCR product DNA dissociates (melts) helps to confirm that the correct product of the correct size is present. Dissociation curves also help identify contaminations in water blanks and primer dimmers (recognised by dissociation peaks with low Tm, typically in the region of 70-75◦C). It was always critical to check for the presence of these peaks after every real-time RT-PCR. In order to measure relative gene expression levels in samples and to compare levels in different samples, expression levels were normalised using a housekeeping gene. Hence two standard curves were generated using gene of interest and housekeeping gene primers and relative gene expression levels of both genes determined in each sample. Each standard curve was analysed using the auto analysis function in the software (auto CT). For both genes of interest and the housekeeping standard curves a line of best fit was generated based on the known dilution factors of the standards. This compares cycle no. to the log of the dilution value. The slope and R2 value of each standard curve was checked to make sure the assay was efficient (the slope should be -3.33 for 100% efficiency and the R2 value should be as close to 1 as possible). Efficiency was calculated using the formula $E = [10^{(-1/\text{slope})}-1] \times 100$. Each sample to be tested was then compared to this line and a value of relative expression for each was determined. This was automatically done with the software package. The quantity value for each sample was taken for use in the relative quantification calculation. For each sample, the relative rhodopsin quantity was normalised to the relative quantity of the house keeping in the same sample.

2.5 Protein techniques

2.5.1 Protein extraction from HeLa cells

Protein was extracted from HeLa cells by adding 500 µl of protein lysis buffer to each well containing cells (work was done on ice at all times). The cells were dislodged from the base of each well using a plastic cell scraper; each cell solution was transferred to an eppendorf. These were stirred for 1 hour at 4°C using small magnetic stir-bars. The contents of each eppendorf was transferred to a fresh eppendorf tube and centrifuged at 12,000 rpm for 30 min at 4°C (Beckman GS-6 centrifuge). The supernatant containing the protein was retained and frozen at -20°C.

2.5.2 Protein extraction from mouse retina

Retinas were extracted from mice eyes and immediately placed in an eppendorf containing ice cold PBS. The lenses were removed from the retina and each retina was added to 200 µl (or 300 µl for both retinas) of protein lysis buffer. Retinas were homogenised by pipetting up and down a number of times with a P1000 pipette tip. In the case of retinal samples that were particularly viscous, the extract was sonicated (Labsonic U, B. Braun Biotech International). Each eppendorf tube was centrifuged at 12,000 rpm for 20 min at RT. The supernatant containing the protein was retained and frozen at -20°C.

2.5.3 Determination of protein concentrations

2.5.3.1 Bicinchoninic acid (BCA) protein assay

BCA assays were carried out to quantify total protein in a sample using Pierce BCA Protein Assay Kit (Thermo Fisher scientific). Albumin Standard, containing bovine serum albumin (BSA) at 2.0 mg/ml in 0.9% saline and 0.05% sodium azide was diluted to prepare a set of protein standards. The BCA working reagent was prepared by mixing 50 parts of BCA reagent A and 1 part of BCA reagent B. Triplicates of each protein standard were

pipetted into a 24 well plate. Then, 200 µl of the BCA working reagent was added to the wells and mixed with the protein standards by pipetting. The microplate was covered and incubated at 37°C for 30 min. The absorbance was measured at 595 nm on a plate reader. The average absorbance of the three replicates for each standard was calculated and those measurements were blank-corrected by subtracting the average of blank measurement containing no albumin. The standard curve was prepared by plotting the average Blank-corrected measurement for each BSA standard vs. its concentration in µg/ml. Retinal lysates were also prepared in the same way, except the blank containing lysis buffer. Concentration of protein samples were calculated based on the standard curve obtained from protein standards.

2.5.3.2 Qubit™ Protein Assay Kits

Only thin-wall, clear 0.5 ml PCR tubes (Invitrogen) were used. Following the manufacturer's instructions, the Qubit™ working solution was made by diluting the Qubit™ protein reagent 1:200 in Qubit™ protein buffer. Three protein standards were prepared by adding 10 µl of each protein standard (1, 2, 3) provided in the kit to 190 µl of the Qubit™ working solution. Each sample tube required anywhere from 180 µl to 199 µl of this working solution as long as the final volume in each assay tube was 200 µl. After adding protein samples and standards into individual assay tubes containing the working solution, each tube was vortexed for 2-3 s without creating any air bubbles. Subsequently, all tubes were incubated for 15 min at room temperature and protein concentrations were measured using the Qubit® 2.0 Fluorometer following the manufacturer's instructions. Using this method, a standard curve was not obtained and sample concentrations were given directly by the Fluorometer.

2.6 Western Blot Protocol

2.6.1 Preparation of SDS PAGE gels

SDS-PAGE gels were cast using the AE-6450 Dual Mini Slab Kit (ATTO Bioscience and Biotechnology Corporation). All gel cast was assembled according to the manufacturer's instructions. A 10/12% resolving polyacrylamide gel was made and approximately 8 ml of this was poured into the gel cast leaving a space of at least 1 mm at the top for the Teflon comb. The resolving gel was left to polymerise for 30 min and then the ddH2O overlay was removed. A 4% stacking polyacrylamide gel was prepared and poured on top of the resolving gel and a Teflon comb was added to the stacking gel. This was left to set for 15 min. The gel electrophoresis apparatus was assembled according to the manufacturer.

2.6.2 Loading samples and electrophoresis

Following quantification with a BCA assay, 40 µl of each protein sample was added to 10 µl Lane Marker Sample Buffer (1/5 dilution). Samples were denatured by heating to 95°C for 10 min unless otherwise stated and loaded directly onto the western gel. The loading buffer contains excess SDS and a thiol reagent to break disulfide bonds. All the proteins were negatively charged by binding to SDS. The reduced polypeptides bind the same amount of SDS on the weight basis (1.4 g SDS/g polypeptide) independent of the amino acid composition and sequence of protein (Hames B.D. 1998). This allows protein to be separated on the basis of their size only. A broad range prestained protein marker was heated at 95°C for 5 min and 10-20 µl was added to the outer most lane of the gel. Maximum of the protein sample loaded onto the gels were 30 µl. All samples were centrifuged briefly and mixed thoroughly by pipetting before being loaded onto the gel. The SDS-PAGE electrophoresis was carried out at 30 mV per gel for 90 min (Consort EV261).

2.6.3 Transfer of proteins

The semi-dried transfer method was used to transfer proteins from the gel into the PVDF membrane. The negatively charged SDS bound proteins were transferred onto the membrane in an electrical field. The PVDF membrane and 8 sheets of the filter paper were cut into the same size as the gel to make membrane-gel sandwich. 4 sheets of the filter papers were soaked with the transfer buffer, and placed on the anode of the electroblot apparatus. On the top of the paper, the membrane was placed and soaked with the transfer buffer. After gel electrophoresis, the gel was taken out from the apparatus, and the stacking gel was removed. The gel was then placed on the membrane and any air bubbles between them removed. The remaining 4 sheets of the filter papers were put on the gel with soaking with the buffer. The apparatus was set to run at 80 mA for 2 hours.

2.6.4 Ponceau S Staining

Following electroblotting, the membrane was stained with Ponseau S solution (Sigma Aldrich), in order to ensure that protein bands had been transferred correctly. Once the presence of protein has been verified, the membrane was washed four times for 15 min (4 x 15 min) with 1x TBS on an orbital shaker (Bellco Biotechnology).

2.6.5 Blocking of immunoblots

The membrane was blocked with 30 ml of 5% blocking solution for 30 mins at room temperature on an orbital shaker. The blocking solution should bind to all non-specific protein binding sites on the membrane, and ensure that non-specific binding of the primary antibody does not occur.

2.6.6 Incubation with antibodies

The membrane was probed with 10 ml of the appropriate dilution of primary antibody (diluted in 5% blocking solution) specific for the protein to be examined. The membrane

was covered in tinfoil to prevent evaporation and subsequently incubated overnight at 4°C. The primary antibody was removed and the membrane was washed 4 x 15 min with 1x TBS on an orbital shaker (Bellco Biotechnology). The blot was probed with the appropriate dilution (in 5% blocking solution) of the corresponding secondary antibody. The membrane was covered in tinfoil and incubated at room temperature for 2 hour. Following this incubation the membrane was washed for 4 x 15 min with 1x TBS.

2.6.7 Chemiluminescent detection of proteins

The rest of the western blot protocol was performed under dark conditions. Chemiluminecence was carried out using the Amersham ECL Western blotting detection reagents. A 1:1 dilution of detection reagent 1: detection reagent 2 was made and added to each immunoblot from which 1x TBS was previously drained. Horseradish-peroxidase (HRP) substrate, which is located on the secondary antibody will oxidise the luminal in the detection solution and this will cause the luminal to be in an excited state and it will emit light. It is this light emission that can be detected by exposure of the blot on a blue light sensitive autoradiography film. The amount of light emitted, correlates to the amount of HRP which in turn is dependent on the amount of primary antibody present and the amount of protein expressed. After 1 min the detection solution was removed from the membrane and the excess removed. The membrane was positioned between two transparent sheets (acetates) and placed in a film cassette. Autoradiography film (Super Rx medical x-ray film, FUJIFILM) was put on top of the membrane and the cassette was closed. After the appropriate amount of exposure time the film was developed. After developing the autoradiography film it was washed with ddH2O, fixed and then washed with ddH2O.

2.6.8 Stripping of immunoblots

In order to reprobe membranes with different antibodies, membranes were stripped with Western Blot Stripping Buffer for 30 min with gentle agitation. After stripping the

membrane was washed 4 x 15 min with 1x TBS and then reprobed overnight with the appropriate antibody.

2.6.9 Quantification of Western blots

Quantification of Western blots was done by using ImageJ software following instructions on the website http://lukemiller.org/index.php/2010/11/analyzing-gels-and-western-blots-with-image-j/. Briefly, the size of protein from each sample was measured and normalized by the size of the house keeping β-actin protein obtained from the sample.

2.7 Animal procedures

2.7.1 Housing of animals

All animals were kept under specific pathogen free (SPF) conditions in individually ventilated racks with 12 hours light and 12 hours darkness at a temperature of 21°C±2°C. All work was carried out in compliance with the European Communities Regulations 2002 and 2005 (Cruelty to Animals Act) and the Association for Research in Vision and Ophthalmology (ARVO) statement regarding animal procedures in ophthalmic and vision research.

2.7.2 DNA isolation from mouse tails

1 cm of tail was isolated from each animal and put in a clean eppendorf tube. 500 µl of tail lysis buffer (50 mM Tris-Cl pH 8.0, 100 mM EDTA pH 8.0, 10 mM NaCl and 1% SDS) and 15 µl of Proteinase K (20 mg/ml) was added. The tube was vortexed briefly and incubated overnight at 55°C. 500 µl of a phenol, chloroform, isoamyl alcohol mixture (25:24:1) was added to the tube which was then centrifuged for 5 mins at 13000 rpm at room temperature. The aqueous phase was placed in a new tube to which 1 ml of 100% ethanol was then added. The tube was inverted several times to precipitate DNA and then

centrifuged for 10 min at 13,000 rpm at room temperature. Ethanol was removed and the tube was left to air dry. DNA was resuspended in 100 µl of sterile water.

2.7.3 Subretinal AAV injection

All subretinal injections were carried out by Dr. Paul F Kenna. Adult mice were anesthetised and the pupils were dilated. AAV contained in a 10 µl syringe (usually 3 µl of AAV for mice and 5 µl of AAV for rats unless otherwise stated) was injected using a blunt-ended microneedle (34-gauge, Hamilton) into the subretinal space via a small incision made under local anaesthetic and a retinal detachment was induced. A reversing agent was administered to the mouse and body temperature was maintained using a homoeothermic heating device. Mice were carefully monitored until recovery. Sub-retinal injections on new born mice were carried out in accordance with Matsuda and Cepko as follows (Matsuda and Cepko, 2004). New born mice were chilled on ice for six min in order to anaesthetise them. A small incision was made into the eye lid and the eye was exposed. The eyes of new born mice are not clearly visible, therefore all sub-retinal injections were performed by touch, rather than visualisation of the needle into the sub-retinal space (The eye was gently touched until a slight movement and resistance was felt at the far wall of the eye). The eye was punctured at the sclera at the edge of the lens with a 30-gauge needle and AAV was then injected into the sub-retinal space of the eye using a blunt ended microneedle (33-gauge, Hamilton). Mice were warmed for 30 min at 33°C. Upon recovery they were returned to their mother.

2.7.4 Electroretinograms (ERG)

ERGs were carried out by Dr. Paul Kenna. Animals were dark-adapted overnight and prepared for electroretinography under dim red light. Pupillary dilation was carried out by instillation of 1 % cyclopentalate and 2.5 % phenylephrine. Animals were anesthetized by intraperitoneal (i.p.) injection of ketamine (2.08 mg per 15 g body weight) and xylazine

(0.21 mg per 15 g body weight). Standardised flashes of light were presented to the mouse in a Ganzfeld bowl to ensure uniform retinal illumination. The ERG responses were recorded simultaneously from both eyes by means of gold wire electrodes (Roland Consulting Gmbh) using Vidisic (Dr Mann Pharma, Germany) as a conducting agent and to maintain corneal hydration. Reference and ground electrodes were positioned subcutaneously, approximately 1 mm from the temporal canthus and anterior to the tail respectively. Body temperature was maintained at 37°C using a heating device controlled by a rectal temperature probe. Responses were analysed using a RetiScan RetiPort electrophysiology unit (Roland Consulting Gmbh). The protocol was based on that approved by the International Clinical Standards Committee for human electroretinography. Rod-isolated responses were recorded using a dim white flash (−25 dB maximal intensity, where maximal flash intensity was 3 candelas/m^2/s) presented in the dark-adapted state. Maximal combined rod-cone response to the maximal intensity flash was then recorded. After a 10-min light adaptation to a background illumination of 30 candelas/m^2, cone-isolated responses were recorded to the maximal intensity flash, presented initially as a single flash and subsequently as 10-Hz flickers. a-waves were measured from the baseline to the trough and b-waves from the baseline (in the case of rod-isolated responses) or from the a-wave to the trough.

2.7.5 Fixation of eyes

The eyes and the optic nerve was removed from the eye cup of each culled mouse by proposing the eye using a forceps and gently pulling upward to detach the eye. Eyes were washed in 1x PBS and subsequently fixed overnight in 4% PFA at 4°C with gentle rotation. Following this, the eye was washed for 3 times x 5 min with 1x PBS and the lenses were removed under a light source (Intralux® 6000-1, Volpi) using a dissection microscope.

2.7.6 Preparation of the eyes for cryosectioning

Eyes were cryoprotected in a series of sucrose gradients (10, 20, 30%) until eyes sank to the bottom of the glass vial. Each eye was placed in plastic moulds containing OCT, and the mould was placed in a container with isopropanol, this container was then submerged in liquid nitrogen and the eyes were frozen. Snap frozen eyes were stored at -20°C and sectioned as soon as possible.

2.7.7 Cryosectioning

Frozen eye blocks were cryo-sectioned on a cryostat (Leica CM 1900 Cryostat, Leica Biosciences) with a head temperature of -25°C and a unit temperature of -20°C. Each eye was cut into sections of 12 μM thickness and the sections were collected on Polysine adhesion slides (Thermo Scientific). All slides were stored in a slide box at 20°C.

2.7.8 Immunohistochemistry

Each slide was removed from the freezer and left to dry at room temperature for 20 min. Using a PAP pen, a mark was drawn around the section on each slide and the PAP stain was left to dry. The slides were then washed for 3 x 5 min with 1x PBS. Each slide was blocked with blocking solution for 1 hour in a humidified chamber. The blocking solution was removed by gently tapping the slide to tissue paper, and the primary antibody was applied at the appropriate dilution. Slides were incubated over-night in a humidified chamber. The following day, the slides were washed 3 x 5 min with 1x PBS and a appropriate secondary antibody was subsequently applied for two hours at room temperature in a humidified chamber (1/500 dilution). The secondary antibody was removed and the slides were washed 1 x 5 min with 1x PBS. Nuclei were counterstained by adding 4', 6-diamidine-2-phenylindoledihydrochloride (DAPI, 1/10,000 dilutions) for 1-2 min at room temperature. Slides were then washed 2 x 5 min with 1 x PBS and mounted using aqueous mounting media. Sections were analysed using the fluorescent microscope (Axiophot microscope, Carl Zeiss LTD). Photographs were taken of sections

using analysis B software. Composite images were produced using Adobe Photoshop (Adobe Systems Europe).

2.7.9 Magnetic Resonance Imaging (MRI)

Animals were anesthetized with isofluorane and were physiologically monitored (ECG, respiration, and temperature) and placed on an MRI-compatible support cradle, which has a built-in system for maintaining the animal's body temperature at 37 °C. The cradle was then positioned within the MRI scanner. Accurate positioning was ensured by acquiring an initial rapid pilot image, which was then used to ensure the correct geometry was scanned in all subsequent MRI experiments. Upon insertion into the MRI scanner, T2-weighted images were acquired (resolution, 0.141 _ 0.141 _5mm_3; matrix, 128 _ 128 _ 36; TR/TE, 4,179.3/36 ms; flip angle, 90°; acquisition time, 1 min 6 sec). iBRB integrity was then visualized in high-resolution T1-weighted MR images (resolution, 0.156 _ 0.156 _ 5 mm_3; field of view _ 20 _20 _ 17.9 mm_3; matrix, 128 _ 128 _ 30; TR/TE, 500/2.7 ms; flip angle, 30°; number of averages, 3; acquisition time, 2 min 24 sec; repetitions, 10) before and after injection of contrast agent Gd-DTPA. A 0.1 mM/L per kg bolus of Gd-DTPA was administered via the tail vein. After injection of Gd-DTPA, repeated T1-weighted scans were performed over a period of 24 min, and images shown are representative of the final scans of this 24-min period.

2.8 Statistical analysis

Statistical analysis was performed on results using GraphPad Prism. The averages and standard error of the mean (SEM) were calculated using Microsoft Excel. Graphs were drawn using both Excel and GraphPad Prism. Unless otherwise stated a two-tailed Student'*t*-test was utilised in order to determine the significance. Differences were considered statistically significant at P values ≤ 0.05.

Chapter 3

Enhanced Systemic Delivery of Calpain inhibitors Prevents Photoreceptor cell death in a murine model of Light-induced Retinal degeneration

3.1 Introduction

Disease processes in the retina can affect a variety of cell types, for example, photoreceptors degenerate in RP and AMD while retinal ganglion cells die in glaucoma and diabetic retinopathy. Interestingly, cells of the INL are more resistant to stress and as a result, diseases associated with this layer have not been identified. Cell loss in RP is caused almost exclusively by the presence of disease-causing mutations, while environmental factors (e.g. smoking, diet and aging) together with a genetic pre-disposition are risk factors associated with AMD. Programmed cell death or apoptosis characterized by nuclear DNA condensation and fragmentation, membrane blebbing, disintegration of dying cells into apoptotic bodies which are engulfed by phagocytotic cells without initiating induction of inflammation or tissue scarring, is the mode of cell death associated with retinopathies as well as various neurodegenerative conditions including Alzheimer's disease, Parkinson's disease and Huntington's disease (Kerr *et al.*, 1972, van Soest *et al.*, 1999, Mattson, 2000, Dunaief *et al.*, 2002). Classically, caspases have been considered central executioners of apoptosis, cleaving a variety of intracellular substrates. However, this view has been challenged in recent years by studies which have suggested the existence of caspase-independent apoptotic pathways. Furthermore apoptosis also involves other cellular compartments such as mitochondria, lysosomes, proteasomes or autophagic vacuoles (Wenzel *et al.*, 2005). In addition, the characteristics of necrosis and apoptosis have also been questioned since lysosomal and cellular proteases including caspases have been found to be involved in both types of cell death (Syntichaki and Tavernarakis, 2003). In this introductory section, mechanisms of the intrinsic and extrinsic pathways of apoptosis will first be outlined, followed by a discussion of the implications of calpain activation during retinal degeneration, since calpains are normally associated with necrotic cell death while retinal cell death has been generally classified as apoptotic nature. In addition, calpain activation in the light-induced retinal degeneration model which has been

developed to study the process of cell death upon light damage has also been outlined. In the context of this chapter, results will be presented from experiments involving a safe method of reversible, transient and size-selective modulation the iBRB via either tail-vein injection of siRNA targeting claudin-5 or subretinal injection of CLDN5 AAV2/9 expressing inducible shRNA targeting claudin-5 which has been employed in tandem with systemic administration of the low molecular weight calpain inhibitors, ALLN and ALLM to investigate their effects on photoreceptor cell death in the Balb/c light ablation model.

3.1.1 Apoptosis in neurodegenerative diseases

The so-called extrinsic pathway of apoptosis occurs upon ligand binding to cell surface receptors, resulting in activation of pro-caspase 8, which then cleaves downstream caspases. On the other hand, cellular stresses such as those caused by oxidative stress, trigger release of cytochrome c from the mitochondria into the cytosol in the intrinsic pathway of apoptosis. Recently, mechanisms associated with apoptosis have been rendered more complex in the light of studies in which caspases were inhibited by pharmacologic inhibition or genetic manipulation, which did not necessarily increase cellular survival. Furthermore, accumulating evidence showing calpain activation during apoptosis (Nath *et al.*, 1996), suggests that apoptosis can occur in a caspase-independent fashion.

3.1.1.1 Caspase-dependent apoptosis

In the classical sense, apoptosis involves activation of various caspases which in turn cleave different intracellular substrates at the carboxyl site of aspartate residues leading to cytoskeletal destruction, DNA fragmentation and autophagocytosis. Caspases have been classified into two major groups: caspases 1, 4, 5, 11, 12 and 14 tend to participate in cytokine cleavage and maturation, whereas caspases 2, 3, 6, 7, 8, 9 and 10 cleave various proteins during apoptosis (Kaufmann *et al.*, 2001). All caspases are synthesized as inactive zymogens which contain an N-terminal pro-domain as well as a large and a small subunit.

Upon cleavage, large and small subunits are released and form the mature caspase in an $\alpha_2\beta_2$ configuration with two large and two small subunits (Kaufmann *et al.*, 2001). The extrinsic pathway is induced when extracellular signals bind to specific transmembrane death receptors belonging to the tumour necrosis factor/nerve growth factor (TNF/NGF) family such as, Fas/cluster of differentiation 95 (CD95) or TNFα receptor (**Figure 3.1**). The ligand-bound death domains of these receptors recruit adaptor molecules such as Fas-associated protein with a death domain, which in turn leads to activation of caspase 8 thereby activating downstream caspases such as caspase 3 (Wenzel *et al.*, 2005, Favaloro *et al.*, 2012).

The intrinsic pathway is activated in response to stress signals including DNA damage, oxidative stress and many others. This pathway results in dissipation of the mitochondrial membrane potential, cessation of ATP production and release of proteins that contribute to caspase activation. The Bcl-2 family of proteins are important regulators of this type of apoptosis and are classified into two types: anti-apoptotic members containing three or four Bcl-2 homology (BH) domains (i.e. Bcl-2, Bcl-xl, Bcl-w and Mcl-1); and pro-apoptotic members with either two or three BH domains (i.e. Bax, Bak, Bcl-xs, Bok) or with just one BH domain (i.e. Bad, Bik, Bid, Bim, Noxa and Puma) (Youle and Strasser, 2008). Pro-apoptotic members mediate apoptosis by disrupting mitochondrial membrane integrity either directly forming pores, or by binding to mitochondrial channel proteins. On the other hand, anti-apoptotic members interfere with the aggregation of pro-apoptotic members thereby preventing apoptosis. Once mitochondrial outer membrane permeabilization occurs, a number of proteins are released including cytochrome c, apoptosis-inducing factor (AIF), endonuclease G (endo G), Direct IAP-binding protein with low PI (DIABLO/Smac) and others (Giam *et al.*, 2008, Youle and Strasser, 2008). Cytochrome c then forms a complex with Apaf-1 inducing apoptosome formation which converts pro-caspase 9 into its active form, thus activating caspase 3 and initiating a caspase cascade

(Favaloro *et al.*, 2012). However, the two apoptosis pathways are not mutually exclusive. Caspase 8 can interact with Bid, a pro-apoptotic protein of the Bcl-2 family which then leads to release of mitochondrial cytochrome c into the cytoplasm (Kaufmann *et al.*, 2012).

3.1.1.2 Caspase-independent apoptosis

An increasing number of studies have suggested that cleavage of proteins during apoptosis does not necessarily involve caspases. For example, lysosomal cathepsin D has been shown to trigger AIF release independent of the caspase cascade and cell death mediated by AIF in Apaf 1 -/- and caspase 3 -/- cells (Susin *et al.*, 2000, Bidere *et al.*, 2003). In addition, the broad caspase inhibitor zVAD-fmk did not prevent the translocation of AIF to the nucleus nor did it prevent its lethal effect, thus indicating an involvement of AIF in caspase-independent apoptosis (Susin *et al.*, 1999, Daugas *et al.*, 2000). AIF may induce cell death by activating chromatin condensation and cleavage of DNA into fragments of 50 kb or larger (Susin *et al.*, 1999) via recruitment and activation of endonucleases upon its entry in the nucleus (Ye *et al.*, 2002). Experiments in transgenic mice lacking DNA fragmentation factor (DFF) 45 or its caspase cleavage site showed that EndoG can induce DNA fragmentation in the complete absence of DFF45, the key caspase-dependent DNA fragmentation factor activated by caspase 3 (Li *et al.*, 2001). Poly (ADP-ribose) polymerase-1 (PARP-1) senses DNA strand breaks and facilitates DNA repair by relaxing the condensed chromatin structure and is also a major substrate for caspase-dependent cell death (Chatterjee *et al.*, 1999). Inhibition of PARP-1 activity or deletion of the PARP-1 gene provides protection against tissue damage in various conditions such as cerebral ischemia, myocardial infarction and streptozotoxin-induced diabetes (Pieper *et al.*, 1999). In addition,Yu *et al.* (2002) reported that excessive calcium influx resulted in over-activation of PARP-1, thus triggering AIF release and subsequent cell death when caspase inhibitors were present.

3.1.2 Calpain activation and retinopathies

Calpain activation has been strongly implicated in various neuronal pathological conditions such as Alzheimer's disease, Parkinson's disease and Huntington's disease (Nixon, 2003, Bizat *et al.*, 2005). In addition, calpain-mediated proteolysis has been observed in retinal degeneration in several animal models of RP and glaucoma (Donovan and Cotter, 2002, Doonan *et al.*, 2003, Paquet-Durand *et al.*, 2006, Huang *et al.*, 2010). The calpain family consists of 14 members of calcium-dependent cysteine proteases, some of which are ubiquitously expressed, such as calpains 1, 2, 4, 5, 7 and 10 whereas others are found in specific tissues: calpain 3 (skeletal muscle), calpain 6 (placenta), calpain 8 (smooth muscle), calpain 9 (stomach), calpain 11 (testes), calpain 12 (skin after birth) and calpain 13 (testes and lung) (Smith and Schnellmann, 2012). In the retina, calpain is present in most layers, including photoreceptor outer segments, plexiform layers (Azarian *et al.*, 1993), ganglion cell and nerve fibre layers (Persson *et al.*, 1993, Azuma and Shearer, 2008). There are two types of calpain present in the brain including calpain 1 (μ-calpain) and calpain 2 (m-calpain) which are activated by micromolar and millimolar Ca^{2+} concentrations respectively (Li *et al.*, 2004, Suzuki *et al.*, 2004). They are heterodimers composed of a regulatory subunit (28 kDa) and a distinct catalytic subunit (80 kDa) (Suzuki *et al.*, 1987). The former is identical for calpains 1, 2 and 9 (Hood *et al.*, 2004, Suzuki *et al.*, 2004). In the endoplasmic reticulum, the catalytic and regulatory subunits are associated with the endogenous calpain inhibitor, calpastatin. Activation of calpain is thought to occur in two steps: calpastatin disassociates from calpain and this leads to its translocation from the lumen to the cytosolic side of the ER or to the cell membrane (Hood *et al.*, 2004, Suzuki *et al.*, 2004). Binding of Ca^{2+} leads to a conformational change which in turn leads to dissociation of the regulatory subunit from the catalytic subunit, thus giving rise to the 76-78 kDa active protease (Li *et al.*, 2004).

Calpains are often associated with necrotic cell death which is an uncontrolled form of death involving a variety of unassociated, degenerative processes. In contrast to energy demanding, active apoptotic cell death, necrosis occurs quickly, needs less energy and exerts negative effects on surrounding cells. However, calpains have also been found to be activated during apoptosis and share many substrates with caspases including cytoskeletal and regulatory proteins. For example, calpains can activate proteins involved in apoptosis such as pro-caspase-12, pro-caspase-3, PARP, Bax, p53, p35, c-Jun N-terminal kinase (JNK) and in translocation of AIF to the nucleus (Wood *et al.*, 1998, McGinnis *et al.*, 1999, Lee *et al.*, 2000, Blomgren *et al.*, 2001, Artus *et al.*, 2006, Tan *et al.*, 2006). In addition, calpain also cleaves alpha-fodrin (α-fodrin), a 240 kDa neuroskeletal protein, the cleavage of which is an important early event in apoptosis, into fragments of 145 and 150 kDa (Vanags *et al.*, 1996, Sakamoto *et al.*, 2000). Calpains and caspases appear to modulate each other via calpain-mediated cleavage of caspases 3, 7, 8, 9, cathepsin and caspase 3-mediated cleavage of calpastatin thereby activating calpains (Chua *et al.*, 2000, Kato *et al.*, 2000, Wang, 2000b, Blomgren *et al.*, 2001). Thus, calpains operate within both forms of cell death; they can inactivate caspases and turn conventional apoptosis into caspase-independent cell death (Chua *et al.*, 2000, Lankiewicz *et al.*, 2000). On the other hand, calpain 1 has been shown to induce apoptosis by cleaving and activating caspase 7 (Gafni *et al.*, 2009). The authors also suggested that the two cell death cascades can directly interact to influence the activity and cellular localization of each other.

The *rd1* mouse is a relatively well studied model for RP and is caused by a mutation in the β subunit of the photoreceptor-specific phosphodiesterase-6 (*PDE-6*) gene (Bowes *et al.*, 1990). In this model, cell death has been characterized as apoptotic based on morphological analysis and evidence of endonuclease activity as seen by DNA fragmentation (Sanyal and Bal, 1973, Chang *et al.*, 1993). However, many attempts at inhibiting conventional apoptosis through caspase inhibition in this and many other

retinopathy models have failed to show any significant protection (Donovan and Cotter, 2002, Zeiss *et al.*, 2004, Gomez-Vicente *et al.*, 2005). In addition, cell death in the *rd1* mouse and other models is associated with high levels of Ca^{2+} influx, membrane depolarization and an energetic collapse (Fox *et al.*, 1999, Delyfer *et al.*, 2004). Therefore, the energy source required for apoptosis is no longer available and apoptosis should be impaired. Indeed, it has been shown in recent years that other death mechanisms may be present in retinal degeneration (Zeiss, 2003, Doonan *et al.*, 2005, Gomez-Vicente *et al.*, 2005). Moreover, typical calpain cleavage of PARP was observed in the *rd1* mouse at P11 suggesting activation of this protease in this model (Doonan *et al.*, 2003). In addition, Paquet-Durand *et al.* (2006) demonstrated that increased calpain activity in *rd1* was localized to the outer nuclear layer of photoreceptors. In Wistar Bonn/Kobori (WBN/Kob) rats, a spontaneously diabetic rat, retinal degeneration is coupled with an increase in calpain 1 and 2 activity (Azuma *et al.*, 2004). It has also been reported that calpain activity led to the rupture of lysosomal membranes and subsequent release and activation of cathepsins thus triggering autolytic digestion of the cell (Leist and Jaattela, 2001, Yamashima, 2004). Moreover, calpain has been suggested to play a major role in the opening of mitochondrial permeability transition pores thereby allowing co-translocation of AIF and caspase 12 to the nucleus (Sanges and Marigo, 2006).

Calpain activation due to high intracellular Ca^{2+} concentrations has been implicated in various pathological conditions, thus inhibition of calpain has been investigated in the development of treatments for these diseases. Calpastatin is a highly specific endogenous calpain inhibitor which binds to calpain in its inactive form in the ER. Interestingly, the calpain-calpastatin association has been shown to be both dependent (Goll *et al.*, 2003) and independent (Melloni *et al.*, 2006) on Ca^{2+} concentrations. Intravitreal injection of calpastatin into the *rd1* mouse model for RP reduced photoreceptor cell death (Paquet-Durand *et al.*, 2010). This study was further supported by another observation which

demonstrated that the peptidic calpain inhibitor CAST, based on the sequence of calpastatin, prevented calpain activation and counteracted photoreceptor cell death in the *rd1* mouse (Paquet-Durand *et al.*, 2010). However, treatment of *rd1* mouse retinal explants with the calpain inhibitor I ALLN effectively reduced cleavage of α-fodrin (an initial step in apoptosis) but did not protect photoreceptor survival (Doonan *et al.*, 2005). Calpain activation has been shown to be involved in glaucoma and the calpain inhibitor II (ALLM) significantly reduced damage to the optic nerve in opossum (Araujo Couto *et al.*, 2004). In addition, ALLM and SNJ-1945, a novel oral calpain inhibitor, significantly reduces cell loss in the ganglion cell layer and thinning of the inner plexiform layer induced by NMDA (Chiu *et al.*, 2005, Shimazawa *et al.*, 2010).

3.1.3 Light ablation model

Photoreceptor cell death is a key feature of retinal degenerative diseases and thus various transgenic models have been developed to provide a better understanding of this process and to enable therapeutic strategies to be evaluated (Chader, 2002, Dejneka *et al.*, 2003, Fletcher *et al.*, 2011). In addition, the light-induced model of retinal degeneration has also been used for studying photoreceptor cell death and has many advantages. Light exposure triggers apoptosis in a highly synchronized fashion in which photoreceptors undergo apoptosis at more or less the same stage, thereby allowing detection of biomarkers and their functions in the different phases of cell death. By contrast, in transgenic models, photoreceptors undergo cell death at different stages and the numbers of affected cells are much smaller compared to the light induced degeneration model at any given time. Moreover, the light induced retinal degeneration model has a faster rate of photoreceptor cell death which takes only 10 days or less from light exposure to complete loss of photoreceptors. Furthermore, the severity of light induced retinal damage can be altered by light intensity and duration of light exposure (Wenzel *et al.*, 2005). Since the discovery of light damage in laboratory animals, several protocols have been developed using

fluorescent white light mimicking excessive exposure to daylight, broadband green light matching the absorbance spectrum of rhodopsin and narrow band blue harmful energy-rich light (Noell *et al.*, 1966, Wenzel *et al.*, 2005, Grimm and Reme, 2013). Moreover, exposure duration and intensity can be varied depending on the light source and the animals exposed. For example, very short exposure periods (i.e minutes) are employed in experiments using harmful energy-rich blue light whereas longer exposure periods varying from hours to weeks can be applied in the case of broadband green and white light. Thus, variation of these protocols has helped to identify different pathways of photoreceptor apoptosis induced by light. In addition, the different animal models used in these light damage experiments also complicate attempts to define a general pathway of light-induced retinal degeneration. For example, it has been reported that photoreceptor cell death in light-induced retinal degeneration Balb/c mice did not involve activation of various caspases including caspase 3 (an important apoptosis executioner), caspases 8, 9, 7 and 1 (Donovan *et al.*, 2001, Donovan and Cotter, 2002). The authors also suggested that zVAD-fmk, a pan-caspase inhibitor did not protect photoreceptors from apoptosis indicating that light-induced retinal degeneration is caspase independent. On the other hand, they showed that the Ca^{2+} channel blocker D-*cis*-diltiazem inhibited calpain activity and photoreceptor apoptosis in this light-induced damage model. In contrast, caspase 3 was shown to be upregulated in the retina after exposure of Sprague-Dawley rats to blue light (Wu *et al.*, 2002) while calpain was observed to be highly upregulated but played no vital role in photoreceptor apoptosis in retinas from light-ablated Wistar rats (Perche *et al.*, 2007, Perche *et al.*, 2009). Thus, these studies indicate that apoptosis is a complicated process involving not only caspases but also other proteins including calpains and that the mechanism varies depending on the model.

3.1.4 Objectives

In this chapter, two low molecular weight calpain inhibitors ALLM (401.6 Da) and ALLN (383.5 Da) that cannot efficiently diffuse across the iBRB and yet have been used to protect against photoreceptor cell death when delivered by direct intraocular injection (Sanges *et al.*, 2006), were administered systemically and tested for efficacy in prevention of light induced photoreceptor cell death in Balb/c mice in tandem with modulation of the iBRB by systemic administration of CLDN5 siRNA. In addition, the doxycycline inducible AAV2/9 expressing shRNA targeting CLDN5 (CLDN5 AAV2/9) was also subretinally injected into the retinas of Balb/c mice to facilitate a more localized approach of specifically targeting claudin-5 in the retina in order to investigate the effect of systemic administration of ALLM and ALLN in a light induced retinal degeneration model. Data presented in this chapter have been published (Campbell *et al.*, 2009, Campbell *et al.*, 2010, Campbell *et al.*, 2011, Nguyen *et al.*, 2012).

3.2 Methods

3.2.1 siRNA and AAV production

siRNA was kindly provided by Dr. Matthew Campbell (Campbell *et al.*, 2008). Sequences of the claudin-5 siRNA used in this study were as follows. Sense sequence: CGUUGGAAAUUCUGGGUCUUUdTdT. Antisense sequence: AGACCCAGAAUUUCCAACGUUdTdT. Non-targeting (NT) control siRNA targeting luciferase was used as a non-targeting control Sense sequence: CUUACGCUGAGUACGUCGAdTdT. Antisense sequence: UCGAAGUACUCAGCGUAAGdTdT.

shRNAs designed to target transcripts derived from mouse claudin-5 were cloned into the pSingle-tTS-shRNA (Clontech) vector and incorporated into AAV2/9 vectors by Dr. Marian Humphries in the laboratory. The plasmid incorporating the inducible system with claudin-5 shRNA was cloned into the plasmid pAAV-MCS, such as to incorporate left and right AAV inverted terminal repeats (L-ITR and R-ITR). AAV2/9 was then generated using a triple transfection system in a stably transfected HEK-293 cell line for the generation of high-titre viruses as previously described by this laboratory. tTS is a fusion of the Tet repressor and the Kid-1 KRAB-AB silencing domain. In the absence of doxycycline, tTS repressor binds to tet operator (tetO) elements in a modified polIII promoter (pTRE-U6), inhibiting expression of claudin-5 (or non- targeting luciferase) shRNAs. In the presence of doxycycline, tTS no longer binds to the promoter, allowing expression of shRNA (**Figure 3.1**). All AAVs were assessed for viral purity using a 10% SDS-PAGE gel analysis.

3.2.2 *In vivo* delivery of siRNA to retinal capillary endothelial cells

Rapid high pressure, high volume tail vein injections were carried out in conjunction with Dr. Matthew Campbell essentially as previously successfully used at this laboratory (12, 47). Mice of weight 20-30 g were individually restrained inside a 60-ml volume plastic tube. The protruding tail was warmed for 5 min prior to injection under a 60-W lamp and the tail vein clearly visualized by illumination from below. 20 μg of targeting siRNA, or non-targeting siRNA made up with PBS to a volume in mls of 10 % of the body weight in grams or PBS alone was injected into the tail vein at a rate of 1 ml/sec using a 26-guage (26G 3/8) needle.

3.2.3 Light ablation methodology

Three month old Balb/c mice were injected with either CLDN5 or NT siRNA by hydrodynamic tail vein injection and 48 h later with ALLM (20 mg/kg), ALLN (100 mg/kg) intra-peritoneally (Calbiochem, Germany). Immediately prior to light exposure, their pupils were dilated with 1% cyclopentalate. Mice were then placed in cages with reflective interior and exposed to white light of 7900 lux for 2 h. The mice were left in the dark and sacrificed by CO_2 asphyxiation 12, 24 and 48 h post 2 h light ablation. In another set of experiments, 3 month old Balb/c mice were subretinally injected with 3 μl of 5 x 10^{11} vp/ml CLDN5 AAV2/9 in the right eye and of NT AAV2/9 in the left eye. Mice were then supplemented with 2 mg/ml doxycycline with 5% sucrose in their drinking water for 3 weeks. Twenty four hours prior to light ablation, mice were intra-peritoneally (i.p.) injected with ALLM (20 mg/kg). Mice were dark adapted for 24 h. Immediately prior to light exposure, their pupils were dilated with 1% cyclopentalate. Mice were then exposed to white light of 7900 lux for 2 h and put down at 24 h post light exposure (**Figure 3.3**).

3.2.4 TdT-mediated dUTP nick end labeling (TUNEL) staining

Eyes from mice were fixed in 3.5% formaldehyde (PFA) for 4 h followed by 3 washes in PBS. The lenses were removed. Eyes were cryoprotected using a sucrose gradient (10, 20 and 30%), and subsequently embedded in optimum cutting temperature (OCT) embedding compound (Sigma Aldrich). Cryostat sections (12 μm) were cut onto Polysine adhesion slides (Menzel-Glazer, Thermo Scientific). Sections were air dried, and washed 3 times in PBS. Sections were subsequently incubated in Proteinase K (20 μg/ml) (Boehringer Mannheim) for 5 min at 37°C followed by 2 washes in PBS. Sections were treated with 70% ethanol/30% acetic acid mix for 5 min at 4°C. Following 2 washes in PBS, sections were incubated again with Proteinase K (20 μg/ml) for 5 min at 37°C, then washed twice in PBS. Sections were re-fixed with 4% PFA (pH 7.4) for 5 min at 4°C, and washed 3 times in PBS. Positive controls were treated with DNaseI (50 U/ml) (Qiagen) in 50 mM Tris-HCl (pH 7.5) for 10 min at room temperature. Control slides were washed with PBS for 5 min. To detect cell death, sections were then incubated with staining mix (*in situ* cell death detection kit, TMR red, Roche) according to manufacturer's instructions for 1 hour at 37°C in the dark, followed by 2 washes in PBS for 5 min each in the dark. Nuclei were counterstained with DAPI (1:10,000 in PBS) and mounted using Aqua-Polymount® mounting medium (Polysciences). Only sections located at the central of the retina were used. On average, 7 sections were used per retina to calculate the average number of TUNEL positive cells.

3.2.5 Western Blot Analysis

After 12, 24 and 48 h, protein was isolated from total retinal tissue. Antibodies for Western blots were as follows: rabbit polyclonal anti claudin-5 (1:500) (Zymed Laboratories), mouse monoclonal anti α-fodrin (1:500) (Millipore), mouse monoclonal anti β-actin (1:2000) (Sigma Aldrich). Membranes were washed with TBS and incubated with a

secondary anti-rabbit (IgG) antibody (1:2000), or anti mouse (IgG) antibody (1:1000) (Sigma Aldrich) with HRP conjugates.

3.2.6 Statistical Analysis

Statistical analysis was performed using paired Student's *t*-test, with significance represented by a P value of < 0.05.

3.3 Results

3.3.1 Safety of systemic administration of CLDN5 siRNA

Firstly, the safety of CLDN5 siRNA systemic administration was assessed by photoreceptor cell death analysis using TUNEL staining of retinal sections at 24, 48 and 72 h post tail vein injection of CLDN5 siRNA in wild type C57BL/6J mice. TUNEL staining is a method to detect fragmented DNA resulting from apoptosis or necrosis. The assay uses terminal deoxynucleotidyl transferase which catalyzes labeled dUTPs to identified nicks in the DNA. **Figure 3.4** showed that no TUNEL positive cells were present in retinal cryosections of mice injected with CLDN5 siRNA at 24, 48 and 72 h post injection compared to both negative and positive control groups. In the positive control group, DNA fragmentation was induced by addition of DnaseI to the retinal section before TUNEL labelling. In addition, using MRI images, the study also showed that no oedema occurred in either the brain or retinas of animals after injection of CLDN5 siRNA (Campbell *et al.*, 2009). Thus, the results showed that systemic administration of CLDN5 siRNA did not cause any adverse effect on the retina.

Since the level of claudin-5 suppression was previously measured in only C57BL/6J mice (Campbell *et al.*, 2009), and since Balb/c mice are needed in light ablation studies, retinal lysates of Balb/c mice tail vein injected with CLDN5 siRNA or NT siRNA were taken 48 h post injection for CLDN5 analysis by western blot. Because it was previously shown that maximum suppression of CLDN5 protein in BBB was obtained at 48 h post injection, this timepoint was chosen to look at suppression of CLDN5 in the light ablation model. As expected, the level of CLDN5 in the retina was greatly reduced in mice injected with CLDN5 siRNA compared to those injected with NT siRNA 48 h post injection (**Figure 3.5**).

3.3.2 Effect of ALLM and CLDN5 siRNA on light-induced photoreceptor cell death

In order to determine whether claudin-5 suppression would lead to a reversible and size-selective opening of the iBRB thus allowing administration of the calpain inhibitor ALLM, Balb/c mice were systemically tail vein injected with either CLDN5 siRNA or non targeting siRNA 48 h prior to i.p. injection with ALLM (20 mg/kg). Mice were then dark adapted for 24 h followed by exposure to white light of 7900 lux for 2 h. Mice were left in the dark room and their retinas were then taken at 12, 24 and 48 h post light ablation for TUNEL staining and western blot analysis. Analysis of end stage cell death through TUNEL staining of photoreceptor nuclei showed that there were less TUNEL positive photoreceptor cells in mice injected with CLDN5 siRNA together with ALLM delivery compared to those injected with NT siRNA by up to 29.12% at 12 h (** P = 0.0011) and 49.07% at 24 h (* P = 0.0252) post light ablation (**Figures 3.6A, B**). Thus, these data suggest that there was less photoreceptor cell death in animals administered with CLDN5 siRNA and the calpain inhibitor ALLM at 12 and 24 h post light exposure. However, ALLM did not seem to provide full protection against light induced retinal damage in these animals because the amount of TUNEL positive photoreceptor cells appears to be significantly increased in the treated group compared to the control group at 48 h post light ablation (* P = 0.0191) (**Figure 3.6C**). Western blot data for α-fodrin cleavage due to calpain activation during light induced apoptosis showed that there was less cleaved α-fodrin in retinal lysates of mice injected with CLDN5 siRNA and ALLM than in those injected with NT siRNA and ALLM at 12 h post injection. Calpains typically cleave α-fodrin into fragments of 145 kDa and 150 kDa whereas cleavage by caspase 3, results in the generation of 120 kDa and 150 kDa fragments (Janicke *et al.*, 1998, Wang, 2000a). Levels of 150 and 145 kDa α-fodrin fragments were statistically significantly decreased by 95.4% (* P = 0.049) and 96.5% (* P = 0.0127) respectively in retinas of mice injected with

CLDN5 siRNA and ALLM compared to control levels (**Figure 3.7A**). Interestingly, the level of the 120 kDa caspase 3 cleaved fragment was also significantly reduced by 65.7% in retinas of mice injected with CLDN5 siRNA and ALLM compared to control retinas (* P = 0.0174) (**Figure 3.7A**). However, the level of α-fodrin cleavage appeared similar in both groups at 24 and 48 h post light damage (**Figures 3.7B, C**). Cleavage of α-fodrin protein is one of the starting points of apoptotic cell death. Thus, the western blot data suggests that maximal levels of α-fodrin cleavage at 24 h post light damage led to widespread cell death in mice injected with CLDN siRNA and ALLM observed at 48 h post light damage. Overall, systemic administration of CLDN5 siRNA together with ALLM provided light-exposed Balb/c mice with some protection from retinal degeneration but only up to 24 h after light exposure.

3.3.3 Effect of ALLN and CLDN5 siRNA on light-induced photoreceptor cell death

Sanges *et al.* (2006) showed that ALLN had a stronger inhibitory effect than ALLM in preventing apoptosis in the *rd1* retina. Thus, in this study, the same experimental set up as in ALLM treatment in light ablated Balb/c mice was used to determine whether intra-peritoneal injection of ALLN (100 mg/kg) could also improve protection of the retina from undergoing light induced degeneration. **Figure 3.8** showed TUNEL data in animals (n = 5) systemically injected with CLDN5 siRNA or NT siRNA together with ALLN, 12, 24 and 48 h post light ablation. The amount of TUNEL positive cells were significantly reduced by up to 21.69% in mice injected with CLDN5 siRNA compared to the control group at 12 h post light exposure (*** P = 0.0003). However, western data showed no differences in α-fodrin cleavage between the two groups of animals at all timepoints post light ablation (**Figure 3.9**). In addition, α-fodrin fragments seemed to increase though not significantly in retinas of mice injected with CLDN5 siRNA compared to those injected with NT siRNA at 12 h post light exposure.

3.3.4 Effect of subretinal delivery of CLDN5 AAV2/9 and systemic administration of ALLM

Since hydrodynamic administration of siRNA is delivered in a volume of 10% of total weight of an animal to allow a sufficient amount of siRNA to reach the iBRB, this approach would not be feasible for treating retinopathies in the clinic. Thus, a doxycycline inducible AAV2/9 system expressing CLDN5 or NT shRNA which can be given as a once-off subretinal injection, was developed. In fact, the data presented here have been recently published by our group (Campbell *et al.*, 2011). This study also reported that inducible iBRB modulation is safe and has no impact on either visual function or oedema in any of the experimental animals. Based on the methods used for systemic delivery of CLDN5 siRNA and calpain inhibitors in the light ablation model, similar experiments were conducted except that the doxycycline inducible CLDN5 AAV2/9 was used instead of CLDN5 siRNA. Since it was suggested earlier that protection of retinal degeneration reached a maximum at 24 h post light ablation in animals injected with CLDN5 siRNA and ALLM, the same timepoint was used in this study to investigate whether subretinal administration of CLDN5 AAV2/9 could also provide protection from light-induced damage.

In brief, Balb/c mice (n = 5) received a subretinal inoculation of 3 µl of 5 x 10^{11} viral particles/ml of CLDN5 AAV2/9 in the right eye and NT AAV2/9 in the left eye. These animals were then supplemented with 2 mg/ml doxycycline and 5% sucrose in their drinking water for 3 weeks post injection. Twenty-four hours prior to light ablation, mice were *i.p.* injected with ALLM (20 mg/kg). Retinas of these animals were taken either for TUNEL staining of photoreceptor cell death or western blot analysis of α-fodrin cleavage 24 h after light exposure. Up to 70% protection was observed in retinas of mice receiving CLDN5 AAV2/9 compared to the retinas of mice injected with NT AAV2/9 (*** P = 0.0006) (**Figure 3.10**). In addition, systemic administration of ALLM together with

inoculation of CLDN5 AAV2/9 appeared to provide a higher efficiency in preventing retinal degeneration compared to hydrodynamic injection of CLDN5 siRNA in terms of α-fodrin fragments (**Figure 3.11**). Specifically, levels of 150, 145 and 120 kDa α-fodrin fragments were significantly reduced by up to 86.91, 89.04 and 85.99% respectively in retinas injected with CLDN5 AAV2/9 compared to those injected with NT AAV2/9 (* P = 0.0254, * P = 0.0391 and ** P = 0.0097; respectively).

3.4 Discussion

Intra-ocular injection of therapeutic agents is widely used experimentally in rodent models of retinal degeneration, however in humans this poses a low, but significant risk of severe endophthalmitis and is a far from optimal treatment for retinopathies given that repeated injections would be required over long periods of time. Using an RNAi approach, it was shown that hydrodynamic injection of siRNA targeting the tight junction protein claudin-5 results in a transient opening of the iBRB to molecules of up to 1 kDa in a reversible manner in mice (Campbell *et al.*, 2009, Campbell *et al.*, 2010). In these studies, we also reported that levels of CLDN5 expression in the iBRB were significantly reduced at 24 and 48 h and returned to normal levels at 72 h post systemic delivery. The process has no negative impact on neuronal transcription or visual function and does not induce neuronal or retinal oedema based on MRI analysis. In this study, TUNEL staining demonstrated that tail vein injection of CLDN5 siRNA did not have any adverse effect on photoreceptors, thus strengthening the safety profile of this barrier modulation approach (**Figure 3.4**). Moreover, western blot analysis of retinal CLDN5 protein levels in Balb/c mice tail vein injected with CLDN5 siRNA showed that claudin-5 was indeed suppressed 48 h post injection thereby potentially facilitating the delivery of small molecular weight compounds to the retina at this timepoint (**Figure 3.5**).

The light ablation model in this study was well characterised by Donovan *et al.* (2001 and 2002) and consists of exposing Balb/c mice to a white fluorescent light at 7900 lux for 2 h. To study the effect of increased delivery in photoreceptor cell survival, low molecular weight calpain inhibitors, ALLM (20 mg/kg) or ALLN (100 mg/kg) was injected i.p. into Balb/c mice 24 h prior to light exposure with or without iBRB modulation. After a hydrodynamic tail vein injection of CLDN5 siRNA, systemic administration of ALLM substantially protected murine retinas from light induced photoreceptor degeneration (**Figures 3.6**). Although TUNEL staining became apparent 12 h post light exposure, significantly less cell death was observed in the group of mice that received ALLM when

the iBRB was modulated with CLDN5 siRNA compared to control mice up to 24 h post light ablation. In contrast to ALLM, systemic administration of ALLN seemed to be less effective in protecting from light induced damage in light ablated Balb/c animals (**Figures 3.8**). This is not in agreement with a previous study by Sanges et al (2006) which reported that ALLN was a much more potent calpain inhibitor than ALLM. However, differences in animal models and route of administration of calpain inhibitors might have contributed to the differing results.

In order to investigate the effect of calpain inhibitors on the mechanism of photoreceptor cell death, levels of cleaved α-fodrin fragments, which contribute to dramatic plasma membrane blebbing and reorganization during apoptosis, were measured in experimental animals. Although it has been suggested that cell death in this light ablation model was caspase independent, levels of caspase cleaved α-fodrin fragment (120 kDa) were also reduced significantly by up to 66% in retinas treated with ALLM and CLDN5 siRNA compared to control retinas at 12 h post light exposure (**Figure 3.7**). Despite ALLN not offering any protection against α-fodrin cleavage in treated retinas, western blot analysis still showed the presence of the 120 kDa fragment at all timepoints post light exposure (**Figure 3.9**). Therefore, the data suggest that both calpain and caspase 3 are involved in this light ablated Balb/c model. In contrast, it has been reported that photoreceptor cell death in light ablated Balb/c mice is independent of caspases 1, 3, 7, 8, and 9 and could only be prevented by calcium channel blocker D-*cis*-diltiazem which inhibited calpain activation (Donovan *et al.*, 2001, Donovan and Cotter, 2002). However, calpain inhibition had no neuroprotective effect against light damage whereas the mechanism of photoreceptor cell death was caspase-dependent in light induced retinal damage in Wistar albino rats (Perche *et al.*, 2007, Perche *et al.*, 2009). In addition, all of the above studies reported that calpain activity was highly upregulated up to 1 day post light exposure

whereas in this study α-fodrin cleavage was still observable at 48 h post light damage suggesting longer activation of calpain in this model.

Both ALLN and ALLM have been shown to suppress calpain 1, calpain 2, cathepsins and caspases (Sasaki *et al.*, 1990, Ravid *et al.*, 2000, Gomez-Vicente *et al.*, 2005). The current study also demonstrated that these two calpain inhibitors inhibited caspase 3 leading to a reduction in 120 kDa α-fodrin fragment post light exposure in Balb/c mice. In fact, many so called caspase specific inhibitors such as zVAD-fmk and z-DEVD-fmk, pan-caspase and caspase 3 specific inhibitors respectively, also potently inhibit calpains (Knoblach *et al.*, 2004, Bizat *et al.*, 2005). Moreover, caspases and calpains work independently or cooperatively to cause neuronal cell death (Wang, 2000b, Ray *et al.*, 2006).

Due to better neuroprotection provided by ALLM when mice had their iBRB modulated with CLDN5 siRNA, ALLM was chosen to be the main calpain inhibitor in experiments using the inducible CLDN5 AAV2/9 approach. As expected, significantly less TUNEL positive cell staining of up to 70% was observed in eyes injected with CLDN5 AAV2/9 compared to eyes injected with NT AAV2/9 in mice injected with ALLM 24 h prior to light ablation (**Figure 3.10**). In addition, levels of α-fodrin cleavage were also statistically significantly reduced by 86-90% in treated retinas compared to control retinas at 24 h post light ablation (**Figure 3.11**).

In summary, these findings have shown that modulation of the permeability of the iBRB by down-regulation of claudin-5 results in enhanced delivery of both ALLM and ALLN to the retina and also highlight the influence that increased delivery of these calpain inhibitors has on the rate of photoreceptor cell death. The study provides a proof of principle for size selective, transient, localized and inducible modulation of the iBRB by using CLDN5 AAV2/9.

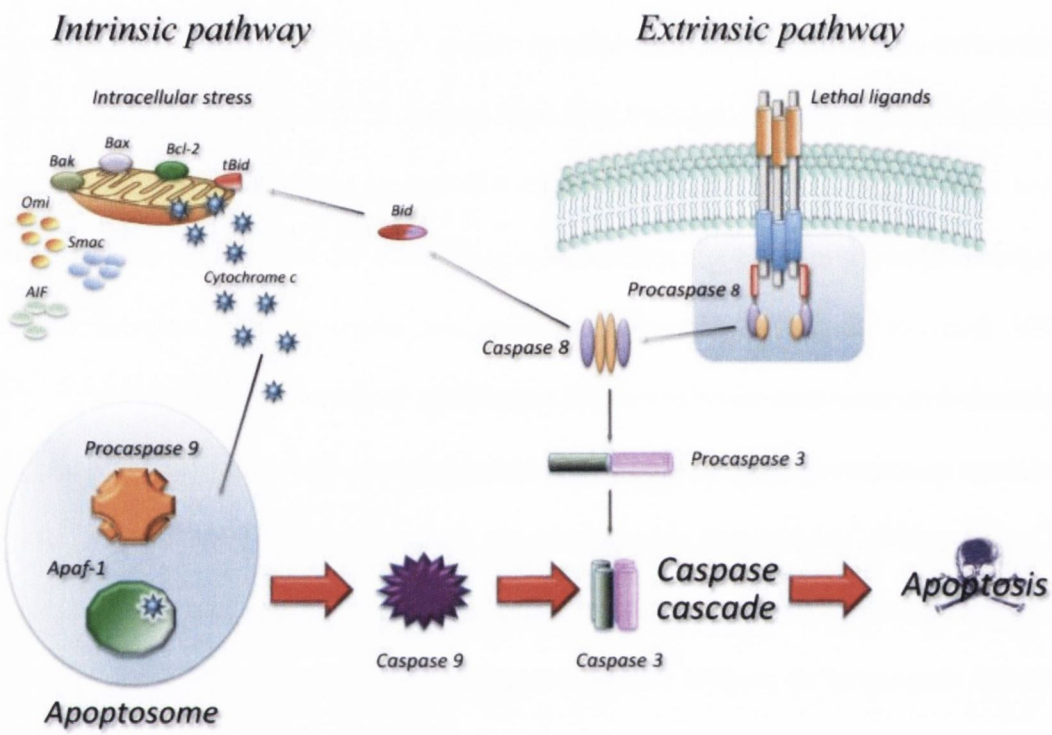

Figure 3. 1: Overview of the main molecular pathways leading to apoptosis.

In the intrinsic pathways, release of cytochrome c from mitochondria results in the formation of the apoptosome and activation of caspase 9. In the extrinsic pathway, upon ligand binding to specific receptors, caspase 8 is activated. Caspase 8 and 9 then activate downstream caspases such as caspase 3 initiating a caspase cascade leading to cell death. Caspase 8 can also cleave Bid which is involved in the intrinsic pathway. Figure is obtained from Favaloro *et al.* (2012).

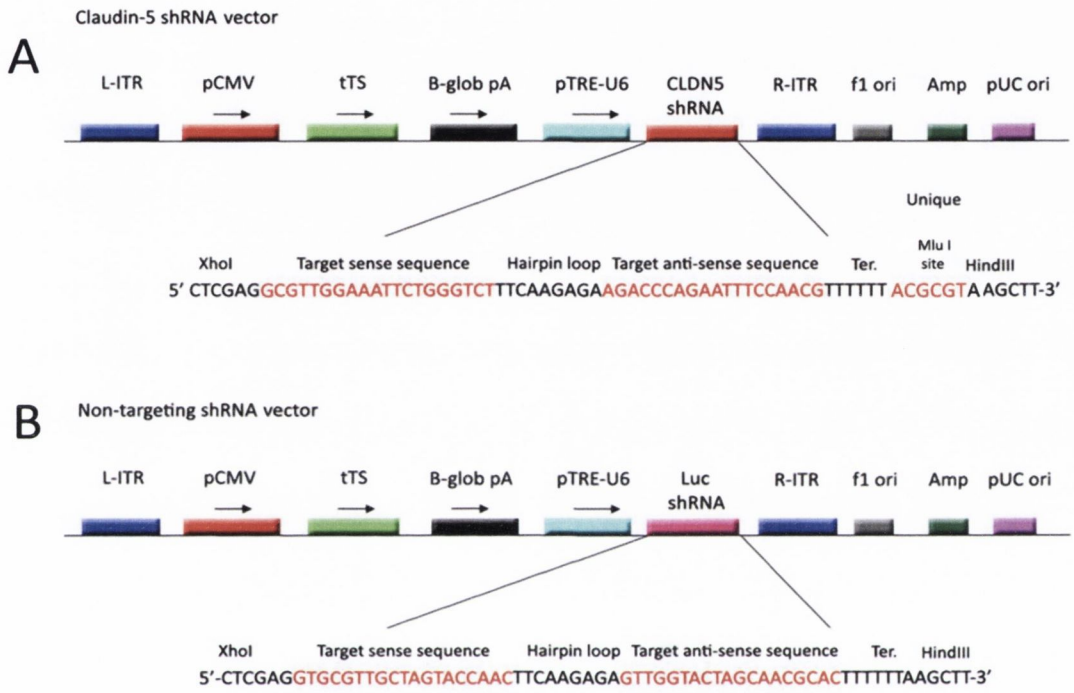

Figure 3. 2: CLDN5 and NT shRNA vector constructs.

The plasmid incorporating the inducible system with claudin-5 shRNA (A) or a non-targeting (NT) luciferase shRNA (B) was cloned into the plasmid pAAV-MCS, such as to incorporate left and right AAV inverted terminal repeats (L-ITR and R-ITR). Abbreviations: tetracycline inducible transcriptional suppressor (tTS); Beta-globin polyA (B-glob pA); Tet-responsive U6 promoter (pTRE-U6); f1 origin of replication (f1 ori); ampicillin selection (Amp); pUC origin of replication (pUC).

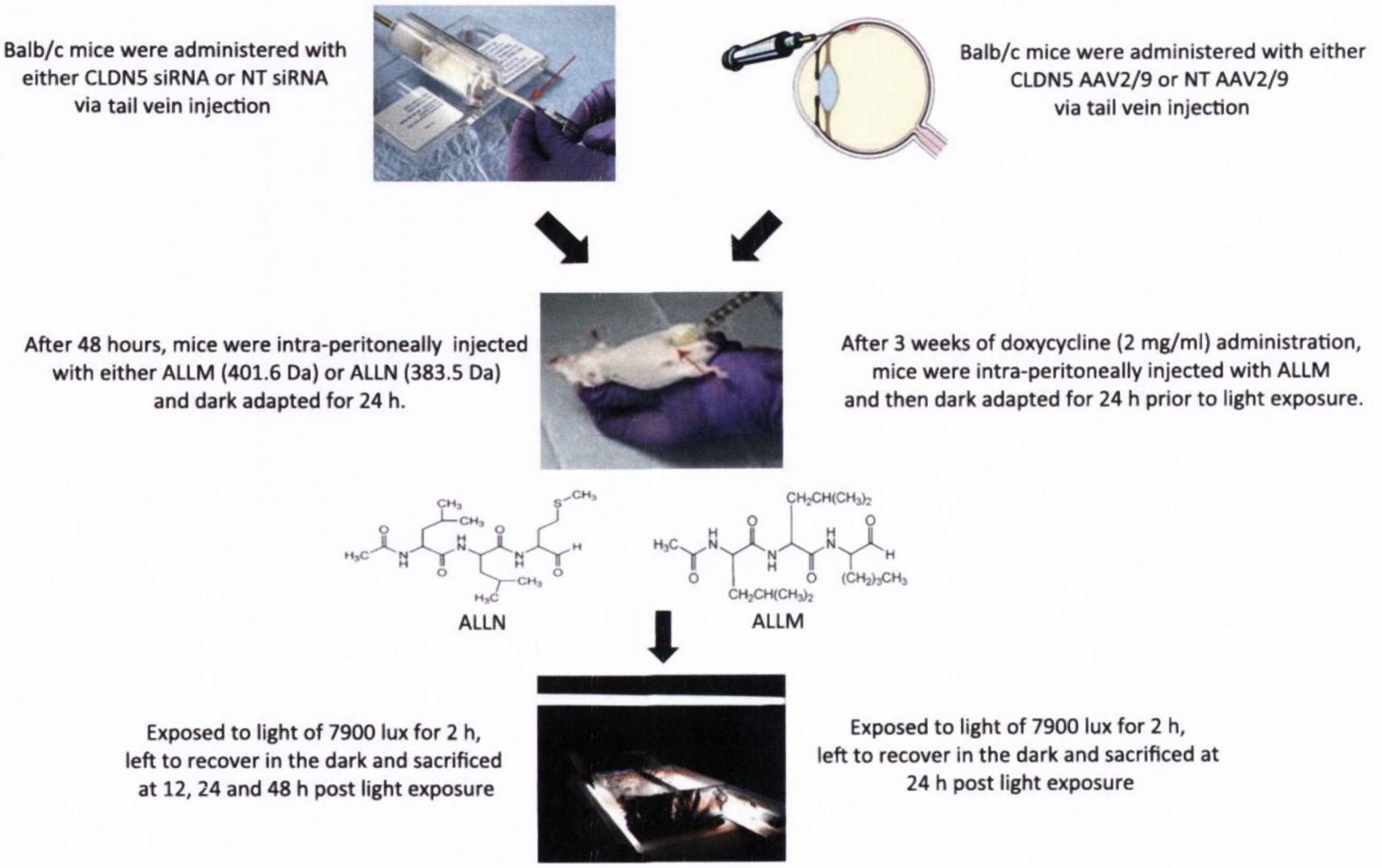

Figure 3. 3: Overview of light ablation experiments in Balb/c mice.

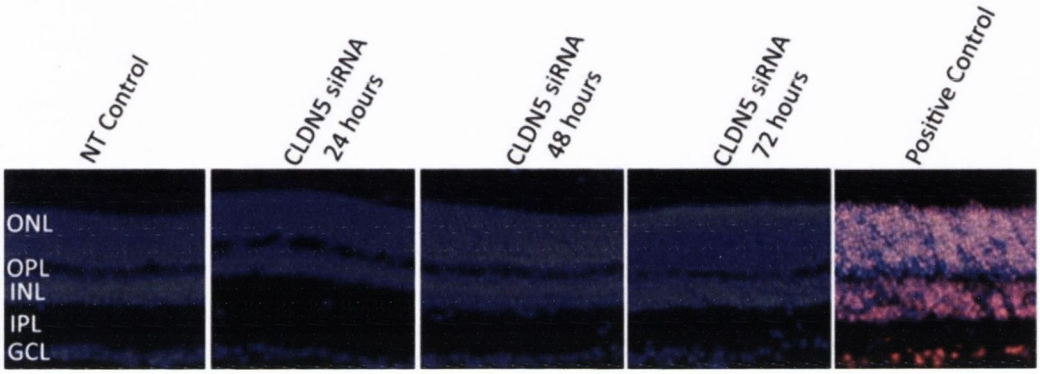

Figure 3. 4: Safety assessment for CLDN5 siRNA.

Delivery of siRNA did not appear to cause neuronal cell death in any experimental group using TUNEL staining. In contrast, almost every single cell was labelled with TUNEL in the control group treated with DnaseI. (40x objective).

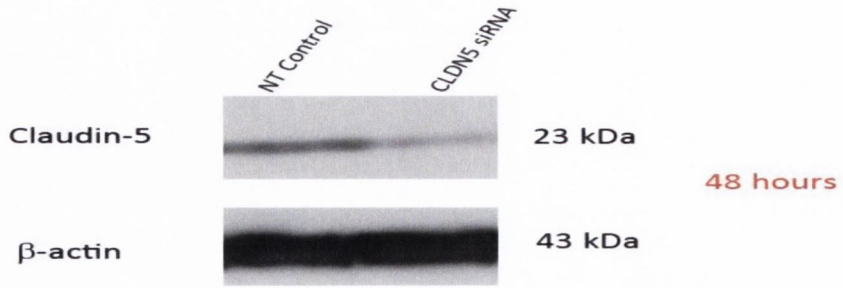

Figure 3. 5: Suppression of CLDN5 expression.

Balb/c mice were tail vein injected with either CLDN5 siRNA or NT siRNA (n = 5 in each group) and their retinas were taken 48 h later for CLDN5 detection by Western blot. The data clearly showed a suppression of CLDN5 protein in retinas of mice injected with CLDN5 siRNA compared to those injected with NT siRNA.

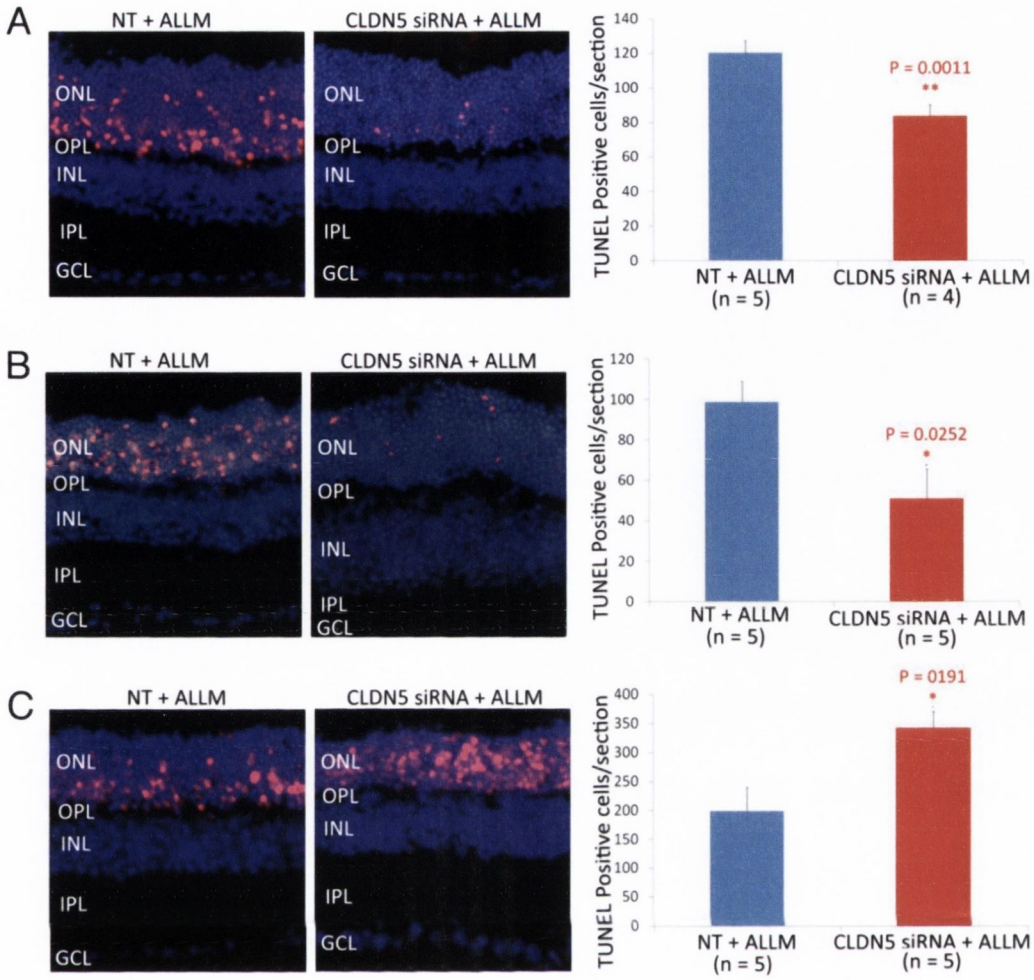

Figure 3. 6: Effects of CLDN5 and ALLM on cell death.

CLDN5 and NT siRNAs were administered to Balb/c mice 48 h prior to I.P injection of ALLM. Mice were dark adapted for 24 h prior to exposure to white light of 7900 lux for 2 h. A) and B) At 12 and 24 h after light ablation, TUNEL positive nuclei present in retinal ONL of mice injected with CLDN5 siRNA were significantly less than those injected with NT siRNA (** P = 0.0011) and (* P = 0.0252). C) However, there were significantly more TUNEL positive nuclei in CLDN5 sections compared to NT sections at 48 h post light exposure (* P = 0.0191). Error bars denote ± SEM. (40x objective).

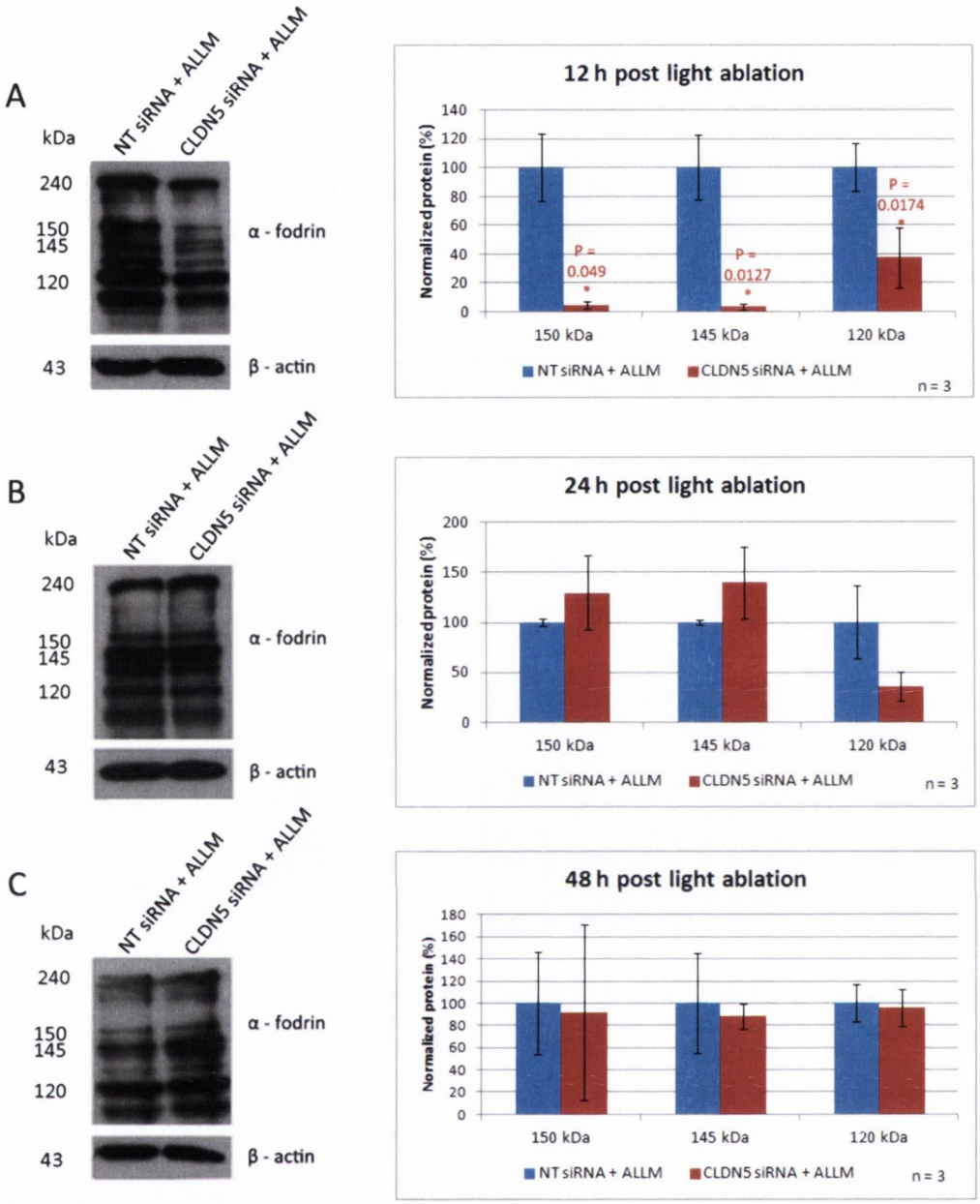

Figure 3. 7: Effect of CLDN5 siRNA and ALLM on α-fodrin cleavage.

Balb/c mice were treated similarly as described in **Figure 3.6**. Western blots for α-fodrin protein showed different amounts of α-fodrin cleaved fragments at three different timepoints (12, 24, and 48 h) post light ablation (n = 3 in each group). A) There were significantly less α-fodrin cleaved fragments (150, 145 and 120 kDa) in retinal lysates of mice treated with CLDN5 siRNA than in those injected with NT siRNA at 12 h post light exposure (* P = 0.049, * P = 0.0127 and *P = 0.0174 respectively). B and C) In contrast, the amount of α-fodrin fragments appeared to be similar between the two experimental groups at 24 and 48 h post light exposure. β-actin immunoreactivity was used for determination of equal loading. Error bars denote ± SEM.

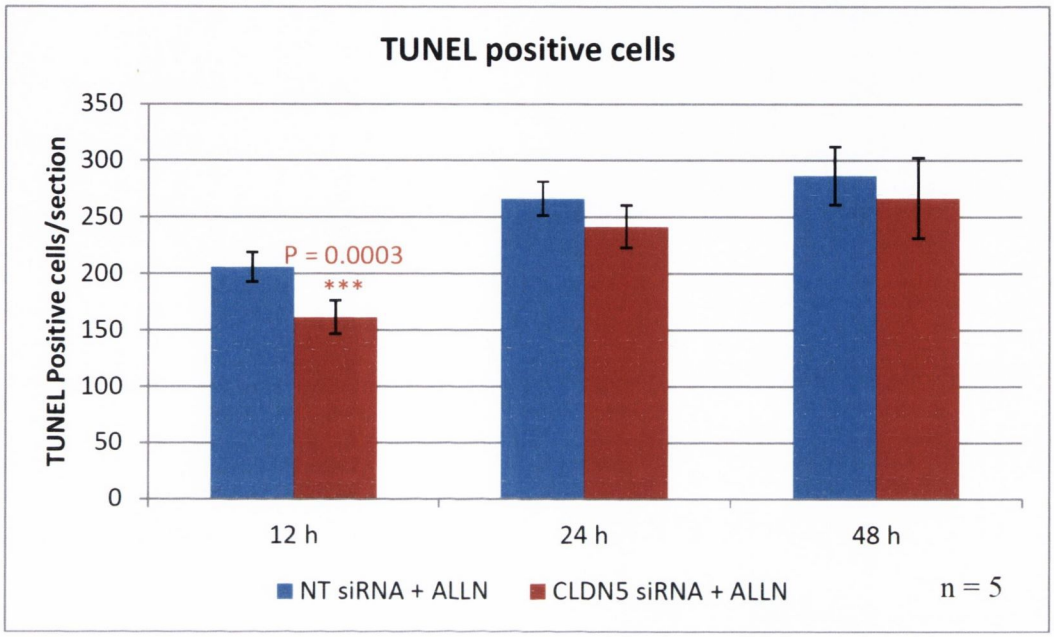

Figure 3. 8: Effect of CLDN5 siRNA and ALLN on cell death.

CLDN5 and NT siRNAs were administered to Balb/c mice (n = 5) 48 h prior to injection of ALLN. Mice were dark adapted for 24 h prior to exposure to white light of 7900 lux for 2 h. There was significantly less cells that are positive for TUNEL staining in mouse retinas injected with CLDN5 siRNA compared to those injected with NT siRNA at 12 h post light exposure (*** P = 0.0003). However, no statistical difference was observed in both experimental groups at 24 and 48 h post light exposure. Error bars denote ± SEM.

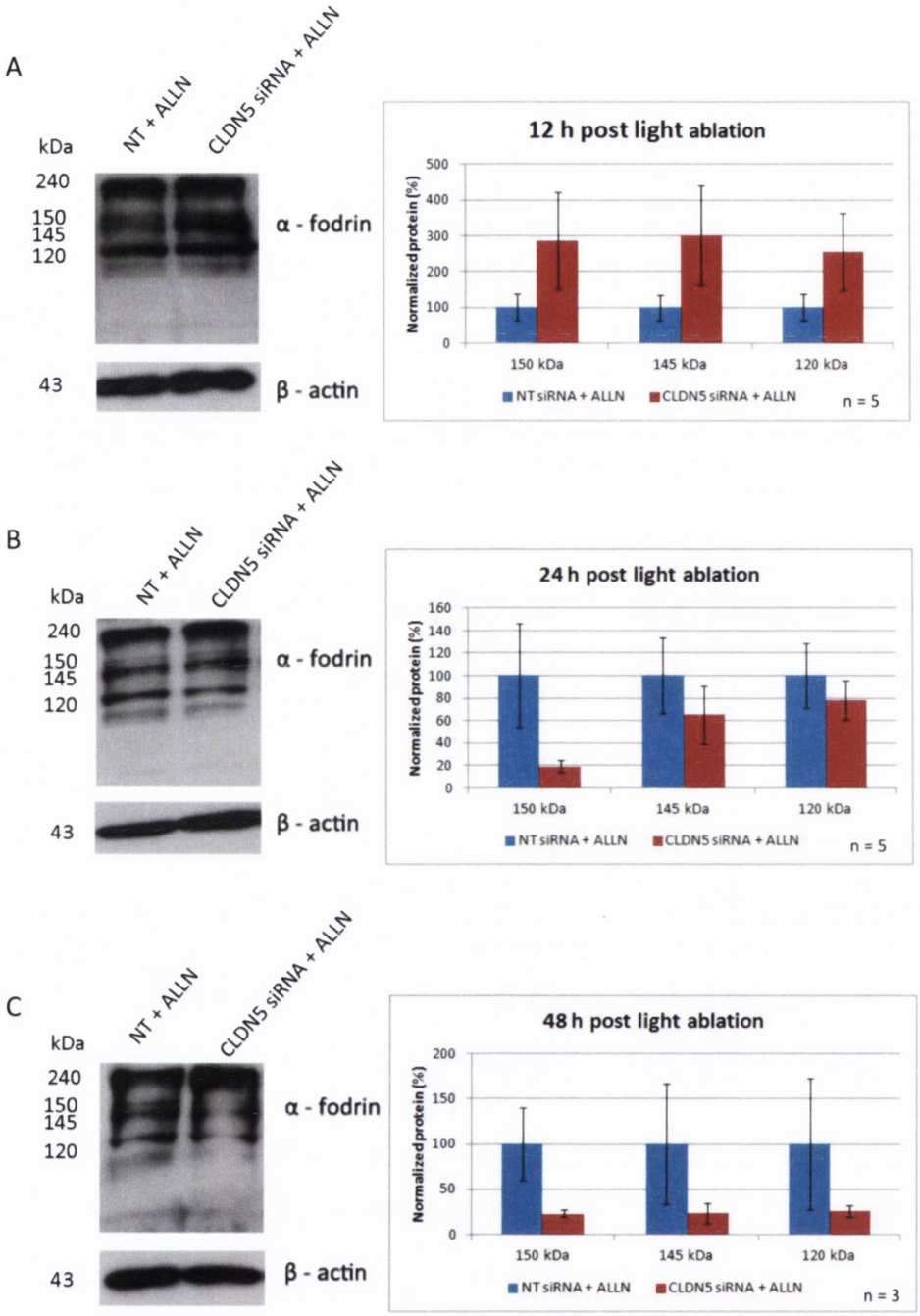

Figure 3. 9: Effect of CLDN5 siRNA and ALLN on α-fodrin cleavage.

Balb/c mice were treated as described in **Figure 3.8**. Western blots for α-fodrin cleavage showed no significant difference between the two groups of animals at three different timepoints. β-actin immunoreactivity was used for determination of equal loading. Error bars denote ± SEM.

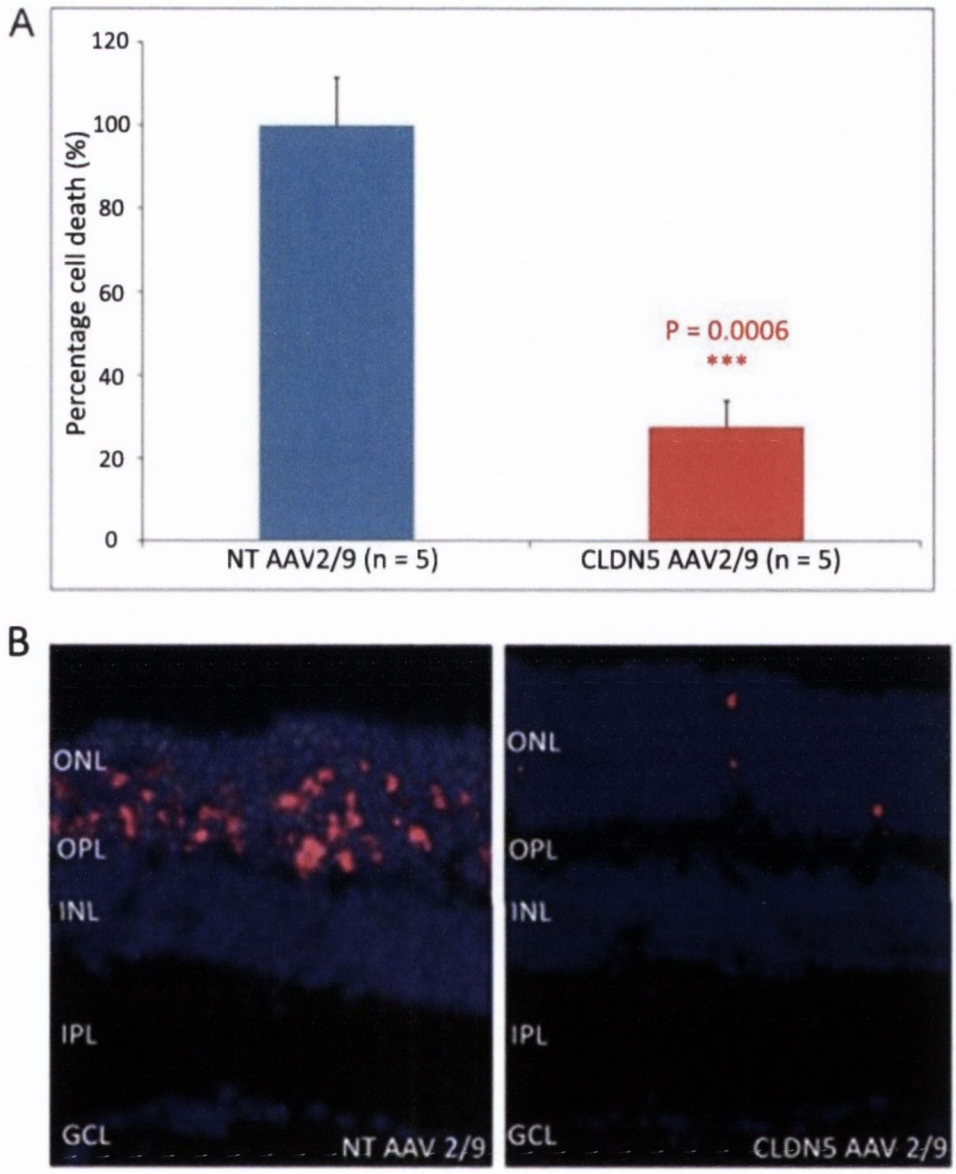

Figure 3. 10: Effect of CLDN5 AAV2/9 and ALLM on photoreceptor degeneration in Balb/c mice 24 h post light ablation.

Mice (n = 5) were injected with NT AAV2/9 in the left eye and CLDN5 AAV2/9 in the right eye sub-retinally. Mice were supplemented with the inducing agent doxycycline in their drinking water for 3 weeks. All mice received an *i.p.* injection of ALLM 24 h prior to light ablation. A) and B) TUNEL staining showed up to 70% protection in the retinas injected with CLDN5 AAV2/9 compared to the NT AAV2/9 injected retinas with *i.p.* injection of ALLM (*** P = 0.0006). Error bars denote ± SEM. (40x objective).

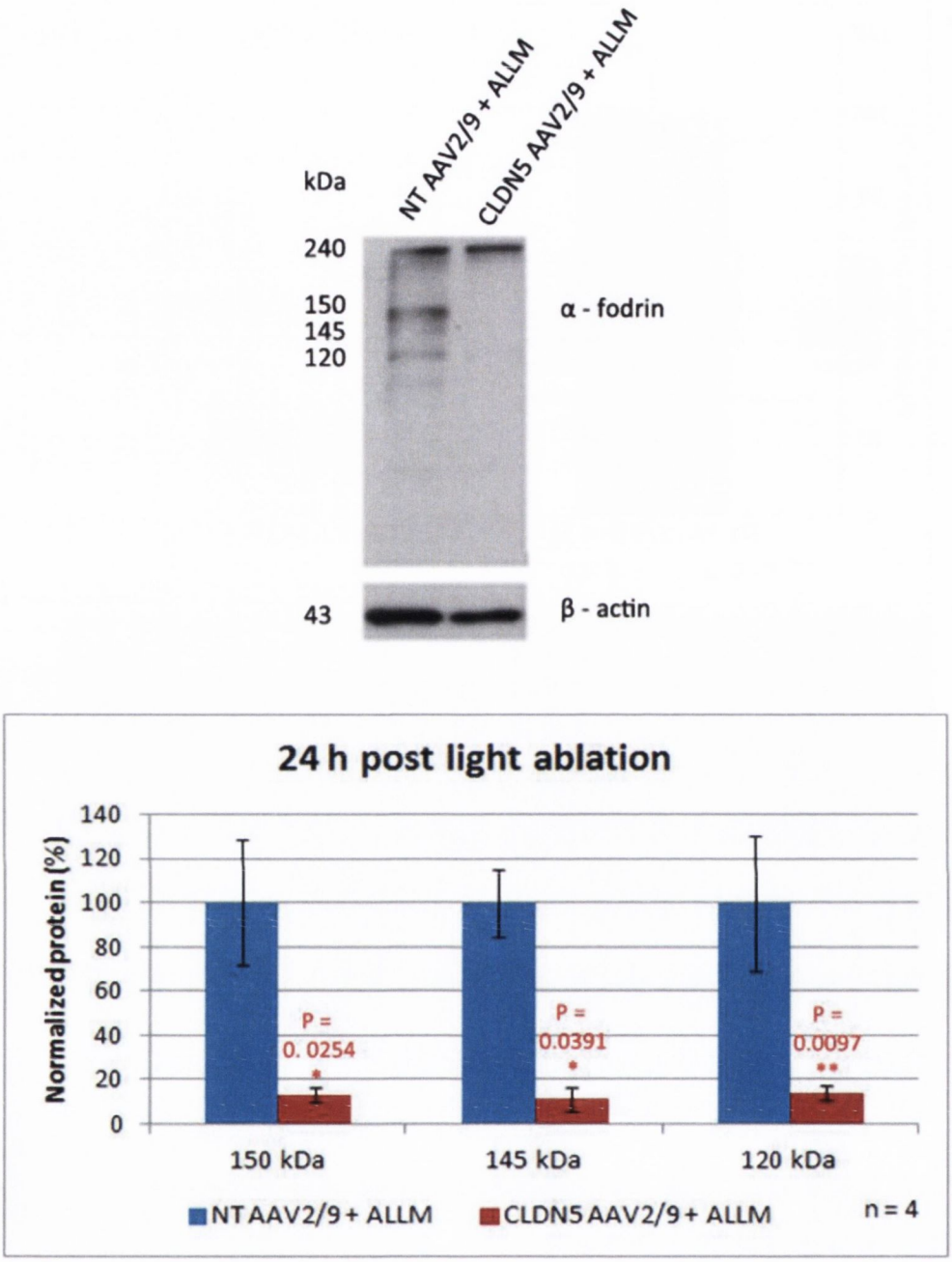

Figure 3. 11: Effect of CLDN5 AAV2/9 and ALLM on α-fodrin cleavage.

Balb/c mice were treated as described in **Figure 3.9**. Western blot analyses showed that levels of different cleaved α-fodrin fragments 150, 145 and 120 kDa were significantly reduced in CLDN5 AAV2/9 injected retinas compared to the NT AAV2/9 injected retinas with I.P injection of ALLM at 24 h post light exposure (* P = 0.0254, * P = 0.0391 and ** P = 0.0097; respectively). Error bars denote ± SEM.

Chapter 4

Effects of 17-AAG on Retinal degeneration in a mouse model of RP10 and Partial characterization of a new RP10 model

4.1 Introduction

Mutations in the *IMPDH1* gene have been associated with the RP10 form of adRP. In this introductory section, an outline of IMPDH1 function and its expression levels within photoreceptors will be discussed. In addition, a comparison between IMPDH1 and other proteins which function similarly to IMPDH1 but do not cause the RP10 form of adRP will also be discussed. Subsequently, mechanisms of cytosolic molecular chaperones which ensure correct folding of nascent polypeptide chains, maintain protein quality control and refold misfolded proteins in addition to studies investigating inhibition of Hsp90 which has been shown to reduce protein aggregation and target misfolded proteins for degradation, will also be outlined. Novel experimental data reported in this chapter, arises from the observation that a point mutation at position 224 of the *IMPDH1* gene has been linked with protein aggregation due to misfolding thus causing photoreceptor cell death and from the investigation of a therapeutic strategy involving systemic administration of an Hsp90 inhibitor, 17-AAG, in tandem with modulation of iBRB via the CLDN5 AAV2/9 system to prevent photoreceptor apoptosis in an AAV-induced mouse model of RP10.

4.1.1 Mutations in *IMPDH1* gene cause the RP10 form of autosomal dominant RP

The majority of mutations identified as causative in autosomal dominat RP (adRP), occur in genes which encode photoreceptor proteins (Kennan *et al.*, 2002) including components of the phototransduction cascade, for example, rhodopsin (Dryja *et al.*, 1990), or structural proteins such as rod outer segment protein (*ROM1*) (Kajiwara *et al.*, 1991) and retinal fascin protein (*FSCN2*) (Wada *et al.*, 2001). In addition, mutations within genes expressed systematically have also been implicated with adRP such as genes encoding mRNA splicing factors (*PRPC8* and *PRPF31*) (McKie *et al.*, 2001, Vithana *et al.*, 2001), the mitochondrial *MTTS2* gene (Mansergh *et al.*, 1999). Although these genes are widely

expressed in different tissues in addition to photoreceptor cells, in general, mutations within them have only been implicated in retinal diseases. In particular, mutations within the inosine 5'-monophosphate dehydrogenase type 1 (*IMPDH1*) gene, which is involved in nucleotide biosynthesis, cause a rare type of dominant Leber congenital amaurosis (LCA) and also the RP10 form of adRP (Bowne *et al.*, 2002, Kennan *et al.*, 2002, Bowne *et al.*, 2006b) which is estimated to account for 3-5% of all adRP cases (Daiger *et al.*, 2003).

Based on genetic linkage studies performed on families with the RP10 form of adRP, IMPDH1 was mapped to chromosome 7q32.1 and codes for the enzyme IMPDH type 1 (Jordan *et al.*, 1993, McGuire *et al.*, 1995, Bowne *et al.*, 2002, Kennan *et al.*, 2002). The gene is comprised of 17 exons, the first three of which are non-coding. The remaining 14 coding exons span about 18 kb and encode a protein subunit of 514 amino acid residues. The active IMPDH1 enzyme functions as a tetramer with these four identical subunits, each of which is composed of an eight-stranded α/β barrel structure which performs the enzymatic function, and a flanking subdomain composed of two cystathionine β-synthase-like (CBS) regions (Carr *et al.*, 1993). Enzymes in the nucleotide biosynthesis pathways play critical roles in cell growth and proliferation. Normally, cells can synthesize nucleotide through two pathways: the *de novo* pathway which involves assembly of purines and pyrimidines in a step-wise manner and the so-called salvage pathway which recycles preformed nucleobases, nucleosides and nucleotides (Kornberg and Baker, 1992). IMPDH1 is the rate-limiting enzyme of the *de novo* pathway of guanine nucleotide synthesis (**Figure 4.1**). It catalyzes the conversion of inosine monophosphate (IMP) to xanthosine monophosphate (XMP) with the concomitant reduction of NAD to NADH. XMP is converted into guanosine monophospate (GMP), diphosphate (GDP) and subsequently triphosphate (GTP). GTP then gives rise to dGTP, a building block of DNA and also plays an essential role in intracellular signalling, normal cell proliferation and function (Kennan *et al.*, 2002), whereas GTP can enter the RNA and glycoprotein

synthesis pathways. Therefore, IMPDH1 controls the pool of guanine nucleotides and thus controls proliferation and many other important cellular processes.

In addition to IMPDH1, there are other enzymes with similar function including IMPDH2 and hypoxanthine phosphoribosyl transferase (HPRT). HPRT synthesizes guanine nucleotides through the salvage pathway, while IMPDH2 functions in the *de novo* pathway. IMPDH1 and IMPDH2 share 84% identity at the amino acid level although IMPDH2 is a product of a different gene located on chromosome 3q21 (Natsumeda *et al.*, 1990). IMPDH1 and IMPDH2 have indistinguishable substrate affinities and catalytic activities, although they differ in inhibitor binding (Carr *et al.*, 1993, Hager *et al.*, 1995). Both isoforms appear to express in many different tissues but their regulation and expression levels differ considerably (Senda and Natsumeda, 1994). IMPDH1 is abundant in the lung, thymus and brain while it is barely detected in the liver and testis (Gu *et al.*, 2003). On the other hand, IMPDH2 expression is inducible and is increased in proliferating and cancerous cells (Nagai *et al.*, 1991, Jayaram *et al.*, 1999). Data analyses from the EyeSAGE database (National Center for Biotechnology Information, Bethesda, MD) showed that on average IMPDH1 expression in the retina is three times higher than that in other tissues and that it is also much higher than retinal IMPDH2 expression even though IMPDH2 levels are more than two-fold higher than those of IMPDH1 in most other tissues (Bowne *et al.*, 2006a).

Interestingly, Aherne *et al.* (2004) showed that the IMPDH1 transcripts are relatively abundant in photoreceptors compared to those from the IMPDH2 and HPRT genes based on *in situ* hybridization, expression in bacterial and mammalian cells, and computational simulations. Thus, it is probable that IMPDH1 is responsible for providing photoreceptors with GTP for which visual transduction has a high requirement (La Cour, 2002). In contrast to the expected severe symptoms of RP seen in humans, a knock-out mouse model lacking the *IMPDH1* gene displays a slowly progressive form of RP in which visual

transduction becomes gradually reduced although most photoreceptors remain intact at 12 months of age (Aherne *et al.*, 2004). Thus, IMPDH1 appears to be non-essential for normal retinal development or early visual function. This also implies that the disease is possibly caused by a dominant negative effect exerted by the mutant proteins (Aherne *et al.*, 2004). In contrast, loss of both copies of the *IMPDH2* gene causes early embryonic lethality in mice demonstrating that this isoform is essential for mouse development (Gu *et al.*, 2000). These workers also showed that expression levels of *IMPDH2* and *HPRT* genes were not increased to compensate for the deficiency of *IMPDH1* expression (Gu *et al.* (2003). Furthermore, the fact that human and mouse IMPDH1 protein sequences share 98% identity and that microarray analysis indicates that IMPDH1 is expressed at a higher level in photoreceptors (being found predominately in the inner segment and synaptic terminals of photoreceptors (Bowne *et al.*, 2006a) than in other retinal cell types (Kennan *et al.*, 2002)) suggests that retinal IMPDH1 function is highly conserved among species and is largely responsible for providing the visual transduction cycle with GTP in photoreceptor cells. In addition, these findings also explain the tissue-specific nature of the disease which involves degeneration of photoreceptors.

Initially, three different IMPDH1 transcripts were identified in human cells and tissues (Gu *et al.*, 1997). These transcripts differ in size (4.0, 2.7, and 2.5 kb) but contain identical coding sequences derived from the 14 exons and identical 3' unstranslated regions (Bowne *et al.*, 2006a). Their differences in size are due to alternate splicing of three untranslated 5' exons. Despite this, each of these transcripts encodes an identical protein, also called "canonical" IMPDH1 which is 514 amino acids in length (**Figure 4.2A**). However, it is interesting that the predominant RNA and protein isoforms of IMPDH1 in the retina have been found to be significantly different from those in other tissues (Bowne *et al.*, 2006a). These unique and distinct retinal isoforms are created by alternate splicing and/or the use of an in-frame, upstream initiation codon; and inclusion of a novel exon, exon 13b. Mouse

retina also contains the same protein isoforms called IMPDHα and IMPDHγ as human retina although the ratios of these isoforms are dramatically different from those in human retina which mainly contains IMPDHα (Bowne *et al.*, 2006a) (**Figure 4.2B**). Both isoforms contain a 32 residue C-terminal extension while IMPDHγ has an additional 49 residues on the N-terminus. This difference might explain why the IMPDH1 knockout mice only develop mild symptoms of retinitis pigmentosa even at an advanced age (12 months) while patients with mutant IMPDH1 have an early age of onset and rapid progression of disease (Kozma *et al.*, 2005, Schatz *et al.*, 2005). Moreover, the presence of unique retinal isoforms exhibiting variable levels of IMPDH1 expression in the retina could probably explain the tissue-specific nature of the disease despite IMPDH1 being a widely expressed house-keeping gene. However, the exact function and mechanisms of disease of these unique isoforms remain to be elucidated. Of special note, mutations in canonical IMPDH1 do not affect enzyme activity (Aherne *et al.*, 2004, Mortimer and Hedstrom, 2005). Thus, it is not obvious that mutations in unique IMPDH1 isoforms will alter enzyme activity in photoreceptor cells. In addition, many studies have reported that IMPDH proteins bind single stranded nucleic acids of approximately 100 nucleotides via reaction with CBS domain both *in vivo* and *in vitro* but the biological role of this property remains unknown (Cornuel *et al.*, 2002, McLean *et al.*, 2004). However, Xu *et al.* (2008) reported that unlike the canonical IMPDH1, the two predominant IMPDHα and IMPDHγ isoforms in the retina bind only poorly to nucleic acid possibly due to the presence of the C-terminal extension which might interact with other factors regulating nucleic acid binding.

Many mutations in IMPDH1 protein have been identified the most common one being Asp226Asn. This mutation has been identified in many families including two out of three families used to identify and localise the RP10 locus (Bowne *et al.*, 2002, Wada *et al.*, 2005). Another causative mutation identified from 45 members of a large Spanish family,

FA84, is Arg224Pro (Kennan *et al.*, 2002). The arginine at codon 224 of the IMPDH1 protein is conserved in human, mouse, Drosophila and Chinese hamster and is notably also highly conserved in both IMPDH1 and IMPDH2 proteins. In contrast to previous expectations, Aherne et al (2004) and Mortimer and Hedstrom (2005) have demonstrated that these two mutations do not affect enzyme activity of IMPDH1 protein. Furthermore, other potentially pathogenic mutations including Thr116Met, Val268Ile, Gly324Asp and His372Pro have also been identified in families with adRP while Arg105Trp and Asn198Lys mutations have been found in patients suffering from isolated Leber congenitial amaurosis (Bowne *et al.*, 2006b) (**Figure 4.3**). These mutations were not found to be present in unaffected controls and none of these mutations affected IMPDH1 enzyme activity. However, they do decrease the affinity and the specificity of single stranded nucleic acid binding. For example, Asn198Lys and Arg105Trp mutations are located on the CBS domain and thus alter the nucleic acid binding properties of IMPDH1 (Bowne *et al.*, 2006b).

4.1.2 Molecular chaperones

Molecular chaperones are a set of highly conserved endogenous cellular facilitators and regulators of protein conformational change within cells (Ellis and Hartl, 1999). Their functions include the correct folding of nascent polypeptide chains, protein transport and translocation across membranes, signal transduction, protein quality control, refolding of proteins denatured by environmental stress and protein degradation (Hartl and Hayer-Hartl, 2002, Nollen and Morimoto, 2002, Rapoport, 2007). Many chaperones with the ability to respond to cellular stress are known as heat shock proteins (Hsp) such as Hsp90 and Hsp70.

More than 20 different families of chaperone proteins have been identified. The major chaperone families classified according to weight include the Hsp90, Hsp70, Hsp60 (chaperonins), Hsp40 (DnaJ) and small heat shock proteins (sHsps) (Kosmaoglou *et al.*,

2008). These chaperones ensure the proper folding of proteins by recognizing and binding to exposed hydrophobic regions of unfolded or partially folded polypeptides thus preventing them from aggregating and maintaining them in a stable folded state until release. In addition, transient interaction between chaperones and newly synthesized polypeptide ensures efficient folding and prevents unwanted inter- and intra- protein interactions at hydrophobic regions thus avoiding protein aggregation (Dobson, 2004).

4.1.2.1 Hsp70

The Hsp70 family comprises several members some of which are stress-inducible (Hsp70, Hsp70i) while others are constitutively expressed (Hsc70). They are present in most cellular compartments including the cytoplasm and nucleus (Hsc70), mitochondria (Hsp75, mortallin/mtHsp70) and the endoplasmic reticulum (Grp78/BiP). Increasing levels of Hsp70 have been proven to be effective against toxic protein aggregation in disease models (Auluck *et al.*, 2002). The ATP-dependent reaction cycle of Hsp70 is regulated by chaperones of the Hsp40 (also known as DnaJ) family and nucleotide exchange factors, some of which are involved in linking chaperone functions with the unfolded protein response and autophagy for the removal of the misfolded proteins (Arndt *et al.*, 2010, Kampinga and Craig, 2010, Mayer, 2010). Binding and release of nascent protein by Hsp70 is achieved through the coupling of a conserved N-terminal ATPase domain with a C-terminal peptide binding domain, which consists a β-sandwich subdomain and an α-helical lid segment (Mayer, 2010). The latter recognizes about seven residue segments enriched in hydrophobic amino acids, preferentially when they are framed by positively charged residues. These segments tend to occur every 50-100 amino acids in proteins and exposure of these fragments has been associated with protein aggregation (Rousseau *et al.*, 2006). The C-terminal peptide binding domain regulates affinity of peptide binding in an ATP-dependent manner. In the ATP-bound state, the lid has an open confirmation. Hydrolysis of ATP to ADP is strongly accelerated by Hsp40, leading to lid closure and

stable peptide binding (Mayer, 2010). Hsp40 can also interact directly with unfolded polypeptides and can recruit Hsp70 to protein substrates (Kampinga and Craig, 2010). After ATP hydrolysis, a nucleotide-exchange factor binds to Hsp70 ATPase domain and facilitates ADP-ATP exchange, thereby causing lid opening and substrate release. Molecules requiring longer folding time will rebind Hsp70 thereby avoiding aggregation by exposure of hydrophobic residues (Sharma *et al.*, 2010). After being folded by Hsp70, certain proteins with high energy folding requirement (i.e. actins, tubulins) may be transferred into specialized chaperonin complexes, such as Hsp60s, for further folding in order to reach their native states (Frydman, 2001).

4.1.2.2 Hsp90

One of the most abundant eukaryotic and prokaryotic heat shock proteins is Hsp90 which is a highly conserved 90 kDa protein and accounts for 1 - 2% of total cellular proteins in normal conditions or to 4 - 6% under stress (Messaoudi *et al.*, 2011). The abundance of Hsp90 in cells suggested that it is an important regulator of folding, activation and assembly of a wide array of 'client' proteins including transcription factors and tyrosine kinases. Hsp90 chaperones are present in most cellular compartments such as the cytosol, the ER, mitochondria and chloroplasts in plants. In humans, there are four Hsp90 family members including glucose-regulated protein 94 (Grp94), tumor necrosis factor receptor-associated protein 1 (Trap-1), Hsp90α and Hsp90β. All these family members function similarly but interact with different client proteins due to their localization within the cell. Grp94 is present in the endoplasmic reticulum whereas Trap-1 is localized in mitochondria. Hsp90α and Hsp90β are closely related cytoplasmic isoforms. In unstressed cells, Hsp90 plays a number of important roles which include assisting folding, intracellular transport, maintenance and degradation of proteins as well as facilitating cell signalling. On the other hand, under pathological and stressed conditions Hsp90 ensures correct folding, stability and trafficking of denatured proteins (Messaoudi *et al.*, 2011).

Hsp90 functions downstream of Hsp70 in the structural maturation and conformational regulation of numerous signal-transduction molecules such as kinases and steroid receptors. Several regulators and co-chaperones are involved in this process, many of which use the tetratricopeptide repeat (TPR) domains to bind to Hsp90. For example, the TPR protein Hop provides a direct link between Hsp70 and Hsp90 thus allowing substrate transfer. There are three domains in an Hsp90 monomer: an N-terminal nucleotide binding ATPase domain (NBD), a middle domain (MD) and a C-terminal dimerization domain (CDD). In addition, the charged domain serves as a linker region (Kim *et al.*, 2013). Cytoplasmic Hsp90 exists as a homodimeric structure which is formed through CDD domains and crucial for Hsp90 chaperone activity. The MD domain is involved in substrate binding and interacts with the co-chaperone AHA1. ATP binding leads to dimerization of the NBD domains forming the Hsp90 molecular clamp leading to the structure of the Hsp90 dimer in which the individual monomers are twisted around each other. After ATP hydrolysis, the NBD domains dissociate and the Hsp90 monomers separate at the N-terminus. This process is regulated by various cofactors such as CDC37 which delivers certain kinase substrates to Hsp90 and inhibits ATPase activity. In addition, Hop directly inhibits NBD dimerization while AHA1 stimulates ATP hydrolysis and p23 stabilizes dimerization of Hsp90 prior to ATP hydrolysis.

4.1.2.3 Hsp70/Hsp90 complex and misfolded protein

In eukaryotes, the functional cytosolic Hsp90/Hsp70 chaperone complex is regulated with protein cofactors known as co-chaperones. This chaperone complex can either assist protein folding of newly synthesized polypeptides or refolding of misfolded proteins, or can target misfolded/damaged proteins for ubiquitin-mediated proteasome degradation (Pratt and Toft, 2003). Under normal condition, the client protein is presented to Hsp70 by Hsp40, or Hsp40 attached to ribosomes, activates and recruits cytosolic Hsp70 to associate with newly synthesized polypeptide chains (Cheetham and Caplan, 1998). The bound

protein can be stabilized on Hsp70 by the Hsp70 interacting protein (Hip) or its release can be stimulated by an exchange factor such as HspBP1 (Hohfeld and Jentsch, 1997, Kabani *et al.*, 2002). This chaperone complex is ATP dependent and is possibly sufficient to fold some polypeptide chains. The released protein may fold into a native state or enter another cycle of chaperone binding and release. In addition, many polypeptide chains may be passed onto the Hsp70/Hsp90 complex for further folding with the help of a co-chaperone, the Hsp70/Hsp90 organizing protein (Hop) (Scheufler *et al.*, 2000). In the case of proteins with significant structural instability, Hsp70 can recruit the co-chaperone CHIP (carboxyl terminus of Hsp70-interacting protein) which is docked to Hsp70 or Hsp90 holding a misfolded protein thus recruiting an E2 enzyme to initiate ubiquitinylation. The anti-apoptotic Bcl-2 associated athanogene-1 (BAG-1) protein regulates the ATPase cycle of Hsp70 and also contains a ubiquitin-like domain that links the chaperone to proteasomes to release ubiquitylated polypeptides for degradation (Young *et al.*, 2004). Adverse conditions such as destabilizing mutations can cause aberrant proteins to manifest which may lead to either clearance of mutant proteins via proteasome degradation with a consequent 'loss of function' phenotype or accumulation of misfolded protein resulting in the aggregation or the formation of insoluble proteinaceous deposits causing 'gain of function' toxicity (Tam *et al.*, 2010) (**Figure 4.4**).

4.1.3 Protein aggregation and diseases

Given the important functions of chaperones, it is not surprising that highly negative consequences such as retinal- and neuro- degeneration could ensue should this machinery be overwhelmed by dominant negative aggregation of misfolded proteins. In the case of retinopathies, a missense at amino acid position 23 (P23H) is the most common rhodopsin mutation leading to autosomal dominant retinitis pigmentosa in North America. Various studies suggested that P23H protein is misfolded in the ER, is extremely prone to aggregation, can recruit cellular chaperones and result in the targeting of wild type

rhodopsin for degradation by the ubiquitin proteasome degradation (Saliba *et al.*, 2002). Thus, ER stress caused by overloading of mutant opsins could initiate a detrimental cascade leading to photoreceptor apoptosis. In addition, some mutations in the *RDS-peripherin* gene (e.g missense mutation N244K) have also been implicated in protein misfolding (Conley *et al.*, 2010). Moreover, Marmorstein *et al.* (2002) showed that inefficient secretion and accumulation of epidermal growth factor-containing fibulin-like extracellular matrix protein 1 (EFEMP1) in RPE cells could lead to EFEMP1 aggregation, apoptosis cell death in age related macular degeneration. Additionally, the Arg224Pro missense mutation in *IMPDH1* responsible for the RP10 form of RP causes misfolded and insoluble aggregation of mutated proteins in the cell cytosol (Aherne *et al.*, 2004). Recently, Wang et al. (2011) showed that the two missense mutations Arg224Pro and Asp226Asn were not only impaired the folding of their own mutant proteins but were also able to impede correct assembly of the normal enzyme into active tetramers, structure of which provides an opportunity for faulty monomers to hinder proper folding and function of their neighbours. It is of note that protein aggregation has been also observed in many common neurodegenerative disorders such as Alzheimer's disease, Parkinson's disease as well as Huntington's disease, amyotrophic lateral sclerosis, prion diseases and others (Sherman and Goldberg, 2001, Bucciantini *et al.*, 2002, George, 2002).

4.1.4 Hsp90 inhibitors

It is widely accepted that chaperones are important regulators of protein folding and can be manipulated to combat protein misfolding diseases. Molecular chaperones have been shown to suppress aggregation of mutant proteins that cause neurodegenerative diseases such as spinal and bulbar muscular atrophy, Huntington's disease and familial amyotrophic lateral sclerosis (Jana *et al.*, 2000, Kobayashi *et al.*, 2000, Takeuchi *et al.*, 2002). In addition, the use of Hsp90 inhibitors/Hsp70 inducers has been reported to reduce protein aggregation in various models of neurodegenerative diseases. One of the first classes for

Hsp90 inhibitors, geldanamycin (GA), was originally developed to use as an anti-tumor drug based on its ability to induced protein degradation of proto-oncogenic protein kinases and nuclear hormone receptors (Fukuyo *et al.*, 2010). This natural compound was isolated from the broth of Streptomyces *hygroscopicus* in the 1970s and was already known for its antibiotic activity. The antitumor activity of GA was reported nearly 20 years after its discovery and subsequent studies revealed that GA binds to the NBD site of Hsp90, thereby altering its function and mediating ubiquitin proteolytic degradation of Hsp90 client proteins (Messaoudi *et al.*, 2011). However, GA is highly hepatoxic and displays unfavorable pharmacokinetics properties such as poor solubility, limited *in vivo* stability, and activation of drug-efflux pumps thus making it unsuitable for clinical use. Many efforts have been put into development of safer derivatives of GA such as 17-allylamino-17demethoxylgeldanamycin (17-AAG, MW: 585.69) which shows a better toxicity profile than GA and was the first Hsp90 inhibitor to enter clinical trials for various cancers (clinicaltrias.gov) (**Figure 4.4**).

Under normal conditions, inactive monomeric HSF-1 is associated with the Hsp90 mutichaperone complex in the cytosol. Upon exposure to cellular stress or stress inducers such as 17-AAG which binds to the ATP pocket of Hsp90, HSF-1 dissociates from the Hsp90 complex and is activated via trimerization and phosphorylation. Activated HSF-1 then translocates into the nucleus and induces expression of various chaperones including Hsp70, Hsp90 and Hsp40. Thus, upregulation of the chaperone complex leads to further binding to misfolded proteins which are then targeted for proteasome degradation (Tam *et al.*, 2010). Recently, 17-AAG has shown a high efficiency in reduction of protein aggregation in animal models of polyglutamine-induced neurodegeneration and spinal and bulbar muscular dystrophy (Waza *et al.*, 2005, Fujikake *et al.*, 2008). Interestingly, it was illustrated that administration of 17-AAG in mammalian cells enhanced P23H folding and reduced the dominant negative effect on WT opsin, as well as reducing toxic gain of

function effect (Mendes and Cheetham, 2008). Moreover, it has been shown in our laboratory that administration of 17-AAG significantly reduced aggregation of IMPDH1 protein and protected against photoreceptor apoptosis in a mouse model of RP10 (Tam *et al.*, 2010). Thus, all these data suggest that a common therapy for retinopathies and neurodegenerative diseases associated with protein aggregation could be developed based on the use of Hsp90 inhibitors.

4.1.5 Objectives

It has been shown previously in our laboratory that subretinal injection of AAV2/5 expressing a human mutant Arg224Pro IMPDH1 fusion with hrGFP (IMP224-hrGFP) into WT C57BL/6J mice provided a good mouse model for RP10 retinitis pigmentosa (Tam *et al.*, 2008). It was also reported that mutant IMPDH1 proteins expressed from this construct were highly prone to aggregation in both *in vivo* and *in vitro* models (Aherne *et al.*, 2004, Tam *et al.*, 2010). Recently, systemic use of a heat shock protein inhibitor 17-AAG together with systemic administration of CLDN5 siRNA significantly reduced the amount of insoluble protein in retinas expressing the mutant IMP224 and protected these retinas from undergoing degeneration (Tam *et al.*, 2010). Thus, following the successful outcome of iBRB modulation in conjunction with delivery of calpain inhibitors in the light ablation model mentioned in **Chapter 3**, the objective of this study was to determine whether localised and inducible modulation of the iBRB with CLDN5 AAV2/9 together with systemic use of 17-DMAG would offer increased protection from mutant IMP224 protein aggregation in the RP10 mouse model in addition to being a more clinically relevant approach. Moreover, a transgenic model expressing the mutant *IMP224-hrGFP* gene based on the IMP224 AAV2/5 construct used in previous studies in the laboratory was also developed and characterized.

4.2 Materials and Methods

4.2.1 17-AAG treatment

Adult C57BL/6J mice (about 3 months old) were subretinally injected with 2 µl of 1 x 10^{12} vp/ml IMP224 AAV2/5 and 1 µl of 5 x 10^{11} vp/ml CLDN5 AAV2/9 in the right eye and 2 µl of IMP224 AAV2/5 and 1 µl of 5 x 10^{11} vp/ml NT AAV2/9 in the left eye. One week post subretinal injection, animals were administered with doxycycline drinking water (2 mg/ml) and one week later, each animal received an intraperitoneal injection (I.P) of 17-AAG (31.25 mg/kg) (Selleck Chemicals) in PBS twice weekly for 1, 2, 5 and 7 weeks while being continuously administered with doxycycline.

In a second experimental protocol, animals were subretinally injected with 3 µl of 1 x 10^{12} vp/ml IMP224 AAV2/5 in both eyes. One week later, they were subretinally injected with 3 µl of 5 x 10^{11} vp/ml CLDN5 AAV2/9 in the right eye and NT AAV2/9 in the left eye. After 2 weeks, these animals were provided with doxycycline (2 mg/ml in drinking water) and received I.P injections of 17-AAG twice a week.

4.2.2 Doxycycline intake measurements

Each red cap tube (50 ml) was filled with 30 ml of doxycycline (2 mg/ml) and 5% sucrose in water and then wrapped in tin foil to avoid oxidization of doxycycline. Every three days, volumes of doxycycline taken by each mouse were noted and variation analysed by ANOVA.

4.2.3 Measurements of transduced ONL area per unit length

Transduced outer nuclear layer per unit length of retinal sections (12 µm) were analyzed using ImageJ software. Retinal sections were viewed and photographed on a fluorescent microscope (Zeiss Axioplan 2, Oberkochen, Germany) using the 5x objective lens. The scale of the sections was then converted into pixels (1.152 pixel = 1 µm) using ImageJ

software. The average transduced ONL area per unit length was calculated by dividing the area of the whole ONL (μm^2) by the ONL length (μm).

4.2.4 Immunohistochemistry

Cryostat sections (12 μm) were blocked with 5% normal goat serum and 1% triton X-100 in PBS for 20 min at room temperature. Sections were incubated with primary rabbit polyclonal anti hrGFP antibody (1:400) (Stratagene) at 4°C overnight. Sections were then incubated with secondary rabbit IgG-Cy3 antibody for 2 h at room temperature. All sections were counterstained with DAPI (1:5000) for 30 s. Analysis of all sections was performed using an epifluorescence microscope (Zeiss Axioplan 2, Oberkochen, Germany).

4.2.5 Genotyping for transgenic animals (PCR)

DNA samples from transgenic mouse tails (**Section 2.8.2**) were taken for genotyping. Briefly, 25 μl of PCR reaction mix was made up for each transgenic mouse DNA as followed: 1.5 μl DNA, 0.25 μl each primer (100 pmoles/μl stock), 0.4 μl dNTP mix, 2.5 μl 10x buffer, 0.125 μl Taq polymerase and 19.975 μl water. The PCR reaction conditions were as follows: 34 cycles (94°C for 1 min, 58°C for 1 min, 72°C for 1 min), then 72°C for 5 minutes. The 2 pairs of PCR primers used for IMP224 transgenic animals were as followed:

Pair 1. From the Rhodopsin promoter to IMP224 gene (660 base pairs)

Forward primer: 5'-AGCCTTGGTCTCTGTCTAC

Reverse primer: 5'-ATCAGGTAGTCCGCCATCT

Pair 2. From IMP224 gene to hrGFP (1536 base pairs)

Forward primer: 5'-TTGGAGCCTCCACAGTGATG

Reverse primer: 5'-TGGTCTTCTTCATCACGGGG

4.2.6 Quantitative PCR on genomic DNA from transgenic animals

In brief, four primers specific for the IMP224 transgene were used (see below), three of which were designed using GenScript software. Specific human IMPDH1 primers were previously designed by Dr. Lawrence Tam.

Name	Forward (5' -> 3')	Reverse (5' -> 3')
RHOpromoter-βglobin	AAGCAGCCTTGGTCTCTGTC	ACTCTTGGCACGGGGAAT
IMPDH1-MCS	GTTTGAGAAGCGGACCATGT	CCTTGTCATCGTCATCCTTG
hrGFP-PolyA	GTGGAGCAGCACGAGACC	GGGCGAATTGGGTACACTTA
humanIMPDH1	TGCCTATCGTCAATGATTGC	TCCCTTGGGACGAGTCCAAG

Primers used to amplify house-keeping genes were as follows:

Name	Forward (5' -> 3')	Reverse (5' -> 3')
Mouse β-actin	AGAGCAAGAGAGGTATCC	TCATTGTAGAAGGTGTGGTGCC
C5AR	GTCCTGTTCACGACCGTTTT	ACGGTCGGCACTAATGGTAG

Each primer was resuspended in nuclease free water to give a final concentration of 100 pmol/μl. Based on a previous study done by Haurogne *et al.* (2007) and various optimization experiments, DNA samples were tested for copy number of the IMP224 transgene using the following parameters. Plasmid encoding IMP224 (IMP224 pAAV) at 5 different concentrations (10^{-1}, 10^{-2}, 10^{-3}, 10^{-4}, and 10^{-5}) was used in PCR reactions to generate a standard curve , while that for the house-keeping genes was generated using DNA from a WT animal at concentrations of 50, 10, 2, 0.04 and 0.08 ng. A total of 12.5 ng of each experimental DNA sample was added into each well. Each reaction contained 10 μl SYBR® Green mix, 2 μl primer stock (10 μl of each primer (100 pmol/μl) in 80 μl water), 5 μl DNA and water for a total of 20 μl reaction. All reactions were performed in duplicate for standard curve samples and in triplicate for experimental DNA samples and carried out in the GeneAmp® 7300 instrument (Applied Biosystems) with the following

parameters: 95°C for 5 min, followed by 40 step cycles of 95°C for 15 s, 60°C for 1 min and 72°C for 1 min, followed by a dissociation stage of 95°C for 15 s, 60°C for 1 min, 95°C for 15 s, 60°C for 15 s.

4.2.7 Statistical Analysis

Statistical analysis was performed using Student's t-test, with significance represented by a P value of ≤ 0.05 (n = 5 mice per treatment). For multiple comparisons, One-way ANOVA was used with a Tukey post-test and significance represented by a P value of < 0.05.

4.3 Results

4.3.1 Delivery of hsp90 inhibitor in a murine model of RP10 retinitis pigmentosa

C57BL/6J mice (n = 12) were subretinally injected with 2 µl of 1 x 10^{12} vp/ml IMP224 AAV2/5 and 1 µl of 5 x 10^{11} vp/ml CLDN5 AAV2/9 in the right eye and 2 µl of IMP224 AAV2/5 and 1 µl of 5 x 10^{11} vp/ml NT AAV2/9 in the left eye. Doxycycline was introduced into their drinking water one week post injection. Two weeks after injection, mice were *i.p.* injected with 17-AAG (31.25 mg/kg) in 1x PBS twice a week for 1, 2, or 7 weeks. The concentration of 17-AAG was based on a previous study (Tam *et al.*, 2010). ERG measurements were also taken after 1 and 2 weeks of 17-AAG treatment. **Figure 4.5** shows that rod photoreceptor b-wave amplitudes in the group of animals treated for 2 weeks with 17-AAG (n = 8) were lower than those treated for 1 week with 17-AAG (n = 4) and that no significant difference was observed between the treated and control eyes for either treatment regimes although there was a trend towards higher ERGs in the CLDN5 AAV2/9-treated eyes. In addition, transduced outer nuclear layer per unit length was also measured from retinal sections of these animals following treatment with 17-AAG for a total of 7 weeks. The transduced outer nuclear layer per unit length is typically measured at regions of the retina which have been transduced by IMP224 AAV2/5 and calculated by dividing transduced ONL area by length of the transduced region (Tam *et al.*, 2008). However, positively transduced cells were observed pan-retinally in addition to the injection site in this study (**Figure 4.6**). In addition, some retinal sections had various extents of thinning regions where only 1-3 rows of photoreceptors were present, possibly due to the effect of subretinal injection. Thus, the transduced ONL area per unit length was measured by taking into account the entire retinal ONL area. **Figure 4.7** shows that no differences were observed in the transduced ONL area per unit length between the treated and non treated eyes as would be expected from the ERG data.

During the experiment, it was noticed that consumption of drinking water containing doxycycline varied between mice in different animal cages. Since this could negatively impact on a factor on the true ONL per unit length values, another 7 animals were treated in the same way as the above animals except that their doxycyline drinking water was monitored in order to establish whether differences in consumption of drinking water (and therefore of doxycycline intake) correlates with variations in transduced ONL area per unit length. Animals were separated into individual cages so that their water intake was measured every 3 days. Similar to the first experiments, no statistical differences in either transduced ONL area per unit length or ERG of rod isolated responses were observed between the CLDN5 AAV2/9-treated and NT AAV2/9-treated eyes 5 weeks post 17-AAG treatment (**Figure 4.8 and 4.9**) although again there was a clear trend showing some retinal protection in the CLDN5 AAV2/9-treated eyes. In addition, intake of doxycycline water appeared similar between animals following ANOVA statistical analysis (**Figure 4.10**).

In order to ascertain whether injecting a mixture of AAVs (i.e. IMP224 AAV2/5 together with CLDN5/NT AAV2/9) might have impacted sub-optimally on the outcome of the previous experiments, another group of animals (n = 9) was first subretinally injected with 3 µl of 1 x 10^{12} vp/ml IMP224 AAV2/5 in both eyes and with 3 µl of 5 x 10^{11} vp/ml CLDN5 AAV2/9 in the right eye and NT AAV2/9 in the left eye one week later. During a one-week period they were administered with doxycycline in their water and received two *i.p.* injections of 17-AAG. Despite this, similar b-wave amplitudes of rod isolated response were measured in both eyes after 1 week of 17-AAG treatment (**Figure 4.11**). The ERG readouts in this group of animals were also much lower than those observed in animals injected with a mixture of two AAVs (**Figure 4.5**). Thus, this faster degeneration rate might have been caused by two separate subretinal injections and/or larger volume of IMP224 AAV2/5 (3 µl) injection. In addition, these animals were also separated into

individual cages to enable doxycycline intake to be measured every 3 days. **Figure 4.12** shows that these animals drank the same volume of doxycycline containing water.

4.3.2 RP10 transgenic model

Since AAV-induced models resulting from the expression of a multiple and possibly variable quantity of cDNA molecules are by nature less dependable and less consistent than transgenic models, an RP10 transgenic model was developed. Digestion of the IMP224 pAAV construct with NheI and RsrII enzymes yielded a fragment of 5820 bp which runs from the Rho promoter through IMP224 and hrGFP to the human growth hormone poly A tail sequence (**Figure 4.13 and Appendix Figure 1**). Transgenic mice on a C57BL/6N background were generated following embryonic injection of the 5820 bp fragment by PolyGene Transgenetics (Switzerland). Four founders including 3 females and 1 male were made. Their tail biopsies were tested for the transgene using two different pairs of primers (**Figure 4.14**). In order to study their visual function, ERG was also performed on these founder mice at different intervals. Normally, ERG measurement of the b wave of rod photoreceptors is around 1mV in wild type mice. Variations in the degree of pupil dilation may have caused the differences in ERG readings observed between the two eyes of these founders. Based on the recommendation from Dr. Paul Kenna, an ophthalmologist in the laboratory, higher ERG readings were considered to be more reliable ERG readouts. Thus, founder females had somewhat similar ERG to the WT animals at 9 months old and two of them (females 1 and 3) had severe visual degeneration with b-wave amplitudes of rod-isolated responses being less than 150 μV at 13 months old (**Figure 4.15**). At 7 months old, the ERG of the founder male reduced to 816/769 μV. At 11 months of age, b-wave amplitudes of the founder male did not appear to degenerate at this stage. This could be because each of them received different copy numbers of the transgene.

Four different pairs of primers were designed to determine the transgene copy number in each animal using real time PCR on their tail DNA samples in an effort to examine whether this might directly correlate to the difference in rate of retinal degeneration as demonstrated by ERGs for each animal. These four pairs of primers are called RHOpromer-βglobin, hrGFP-GPA, IMPDH1-MCS (which stands for their start and end positions within the IMP224 pAAV construct) and human IMPDH1 which distinguishes human IMPDH1 from mouse IMPDH1. Two pairs of primers for house-keeping gene were C5AR (complement component 5a receptor) and mouse β-actin. Preliminary quantitative PCR data using dilutions of IMP224 pAAV DNA for the transgene primers and wild type DNA for the house keeping primers rendered reliable, accurate standard curves (**Appendix Table 1 and Figure 2**). Slopes for the standard curves of human IMPDH1, hrGFP-polyA, C5AR and mouse β-actin were -3.22, -3.19, -3.14 and -3.01, respectively. Therefore, the efficiencies of these primers are within the range of 104-114% which is acceptable for real time PCR. In addition, DNA of control samples for hrGFP-polyA and humanIMPDH1 were not amplified during the reaction, indicating specificity of these primers. Contamination in water and primer dimer formations were also not detected in all reactions. In contrast, the remaining two pairs of primers which were designed to amplify the transgene did not work well, thus they were not used in ongoing studies. However, further attempts will be required to establish the real copy number of transgene in each animal since difficulty in obtaining acceptable real time PCR efficiencies, the main factor required for correct quantification, rendered the data erroneous. In fact, the tried and tested classical technique of Southern blotting may be a more appropriate technique to be used in future studies.

ERG measurements were also carried out for all offsprings in order to characterize disease progression in these transgenic mice. Unfortunately, due to crossed communications with staff in the animal breeding unit, founder animals were mistakenly mated with each other

initially rather than to WT C57BL/6J mice. These founder animals were then also mated with WT C57BL/6J animals; however, they were too old to produce any offsprings at that stage. Currently, all the IMP224 transgenic animals present in the unit derive from one offspring (animal 16, male) from the initial mating of founder male and founder female 2 REP (**Figure 4.16**). This male was then mated with a WT C57BL/6J to produce animal 8.1 which was then mated with a WT C57BL/6J to produce animal 18.1. All three males descended from the mating of animal 18.1 with a WT C57BL/6J were 35.2, 35.3 and 37.2, each of which are currently mated with a WT C57BL/6J. All animals chosen for mating were done so on the basis of ERG results at different timepoints (**Table 4.1**). Interestingly, ERGs of these offspring decreased at a faster rate compared to those of their transgenic parents.

Since these transgenic animals were originally on the C57BL/6N background which was recently reported to harbour the Rd8 mutation in the *Crb1* gene causing lesions in the retina (Mattapallil *et al.*, 2012), DNA samples of all three animals 35.2, 35.3 and 37.2 were sequenced for the presence of this mutation using a reversed primer by Dr. Marian Humphries in the lab. After three generations of backcrossing with WT C57BL/6J animals, the Rd8 mutation is not present in these fourth generation mice (**Figure 4.17**). Thus, it can be confirmed that degeneration in visual function in mice 35.2, 35.3 and 37.2 is not due to Rd8 mutation and is thus likely to be due to the presence of *IMP224* transgene.

4.4 Discussion

Protein aggregation has been implicated in many retinopathies and is often linked with the heat shock protein chaperone complex containing Hsp90, Hsp70 and Hsp40. The Hsp90 superchaperone complex plays a crucial role in assisting the folding and function of client proteins, many of which are important in cell proliferation and signaling (Workman, 2002). In addition, results from a recent study of spinal and bulbar muscular dystrophy, a late onset of motor neuron disease suggest that 17-AAG significantly inhibited hsp90 leading to degradation of the mutant androgenic receptor. Recently, systemic administration of CLDN5 siRNA together with the Hsp90 inhibitor, 17-AAG have been reported to offer protection against aggregation of mutant IMPDH1 in the RP10 mouse model (Tam *et al.*, 2010). This therapeutic strategy was further extended in this study to encompass a more clinically relevant long-term chronic dosing strategy in which a localized and inducible AAV-mediated expression of CLDN5 shRNA, rather than a transient CLDN5-targeting siRNA, was used to modulate the inner blood retinal barrier. Statistically both ERG and transduced ONL area per unit length were not improved in animal eyes injected with IMP224 AAV2/5 and CLDN5 AAV2/9 compared to eyes injected with IMP224 AAV2/5 and NT AAV2/9 post 17-AAG treatment although the existence of a trend for improvement could be argued (**Figures 4.5 and 4.7**). Of special note, IMP224 AAV2/5 used in this experiment transduced the whole retina instead of being localized around the injection site as previously observed by Tam *et al.* (Tam *et al.*, 2008, Tam *et al.*, 2010). Since the AAVs used in the latter two studies were made in our laboratory whereas for this research they were made commercially by Vector Biolabs, improved purity of the viruses might have contributed to the enhanced retinal transduction observed. In a similar repeat experiment, animals were also separated into individual cages to ensure that they got equal amounts of doxycycline containing water. However, statistical analysis of both ERG data and ONL analysis of retinal sections implies that carefully monitoring doxycycline intake

did not increase the efficiency of the treatment although there was again a trend towards retinal protection in CLDN5 AAV2/9-injected eyes (**Figures 4.8 and 4.9**). Since others in the laboratory have found that the AAV-induced RP10 model can be quite variable as regards the severity of retinal degeneration even between eyes of an individual mouse (Drs. L Tam and A-S. Kiang, personal communication), it is probable that should these experiments be repeated with larger numbers of mice a statistically significant positive effect may have been achieved.

In order to reduce any complications resulting from a mixture of two different AAVs, another experiment in which animals were injected with IMP224 AAV2/5 in both eyes a week before being injected with CLDN5 AAV2/9 in the right eye and NT AAV2/5 in the left eye, were set up. Yet again, the ERG data showed no improvement in eyes injected with CLDN5 AAV2/9 and IMP224 AAV2/5 compared to control eyes (**Figure 4.11**). However it is probable that two consecutive subretinal injections might have been too harsh for the animals since retinal detachment from initial injection of IMP224 AAV2/5 may not have completely settled in the 7 days after which the second subretinal injection of CLDN5 or NT AAV2/9 was administered. It was also possible that longer-term treatment with 17-AAG may be necessary or that the dose was too high and caused some retinal toxicity resulting in degeneration. Ideally a dose de-escalation study of 17-AAG should be carried out in this model. Additionally, due to the variable nature of the IMP224 AAV2/5-induced model, pre-treatment ERGs should have been taken to compare with the post-treatment ERG data between individual eyes. Moreover, more controls could also be used in future experiments to interpret the data observed from ONL measurements. For example, mice injected with IMP224 AAV2/5 in one eye and DMSO or sham injected in the other eye, could be used to measure the maximum transduced ONL area per unit length for a better comparison between the treated eye and non treated eye. Controls where mice were injected with IMP224 AAV2/5 and NT AAV 2/9 in one eye and IMP224 AAV2/5

and sham injected in the other eye could be included to determine the effect of NT AAV2/9 on the treatment of these animals. Despite 17-AAG being under clinical trials, it nonetheless has a number of disadvantages including high metabolism, potential to form toxic metabolites and limited aqueous solubility which requires the use of dimethyl sulfoxide and egg phospholipid for solubilization (Egorin *et al.*, 1998). In fact, Bristol-Myers Squibb, the pharmaceutical company which produces 17-AAG for clinical trials of cancers has decided to stop manufacturing the drug due to its toxicity – a factor which may have contributed to the negative results obtained here. Thus, many efforts have been made to search for improved derivatives of geldanamycin. One of these new improved compounds is 17-(dimethylaminoethylamino)-17-demethoxygeldanamycin (17-DMAG) which is also under clinical trials for various types of cancer. In contrast to 17-AAG, 17-DMAG is water soluble and can be formulated in saline or 5% dextrose in water. 17-DMAG undergoes limited metabolism compared to 17-AAG and has higher oral bioavailability in mice than 17-AAG. Also, less 17-DMAG (30-45%) is bound to plasma proteins as compared to 17-AAG (90%) (Egorin *et al.*, 2001, Egorin *et al.*, 2002). Finally, *in vivo* and *in vitro* studies have demonstrated that 17-DMAG is more efficaceous than 17-AAG. However, like 17-AAG, 17-DMAG (MW = 653.21) does not cross the BBB/iBRB. Thus, 17-DMAG shows promise as an improved Hsp90 inhibitor and has been used in further experiments involving drug delivery by modulation of iBRB in models of retinal degeneration as outlined in **Chapters 5** and **6**.

The induced model of RP10 resulting from IMP224 AAV2/5 may not be the optimal model for this particular disease due to variations in subretinal injections and quality and concentration of IMP224 AA2/5, which leads to large variation in the degree of retinal degeneration in any given eye. Thus, a transgenic model expressing human mutant IMP224 is being developed and characterized. The founder animals exhibited only minor degeneration at 6 months old. Since founder animals were initially mated with each other

instead with WT animals, the current animals are offspring of a mating between two founders. Although all later offspring were descendents from a mating between an IMP224 trangenic F1 from the initial mating of two founders and a WT C57BL/6J, it still proves a challenge to establish a pure line of RP10 transgenic model. In addition, the rd8 mutation of the *Crb1* gene has been found to be present in mice with a C57BL/6N background from which founder IMP224 transgenic animals were generated (Mehalow *et al.*, 2003, Mattapallil *et al.*, 2012). This mutation which involves a single base C deletion leads to ocular lesions which have been associated with several induced mutant mouse lines and is present in homozygous form in all C57BL/6N substrains and embryonic stem cells of C57BL/6N origin, but not in the C57BL/6J substrains. It appears that the current IMP224 animals do not have the rd8 mutation perhaps due to mating of transgenic mice with C57BL/6J mice for three generations. Therefore, degeneration in visual function in the current transgenic animals is most likely caused by the presence of the mutant IMP224 gene. Hopefully, in the future, these transgenic animals will provide a better model for RP10 retinitis pigmentosa than that induced by AAV IMP224 and that treatment of these animals with 17-DMAG in conjunction with iBRB modulation will result in an improved therapeutic outcome.

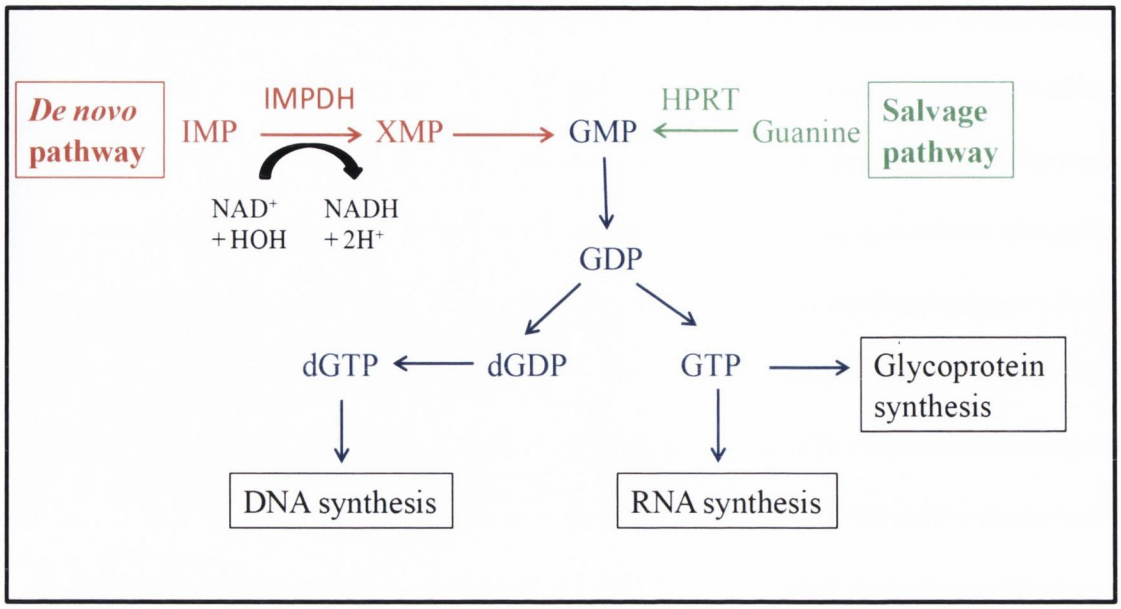

Figure 4. 1: Guanine nucleotide biosynthesis.

Guanine nucleotides are synthesized through *de novo* and salvage pathways. In the *de novo* pathway, IMPDH catalyzes the conversion of IMP to XMP which is then eventually converted into dGTP and GTP which are important in different cellular processes. On the other hand, HPRT catalyzes the conversion of guanine to GMP in the salvage pathway.

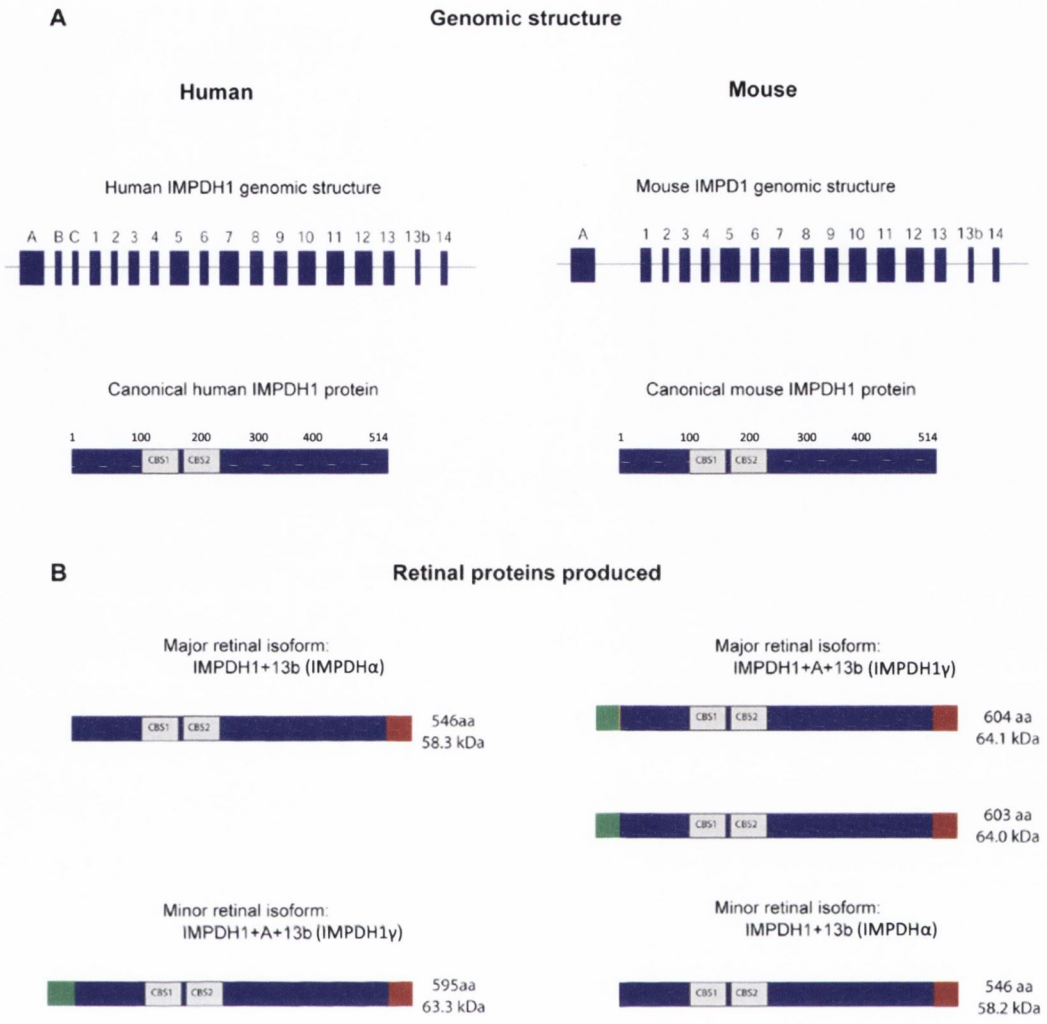

Figure 4. 2: Genomic structure and retinal isoforms of IMPDH1 in mouse and human.

A) Canonical IMPDH1 has similar structure in both mouse and human tissues. B) However, the retinal isoforms are different from the canonical IMPDH1 and are produced through alternate starts of translation and alternate splicing leading to inclusion and/or exclusion of amino acid residues encoded by exons A and 13b. Green indicates exon A encoded residues while red indicates exon 13b encoded residues. IMPDHα (IMPDH1 + 13b) is the major isoform in human retina whereas IMPDHγ (IMPDH1 + A + 13b) is the major isoform in mouse retina. The two major IMPDHγ isoforms in mouse differ by only one amino acid (orange) which results from alternate splicing of exon 1 adding 3 additional bases. The figure was obtained from Spellicy *et al.* (2007).

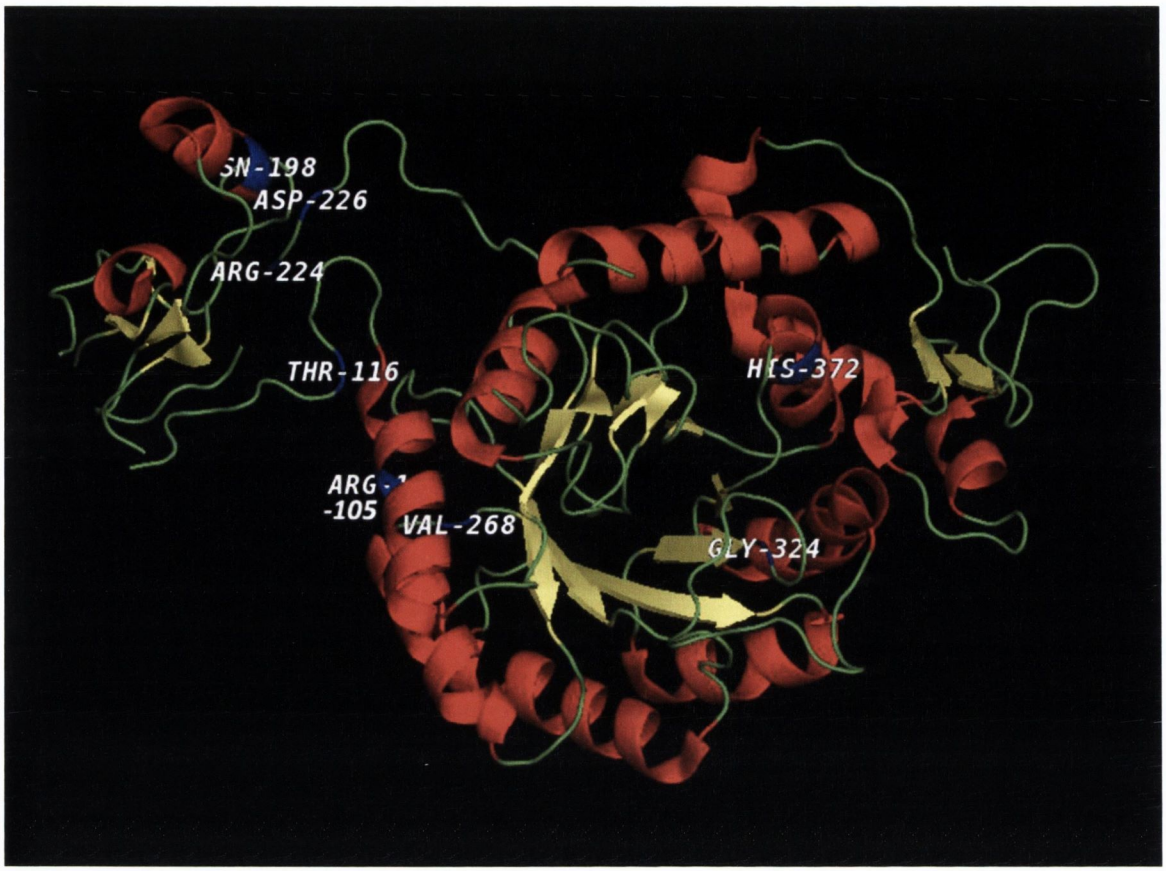

Figure 4. 3: Mutations identified in IMPDH1 protein.

Protein structure (PDB ID: 1CJN) was modified using PyMOL software. Eight different mutations have been identified so far, six of which are from families with adRP whereas Arg105Trp and Asn198Lys were found in patients with isolated Leber's congenitial aumorausis. Blue: mutations, Red: α-helix, Yellow: β-sheet.

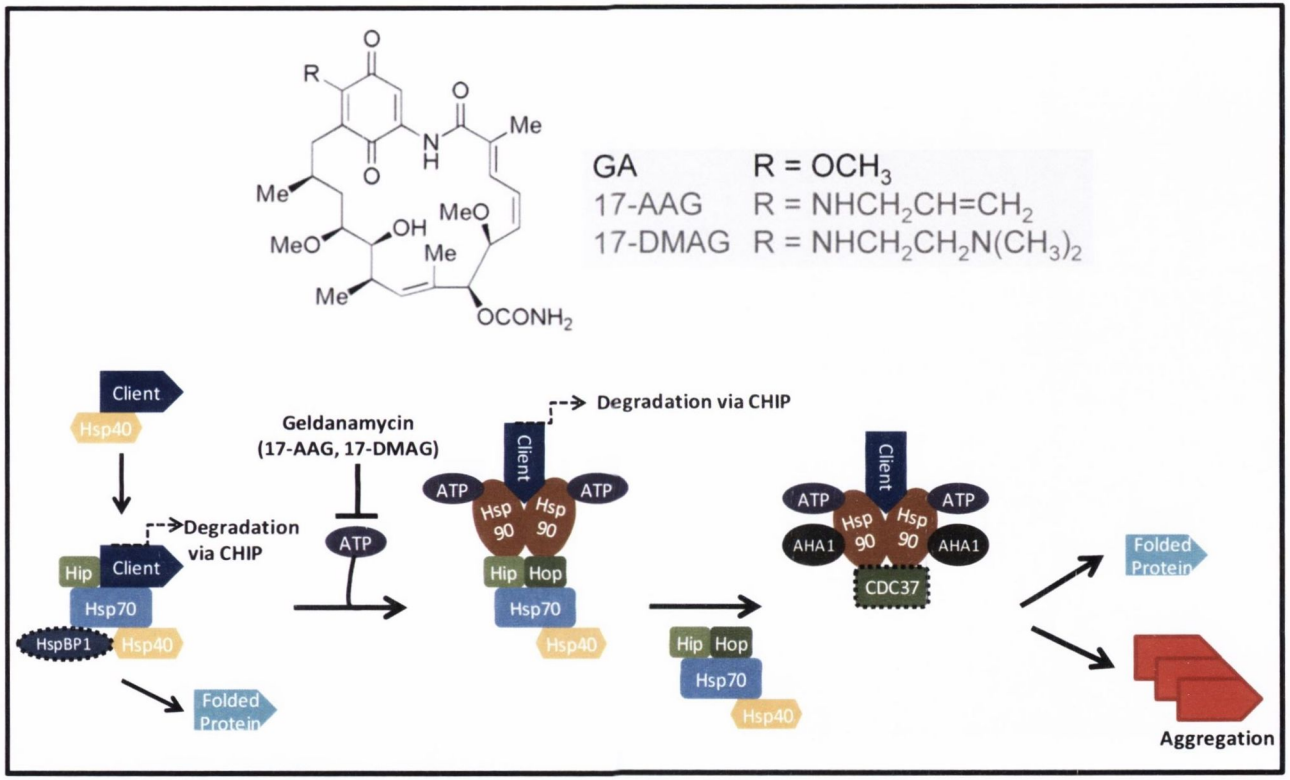

Figure 4. 4: Roles of heat shock protein chaperons in protein folding in eukaryotic cells.

The client protein is presented to Hsp70 by Hsp40, or Hsp40 attached to ribosomes, activates and recruits cytosolic Hsp70 to associate with newly synthesized polypeptide chains under normal conditions. The bound protein can be stabilized on Hsp70 by the Hsp70 interacting protein (Hip) or its release can be stimulated by an exchange factor such as HspBP1. The released protein may fold into a native state or enter another cycle of chaperon

binding and release. However, in the case of misfolded protein, the protein can be targeted for proteasomal degradation via CHIP. In addition, many polypeptide chains may be passed onto the Hsp70/Hsp90 complex for further folding with the help of a co-chaperone Hop. ATP binding leads to dimerization of Hsp90 forming the molecular clamp. AHA1 stimulates ATP hydrolysis and the release of folded client protein whereas CDC37 inhibits this process. In the case of proteins with significant structural instability, Hsp70 in the Hsp70/Hsp90 complex can recruit the co-chaperone CHIP which is docked to Hsp70 or Hsp90 holding a misfolded protein thus recruiting an E2 enzyme to initiate ubiquitinylation. BAG-1 protein links the chaperone to proteasomes to release ubiquitylated polypeptides for degradation. In certain adverse conditions involving destabilizing mutations, accumulation of misfolded protein can also occur leading to aggregation or the formation of insoluble deposits causing 'gain of function' toxicity. Moreover, geldanamycin (GA) and its derivatives (17-AAG, 17-DMAG) have been found to inhibit the function of Hsp90 by binding to the ATP binding pocket, thereby leading to degradation of misfolded proteins via proteasomes.

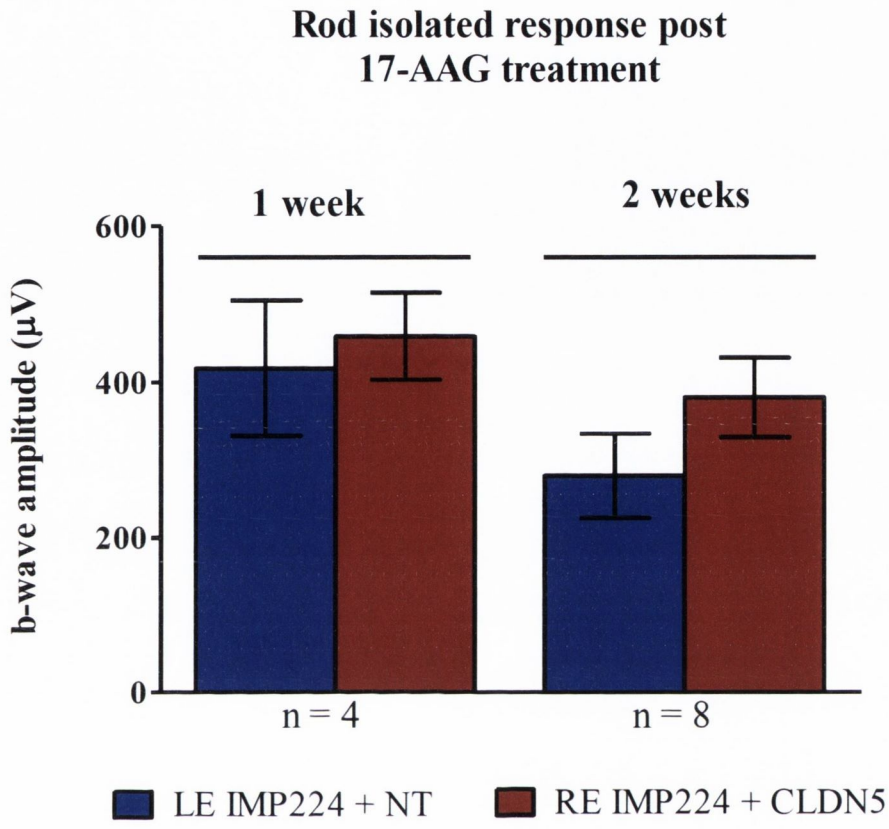

Figure 4. 5: Rod isolated response in mice treated with 1 and 2 weeks of 17-AAG. Adult mice were subretinally injected with CLDN5 AAV2/9 and IMP224 AAV2/5 in the right eye and NT AAV2/9 and IMP224 AAV2/5 in the left eye and I.P injected with 17-AAG twice weekly. ERG was measured post 1 (n = 4) and 2 (n = 8) weeks of 17-AAG treatment. No significant differences in b-wave amplitude were observed between left and right eyes after each treatment. Error bars denote ± SEM.

A)

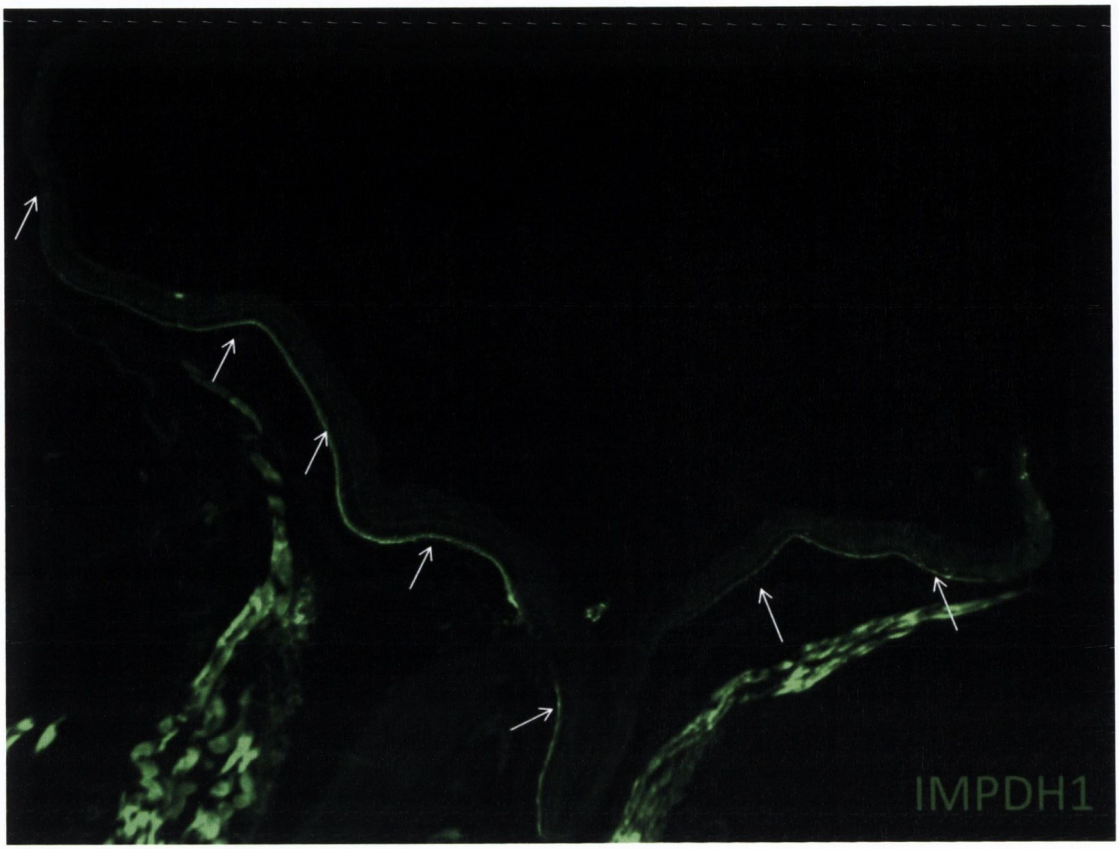

Figure 4.6

B)

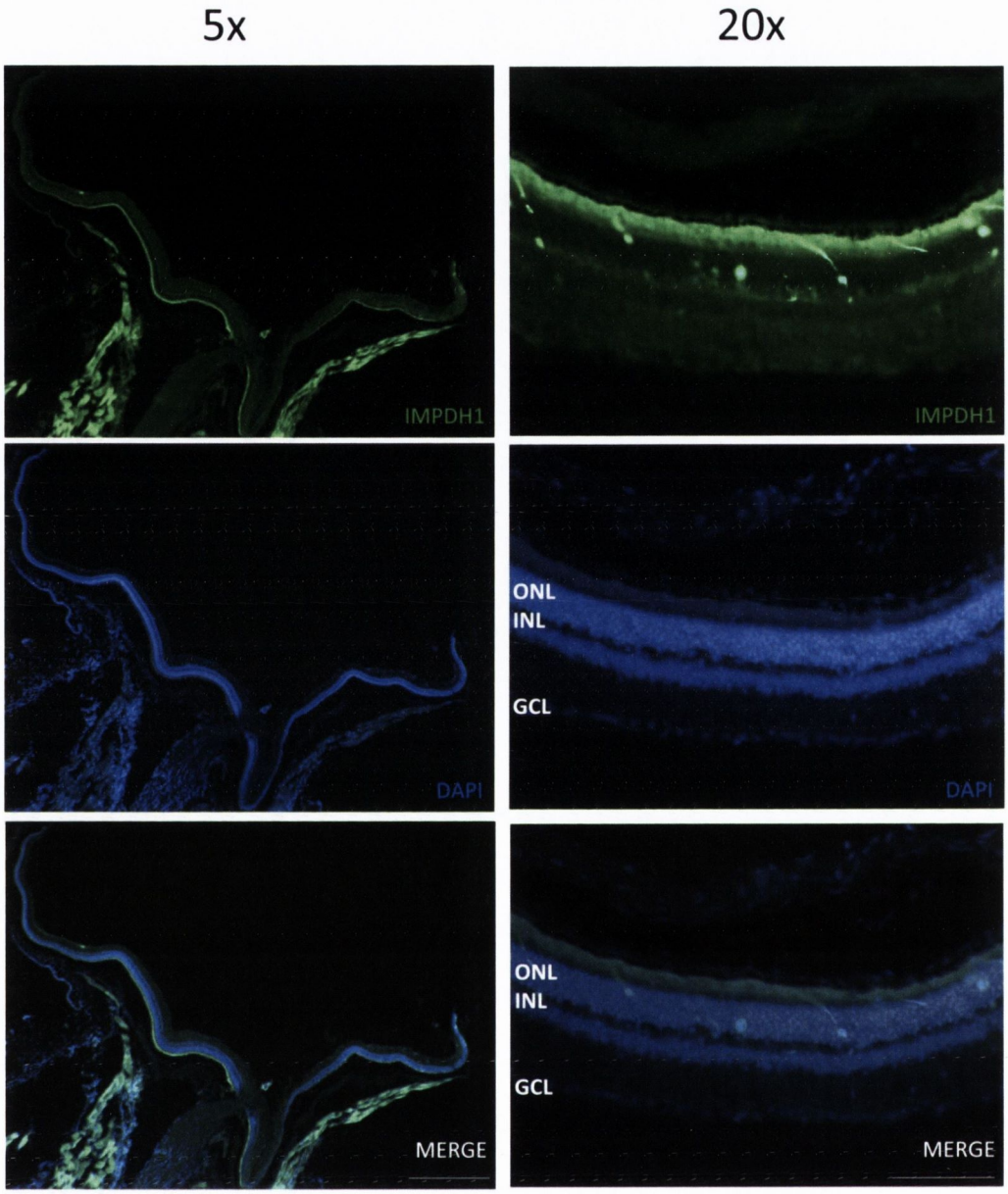

Figure 4. 6: Representative images of IMP224-hrGFP staining.

A retinal section from one animal in **Figure 4.5** was immuno-stained for IMP224-hrGFP and counterstained with DAPI at 7 weeks post 17-AAG treatment. A) 5x image of IMP224-hrGFP retinal section shows that IMP224 AAV2/5 transduces pan-retinally (white arrows). B) 5x and 20x images of the same retinal section. Green: IMP224-hrGFP, Blue: DAPI Error bar: 250 μm (5x images), 150 μm (20x images).

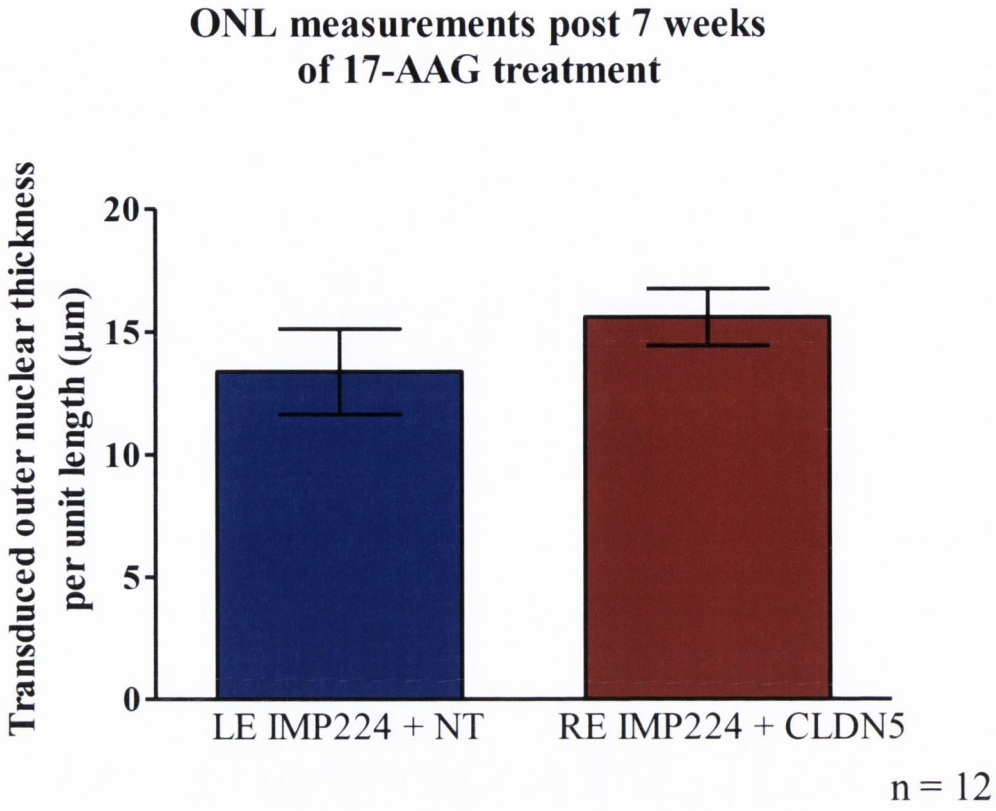

Figure 4. 7: Transduced outer nuclear thickness per unit length post 7 weeks of 17-AAG treatment.

Retinas of the same group of animals (n = 12) in **Figure 4.6** were taken and sectioned after the course of treatment. The transduced ONL per unit length was calculated by ImageJ software using 5x images under fluorescence microscope. The average transduced ONL area per unit length of the whole retina was similar between the left and right eyes post 17-AAG treatment. Error bars denote ± SEM.

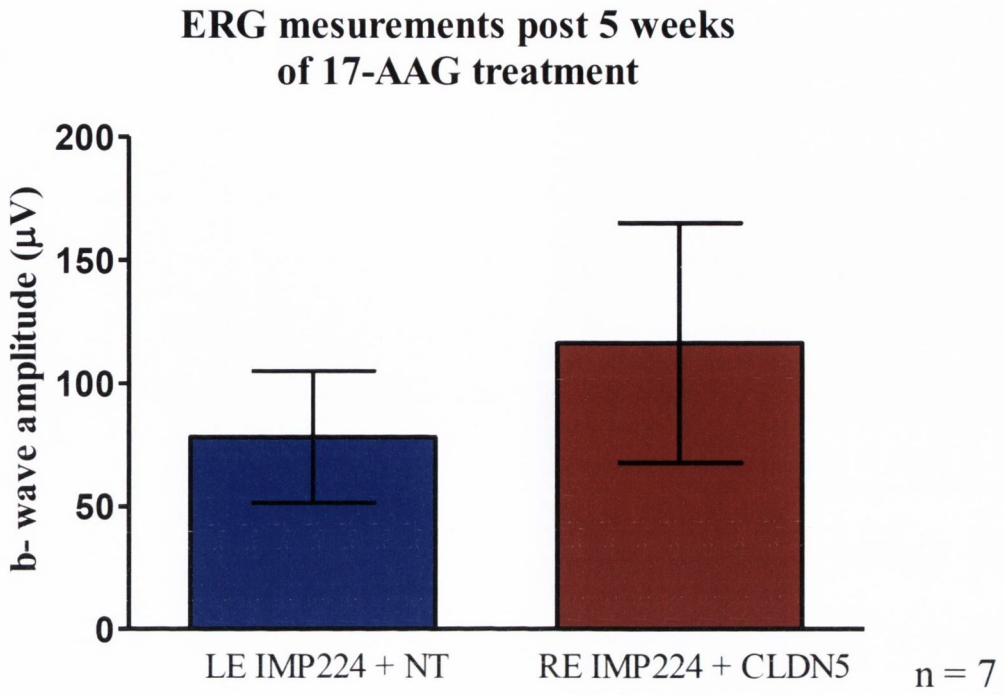

Figure 4. 8: Rod isolated response post 5 weeks of 17-AAG treatment.

Adult mice (n = 7) were subretinally injected with CLDN5 AAV2/9 and IMP224 AAV2/5 in the right eye and NT AAV2/9 and IMP224 AAV2/5 in the left eye and I.P injected with 17-AAG twice weekly for 5 weeks. No statistically significant improvement in b-wave amplitudes of the right treated eye was observed compared to control. Error bars denote ± SEM.

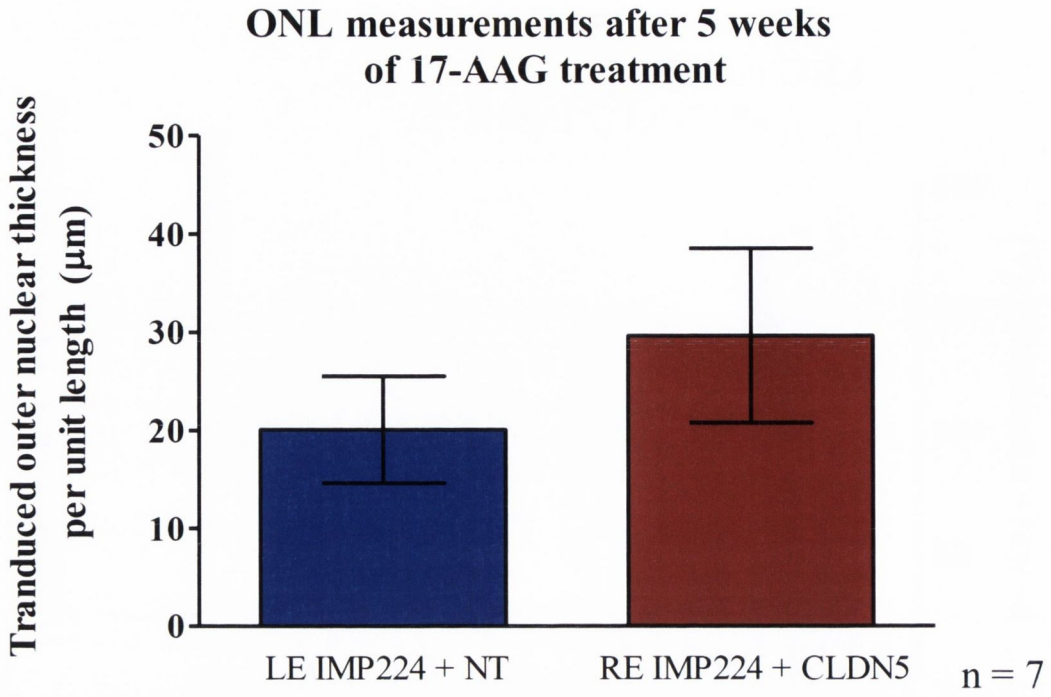

Figure 4. 9: Transduced ONL area per unit length of retinal sections 5 weeks post 17-AAG treatment.

5x images of retinal sections of the same mice in **Figure 4.9** were measured for average whole transduced ONL area per unit length. No significant differences were observed between two eyes. Error bars denote ± SEM.

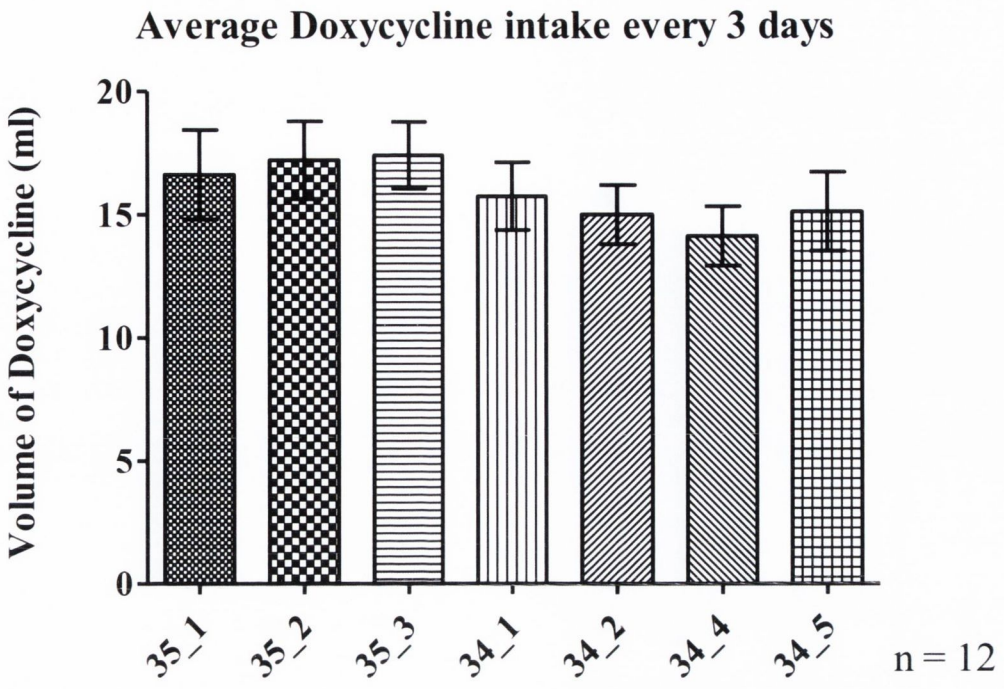

Figure 4. 10: Average doxycycline intake by each mouse every 3 days.

The same animal groups are presented here as in **Figure 4.9**. During the course of 5 weeks of 17-AAG treatment, 12 measurements were carried out. Using ANOVA algorithm, no statistically significant differences were observed in the amount of doxycycline taken by individual animals. Error bars denote ± SEM.

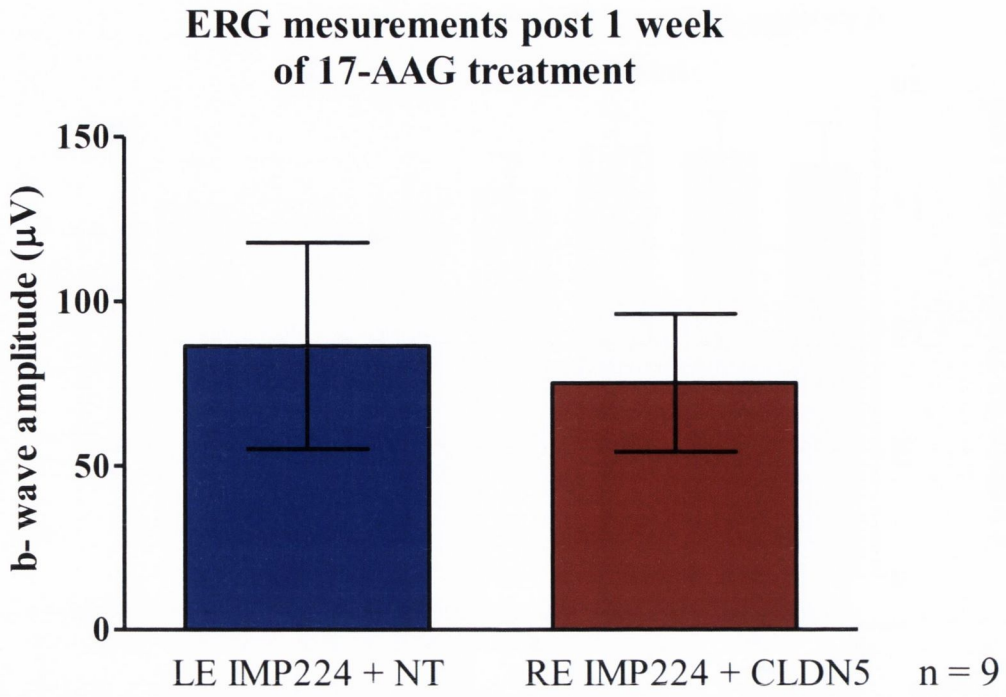

Figure 4. 11: ERG measurements post 1 week of 17-AAG treatment.

Adult mice (n = 9) were subretinally injected with IMP224 AAV2/5. One week later, these mice were subretinally injected with CLDN5 AAV2/9 in the right eye and NT AAV2/9 in the left eye. Mice were also I.P injected with 17-AAG twice weekly for 1 week during which doxycycline drink was administered to these mice. b-wave amplitudes of isolated rod response showed no differences between the left and right eyes post 17-AAG treatment. Error bars denote ± SEM.

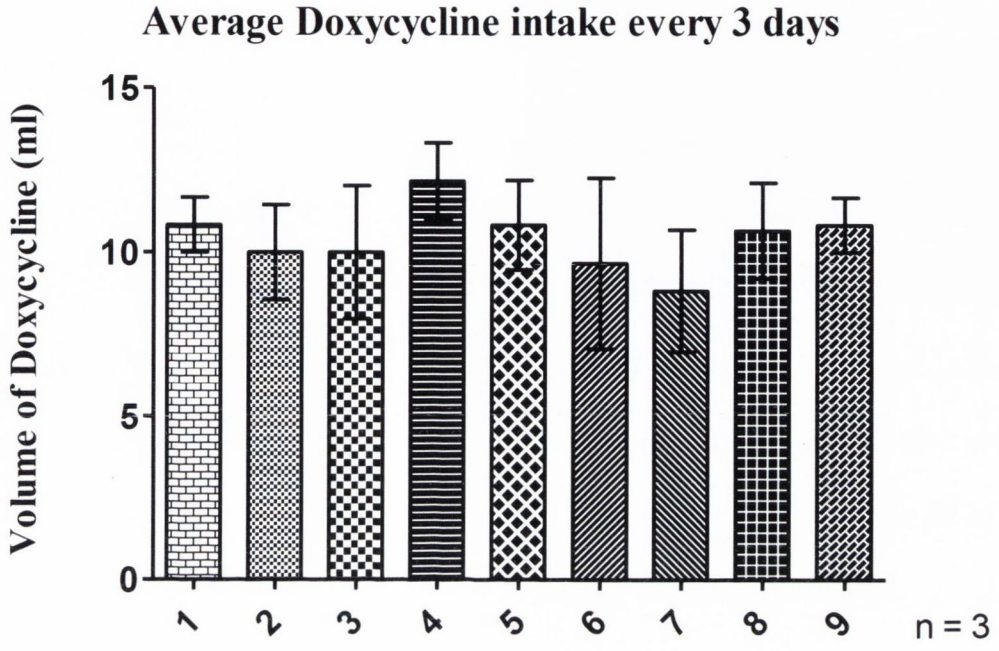

Figure 4. 12: Average intake of doxycycline every 3 days.

Volumes of doxycycline taken by each mouse from the same group of mice as in **Figure 4.11** were measured every 3 days. ANOVA analysis showed each mouse drank similar amount of doxycycline. Error bars denote ± SEM.

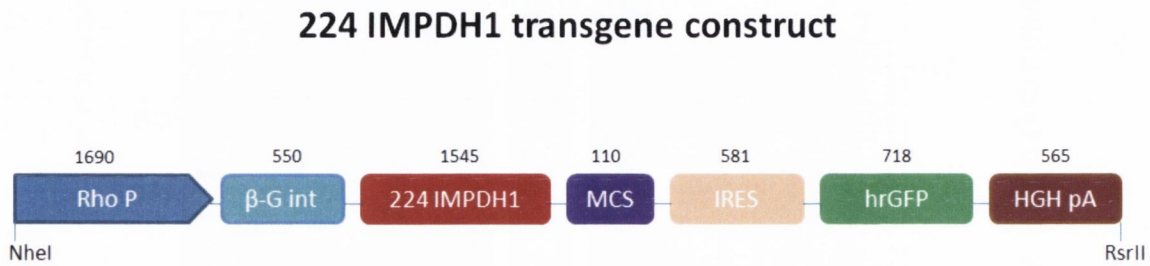

Figure 4. 13: Transgene construct for RP10 mouse model.

The IMP224 pAAV was digested with NheI and RsrII enzymes to produce a 5820 bp transgene. The transgene consists of the Rhodopsin promoter, β globin intron, 224 IMPDH1 coding sequence, multiple cloning site, IRES sequence, hrGFP and HGH poly A tail sequence.

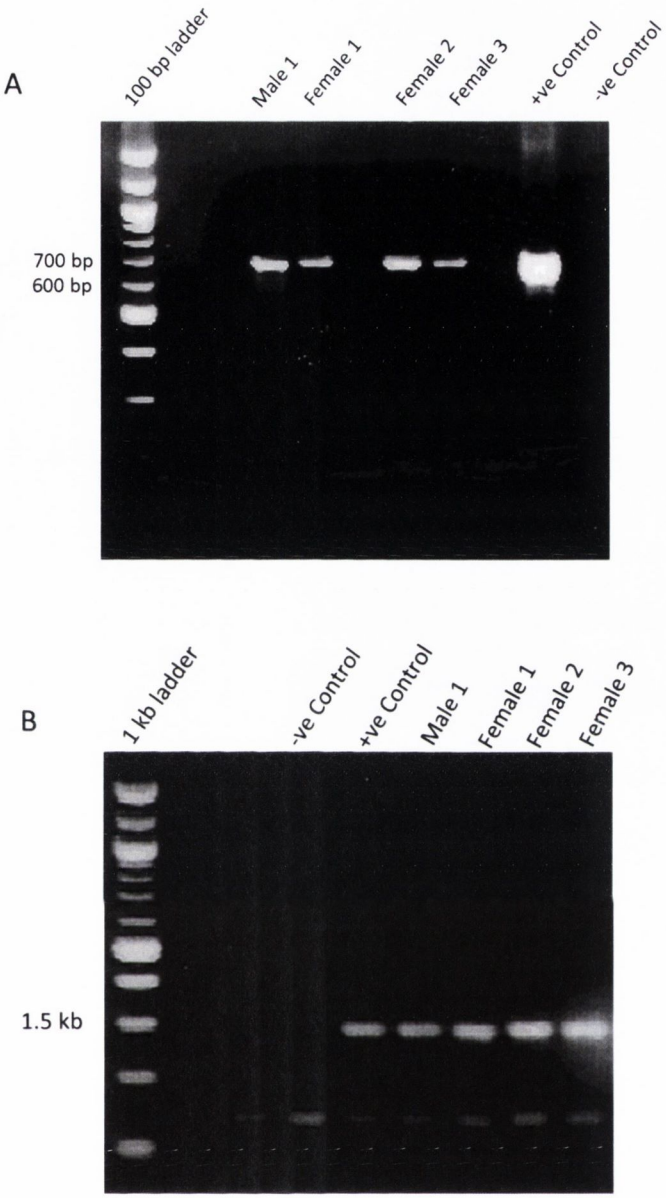

Figure 4. 14: Gel electrophoresis for transgene in founder animals.

Founder DNA samples were tested using 2 different pairs of primers. A) Pair 1 amplifies the region from the Rhodopsin promoter to the IMP224 gene producing a fragment of 660 base pairs and B) Pair 2 amplifies the region from the IMP224 gene to the hrGFP gene producing a fragment of 1536 base pairs. All founders had bands of 660 and 1536 base pairs. IMP224 pAAV plasmid DNA was used as the positive control, while water was used as the negative control.

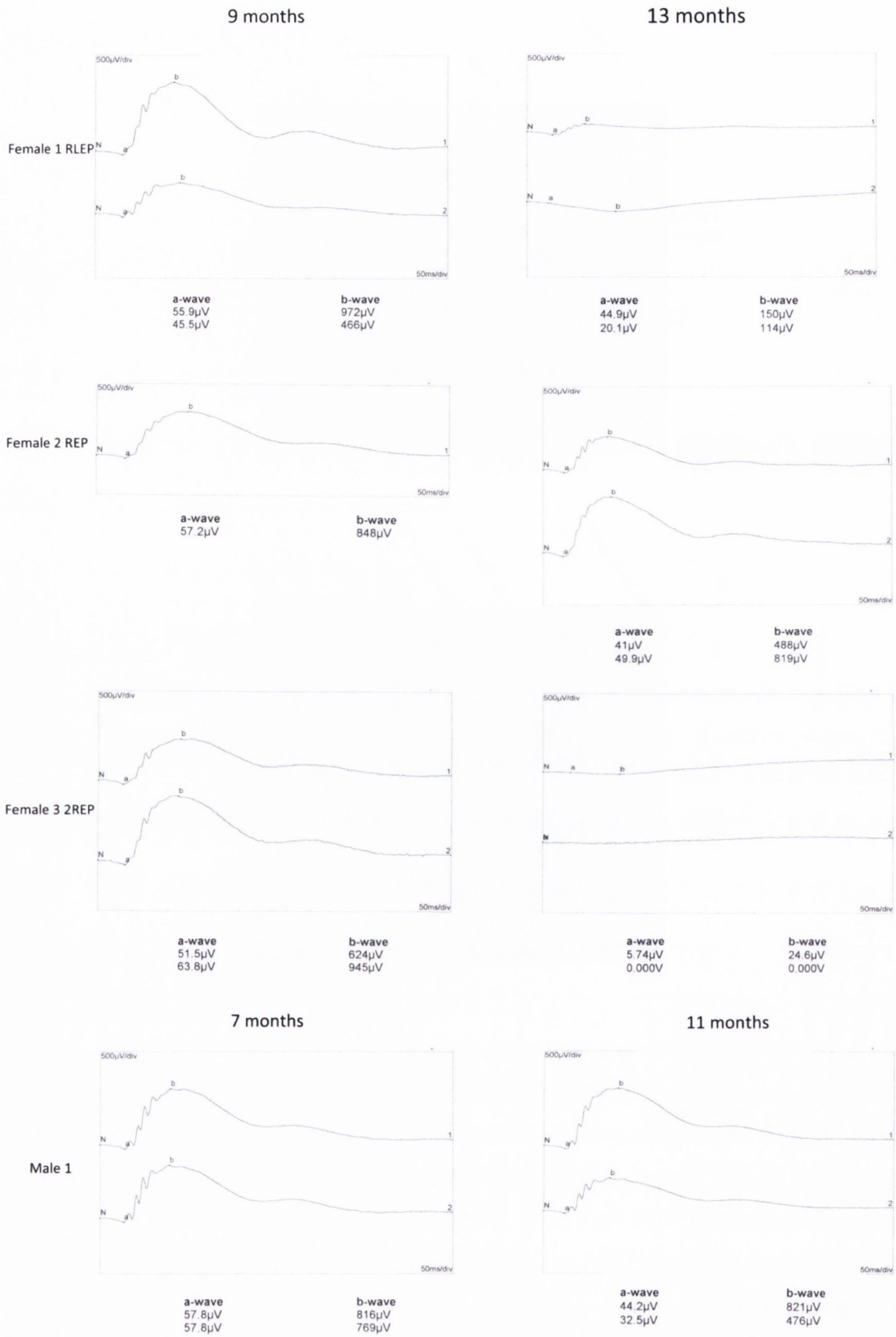

Figure 4. 15: ERG measurements of rod photoreceptors in founder animals.

Founder females had somewhat similar ERG to the WT animals at 9 months old and two of them (females 1 and 3) had severe visual degeneration with b-wave amplitudes of rod-isolated responses being less than 150 μV at 13 months old. However, this was not the case for the remaining founder female and the founder male. Their visual functions seemed to reduce at a slower rate than in the other founder females. At 13 months of age, female 2 had similar ERG compared to female 1 and 3 at 9 months old. Also, ERG of the founder male did not appear to significantly reduce at 11 months old.

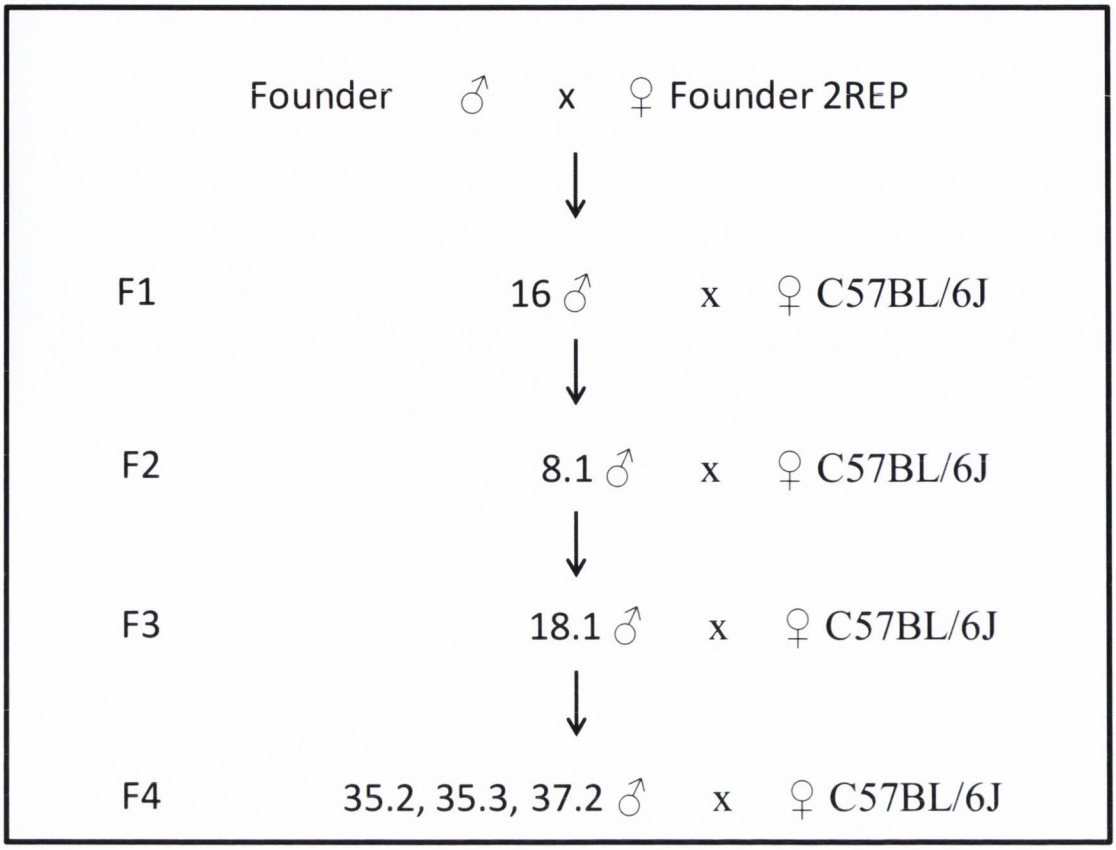

Figure 4. 16: Schematic diagrams of different IMP224 transgenic generations.

Abbeviations: F: generation, ♂: male, ♀: female.

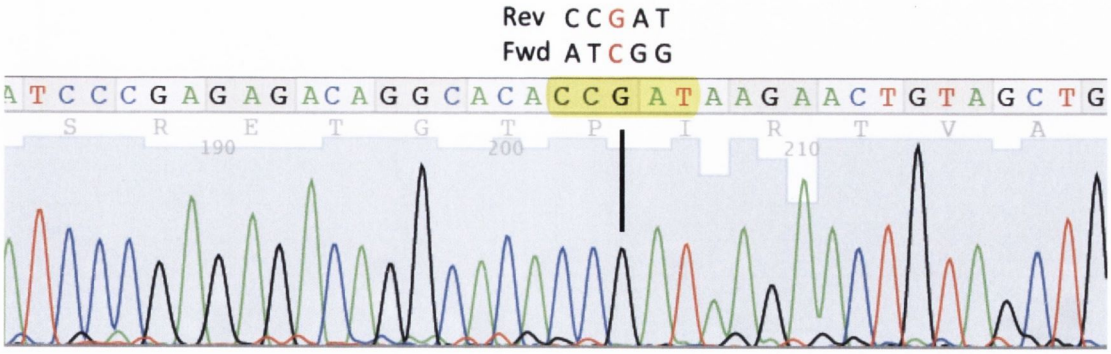

Figure 4. 17: Sequencing for presence of rd8 mutation.

Representative result shows that the animal DNA resembles WT DNA with the presence of the cytosine nucleotide (labelled red in the Forward sequence and obtained by reverse complementation of the reverse primer-sequenced DNA).

		b - wave amplitudes of rod isolated response (μV)							
Animals	Time	16 wks	19 wks	26 wks	27 wks	32 wks	51 wks	54 wks	72 wks
16	RE				671				
	LE				817				
8.1	RE		528				404		
	LE		624				446		
18.1	RE	488						221	274
	LE	458						189	124
35.2	RE			227					
	LE			336					
35.3	RE			316					
	LE			309					
37.2	RE					186			
	LE					276			

Table 4. 1: b-wave amplitudes of rod isolated response (μV).

Animal 8.1 was an offspring of animal 16 x WT C57BL/6J, animal 18.1 was an offspring of animal 8.1 x C57BL/6J. All three animals 35.2, 35.3 and 37.2 (labelled yellow) were descendents of 18.1 x C57BL/6J. All animals were male.

Chapter 5

Prevention of Retinal Degeneration in a P23H rat model of Retinitis Pigmentosa by Systemic Administration of 17-DMAG

5.1 Introduction

Nearly all resident proteins of organelles along the secretory pathway as well as transmembrane and secretory proteins are first translocated to the ER as unfolded polypeptide chains. Upon entering the ER, they are often modified with N-linked glycans, folded into their correct secondary and tertiary structures which are stabilized by disulfide bonds, and then assembled into quaternary structures in many cases. These processes are highly regulated and aided by a complex network of chaperones, co-chaperones and folding enzymes within the ER. When cells experience conditions that disrupt ER homeostasis such as accumulation of misfolded proteins, a transduction cascade termed the unfolded protein response (UPR) is triggered and expressions of chaperones and associated proteins are upregulated in order to cope with a large amount of unfolded proteins. Thus, specific chaperones can also be involved in the regulation of stress signalling and protein degradation pathways to prevent cellular apoptosis and re-establish the balance of ER homeostasis. In this introductory section, I will outline mechanisms of different chaperone systems in the ER, especially the BiP/Grp94 chaperone complex and how UPR is activated upon ER stress caused by accumulation of misfolded proteins through three transduction cascades termed PERK, IRE1 and ATF6. Additionally, about 30-40% of adRP cases involve mutations in the RHO gene, the most common and best studied of which is the P23H mutation which has been associated with aggregation within the ER and thus triggering of the UPR response. Thus, I will also outline current therapeutic strategies for P23H RHO linked RP. As mentioned in **Chapter 4,** 17-DMAG, an Hsp90 inhibitor, is an excellent candidate for the iBRB modulation method due to its low molecular weight. In the context of this chapter, 17-DMAG which has also been shown to inhibit the ER-resident Hsp90 chaperone Grp94 was used to investigate whether its administration would alleviate ER stress in cells expressing P23H RHO and in the P23H-line 3 rat model.

5.1.1 Endoplasmic reticulum stress and protein folding

5.1.1.1 Chaperones in the ER

The ER chaperones can be divided into three categories a) chaperones of the heat shock protein family including glucose-related proteins (Grp) such as Grp78, Grp94 and co-chaperones; b) lectin-like chaperones including calnexin, calreticulin and ER degradation-enhancing α-mannosidase-like protein (EDEM); c) substrate-specific chaperones such as Hsp47. In addition, there are two groups of folding enzymes known in the ER, thiol oxidoreductases from the protein disulfide isomerase (PDI) family (i.e. PDI, Grp58/ERp57) and peptidyl prolyl isomerases (PPIs). The two major chaperone systems which have been best studied in the ER are calnexin/calreticulin and Grp78/Grp94 (Ni and Lee, 2007).

a) Calnexin/Calreticulin chaperone system

After newly synthesized polypeptide chains enter the lumen of the ER, they are often modified with N-linked glycans ($Glc_3Man_9GlcNAc_2$) and glucoses are rapidly removed by glucosidases I and II (Parodi, 2000). The nascent proteins with monoglucosylated N-linked glycans ($Glc_1Man_9GlcNAc_2$) become substrates for the calnexin/calreticulin chaperone system for subsequent folding and assembly. Removal of the last glucose destroys the binding sites of these chaperones, thus nascent proteins are transported to the Golgi once they have been folded properly (Hebert *et al.*, 1995). Grp58/ERp57, a member of the PDI family which contains two thioredoxin motifs also interacts with the chaperone complex to stabilize protein folding by catalyzing the formation of disulfide bonds of the loaded glycoproteins (High *et al.*, 2000). If the glycoprotein cannot be folded properly, another ER protein, UGGT (UDP-glucose glycoprotein-glucosyltransferase) binds to the unfolded glycoprotein and adds a single glucose to the deglucosylated glycan, thereby providing the binding site for the calnexin/calreticulin complex (Sousa and Parodi, 1995). Studies have shown that UGGT recognizes surface exposed hydrophobic regions, a local subtle

alteration caused by a single point mutation, or N glycans close to or within the unfolded sites (Caramelo *et al.*, 2003; Ritter *et al.*, 2005; Taylor *et al.*, 2004). The monoglucosylated N-glycan protein is then refolded and exits the ER to its final destination. However, if refolding is unsuccessful, the whole process will repeat itself until a decision is made to destroy the protein (Sousa *et al.*, 1992).

a) BiP/Grp94 system

The second major chaperone system recognizes and binds to aromatic and hydrophobic residues of unfolded proteins and is composed of the BiP/Grp94 system in a large multi protein complex which includes ER chaperones such as PDI, Erp72, Grp170/ORP150, UGGT, CaBP1, cyclophilin B and SDF2-L1 which together form a network to process unfolded proteins (Meunier *et al.*, 2002). In addition, some calreticulin/calnexin substrate could bind to this BiP/Grp94 system when the N-glycosylation is blocked.

BiP, originally termed immunoglobulin heavy chain binding protein for its role in the assembly of immunoglobulins (Haas and Wabl, 1983), is the most abundant member of the heat shock protein 70 kDa family in the ER lumen with a concentration reaching millimolar range. It consists of two domains: a 44 kDa N-terminal ATPase domain and a 20 kDa C-terminal polypeptide binding domain (Guth *et al.*, 2004). In addition, BiP also contains a highly helical and variable 10 kDa C-terminal domain with unknown function (Chevalier *et al.*, 2000). These domains interact to regulate the binding and duration of binding of BiP to substrate polypeptides. Like all Hsp70 proteins, BiP binds both ADP and ATP which regulate its binding and release of nascent polypeptides. In mammalian cells, ER resident DnaJ like (ERdj) co-chaperones, of which there are seven (ERdj1-7) bind to BiP when it is in an "open" ATP-bound state catalyzing the rapid hydrolysis of ATP to ADP thus leading to binding of BiP to the unfolded substrates (Liberek *et al.*, 1991; Otero *et al.*, 2010). In contrast to ERdj, nucleotide exchange proteins such as BiP associated protein (BAP)/Sil1, and Grp170 induce ADP release and exchange for ATP which reopen

BiP and release the proteins (Hendershot, 2004; Maattanen *et al.*, 2010). It is believed that nucleotide exchange proteins together with ERdjs continuously regulate the ATPase cycle of binding and release of polypeptide chains allowing them to progress towards an increasingly folded state with folding occurring during the release cycle (Hendershot *et al.*, 1996).

BiP is usually the first chaperone to bind the nascent chains with alternating aromatic and hydrophobic residues, and the binding of BiP to these chains is usually facilitated by ERdj1 and 2, homologs of yeast Sec63. BiP is predicted to recognize a frequently existing protein sequence which occurs about every 36 amino acids thereby facilitating translocation of nascent chains into the ER lumen (Matlack *et al.*, 1999). However, the actual specificity of BiP *in vivo* is not yet clear because translocation of nascent chains into the ER more likely involves multiple weak affinity interactions between BiP and nascent chains (Maattanen *et al.*, 2010). In general, ERdj co-chaperones direct BiP activity towards specific substrates while ERdj3-6 are induced by the unfolded protein response and thus are believed to have roles in protein folding and quality control. For example, ERdj3 is found in a multi protein complex binding to IgG during its folding in the ER and is only found when IgG is also present. In addition, ERdj3, 4 and 6 have also been shown to be able to bind directly to unfolded protein substrates both *in vivo* and *in vitro*, and in doing so, recruit BiP to the substrate also (Dong *et al.*, 2008; Jin *et al.*, 2008; Jin *et al.*, 2009; Petrova *et al.*, 2008). It is of interest that while the interaction of BiP with nascent chains is immediate and transient during synthesis, the association with misfolded proteins tends to be prolonged suggesting that this might be a signal for degradation of these proteins. Indeed, prolonged association of BiP with misfolded substrates such as ΔF508-CFTR and mutant SP-C leads to degradation of these proteins (Dong *et al.*, 2008; Farinha and Amaral, 2005).

Grp94 is an ER resident Hsp90 protein and encoded by the HSP90B1 gene. It is also commonly known as gp96, endoplasmin, Tra-1 or Hsp108. Interestingly, Grp94 is the only Hsp90 protein found within the ER in all organisms characterised so far; and is ubiquitously expressed and found in high levels in secretory tissues (Eletto *et al.*, 2010). Although Grp94 exists exclusively as a dimer both *in vitro* and *in vivo*, individual monomers have also been found to be able to bind ATP and peptide (Vogen *et al.*, 2002; Wassenberg *et al.*, 2000). However, it is not yet fully understood whether Grp94 monomers can act as a chaperone or is associated with an ATPase cycle which could facilitate substrate binding. In contrast to Hsp90 in the cytosol, the substrate proteins of Grp94 tend to have distinct folds such as the immunoglobulin domain fold which is found in a large fraction of secretory but not in cytosolic proteins, contain disulfide bonds and rely on proper oxidative folding due to a 30-fold higher oxidizing environment in the ER compared to the cytosol (Marzec *et al.*, 2012). Like all Hsp90, Grp94 consists of 4 domains: an N-terminal domain, an acidic link domain, a middle domain and a C-terminal domain. The N-terminal domain mediates ATP association while hydrolytic activity requires the linker and middle domains (Eletto *et al.*, 2010). Unlike Hsp90, Grp94 has no known co-chaperone which would assist its ATPase cycle, thus helping the loading of substrate or affecting the conformational equilibrium of the chaperone. In terms of its function in protein folding, Grp94 is quite selective to specific substrates compared to PDI, calreticulin or BiP.

Meunier *et al.* (2002) have suggested the existence of a multi-protein complex in the ER in which BiP and Grp94, the most abundant components, act in concert with each other. Specifically, it is thought that BiP transfers substrates including immunoglobulins and thyroglobulin to Grp94 for later stages of folding (Melnick *et al.*, 1994; Muresan and Arvan, 1997). This indicates that the folding of some proteins requires one chaperone system to fold early intermediates and another to continue the process of folding at later

stages. On the other hand, some proteins do not require both of these chaperones: many proteins associate with BiP but not with Grp94 whereas IGF interacts exclusively with Grp94 and not with BiP (Ostrovsky *et al.*, 2009a; Ostrovsky *et al.*, 2009b).

5.1.1.2 Unfolded protein response

Once ER homeostasis is unbalanced due to cellular toxicity associated with aggregation of misfolded proteins, a signal transduction cascade termed UPR or ER stress response is activated in order to alleviate ER stress. Although ER stress is the precursor of UPR, these terms have been used interchangeably in various publications. In addition, the UPR has been shown recently to be activated during normal cellular events such as B-cell differentiation, muscle differentiation, or viral infections as well as being associated with a variety of disorders such as those caused by protein misfolding, so-called conformational diseases (Benali-Furet *et al.*, 2005; Nakanishi *et al.*, 2005; Reimold *et al.*, 2001). Typically, the UPR transduction cascades are composed of translation attenuation to prevent further production of unfolded proteins, transcriptional induction of various ER resident proteins such as chaperones to further assist folding, induction of ER-associated degradation (ERAD) to target misfolded proteins for degradation via ubiquitination, and enlargement of the ER to handle the accumulation of unfolded proteins (Haeri and Knox, 2012).

There are three main trans-membrane proteins within the ER that respond to prolonged ER stress: inositol requiring kinase 1 (IRE1), activating transcription factor 6 (ATF6), and double stranded RNA activated protein kinase-like endoplasmic reticulum kinase (PERK). These proteins have a transmembrane domain that spans the ER, a cytosolic domain and an ER luminal domain and upon ER stress activate transcription of ER resident chaperones, reduce synthesis of new proteins and enhance degradation of misfolded proteins. However, cyto-protective and pro-apoptotic outputs coexist in the UPR cascade. Under prolonged ER stress where ER homeostasis cannot be re-established, UPR signalling eventually induces

cell death by apoptosis. Downstream UPR target genes are regulated by two distinct consensus response elements within their promoters, the unfolded protein response element (UPRE) and the cis-acting ER stress element (ERSE) (Yoshida *et al.*, 1998). Under prolonged ER stress, sustained PERK signalling has been associated with apoptosis due to induction of CHOP, a bZIP transcription factor, whereas IRE1 and ATF6 signalling are attenuated (Lin *et al.*, 2007; Lin *et al.*, 2009). On the other hand, expression of ER chaperone BiP seems to protect cells from ER stress (Gorbatyuk *et al.*, 2010) (**Figure 5.1**).

a) PERK

PERK is a type I transmembrane protein kinase receptor which is activated during ER stress by the release of BiP from its ER luminal domain. Similar to IRE1, this leads to oligomerization and subsequent autophosphorylation of its cytoplasmic domain. Activated kinase PERK phosphorylates the α subunit (S51) of eukaryotic translation initiation factor 2 (eIF2α), thus inhibits 80S ribosome assembly and consequently attenuates protein translation and alleviates ER protein overload (Harding *et al.*, 1999). In contrast, phosphorylated eIF2α also selectively activates expression of ATF4, a transcription factor that controls the upregulation of chaperones, ERAD machinery and some UPR target genes which function in redox homeostasis, amino acid metabolism, apoptosis (i.e. CHOP, GADD34) and autophagy (Ameri and Harris, 2008; Matus *et al.*, 2011).

b) IRE1

IRE1 is a type I transmembrane Serine/ Threonine kinase receptor which has a site-specific endoribonuclease (RNase) activity in its cytoplasmic domain. IRE1 is highly conserved among eukaryotes. In mammals, two types of IRE1 have been found, IRE1α and IRE1β. IRE1α is expressed ubiquitously in all tissues while IRE1β is limited to the gastrointestinal tract. Lack of IRE1α is lethal while IRE1β deficient mice are viable (Haeri and Knox, 2012). Upon accumulation of unfolded protein, BiP is released from the luminal domain of IRE1 leading to dimerization and autophosphorylation of IRE1. Once endoribonuclease

activity is triggered by autophosphorylation, IRE1 will directly regulate the unconventional splicing of a 26 nucleotide segment from the mRNA coding X-box binding protein -1 (Xbp1) creating a translational frameshift (Yoshida *et al.*, 2001). Spliced Xbp1 (Xbp1s) is a bZIP (basic region and leucine zipper) domain containing transcription factor of the ATF/CREB (cyclic-AMP-responsive-element-binding protein) family. Xbp1s is then translocated to the nucleus and activates expression of genes involved in protein quality control, folding, the ERAD system and ER and Golgi biogenesis (Ron and Walter, 2007). Xbp1 splicing also activates transcription of UPR target genes such as BiP (Travers *et al.*, 2000).

c) ATF6

ATF6 is a type II transmembrane protein with both a cytosolic/nucleoplasmic and an ER luminal domain. Mammals have two ATF6 homologs, ATF6α and ATF6β (Haze *et al.*, 2001). There are two ER stress regulated Golgi localization sequences (GSL1 and GSL2) in the luminal domain of ATF6α and one GSL2 in that of ATF6β. BiP is released from the GSL1 region of ATF6 luminal domain upon ER stress leading to ATF6 translocation to the Golgi where it is cleaved by site-1 proteases (S1P and S2P) to become cleaved ATF6, a bZIP transcription factor that interacts with nuclear factor-Y and Xbp1s, binds to ERSE and UPRE elements and activates many ER chaperones such as BIP, Grp94 and PDI, and to ERAD related genes and Xbp1 mRNA (Haze *et al.*, 1999).

5.1.1.3 ER stress signaling and ER chaperones

In addition to being one of the first targets for upregulation to assist protein folding upon ER stress, BiP also acts as a sensor for unfolded proteins in the ER. Under normal conditions, BiP binds to each of the three main ER stress sensors (IRE1α, ATF6α and PERK) **(Figure 5.1).** When misfolded proteins are accumulated within the ER, BiP is dissociated from these three transmembrane proteins in order to bind to misfolded proteins which results in activation of these transmembrane proteins leading to activation of the

UPR response. Recently, the ERSE has been indicated to be the most important element of the BiP promoter in upregulation of BiP during ER stress. BiP activation is mainly regulated at the transcriptional level and mediated by three copies of the ERSE with the evolutionary conserved sequence of CCAAT(N_9)CCACG located upstream of the TATA box (Li and Lee, 2006). However, upregulation of BiP is also mediated through a non ERSE element pathway which involves ATF4 and CREB1 complex (Luo *et al.*, 2003; Roy and Lee, 1999). Transcription factors that bind to ERSE element include NF-Y, YY1, TFII-1, Sp1 and especially the cleaved form of ATF6 which is the most potent activator of BiP upregulation. Cleaved ATF6 binds to the ERSE element by forming a complex with NF-Y (Yoshida *et al.*, 2001). However, ATF6 function in induction of BiP remains controversial. It was reported that ER stress induction of BiP was unaffected in MEF cells treated with ATF6α siRNA (Lee *et al.*, 2003a). In contrast, other studies *in vivo* have shown that ATF6α targeting siRNA or mutations within ATF6α dramatically reduced induction of BiP (Baumeister *et al.*, 2005; Thuerauf *et al.*, 2004). Thus, an animal model for ATF6α is needed to study the effect of this protein towards BiP expression upon ER stress.

In addition to ATF6, Xbp1 and ATF4 are also involved in the induction of BiP upon UPR. A conserved ATF4 binding site (5'-TGACGTGA-3') upstream of the ERSE elements has been identified in the promoter region of BiP. Upon ER stress, ATF4, upregulated through the activation of PERK pathway, forms a complex with the nuclear co-factors ATF1 and CREB1 *in vivo* which in turn bind to the ATF/CRE binding site in the BiP promoter (Harding *et al.*, 2000). Similar to ATF6, induction of BiP by ATF4 is not yet fully understood and has been found to be dispensable in certain experimental studies.

Many studies have shown that overexpression of BiP decreases the level of Aβ4 and Aβ42 amyloids in cells expressing β-amyloid precursor mutant (Hoshino *et al.*, 2007) reduces apoptosis in Chinese hamster ovary cells (Morris *et al.*, 1997) and cardiomycytes (Fu *et al.*,

2008) and increases the Ca^{2+} concentration within the ER in Hela cells (Lievremont *et al.*, 1997). In addition, increased expression of BiP also protects photoreceptors from ER stress induced by accumulation of P23H RHO in a rat model of retinitis pigmentosa (Gorbatyuk *et al.*, 2010).

Similar to BiP, human Grp94 promoter also contains 4 cis-acting ERSE elements and the main mechanism controlling its expression is transcriptional regulation upon ER stress (Marzec *et al.*, 2012). In additon, NF-Y binds to the CCAAT motif of the ERSE whereas cleaved ATF6 has a specific binding site at CCAGG motif of the ERSE. While the binding of NF-Y is required for the activity of Grp94 promoter, the binding of cleaved ATF6 to ERSE is more specific and sufficient than that of NF-Y. The 9bp GC rich linker of the ERSE is also important in induction of Grp94 during stress response (Yoshida *et al.*, 1998). Furthermore, the Grp94 promoter can also be activated by another transcription factor involved in UPR, Xbp1. In yeast, the ER stress responsive element (UPRE) with a consensus sequence TGACGTGG/A is targeted by Xbp1. Although the promoter of Grp94 and many other chaperones do not contain canonical UPRE, Xbp1, however, has been observed to bind the CCACG motif in the ERSE at a lower affinity than cleaved ATF6 (Yoshida *et al.*, 2001).

In addition, UPR activation also increases expression of other ER localised stress proteins such as PDI, Erp72, GRP170, and calreticulin. The coordinated transcriptional regulation of these proteins suggests they form a functional network to increase the folding efficiency and reduce the chances of misfolded protein escaping. Such an ER network is equivalent to the cytosolic folding factors that also form a dynamic complex mentioned in **Section 4.1.2.3**. Therefore, it is not surprising that depletion of one chaperone would affect activities or levels of expression of other chaperones in the complex. Indeed, the IRE1 branch of the UPR is activated leading to BiP induction when Grp94 is suppressed by RNAi in C. elegans (Kapulkin *et al.*, 2005). BiP is also upregulated when *C.elegans* E3

ubiquitin ligase HRD-1 is silenced indicating that the ERAD component also importantly functions in the quality control network (Sasagawa *et al.*, 2007). In mammalian cells, knockdown or inactivation of BiP induces expression of Grp94, PDI, calreticulin and ERp57 while silencing of calreticulin mediates expression of Grp94 and PDI (Maruri-Avidal *et al.*, 2008). On the other hand, knocking out Grp94 in mice results in embryonic lethality at the stage when mesoderm formation occurs, while complete deletion of BiP, ERp57 and calreticulin also leads to lethality in mouse embryo thus indicating that these chaperones are essential in early development of the mouse embryo (Hendershot, 2004; Ni and Lee, 2007).

5.1.1.4 ER chaperones facilitate ER-associated protein degradation

In vitro studies using a reversible ER stress inducer (i.e. dithiothreitol (DTT)) suggested that during transient stress the chaperones bind to nascent proteins and allow them to fold later when the stress condition is resolved (Ma and Hendershot, 2004). However, many unfolded proteins will be targeted for ERAD to reduce the protein load and accumulation of these proteins within the ER if the stress is prolonged. During ERAD, the targeted proteins are retrotranslocated to the cytosol and degraded by the ubiquitin proteasome system. ER chaperones play a key role in targeting substrates for the ERAD process by recognizing substructures such as hydrophobic patches, unpaired cysteines, and partially de-mannosylated N-glycans within misfolded proteins (Ni and Lee, 2007). As mentioned above, the calnexin/calreticulin chaperone complex tends to repeat the folding cycle with the help of UGGT until its substrate is properly folded. However, these glycoprotein substrates will eventually be subjected to terminal mannose trimming (from $Man_9GlcNAc_2$ to $Man_8GlcNAc_2$ or extensively to $Man_6GlcNAc_2$ or $Man_5GlcNAc_2$) by ER α 1,2-mannosidases (Lederkremer and Glickman, 2005). As a result, EDEM will target these proteins for degradation. In addition, three EDEM homologs (EDEM1-3) are transcriptionally induced upon ER stress by the activation of IRE1 while overexpression of

EDEM facilitates faster release of unfolded proteins from the calnexin/calreticulin chaperon complex for degeneration (Molinari *et al.*, 2003; Yoshida *et al.*, 2003).

On the other hand, BiP with its co-chaperones target proteins for degradation through the recognition of hydrophobic regions in nascent polypeptides which are usually exposed on the surface of misfolded or unfolded proteins. They also simultaneously hold the proteins in soluble conformations to prevent their aggregation within the ER. Indeed, all known soluble ERAD targeted proteins require BiP and its co-chaperones for degradation (Fewell *et al.*, 2001; Nishikawa *et al.*, 2005). Recently, Grp94 has been found to cooperate with osteosarcoma amplified 9 (OS-9), a soluble ER resident protein which can distinguish between folded and misfolded protein through an as yet unidentified sensing mechanism (Alcock and Swanton, 2009; Szathmary *et al.*, 2005). However, it is thought that OS-9 uses polypeptide based signals to bind glycoproteins and target them to ERAD degradation (Christianson *et al.*, 2008). Together, Grp94 and OS-9 can deliver the mutant 1-antitrypsin to the Hrd-1 ubiquitin ligase complex in the ER membrane for retrotranslocation by the ERAD machinery (Bernasconi *et al.*, 2008; Christianson *et al.*, 2008). In addition to the enzymatic activity, PDI is also a chaperone playing an important role in ERAD targeting. PDI interacts specifically with disulfide-free, misfolded secretory protein in yeast and targets them for degradation (Gillece *et al.*, 1999).

5.1.1.5 ER stress and Apoptosis

In cell culture, prolonged ER stress, a pathological factor in neurodegenerative diseases, diabetes, renal diseases and atherosclerosis appears to stimulate IRE1, ATF6 and PERK pathways sequentially and deactivates them in the same order triggering apoptosis (Lin *et al.*, 2007). Four pro-apoptotic pathways are associated with ER stress: 1) activation of ASK1 (apoptosis signal regulating 1) mediated by IRE1α, 2) caspase-12, 3) PERK induction of CHOP, and 4) release of Ca^{2+} from the ER which mediates pro-apoptotic Bak/Bax (Haeri and Knox, 2012).

The IRE1/TRAF2/ASK1/JNK pathway is the dominant pro-apoptotic pathway in ER stress. IRE1α recruits TNF receptor-associated factor 2 (TRAF2) to its cytosolic domain which can in turn activate apoptosis signal-regulating kinase (ASK) 1, p38 and finally c-Jun amino-terminal kinase (JNK) (Nishitoh *et al.*, 2002; Urano *et al.*, 2000). Upregulation of ASK1 and JNK leads to phosphorylation and inactivation of anti-apoptotic Bcl-2 (Yamamoto *et al.*, 1999). In addition, JNK has been shown to translocate to the mitochondria and mediate phosphorylation of Bim leading to Bax-dependent release of cytochrome c (Lei and Davis, 2003; Putcha *et al.*, 2003). Also, IRE1α can interact with TNF receptor 1 (TNFR1) and TRAF2/ASK1 thus activating JNK, or TRAF2 and the inhibitor of κB kinase (IKK) leading to activation of nuclear factor κB, both of which trigger apoptosis in cells (Yang *et al.*, 2006).

The PERK/ATF4/CHOP pathway is the second pro-apoptotic pathway induced during prolonged ER stress. CHOP is minimally expressed during normal conditions and upregulated moderately upon ER stress (Haeri and Knox, 2012). Actually, all three UPR pathways are able to induce CHOP transcriptionally (Oyadomari and Mori, 2004) **(Figure 5.1)**. It has been shown that CHOP activation triggers cells towards apoptosis by downregulation of Bcl-2 and/or depletion of glutathione leading to accumulation of reactive oxygen species within the cell (McCullough *et al.*, 2001). In addition, CHOP also activates other pro-apoptotic factors such as DR5, TRB3, BIM, and GADD34 (Ohoka *et al.*, 2005; Puthalakath *et al.*, 2007; Song *et al.*, 2008; Yamaguchi and Wang, 2004). Indeed, CHOP has been associated with neurodegenerative diseases (i.e. Parkinson's disease), retinitis pigmentosa, colitis, cardiac overload, renal dysfunction, etc. Therefore, CHOP is a major pro-apoptotic factor in ER stress and is thus a major target therapeutic target.

Protein folding is an energy demanding process and can involve the formation of disulfide bonds which are necessary for proper folding of some proteins. Therefore, this process

produces a lot of reactive oxygen species which are accumulated greatly during ER stress. The PERK pathway of UPR has been found to upregulate the transcription of glutathione S-tranferase, NAD(P)H:quinine oxidoreductase-1, γ-glutamate cysteine ligase, and hemeoxygenase in order to mininse oxidative stress; a potent disease causing factor associated with AMD, retinitis pigmentosa and other ocular diseases (Cullinan and Diehl, 2004; Lee *et al.*, 2003b).

Moreover, activation of ER localized caspase 12 is highly specific to the UPR response since caspase 12 null mice are resistant to apoptosis induced by ER stress including disruption of ER calcium storage and accumulation of excess proteins within the ER but not to other pro-apoptotic signals (Nakagawa *et al.*, 2000). Caspase-12 is a member of the group I family of caspases consisting of caspase-1, 4, 5, 11 and 13. As mentioned above, during ER stress IRE1α can recruit TRAF2 adaptor protein which in turn can also bind to procaspase 12 during ER stress and induce activation via proteolytic cleavage (Yoneda *et al.*, 2001). Caspase 12 is located in the cytoplasmic side of the ER membrane and caspase 7 can be translocated to the ER membrane and interact with procaspase 12 during ER stress leading to its cleavage and activation. Activated caspase 12 is then translocated to the cytosol where it activates caspase 9 and caspase 3 in a cytochrome c-independent manner (Rao *et al.*, 2002). Indeed, the authors also suggested that BiP can be present as a transmembrane protein within the ER or in the cytosol and can form a complex with caspase 12 and caspase 7 thus preventing their activation upon ER stress. Prolonged ER stress might lead to disruption of the complex and release of active caspase 12 to the cytosol. However, functional caspase 12 is lost in humans due to deletion during evolution, thus other caspases might play a role in apoptosis induced by ER stress such as caspase 8 (Fischer *et al.*, 2002; Momoi, 2004).

Lastly, ER stress also activates pro-apoptotic member of Bcl-2 family such as BAD, BAX and BAK and down-regulates anti-apoptotic like Bcl-2 in mitochondria. This in turn triggers the release of cytochrome c from mitochondria leading to apoptosis.

5.1.2 Rhodopsin and adRP

Rhodopsin is the most abundant protein in photoreceptors, accounting for nearly 30% of the entire proteome of these cells and over 90% of all proteins in the outer segment region (Hargrave, 2001). RHO is critical in phototransduction and is expressed only in rod photoreceptors. RHO is a transmembrane G-protein coupled receptor (348 aa), organized into 7 transmembrane alpha helices connected by six loops of various lengths and contains a binding pocket for light sensitive 11-cis-retinal (Palczewski *et al.*, 2000). Being a transmembrane protein, RHO synthesis occurs in the ER where nascent RHO polypeptide is co-translationally transported to the ER and subjected to post-translational modifications including disulfide bond formation and glycosylation at asparagines-2 and 15 residues with Asn-15 glycosylation being important in signal transduction (Fukuda *et al.*, 1979; Kaushal *et al.*, 1994; Krebs *et al.*, 2004). Once properly folded, RHO exits the ER and undergoes additional sugar modifications within the Golgi from where it is finally transported to the rod photoreceptor outer segment (Liang *et al.*, 1979). In the outer segment, 11-cis-retinal (the aldehyde form of Vitamin A) covalently binds to opsin (the apoprotein of RHO) via a protonated Schiff based at Lysine-296 residue in transmembrane helix VII forming a RHO chromophore. This protonated Schiff base linkage is stabilized by the negatively charged Glu-113 in transmembrane helix III. In addition, many polar or polarisable groups (i.e. Tyr-43, Met-44, Leu-47 in helix I, Thr-94 in helix-II, Phe-293 and Phe-294) surrounding the hydrophobic chain of the retinal chromophore help to ensure correct positioning of the Lysine-296 side chain (Hwa *et al.*, 2001; Janz *et al.*, 2003).

When light strikes RHO, absorption of a photon causes 11-cis-retinal to isomerize to all-trans-retinal which changes the conformation of RHO leading to activation of the G

protein, transducin and downstream signal transduction cascades which causes closure of the cyclic GMP-gated cation channel in the plasma membrane and hyperpolarization of the photoreceptor cell. This process, termed the visual phototransduction cascade, generates an electrical signal and activates the neural circuitry of vision (**Figure 5.3**). After isomerisation and release from the opsin protein, all-trans-retinal is reduced to all-trans-retinol and travels to the RPE for recycling via the visual cycle. During this process, all-trans-retinol is first esterified by lecithin-retinol acyltransferase (LRAT) and converted to 11-cis-retinol by RPE65 and then finally oxidized to 11-cis-retinal before being transported to the rod outer segment where it is covalently linked to an opsin protein to form a new functional RHO molecule.

Mutations in the *RHO* gene are the most common cause of RP and account for ~30-40% of adRP (Dryja *et al.*, 2000; Noorwez *et al.*, 2008). So far, over 120 distinct missense mutations of the RHO gene have been found (http://www.sph.uth.tmc.edu/Retnet/). Some of these mutations cause recessive RP and congenital stationary night blindness; however, the vast majority of them are associated with adRP. Studies of these mutations in cells and transgenic models suggested there are two major types of RHO mutations based on the mechanisms of pathogenesis. Class I mutations often occur in the C-terminus of the protein, resemble wild type RHO (WT RHO) in expression level, have the ability to bind with 11-cis-retinal, and to fold correctly but exhibit impairment in normal targeting to photoreceptor outer segments (Kaushal and Khorana, 1994; Sung *et al.*, 1994; Tam *et al.*, 2000). On the other hand, class II mutants, the most common adRP mutations and characterised by mutations in the intradiscal, transmembrane, and cytoplasmic domains of RHO, have much lower expression levels compared to the WT protein, variable or no ability to bind to 11-cis-retinal and are inefficiently transported to the membrane. This class of mutant also tends to be misfolded and retained within the endoplasmic reticulum (Mendes *et al.*, 2005; Sung *et al.*, 1991). In addition, Mendes *et al.* (2005) proposed four

extra classes of RHO mutations based on different biochemical and cellular defects. Class III mutations include those that affect endocytosis such as R135L (Chuang *et al.*, 2004), while class IV mutations (i.e. T4R mutation in dogs) are thought to affect protein stability and posttranslational modification but do not affect RHO folding (Zhu *et al.*, 2004). Similar to class IV, class V mutations do not seem to affect folding but cause an increase in transducin activation (Andres *et al.*, 2003). Finally, class VI consists of mutations which lead to constitutive activation of opsin in the absent of chromophore and in the dark (**Figure 5.4**).

The first adRP mutation to be identified and a leading cause of adRP in North America is the substitution of proline to histidine at position 23 of the *RHO* gene (P23H RHO) (Dryja *et al.*, 1991). This proline residue at position 23 is highly conserved among vertebrates and invertebrate opsins and in other G protein coupled receptors such as beta-2-adrenergic receptor (Applebury and Hargrave, 1986). This class II mutant is misfolded at the N terminal plug, the binding site for 11-cis-retinal chromophore. Many biochemical studies have demonstrated that P23H mutation induces RHO misfolding. Mutant RHO forms oligomeric aggregates, and instead of being properly glycolysated as WT RHO, P23H RHO is complexed with endoplasmic reticulum chaperones such as BiP or Grp94 (Anukanth and Khorana, 1994; Liu *et al.*, 1996; Noorwez *et al.*, 2004). Furthermore, unlike WT RHO which is translocated to the surface membrane, P23H RHO is localized to the ER/Golgi (Tam and Moritz, 2006). Several studies also suggested that P23H has a dominant negative effect over wild type RHO. For example, co-expression of WT and P23H RHO resulted in the formation of microscopically visible inclusion bodies containing WT RHO and in the disruption of normal trafficking of WT RHO synthesized in the same cell (Illing *et al.*, 2002; Saliba *et al.*, 2002), while the P23H mutant enhanced proteasome mediated degradation of the WT protein (Rajan and Kopito, 2005). The chaperone folding machinery is expected to be highly efficient in photoreceptor cells since

RHO is continuously synthesised in large amount of up to 10^7 molecules per day per photoreceptor. Therefore, accumulation of misfolded P23H RHO in the ER can induce ER stress leading to unfolded protein response (UPR) and ultimately photoreceptor degeneration (Chapple *et al.*, 2001). Indeed, more than 140 RP-linked RHO mutations have been identified and those that result in protein misfolding and ER retention are the most prevalent (Mendes *et al.*, 2005). Li *et al.* (1996) also suggested that most of point mutations in the intradiscal domain linked to adRP lead to either complete or partial misfolding of RHO.

Misfolded P23H RHO is detected by BiP and Grp94 within the ER; whereas DnaJ-containing protein 1B (HSJ1B), a cytoplasmic chaperone, recognizes parts of misfolded protein that face the cytosol (Chapple and Cheetham, 2003). Misfolded RHO also interacts with calnexin, overexpression of which has been shown to promote partial folding of misfolded P23H protein and to reduce degradation via ERAD in the presence of 11-cis-retinal in mammalian cells (Noorwez *et al.*, 2009). In contrast, P23H RHO undergoes the same degeneration as observed in WT RHO in cells exhibiting dysfunctional calnexin suggesting that calnexin might not be required in RHO biogenesis but its upregulation could increase its interaction with P23H RHO (Kosmaoglou and Cheetham, 2008). Moreover, EDEM1 has also been found to interact with P23H RHO, promoting its degradation via ERAD and also enhancing the folding and transportation of P23H RHO (Kosmaoglou *et al.*, 2009).

In addition, P23H RHO also leads to an increase in the chaperone BiP. Expression levels of heat shock cognate protein 3 (Hsc3), the Drosophila BiP homolog, has been shown to increase in transgenic Drosophila expressing the class II mutant rhodopsin1 G69D and P37H (the fly homolog of mammalian P23H RHO), or in flies deficient for ninaA, a chaperone which functions in maturation of fly RHO (Mendes *et al.*, 2009; Ryoo *et al.*, 2007). BiP expression levels also increase in mammalian cells overexpressing P23H RHO

but not WT RHO (Lin *et al.*, 2007). Accumulation of P23H RHO also triggers UPR in the ER (Mendes and Cheetham, 2008). For example, flies expressing P37h rh1 or G69D rh1, or lacking ninaA experiences an increase in Xbp1 splicing (Ryoo and Steller, 2007). Similarly, rats expressing P23H RHO have an increased activation of all three UPR pathways IRE1, PERK and ATF6, culminating in high expression levels of CHOP and caspase 7, critical executioners of UPR-induced apoptosis (Gorbatyuk *et al.*, 2010). Furthermore, these animals also exhibit a decrease in BiP expression level simultaneously with an increase in CHOP expression levels with age; thus implicating prolonged ER stress caused by accumulation of misfolded P23H RHO as the main factor leading to photoreceptor cell death (Lin *et al.*, 2007).

Protein aggregation is also a hallmark of pathology in other diseases of retinal degeneration. For example, mutations in the gene encoding ELOVL4 (elongation of very long chain fatty acids protein 4) have been identified in Stargardt-like macular degeneration. ELOVL4 is a transmembrane protein which functions specifically in photoreceptor lipid biosynthesis and resides within the ER. Similar to P23H RHO, mutant ELOVL4 misfolds and binds to WT ELOVL4 forming aggregates in a dominant negative fashion (Karan *et al.*, 2005; Vasireddy *et al.*, 2005). Mutant ELOVL4 also activates UPR through BiP and CHOP upregulation *in vitro* thus suggesting a possible mechanism for photoreceptor cell death in this disease (Karan *et al.*, 2005). Another example is the *rd1* mutant caused by mutation in cytosolic PDE6-β protein which regulates cGMP levels in photoreceptors in response to light activation which disrupts the function of this protein causing accumulation of cGMP which leads to a significant increase of intracellular calcium and ultimately photoreceptor cell death. Indeed, retinal degeneration in the *rd1* mouse is coupled with an increase in both CHOP and peIF2α (Yang *et al.*, 2007). However, the reason why this mutation appears to activate the UPR in the ER still needs to be elucidated. It might be because ER stress is also triggered by calcium concentration,

thus calcium dysregulation in rd1 or other retinal diseases may cause UPR activation (Lin and Lavail, 2010).

To summarize, these data suggest that a common potential therapy for this type of disease could be developed based on promotion of correct protein folding, inhibition of aggregation and increase of degradation.

5.1.2.1 Current therapeutic strategies for P23H RHO linked RP

There are three main ways to reduce apoptosis due to prolonged ER stress caused by expression of P23H RHO: 1) upstream of ER stress by promoting partial folding and trafficking of misfolded protein; 2) at the level of ER stress sensors by attenuating their activation; 3) downstream of the UPR by manipulating the complex network of different factors that execute the apoptotic signal (Griciuc *et al.*, 2011).

1) Upstream of ER stress

Pharmacological chaperones such as 11-cis-retinal and its isomer 9-cis-retinal have been found to promote correct folding of P23H RHO and improve its ability to bind to retinal and trafficking to the plasma membrane in mammalian cells (Krebs *et al.*, 2010; Noorwez *et al.*, 2004). Moreover, 11-cis-7-ring-retinal, a modified form of retinal that cannot undergo isomerisation upon light exposure has a higher binding affinity for P23H RHO than for WT RHO and increase P23H RHO folding in mammalian cells (Noorwez *et al.*, 2003). Indeed, the retinal precursor vitamin A palmitate has been used as a nutritional supplement for RP patients (Berson *et al.*, 1993b). Although there is no effective cure for RP or any beneficial effects on functional vision such as visual acuity or visual field, this therapy has been shown to delay the rate of retinal degeneration thus slowing progression of the disease in RP patients (Berson *et al.*, 1993b; Shintani *et al.*, 2009). However, potential disadvantages of retinal derivatives are their chemical instability, photolability and the potential toxic effects of their metabolites (such as retinoic acid) on other tissues. The recommended dose of 15000 IU/day in RP patients is far beyond the daily

recommendation of about 5000 IU/day of vitamin A (Berson *et al.*, 1993a). This high dose of vitamin A could be teratogenic and might also cause liver damage and elevated blood lipids in these patients (Shintani *et al.*, 2009). Moreover, 11-cis-retinal was only effective in rescuing P23H and T17M mutations and had little effect on other mutations in the RHO gene (Krebs *et al.*, 2010), which may partially explain the modest clinical efficacy of vitamin A therapy when used in the treatment of a broad range of RP mutations (Berson *et al.*, 1993b).

Recently, retinobenzaldehydes have been developed and they represent a class of more stable RHO ligands with distinct structure and less toxicity compared to retinals. These potential chaperones (CF35Es and CF35EsC) also promote P23H RHO trafficking in HEK293 cells (Ohgane *et al.*, 2010). In a recent high-throughput screen in HEK293 cells, novel pharmacological chaperones such as β-Ionone and NSC45012 have also been found to improve P23H RHO folding to certain extent by occupying the same hydrophobic region of the retinal binding site (Noorwez *et al.*, 2008). Excitingly, the use of natural cytoprotective compounds such as tauroursodeoxycholic acid (TUDCA), curcumin and safranal have been tested recently in rat models of P23H (Fernandez-Sanchez *et al.*, 2012; Fernandez-Sanchez *et al.*, 2011; Vasireddy *et al.*, 2011). These compounds were shown to disrupt protein aggregation, facilitate protein trafficking to the plasma membrane *in vitro* and provide beneficial effects on retinal degeneration in terms of retinal morphology and physiology *in vivo*.

A second strategy to restore ER homeostasis is to target the mutant RHO at the genetic level. Currently, gene therapy for some forms of RP has been successfully used in both animals and humans (Acland *et al.*, 2005; Maguire *et al.*, 2009; Mihelec *et al.*, 2011; Tan *et al.*, 2009). However, therapy for P23H linked RP represents a challenging task due to its autosomal dominant nature. Nevertheless, some groups have developed different methods to tackle this problem. Mutation independent therapies including ribozymes or RNAi are

useful in suppressing both mutant and wild type RHO, whereas gene replacement can be used in parallel to introduce WT RHO cDNA (Farrar *et al.*, 2002). For examples, subretinal injection of AAV2/5 expressing shRNAs targeting both WT and mutant RHO in combination with WT RHO cDNA shows suppression of retinal degeneration in mice expressing P23H RHO (O'Reilly *et al.*, 2007; Palfi *et al.*, 2010). On the other hand, a recent report showed that AAV2/5 delivery of WT RHO alone is sufficient to suppress the disease progression in mice expressing P23H RHO (Mao *et al.*, 2011).

2) At the level of ER stress sensors

As mentioned above, BiP is an important sensor in unfolded protein induced ER stress. Indeed, administration of AAV2/5 expressing BiP has been found to delay retinal degeneration and lead to better ERG measurement in a rat model of P23H (Gorbatyuk *et al.*, 2010). Although, addition of BiP does not seem to promote proper trafficking of P23H to the plasma membrane *in vitro,* it does alleviate ER stress by reducing the production of peIF2α and cleaved ATF6 which are important in the UPR transduction cascade in both *in vivo* and *in vitro.* In addition, BiP also interacted with caspase-12 and pro-apoptotic Bik, and suppressed ER stress induced CHOP regulation *in vivo.*

In addition to BiP and Grp94, calnexin is an important chaperone which functions in quality control of glycoproteins. Noorwez *et al.* (2009) recently demonstrated that upregulation of calnexin in the presence of 11-cis-retinal increased both the efficacy and the accuracy of P23H RHO folding. They also showed that misfolded RHO is a substrate for calnexin expression of which can be upregulated to increase the folding efficacy of misfolded protein.

3) Downstream of ER stress response

IRE1 activation can promote apoptosis via ASK1-JNK signalling and caspase-12 activation. Therefore, suppression of ASK1-JNK signalling by a JNK inhibitor such as

SP600125 might inhibit cell death in retinitis pigmentosa since it has been shown to reduce ganglion cell loss in a rat model of acute glaucoma attack (Sun *et al.*, 2011).

In addition to proteasomal degradation, autophagy also plays an essential role in clearing up protein aggregation. This cellular process can be induced by stimuli toxic to the cell such as aggregation of misfolded protein, accumulation of damaged organelles or amino acid derivation. Indeed, rapamycin targeting the mTOR signalling pathway, has been found to induce autophagy in cells expressing P23H RHO and specifically reduce mutant RHO while leaving the WT protein intact (Kaushal, 2006).

5.1.3 Objectives

It was shown in the previous chapters that subretinal inoculation of AAV2/9 expressing a doxycycline-inducible shRNA targeting transcripts encoding the neuronal vascular endothelial tight junction protein claudin-5 results in iBRB modulation for the period of time during which the inducing agent is administered, providing a means of systemic drug delivery specifically to the retina, avoiding access to the brain. In the context of this chapter, I wish to describe here a minimally invasive therapy for adRP, validated in transgenic rats expressing P23H mutation within the human RHO gene. The rat model used in the experiments has the slowest photoreceptor degeneration rate in three lines of rats created with P23H transgene (Machida *et al.*, 2000). Therefore, they are the most suitable model to study the disease progression which is equivalent to that in humans. In addition, GA and 17-AAG have been shown previously to have a positive effect in reducing insoluble P23H RHO *in vitro* although they did not seem to promote P23H RHO trafficking to the cell membrane or increase the levels of soluble P23H (Mendes and Cheetham, 2008). Administration of 17-AAG enhances P23H folding and reduces the dominant negative effect on WT RHO processing and also decreases protein aggregation in a model of RP10 dominant RP (Tam *et al.*, 2010). On the other hand, 17-DMAG has been shown to be a safer derivative of GA and to inhibit Grp94 (Lawson *et al.*, 1998) (**Figure**

5.5). Therefore, experiments were set out to test the hypothesis that systemic administration of 17-DMAG in conjunction with the CLDN5 AAV2/9 system in rats expressing P23H would lead to inhibition of Grp94 and increased level of BiP which was previously shown to be protective against ER stress-induced apoptosis in the same rat model (Gorbatyuk *et al.*, 2010) (**Figure 5.6**).

5.2 Materials and Methods

5.2.1 Animal and Experimental Groups

Homozygous P23H-3 albino rats were originally sourced from Dr. Matthew LaVail Laboratory, USA (University of San Francisco, School of Medicine; http://www.ucsfeye.net/mlavailRDratmodels.shtml) and bred on-site with wild type albino Wistar rats to produce heterozygous P23H-3 rats at the Ocular Genetics Unit in TCD.

5.2.2 Subretinal and intravitreal AAV injection

Animals were anesthetized by i.p. injection of ketamine (100 mg/kg) and Domitor (100 μg/kg) and later reversed with Antisedan (500 μg/kg). Each eye received a single subretinal injection of 5 μl dose of 5 x 10^{11} vp/ml AAV (Vector Biolabs) to the subretinal space and a retinal detachment induced. Rats were injected with NT AAV2/9 in the left eye and CLDN5 AAV2/9 in the right eye. Rats were subsequently administered doxycycline (2 mg/ml) and 17-DMAG (Selleckchem) at three different concentrations (0.2 mg/kg/day, 2 mg/kg/day or 4 mg/kg/day) in their drinking water.

For intravitreal injection, each rat received a single injection of 5 μl of 17-DMAG (1 mg/ml or 0.2 mg/ml) in the treated eye and saline in the contralateral eye.

5.2.3 Generation of P23H pcDNA3 construct

The human WT RHO sequence was originally cloned into pcDNA3 plasmid **(Figure 5.7)** using EcoRI and HindIII restriction sites. WT RHO pcDNA3 was provided by Dr. Sophia Kiang. Mutagenesis was carried out using QuikChange II site-directed mutagenesis kit as manufacturer's protocol (Agilent Technologies). The P23H mutagenesis primers used were:

Forward: 5'-GTGTGGTACGCAGCCACTTCGAGTACCCAC-3'

Reverse: 5'-GTGGGTACTCGAAGTGGCTGCGTACCACAC-3'

The treated DNA sample was then transformed into XL-1 Blue supercompetent cells and sequenced using CMVF_pcDNA3 forward primer by SourceBioscience. Sequences were viewed using FinchTV software.

5.2.4 QuikChange Site-Directed Mutagenesis

Reactions for both sample and control DNA were set up following the manufacturer's protocol. Sample reaction consisted of 1 µl of WT RHO DNA (20 ng/µl), 5 µl of 10x reaction buffer, 1.263 µl of each forward and reverse primer (100 pmol/µl), 1 µl of dNTP mix, and 39.474 µl dH_2O to a final volume of 50 µl. Sample reaction was prepared in duplicates. Control reaction consisted of 2 µl of pWhitescript template (5 ng/µl), 5 µl of 10x reaction buffer, 1.25 µl of each oligonucleotide control primer #1 and #2 (100 ng/ µl), 1 µl of dNTP mix and 38.5 µl of dH_2O to a final volume of 50 µl. In addition, 1 µl of *PfuTurbo* DNA polymerase (2.5 U/ µl) was then added to each reaction which was later overlaid with 30 µl of mineral oil. Cycling parameters for each reaction were: 95°C for 30 s and 12 cycles of 95°C for 30 s, 55°C for 1 min and 68°C for 3 min 30 s. Subsequently, 1 µl of the *Dpn* I restriction enzyme (10 U/µl) was added below the mineral oil overlay. Each reaction was then mixed gently and thoroughly, centrifuged for 1 min, and incubated at 37°C for 1 h to digest the parental supercoil dsDNA. Later on, 1 µl of treated DNA from each sample and control reaction was transformed into 50 µl aliquots of XL1-Blue supercompetent cells.

5.2.5 Cell culture and cell transfection

Twenty four hours prior to transfection, either 2.4 x 10^5 were plated out in each well of a 12-well plate for RNA studies or 6 x 10^5 cells were plated out in each well of 6-well plate for protein studies. Quantities of plasmid ranging from 400 ng in each of a 12-well plate to 1 ug in each of a six well plate were transfected using Lipofectamine 2000 as outlined by the manufacturer (Invitrogen). Plasmids used were WT RHO pcDNA3, P23H RHO pcDNA3 and empty plasmid pcDNA3.1 (+) (**Figure 5.8**). Five hours post transfection,

media in these plates were changed and either 4 μM 17-DMAG or nuclease-free water was added to each well.

5.2.6 Western blot analyses

Whole cell and nuclear protein lysates were extracted from cultured cells based on a protein isolation protocol previously described in (Aherne *et al.*, 2004). Total retinal tissues were harvested in protein lysis buffer. The homogenate was centrifuged at 13000 rpm for 20 min at 4°C, and the supernatant was removed for western blot analysis. All protein samples were incubated at 95°C for 10 min, or 60°C for 30 min in the case of RHO analysis to ensure separation of different types of RHO oligomers (Vihtelic *et al.*, 1999) Antibodies for Western blots were as follows: rabbit polyclonal against GRP78 BiP (1:1000), rabbit polyclonal anti GRP94 (1:1000), rabbit polyclonal anti eIF2A (phosphor S51) (1:500), mouse monoclonal anti RHO 1D4 (1:1000) (Abcam), rabbit polyclonal anti ATF6α (H-280) (1:500), CHOP/GADD153 (R20) (1:200) (Santa Cruz Biotechnology), mouse monoclonal anti β-actin (1:2000) (Sigma Aldrich). Membranes were washed with TBS and incubated with a secondary anti-rabbit (IgG) antibody with HRP conjugates (1:2500), or anti mouse antibody (1:1000) (Sigma Aldrich). All Western blots were repeated a minimum of three times.

5.2.7 Xbp1 PCR analysis

Total RNA was extracted either from transfected cells using TRIzol reagent (MRC) or tissues using RNeasy Mini Kit (Qiagen) according to manufacturers' protocols (**Sections 2.4.2 and 2.4.3**). PolyA mRNA was reserve-transcribed using the SuperScript® Reverse Transcriptase system (Invitrogen). cDNA was used as a template for PCR amplication across the fragment of the Xbp1 cDNA containing the intron target of IRE1α ribonuclease activity. PCR conditions used for human Xbp1 cDNA were: 95°C for 5 min, 95°C for 1 min, 60°C for 1 min, 72°C for 1 min, 72°C for 5 min with 35 cycles of amplification. PCR products were resolved on a 2.5% agarose gel. Two products observed were a 289 bp band

generated from unspliced Xbp1 and a 263 bp band generated from spliced Xbp1. A minor hybrid amplicon generated when unspliced and spliced Xbp1 annealed together which appeared above the unspliced Xbp1 in the agarose gel.

PCR conditions for rat Xbp1 cDNA were 94°C for 30 s, 57°C for 30 s, 72°C for 30 s, 72°C for 7 min with 35 cycles of amplification. Quantification of the spliced Xbp1 was performed by digestion with Pst1 endonuclease restriction enzyme which is a site unique for unspliced Xbp1 (New England Biolabs). PCR products were resolved on a 2.5% gel and unspliced Xbp1 band is 486 bp while spliced Xbp1 band is 459 bp.

Primers used for Xbp1 PCR reactions (Gorbatyuk *et al.*, 2010; Lin *et al.*, 2007):

Species	Forward (5'-3')	Reverse (5'-3')
Human	TTACGAGAGAAAACTCATGGC	GGGTCCAAGTTGTCCAGAATGC
Rat	AGAGTAGCAGCACAGACTGCGCGAGA	GGAACTAGGTCCTTCTGGGTAGACCT

5.2.8 SuperScript® Reverse Transcriptase system (Invitrogen)

Each mRNA sample was reversed to cDNA by using 2 µl of 10x reversed transcriptase buffer, 0.8 µl of 25x dNTPs, 2 µl of 10x random primers, 1 µl of Multiscribe reverse transcriptase, 4.2 µl of H_2O and 10 µl of RNA (2-200 ng/µl recommended by Invitrogen) to the total of 20 µl per reaction. Reaction conditions were as follows: 25°C for 10 min, 37°C for 120 min, 85°C for 5 min and hold at 4°C.

5.2.9 RT-PCR analysis

Taqman® Gene Expression Assays (Applied Biosystems) were used to measure transcriptional changes in Grp94, BiP, CHOP, Xbp1, Hsp40, Hsp70 and Hsp90. Transcriptional changes for these genes were measured in a StepOne Plus machine (Applied Biosystems), using Taqman® Gene Expression Assays (Applied Biosystems) with the following IDs: Xbp1 (Rn01443523_m1), BiP (Rn00565250_m1 and Hs00946084_g1), Grp94 (Rn01760569_m1 and Hs00427665_g1), CHOP

(Rn00492098_g1 and Hs01090850_m1), Hsp40 (Hs00356730_g1), Hsp70 (Hs00359147_s1), Hsp90 (Hs00743767_sH). All target genes used a FAM reporter. Each well of the 96 well plate was added with 4 μl diluted cDNA (1-100 ng per reaction recommended by Invitrogen), 5 μl Taqman mix, 0.5 μl testing primer and 0.5 μl β-actin primer.

Reaction conditions were as follows: 50°C for 2 min, 95°C for 20 s, [95 °C forl s, 60 °C for 20 s] with 40 cycles of amplification. Transcript levels were standardized using β-actin (Rn00667869_m1, Hs01060665_g1) with a VIC reporter in the same well, and calculated using the ΔΔCT method recommended by Applied Biosystems. Untransfected samples or samples transfected with pcDNA3.1 (+) treated with nuclease-free water were used as controls for the calculation of gene expression in tissue culture samples. Uninjected rats were used as controls.

Human RHO expression levels in HeLa cells were measured by RT-PCR method using QuantiTect®SYBR® Green RT-PCR kit (**Section 2.4.7**). Primers used were as followed:

Name	Forward (5'-3')	Reverse (5'-3')
Human RHO	CTTTCCTGATCTGCTGGGTC	GGCAAAGAACGCTGGGATG
Human β-actin	AGAGCAAGAGAGGCATCC	TCATTGTAGAAGGTGTGGTGCC

5.2.10 MRI

Seven weeks after sub retinal inoculation of AAV2/9, iBRB integrity to the contrasting agent Gd-DTPA (MW = 742 Da) was assessed via MRI using a dedicated small rodent Bruker BioSpec 70/30 magnet system (i.e., 7-T field strength, 30-cm bore diameter) with an actively shielded USR magnet (**Section 2.8.7**).

5.2.11 Therapeutic agent

17-DMAG or also called Alvespimycin was supplied by Selleck Chemicals and reconstitute in deionised water to give a final stock solution of 0.2, 2 or 4 mg/kg/day.

Animals was supplemental with doxycycline (2 mg/ml) (Sigma Aldrich) 2 days/week, doxycycline together with 17-DMAG 1 day/week and 17-DMAG 2 days/week in their drinking water. Animals were given normal drinking water in the remaining two days of the week. On average, an adult rat drinks 10 ml for 100 g body weight. This was used to calculate the volume of drink taken by each rat to ensure the correct dose of 17-DMAG was consumed per animal per day.

Timetable for doxycycline and 17-DMAG treatment:

Date	Mon	Tues	Wed	Thurs	Fri	Sat	Sun
Doxycycline	+	+	+	-	-	-	-
17-DMAG	-	-	+	+	+	-	-

5.2.12 Immunohistochemistry

Cryostat sections (12 μm) were blocked with 5% normal goat serum and 1% triton X-100 in PBS for 20 min at room temperature. Sections were incubated with primary antibodies: mouse monoclonal anti 1D4 RHO (1:1000) (Abcam) and rabbit polyclonal anti claudin-5 (1:500) (Zymed Laboratories) at 4°C overnight. Sections were then incubated with either secondary mouse IgG-Cy3 or secondary rabbit IgG-Cy3 for 2 h at room temperature. All sections were counterstained with DAPI (1:5000) for 30 s. Analysis of all sections was performed using an epifluorescence microscope (Zeiss Axioplan 2, Oberkochen, Germany) and Confocal Microscope (FV1000, Olympus).

5.2.13 Determination of the outer nuclear layer thickness

10x images of 10 retinal sections containing the optic nerve and both the temporal and the nasal ora serrate stained with DAPI were used for measuring the average outer nuclear thickness from each eye. ImageJ software was used to measure the outer nuclear thickness of the retinas at distances of 0.25, 0.5, 0.75, 1, 1.25, 1.5, 1.75, 2, 2.25, 2.5 and 2.75 mm from the optic nerve toward each ora serrata. Each measurement was calculated based on the average thickness of 10 sections per retina.

5.2.14 ERG analysis

Animals were anesthetized by i.p. injection of ketamine (100 mg/kg) and Domitor (100 μg/kg) and later reversed with Antisedan (500 μg/kg). ERG was measured as described in **Section 2.8.4.**

5.2.15 Dose calculation from animal to human

Based on FDA guidelines for drug calculation (http://www.fda.gov/downloads/Drugs/Guidances/UCM078932.pdf) and Reagan-Shaw *et al.* (2008), dose translation from animal dose to human dose was calculated as followed:

$$\text{Human equivalent dose (HED) (mg/kg)} = \text{Animal dose (mg/kg)} \times \frac{\text{Animal } K_m}{\text{Human } K_m}$$

In addition, dose conversion from mg/kg to mg/m^2 was calculated by multiplying mg/kg dose with *Km* factor of the corresponding species as in the following table:

Species	Reference Weight (kg)	Working Weight Range (kg)	K_m factor
Human			
Adult	60	---	37
Child	20	---	25
Rat	0.15	0.080 – 0.270	6
Mouse	0.02	0.011 – 0.034	3

For example, 2 mg/kg in a rat of 0.15 kg is equivalent to 2 x 6 = 12 mg/m^2. Using the K_m factor for the working weight range of rats, the human equivalent dose is 2 x 6/37 = 0.324 mg/kg and 0.324 mg/kg x 37 = 12 mg/m^2 for a 60 kg person.

However, K_m is not constant but changes with weight of animals. Thus, a more accurate method proposed in the FDA guidelines took into account the actual weight of animals using the formula:

$K_m = 100/K \times W^{0.33}$ where K is a value unique to each species (Freireich *et al.*, 1966)

Taking account of the animal weight and given the K value for rats is 9.041, a 0.3 kg rat has a $K_m = (100/9.041) \times 0.3^{0.33} = 7.434$. Thus, 2 mg/kg in a rat of 0.3 kg is equivalent to 2 x 7.434 = 14.868 mg/m^2.

The human equivalent dose is 2 x 7.434 ÷ 37 = 0.402 mg/kg and 0.402 mg/kg x 37 = 14.874 mg/m^2 for a 60 kg person.

Generally, the standard K_m factor is used for animals with weights within the standard working weight range which encompasses the animal weights expected for the majority of studies used to support starting doses in humans. The actual K_m factors calculated for animals within the working weight range are within 20 percent of the standard K_m. Thus, it is important to take into account of the animal weight outside the working weight range to get a more accurate dose calculation.

5.2.16 Statistical analysis

Student's paired *t*-test was performed for all statistical analyses. $P \leq 0.05$ was considered statistically significant. Data were plotted as the average ± SEM. For *in vitro* data, one way ANOVA and Tukey post tests were carried out to compare three treatments at the same time. For *in vivo* data, repeated measures ANOVA and Tukey post tests were used to compare more than two values at the same time. Statistical analyses of densitometric results after MRI were from combined regions of the whole eye and were performed by using ANOVA. GraphPad Prism does not generate exact P values for ANOVA test, thus asterisks were used in these cases (i.e. * $P \leq 0.05$, ** $P < 0.01$, *** $P < 0.001$).

5.3 Results

5.3.1. P23H point mutation and RHO structure

Using two computer based algorithms, the P23H mutant was tested for folding capacity and aggregation hot spots. Interestingly, the wild type human RHO protein (NP_000530.1) does not have an aggregation hotspot at amino acid 23 when tested with the algorithm Aggrescan which predicts aggregation prone segments in protein sequence (Conchillo-Sole *et al.*, 2007). When proline is mutated to histidine, an aggregation hotspot is generated at this position in the RHO sequence. In addition, the program PoPMuSiC version 2.1 was used to predict thermodynamic stability changes upon point mutation P23H in RHO (structure is predicted to be based on 1u19, the protein data bank number of bovine RHO by SWISSMODEL program) (Dehouck *et al.*, 2009). The result of a positive folding free energy change ($\Delta\Delta G$ = 0.11 kcal/mol) suggested that this point mutation creates a destabilizing folding effect in the RHO protein structure (**Figure 5.9**).

5.3.2 Effect of 17-DMAG *in vitro*

5.3.2.1 Effect of 17-DMAG in untransfected cells

Firstly, to assess the effect of 17-DMAG on ER stress responses under normal conditions, HeLa cells treated with 17-DMAG (4 μM) or nuclease-free water were harvested at 2, 4, 8, 12, 16, 20 and 24 h after 17-DMAG administration for RNA analysis. **Figure 5.10** shows time course of expression levels of BiP (A), CHOP (B) and Grp94 (C). In general, 17-DMAG addition led to upregulation of all these ER stress response components as early as 2 h post 17-DMAG treatment compared to control samples. In particular, BiP expression level was significantly increased by 2.15, 4.02 and 3.6-fold at 2, 4, 8 h post 17-DMAG addition in 17-DMAG treat cells compared to control cells (* P = 0.0126, * P = 0.0145 and * P = 0.0156, respectively). Similarly, CHOP expression levels were also significantly higher by 6.41 and 5.97-fold in cells treated with 17-DMAG compared to control cells at 2

and 4 h post 17-DMAG treatment (** P = 0.0023 and * P = 0.0423, respectively). CHOP expression levels then decreased to similar levels as control cells at 8 and 12 h post treatment and statistically increased again at 16, 20, 24 h in 17-DMAG treated cells (** P = 0.0069, * P = 0.0493 and ** P = 0.0073, respectively). On the other hand, BiP expression levels remained similar at 16, 20 and 24 h in treated cells compared to control cells. In contrast to both CHOP and BiP mRNA levels, Grp94 expression levels were higher at most timepoints in 17-DMAG treated cells compared to control cells with significant increases at 16 and 24 h post treatment (* P = 0.0425 and ** P = 0.0075, respectively).

5.3.2.2 Effect of P23H RHO on the UPR

The human WT RHO sequence (NM_000539.3) was previously inserted into pcDNA3 plasmid and was driven by the CMV promoter present in the original pcDNA3 plasmid. Using the WT RHO plasmid, the P23H RHO expressing pcDNA3 plasmid was made and both plasmids were then sequenced by Source BioScience using their commercially available CMVF_pCDNA3 forward primer (**Figure 5.11**).

In order to investigate the effect of P23H RHO in the UPR, HeLa cells were transfected with control plasmid pcDNA3.1 (+), WT RHO and P23H RHO expressing pcDNA3. RNA samples were also isolated from these cells 2, 4, 8, 12, 16, 20 and 24 h post transfection. **Figure 5.12** shows mRNA levels of BiP (A), CHOP (B) and Grp94 (C) in cells transfected with different plasmids at different timepoints. There were no significant differences in mRNA levels of BiP and Grp94 tested between cells transfected with control plasmid and those transfected with WT RHO or P23H RHO. However, compared to control transfected cells, P23H RHO transfected cells exhibited significantly higher expression levels of CHOP 2.58-fold at 16 h post transfection (** $P < 0.01$) while WT RHO transfected cells also had higher levels of CHOP by 1.83-fold at the same timepoint (* $P \leq 0.05$). Given the same RHO expression levels in cells transfected with WT RHO and P23H RHO, this

implies that P23H RHO seems more potent than WT RHO in inducing ER stress (**Figure 5.12D**).

5.3.2.3 17-DMAG alleviates ER stress at mRNA levels

To investigate whether 17-DMAG could alleviate ER stress, HeLa cells were transfected with 400 ng of control plasmid pcDNA 3.1 (+), WT RHO or P23H RHO expressing plasmid pcDNA3 and then treated with 17-DMAG (4 μM) 5 h post transfection. RNA samples were isolated at 2, 4, 8, 12, 16, 20 and 24 h post 17-DMAG treatment and subjected to RT-PCR analysis. **Figure 5.13** shows that cells transfected with control DNA, WT RHO and P23H RHO had similar expression patterns of BiP, CHOP at Grp94 at different timepoints post 17-DMAG treatment when compared to cells treated with control plasmid and nuclease-free water. In fact, no significant differences were observed in levels of BiP, CHOP and Grp94 post transfection at any timepoint. Expression levels of BiP started to increase as early as 4 h and reduced to the normal level 16 h post 17-DMAG treatment in all controls and cells transfected with wild type or mutant RHO (**Figure 5.13A**). The highest fold difference of BiP mRNA level in cells transfected with control DNA and P23H RHO normalized to cells transfected with control DNA and water was observed at 4 h post 17-DMAG treatment; these were 2.95 and 2.37-fold; respectively. However, the highest fold difference (3.5 fold) in cells transfected with WT RHO was observed at 8 h post 17-DMAG treatment. On the other hand, while BiP expression levels remained as similar as the control levels in all samples 2 h post 17-DMAG treatment, CHOP mRNA levels were simultaneouly upregulated post 17-DMAG in all experimental groups compared to control samples (**Figure 5.13B**). The relative fold increase compared to control cells in cells transfected with control DNA, WT RHO and P23H at 2 h post 17-DMAG was 4.47, 5.67 and 3.98; respectively. As BiP expression levels started to increase, CHOP expression levels started to decrease 4 h post 17-DMAG treatment. Fold differences in CHOP expression between 17-DMAG treated and non-treated cells were lowest 8 h post

treatment, even lower than the average CHOP expression level in cells transfected with control DNA and water. In addition, CHOP expression levels increased again at 20 h post 17-DMAG while BiP expression level decreased. Grp94 mRNA expression levels increased from 4 to 24 h post 17-DMAG treatment in all transfected cells (**Figure 5.13C**). Grp94 mRNA levels peaked in cells transfected with WT RHO at 8 h post 17-DMAG treatment (2.59-fold). On the other hand, the highest Grp94 mRNA levels in cells transfected with control DNA and P23H were observed at 12 h post 17-DMAG treatment (2.55 and 2.87-fold higher compared to control samples, respectively).

Figure 5.14 shows expression levels of BiP, CHOP and Grp94 in cells transfected with P23H RHO and treated with either 17-DMAG or nuclease-free water. BiP expression was significantly increased by 2.37-fold in cells treated with 17-DMAG compared to cells treated with water 8 h post treatment (* $P = 0.0247$). In contrast, CHOP expression levels were statistically reduced by 0.68 and 0.52-fold in cells treated with 17-DMAG compared to cells treated with water 12 and 16 h post treatment (* $P = 0.0163$, * $P = 0.0203$; respectively). In addition, Grp94 was significantly higher by 2.14-fold in cells treated with 17-DMAG 12 h post treatment (* $P = 0.0284$). When BiP and Grp94 were upregulated, CHOP was simultaneously downregulated in cells treated with 17-DMAG. Also, expression levels of BiP were only upregulated up to 16 h post 17-DMAG treatment while Grp94 expression level still increased at 20 h post 17-DMAG treatment without being significant.

Similar to cells transfected with P23H RHO, cells transfected with control plasmid or WT RHO showed similar patterns of BiP (**Figure 5.15**), and Grp94 (**Figure 5.17**) expression levels at different timepoints post 17-DMAG treatment. In contrast to cells transfected with P23H RHO, pcDNA3.1 transfected and 17-DMAG treated cells had significantly higher CHOP mRNA levels at 2, 16 and 20 h post treatment compared to control samples (**Figure 5.16**). Similar trends were also observed in cells transfected with WT RHO although no

significant differences in CHOP level were obtained. Thus, a comparison of the data presented in **Figure 5.14** and those from **Figures 5.15, 5.16 and 5.17** may suggest that 17-DMAG alleviates the effect of ER stress under the presence of mutant P23H RHO by upregulating BiP and Grp94 mRNA levels while downregulating CHOP expression levels at certain timepoints post 17-DMAG treatment.

In addition, PCR of cDNA extracted from HeLa cells also showed an increase in Xbp1 mRNA splicing in cells treated with 17-DMAG compared to control cells at 2 and 4 h after 17-DMAG treatment (**Figure 5.18**). There were 3 different amplicons obtained from the PCR reaction including 289 bp (unspliced Xbp1, denoted u), 263 bp (spliced Xbp1, denoted s) and a band amplified from annealing of unspliced and spliced Xbp1 (denoted *). Although Xbp1 mRNA splicing still occurred in all cells transfected with DNA at 8, 12 and 16 h after the control treatment, it was either not observed or present at extremely low levels at those timepoints post 17-DMAG treatment. This might be because increasing levels of BiP and Grp94 due to 17-DMAG treatment may have helped to alleviate ER stress caused by the plasmid DNA transfection. On the other hand, there was no spliced Xbp1 observed at 2 h and 12 h onwards in untransfected cells treated with nuclease-free water.

5.3.2.4 17-DMAG reduces ER stress at protein levels

In order to investigate whether the results observed at the RNA levels would be similar to those at protein levels post 17-DMAG treatment, whole cell and nuclear fractions of proteins were collected at 4, 8, 12, 16, 20 and 24 h post 17-DMAG or water control treatment in cells transfected with P23H RHO. In the whole cell fractions, western blots showed that treatment of 17-DMAG increased expression of BiP and Grp94 at all timepoints post 17-DMAG compared to water control (**Figure 5.19A**). In addition, it was observed that the later the timepoints, the higher the expression of BiP in samples treated with 17-DMAG compared to control. Indeed, densitometry analysis of BiP and Grp94

protein levels showed these proteins were statistically higher in 17-DMAG treated cells compared to non-treated cells (**Figures 5.20A, B**). BiP protein levels were increased by up to 324.89, 267.69, 156.80 and 107.26% at 8, 16, 20 and 24 h post 17-DMAG (* P = 0.0375, * P = 0.0323, * P = 0.0386 and * P = 0.0371; respectively). Furthermore, Grp94 protein level was also significantly higher by 300.34% in cells treated with 17-DMAG 16 h post treatment (* P = 0.027).

However, 17-DMAG appeared to suppress the activation of both PERK and ATF6 pathways by reducing phosphorylation of eIF2α from 8 up to 24 h post treatment and cleavage of ATF6 from 12 up to 24 h post treatment as shown in western blots of whole cell and nuclear fractions; respectively (**Figures 5.19B and 5.21**). Specifically, phosphorylated eIF2α were reduced by 72.26, 80.06 and 81.34% in 17-DMAG treated cells at 16, 20 and 24 h post treatment (** P = 0.0033, * P = 0.0298 and ** P = 0.008; respectively) (**Figure 5.20C**). Likewise, the amount of cleaved ATF6 was statistically lower by up to 83.44% in 17-DMAG treated cells 12 h post treatment (*** P = 0.0002) (**Figure 5.22A**). As a result, CHOP protein levels were also significantly lower by 77.38 and 39.49% in treated cells at 12 and 16 h post 17-DMAG administration (* P = 0.0178 and * P = 0.0478; respectively) (**Figure 5.22B**).

5.3.2.5 17-DMAG reduces aggregation of P23H RHO

HeLa cells were transfected with control DNA, WT RHO and P23H RHO in order to investigate aggregation caused by P23H RHO. Insoluble fractions were obtained from these cells 12, 24, and 48 h post transfection and immune-blotted with 1D4 anti-RHO antibody. The 1D4 RHO antibody used binds exclusively to the C-terminus of the RHO protein; thus eliminating unspecific binding of the antibody to the N-terminus containing the P23H mutation site (MacKenzie *et al.*, 1984; Molday and MacKenzie, 1983). **Figure 5.23** shows a marked increase of RHO protein with time in cells transfected with P23H RHO. There was also some evidence of low RHO protein expression in cells transfected

with WT RHO at 24 and 48 h post transfection. In contrast, no RHO staining was observed in cells transfected with control plasmid.

17-DMAG was then tested for its efficacy in reducing RHO protein levels in the insoluble fractions of cells transfected with DNA and treated with 17-DMAG for 48 h. **Figure 5.24** clearly shows that the amount of RHO protein was greatly decreased in cells transfected with P23H RHO and treated with 17-DMAG. The same result was also observed for the small amount of RHO present in the insoluble fraction in cells transfected with WT RHO.

5.3.2.6 Effect of 17-DMAG on expression levels of Hsp protein in the cytoplasm

Since 17-AAG was mentioned to have an effect on Hsp proteins in the cytoplasm in **Section 4.1.4,** 17-DMAG was also tested for its effect on these heat shock proteins. Indeed, using TaqMan® gene expression assays, **Figure 5.25** demonstrates 17-DMAG greatly increased expression levels of Hsp40, Hsp70 and Hsp90 in untransfected cells and cells transfected with control DNA, WT RHO or P23H RHO with the expression level of Hsp70 being affected the most.

5.3.3 Effect of 17-DMAG *in vivo*

5.3.3.1 Intra-vitreal delivery of 17-DMAG leads to reduction in ER tress in P23H-3 rats

a) RNA levels

In vitro studies suggested that 17-DMAG reduced UPR signalling by upregulating expressions of BiP and Grp94 while downregulating expressions of CHOP, cleaved ATF6, phosphorylated eIF2α and Xbp1 mRNA splicing. The next subject of investigation was to determine the effect of 17-DMAG on ER stress in P23H-3 rats which have been shown to display an age related decline of BiP and an increase of CHOP (Lin *et al.*, 2007) and also have a moderate rate of photoreceptor degeneration which is similar to the disease progression in man (Walsh *et al.*, 2004). Firstly, to optimise the concentration of 17-

DMAG required, two groups of 6 month old rats (n = 5) were intravitreally injected with either 5 µl 17-DMAG (0.2 mg/ml or 1 mg/ml) in the left eye and saline PBS in the right eye. RNA samples were isolated from the retinas of these rats 6 days post injection and TaqMan® gene expression assays were carried out. **Figure 5.26** shows no significant differences in expression levels of BiP, CHOP, Grp94 and Xbp1 when rats were treated with two different concentrations of 17-DMAG. However, Grp94 mRNA levels were statistically higher in eyes injected with 1 mg/ml 17-DMAG compared to control eyes (* P = 0.0132), while this was not observed in eyes injected with 0.2 mg/ml 17-DMAG. In addition, rats did not exhibit any abnormalities in the eye area after injection with the higher dose of 17-DMAG, it was subsequently decided to use 1 mg/ml for 17-DMAG concentration in subsequent experiments.

To investigate a time course study of ER stress response, a group of 6 month old P23H-3 rats were intravitreally injected with 5 µl 17-DMAG (1 mg/ml) in the left eye and saline in the right eye. RNA samples of the retinas were harvested 6 h (n = 4), 24 h (n = 4), 48 h (n = 4) and 6 days (n = 5) post injection. TaqMan® gene expression assays showed that expression levels of BiP, Grp94, CHOP and Xbp1 were significantly upregulated in retinas injected with 17-DMAG compared to control retinas 6 h post injection (**Figures 5.27 and 5.28**). Interestingly, at 6 h post injection, BiP expression levels were 4.34 times higher in retinas injected with 17-DMAG compared to control retinas (** P = 0.006; **Figure 5.27A**). Similarly, the expression levels of Grp94 were increased by 3.13 times (** P = 0.0024; **Figure 5.28A**) while Xbp1 expression levels were 2.07 times higher in retinas injected with 17-DMAG compared to control retinas (* P = 0.017, **Figure 5.28B**). In contrast to the *in vitro* study, CHOP expression levels were increased by 2.08 times in retinas injected with 17-DMAG compared to control retinas in spite of high levels of Grp94 and BiP expressions 6 h post injection (* P = 0.0254) (**Figure 5.27B**). Little effect of 17-DMAG on the expression of these genes was observed after 6 h post injection except for CHOP

mRNA levels which were still significantly higher (1.48 times) in treated retinas compared to control retinas at 24 h post injection (** P = 0.0051, **Figure 5.27B**). On the other hand, BiP, Grp94 and Xbp1 expression levels were either unchanged or greatly reduced in treated retinas compared to control retinas 24, 48 and 6 days post injection. CHOP was also expressed at the same level as in control retinas 48 h and 6 days post 17-DMAG injection. In addition, gel electrophoresis results for Xbp1 mRNA splicing obtained from these rats were inconclusive (**Figure 5.29**). Similar results were also observed in retinal samples collected at 6, 24 and 6 days post injection. Therefore, it was unclear whether there was any difference in Xbp1 splicing level between 17-DMAG and control injected eyes.

b) Protein levels

Protein levels of different UPR signalling pathways were next investigated by western blots. Four month old rats were also intravitreally injected with 5 µl 17-DMAG (1 mg/ml) in the left eye and saline in the right eye. Whole cell fractions were isolated from retinas 12 h (n = 3), 24 h (n = 3) and 48 h (n = 4) post injection. Uninjected retinas were used for extra controls. Western blots show that BiP protein level was increased by up to 77% in retinas treated with 17-DMAG compared to control retinas 24 h post injection (* P = 0.0164) (**Figure 5.30**). However, protein levels of BiP remained the same as in non-treated retinas 12 and 48 h post injection. In contrast, CHOP protein was decreased to a level bordering on statistical significance in treated retinas compared to non-treated retinas 24 h post injection (P = 0.0547) (**Figure 5.31**). In addition, protein levels of Grp94, phosphorylated eIF2α and cleaved ATF6 in treated retinas were similar to those in control retinas 12, 24 and 48 post treatment (**Figures 5.32 and 5.33**).

5.3.3.2 Systemic delivery of 17-DMAG leads to rescue of visual function

Based on the results observed from intravitreal injections of 17-DMAG to the retinas of P23H-3 rats, 17-DMAG appears to have certain effects on the UPR signalling by

increasing BiP and reducing CHOP expression levels, thereby offering some protection from apoptosis in these retinas. However, the potential protective effects obtained by intravitreal injection were somewhat short-lived due to the short half life of 17-DMAG and to the mode of delivery. Therefore, it was of interest to test the efficacy of long-term systemic administration of 17-DMAG using the doxycycline inducible CLDN5 AAV2/9 vector to modulate the iBRB, in protecting photoreceptor structure and function in P23H-3 rats. Given the low molecular weight of 616.75 and its impermeability across the BRB, 17-DMAG is a highly suitable candidate for this systemic delivery approach.

An experimental group of ten 6 month old P23H-3 rats (n = 10) received a subretinal inoculation of 5 µl of 5 x 10^{11} vp/ml of either CLDN5 AAV2/9 in the right eye or NT AAV2/9 in the left eye. These animals were then supplemented with 2 mg/ml doxycycline and 17-DMAG in their drinking water 7 weeks post injection.

Dose 1: 2 mg/kg/day

Based on preclinical studies on 17-DMAG toxicity in rats which suggested the maximum tolerated dose was 2 mg/kg/day via intravenous injection (Glaze *et al.*, 2005) and oral bioavailability was 50% in mice (Egorin *et al.*, 2002), rats were first orally given doxycycline (2 mg/ml) and half of the maximum tolerated dose of 17-DMAG (2 mg/kg/day) in the drinking water 7 weeks after subretinal injection. The treatment regime was as follows: 2 days on doxycycline, 1 day on doxycycline and 17-DMAG, and 2 days on 17-DMAG. The volumes of drink intake were noted at the end of each day to ensure rats were taking the required dose. **Figure 5.34** shows that the b-wave amplitude of the rod photoreceptor response in the eye injected with CLDN5 AAV2/9 was significantly higher by 25.98% compared to contralateral control eyes in 10 animals treated with 2 mg/kg/day 17-DMAG together with doxycycline in drinking water for 5 weeks (* P = 0.0482). In addition, b-wave amplitude of maximum cone and rod response showed a similar trend

with the ERG of the treated eye being statistically elevated by up to 35.69% compared to the control eye (* P = 0.038).

Dose 2: 4 mg/kg/day

The effect of a higher dose of 17-DMAG on the visual function of these animals was then investigated, the same experimental group was given the maximum tolerated dose, 4 mg/kg/day 17-DMAG, suggested by Glaze *et al.* (2005) with doxycycline in drinking water for 4 weeks. Interestingly, all animals had significantly higher b-wave amplitude of rod photoreceptor response by 30.13% in eyes injected with CLDN5 AAV2/9 compared to the control eyes (* P = 0.0224) (**Figure 5.35**). Likewise, b-wave amplitudes of both cone and rod response in the treated eye were increased by up to 32.96% compared to contralateral eyes (* P = 0.0126). In addition, the cone photoreceptor isolated response in treated eyes was also elevated by 31.25% (* P = 0.0174). Since higher doses of 17-DMAG have been complicated with weight loss during preclinical studies, weights of all rats were also measured after each treatment course of 17-DMAG (Glaze *et al.*, 2005). **Table 5.1A** exhibits no significant reduction in weight after rats were treated with 4 mg/kg/day 17-DMAG compared to 2 mg/kg/day 17-DMAG.

Phenotyic analysis of the modulated iRBR in P23H rats

After 9 weeks of ERG monitoring, a series of magnetic resonance imaging (MRI) experiments were carried out to assess the phenotype of the CLDN5 AAV2/9 system. A contrasting agent, Gd-DTPA (742 Da), which does not passively diffuse across the iBRB under normal conditions was used to test for modulation of the iBRB by AAV2/9. Contrast enhanced MRI showed significant extravasation of Gd-DTPA (742 Da) specifically in eyes injected with CLDN5 AAV2/9 compared to contralateral control eyes (**Figure 5.36A**). This extravasation was greatest at the site of subretinal inoculation of CLDN5 AAV2/9. This observation was consistent in all experimental animals (n = 6), the relative intensity of this region when the background intensity from the NT AAV 2/9 injected eye was

subtracted from the CLDN5 AAV2/9 injected eye was significant (** P = 0.0029) (**Figure 5.36C**). In addition, no oedema or abnormalities in the injected retinas was observed.

5.3.3.3 Systemic delivery of 17-DMAG leads to preservation of retina structure

After MRI imaging, rats were euthanized and their eyes were harvested for histological analysis. The outer nuclear thickness (ONL) was measured after DAPI staining. Morphometric analysis of these retinas showed a trend towards a thicker ONL in CLDN5 AAV2/9 injected eyes, especially in the area of its subretinal injection compared to control eyes (**Figure 5.37**). In addition, the differences in ONL thickness were statistically higher in the inoculation region of CLDN5 AAV2/9 at 1, 1.25 and 1.25 mm from the optic nerve by 38.84, 39.69 and 47.73% (* P = 0.049, * P = 0.0429 and * P = 0.0478, respectively). Moreover, significant differences in ONL were also observed in the treated eye compared to the control eye in the opposite region at 2 and 2.75 mm away from the optic nerve by 80.49 and 28.29% (* P = 0.0474 and * P = 0.0282, respectively). On average, the ONL of treated eyes was 1 to 2 rows of photoreceptor thicker than non-treated eyes (**Figure 5.38**). Retinal sections were also stained with RHO and CLDN5 antibodies. Rhodopsin staining shows RHO was localised mainly in the outer segment region with some staining in the ONL of the CLDN5 AAV2/9 injected retina (**Figure 5.39**). However, RHO was present to a much lesser extent and mainly in the inner segment and the ONL region of the NT AAV2/9 injected retina. In addition, **Figure 5.40** shows stark contrast in CLDN5 staining between non-treated and treated eyes. There was a greater amount of CLDN5 staining exhibiting clear structure of microvessels in the NT AAV2/9 injected retina; however, there was patchy staining of CLDN5 without any clear structure in the CLDN5 AAV2/9 injected retina. These results are consistent with the MRI data showing extravasation of the contrasting agent Gd-DTPA in the CLDN5 AAV2/9 injected eyes compared to control eyes (**Figure 5.36**).

5.3.3.4 Minimum dose of 17-DMAG for the systemic approach

Since 17-DMAG would be ideally taken on a regular basis over a long period of time to maintain its effect in patients with RP, a much lower dose of 17-DMAG (0.2 mg/kg/day) was also tested in P23H rats. Six P23H-3 rats were injected with NT AAV2/9 in their left eye and CLDN5 AAV2/9 in their right eye at 1 month old. These rats were then given the 17-DMAG and doxycycline treatment 2 weeks post subretinal injection. Their ERGs were measured every month for up to 4 months post treatment. **Figure 5.41** shows b-wave amplitudes of rod response in both treated and non-treated eyes over the 4 month period with 17-DMAG (0.2 mg/kg/day) treatment. Although the ERG readouts decreased with time in both eyes, no statistical difference was observed between the NT AAV2/9 and CLDN5 AAV2/9 injected eyes at each timepoint (**Figure 5.41A**). Furthermore, ERG readings were significantly reduced by 39.82 and 35.42% in NT AAV2/9 injected eyes and CLDN5 AAV2/9 injected eyes, respectively after 4 months of 17-DMAG treatment compared to 1 month (** $P < 0.01$ and * $P \leq 0.05$, respectively) (**Figure 5.41B).** Moreover, ERG readouts were also steadily reduced in eyes injected with NT AVV2/9 post 2 and 3 months compared to 4 months of 17 DMAG treatment (** $P < 0.01$ and * $P \leq 0.05$, respectively). In addition to rod isolated response, ERG readouts obtained from cone and rod response showed no effect of 17-DMAG to the visual function in eyes injected with CLDN5 AAV2/9 compared to control eyes 4 months post treatment (**Figure 5.42**). Histology analysis of ONL thickness was also carried out for these rats and both treated and control retinas had similar ONL measurements (**Figure 5.43**). Lastly, weights of all rats were also taken every month during 17-DMAG treatment. **Table 5.1B** shows 17-DMAG had no adverse effect on the development of these rats over the period of 4 months. Using repeated measures ANOVA and Tukey post tests, weights of these animals increased significantly with age (*** $P < 0.001$).

5.4 Discussion

As mentioned in **Chapter 4**, protein aggregation has been implicated in many retinopathies and is often linked with the heat shock protein chaperone complex containing Hsp90, Hsp70 and Hsp40 which plays a crucial role in assisting the folding and function of client proteins, many of which are important in cell proliferation and signalling (Workman, 2002). Recently, systemic administration of CLDN5 siRNA together with the therapeutic Hsp90 inhibitor, geldanamycin derived 17-AAG has been reported to offer protection against the dominant negative effect of aggregation of mutant IMPDH1 in the RP10 mouse model (Tam *et al.*, 2010). In addition, BiP, an ER homologue of Hsp70 chaperone has been found to play an important role in the UPR signalling during ER stress. It has been previously shown that BiP mRNA levels were reduced while CHOP mRNA levels were increased in animals undergoing retinal degeneration such as P23H-3 rats, a model of adRP (Lin *et al.*, 2007). Overexpression of BiP in these animals led to the rescue of their visual function and preservation of the retina structure (Gorbatyuk *et al.*, 2010). In addition, geldanamycin was shown to also bind Grp94, the ER homologue of Hsp90 leading to transcriptional upregulation of the ER chaperones including BiP (Chavany *et al.*, 1996; Lawson *et al.*, 1998). Moreover, Mendes and Cheetham (2008) previously showed both geldanamycin and 17-AAG had a positive effect on cell death in cells transfected with P23H RHO reducing inclusion formation, the amount of insoluble P23H RHO, LDH release and caspase 3 activation. In the present study, it was hypothesized that 17-DMAG could have a similar effect as geldanamycin on Grp94 and thus increase expression of BiP thereby providing protection against P23H RHO, a mutation known to cause misfolding of RHO that leads to its retention in the ER. Indeed, a recent quantitative proteomic study suggested that inhibition of Grp94 by 17-DMAG does indeed potentially upregulate BiP protein level (Sharma *et al.*, 2012).

Upon ER stress as a result of accumulation of misfolded protein, three signalling pathways of the unfolded protein response are activated including IRE1, ATF6 and PERK. Activation of the UPR can promote neuronal protection by increasing the efficiency of protein folding and quality control or elicit a degenerative trigger if ER stress is prolonged. Under normal conditions, activity of the three branches of the UPR is blocked due to the binding of BiP at the active sites of these molecules. Once the ER homeostasis is disturbed, BiP is released and the three signalling pathways are activated, all of which are capable of inducing CHOP expression, considered a key factor inducing apoptosis (Oyadomari and Mori, 2004). However, BiP has been shown to also have an important cytoprotective output that could outweigh effects of proapoptotic CHOP, leading to cellular protection (Rutkowski *et al.*, 2006). Misfolded P23H RHO is detected by BiP and Grp94 within the ER (Chapple and Cheetham, 2003). BiP also assists the normal processing of RHO by binding to the RHO intradiscal loops to prevent these domains from aggregating; the absence of BiP led to misfolding of WT RHO to such an extent that ubiquitination was reported to be initiated in the ER (Athanasiou *et al.*, 2012). Although overexpression of BiP does not promote proper folding of the mutant P23H RHO or its trafficking to the cell membrane, BiP has been shown to affect the mobility of mutant RHO and enhance its dislocation into the cytosol for proteasomal degradation (Athanasiou *et al.*, 2012; Gorbatyuk *et al.*, 2010).

In this chapter, the *in vitro* studies showed that P23H RHO did upregulate the UPR response compared to control DNA (**Figure 5.12**) and administration of 17-DMAG induced expressions of both BiP and Grp94 in cells transfected with P23H RHO while concomitantly reducing CHOP mRNA (**Figure 5.14**). Specifically, BiP and Grp94 mRNA levels increased significantly as much as 2.37 and 2.14-fold respectively post 17-DMAG treatment compared to control samples. In contrast, CHOP mRNA levels in 17-DMAG treated samples were statistically reduced by 0.52-fold post 17-DMAG treatment (**Figure**

5.14). Moreover, activation of the IRE1 signalling pathway was also detected by measuring levels of Xbp1 mRNA splicing. Although, Xbp1 mRNA splicing also occurred in control samples transfected with P23H RHO and treated with water at 2 to up to 16 h post control water treatment, the amounts of spliced Xbp1 mRNA were higher in samples treated with 17-DMAG at 2 and 4 h post treatment (**Figure 5.18**). Since IRE1 signalling is also capable of reducing CHOP production, the results observed in this present study indicate that increased activity of IRE1 at the early timepoints post 17-DMAG treatment upregulated Xbp1 splicing leading to production of chaperones and components of ERAD which alleviated ER stress. However, the IRE1 signalling was attenuated at very early timepoints instead of being continually upregulated. This observation is contrary to that reported in previous studies which showed that attenuation of IRE1 signalling by persistent ER stress led to cell death (Lin *et al.*, 2007). Therefore, further experiments are necessary to confirm whether attenuation of IRE1 signalling is necessary to reduce CHOP production in this case.

Similar to mRNA levels, BiP was significantly elevated by up to 325% in treated samples compared to control samples as early as 8 h post 17-DMAG treatment and remained upregulated until the 24 h timepoint (**Figure 5.20A**). Likewise, Grp94 protein was also highly elevated post 17-DMAG treatment with the most significant difference being 300% 16 h post 17-DMAG compared to control (**Figure 5.20B**). Gorbatyuk *et al.* (2010) demonstrated that the increase in BiP protein led to down-regulation of the ATF6 and PERK pathways. Furthermore, it was also shown that PERK signalling persisted much longer than IRE1 and ATF6 signalling pathways under prolonged ER stress (Lin *et al.*, 2007). As a result, this is thought to have led to an imbalanced environment within the ER in which cells were guided towards destruction by other factors such as CHOP production. Herein, suppression in PERK signalling was observed by investigating phophorylated eIF2α protein levels which decreased by over 70-81% at 12 to 24 h post 17-DMAG

treatment (**Figure 5.20C**). Interestingly, the amount of cleaved ATF6, the third arm of the UPR response, was also downregulated by 83% at 12 h post 17-DMAG (**Figure 5.22A**). In brief, *in vitro* studies indicated a link between 17-DMAG and UPR response. Administration of 17-DMAG to cells with accumulation of P23H RHO led to upregulation of BiP and Grp94 thus eventually reducing the activity of three UPR signalling pathways. Specifically, the data obtained here suggested that upregulation of IRE1 signalling was swift but short-lived post 17-DMAG treatment. The results also indicated that the PERK signalling pathway is a major ER stress response affected by 17-DMAG treatment in cells expressing P23H RHO since peIF2α protein levels remained suppressed until 24 h post 17-DMAG. As a result, attenuations of all three UPR signalling pathways led to reduction of CHOP protein levels by up to 77 and 39.5% at 12 and 16 h post 17-DMAG. This result is consistent with studies which have shown that overexpression of BiP attenuates ER stress through suppression of PERK and ATF6 thus downregulates CHOP. For example, elevated BiP was suggested to affect the cleavage of ATF6 upon ER stress by delaying ATF6 translocation to the Golgi via inhibition of Golgi localization signals present in the ATF6 protein (Shen *et al.*, 2002). In addition, BiP attenuated PERK signalling thus reducing CHOP protein levels and protected cells from undergoing apoptosis (Gorbatyuk *et al.*, 2010; Lai *et al.*, 2008). Furthermore, 17-DMAG also led to reduction of insoluble P23H in treated cells compared to non-treated cells at 48 h post 17-DMAG (**Figure 5.24**). A similar result has been obtained in previous work in which the effect of geldanamycin and 17-AAG in a mammalian cell line expressing P23H was studied (Mendes and Cheetham, 2008).

Transgenic P23H rats have been bred to mimic RP found in patients (http://www.ucsfeye.net/mlavailRDratmodels.shtml). Of interest, P23H-3 heterozygous rats which have a single P23H transgene copy and two copies of wild type RHO develop an early onset of retinal degeneration in terms of ERG impairment which begins at 4 weeks

after birth but with minimal change in retinal histology and exhibit a slow rate of photoreceptor dysfunction which is generally consistent with the clinical findings found in patients (Machida *et al.*, 2000). Changes in ERG responses correspond with continuous losses of photoreceptor cells during development and adulthood (Chrysostomou *et al.*, 2009; Yu *et al.*, 2004). In addition, these rats also retain vision for a long period of their lives similar to P23H patients who have significantly better visual acuity and larger ERG amplitudes than patients with other adRP mutations, and may still possess useful vision up to 70 years of age (Berson *et al.*, 1991). Thus, P23H-3 makes the most suitable animal model for the study of this disease in humans compared to other models such as P23H-1 rats which have a much faster rate of retinal degeneration. Moreover, BiP mRNA levels selectively dropped while CHOP mRNA levels concomitantly increased in P23H-3 rats over time compared to wild type rats (Lin *et al.*, 2007) while overexpression of BiP has been shown to protect the degenerating retina in P23H-3 rats (Gorbatyuk *et al.*, 2010), suggesting this model should respond favourably to treatment with 17-DMAG.

In the context of the current study, the efficacy of 17-DMAG was tested in the same model of adRP by first intravitreally injecting a group of P23H-3 rats with 17-DMAG in one eye and saline in the contralateral eye. Originally, two different concentrations of 17-DMAG 0.2 mg/ml and 1 mg/ml were tested with the lower concentration based on a previous study done in the lab (Tam *et al.*, 2010). However, since intravitreal injection with 1 mg/ml and not 0.2 mg/ml 17-DMAG led to a measurable effect on a UPR-associated protein (levels of Grp94 were significantly elevated 6 days post-injection) (**Figure 5.26**), this concentration of 17-DMAG was used in all subsequent intravitreal injections. In contrast to our *in vitro* studies, CHOP mRNA levels did not seem to reduce greatly after the upregulation of Grp94, BiP and Xbp1 splicing in 17-DMAG injected eyes compared to control eyes. On the other hand, western blots showed that BiP protein levels were significantly elevated while CHOP protein levels were reduced in treated eyes compared to non-treated eyes 24 h

post 17-DMAG injection (**Figures 5.30 and 5.31**). In addition, no significant differences were observed for Grp94, cleaved ATF6 and peIF2α protein levels between the treated and control eyes (**Figures 5.32 and 5.33**). The data indicated that 17-DMAG level was not maintained at an optimum level for a necessary period of time to have any effect on the UPR response perhaps due to its short half-life of 24 ± 15 h (Ramanathan *et al.*, 2010) and complications associated with drug administration into the eye as mentioned in **Chapter 1.** Nonetheless, the results demonstrated that 17-DMAG greatly affects BiP levels in the short-term post 17-DMAG treatment, thereby suggesting a positive effect in the UPR response.

The inability of 17-DMAG to diffuse freely across the blood retina barrier together with its low molecular weight of 616.75 Da renders it a suitable candidate for long term systemic administration in tandem with the doxycycline inducible CLDN5 AAV2/9 system which facilitates retinal uptake of drugs of up to 1 kDa in size (Campbell *et al.*, 2011). Thus, employment of this method should help to reduce complications of repetitive intraocular injections of 17-DMAG which would prove necessary in order to produce sustained therapeutic benefit. In order to investigate the long term effect of 17-DMAG in P23H-3 rats, a group of ten 6 month old rats were subretinally injected with CLDN5 AAV2/9 in the right eye and NT AAV2/9 in the contralateral eye. Rats were supplemented with doxycycline (2 mg/ml) in their drinking water to induce barrier modulation and subsequently administered 17-DMAG in their drinking water in a dosing regimen that would reflect a human therapeutic strategy, *i.e.*, 3 days on doxycycline, 3 days on 17-DMAG. Based on a preclinical study on toxicity of 17-DMAG, two different doses of 17-DMAG were used, 2 mg/kg/day for up to 5 weeks and 4 mg/kg/day for up to 4 weeks (Glaze *et al.*, 2005). Electroretinogram results demonstrated 17-DMAG administration led to significant rescue of the visual function in the CLDN5 AAV2/9 injected eyes compared to control eyes (**Figures 5.34 and 5.35**). Specifically, b-wave amplitudes of the rod

isolated response in CLDN5 AAV2/9 injected eyes was statistically higher than those in control eyes by up to ~26 and 30% in the CLDN5 AAV2/9 injected eyes after rats were orally given with 2 mg/kg/day and 4 mg/kg/day 17-DMAG, respectively. Likewise, ERG readouts of mixed cone and rod response were significantly elevated by up to 36 and 33% in the treated eyes after 2 mg/kg/day and 4 mg/kg/day 17-DMAG treatments, respectively. In addition, the cone ERG response was elevated by 31.25% in the treated eye compared to control eyes after 4 mg/kg/day 17-DMAG administration. Cone photoreceptors maintain their integrity for a long time and the onset of cone dysfunction has previously been suggested to be at around P540 (~18 months) in heterozygous P23H-3 rats compared to wild type rats (Chrysostomou *et al.*, 2009). However, our data indicate that despite normal cone abundance and morphology subtle though significant deficits in cone b-wave ERG may occur as early as about P250 (~ 8.3 months) and that these can be negated by 17-DMAG treatment.

17-DMAG administration also led to preservation of the photoreceptor layer which had a greater ONL thickness and an increase in RHO protein in eyes injected with CLDN5 AAV2/9 compared to control eyes, especially in the region of subretinal inoculation of the AAV (**Figures 5.37 and 5.39**). The results obtained from the *in vivo* study were consistent with a previous study which showed localised overexpression of BiP in retinas of P23H-3 rats led to the rescue of the ERG and preservation of retinal structure. (Gorbatyuk *et al.*, 2010). Additionally, since animals were first supplemented with 17-DMAG at 7 months old when extensive photoreceptor cell loss had already occurred in this rat model, it was no surprise that the ONL thickness only differed by 1 to 2 rows of photoreceptors. Undoubtedly, 17-DMAG would offer a better protection if animals were treated at a younger age and for a longer period of time. However, many people with P23H RP already have significant retinal degeneration, thus even at this late stage 17-DMAG treatment may prevent further degeneration and thus help retain vision. Due to insufficient numbers of

animals, the long term effect of 17-DMAG on the three signalling pathways of UPR including IRE1, PERK, and ATF6 could not be determined for this systemic approach. However, *in vitro* data obtained indicated that all three arms of UPR response were downregulated when cells expressing P23H RHO were treated with 17-DMAG.

In an attempt to make this work more clinical relevant, a much lower dose of 17-DMAG (0.2 mg/kg/day) was also tested to see if this had any effect *in vivo*. Thus, one month old rats were injected with CLDN5 AAV2/9 in one eye and NT AAV2/9 in the contralateral eye and administered with doxycycline and 17-DMAG for a period of 4 months. Despite the advantage of a much earlier 17-DMAG treatment, this low dose provided neither functional rescue nor retinal preservation in eyes injected with CLDN5 AAV2/9 compared to control eyes (**Figures 5.41 and 5.43**).

Regarding doses of 17-DMAG used in this study, all calculations were based on guidelines of drug concentration recommended by the FDA (http://www.fda.gov/downloads/Drugs/Guidances/UCM078932.pdf) and Reagan-Shaw *et al.* (2008). Maximum tolerated dose of 17-DMAG was determined to be 12 mg/m^2 per day for 5 days or 60 mg/m^2/week through intravenous administration in rats (Glaze *et al.*, 2005). In addition, 17-DMAG bioavailability was found to be 100% and 50% after intra peritoneal and oral delivery in mice, respectively (Egorin *et al.*, 2002). In this work, rats were given with 0.2, 2 and 4 mg/kg/day of 17-DMAG which worked out to be 1.473, 14.986 and 29.365 mg/m^2 orally per day for 3 days taking account of the animal weight, respectively (**Section 5.2.14** and **Table 5.1**). Since 17-DMAG bioavailability post oral administration is only 50%, it could be argued that these rats were only exposed to 0.737, 7.492 and 14.683 mg/m^2 per day for 3 days every week or 2.211, 22.476 and 44.049 mg/m^2/week. Thus, doses of 17-DMAG used were well under the maximum tolerated dose for rats. Moreover, no mortality, sickness or weight loss was observed in experimental

animals during the study indicating these doses were well tolerated by animals during the long period of treatment.

Hsp90 protein also acts as a chaperone for proteins that are involved in cell signalling, proliferation and survival such as p53, HER-2/neu, raf-1 and Bcr-Abl. Thus, Hsp90 is a popular target for many drug development projects including those of geldanamycin derivatives of which 17-DMAG has proven to be an ideal candidate for Hsp90 inhibition. Currently, 17-DMAG has successfully undergone different Phase I clinical trials either by itself or in combination with trastuzumab testing in patients with advanced solid tumours and acute myeloid leukemia leading to recommendations for the Phase II dose to be 80 mg/m^2 weekly via intravenous infusion (Jhaveri *et al.*, 2012; Lancet *et al.*, 2010; Pacey *et al.*, 2011; Ramanathan *et al.*, 2010). Interestingly, the two efficacious doses used in the present study (2 mg/kg/day and 4 mg/kg/day for 3 days every 4 days) work out to be equivalent to a human dose of 22.478 and 44.048 mg/m^2/week respectively which are much lower than the recommended dose suggested for phase II clinical trials. Additionally, the main difference that sets the present study apart from other studies done on P23H-3 rats is that the treatment targeted a much later stage of the disease which is more clinical relevant to RP patients who suffer from the advanced form of the disease. In contrast, most other studies demonstrated rescue of visual function and preservation of photoreceptor layer after starting the treatment in P23H-3 rats soon after birth such as P15-P21 days old (Fernandez-Sanchez *et al.*, 2012; Fernandez-Sanchez *et al.*, 2011; Gorbatyuk *et al.*, 2010), a scenario which is of little relevance to patients with advanced disease.

In conclusion, data presented here regarding prevention of retinal degeneration in a model of advanced adRP provide proof of principle for transient, localized and inducible delivery of 17-DMAG via modulation of the iBRB following a once-off subretinal injection of CLDN5 AAV2/9. Since 17-DMAG is already approved for clinical trials involving various types of cancer, the technique could, therefore, be used to develop a common

therapy for the treatment of retinopathies and neuropathies which have been associated with ER stress such as diabetic retinopathy, Alzheimer disease, Parkinson's disease.

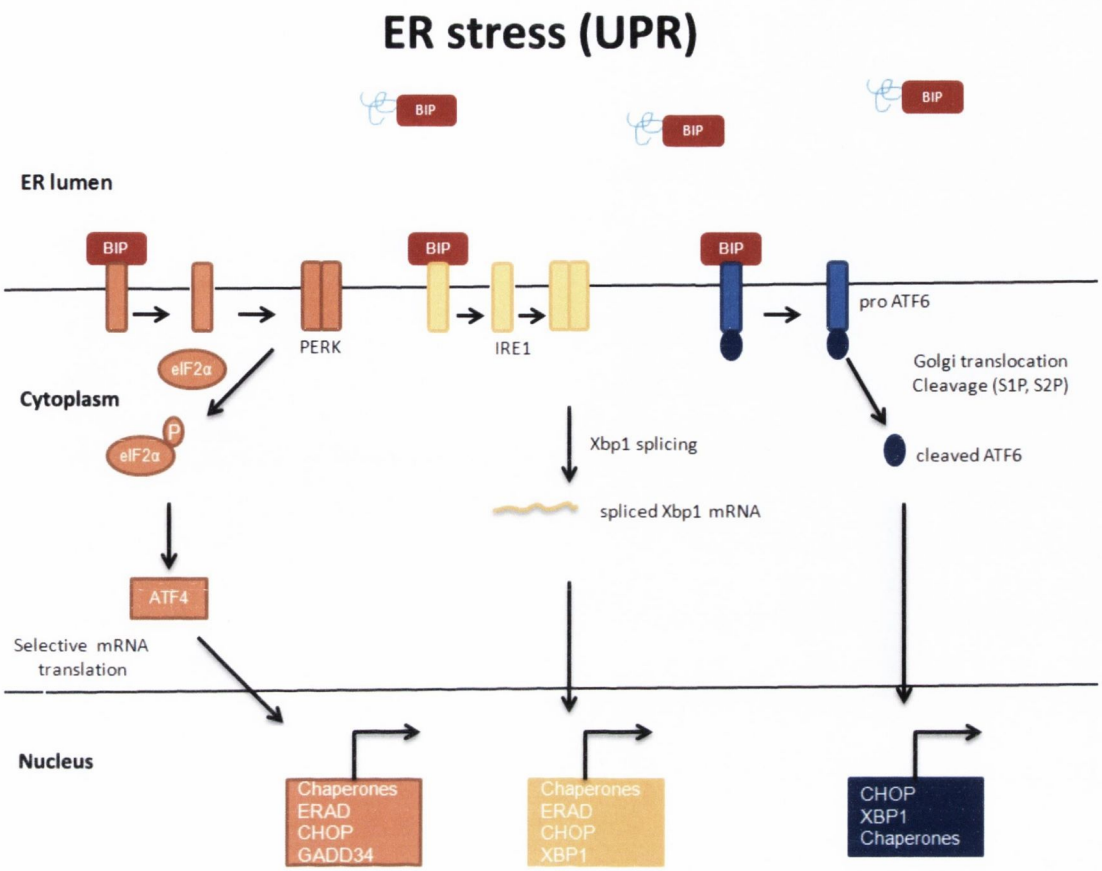

Figure 5. 1: Unfolded protein response (ER stress response).

The ER stress response is mediated by three trans-membrane proteins located in the ER, IRE1, ATF6 and PERK. Under normal conditions, all of these three proteins are bound to BiP thus being inactivated. Upon accumulation of unfolded/misfolded proteins, these proteins become activated after being released from BiP which now binds to unfolded proteins. Dimerization and autophosphorylation of cytoplasmic domains activate PERK which in turn phosphorylates the α subunit of eIF2α, thereby inhibiting its activity and consequently attenuating protein translation which alleviates ER overload. Phosphorylated eIF2α also promotes expression of ATF4 which upregulates chaperones, ERAD machinery and pro-apoptotic proteins such as CHOP and GADD34. Dimerization and autophosphorylation also lead to activation of IRE1 which via its endoribonuclease activity then triggers unconventional splicing of Xbp1 mRNA. Xbp1s then translocates to the nucleus and activates expression of chaperones (e.g. BiP), ERAD-related proteins, Xbp1 and CHOP. In the ATF6 pathway, the disassociation from BiP leads to translocation of ATF6 to the Golgi where it is cleaved by S1P and S2P proteases to become cleaved ATF6 which then upregulates expression of many chaperones such as BIP, Grp94 and PDI, ERAD related proteins and Xbp1 and CHOP.

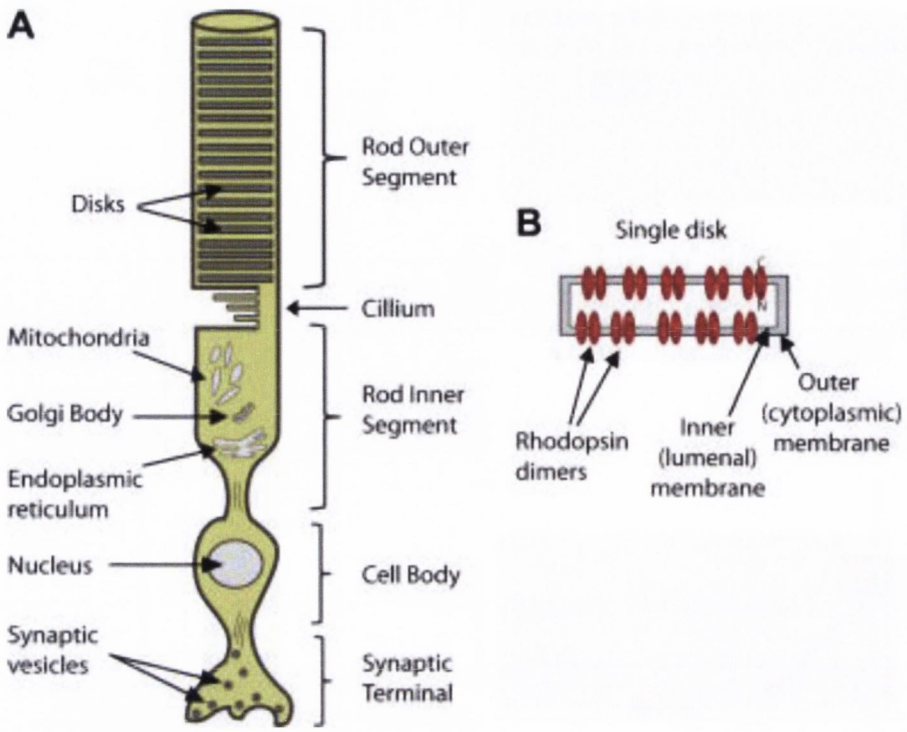

Figure 5. 2: The retinal rod photoreceptor cell.

A) A rod photoreceptor cell with labelled cellular compartments and segments. B) Rhodopsin proteins are folded within the ER in the rod inner segment and then transported to the rod outer segment where they function as rhodopsin dimers in the membrane disks (Jastrzebska *et al.*, 2011).

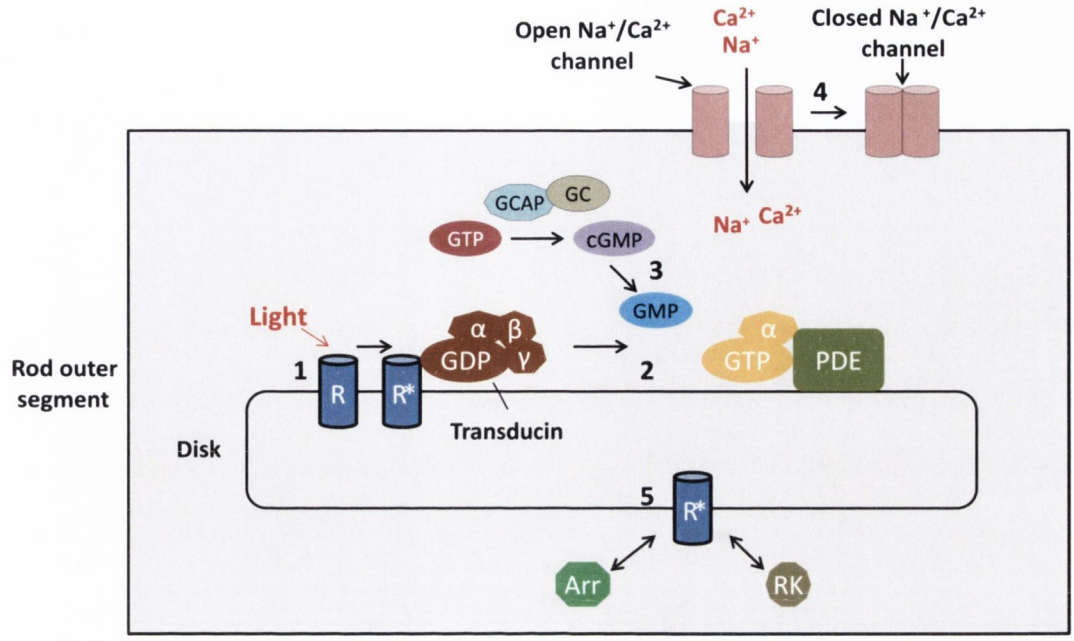

Figure 5. 3: Phototransduction cascade.

When light strikes the retina, 11-cis-retinal undergoes an isomerisation to all-trans form which leads to activation of rhodopsin (R). Activated rhodopsin (R*) interacts with and activates transducin (1). Transducin is a trimeric G-protein consisted of α, β, and γ subunits. Activation of transducin involves the exchange of guanosine diphosphate (GDP) for guanosine triphosphate (GTP), causing disassociation of the α subunit of GTP from the transducin complex and rhodopsin. This activated α-GTP transducin now activates cyclic guanosine monophosphate (cGMP) phosphodiesterase (PDE) (2), leading to the hydrolysis of cGMP to GMP and reduced levels of cGMP in the cytoplasm (3). Decreased levels of cGMP cause the closing of cGMP-gated ion (Na^+/Ca^{2+}) channels which then leads to a decrease in intracellular cations and consequently membrane hyperpolarization (4). The decrease in cation levels also activates guanylate cyclase activating protein (GCAP) which in turn activates guanylate cyclase (GC) and regeneration of cGMP to ensure the continuity of the cycle. Termination of the phototransduction cascade can be regulated by several mechanisms (5). Inactivation of rhodopsin occurs through phosphorylation of rhodopsin kinase (RK) which induces the binding of arrestin (Arr) to inactivated rhodopsin. This in turn prevents the interaction of rhodopsin with transducin, reduces activity of PDE and cGMP levels leading to the opening of the cGMP gated ion channels. This step initiates the recycling process of the chomophore allowing 11-cis-retinal to bind to inactivated rhodopsin and begin the cascade again.

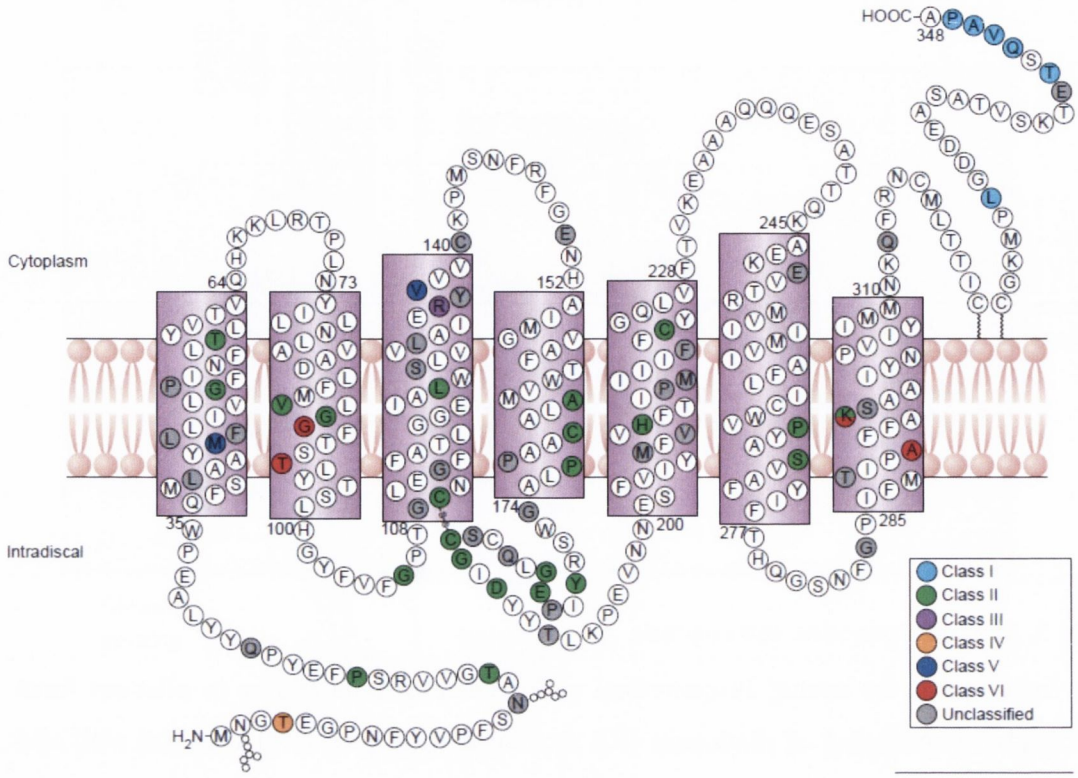

Figure 5. 4: Mutations found in the RHO protein.

Secondary structure of rhodopsin shows point mutations which are categorized into 6 different classes of mutations. Known mutations with no observed biochemical/ cellular defect or not studied in detail are shown as unclassified. A majority of these mutations belong to class II and are present in the intradiscal, transmembrane and cytoplasmic domains of rhodopsin, class I mutations are present predominantly in the C-terminus. Figure was obtained from Mendes *et al.*, (2005).

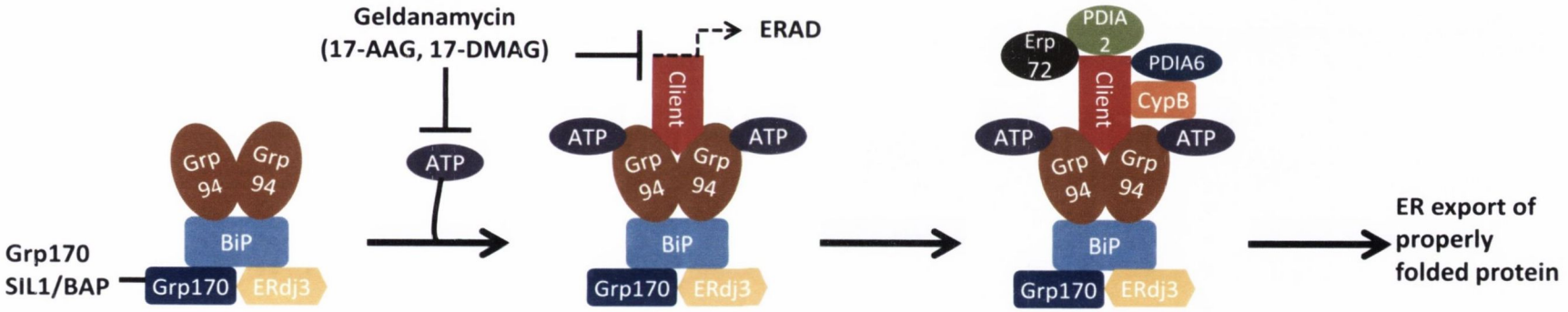

Figure 5. 5: The BiP/Grp94 chaperone system

BiP/Grp94 system is in a large multi-protein complex with a set of ER chaperones including PDI, Erp72, Grp170/ORP150, Sil1/BAP, Hsp40 co-chaperones (ERdj3), cyclophilin B which together form an ER chaperone network processing the unfolded protein. Grp94, BiP and Grp170 have been shown to be present as a pre-existing complex prior to client binding. ER resident Hsp40 co-chaperone, ERdj3 catalyzes the hydrolysis of ATP to ADP thus leading to the binding of BiP to the client. On the other hand, nucleotide exchange proteins associated with BiP, BAP/Sil1, and Grp170 induce ADP release and exchange for ATP leading to the client release. Co-chaperones of Grp94 are not yet known. Presence of client proteins and addition of ATP activate Grp94 and recruit other proteins associated with this complex to properly fold client proteins which are then exported out of the ER. However, addition of geldanamycin inhibits Grp94 ATP binding and thus its association with client proteins leading to their proteasomal degradation via ERAD. Figure was adapted from McLaughlin and Vandenbroeck (2011).

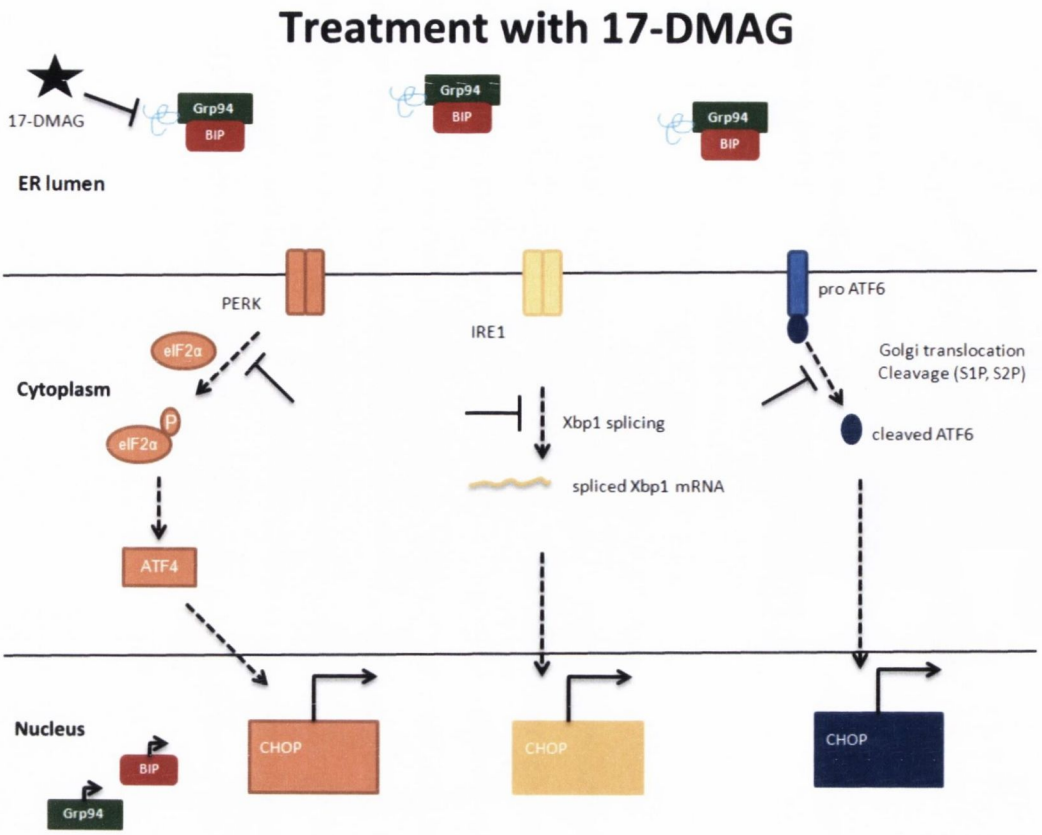

Figure 5. 6: Effect of 17-DMAG in ER stress.

Addition of 17-DMAG leads to upregulation of Grp94 and BiP levels which in turn suppress all three UPR pathways. As a result, expression levels of phosphorylated eIF2α, spliced Xbp1, and cleaved ATF6 are reduced. Thus, CHOP expression is attenuated and ER stress is relieved.

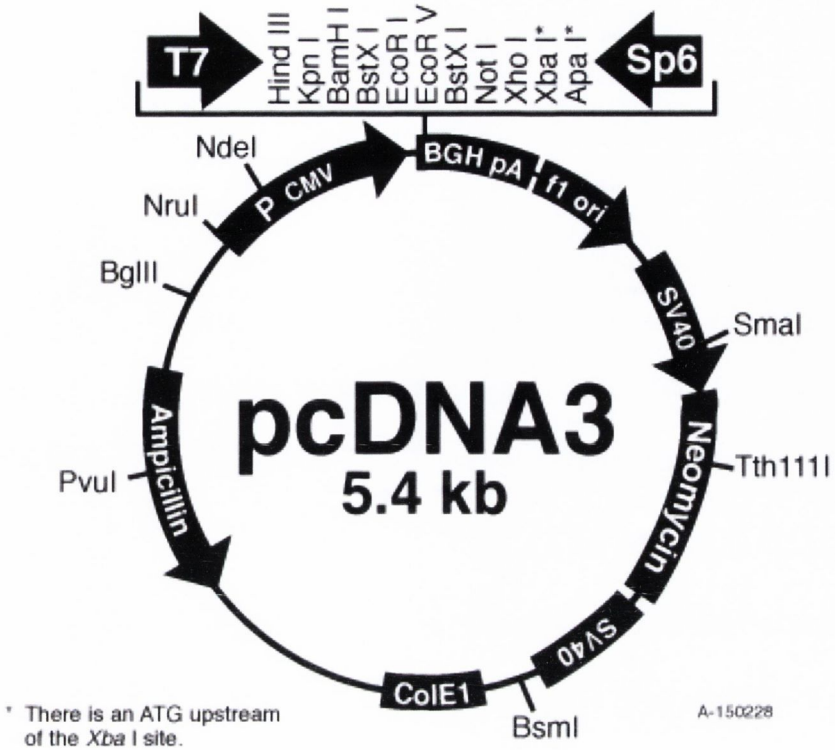

Figure 5. 7: pcDNA3 vector

Map of the pcDNA3 construct illustrating the main restriction enzyme sites (Invitrogen).

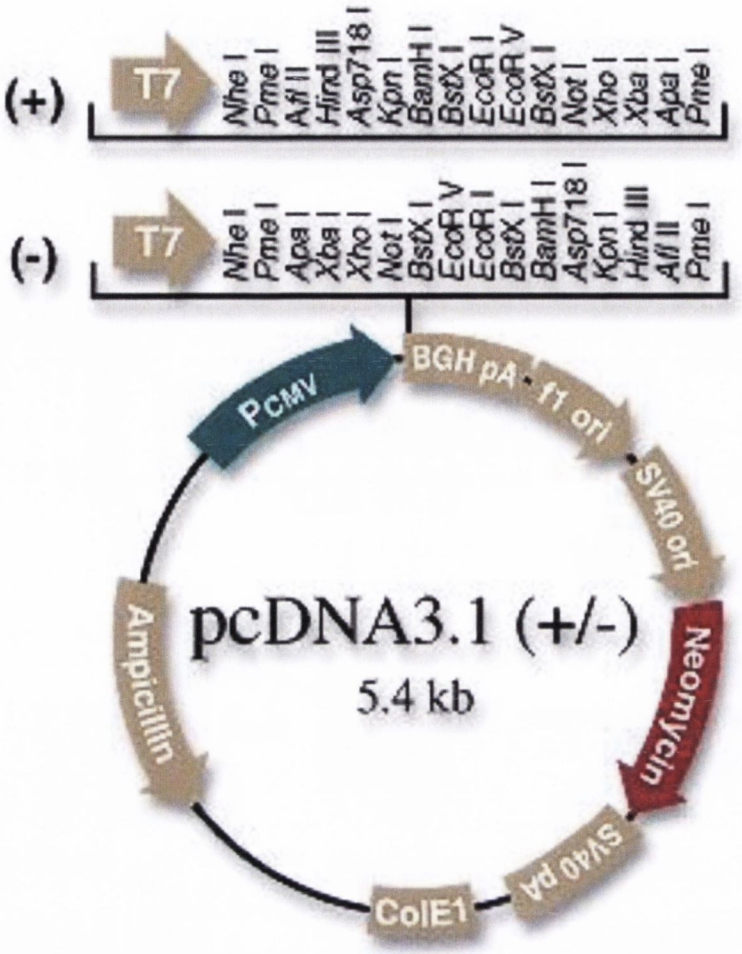

Figure 5. 8: pcDNA3.1 (+/-) vector

Map of the pcDNA3 construct illustrating the main restriction enzyme sites (Invitrogen).

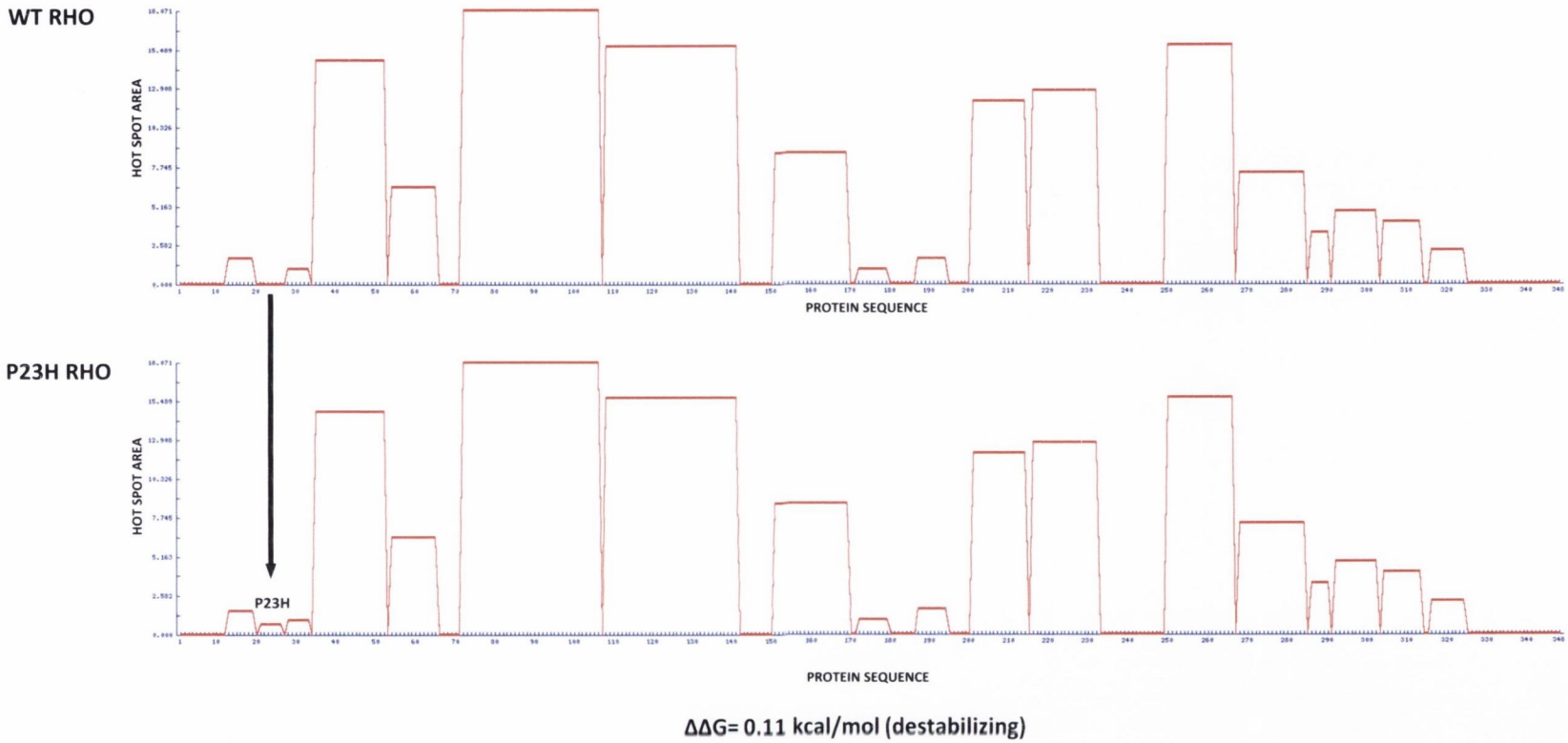

Figure 5. 9: Aggregation hotspots of human WT RHO and P23H RHO protein sequences.

There are 17 aggregation hotspots present in the protein sequence of WT RHO; however, the point mutation at position 23 creates an extra hotspot at that position in the P23H RHO sequence. Also, this mutation leads to a destabilizing energy of 0.11 kcal/mol which makes the protein unstable.

A)

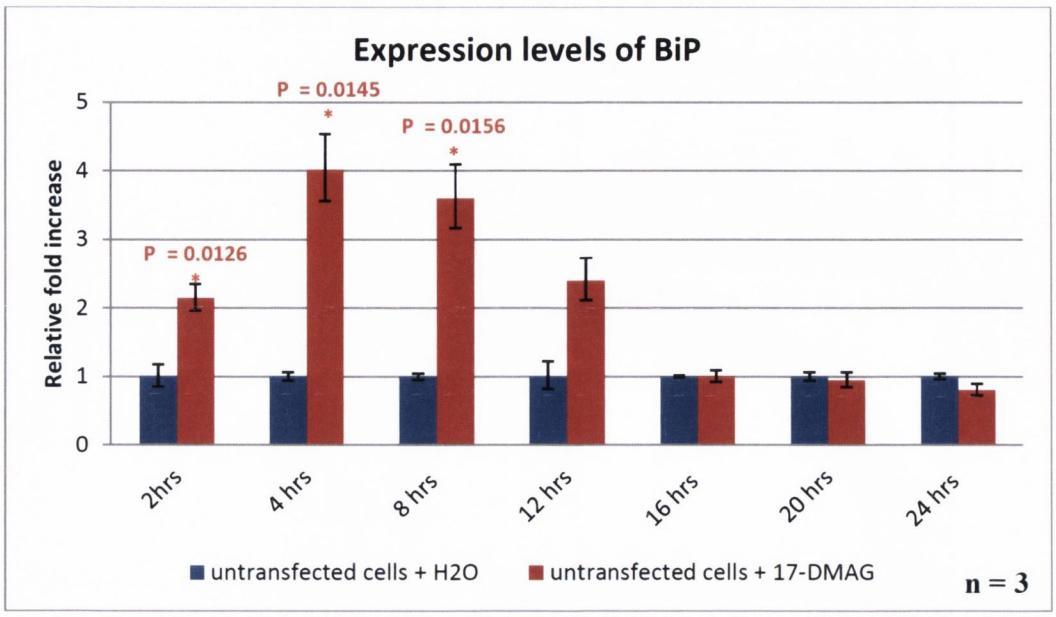

B)

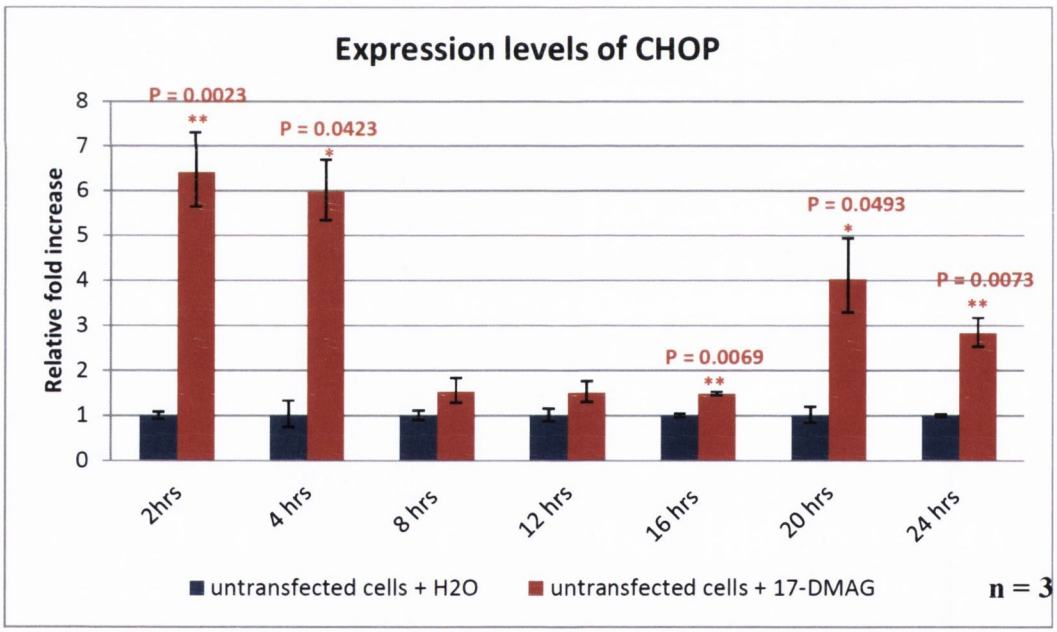

Figure 5.10

C)

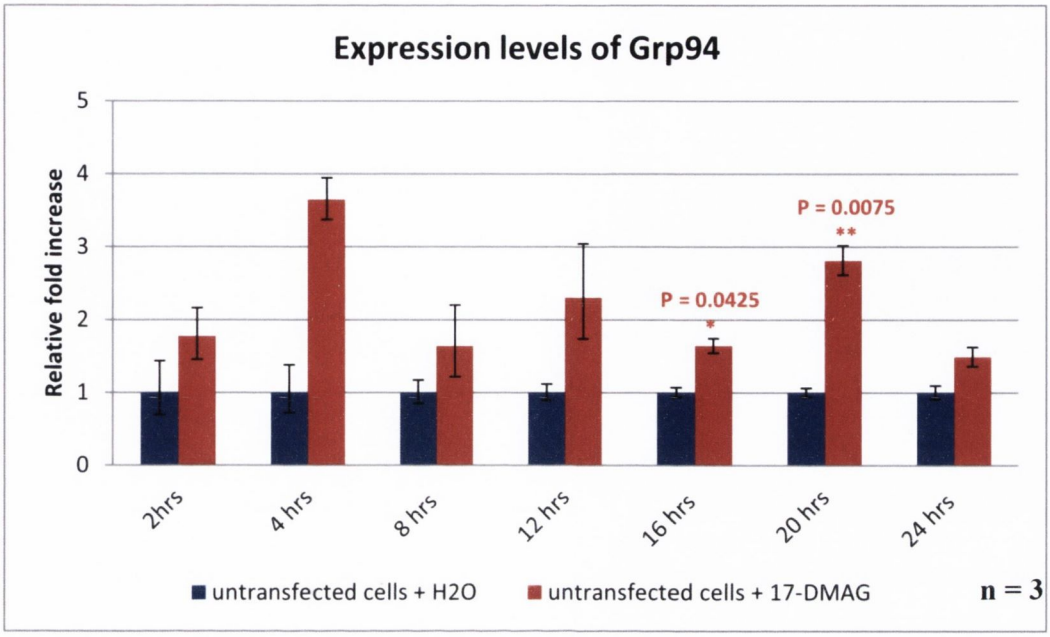

Figure 5. 10: Effect of 17-DMAG on untransfected cells.

Time course analyses of levels of BiP (A), CHOP (B) and Grp94 (C) mRNA in Hela cells treated with 4 μM 17-DMAG or nuclease free water. Untransfected cells treated with nuclease free water were used as the control for ΔΔCt method. Error bars denote ± SEM. All experiments were repeated three times. Administration of 17-DMAG significantly increased A) BiP mRNA levels 2, 4 and 8 h post treatment (* P = 0.0126, * P = 0.0145 and * P = 0.0156, respectively) B) CHOP mRNA levels at 2, 4, 16, 20 and 24 h post treatment (** P = 0.0023, * P = 0.0423, ** P = 0.0069, * P = 0.0493 and ** P = 0.0073, respectively) and C) Grp94 mRNA levels 16 and 20 h post treatment (* P = 0.0425 and ** P = 0.0075, respectively).

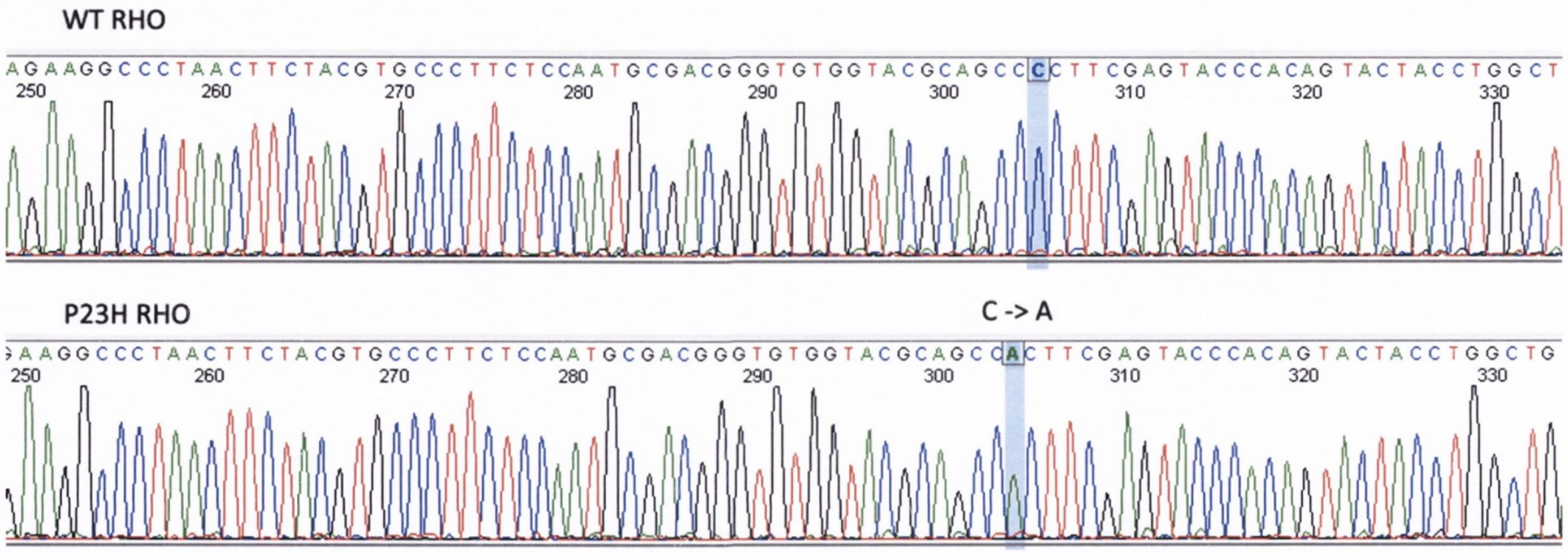

Figure 5. 11: Sequence analysis of WT RHO pcDNA3 and P23H RHO pcDNA3.

Both DNA plasmids were sequenced by Source BioScience using their CMVF_pCDNA3 forward primer. Note the point mutation from C to A nucleotide (labelled blue) in the P23H RHO expressing pcDNA3 plasmid.

A)

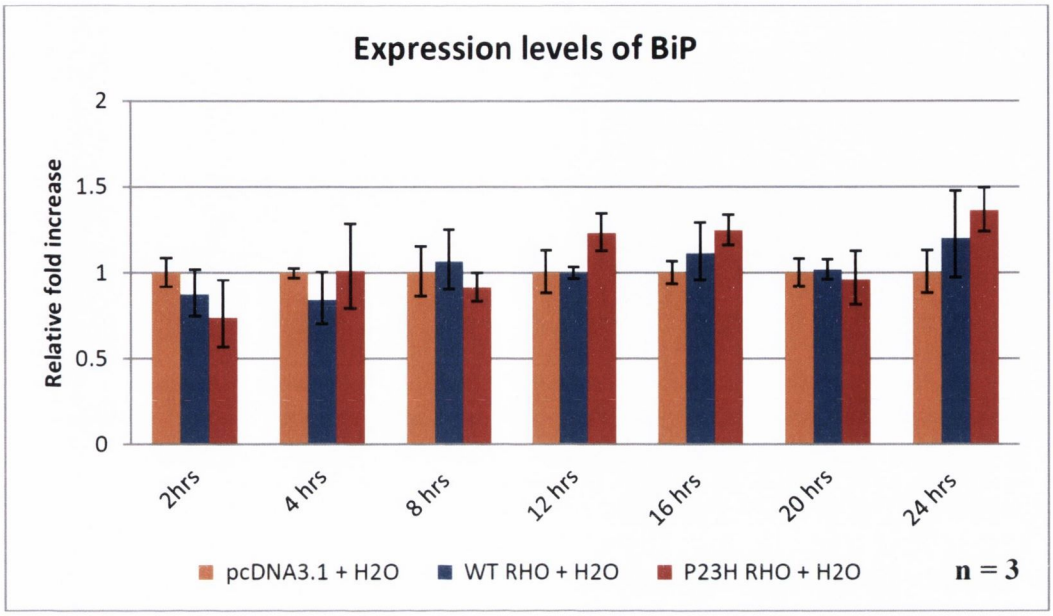

B)

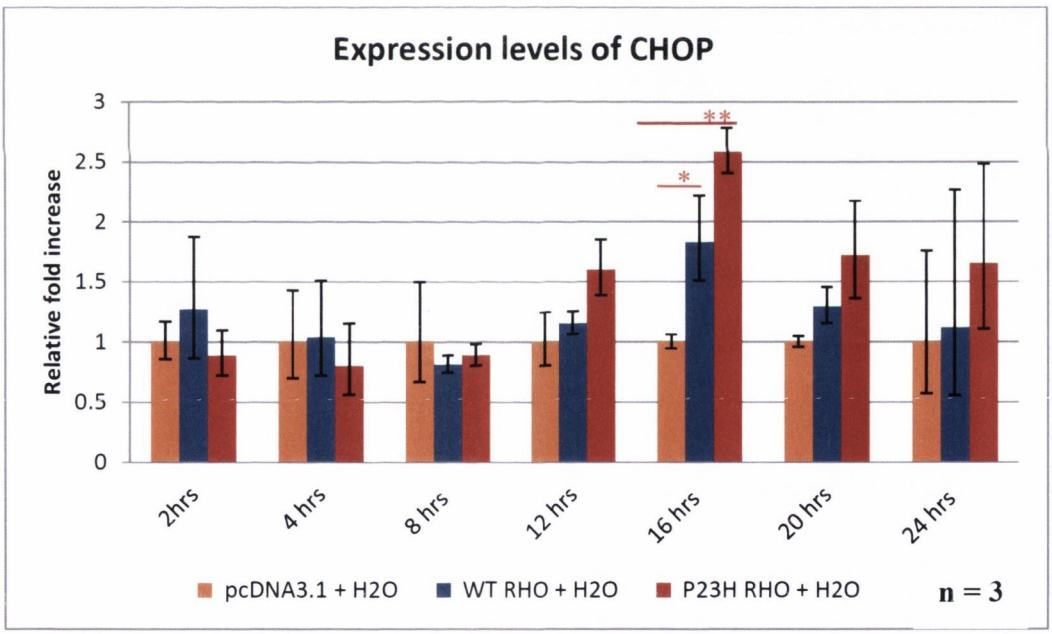

Figure 5.12 ➡

C)

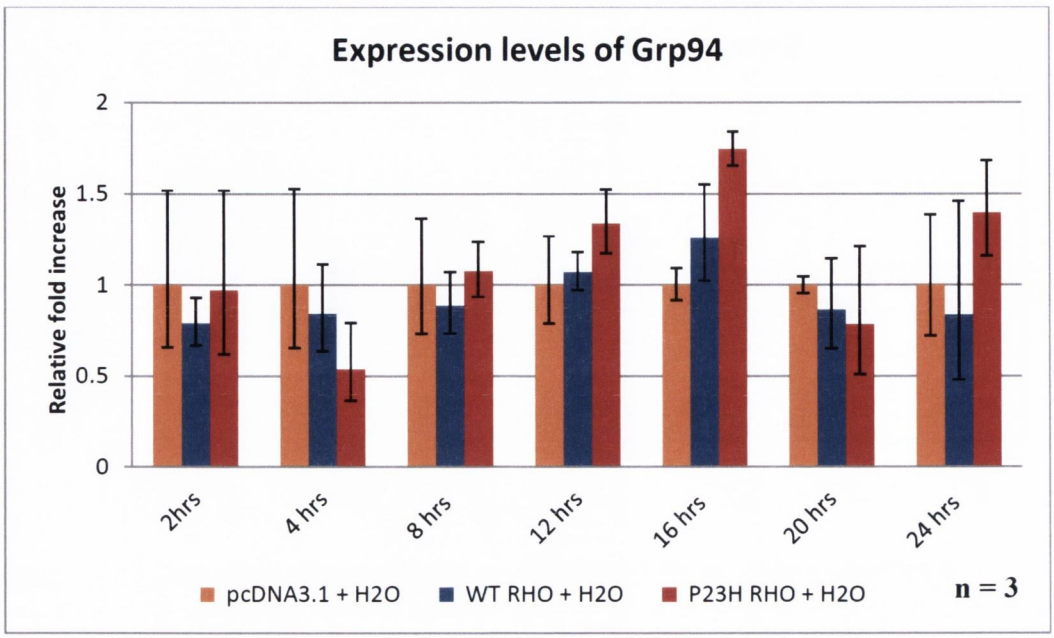

D)

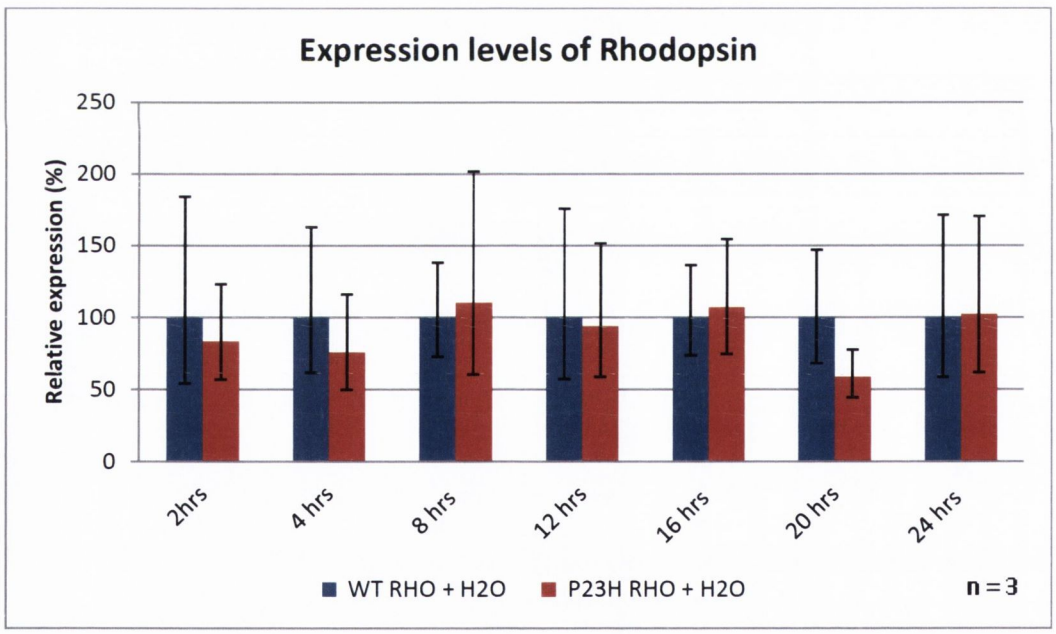

Figure 5. 12: Effect of P23H RHO on ER stress.

Time course analyses of BiP (A), CHOP (B) and Grp94 (C) mRNA levels extracted from HeLa cells which were transfected with 400 ng control plasmid, WT RHO or P23H RHO. Cells transfected with control DNA were used as control samples for ΔΔCt calculation method. All experiments were repeated three times. Error bars denote ± SEM. In general, there were no significant differences in ER stress levels between cells transfected with

control DNA and those with WT RHO, or cells transfected with WT RHO and those with P23H RHO. However B) Using one way ANOVA and Tukey post tests, CHOP mRNA levels were significantly higher in cells transfect with P23H RHO or WT RHO compared to control cells at 16 h (** $P < 0.01$, * $P \leq 0.05$, respectively). D) Rhodopsin expression levels were similar between cells transfected with P23H RHO and WT RHO at all timepoints.

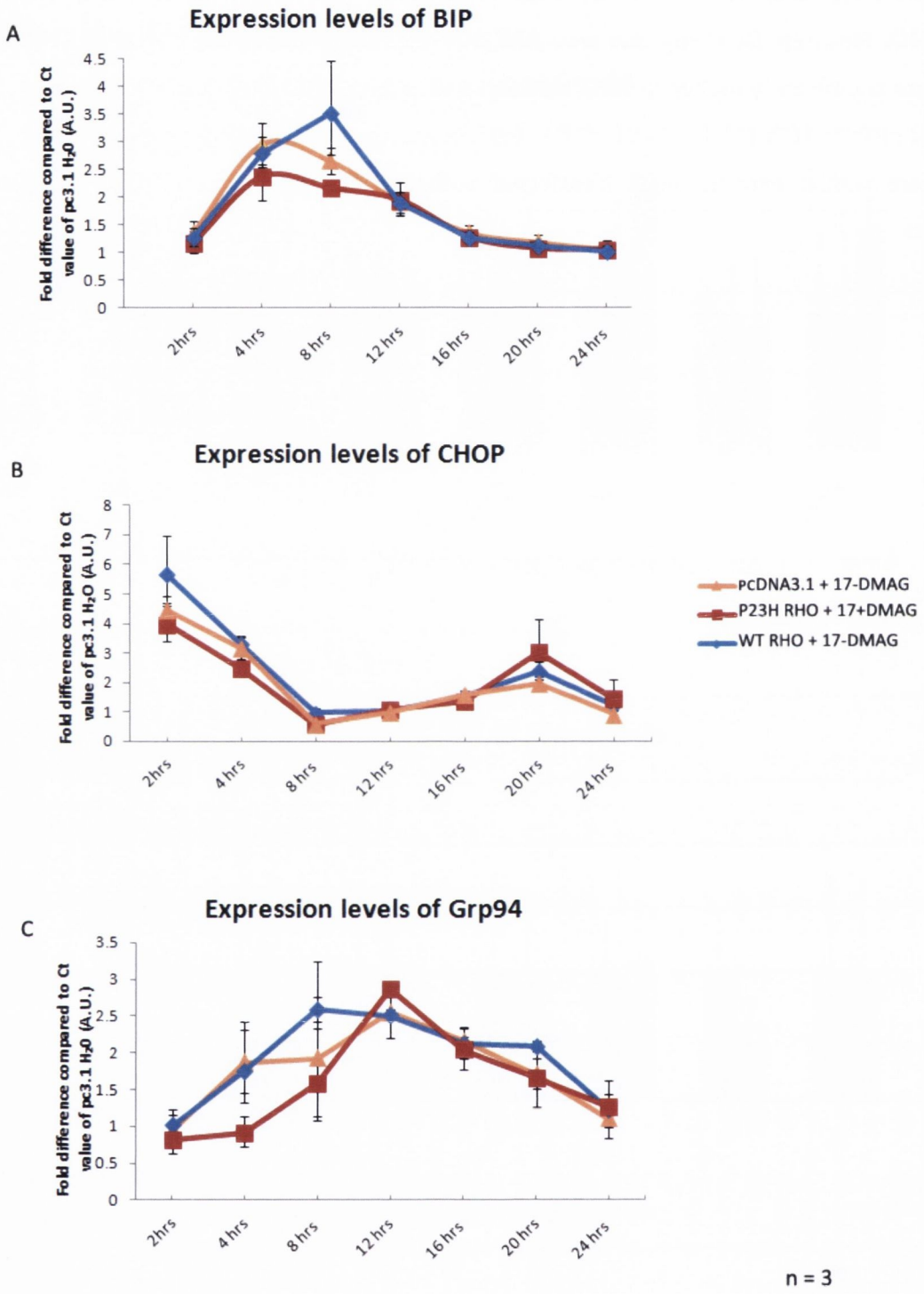

Figure 5. 13: Effect of 17-DMAG on ER stress in cells transfected with plasmid DNAs.

TaqMan® gene expression assay analyses of BiP (A), CHOP (B) and Grp94 (C) mRNA levels extracted from HeLa cells which were transfected with control DNA, WT RHO or P23H RHO and then treated with 17-DMAG 5 h later. Cells transfected with control DNA and treated with nuclease water were used as control samples for ΔΔCt calculation method.

All experiments were repeated three times. Error bars denote ± SEM. In general, these cells had similar patterns in expression profiles of BiP, Grp94 and CHOP. No significant differences were observed in levels of BiP, CHOP and Grp94 post transfection at any timepoint.

A)

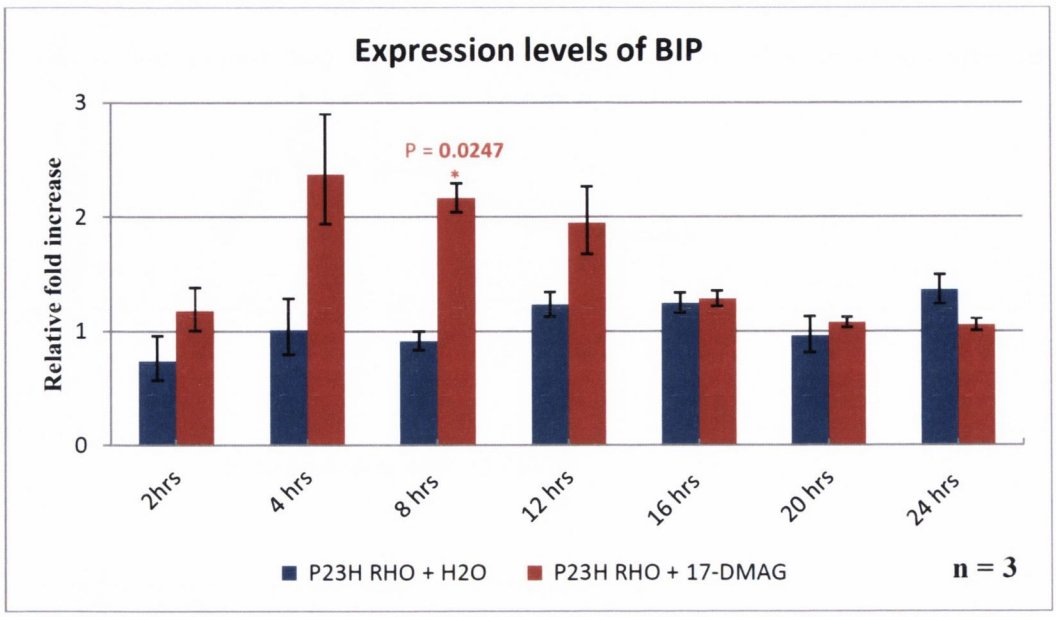

B)

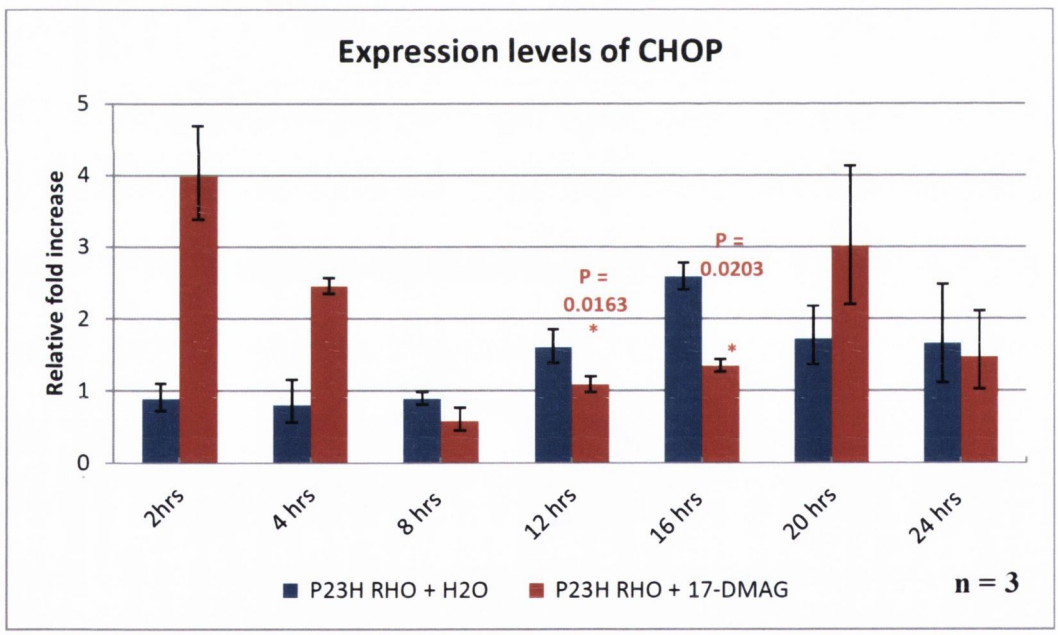

Figure 5.14

C)

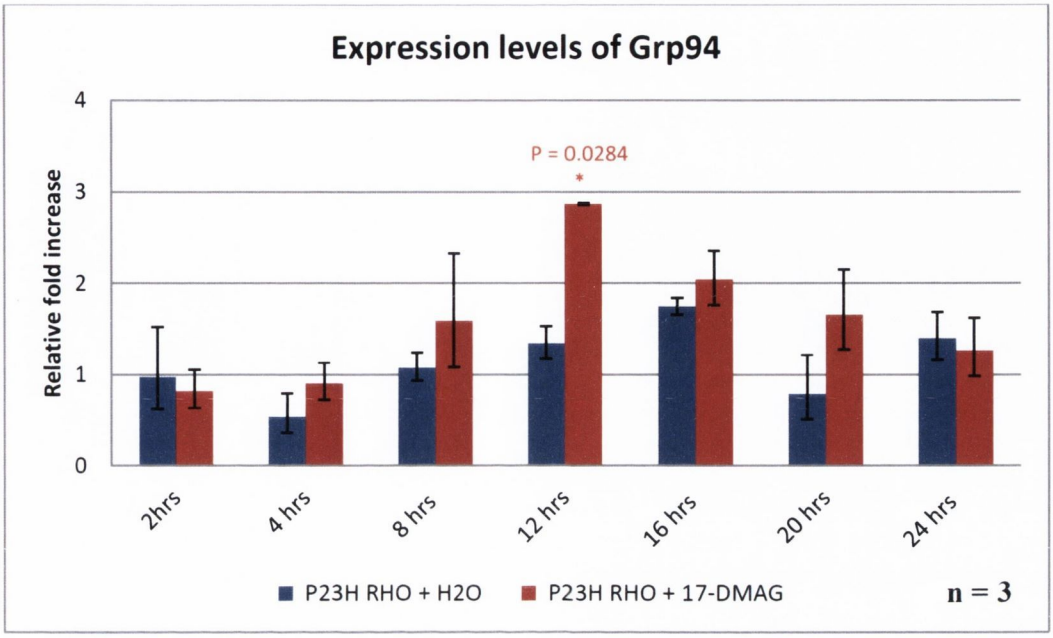

Figure 5. 14: 17-DMAG treatment in cells transfected with P23H RHO.

Cells were transfected with P23H RHO and treated with 4 μM 17-DMAG or nuclease free water for controls. mRNA levels were normalized against cells transfected with control DNA and nuclease free water. Error bars denote ± SEM. A) The graph shows a trend of BiP mRNA increasing from 4 to 12 h post 17-DMAG treatment in treated cells compared to control cells. BiP mRNA levels were significantly increased in treated cells compared to non-treated cells 8 h post 17-DMAG treatment (* P = 0.0247). B) CHOP mRNA levels first increased in treated cells compared to non-treated cells at 2 and 4 h post 17-DMAG treatment. CHOP then decreased when BiP and Grp94 mRNA levels started to increased. CHOP mRNA levels were significant lower in treated cells compared to non-treated cells at 12 and 16 h post 17-DMAG treatment. (* P = 0.0163 and * P = 0.0203, respectively). C) Similar to BiP mRNA levels, Grp94 mRNA levels started to increase in treated cells compared to non-treated cells 4 h post 17-DMAG treatment. At 12 h post 17-DMAG, Grp94 mRNA levels were significantly higher in cells treated with 17-DMAG compared to control cells (* P= 0.0284).

A)

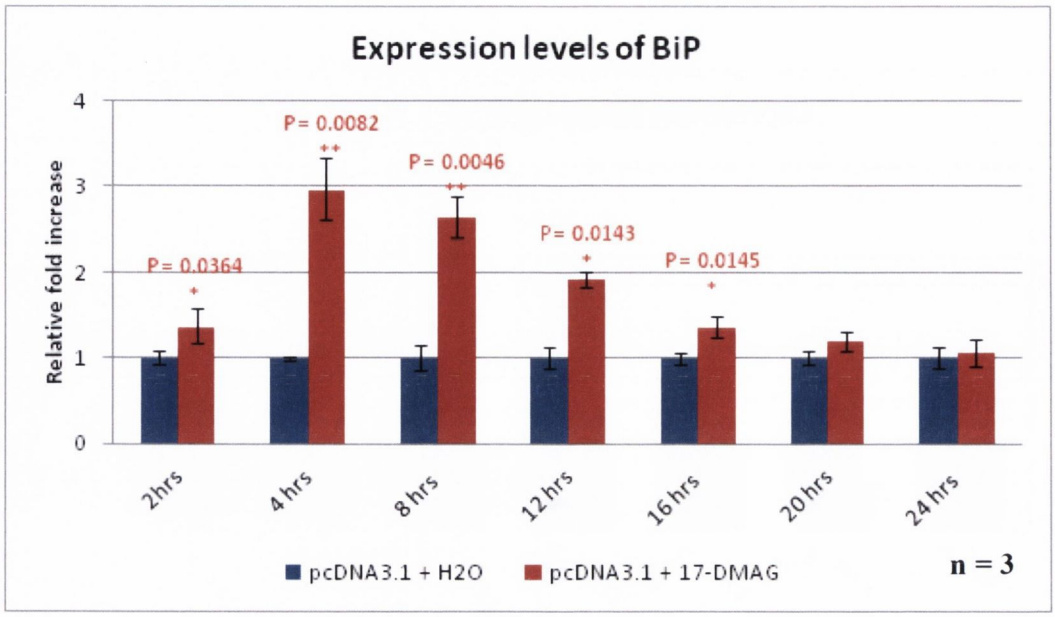

B)

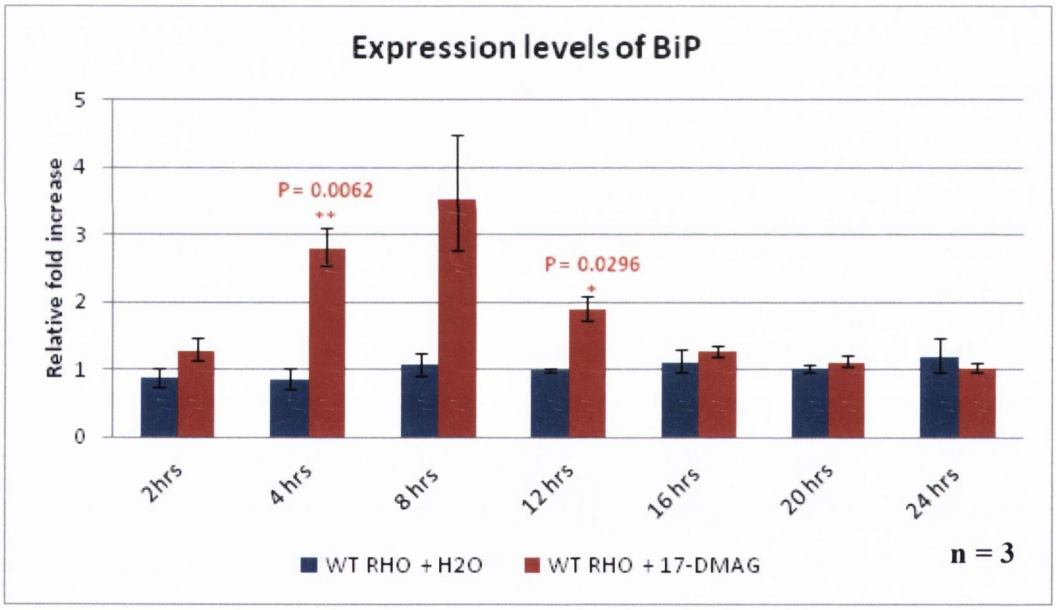

Figure 5. 15: 17-DMAG treatment and BiP expression levels in cells transfected with control DNA and WT RHO.

Cells were transfected with either control plasmid or WT RHO and then treated with 4 μM 17-DMAG or nuclease free water 5 h post transfection. A) BiP expression levels were significantly increased in pcDNA3.1(+) transfected cells treated with 17-DMAG at 2, 4, 8, 12, 16 h post 17-DMAG treatment (* P = 0.0364, ** P = 0.0082, ** P = 0.0046, * P = 0.0143, and * P = 0.0145, respectively). B) BiP expression levels were significantly increased in WT RHO transfected cells treated 17-DMAG compared to control cells

treated with nuclease free water 4 and 12 h post 17-DMAG treatment (** P = 0.0062 and * P = 0.0296, respectively).

A)

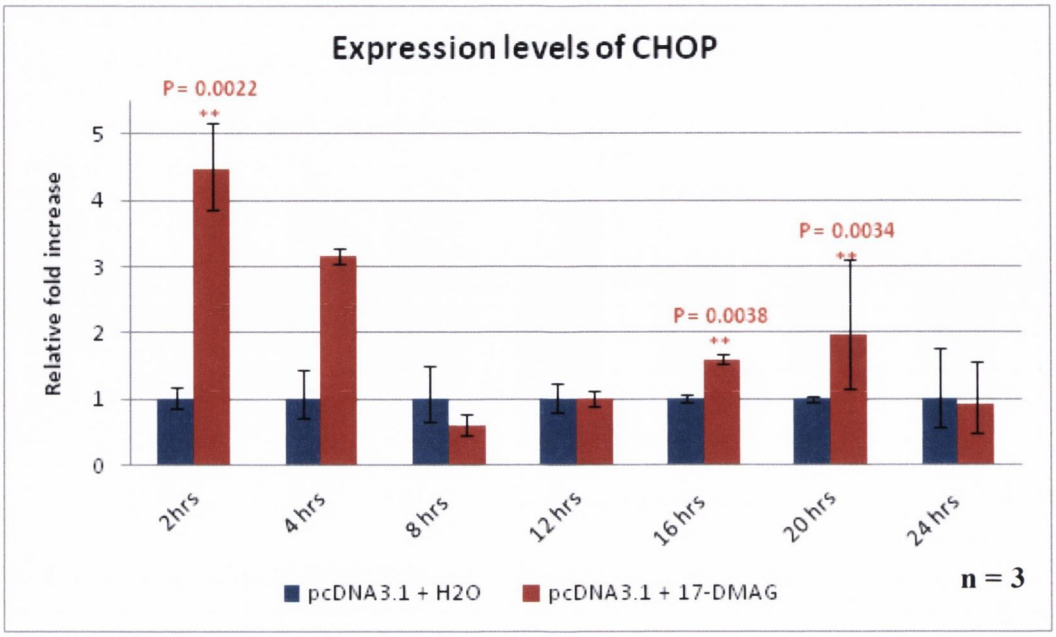

B)

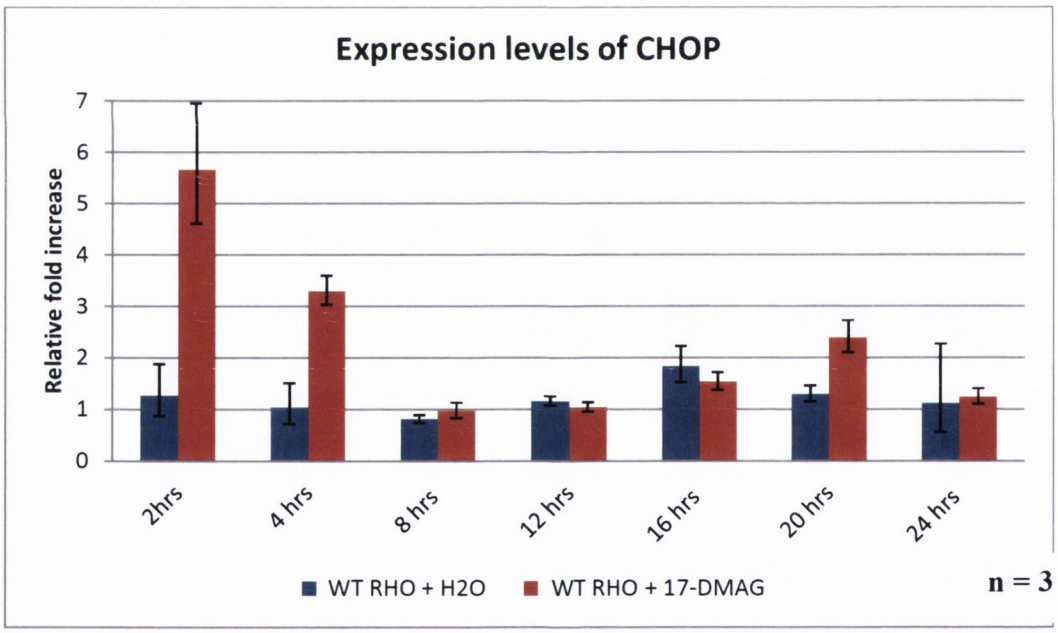

Figure 5. 16: 17-DMAG treatment and CHOP expression levels in cells transfected with control DNA and WT RHO.

Cells were transfected with control plasmid or WT RHO and then treated with 17-DMAG or nuclease free water. A) CHOP expression levels were significantly increased in pcDNA3.1(+) transfected cells treated 17-DMAG compared to control cells treated with nuclease free water 2, 16 and 20 h h post 17-DMAG treatment (** P = 0.0022, ** P = 0.0038, and ** P = 0.0034; respectively). B) CHOP expression levels in WT RHO

transfected cells treated 17-DMAG had similar pattern compared to cells transfected with pcDNA3.1(+) and 17-DMAG. Error bars denote ± SEM.

A)

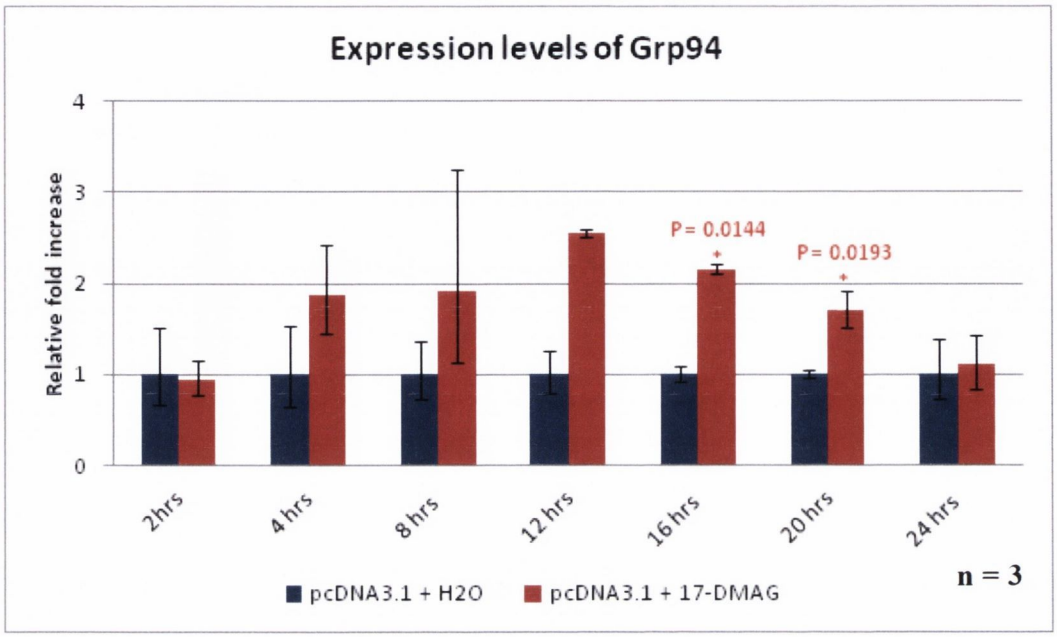

B)

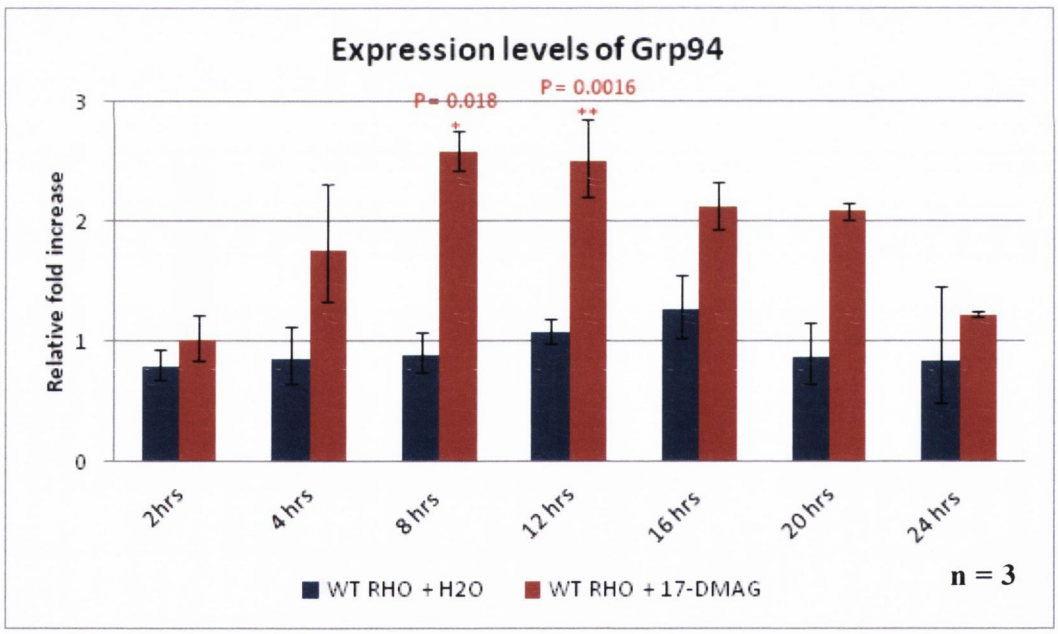

Figure 5. 17: 17-DMAG treatment and Grp94 expression levels in cells transfected with control DNA and WT RHO.

Cells were transfected with control plasmid or WT RHO and then treated with 17-DMAG or nuclease free water. A) Grp94 expression levels were significantly increased in pcDNA3.1 (+) transfected cells treated with 17-DMAG compared to control cells at 16 and 20 h post 17-DMAG treatment (* P = 0.0144, and * P = 0.0193; respectively). B) Grp94 expression levels were significantly increased in WT RHO transfected cells treated with

17-DMAG compared to control cells at 8 and 12 h post 17-DMAG treatment (* P = 0.018 and ** P = 0.0016, respectively). Error bars denote ± SEM.

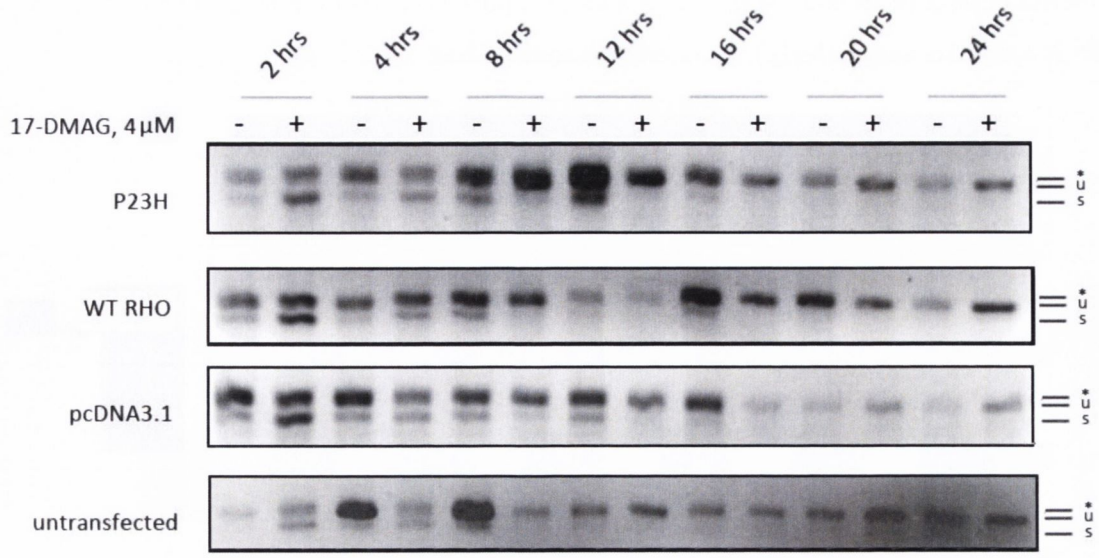

Figure 5. 18: Gel electrophoresis of PCR products of Xbp1 cDNA obtained from mRNA in cells.

Cells were transfected with control plasmid, WT RHO or P23H RHO and then treated with 4 µM 17-DMAG or water. PCR reactions were then carried out for Xbp1 cDNA obtained from RNA samples of these cells at different timepoints. There were three different bands including unspliced Xbp1 (denoted u), spliced Xbp1 (denoted s) and a by product created from annealing of spliced (263 bp) and unspliced Xbp1 (289 bp) (denoted *). The results are similar in all transfected cells. The amounts of spliced Xbp1 compared to unspliced Xbp1 were higher in treated cells 2 and 4 h post 17-DMAG. From 8 to 16 h post 17-DMAG treatment, spliced Xbp1 was detected in non-treated samples while this was not the case in treated cells transfected with P23H and WTRHO. There was a very faint band of spliced Xbp1 at 16 h in cells transfected with pcDNA3.1 and treated with water. In untransfected cells, 17-DMAG also led to an increase in spliced Xbp1 2 and 4 h post 17-DMAG. However, these cells also had a baseline of spliced Xbp1 at 4, and 8 h post nuclease free water treatment.

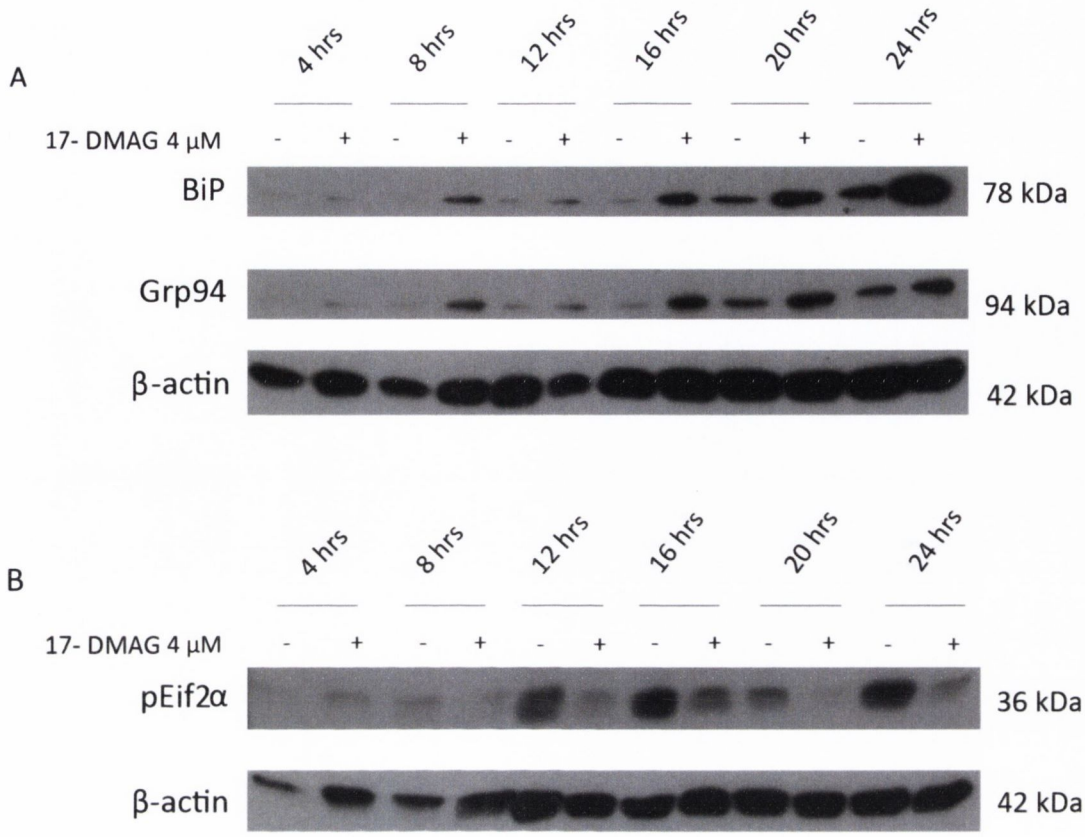

Figure 5. 19: Effect of 17-DMAG on BiP, Grp94 and peIF2α protein levels in cells transfected with P23H RHO.

HeLa cells were first transfected with P23H RHO and then treated with 17-DMAG or nuclease free water 5 h post transfection. A) whole cell lysates were used for western blots. Treatment of 17-DMAG increased BiP and Grp94 protein levels in treated cells compared to control cells from 4 h up to 24 h post 17-DMAG. B) On the other hand, levels of phosphorylated eIF2α were reduced in treated cells compared to non-treated cells from 8 to up to 24 h post 17-DMAG treatment. β-actin was used for equal loading control.

A)

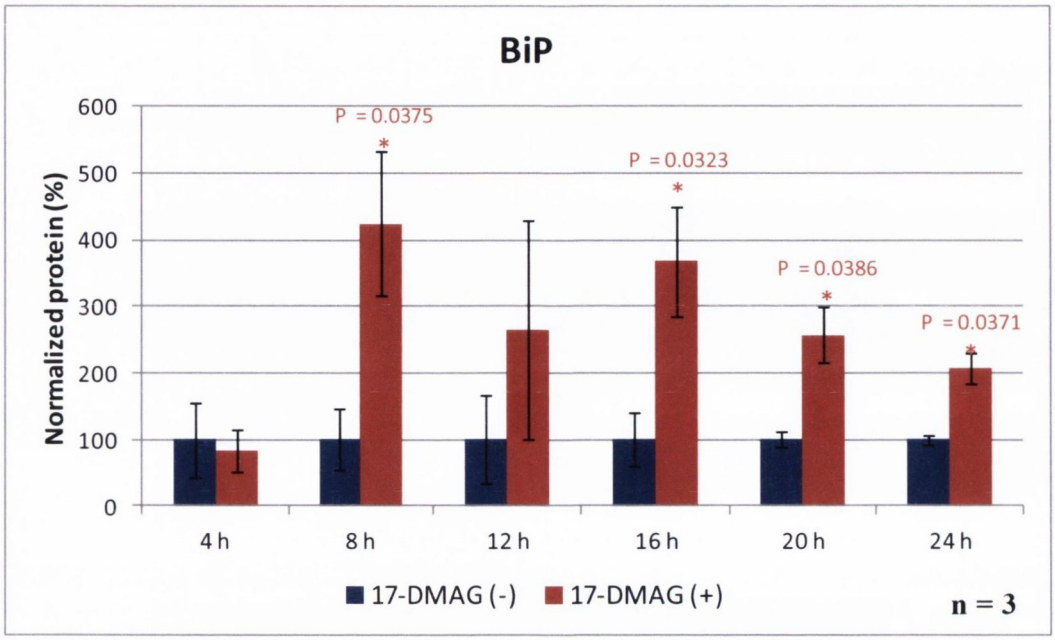

B)

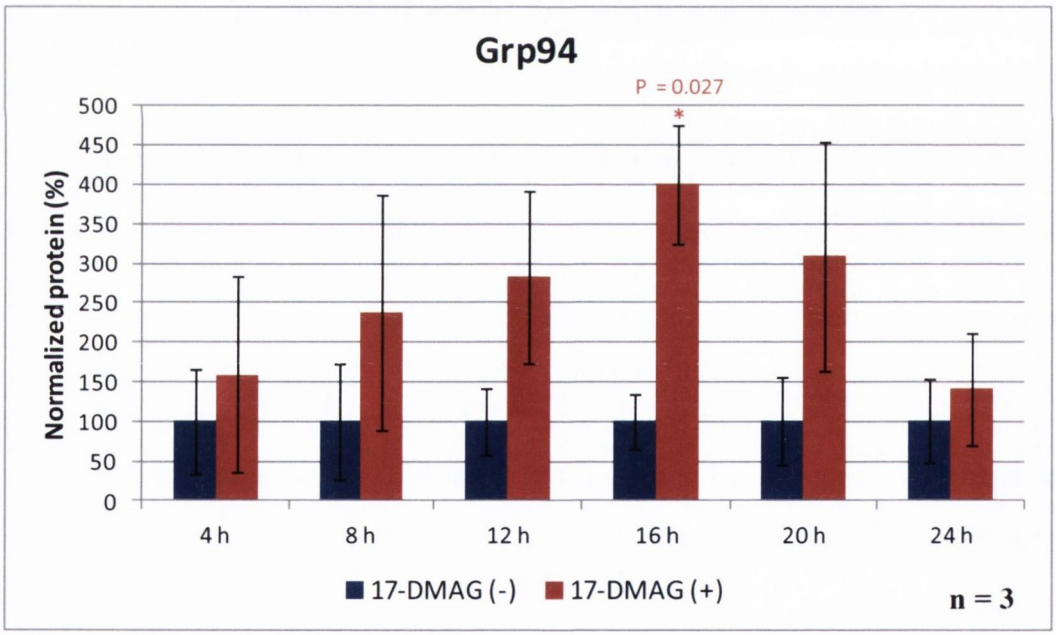

Figure 5.20

C)

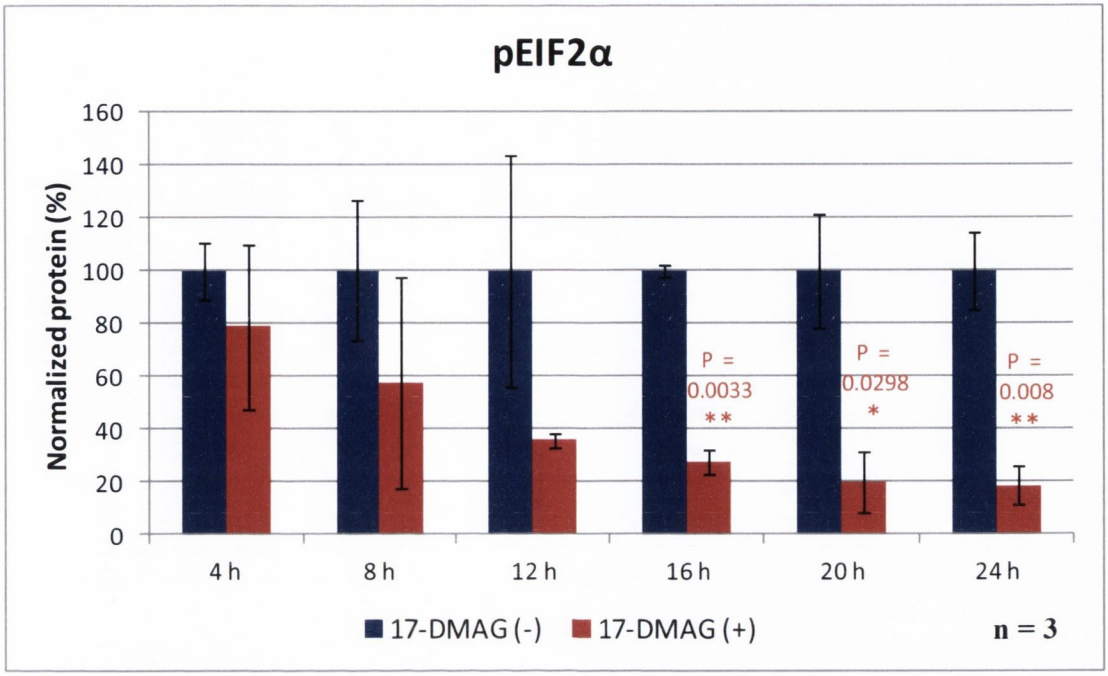

Figure 5. 20: Quantification of BiP, Grp94 and pEIF2α protein levels from figure 5.19.

A) Protein levels of BiP were significantly increased in P23H RHO transfected cells treated with 17-DMAG at 8, 16, 20 and 24 h post treatment compared to non-treated cells (* P = 0.0375, * P = 0.0323, * P = 0.0386 and * P = 0.0371; respectively). B) Protein levels of Grp94 were significantly increased in P23H RHO transfected cells treated with 17-DMAG at 16 h post treatment compared to non-treated cells (* P = 0.027) and C) On the other hand, levels of phosphorylated eIF2α were significantly reduced at 16, 20 and 24 h post treatment compared to non-treated cells (** P = 0.0033, * P = 0.0298, ** P = 0.008; respectively). All experiments were repeated three times. Error bars denote ± SEM.

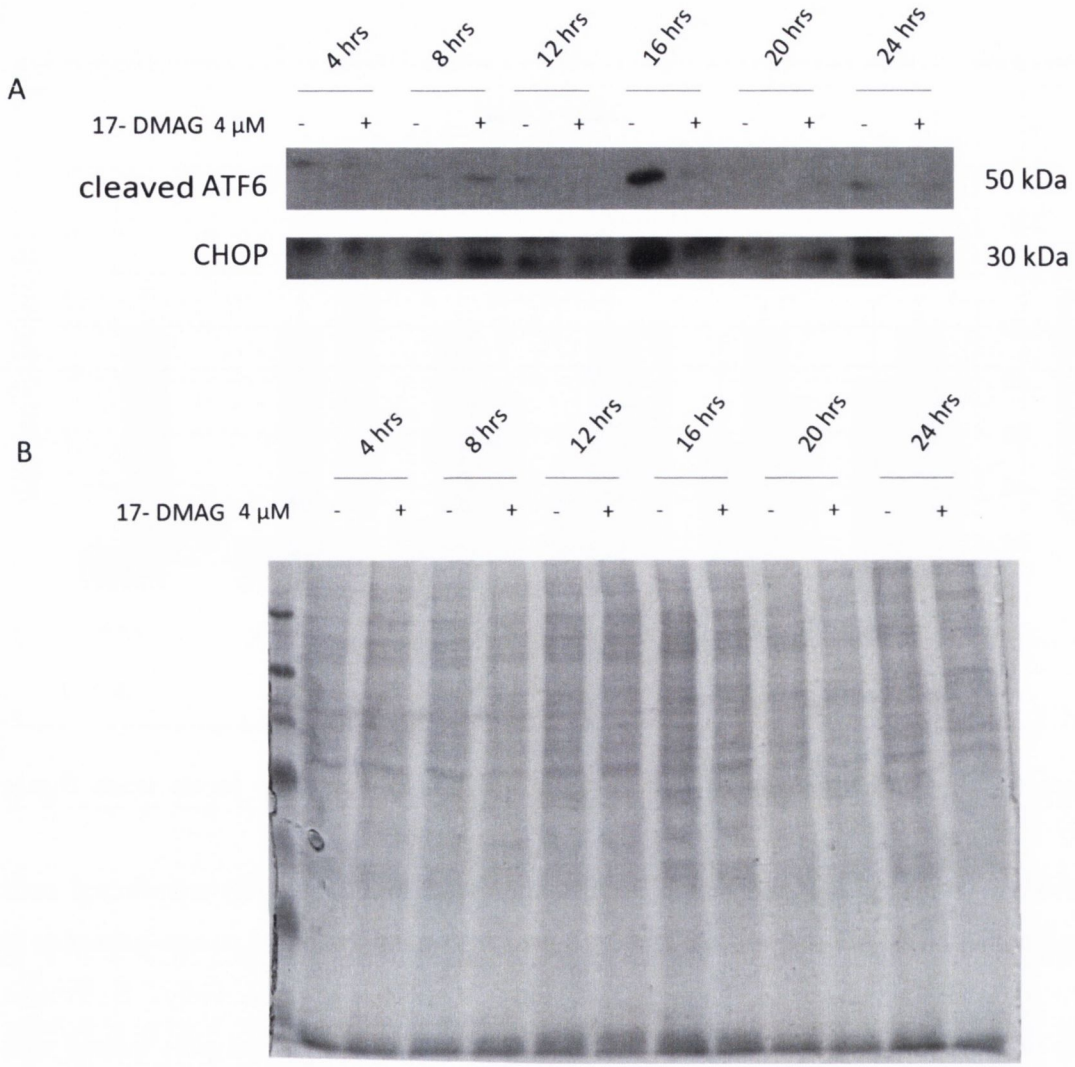

Figure 5. 21: Effect of 17-DMAG on CHOP and cleaved ATF6 protein levels in cells transfected with P23H RHO.

HeLa cells were first transfected with P23H RHO and then treated with 17-DMAG or nuclease free water 5 h post transfection. Nuclear fractions were prepared for western blots. Cleaved ATF6 and CHOP protein levels started to decrease in treated cells compared to non-treated cells from 12 h up to 24 h post 17-DMAG treatment. Coomassie blue staining of the identical gel was used as loading control for the nuclear fraction.

A)

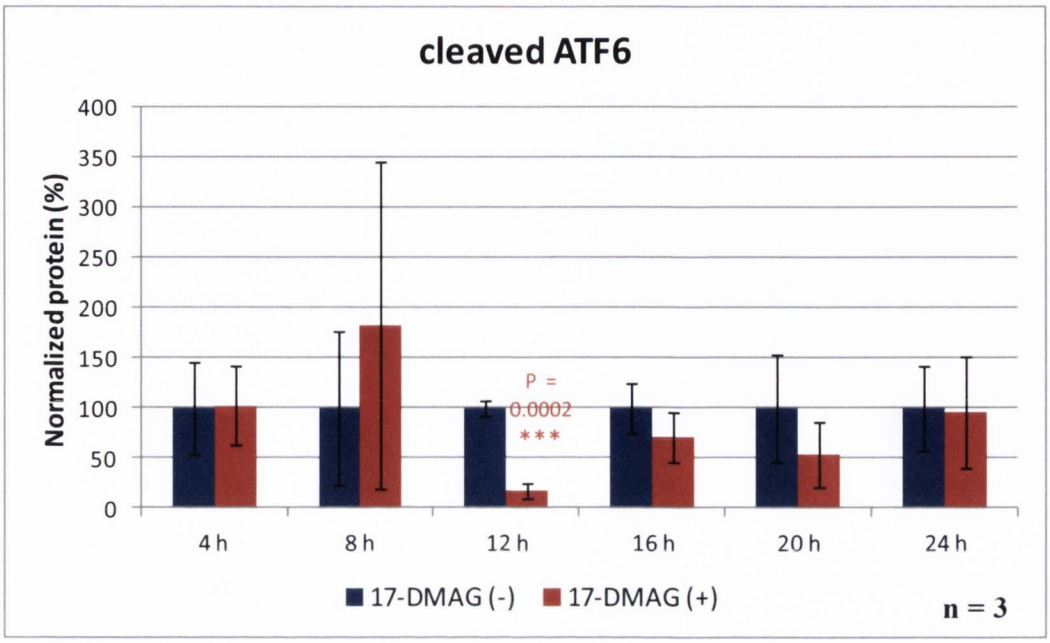

B)

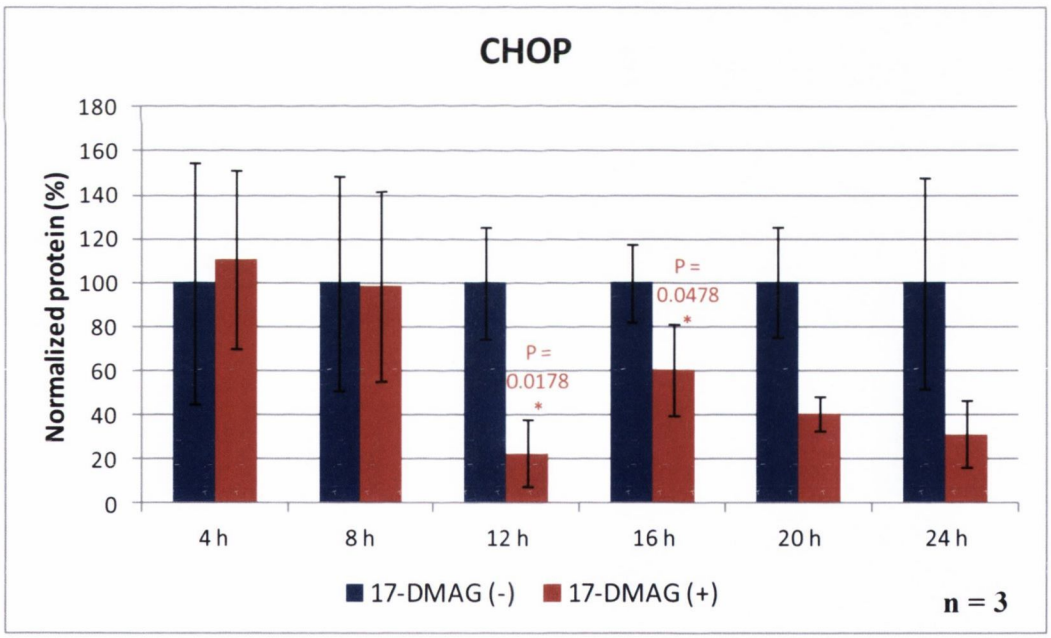

Figure 5. 22: Quantification of cleaved ATF6 and CHOP protein levels from figure 5.21.

A) Protein levels of cleaved ATF6 were significantly reduced in P23H RHO transfected cells treated with 17-DMAG at 12 h post treatment compared to non-treated cells (*** P = 0.0002). B) Similarly, protein levels of CHOP were significantly lowered in P23H RHO transfected cells treated with 17-DMAG at 12 and 16 h post treatment compared to non-

treated cells (* P = 0.0178 and * P = 0.0478; respectively). All experiments were repeated three times. Error bars denote ± SEM.

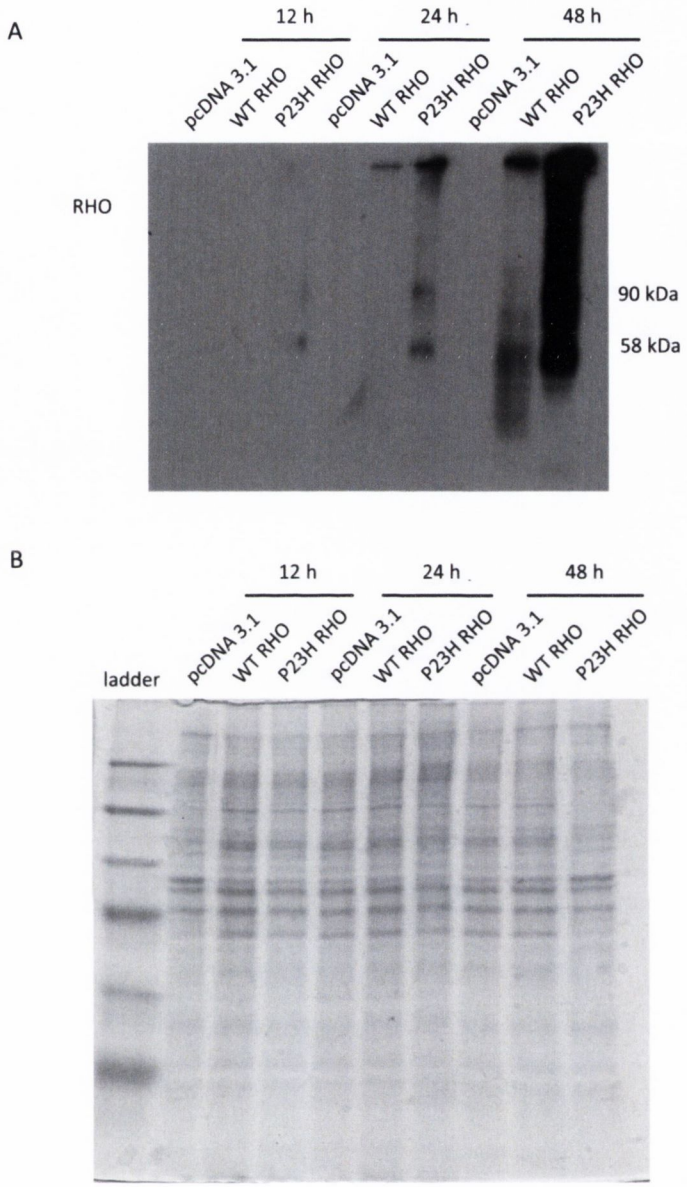

Figure 5. 23: Aggregation of P23H RHO in cells.

Insoluble fraction of HeLa cells transfected with pcDNA3.1(+), WT RHO or P23H RHO. Protein samples were harvested at 12, 24 and 48 h post tranfection and the insoluble fractions were blotted with anti rhodopsin antibody. A) There was a clear increase in RHO protein levels in cells transfected with P23H RHO compared to cells tranfected with WT RHO at all timepoints. No RHO protein expressions were detected in lanes containing protein samples isolated from pcDNA3.1 (+) transfected cells. B) Coomassie blue staining was used for loading control.

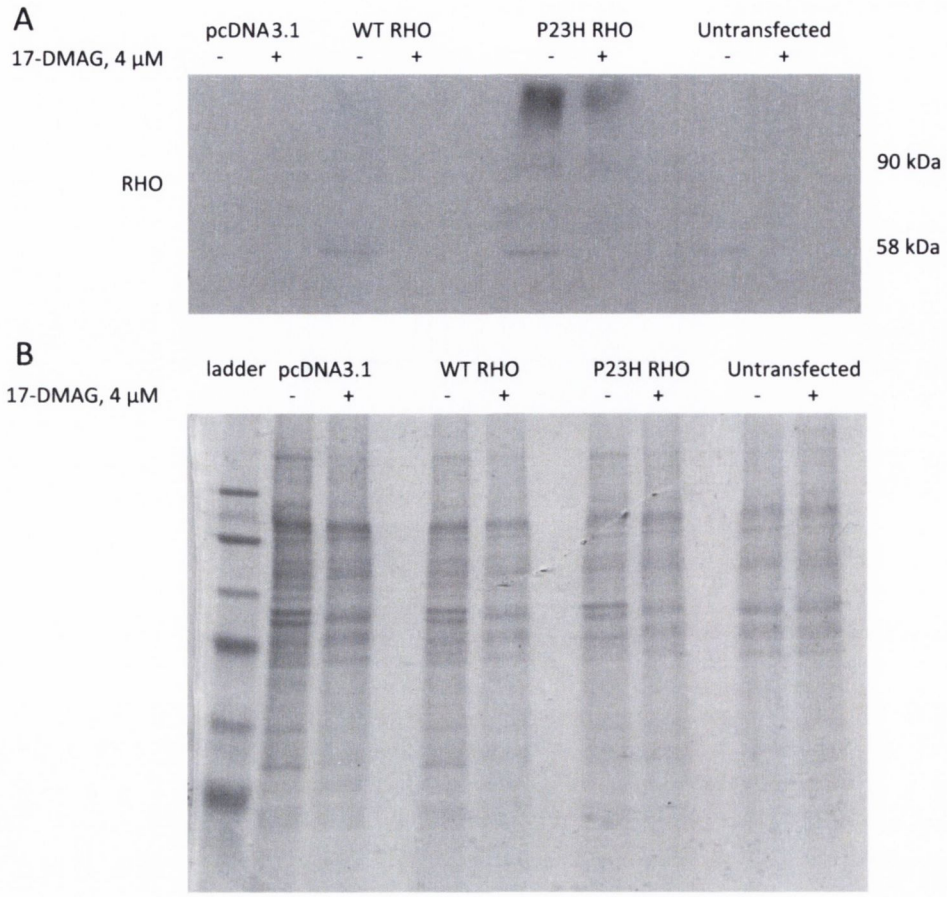

Figure 5. 24: Effect of 17-DMAG on RHO protein level in the insoluble fractions.
HeLa cells were transfected with pcDNA3.1(+), WT RHO or P23H RHO and then treated with 17-DMAG (4 µM) or nuclease free water 5 h post transfection. Insoluble protein fractions were then harvested 48 h post 17-DMAG treatment. A) The amounts of rhodopsin protein were clearly reduced in treated cells transfected with P23H RHO versus control cells. Also, there was a small amount of rhodopsin protein in the insoluble fraction of cells transfected with WT RHO which also had its rhodopsin levels reduced after being treated with 17-DMAG. B) Coomassie blue staining was used for equal loading control.

A)

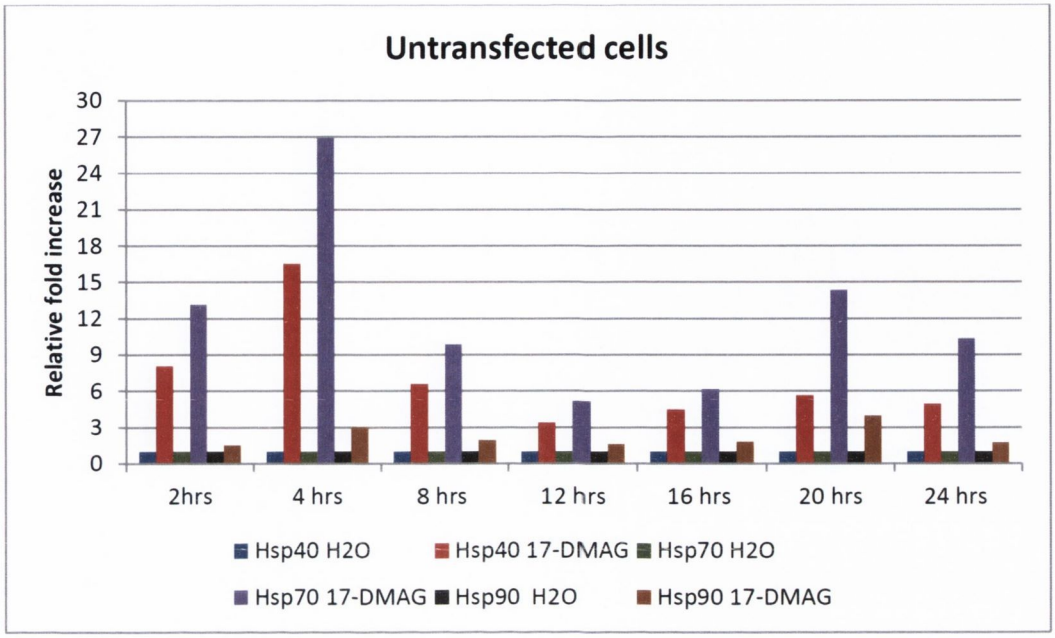

B)

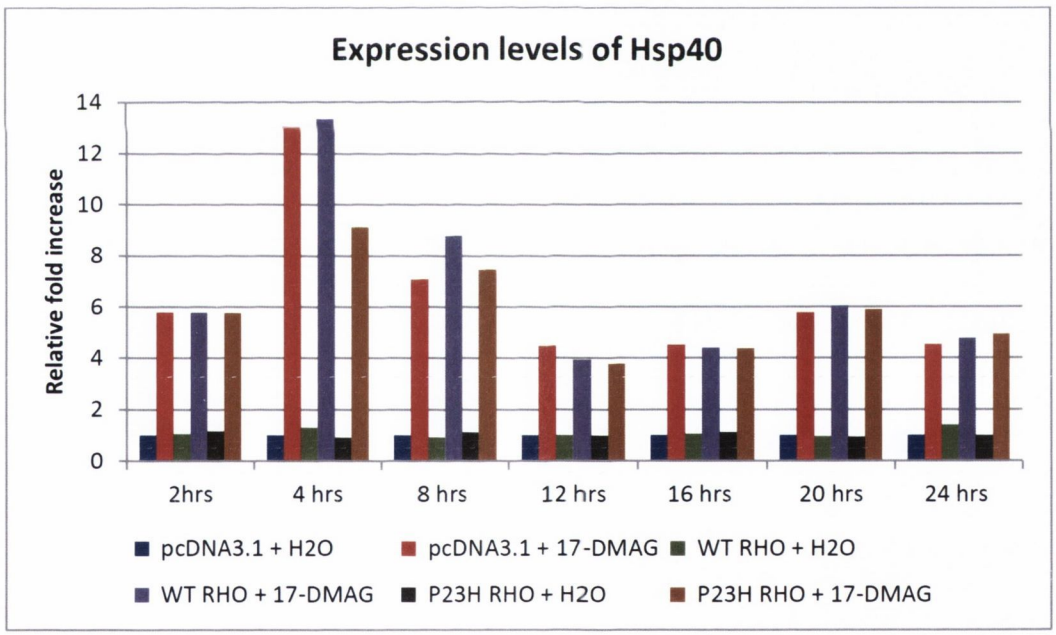

Figure 5.25

C)

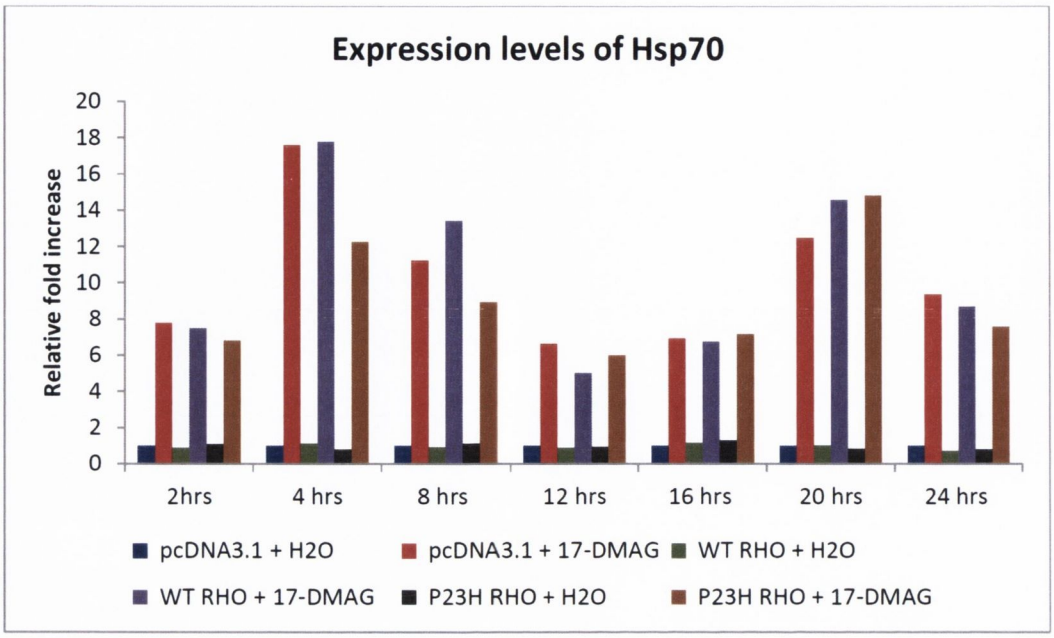

D)

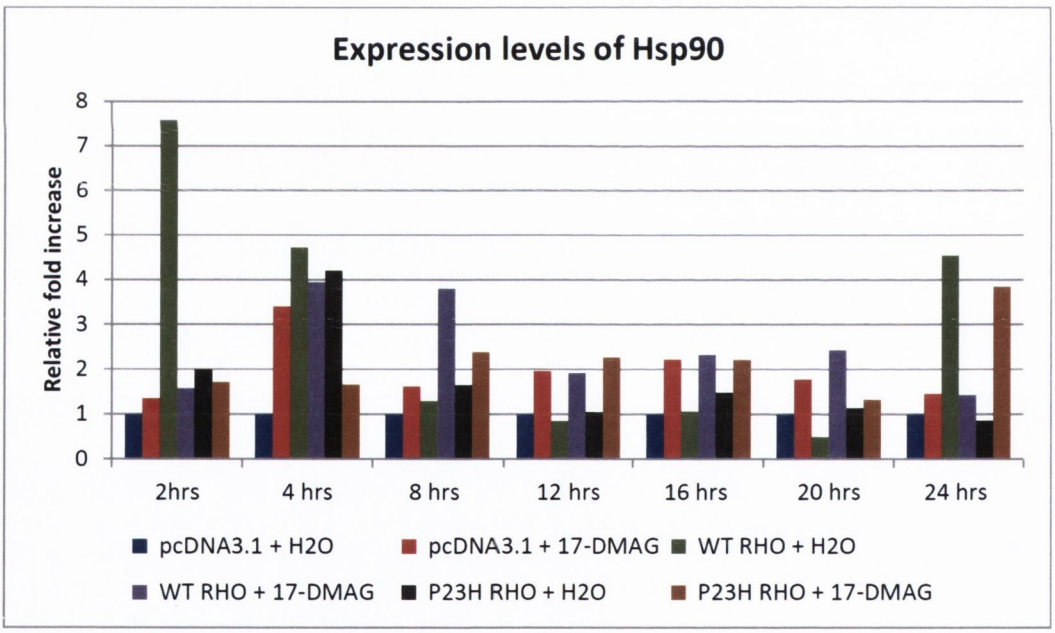

Figure 5. 25: Effect of 17-DMAG on Hsp40, Hsp70 and Hsp90 expression levels.

Cells were transfected with control DNA, WT RHO or P23H RHO and then treated with 17-DMAG. Only one RT-PCR reaction was carried out in each case, therefore there was no statistical analysis. A) In untransfected cells, 17-DMAG treatment led to increased expression levels of all three Hsp40, Hsp70 and Hsp90 in treated cells compared to control cells treated with nuclease free water at all timepoints. Similar to results obtained from untransfected cells, cells transfected with WT, P23H RHO or control plasmid showed

similar trends of Hsp40 (B) and Hsp90 (C) expression levels post 17-DMAG treatment compared to control treatment. D) Expression levels of Hsp90 in cells transfected with WT or P23H RHO and treated with 17-DMAG were different from those in cells transfected with control plasmid.

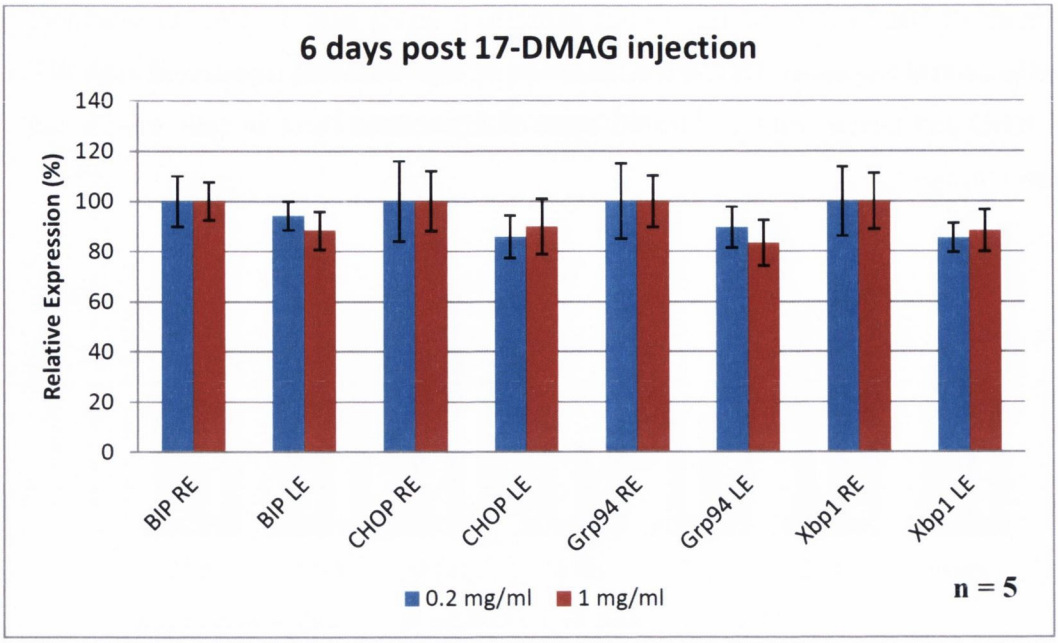

Figure 5. 26: 17-DMAG concentrations and ER stress response in P23H-3 rats.

Two groups of 6 month old P23H-3 rats (n = 5 in each group) were intravitreally injected with 5 µl of 0.2 mg/ml or 1 mg/ml 17-DMAG into their LE, and saline PBS into their RE. Uninjected P23H-3 rats were used as controls for ΔΔCt method. Error bars denote ± SEM. There were no significant differences in BiP, CHOP, Grp94 and Xbp1 expression levels 6 days post injection in two groups of animals. However, there was a statistically difference in Grp94 mRNA levels in eyes injected with 1 mg/ml 17-DMAG compared to control eyes (* P = 0.0132) while this was not the case for eyes injected with 0.2 mg/ml 17-DMAG.

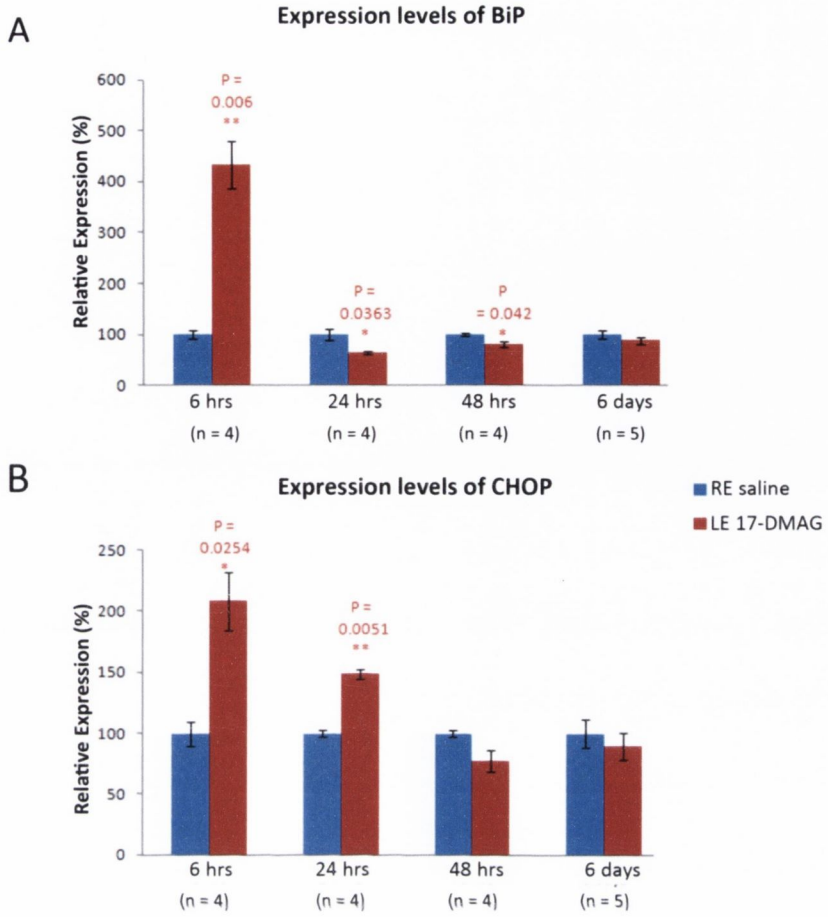

Figure 5. 27: Effect of 17-DMAG on BiP and CHOP expression levels in P23H-3 rats. Six month old P23H-3 rats were intravitreally injected with 5 µl 17-DMAG (1 mg/ml) in the left eye and saline in the right eye. TaqMan® gene expression assays were used to measure different mRNA levels in the retinas which were harvested at 6, 24, 48 h and 6 days post injection. Non injected P23H-3 rats were used as controls for ΔΔCt method. Error bars denote ± SEM. A) BiP mRNA levels were significantly higher in 17-DMAG injected retinas compared to saline injected retinas 6 h post injection (** P = 0.006). However, BiP mRNA levels were significantly decreased in 17-DMAG injected retinas compared to saline injected retinas 24 and 48 h post injection (* P = 0.0363 and * P = 0.042, respectively). B) CHOP mRNA levels were significantly higher in 17-DMAG injected retinas compared to saline injected retinas 6 and 24 h post injection (* P = 0.0254 and ** P = 0.0051, respectively).

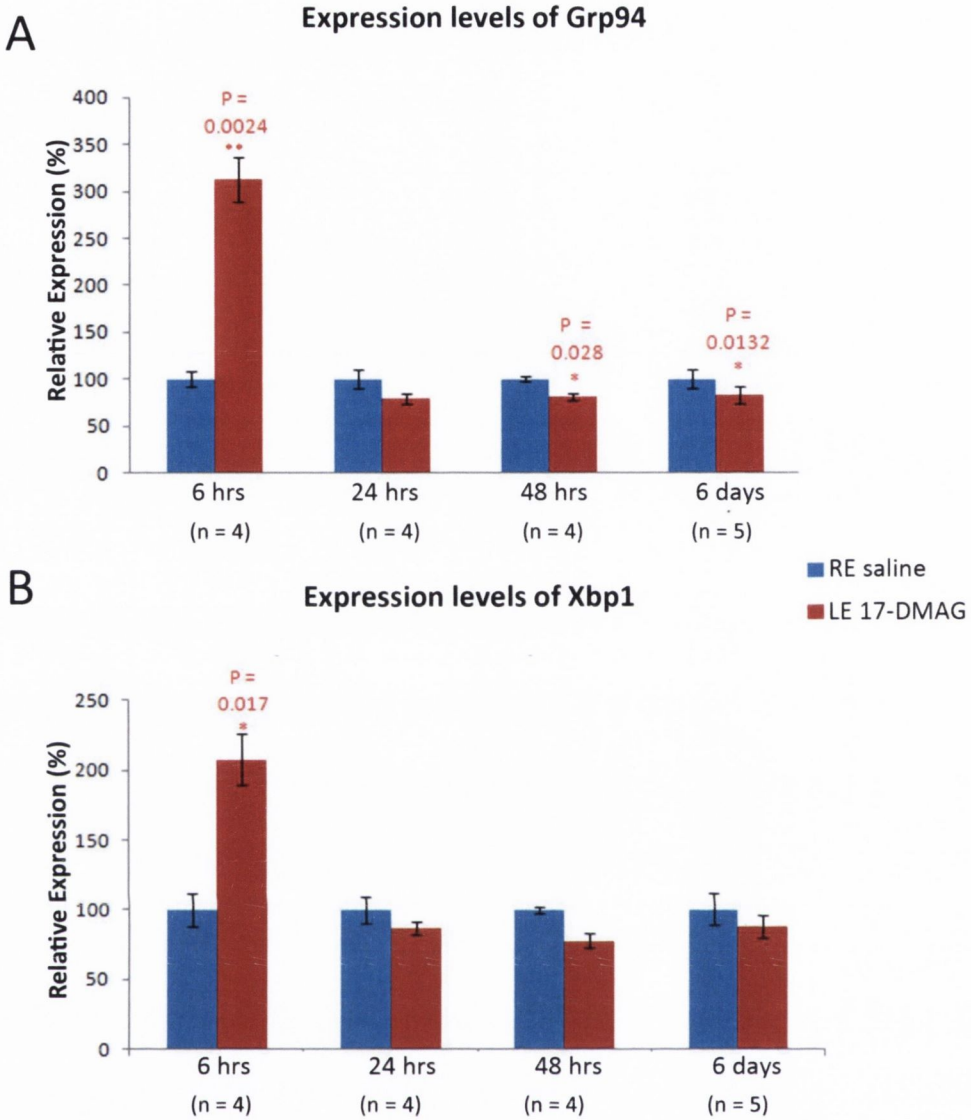

Figure 5. 28: Effect of 17-DMAG on Grp94 and Xbp1 expression levels in P23H-3 rats.

These were the same animals as in **Figure 5.27**. Error bars denoted ± SEM. A) Grp94 mRNA levels were higher in 17-DMAG injected retinas compared to control retinas 6 h post injection (** P = 0.0024). However, Grp94 mRNA levels were significantly lower in 17-DMAG injected retinas compared to saline injected retinas 48 h and 6 days post injection (* P = 0.028 and * P = 0.0132, respectively). B) Xbp1 mRNA levels were significantly higher in 17-DMAG injected retinas compared to saline injected retinas 6 h post injection (* P = 0.017).

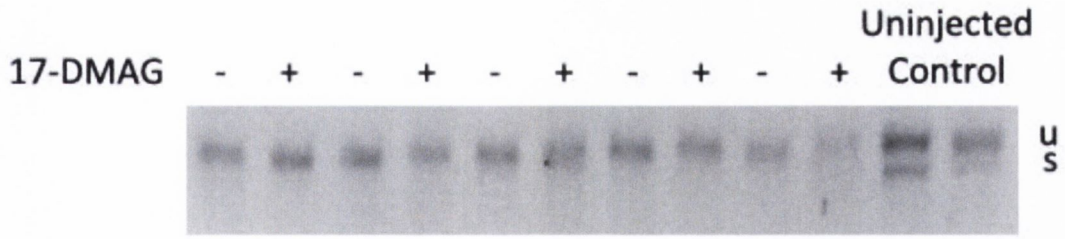

Figure 5. 29: Xbp1 splicing in P23H rats treated with 17-DMAG.

Five 6 month old P23H-3 rats were intra-vitreally injected with 17-DMAG (1 mg/ml) in the left eye and saline in the right eye. The retinas were then processed for RNA 48 h post injection and PCR were carried out to quantify spliced Xbp1 level. Unspliced (u) Xbp1 is 486 bp while spliced (s) Xbp1 is 459 bp. The result obtained here was inconclusive since no spliced Xbp1 band was detected in all experimental animals with the exception in uninjected controls.

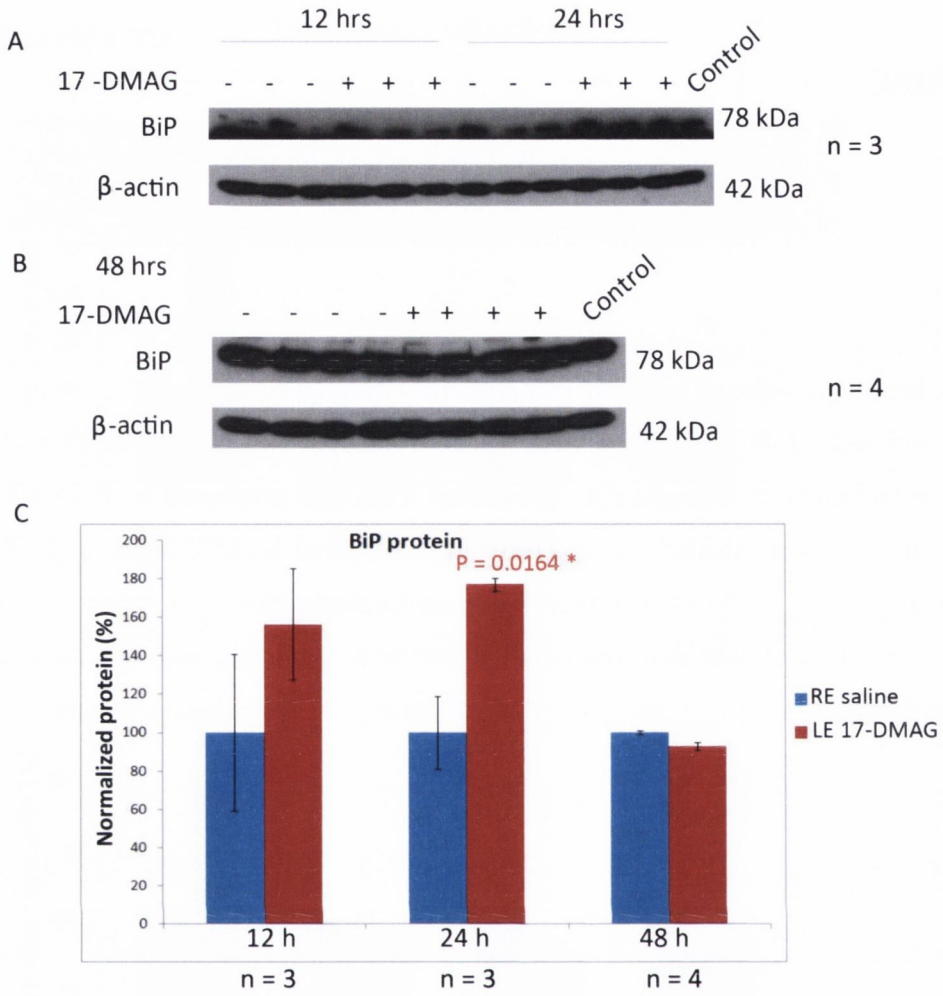

Figure 5. 30: Western blot analyses of BiP in P23H-3 rats treated with 17-DMAG.

Four month old P23H-3 rats were intravitreally injected with 17-DMAG in the left eye and saline in the right eye. Uninjected P23H-3 rats were used as controls. Proteins were collected from the retinas 12, 24 and 48 h post injection and whole cell lysates were isolated. β-actin was used for equal loading control. A) Western blots showed higher BiP protein levels in 17-DMAG injected retinas compared to saline injected retinas 12 and 24 h post injection. B) No differences in protein levels of BiP were observed between 17-DMAG treated and non-treated eyes 48 h post injection. C) Bar charts illustrate the densitometry measurements of percentage of BiP and CHOP proteins in 17-DMAG injected retinas compared to saline injected controls 12, 24 and 48 h post injection. BiP protein levels were significantly increased in 17-DMAG retinas compared to control retinas 24 h post injection (* P = 0.0164). Error bars denote ± SEM.

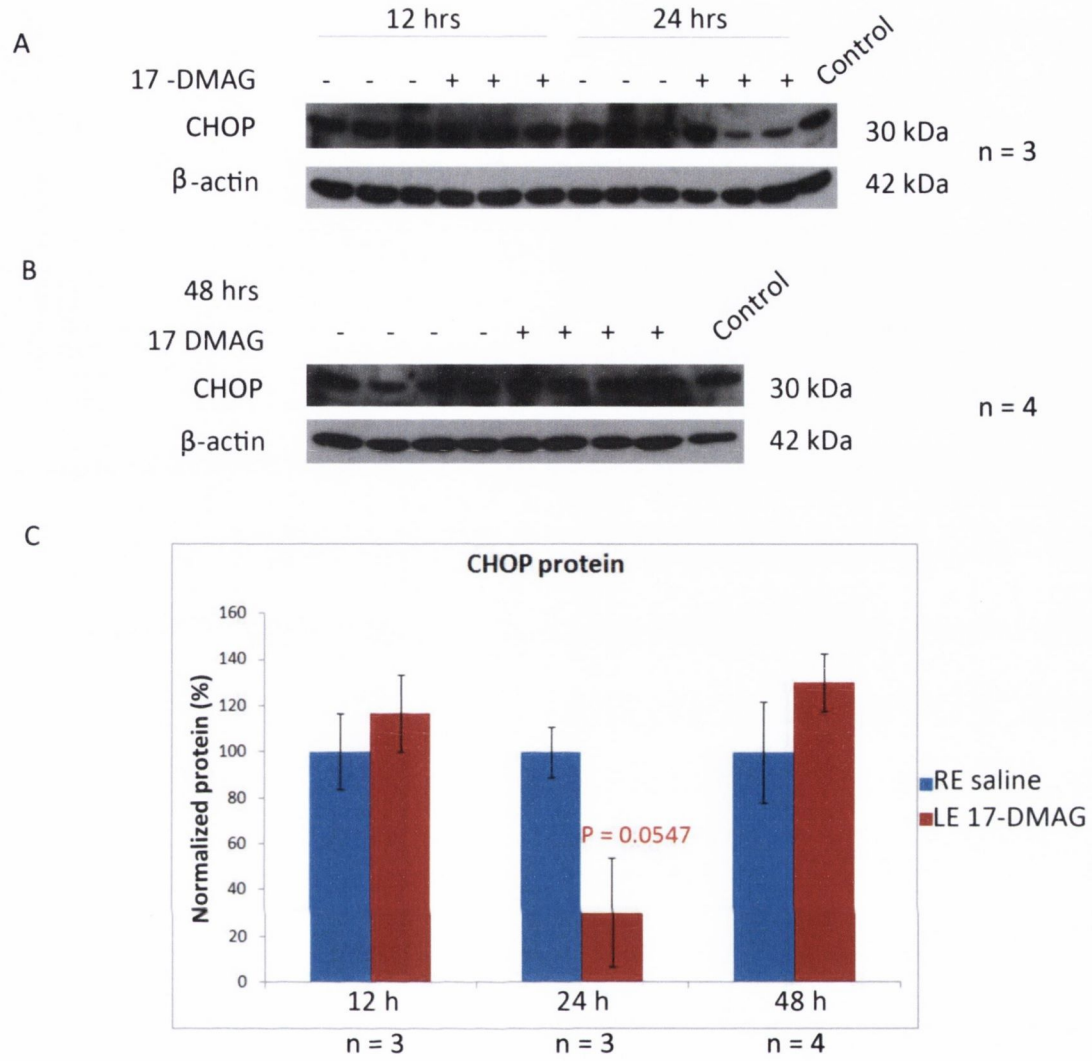

Figure 5. 31: Western blot analyses of CHOP in P23H-3 rats treated with 17-DMAG. Protein samples of the same rats in **Figure 5.30** were blotted with antibody against CHOP. β-actin was used for equal loading control. A) CHOP protein levels were lower in two out of three retinas injected with 17-DMAG compared to saline injected retinas 24 h post injection. B) Western blots showed no differences in protein levels of CHOP 48 h post injection. C) CHOP was greatly reduced in 17-DMAG injected retinas compared to control retinas at the same timepoint post injection (P = 0.0547). Error bars denote ± SEM.

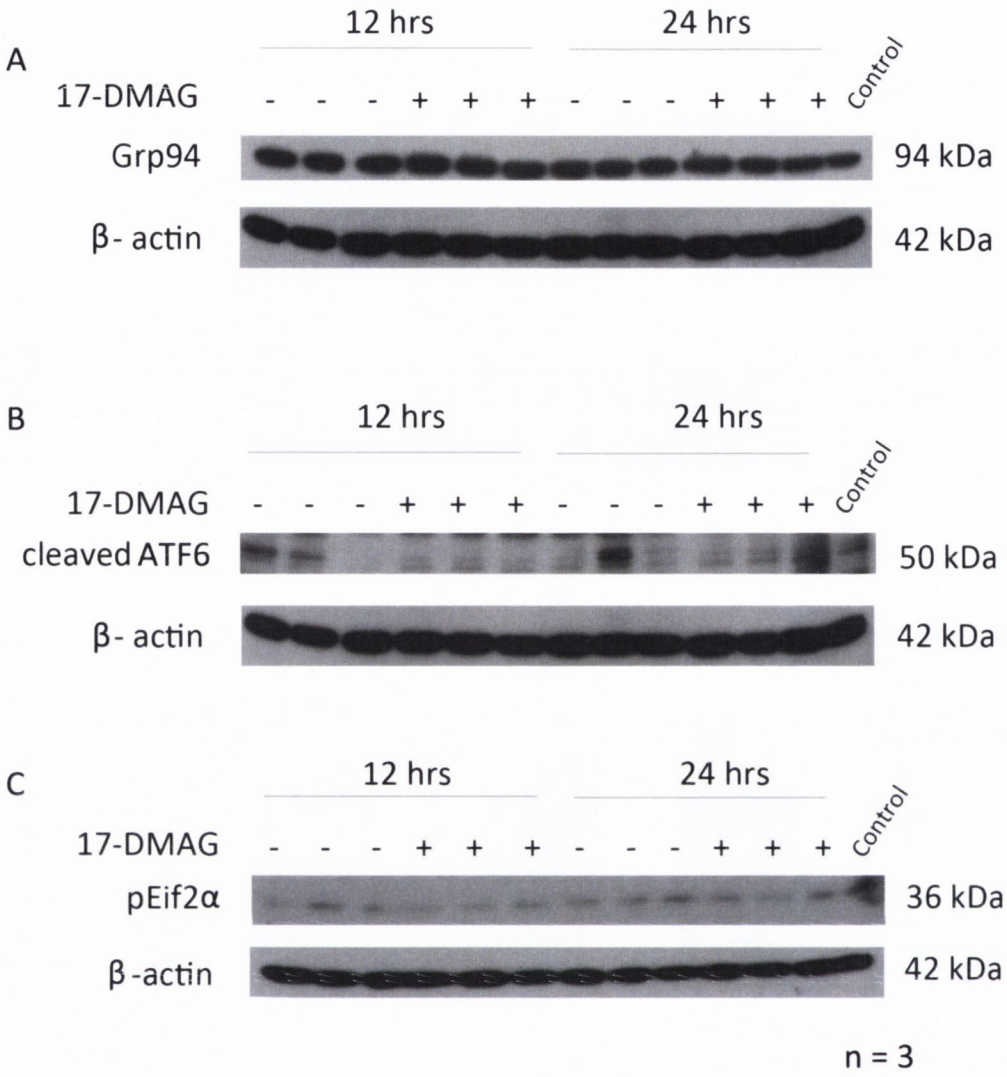

Figure 5. 32: Western blot analyses of Grp94, cleaved ATF6, peIF2α in P23H-3 rats treated with 17-DMAG.

Protein samples of the same rats in **Figure 5.30** were blotted with antibodies against Grp94, cleaved ATF6 and peIF2α. β-actin was used for equal loading control. There were no differences in protein levels of Grp94 (A), cleaved ATF6 (B) and phosphorylated eIF2α (C) between 17-DMAG injected retinas and saline injected retinas at both timepoints post injection.

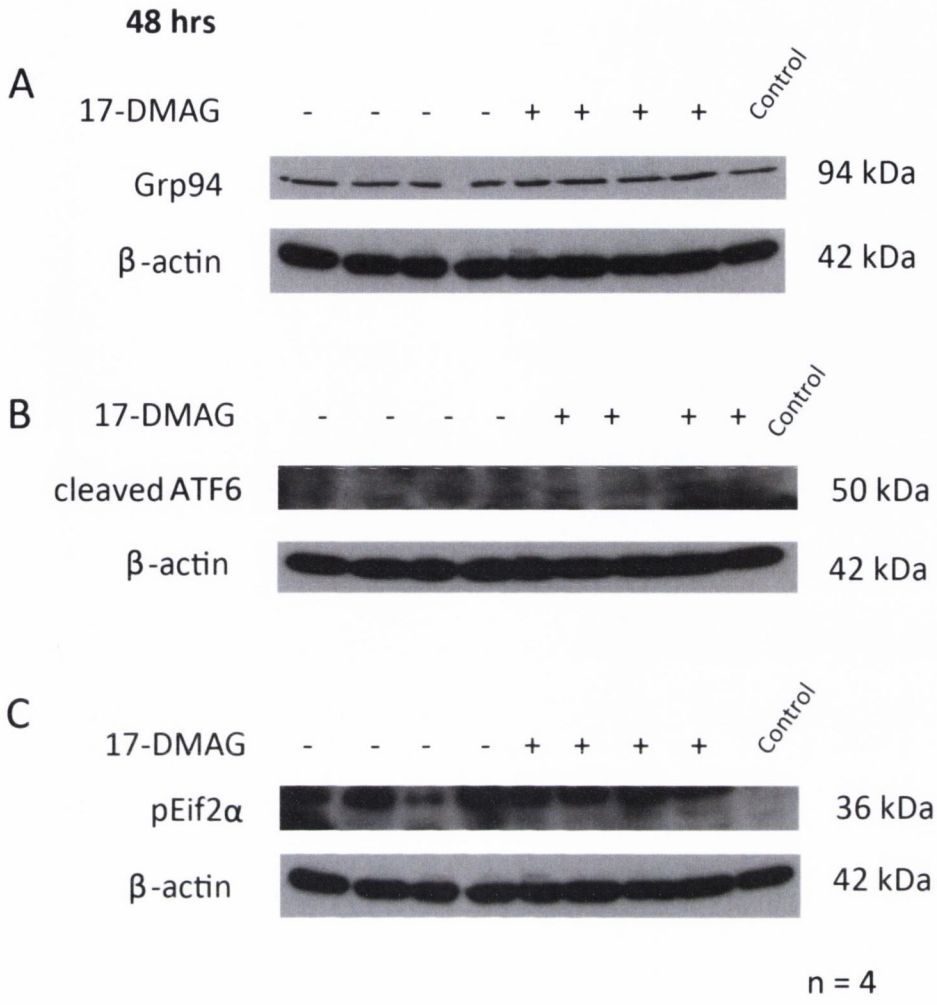

Figure 5. 33: Western blot analyses of Grp94, cleaved ATF6, peIF2α in P23H-3 rats treated with 17-DMAG.

Protein samples of the same rats in **Figure 5.30** were blotted with antibodies against Grp94, cleaved ATF6 and peIF2α. β-actin was used for equal loading control. Western blots showed no differences in protein levels of Grp94 (A), cleaved ATF6 (B), peIF2α (C) between 17-DMAG injected retinas and saline injected retinas 48 h post injection.

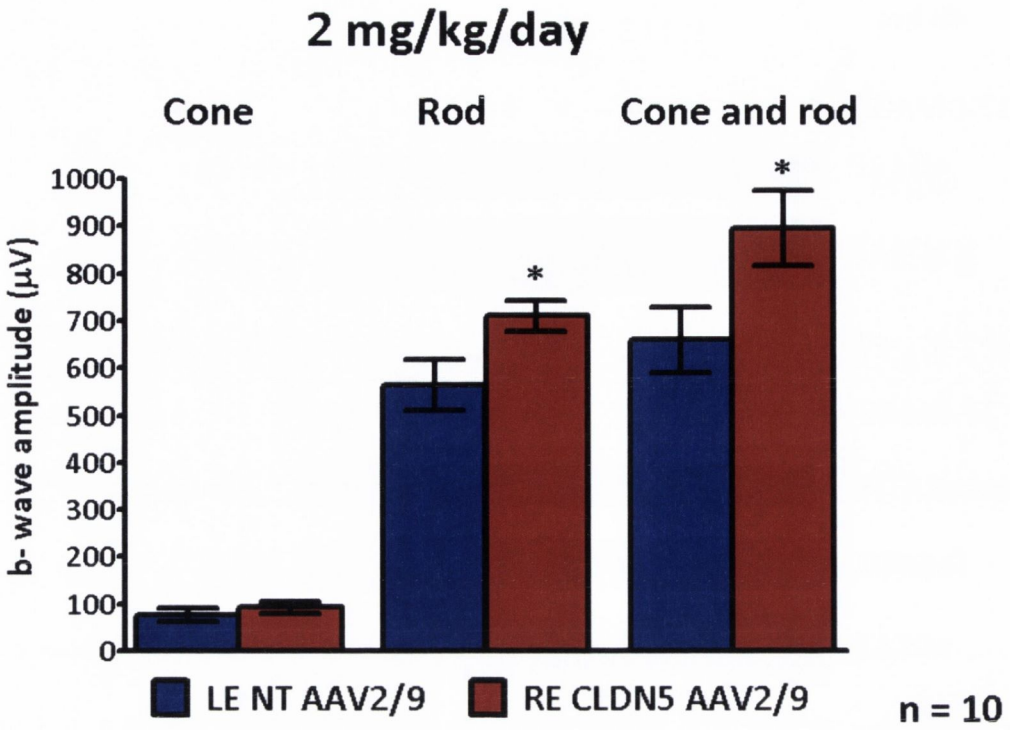

Figure 5. 34: Effect of 2 mg/kg/day 17-DMAG on the degenerating P23H-3 rat retina. After being injected with CLDN5 AAV2/9 in the right eye and NT AAV2/9 in the left eye, 6 month old rats (n = 10) were supplemented with doxycycline (2 mg/ml) and 17-DMAG (2 mg/kg/day) in their drinking water for 5 weeks. ERG measurements showed that b-wave amplitude of the rod isolated and mixed cone and rod responses were significantly better in CLDN5 AAV2/9 injected eyes compared to control eyes (* P = 0.0482 and * P = 0.038; respectively). Error bars denote ± SEM.

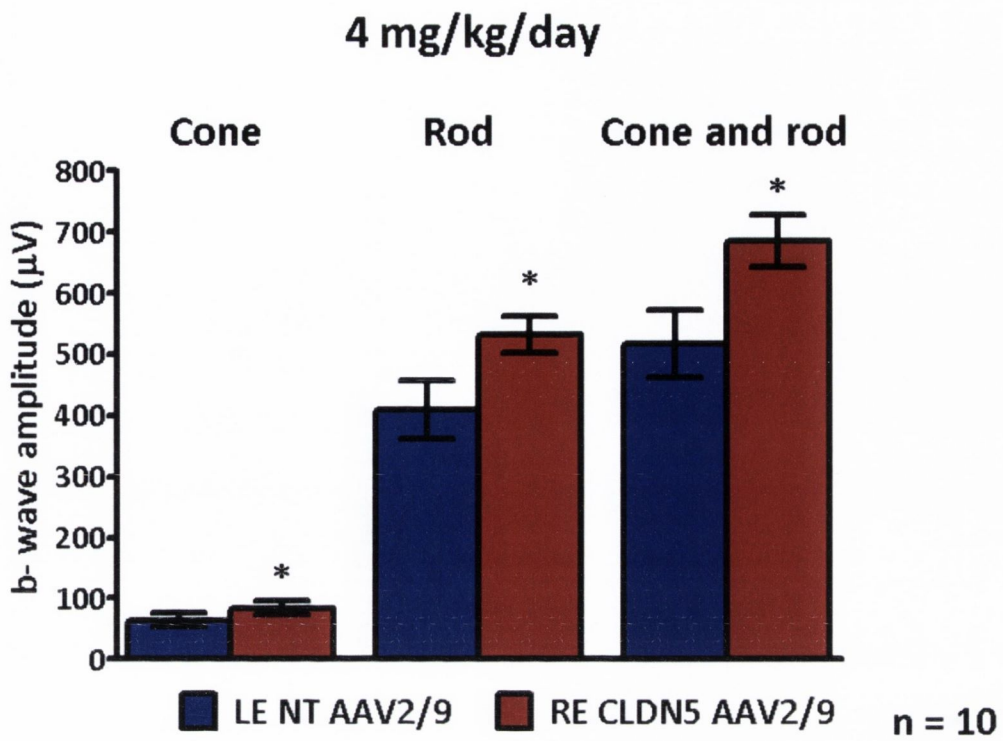

Figure 5. 35: Effect of 4 mg/kg/day 17-DMAG on the degenerating P23H-3 rat retina. The same rats as in **Figure 5.34** were then supplemented with 4 mg/kg/day 17-DMAG and doxycycline (2 mg/ml) in their drinking water for 4 weeks. There were significant differences in ERG readouts of the cone isolated, rod isolated and cone and rod responses in eyes injected with CLDN5 AAV2/9 compared to contra lateral control eyes (* P = 0.0174, * P = 0.0224 and * P = 0.0126; respectively) (n = 10). Error bars denote ± SEM.

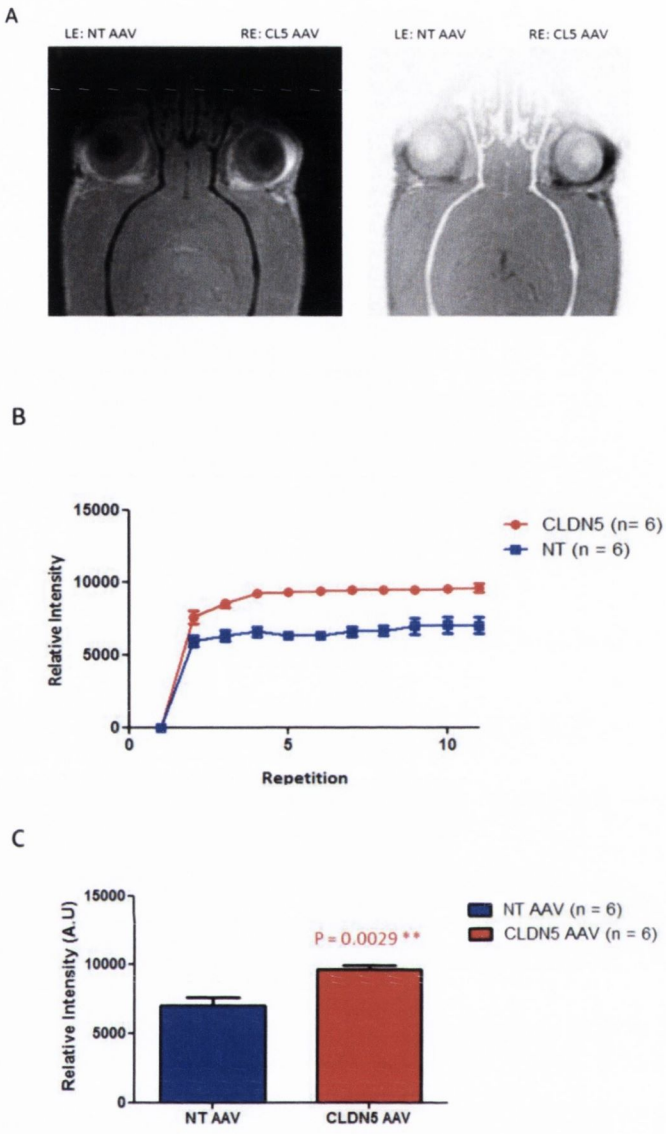

Figure 5. 36: Phenotypic analysis of the modulated iRBR in P23H-3 rats.

The same rats in **Figures 5.34 and 5.35** were used in this experiment after being supplemented with 17-DMAG and doxycycline for 9 weeks (n = 6) A) Contrast-enhanced MRI showed extravasation of the MRI contrasting agent Gd-DTPA (MW 742 Da) in the right eye injected with CLDN5 AAV2/9, but not in the left eye injected with NT AAV2/9. The inverted image highlights the localised extravasation of Gd-DTPA in the right eye compared to the control eye. B&C) This extravasation was consistently observed in all rats (n = 6), with the background pixel intensity from the NT AAV2/9 injected eye being subtracted from the CLDN5 AAV2/9 injected eye (** P = 0.0029). Error bars denote ± SEM.

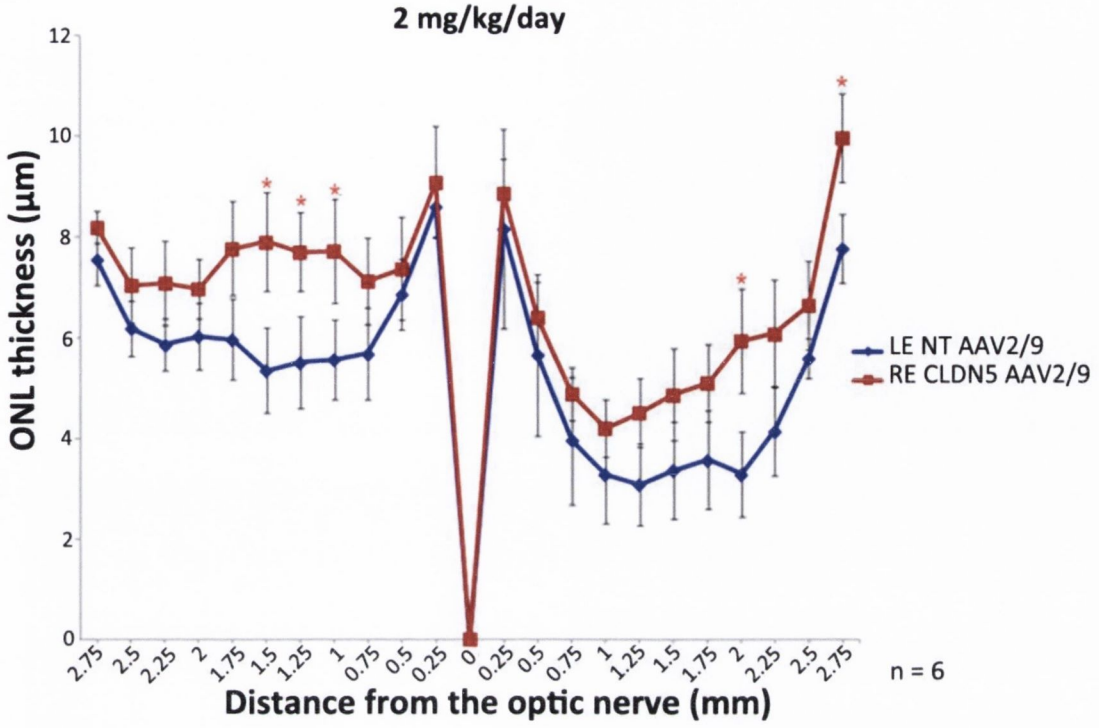

Figure 5. 37: Measurements of ONL thickness in P23H-3 rats treated with 17-DMAG. Systemic delivery of 17-DMAG using the inducible CLDN5 AAV2/9 system led to preservation of the photoreceptors at the site of AAV2/9 inoculation (* $P \leq 0.05$). Interestingly, the outer nuclear layer thickness was also significantly greater at the opposite region in the untreated eyes compared to the control eyes (* $P \leq 0.05$). Error bars denote ± SEM.

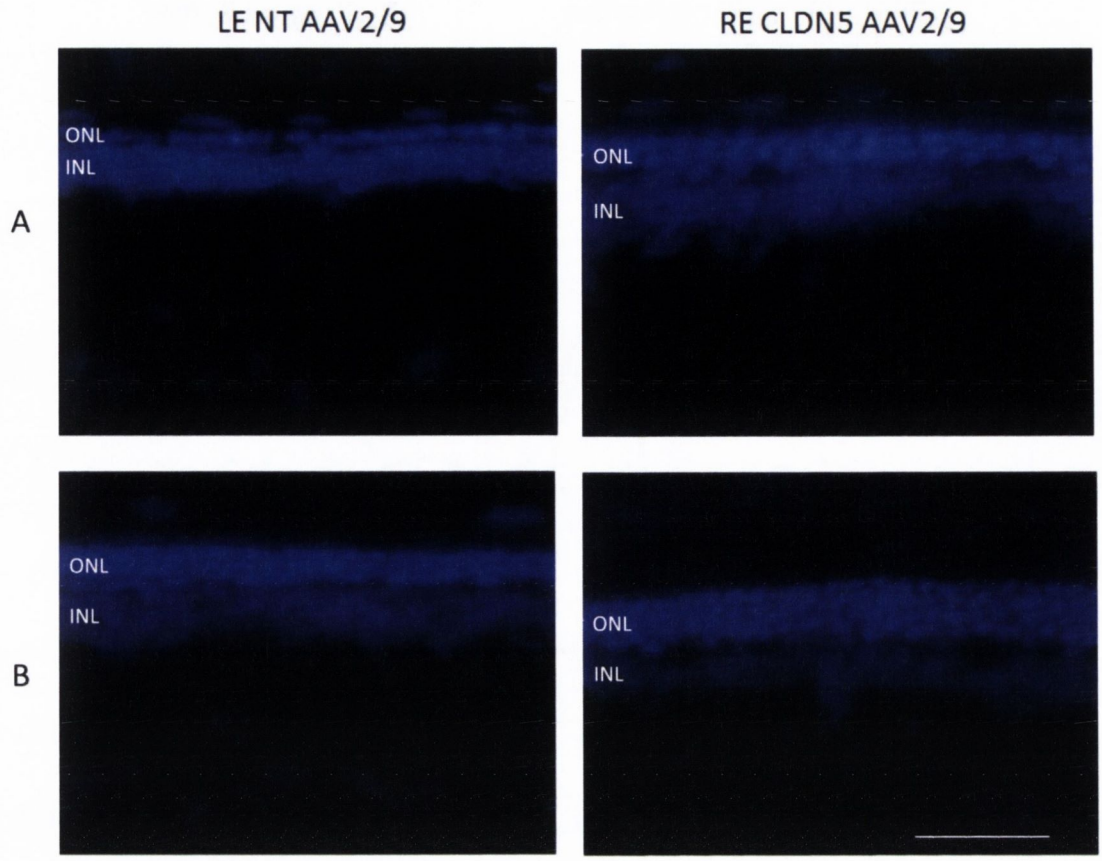

Figure 5. 38: Histological analysis of retinas of P23H-3 rats supplemented with 17-DMAG and doxycycline for 9 weeks.

DAPI staining of retinal sections showed on average the right eye injected with CLDN5 AAV2/9 had 1 or 2 more rows of photoreceptors compared to the left eye injected with NT AAV2/9. A) Thinner and B) thicker regions of the ONL were compared between NT AAV2/9 and CLDN5 AAV2/9 injected eyes. Scale bar represents 50 μM.

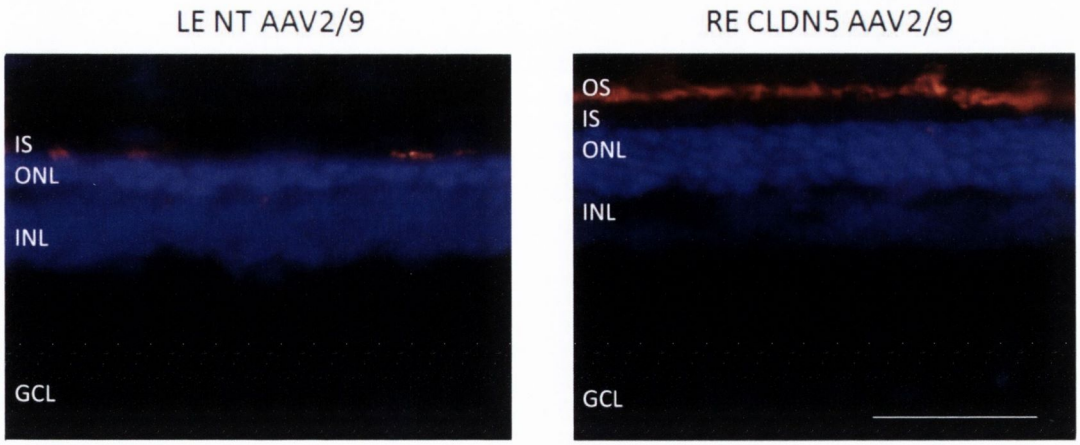

Figure 5. 39: Rhodopsin staining of retinas of P23H-3 rats supplemented with 17-DMAG and doxycycline for 9 weeks.

Images showed patchy staining of Rhodopsin in the IS and ONL regions in the eye injected with NT AAV2/9. On the other hand, Rhodopsin was localised in the OS and ONL regions in the eye injected with CLDN5 AAV2/9. All sections were counterstained with DAPI. Scale bar represents 50 μM.

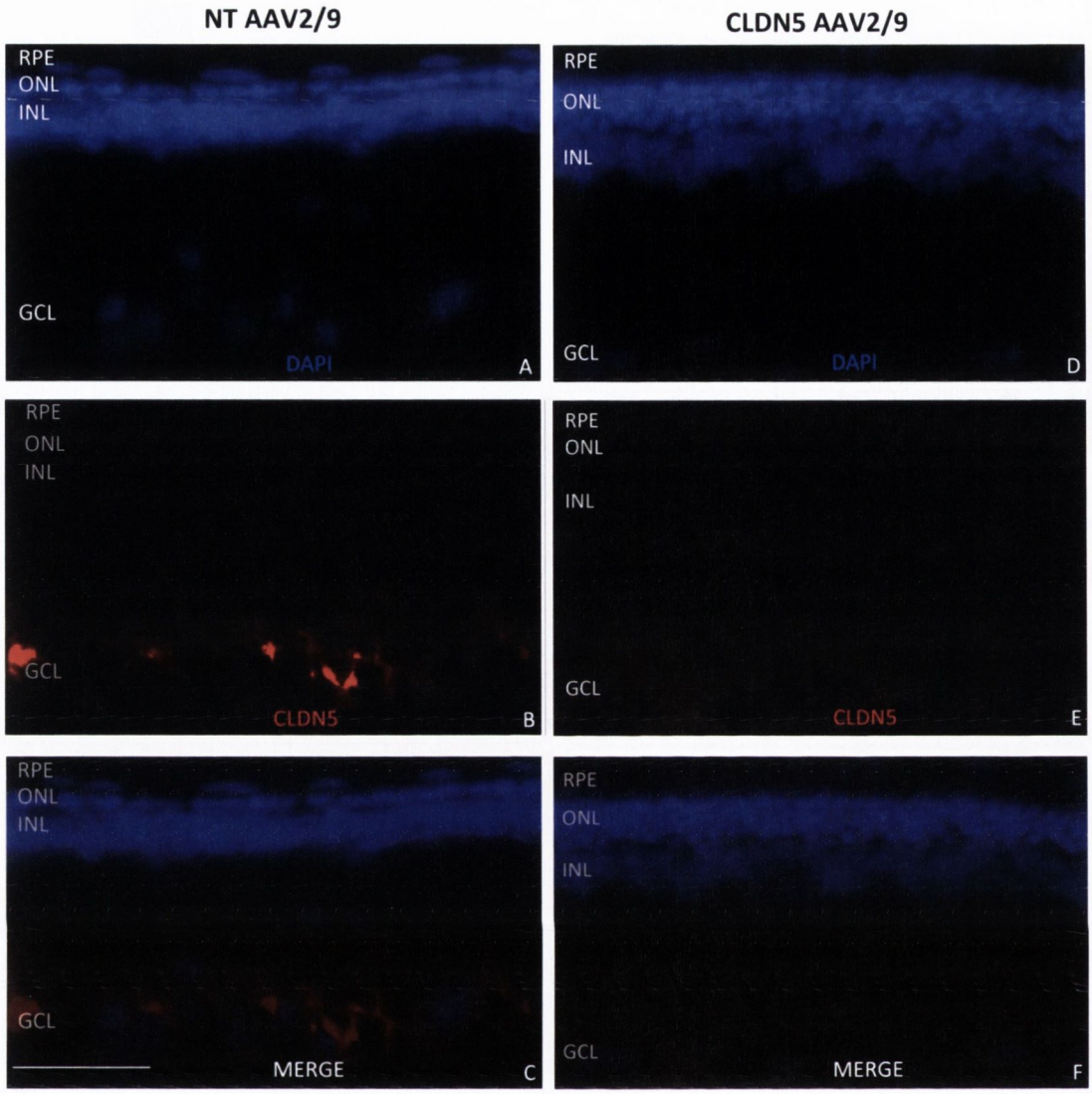

Figure 5. 40: CLDN5 staining of retinas of P23H-3 rats supplemented with 17-DMAG and doxycycline for 9 weeks.

A) & D) Thicker ONL was observed in CLDN5 AAV2/9 injected retina compared to NT AAV2/9 injected retina. B) & E) Higher amounts of CLDN5 staining with clear structure of microvessels were observed in the left eye injected with NT AAV2/9 compared to the right eye injected with CLDN5 AAV2/9. All sections were counterstained with DAPI. Scale bar represents 50 μM.

A)

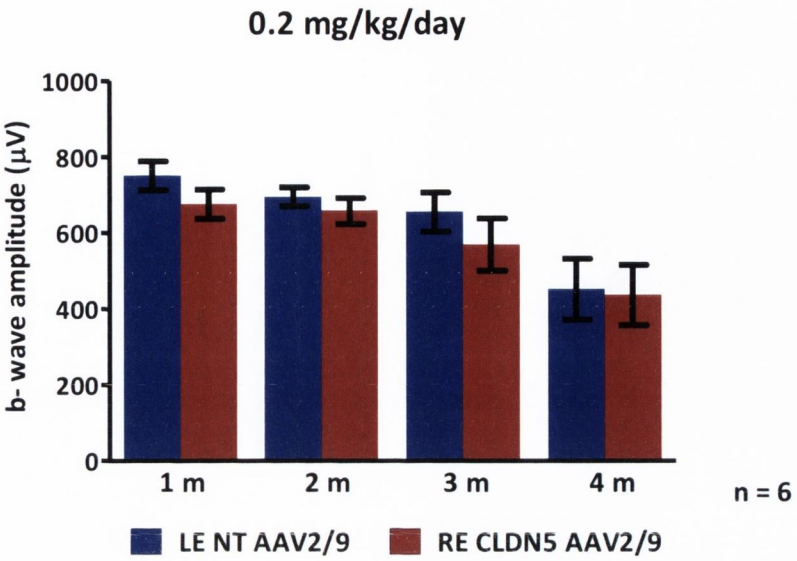

B)

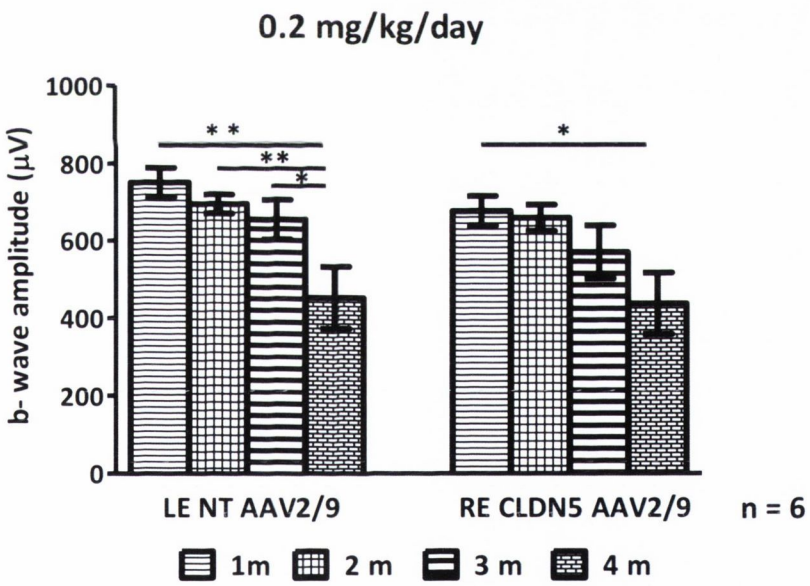

Figure 5. 41: ERG measurements of rod isolated response in P23H-3 rats treated with 0.2 mg/kg/day 17-DMAG.

Six rats were injected with NT AAV2/9 in their left eye and CLDN5 AAV2/9 in their right eye at 1 month old. These rats were then administered with 17-DMAG and doxycyline 2 weeks post injection and ERGs were measured at 1, 2, 3 and 4 months post treatment. A) b-wave amplitudes of the isolated rod response. No significant difference was observed in b-wave amplitudes between LE and RE at all timepoints. B) Using repeated measures ANOVA and Tukey post tests, there were statistical differences in b-wave amplitude of rod

response in LE NT AAV2/9 of rats treated with 17-DMAG and doxycycline for 1, 2 or 3 months compared to those treated for 4 months (** $P < 0.01$ and * $P \leq 0.05$). Likewise, ERG readouts were significantly reduced in eyes injected with CLDN5 AAV2/9 after 4 months compared to 1 month post 17-DMAG (* $P \leq 0.05$). Error bars denote ± SEM.

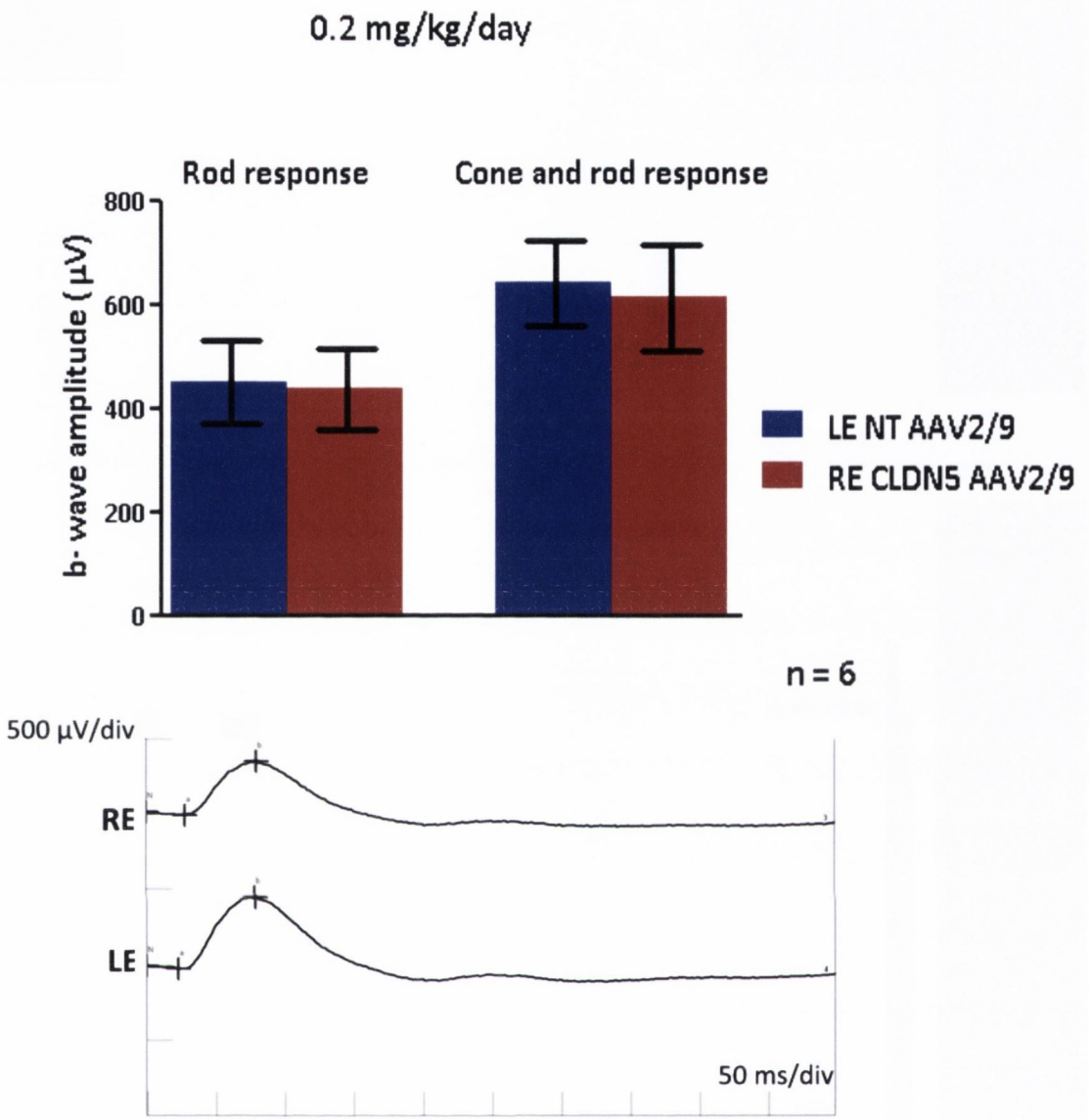

Figure 5. 42: Effect of 0.2 mg/kg/day 17-DMAG on the degenerating P23H-3 rat retina.

ERG readouts of the same rats as in **Figure 5.41** 4 months post 17-DMAG (0.2 mg/kg/day) treatment. There was no significant difference in b-wave amplitudes of both rod isolated response and cone and rod response in eyes injected with CLDN5 AAV2/9 compared to contra lateral control eyes (n = 6). The graph shows representative ERG tracing of rod isolated response. Error bars denote ± SEM.

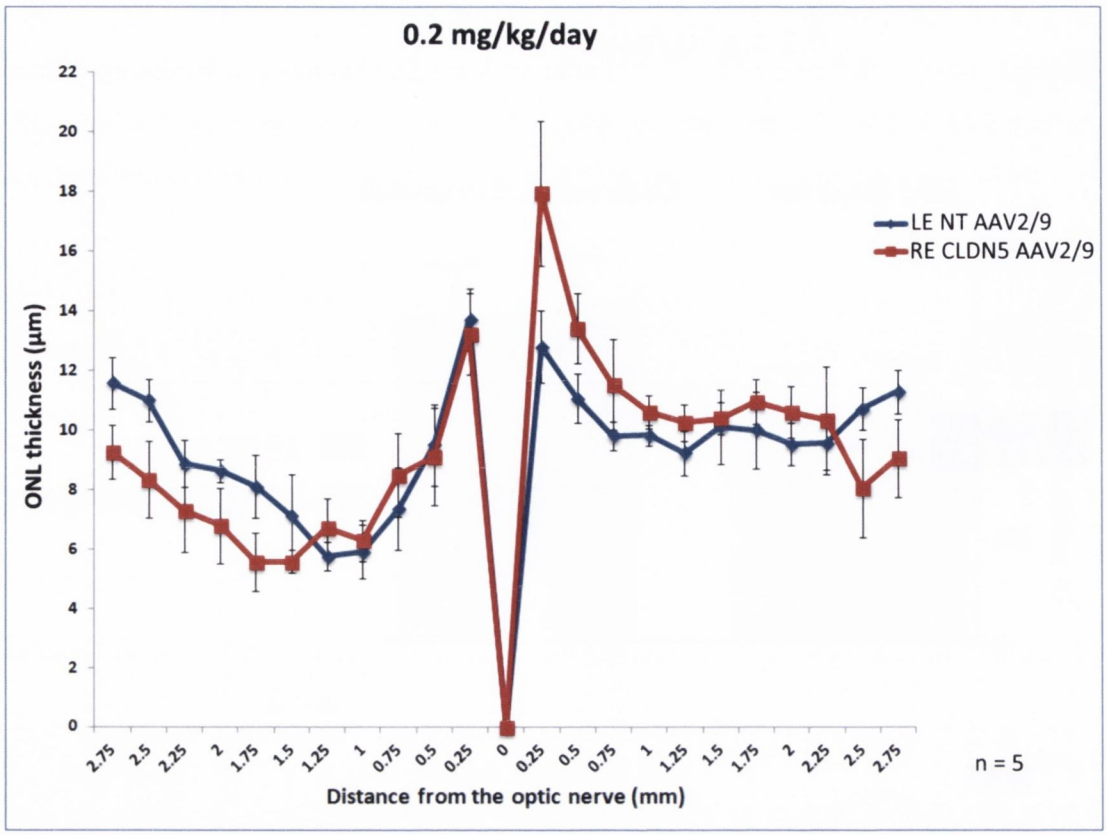

Figure 5. 43: Measurements of ONL thickness in rats treated with 0.2 mg/kg/day.

No statistical difference in ONL thickness between treated and non-treated eyes of the same rats as in **Figures 5.41 and 5.42**.

A) 4 mg/kg/day

Animal	Before (g)	After (g)
1	360	272
2	313	301
3	294	268
4	283	285
5	303	304
6	310	296
7	313	293
8	297	288
9	292	292
Average	**307.22**	**288.78**

B) 0.2 mg/kg/day

Animal	1 m (g)	2 m (g)	3 m (g)	4 m (g)
1	235	270	286	299
2	211	252	261	272
3	244	280	283	295
4	234	286	297	310
5	220	260	274	282
Average	**228.80**	**269.60**	**280.20**	**291.60**

Table 5. 1: Weight of P23H-3 rats treated with A) 4 mg/kg/day and B) 0.2 mg/kg/day 17-DMAG.

Table shows that the treatment did not affect weight of these rats in general. A) No significant difference in weight between before and after 17-DMAG treatment. B) Weight of rats continued to increase as they grew older. In fact, repeated measures ANOVA and Tukey post tests showed that weights of these animals increased significantly with age (*** $P < 0.001$).

Chapter 6

Studies on Murine Models of P23H Rhodopsin

1. Characterisation of models generated by AAV2/5 Delivery of WT and P23H Rhodopsin

2. Effect of 17-DMAG in a P23H Transgenic mouse model exhibiting Rapid degeneration

6.1 Introduction

The need for effective therapy for adRP has led to the development of several animal models including transgenic mice and rats expressing the rhodopsin mutations P23H, T17M, P347S and S334X in addition to fly and frog mutants carrying P23H rhodopsin. Although spontaneously arising mice mutants mimicking the course of human autosomal dominant RP have not been described, there are two such mutants, *rd* and *rds*, which model recessive retinopathies, having defects in the cGMP phosphodiesterase β-subunit gene and in the peripherin gene, respectively (Bowes *et al.*, 1990, Connell *et al.*, 1991, Pittler and Baehr, 1991, Travis *et al.*, 1991). Large animal models include a dog harbouring the T4R rhodopsin mutation and transgenic P23H miniature pigs which are also available for investigators to explore disease pathogenesis and therapeutic interventions for adRP (Kijas *et al.*, 2002, Zhu *et al.*, 2004, Cideciyan *et al.*, 2005, Ross *et al.*, 2012). In this introductory section, various mouse models expressing either human or mouse P23H transgene and their differences in expression levels and localization of rhodopsin within photoreceptors will be outlined. Since the P23H rat model used in **Chapter 5** has a slow rate of retinal degeneration, a P23H AAV2/5-induce mouse model was simultaneously developed in this study in order to test the effect of 17-DMAG on photoreceptor cell death. In addition, systemic administration of 17-DMAG in tandem with iBRB modulation via subretinal injection of CLDN5 AAV2/9 was also investigated in a P23H mouse model.

The first transgenic animal models for retinal research carrying either a normal or a mutant human rhodopsin (abbreviated henceforth RHO) allele on a B6D2F1 background were created by Olsson *et al.* (1992) two years after the discovery of the P23H mutation in the *RHO* gene in man (Dryja *et al.*, 1990). Three lines carrying P23H rhodopsin designated P23H-D, P23H-E and P23H-L had ratios of mouse rhodopsin (abbreviated henceforth Rho) to human P23H RHO mRNA of 1:3, 1:1 and 6:1, respectively. Although all of these lines exhibit retinal degeneration, the variation in the severity of the phenotype correlates with

the amount of mutant RHO expression compared to WT mouse Rho expression. Despite the level of mouse Rho mRNA being far greater than that of mutant RHO in the P23H-L line, these mice still suffered from a moderate retinal degeneration which was strikingly apparent by P20. In addition, Olsson *et al.* (Olsson *et al.*, 1992) also created two transgenic lines carrying a normal human allele (NHR), NHR-A and NHR-E which differed in the ratio of mouse Rho expression versus human RHO expression. The NHR-A strain which expresses 5-fold more human RHO than murine Rho expression level had severe photoreceptor degeneration similar to that observed in the P23H-D and P23H-E lines. On the other hand, the NHR-E line with equal amounts of both human and mouse rhodopsin mRNA was nondegenerating and had similar photoreceptor structures and ERG readouts as WT mice. However, in general, studies regarding the effect of overexpression of WT rhodopsin have been met with conflicting results. For example, Sung *et al.* (1994) showed that in mice expressing as little as ~ 10% more mouse Rho transcripts, the average time for loss of more than 50% of photoreceptors occurred after only 8 weeks of age. In addition, photoreceptor degeneration evident at P30 was induced by ~23% overexpression of WT mouse Rho (Tan *et al.*, 2001).

In this laboratory, Rho knockout mice on a mixed C57BL/6J-129Sv genetic background were generated back in the 1990s to provide a useful tool for the study of RP (Humphries *et al.*, 1997). These Rho-/- mice initially develop normal numbers of photoreceptor nuclei but do not elaborate rod outer segments and thus do not have rod ERG responses. Photoreceptor degeneration was relatively uniform across the retina and was almost completed at 3 months of age at which time only one row of photoreceptor nuclei (probably from cone cells) remained. On the other hand, Rho+/- animals retained the majority of their photoreceptors albeit with structural disorganization and shorter outer and inner segments compared to those of WT animals. Both Rho+/- and WT mice had similar cone and rod ERG responses at 13 weeks old. Moreover, the severity of the retinopathy

also varied depending on genetic background (Humphries *et al.*, 2001). By three months of age, the rate of photoreceptor cell loss was significantly slower in C57BL/6J Rho-/- compared to 129Sv Rho-/- mice whereas WT mice on these two backgrounds had similar number of photoreceptor nuclei at this age. In addition, TUNEL staining results also showed that photoreceptor apoptosis started to occur at a later stage (P28) in Rho-/- mice on 129Sv background but increased over a longer period of time and had a more devastating effect. From 45 days of age, b-wave amplitude of cone isolated response also declined significantly faster in 129Sv Rho-/- mice than in C57BL/6J Rho-/- mice. Further studies on Rho-/- mice demonstrated that retinas of both P23H+/- Rho-/- and P23H+/- Rho+/- showed marked degeneration with a complete loss of photoreceptors by 2 weeks old, and reduced a- and b-wave ERG readouts (O'Reilly *et al.*, 2007).

Another mouse model was created which expresses a mutated mouse *Rho* transgene containing three amino acid substitutions near the N terminus of rhodopsin V20G, P23H and P27L and is thus known as the VPP mouse. V20G and P27L mutations have not been observed in human adRP and these amino acid positions are much less conserved than Pro23. These mice simultaneously express mutated and WT murine *Rho* genes at comparable levels and exhibit retinal degeneration mimicking severe human adRP, degeneration being essentially complete by P30 (Naash *et al.*, 1993, Goto *et al.*, 1995, Frederick *et al.*, 2001) . In particular the rate of retinal degeneration observed in the presence of one wild type endogenous allele (Rho +/-) was significantly faster than that in the normal Rho +/+ background (Frederick *et al.*, 2001).

Murine models expressing P23H rhodopsin have also been used to investigate mutant protein localization. However, although studies carried out using these mouse models are in agreement that retinal degeneration correlates with the level of P23H expression, they differ significantly in the localization of mutant P23H rhodopsin. For example, in models expressing high levels of P23H RHO, the mutant RHO was localised in the inner and outer

segments, with significant levels in the ONL and in the OPL (Olsson *et al.*, 1992, Roof *et al.*, 1994). On the other hand, in models exhibiting slower degeneration most P23H RHO was found in the rod OS although a small fraction was initially present in the OPL and in the ONL (Olsson *et al.*, 1992, Roof *et al.*, 1994). In the VPP mice with the Rho-/- background, the VPP Rho was localized in the ER around the rod cell nuclei in the ONL and failed to support OS formation (Frederick *et al.*, 2001). In contrast, mutant Rho was present mostly in the rod OS but with some mislocalization to the OPL in the presence of endogenous mouse Rho (Wu *et al.*, 1998). Recently, two P23H RHO knock-in mouse models were generated, in which the endogenous mouse rhodopsin locus was modified to carry either a mouse *P23H Rho* or a human *P23H RHO-GFP* fusion gene (Price *et al.*, 2011, Sakami *et al.*, 2011). In mice heterozygous for mouse *P23H Rho* and normal mouse *Rho* generating a phenotype mimicking changes in the retina of patients with P23H adRP, all rhodopsin was found in the rod OS (Sakami *et al.*, 2011). In contrast, in mice heterozygous for the human *P23H RHO-GFP* fusion gene, expression of which was at such a low level that no significant retinal dysfunction could develop, the P23H RHO-GFP fusion protein was substantially degraded and mostly mislocalized to the ONL and the rod IS (Price *et al.*, 2011).

Although murine and human rhodopsin differ in their amino acid sequence at 18 residues, the presence of *NHR* transgene, expressing at the same level as WT mouse rhodopsin, rescued severe retinal degeneration in Rho-/- mice and displayed a WT phenotype (McNally *et al.*, 1999). Similarly, mice expressing a codon-modified human *RHO* transgene designed to avoid targeted suppression by siRNA on a Rho-/- background also had ERG responses and retinal histology equivalent to WT and NHR+/- Rho -/- mice (O'Reilly *et al.*, 2007, O'Reilly *et al.*, 2008). Indeed, the presence of normal rhodopsin does appear to influence localization of mutant P23H rhodopsin and the extent of retinal degeneration in mutant mouse models, since it has also been shown that increasing the

amount of WT rhodopsin up to a limit where it is toxic on its own, improved long term photoreceptor survival and visual function in mice expressing a P23H transgene (Mao *et al.*, 2011, Mao *et al.*, 2012, Price *et al.*, 2012).

6.1.1 Objectives

Recently, recombinant AAV serotypes have been the predominant vectors used for gene delivery to photoreceptors because of efficient transduction, low toxicity and long term gene expression compared to adeno- and lenti-viral vectors (Lebherz *et al.*, 2008, Surace and Auricchio, 2008, Stieger *et al.*, 2009, Watanabe *et al.*, 2013). Moreover, the safety and efficacy of AAV for retinal gene therapy has been further enhanced by results from four independent human clinical trials using AAV2 in the human eye (Bainbridge *et al.*, 2008, Cideciyan *et al.*, 2008, Maguire *et al.*, 2008, Banin *et al.*, 2010), and so far the treatment has resulted in substantial improvement in vision for at least 3 years (Jacobson *et al.*, 2012). In addition, these viral vehicles are also promising for *in vivo* functional analysis of retinal genes. AAV-mediated expression of human mutant IMPDH1 containing the Arg224Pro mutation but not WT IMPDH1 in retina has been shown to produce rapid structural and functional retinal degeneration in IMPDH1+/- mice (Tam *et al.*, 2008). Similarly, adenovirus or AAV-mediated delivery of vascular endothelial growth factor to rat and mouse retinas induces choroidal neovascularisation, a hallmark of wet AMD (Baffi *et al.*, 2000, Wang *et al.*, 2003, Cashman *et al.*, 2006). Moreover, adenovirus-mediated delivery of complement component 3 to the RPE of murine retinas leads to significant functional and structural changes resembling many features of AMD as well as those of other retinal diseases such as proliferative diabetic retinopathy and proliferative vitreoretinopathy (Cashman *et al.*, 2011). In the context of this chapter, AAV2/5 vectors expressing human P23H or WT RHO were designed to generate viral-mediated WT and P23H RHO murine models for studies involving the characterization of P23H disease progression. In addition, similar to research carried out and described in **Chapter 5**, the

efficacy of 17-DMAG in alleviating ER stress was also tested in human P23H+/- Rho+/- and P23H+/- Rho-/- mouse models due to their faster photoreceptor degeneration rate compared to the rat model. Thus, it was envisaged that the results obtained from these mice may also confirm the effect of 17-DMAG in ER stress-induced apoptosis.

6.2 Materials and Methods

6.2.1 AAV construction

Based on the replacement human RHO complementary DNA sequence in the pAAV-BB24 vector, the human WT RHO DNA sequence (758 bp) was constructed by synthesizing the whole sequence starting from the HindIII restriction site in the murine Rho promoter and finishing at the BsaBI restriction site in the replacement RHO pAAV-BB24 vector and modifying wobble (modified) sites at nucleotides 254-274 back to the original WT RHO sequence (NM_000539.2) (Palfi *et al.*, 2010). The pAAV-BB24 vector was kindly provided by Prof. Jane Farrar. The DNA sequence generated by GeneArt contained an extra sticky KpnI site at the 3' end right after the original BsaBI site which generated a blunt end thus being unsuitable for ligation to the GeneArt plasmid. The pRHO-GeneArt vector consisted of 758 bp WT RHO sequence, 668 bp Col E1 origin and 798 bp Kanamycin resistance sequence (**Figure 6.1**).

Using the same pair of P23H mutagenesis primers (**Section 5.2.4**), QuikChange Site-Directed Mutagenesis was then carried out on the WT RHO vector synthesized by GeneArt (Invitrogen) to create the P23H RHO vector. These two GeneArt vectors were then digested with HindIII and BsaBI restriction enzymes to release the human P23H and WT RHO DNA sequences which were later ligated back into pAAV-BB24 vector also previously digested with HindIII and BsaBI to remove the original replacement RHO sequence. Both WT RHO pAAV-BB24 and P23H pAAV-BB24 contained a 1812 bp mouse rhodopsin promoter (Rho-P) together with two conserved Rho-P elements (66 bp Enhancer Element and 76 bp B region), a 0.4 kb fragment of the endogenous 3'-UTR (168 bp polyA region F and 253 bp polyA region G), and a 49 bp minimal polyadenylation signal (**Figure 6.1**).

Sequencing primers for detecting P23H and WT sequence in pRHO-GeneArt after mutagenesis were: Forward: 5'-GCCTCTTCGCTATTACGCCAG-3' and Reverse: 5'-

TTAGGCACCCCAGGCTTTAC-3' (GeneArt), or Reverse: 5'-CATGCAGAGAGGTGTAGAGGG-3' (GenScript). Sequencing primer for detecting P23H and WT sequence in pAAV-BB24 was Forward: 5'-ATGTCACCTTGGCCCCTCT-3' (GenScript).

The two P23H pAAV-BB24 and WT RHO pAAV-BB24 plasmids were then used to generate P23H AAV2/5 and WT RHO AAV2/5 by Vector Biolabs.

6.2.2 Ligation

Ligations were carried out in 20 µl reaction volumes at a vector to insert ratio of 1:5 (w/w) and incubated at 16°C overnight. Negative controls were also included to verify the complete digestion of the pAAV-BB24 vector. The components of a ligation reaction included the following:

Component	Experiment (µl)	Negative control (µl)	Negative control (µl)	Negative control (µl)
pAAV-BB24	1	1	-	1
Insert	4	-	4	4
T4 Ligase	1	1	1	-
T4 10x Ligase buffer	4	4	4	4
ddH_2O	11	14	11	11
Total Volume	20	20	20	20

3 µl of each ligation reaction was then used for the transformations of 150 µl of XL1 Blue competent cells which were then plated on a petri dish containing Ampicillin and Tetracycline antibiotics. Clones were mini prepared, double digested with HindIII and BsaBI enzymes and analyzed with gel electrophoresis to ensure positive results. Two samples were chosen for further evaluation with sequencing and later being maxi prepared.

6.2.3 RT-PCR for expression level of human RHO

mRNA was isolated from mouse retinas and measured for levels of human RHO using QuantiTect®SYBR® Green RT-PCR kit as in **Section 2.4.7**. Human RHO specific primers used were the same as in **Section 5.2.10.** Human RHO expression levels were standardized against mouse β-actin. Primers for mouse β-actin were: Forward 5'-AGAGCAAGAGAGGTATCC- 3' and Reverse 5'- TCATTGTAGAAGGTGTGGTGCC-3'.

6.2.4 Determination of AAV titer (Rohr *et al.*, 2002)

Before determining viral titre, 2 µl from each viral fraction was diluted with 28 µl nuclease free water and 15 µl of this was mixed with 5 µl RQ1 DNase 10x reaction buffer, 1 µl RQ1 RNase free-DNase enzyme and 29 µl nuclease free H_2O (Promega). The reaction was incubated at 37°C for 30 min and later at 65°C for 10 min. After this step, 1 µl Proteinase K (Invitrogen) was added and the reaction was incubated at 50 °C for 1 hour and inactivated at 95°C for 20 min.

Quantitative PCR (qPCR) analysis was carried out with human RHO specific primers. Either WT RHO pcDNA3 or P23H RHO pcDNA3 was used for preparation of a standard curve. For example, the concentration of P23H RHO pcDNA3 was 895.4 ng/µl and the length of the plasmid was 7.323 kb containing 1.923 kb insert of P23H RHO between EcoRI and HindIII site, these values were used to calculate number of molecules available in 1 ng of plasmid. Using the website http://www.uri.edu/research/gsc/resources/cndna.html, each ng of P23H RHO pcDNA3 contained 1.13×10^{11} molecules of P23H RHO pcDNA3. A serial 10-fold dilution of pcDNA3 containing the human RHO was made consisting of between 10^3-10^8 molecules of the plasmid. These dilutions were used to generate a standard curve for determining viral titre. qPCR was performed on 100-fold dilution of each AAV treated with DNase and Proteinase K using the two-step RT-PCR SYBR green PCR kit (Qiagen) and each reaction

well contained 5 µl diluted AAV2/5, 10 µl SYBR green, 1 µl primer stock (10 pmol/µl) and 4 µl nuclease-free H_2O. Reactions were carried out as follows:

1. **Activation of DNA polymerase:** 95°C for 15 min

2. **cDNA amplification:** 36 cycles at 95°C for 15 s and 60°C for 1 min.

Titre of each AAV2/5 (viral genomes/ml) was calculated by multiplying results obtained with 10^6.

6.2.5 Genotyping

Primers for mouse Rho (GenBank M55171.1) genotyping were as follows: MuRho3109Forward 5'-GAGCTTCTGTTTTGGCACAC-3' (position 3109-28 intron 1), MuRho3536Reverse 5-TTATGCCTGGAACCAATCCG-3' (position 3536-17 intron 2) and NeoR 5'-TTCAAGCCCAAGCTTTCGCG-3'. MuRho3109Forward and MuRho3536Reverse gave a fragment of 428 bp in a Rho+/+ mouse. However, the neo^R gene was inserted at the Eco47111 site in exon 2 of the rhodopsin gene in a Rho-/- mouse. The fragment amplified with MuRho3109Forward and NeoR is 251 bp. All three primers were used together in the following amplification reaction: 1 µl of crude DNA extracted from tail or ear biopsy (**Section 2.8.2**), 0.25 µl each of primers (100 pmol/µl), 0.4 µl dNTP mix (12.5 pmol/µl, 2.5 µl 10x reaction buffer, 0.125 µl *Taq* polymerase in a total reaction volume of 25 µl. PCR conditions: 94°C for 1 min, 35 cycles at 94°C for 1 min, 55°C for 1 min and 72°C for 1 min; and 72°C for 5 min. PCR products were resolved on a 2% agarose gel, fragments of 428 and 251 bp being diagnostic of the WT and mutant alleles respectively.

Primers for human P23H genotyping were as follows: Forward: 5'-CATTCTTGGGTGGGAGCAG-3'and Reverse: 5'-GGACAGGAGAAGGGAGAAGG-3'. Amplification reaction included 1 µl of crude DNA extracted from tail or ear biopsy, 0.25 µl each of primers (100 pmol/µl), 0.4 µl dNTP mix (12.5 pmol/µl), 0.125 µl Taq polymerase in a total reaction volume of 25 µl. PCR conditions: 95°C for 1 min, 35 cycles

at 95°C for 30 s, 57.5°C for 30 s and 72°C for 1 min 20 s; and 72°C for 10 min. PCR products were resolved on a 2% agarose gel, a fragment 518 bp being diagnostic of the presence of human P23H transgene.

6.2.6 TaqMan® gene expression analysis

After being intravitreally injected with 17-DMAG or PBS, mRNA were isolated from the retinas of P23H+/- Rho-/- mice at 3 and 5 days post injection. mRNA samples were converted to cDNA samples which were then used in Taqman® Gene Expression Assays (**Section 5.2.9**). IDs for these assays were: CHOP (Mm_00492097_m1), BiP (Mm_00517691_m1), Xbp1 (Mm_00457357_m1), Grp94 (Mm_00441926_m1) and β-actin (Mm_00607939_s1).

6.2.7 Statistical analysis

Two-tailed paired student's *t* test was used for comparison between results obtained from the left and right eyes of the same animals. Unpaired two-tailed student's *t* test was used for comparison between different strains of animals. $P \leq 0.05$ was considered being significant.

6.3 Results

6.3.1 Generation of AAV constructs

The aim of this section was to develop an induced mouse model of P23H adRP by subretinal injection of AAV2/5 expressing P23H RHO which would exhibit a moderate rate of retinal degeneration so that a full spectrum of P23H models encompassing slow (P23H-line 3 rat), moderate (P23H AAV2/5-induced mouse) and fast (P23H+/- Rho-/- mouse) rates of retinal degeneration would be available for testing therapeutics. A range of AAV2/5 constructs for gene replacement therapy of adRP was investigated for efficacy in transduction and retinal improvement in Rho-/- mice (Palfi *et al.*, 2010). In one particular vector design called AAV-BB24, the authors indicated that murine Rho promoter containing highly conserved elements across different species provided a high level of WT RHO mRNA expression which represented approximately 40% of endogenous mouse rhodopsin found in WT mice. ERG measurements at 6 and 12 weeks post subretinal delivery of AAV-BB24 to P0 Rho-/- mice showed evidence of rod derived ERG responses in the injected eyes compared to the control eyes. However, there was a decline in both ERG rod response and ONL thickness at 12 weeks compared to 6 weeks post subretinal injection. Nevertheless, ultrastructural analysis of Rho-/- retinas transduced with AAV-BB24 at 6 weeks post injection showed correctly formed rod photoreceptor OS with parallel membrane disks, reaching to the RPE compared to short truncated rod OS extending from the apical membrane of the rod photoreceptor inner segment in uninjected eyes (Palfi *et al.*, 2010).

Given these results, P23H and WT RHO AAV2/5 investigated in this chapter were designed based on the AAV-BB24 construct which contained modified bases in the RHO cDNA sequence for gene suppression and replacement therapy. At first, a short DNA sequence containing the human WT RHO with a HindIII restriction site at the 5' end and a BsaBI restriction site right before a KpnI restriction site at the 3' end were synthesized and

ligated into a plasmid called pRHO-GeneArt by GeneArt (Invitrogen). The HindIII and BsaBI sites are also present in the pAAV-BB24 construct (**Figure 6.1**). The reason to introduce the KpnI site was because BsaBI generated a blunt end which was unsuitable for ligating to the GeneArt plasmid. Next, pRHO-GeneArt expressing P23H RHO was made using the QuikChange site directed mutagenesis kit with the same pair of primers used in **Section 5.3.2.2**. The two pRHO-GeneArt plasmids expressing WT RHO or P23H RHO were then digested with HindIII and BsaBI restriction enzymes to excise a 758 bp band which was then ligated back to pAAV-BB24 previously digested with these two enzymes to generate P23H pAAV-BB24 and WT RHO pAAV-BB24 (**Figure 6.2**). These two plasmids were later used to synthesize P23H AAV2/5 and WT RHO AAV2/5 by Vector Biolabs. All constructs were sequenced at every single step to ensure the correct DNA sequence of WT and P23H RHO (**Figure 6.3**).

6.3.2 Determination of AAV titres

In order to investigate expression levels of WT RHO AAV2/5 and P23H AAV2/5, a group of 5 month old 129Sv WT animals (n = 3) was first injected with 3 µl of WT RHO AAV2/5 in their left eyes and 3 µl of P23H AAV2/5 in their right eyes. 23 days later, mice were put down and mRNA samples were isolated from their retinas and tested for expression levels of human RHO using mouse β-actin expression level as the endogenous control. mRNA of an NHR mouse was used for the standard curve. According to Vector Biolabs, the titres of WT RHO AAV2/5 and P23H AAV2/5 were 1.8×10^{13} and 1.2×10^{13} vp/ml, respectively. However, the expression level of human RHO in retinas injected with WT RHO AAV2/5 was 2.3-fold higher than that in retinas injected with P23H AAV2/5 (* P = 0.0219) (**Figure 6.4**). Therefore, it was necessary to establish whether the inclusion of empty viral particles had resulted in inaccurate titering by Vector Biolabs. In order to do this the actual titres expressed as vector genomes per ml (vg/ml) of the two AAVs were quantified by qPCR. Both WT RHO and P23H AAV2/5 were first digested with DNase

and Proteinase K and then tested for levels of human RHO. The AAV titres measured were roughly 10-fold less than those suggested by Vector Biolabs. In fact, AAV tires of WT RHO AAV2/5 and P23H AAV2/5 were 2.2 x 10^{12} and 9.97 x 10^{11} vg/ml, respectively. Thus the quantity of P23H AAV2/5 injected was 54.64% less (2-fold less) than that of WT RHO AAV2/5 (** P = 0.0057) (n = 3) (**Figure 6.5**) explaining the higher expression level of RHO in eyes injected with WT RHO AAV2/5 (**Figure 6.4**).

6.3.3 Effect of AAV2/5 – mediated delivery of WT and P23H RHO in 129Sv WT mice

In order to investigate the effect of P23H AAV2/5 in WT mice, a group of 3 month old 129Sv mice (n = 3) were injected with 3 µl PBS in the left eye and 3 µl of P23H AAV2/5 (9.97 x 10^{11} vp/ml) in the right eye. **Figure 6.6** shows that b-wave amplitudes of rod isolated response were significantly reduced by up to 49.87% and 62.02% in the right eye injected with P23H AAV2/5 compared with the control eye at 2 and 4 weeks post injection (* P = 0.0306 and * P = 0.0233, respectively). In addition, expression of P23H also led to a decrease of approximately 60% of both dimer and monomer levels of total rhodopsin protein in eyes injected with P23H AAV2/5 compared to control eyes at 6 weeks post injection (* P = 0.0322 and * P = 0.015 respectively) (**Figure 6.7**).

Since the presence of WT RHO has complicated analyses of retinal degeneration, as mentioned above, two different doses of P23H and WT RHO AAV2/5, termed Dose 1 and 2 were tested for induction of retinal degeneration. A group of 4 month old 129Sv WT mice were subretinally injected with 3 µl of either Dose 1 (9.97 x 10^{11} vg/ml P23H AAV2/5 in the right eye and 1.1 x 10^{12} vg/ml WT RHO AAV2/5 in the left eye) or Dose 2 (9.97 x 10^{10} vg/ml P23H AAV2/5 in the right eye and 1.1 x 10^{11} vg/ml WT RHO AAV2/5 in the left eye). Although the titres of both virus were reduced by 10-fold in Dose 2, b-wave amplitudes of rod isolated response in both eyes injected with AAV2/5 still significantly degenerated 6 weeks post injection compared to sham injected animals

(**Figure 6.8**). Specifically, ERG readouts in the left eye injected with Dose 1 (n = 3) and 2 (n = 4) of WT RHO AAV2/5 were statistically reduced by up to 64.46 and 33.9% compared to control (n = 4) (** P = 0.0083 and ** P = 0.0032, respectively). Likewise, ERG readouts in the right eye injected with Dose 1 and 2 of P23H RHO AAV2/5 were statistically lower by 56.77 and 36.24% compared to control (* P = 0.0134 and ** P = 0.0039, respectively). On the other hand, there was no significant difference in ERG readouts in the left eye injected with WT RHO AAV2/5 compared to the right eye injected with P23H AAV2/5 of both Dose 1 and 2.

6.3.4 Effect of WT RHO and P23H AAV2/5 in Rho+/- mice

Based on the results obtained from 129Sv WT mice, both WT RHO AAV2/5 and P23H AAV2/5 exerted a great effect on rod isolated response even at the lower concentration (3 µl of ~10^{11} vg/ml). The next objective was to study whether WT RHO AAV2/5 could alleviate degeneration and P23H AAV2/5 lead to retinal degeneration in 129Sv Rho+/- mice and C57BL/6 Rho+/- mice. First, two groups of Rho+/- animals in either C57BL/6 or 129Sv background (n = 7 for each group) were subretinally injected with 0.8 µl of 9.97 x 10^{11} vg/ml P23H AAV2/5 in the right eye and 0.8 µl of 1.1 x 10^{12} vg/ml WT RHO AAV2/5 in the left eye at P4. ERGs were then measured at 6 weeks post injection. **Figure 6.9** showed that all rod isolated, cone isolated and maximum cone and rod responses in C56BL/6J animals were statistically higher than that in 129Sv animals. In rod derived response, ERG in the left eye injected with WT RHO AAV2/5 and the right eye injected with P23H AAV2/5 were significantly reduced by up to 44.69% and 61.12% in 129Sv mice compared to C57BL/6J mice (** P = 0.0067 and ** P = 0.0014, respectively). As regards cone derived response, ERG in the left eye injected with WT RHO AAV2/5 and the right eye injected with P23H AAV2/5 were statistically reduced by up to 48.94% and 63.03% in 129Sv mice compared to C57BL/6J mice (** P = 0.0065 and ** P = 0.0015, respectively). Likewise, the maximum cone and rod response in WT RHO AAV2/5

injected eyes and P23H AAV2/5 injected eyes were significantly degenerated by 44.33% and 58.22% in 129Sv mice compared to C57BL/6J mice (** P = 0.0082 and ** P = 0.0003, respectively).

ERGs in Rho+/- animals on the C57BL/6J background were measured again 14 weeks post injection. **Figure 6.10** showed that ERG responses in these animals continued to degenerate with time. Rod derived responses in eyes injected with WT RHO AAV2/5 and P23H AAV2/5 were significantly reduced by 48.21% and 37.792% compared to 6 weeks post injection respectively (** P = 0.0015 and ** P = 0.0058, respectively). In cone derived response, the ERG in the left eye injected with WT RHO AAV2/5 was significantly reduced by 41.03% at 14 weeks post injection (*** P = 0.0008). Similarly, maximum cone and rod responses in the left eye injected with WT RHO AAV2/5 and the right eye injected with P23H AAV2/5 were also significantly reduced by 53.63% and 35.7% at 14 weeks post injection (*** P < 0.0001 and ** P = 0.008, respectively). Although no ERG differences were detected between P23H AAV2/5 and WT RHO AAV2/5 injected eyes at 6 weeks post injection, ERG in the left eye injected with WT RHO AAV2/5 were much lower than that in the right eye injected with P23H AAV2/5 at 14 weeks post injection. **Figure 6.12** demonstrates all cone isolated response, rod isolated response and maximum cone and rod response in eyes injected with P23H AAV2/5 were statistically higher by 76.89, 39.22, 53.66% compared to eyes injected with WT RHO AAV2/5 (*** P = 0.0005, * P = 0.0211 and ** P = 0.0034, respectively).

6.3.5 Effect of 17-DMAG in P23H+/- Rho-/- mice

Since transgenic P23H+/- Rho-/- mice have been shown to degenerate at a very fast rate with only one row of photoreceptors by two weeks of age, these mice were used to investigate if 17-DMAG would have any effect given this short therapeutic window. Mice were genotyped using specific primers for mouse Rho and human P23H genes. In brief, PCR products were run on a 2% gel with fragments of 428 and 251 bp being diagnostic of

the WT and mutant alleles respectively. For P23H genotyping, a fragment of 518 bp indicated the presence of the transgene (**Figure 6.13**). P23H+/- Rho-/- pups were intravitreally injected with 0.8 µl of 0.2 mg/ml 17-DMAG in the right eye and PBS in the left eye at P5. Mice were put down and mRNA isolated from retinas 3 (n = 5) and 5 (n = 7) days post injection. Taqman® gene expression analyses were carried out for BiP, Grp94, CHOP and Xbp1 in these samples. No differences were detected in any samples, except for the expression level of Grp94 5 days post injection which was 12.11% higher in the control PBS- injected eye compared to the eye injected with 17-DMAG (**Figure 6.14**).

6.4 Discussion

Both WT and P23H RHO AAV2/5 constructs used in this chapter were based on the design of AAV-BB24 which expresses a codon-modified replacement WT RHO at approximately 40% that of endogenous mouse Rho in WT mice with no adverse effect on ERG (Palfi *et al.*, 2010). In the current project 3 µl of 1.1 x 10^{12} vg/ml (3.3 x 10^{9} vg/eye), approximately three times less WT RHO AAV2/5, was injected and yet rod isolated ERG was reduced by over 60%. Moreover, even when the quantity of WT RHO AAV2/5 injected was reduced ten-fold (3.3 x 10^{8} vg/eye), reduced ERGs were still observed (**Figure 6.8**). This observation was in line with previous studies which suggested that a small amount of overexpression of rhodopsin could lead to retinal degeneration (Sung *et al.*, 1994, Tan *et al.*, 2001, Mao *et al.*, 2011). Interestingly, WT RHO AAV2/5 was as potent as P23H AAV2/5 in having a negative effect on ERG of 129Sv WT animals.

Despite WT animals with both 129Sv and C57BL/6J backgrounds having similar ERG and retinal thicknesses during developmental and adult stages, Rho-/- mutants exhibited different rates of retinal degeneration with a faster rate associated with the 129Sv background (Humphries *et al.*, 2001). In particular, this became apparent at 45 days old which was also the start of a steady decline in cone response (Toda *et al.*, 1999). Although the visual function of Rho+/- mice is similar to that of WT mice until 13 weeks of age (Humphries *et al.*, 1997), the genetic background did correlate with reduced ERG responses following injection with either WT or P23H RHO AAV2/5 in 129Sv Rho+/- mice compared to similarly injected C57BL/6J Rho+/- mice at six weeks post injection (**Figure 6.9**). The ERG reductions were approximately 44 – 49% and 58 - 63% in eyes injected with WT RHO AAV2/5 and P23H AAV2/5 respectively in Rho+/- mice on the 129Sv background compared to the C57BL/6J background. ERG readouts continued to decline in AAV2/5 injected C57BL/6J Rho+/- animals until 14 weeks post injection (**Figures 6.10 and 6.11**). In addition, ERG measurements from eyes injected with either

AAV were similar at 6 weeks post injection. Moreover, unexpectedly, significantly higher ERG readings of cone, rod and maximum cone and rod responses were observed in P23H AAV2/5 compared to WT RHO AAV2/5 injected eyes at 14 weeks post administration. The aim of this study was to determine the optimum titre which would cause retinal degeneration in mice when injected with P23H AAV2/5 but not with WT RHO AAV2/5. However, the negative effect of overexpression of WT RHO even in Rho+/- mice observed here demonstrates that either the viral titres used here, despite being of a smaller magnitude to those employed by others, are excessive. The design of the AAV construct has already been shown to give high transduction efficiency thus triggering OS formation and ERG response in Rho-/- mice (Palfi *et al.*, 2010). Hypothetically, it is possible to assume that WT RHO AAV2/5 would provide the same protection in Rho-/- mice. Therefore, future studies using these AAVs may have to be carried out in Rho-/- mice but will most likely be compromised due to rapidity of the retinal degeneration which P23H AAV2/5 is likely to cause in this background. Additionaly, injection at P0 with PBS alone compromised cone ERG response in Rho-/- while less of a decrease in ERG response was observed in mice injected at P10 (Palfi *et al.*, 2010). Moreover, expression of rhodopsin initiates at appoxiamately P4 postnatally in the murine retina (McNally *et al.*, 1999). Therefore, determination of the precise time of injection will also be necessary to improve this P23H AAV2/5 induced retinal degeneration model which could then be used to investigate whether systemic administration of 17-DMAG provides some protection against expression of P23H RHO.

The second objective of this chapter was to investigate the effect of intravitreal administration of 17-DMAG on expression levels of BiP, CHOP, Grp94 and Xbp1 in P23H+/- Rho-/- mice which exhibit an extremely rapid rate of retinal degeneration which results in less than one row of photoreceptor nuclei remaining by two weeks of age. Unfortunately though, due to the lack of animals (breeding was a problem), it was not

possible to optimise the timing of injection and dosage of 17-DMAG for intravitreal injection. Moreover, due to the short half-life of 17-DMAG, the difficulties of repeated injections in young pups and the rapid nature of the degeneration it would have been difficult to have observed any effect in preventing the thinning of the developing retina in these mice. Thus, after several unsatisfactory attempts, all experiments involving 17-DMAG intravitreal injections into this model were abandoned.

Recently, two knock-in models of P23H mice have been developed for better understanding of expression level, localization and mode of pathology of P23H protein. However, they differ significantly in their conclusion about the localization of P23H mutant protein. Sakami *et al.* (2011) suggested that mutant mouse P23H protein did not accumulate in the rod photoreceptor ER as described in various transgenic rodent rhodopsin mutant models, but instead disrupted rod photoreceptor disks. Moreover, the mouse P23H protein was inadequately glycosylated with levels between 1 and 10% that of WT Rho. It is worth noting that the authors used an antibody that did not distinguish between WT and mutant Rho protein and most P23H protein underwent an extensive rate of degeneration. Therefore, it was unclear whether mislocalization of P23H could have been detected in this study. Contrary to the above knock-in mouse model, the model developed by Price *et al.* (2011) contained one copy of a mutant human *RHO* gene fused with an enhanced *GFP* gene, thus replacing one copy of the endogenous mouse *Rho* gene. The study also indicated substantial degradation of P23H RHO in mouse rod cells and most of the remaining mutant P23H protein was mislocalized to the IS and ONL layers with only ~ 20% in the rod OS. It was also suggested that the toxic site of action of P23H protein was in the rod OS since retinal health improved with loss of P23H protein from the OS and gains in the IS and ONL layers, thus suggesting that in this model ER stress was not the cause of cell death (Price *et al.*, 2012). In addition, increasing the level of WT RHO in a retina heterozygous for a mutant P23H rhodopsin allele protected the retina from

degeneration (Mao *et al.*, 2011, Mao *et al.*, 2012, Price *et al.*, 2012). Given these results, it would be interesting to investigate the effect of 17-DMAG in these knock-in models to determine if induction of the unfolded protein response has any effect on retinal degeneration in these mouse models in which ER stress appears not to be the primary disease mechanism.

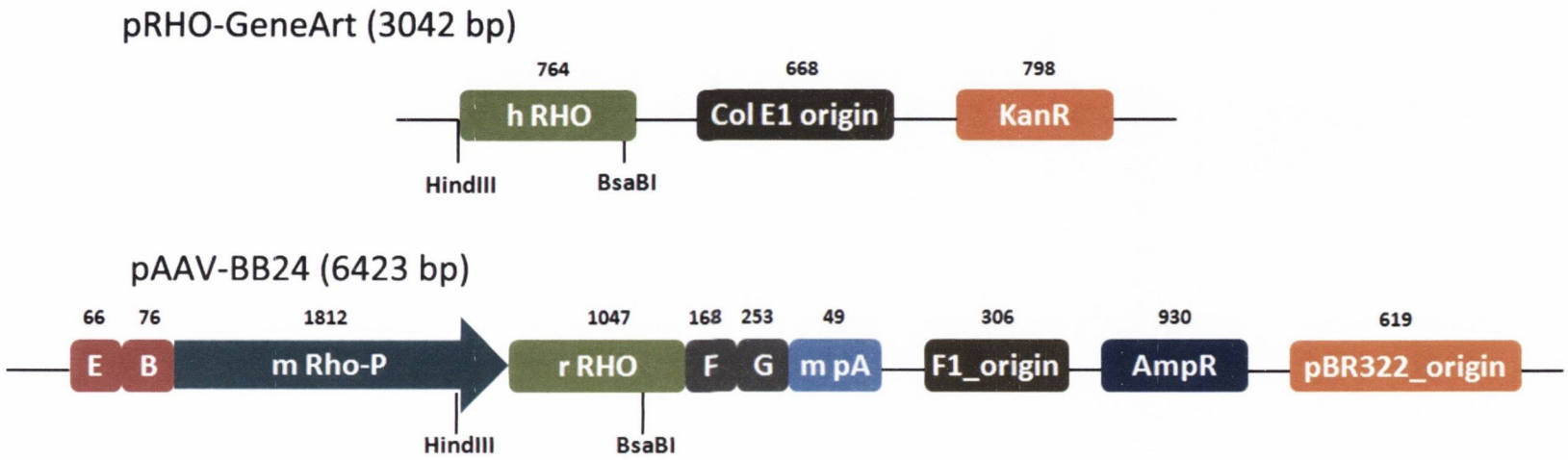

Figure 6. 1: Schematic presentations of DNA construct.

The pRHO-GeneArt vector consists of 758 bp WT RHO sequence, 668 bp Col E1 origin and 798 bp Kanamycin resistance sequence. The pAAV-BB24 vector was kindly provided by Prof. Jane Farrar Lab. Both WT RHO pAAV-BB24 and P23H pAAV-BB24 contain a 1812 bp mouse rhodopsin promoter (Rho-P) together with two conserved Rho-P elements (66 bp Enhancer Element and 76 bp B region), a 0.4 kb fragment of the endogenous 3'-UTR (168 bp polyA region F and 253 bp polyA region G), and a 49 bp minimal polyadenylation signal.

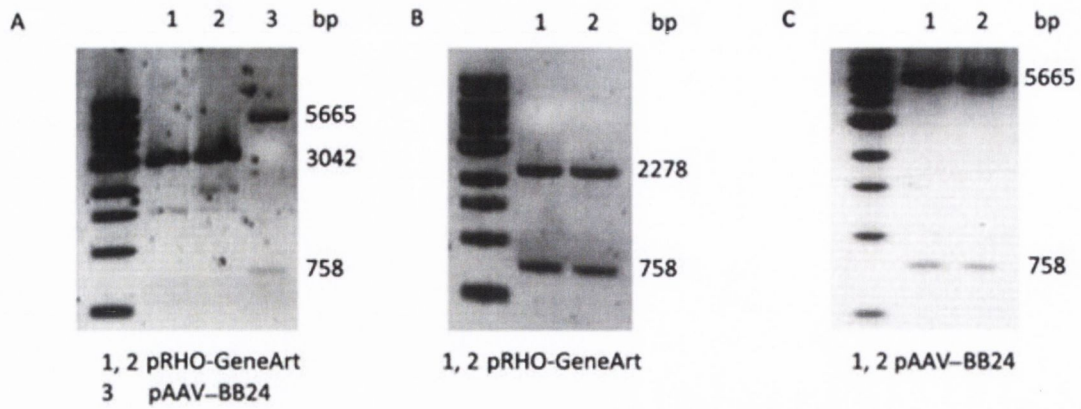

Figure 6. 2: Gel electrophoresis of DNA fragments important for the generation of P23H and WT RHO pAAV-BB24 constructs.

A) Two GeneArt vectors containing either WT RHO or P23H RHO DNA sequences were double digested with HindIII and BsaBI and then run on a 2% gel as lane 1 and lane 2 respectively to give a band of 3042 bp. The original pAAV-BB24 provided by Prof. Jane Farrar lab was digested with HindIII and BsaBI to excise two fragments of 5665 and 758 bp (lane 3). B) Two pRHO-GeneArt vectors expressing either WT RHO or P23H RHO were double digested with both restriction enzymes HindIII and BsaBI and run on a 2% gel to release two bands of 2278 and 758 bp. C) Gel analysis of pAAV_BB24 vectors post ligation and double restriction digestion with both HindIII and BsaBI to test for positive clones. 1 kb DNA ladder was loaded in all gels.

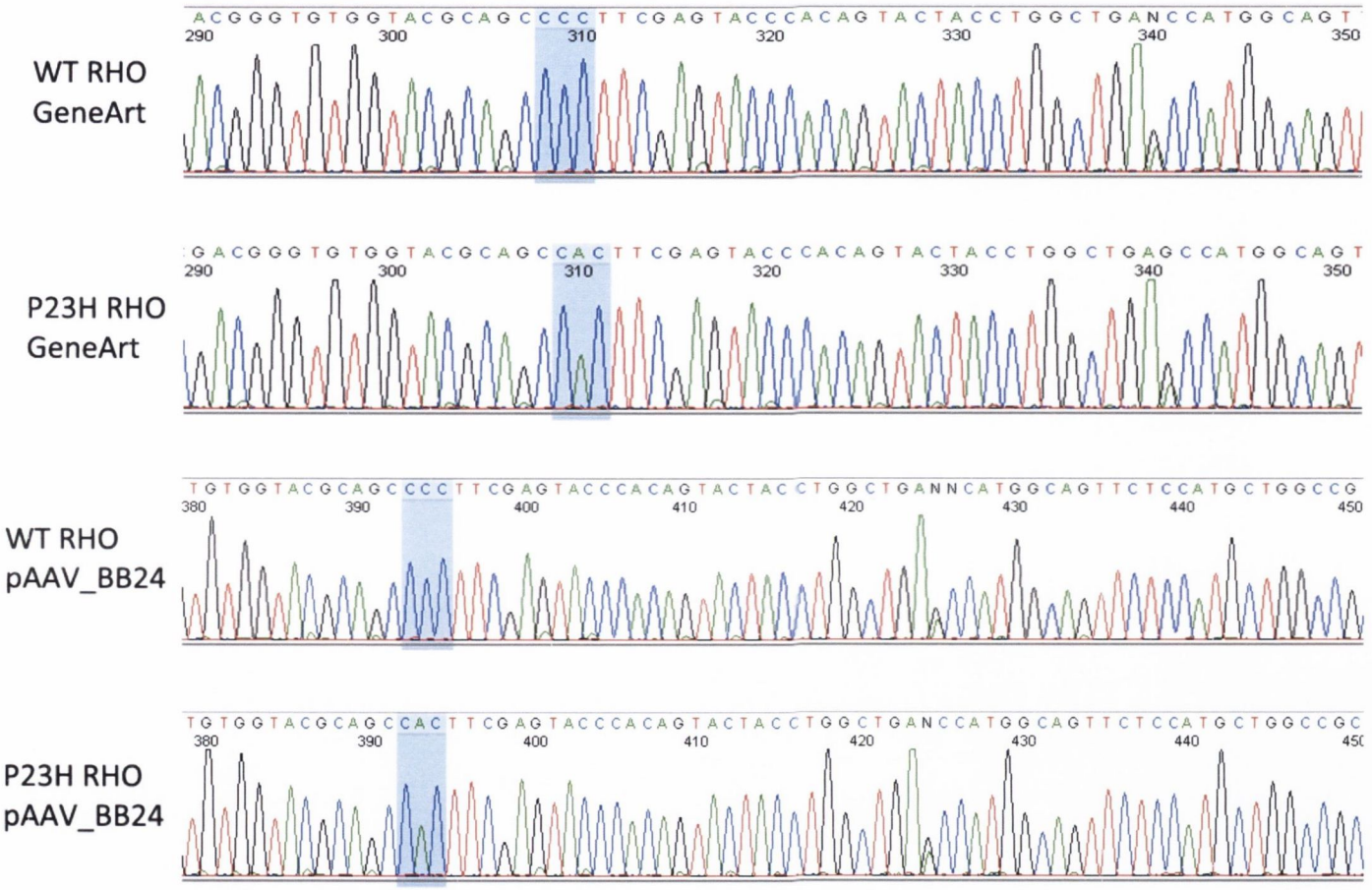

Figure 6. 3: Sequencing results for WT RHO and P23H constructs.

Blue labelled boxes show region of the DNA of interest to determine whether the construct is wild type or mutant RHO (CCC -> CAC).

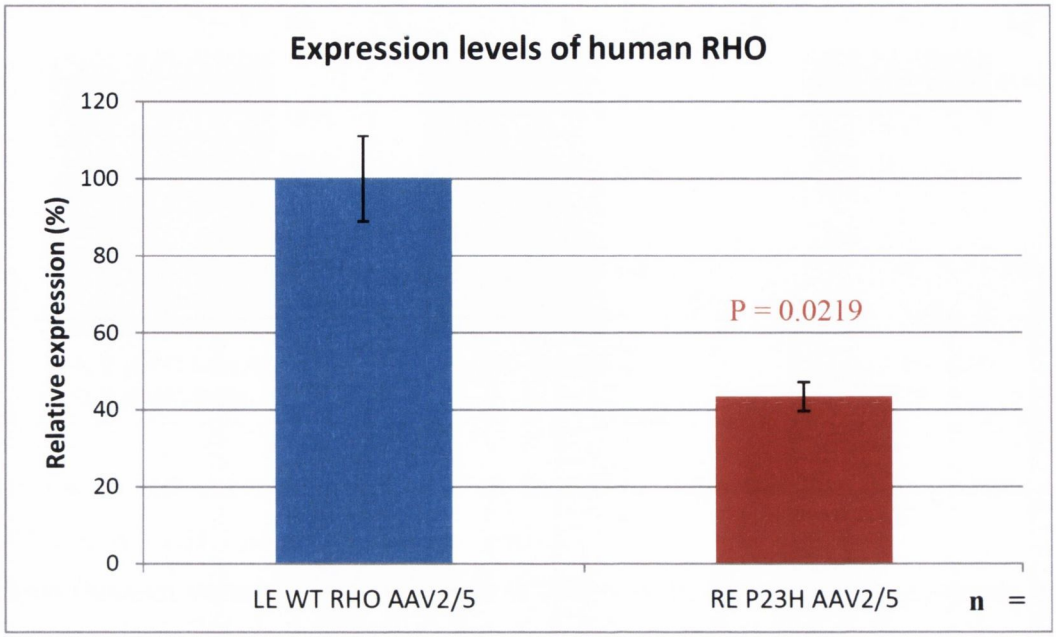

Figure 6. 4: Expression levels of human RHO in adult 129Sv WT mice injected with WT RHO and P23H AAVs.

Mice were injected with 3 µl of WT RHO AAV2/5 in their left eyes and 3 µl of P23H AAV2/5 in their right eyes (n = 3). 23 days later, mRNA were isolated from their retinas and measured for levels of human RHO expression. mRNA levels of human RHO in the left eye injected with WT RHO AAV2/5 were significantly higher than that in the right eye injected with P23H AAV2/5 (* P = 0.0219). Error bars denote ± SEM.

A)

	WT RHO AAV2/5	P23H AAV2/5
	2.02E+12	9.21E+11
	2.42E+12	1.04E+12
	2.15E+12	1.03E+12
Average	**2.20E+12**	**9.97E+11**
SEM	1.18E+11	3.81E+10

B)

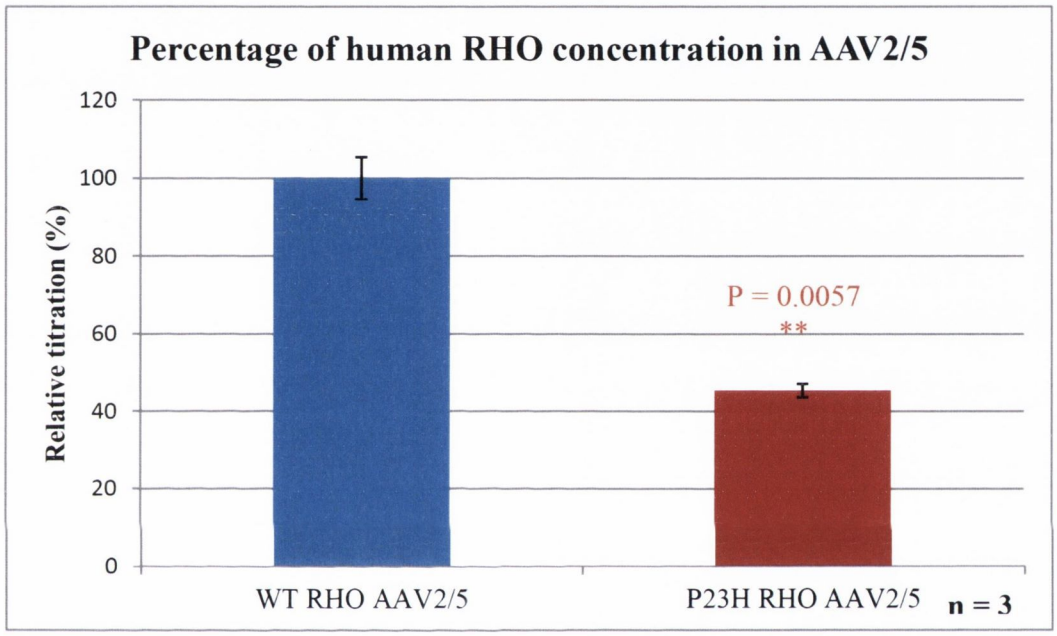

Figure 6. 5: Titres of WT RHO AAV2/5 and P23H AAV2/5.

Both AAV2/5s were first treated with DNase and Proteinase K before being measured for titres by qPCR method. A) AAV titres of WT RHO AAV2/5 and P23H AAV2/5 were 2.2 x 10^{12} and 9.97 x 10^{11} vg/ml, respectively. B) Titre of P23H AAV2/5 was 54.64% less than that of WT RHO AAV2/5 (** P = 0.0057) (n = 3). Error bars denote ± SEM.

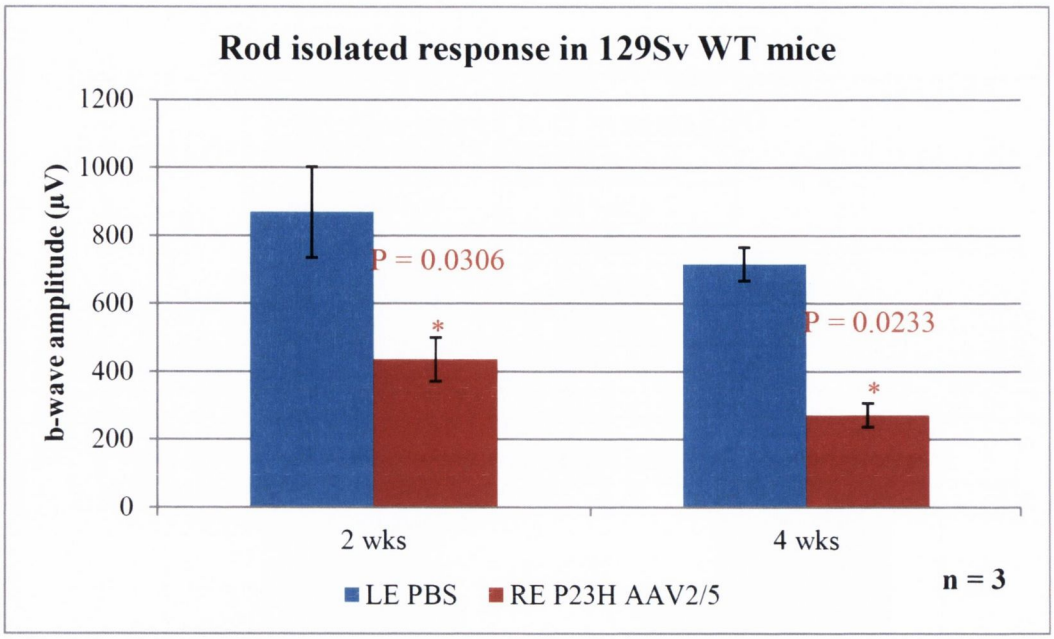

Figure 6. 6: ERG readouts in mice injected with P23H AAV2/5.

A group of 3 month old 129Sv mice (n = 3) were injected with 3 µl of PBS in the left eye and 3 µl of 9.97 x 10^{11} vg/ml P23H AAV2/5 in the right eye. b-wave amplitudes of rod isolated response was significantly reduced in the right eye injected with P23H AAV2/5 compared with the control eye at 2 and 4 weeks post injection (* P = 0.0306 and * P = 0.0233, respectively). Error bars denote ± SEM.

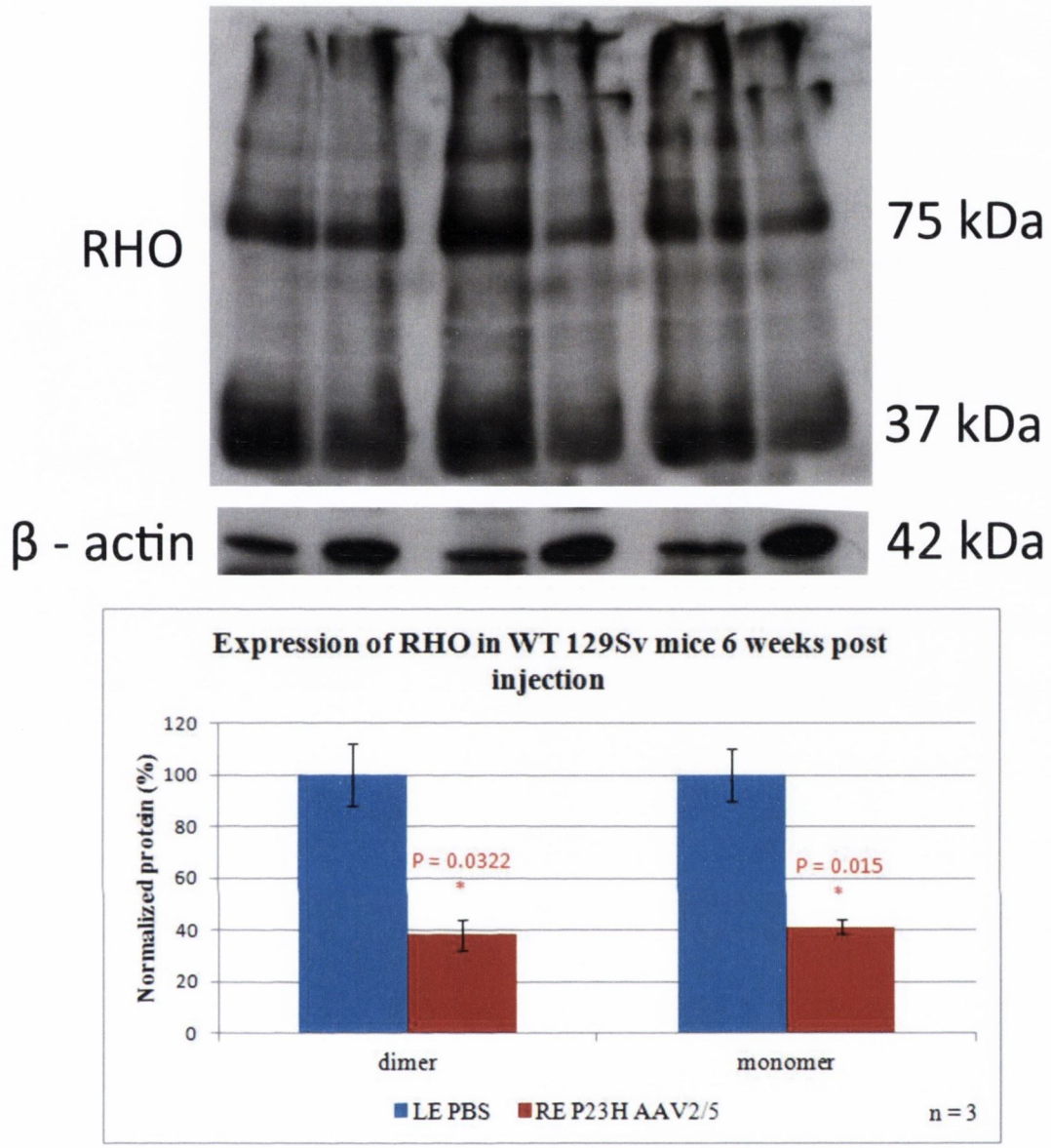

Figure 6. 7Expression of RHO protein in 129Sv WT mice injected with WT RHO and P23H AAVs.

The same group of mice (n = 3) as in **Figure 6.6** were put down 6 weeks post injection and whole cell fractions were measured for the total RHO protein levels using 1D4 anti-rhodopsin antibody. Rhodopsin protein resolved as monomer and dimer on a 12% gel. Both dimer and monomer bands of the protein were significantly fainter in the eye injected with P23H AAV2/5 compared to the left eye injected with PBS (* P = 0.0322 and * P = 0.015, respectively). Error bars denote ± SEM.

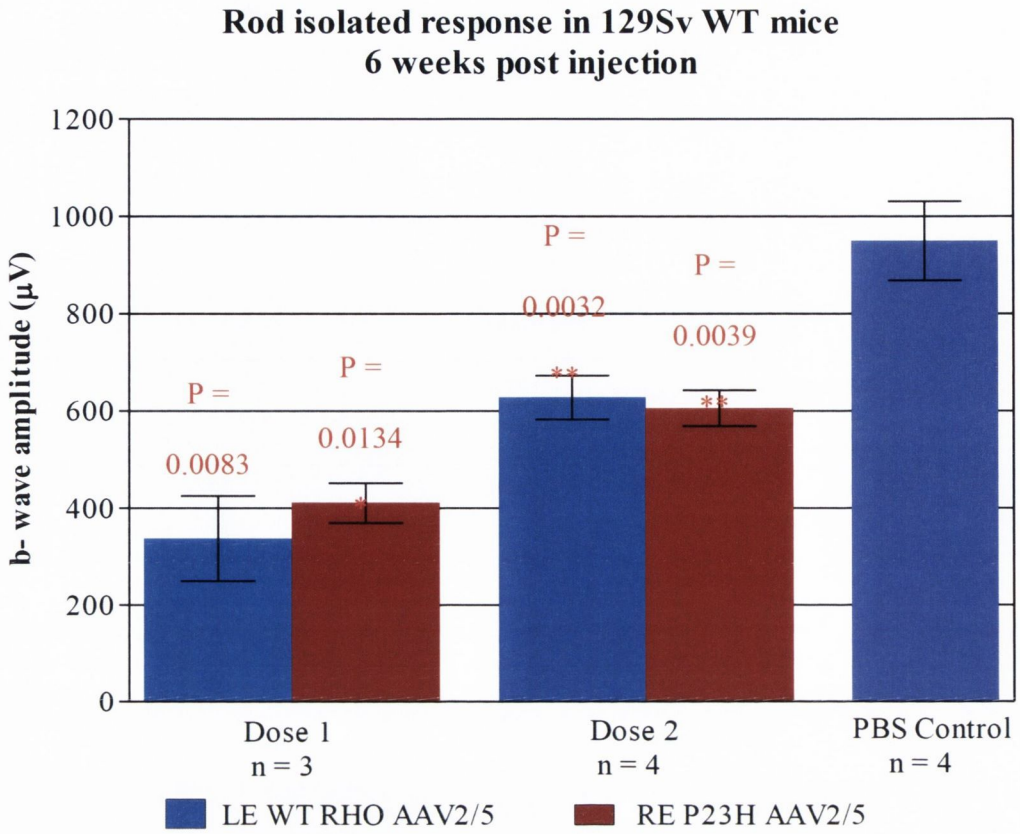

Figure 6. 8: ERG of mice treated with Dose 1 or 2 of AAV2/5.

A group of 4 month old 129Sv WT mice were subretinally injected with 3 µl of either Dose 1 (9.97×10^{11} vp/ml P23H AAV2/5 in the right eye and 1.1×10^{12} vp/ml WT RHO AAV2/5 in the left eye) or Dose 2 (9.97×10^{10} vp/ml P23H AAV2/5 in the right eye and 1.1×10^{11} vp/ml WT RHO AAV2/5 in the left eye). ERG readouts in the left eye injected with Dose 1 and 2 of WT RHO AAV2/5 were statistically reduced compared to control (** P = 0.0083 and ** P = 0.0032, respectively). Likewise, ERG readouts in the right eye injected with Dose 1 and 2 of P23H RHO AAV2/5 were statistically lower compared to control (* P = 0.0134 and ** P = 0.0039, respectively). Error bars denote ± SEM.

A)

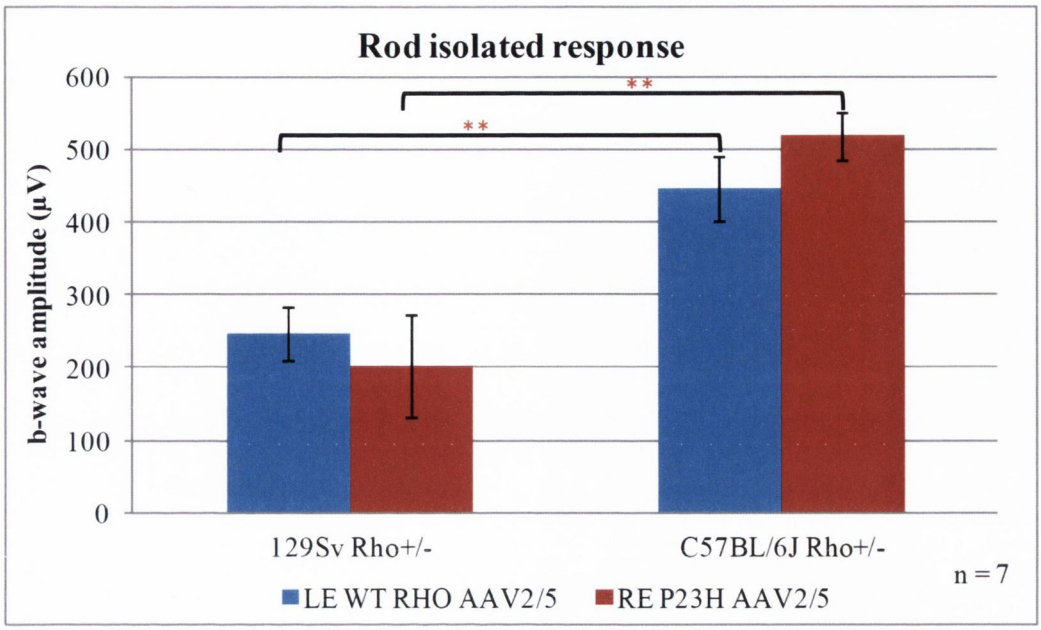
Rod isolated response
b-wave amplitude (µV)
600
500
400
300
200
100
0
**
**
129Sv Rho+/-
C57BL/6J Rho+/-
n = 7
LE WT RHO AAV2/5
RE P23H AAV2/5

B)

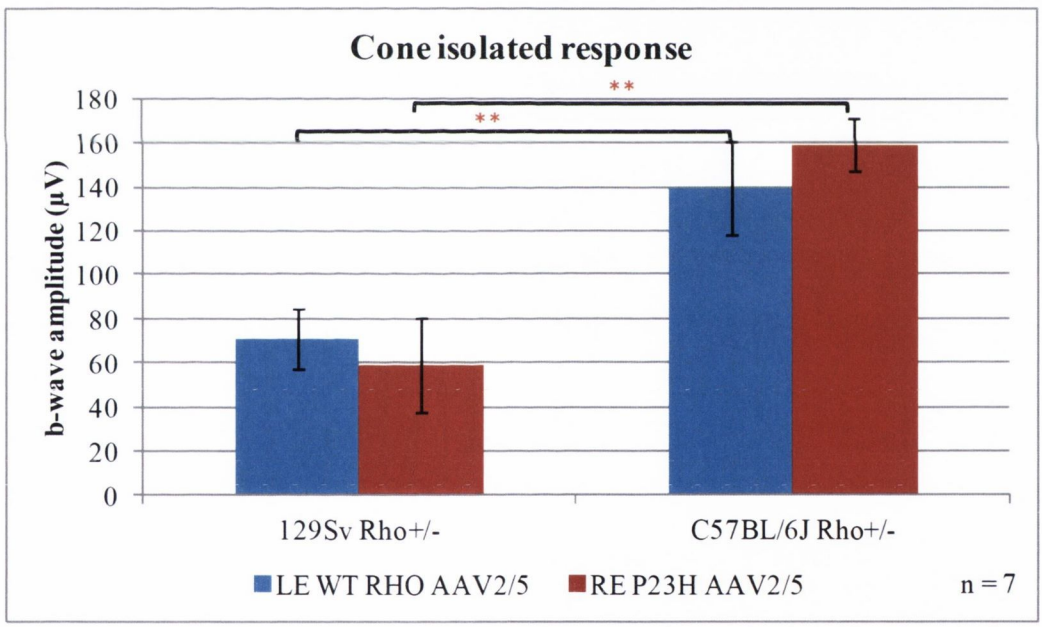
Cone isolated response
b-wave amplitude (µV)
180
160
140
120
100
80
60
40
20
0
**
**
129Sv Rho+/-
C57BL/6J Rho+/-
LE WT RHO AAV2/5
RE P23H AAV2/5
n = 7

Figure 6.9

C)

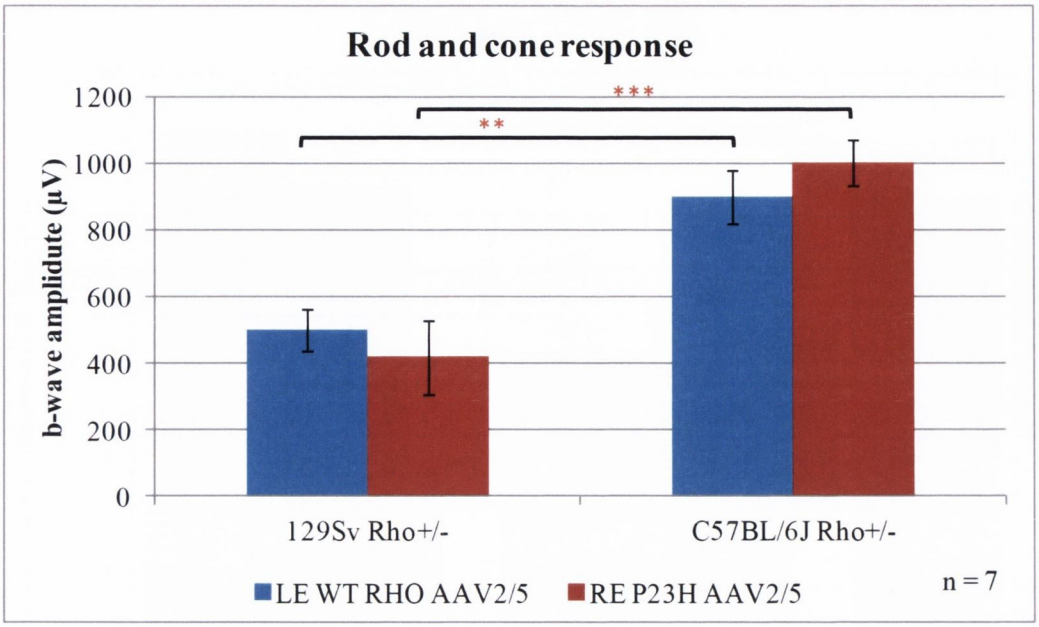

Figure 6. 9: Effect of WT RHO AAV2/5 and P23H AAV2/5 in C57BL/6J and 129Sv Rho+/- mice.

Two groups of C57BL6J and 129Sv Rho+/- mice (n = 7 for each group) were subretinally injected with WT RHO AAV2/5 in the left eye and P23H AAV2/5 in the right eye at P4. ERGs were measured at 6 weeks post injection. A) In rod derived response, ERG in the left eye injected with WT RHO AAV2/5 and the right eye injected with P23H AAV2/5 were significantly reduced in 129Sv mice compared to C57BL/6J mice (** P = 0.0067 and ** P = 0.0014, respectively). B) In cone derived response, ERG in the left eye injected with WT RHO AAV2/5 and the right eye injected with P23H AAV2/5 were significantly reduced in 129Sv mice compared to C57BL/6J mice (** P = 0.0065 and ** P = 0.0015, respectively). Likewise, C) In maximum cone and rod response, ERG in the left eye injected with WT RHO AAV2/5 and the right eye injected with P23H AAV2/5 were significantly reduced in 129Sv mice compared to C57BL/6J mice (** P = 0.0082 and *** P = 0.0003, respectively). Error bars denote ± SEM.

A)

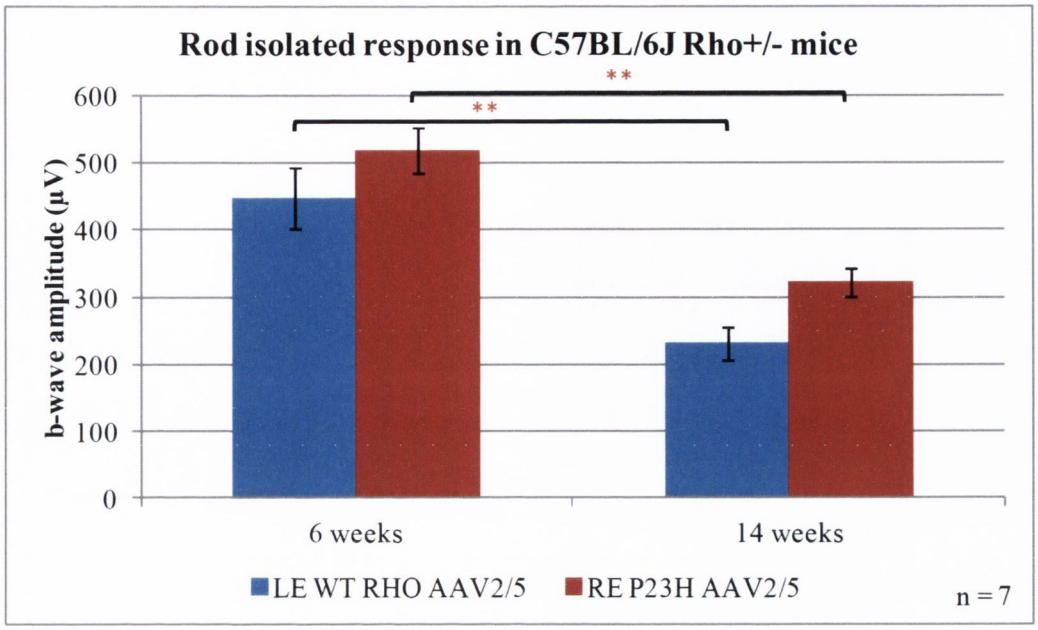

B)

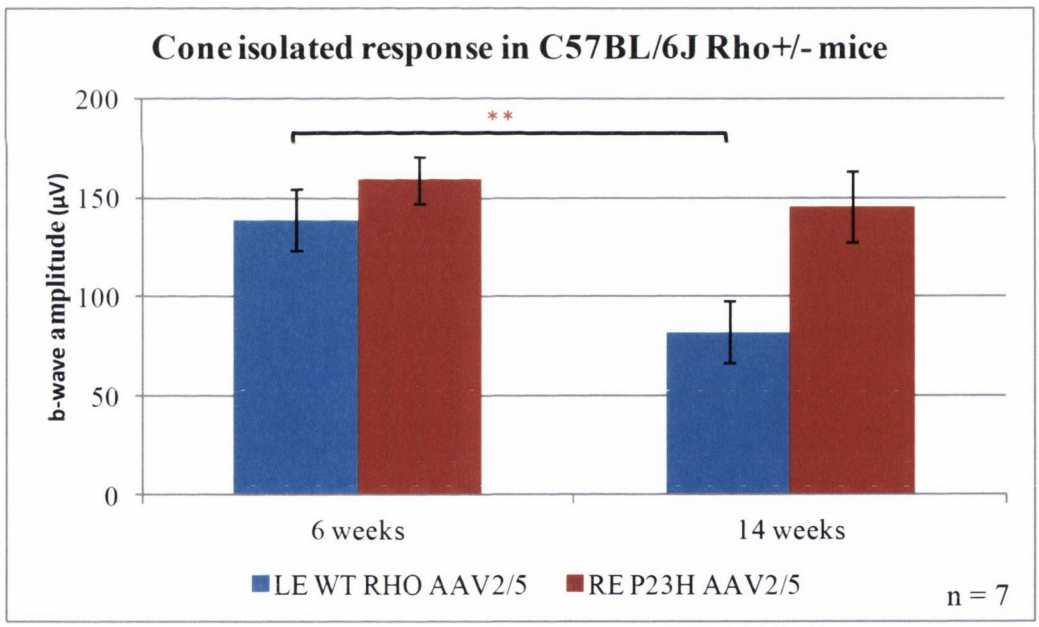

Figure 6.10

C)

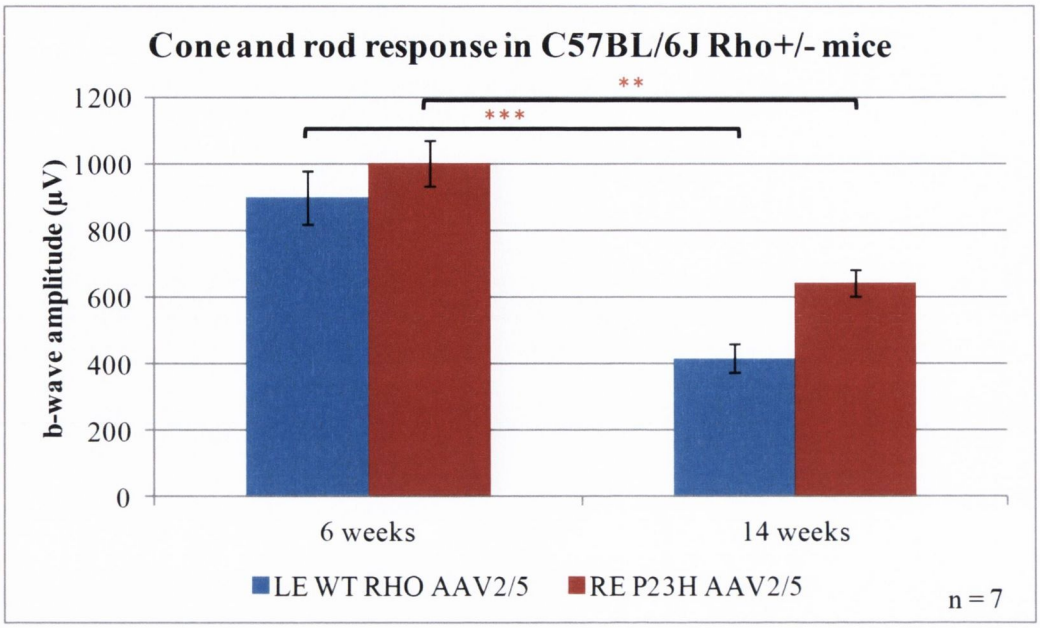

Figure 6. 10: ERG in C57BL/6J Rho+/- mice injected with AAV2/5.

A group of C57BL6J mice (n = 7) were subretinally injected with WT RHO AAV2/5 in the left eye and P23H AAV2/5 in the right eye at P4. ERGs were measured at 6 and 14 weeks post injection. A) In rod derived response, ERG in the left eye injected with WT RHO AAV2/5 and the right eye injected with P23H AAV2/5 were significantly reduced compared to 6 weeks post injection (** P = 0.0015 and ** P = 0.0058, respectively). B) In cone derived response, ERG in the left eye injected with WT RHO AAV2/5 was significantly reduced at 14 weeks post injection (*** P = 0.0008). Likewise, C) In maximum cone and rod response, ERG in the left eye injected with WT RHO AAV2/5 and the right eye injected with P23H AAV2/5 were significantly reduced at 14 weeks post injection (*** P < 0.0001 and ** P = 0.008, respectively). Error bars denote ± SEM.

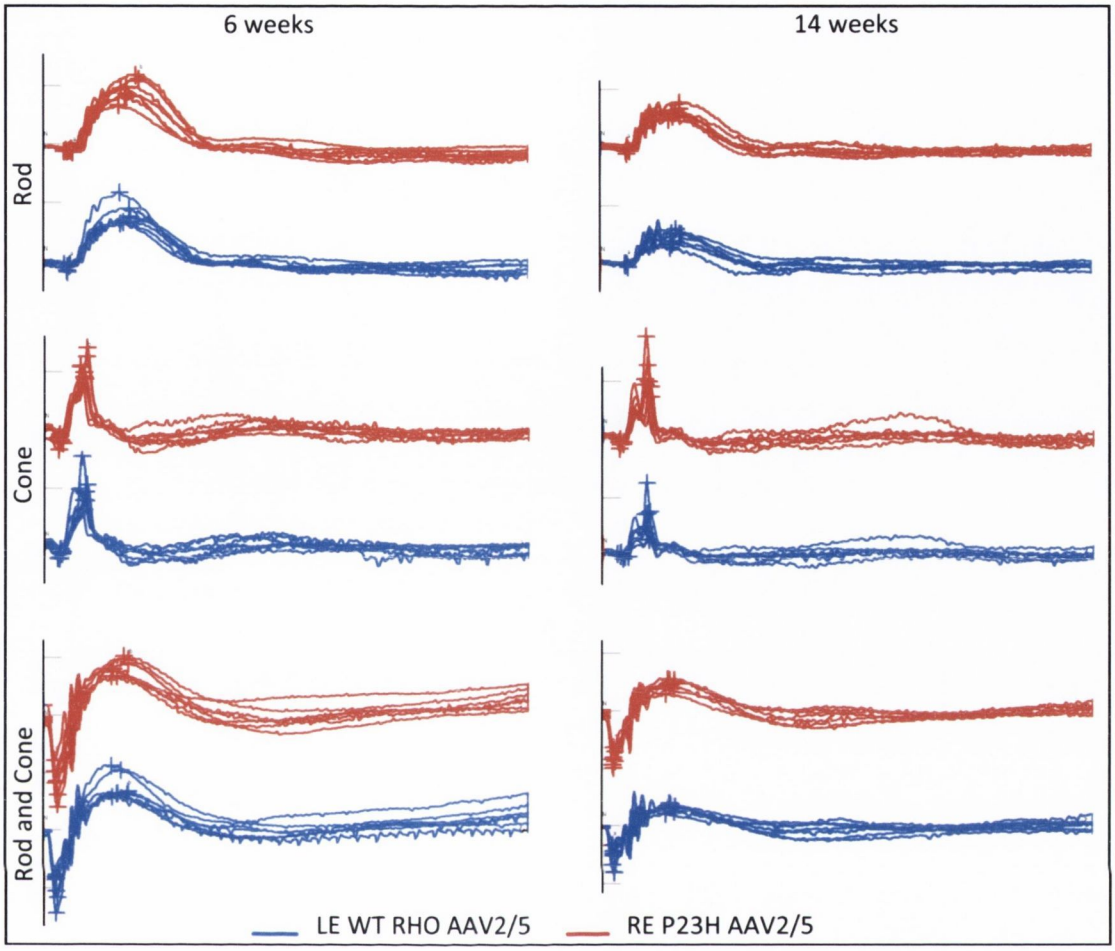

Figure 6. 11: ERG in C57BL/6J Rho+/- mice injected with AAV2/5.

Overlay of ERG readings of rod, cone and cone and rod derived responses from the same animals in **Figure 6.10**.

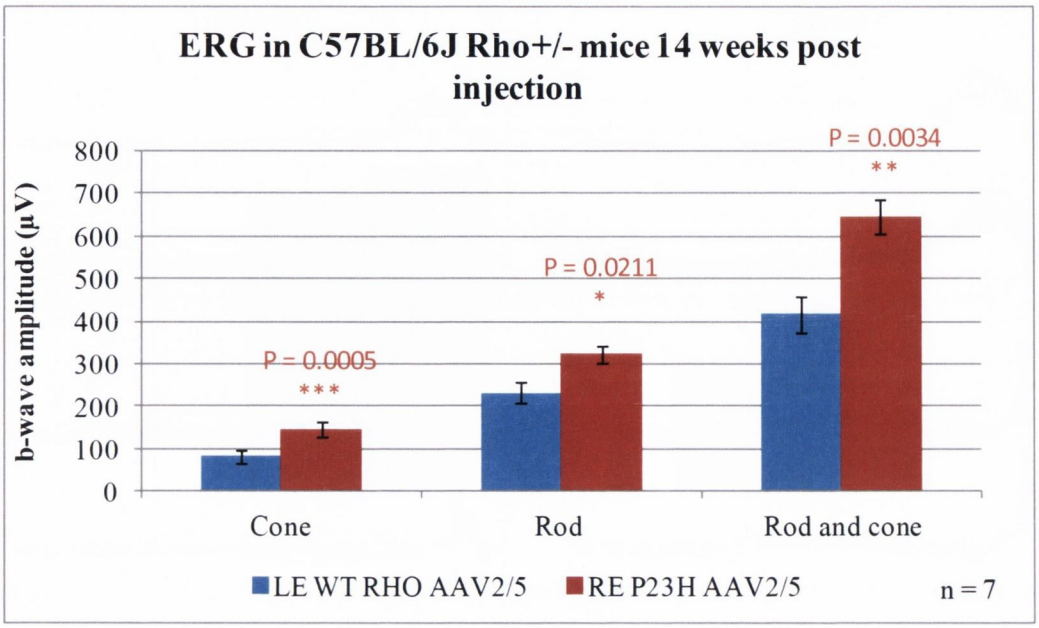

Figure 6. 12: ERG in C57BL/6J Rho+/- mice injected with AAV2/5 at 14 weeks post injection.

The same group of animals as in **Figure 6.8.** All cone isolated, rod isolated and maximum cone and rod responses in eyes injected with P23H AAV2/5 were statistically higher compared to eyes injected with WT RHO AAV2/5 (*** P = 0.0005, * P = 0.0211 and ** P = 0.0034, respectively). Error bars denote ± SEM.

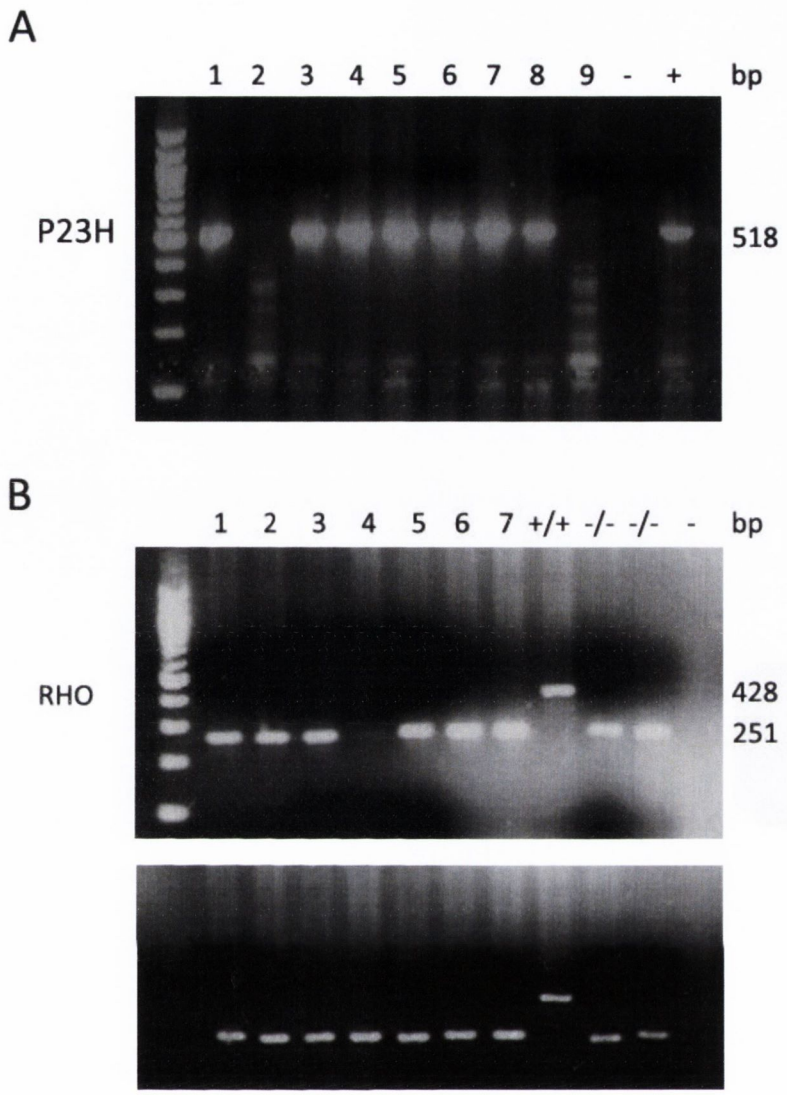

Figure 6. 13: P23H RHO genotyping of transgenic animals.

Pup tails were processed for DNA and PCR reactions were carried out for genotyping. A) Positive results for P23H +/- have a band of 518 bp (lanes 1, 3, 4, 5, 6, 7 and 8). NHR+/- sample was used as a positive control. B) Fragments of 428 and 251 bp are diagnostic of the WT and mutant alleles respectively. Rho+/+ and Rho-/- samples were used as positive and negative controls respectively. All tested samples had a genotype of Rho-/-. Negative water control was used in both gels.

A)

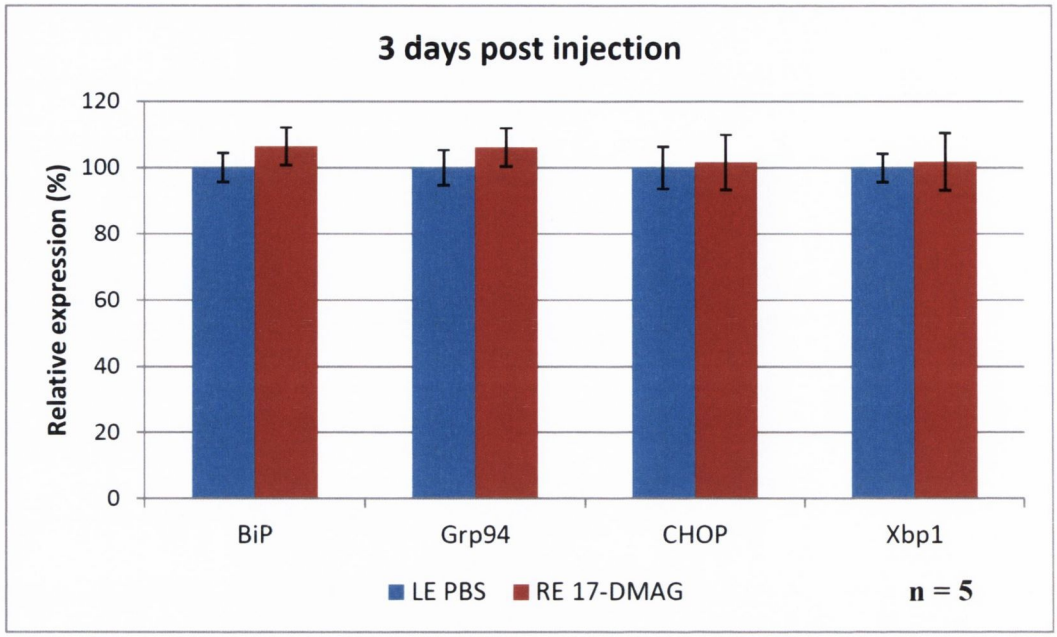

B)

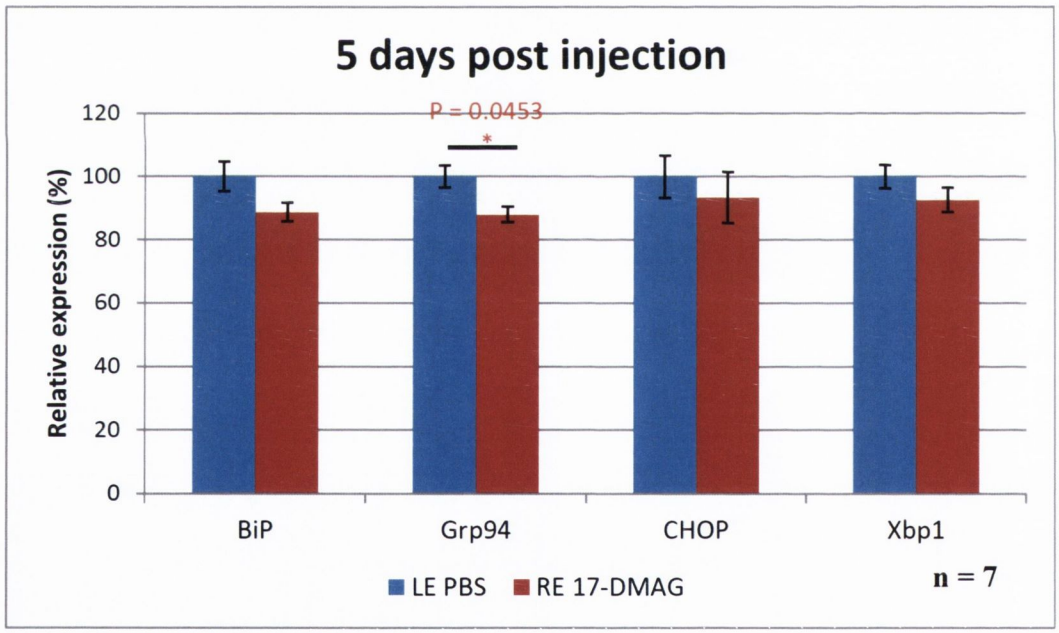

Figure 6. 14: Relative expression of levels of ER stress markers in P23H+/- Rho-/- mice treated with 17-DMAG.

P23H+/- Rho-/- mice were intravitreally injected with PBS in their left eye and 17-DMAG in their right eye at P5 and Taqman® expression analyses were carried out for their retinas 3 days (n = 5) (A) and 5 days (n=7) (B) post injection. There were no significant differences in BiP, CHOP, and Xbp1 expression levels in both groups of animals. However, Grp94 expression differed statistically in LE injected with PBS versus RE

injected with 17-DMAG 5 days post injection (* P = 0.0453) (B). Error bars denote ± SEM.

Chapter 7

Concluding remarks and Future Studies

Based on the discovery of reversible BBB modulation using siRNA targeting CLDN5 expression (Campbell *et al.*, 2008), the studies in this PhD thesis were designed to investigate whether the same principle would be applicable to the iBRB and thus facilitate delivery of small molecular weight drugs across this barrier in various rodent models of retinal degeneration. **Chapter 3** provides proof of principle that suppression of claudin-5 via either tail vein hydrodynamic injection of CLDN5 siRNA or subretinal injection of doxycycline inducible CLDN5 AAV2/9 to the retina, leads to a size selective, reversible and transient modulation of the iBRB which enhances delivery of the calpain inhibitors ALLM and ALLN protecting photoreceptors from undergoing apoptosis in the Balb/c light-induced retinal degeneration model. Indeed, these data presented in **Chapter 3** have been recently published (Campbell *et al.*, 2009, Campbell *et al.*, 2011, Nguyen *et al.*, 2012). In **Chapter 4**, the effect of systemic administration of an Hsp90 inhibitor, 17-AAG, on retinal degeneration was studied in the IMP224 AAV2/5 induced mouse model of RP10 adRP following modulation of the iBRB via CLDN5 AAV2/9. Although there was a trend of higher ERG in eyes post 17-AAG treatment which had been injected with CLDN5 AAV2/9 and IMP224 AAV2/5 compared to eyes injected NT AAV2/9 and IMP224 AAV2/5, no statistically significant difference in transduced ONL area per unit length was observed between treated and non-treated eyes. In addition, it is worth mentioning that since production of medical grade 17-AAG (Tanespimycin) used in clinical trials was recently halted due to its toxicity and unfavourable pharmacological properties, it is possible that some level of toxicity of this compound in the retina may have compromised the outcome. Moreover, in this chapter the construction and development of a transgenic model for RP10 adRP which should provide an improved model for this form of RP, is also detailed. Thus, future studies could include delivery of the less toxic, more soluble geldanamycin derivative, 17-DMAG, in tandem with modulation of the iBRB via CLDN5 AAV2/9 in this new transgenic RP10 model.

To date, P23H line 3 rats have proven to be an excellent model in which to study the effect of P23H rhodopsin-associated adRP due to the slow rate of retinal degeneration which is similar to that observed in human patients (Machida *et al.*, 2000). The main focus of **Chapter 5** was to investigate the efficacy and mechanism of 17-DMAG in alleviating ER stress-induced retinal degeneration. The results suggested that apoptosis was largely reduced via upregulation of BiP and downregulation of CHOP which led to preservation of the photoreceptor layer and rescue of visual function. Following subretinal injection of CLDN5 or NT AAV2/9, rats were treated with three different doses of 17-DMAG: 0.2, 2 and 4 mg/kg/day in their drinking water. Although treatment with 0.2 mg/kg/day 17-DMAG did not slow down disease progression, the remaining two doses of 17-DMAG did offer protection against retinal degeneration. These two efficacious doses (22.5 mg/m^2 and 44 mg/m^2 weekly) are well below the maximum tolerated dose for rats and recommended dose (80 mg/m^2 weekly) suggested for patients with advanced form of cancer in phase II clinical trials (Glaze *et al.*, 2005, Pacey *et al.*, 2011, Jhaveri *et al.*, 2012). However, four patients have been reported to suffer from ocular toxicity (i.e. reversible blurry vision, keratitis, dry eye, conjunctivitis, or ocular surface disease) in a phase I trial of 17-DMAG (Pacey *et al.*, 2011) while two patients receiving a combination of 17-DMAG and trastuzumab also had reversible keratitis (Jhaveri *et al.*, 2012). This drug-related ocular toxicity seems to be dose and schedule dependent, the majority of these cases having occurred at a weekly dose of 80 mg/m^2 or higher. Therefore, a dose de-escalating study should be carried out in the rat model in order to unequivocally establish the minimal effective dose of 17-DMAG, in tandem with regular ophthalmic inspection for the presence of any side effects. Also, in order to correctly assess exactly how much of the drug actually reaches the target tissue the concentration of 17-DMAG present in rat retinas following oral delivery should be quantified via high performance liquid chromatography. Hence, future experiments will involve investigation of pharmacokinetics, tissue

distribution and metabolism of 17-DMAG once taken orally by these P23H rats. Moreover, the result obtained from CHOP protein level in eyes intravitreally injected with 17-DMAG was inconclusive since only 2 out of 3 rats showed reduction of CHOP protein post 17-DMAG injection. This experiment should be repeated with a larger number of animals to determine the effect of 17-DMAG on CHOP protein *in vivo* as presented in **Chapter 5**. In addition, cone photoreceptors survive for a longer period of time than rod photoreceptors and although the onset of cone dysfunction was suggested to be at around 18 months in these rats (Chrysostomou *et al.*, 2009) significant deficits in cone ERG were observed as early as about 8.3 months in this study and were reduced in treated retinas. Thus, administering 17-DMAG to older animals in conjunction with iBRB modulation, for extended periods, could provide important data for the development of a therapeutic strategy which may enable severely affected RP patients to retain some daytime vision.

Due to the slow rate of retinal degeneration observed in P23H rats (**Chapter 5**), a P23H AAV2/5-induced mouse model was simultaneously developed and again used to investigate the effect of 17-DMAG on photoreceptor cell death and visual function. These data are presented in **Chapter 6**. In this study, despite the design of WT RHO AAV2/5 being based on an AAV construct which was previously shown to have no adverse effect on ERG in Rho-/- mice and to express approximately 40% of the level of rhodopsin found in WT mice (Palfi *et al.*, 2010), subretinal inoculation of this virus in Rho+/- mice exerted a negative effect on visual function even at much lower concentrations than those used by Palfi *et al.* (2010). The results obtained further confirm those of others reporting toxicity of WT RHO in mice expressing endogenous rhodopsin (Sung *et al.*, 1994, Tan *et al.*, 2001, Mao *et al.*, 2011). Therefore, future studies using these AAVs may have to be carried out in Rho-/- mice but will most likely be compromised due to rapidity of the retinal degeneration which P23H AAV2/5 is likely to cause in this background. However, recently, two P23H knock-in mouse models have become available (Price *et al.*, 2011,

Sakami *et al.*, 2011) and observations based on the lack of detection of protein aggregates in the ER and retinal health improved with loss of the P23H protein from the OS and gains in the IS and ONL layers suggest that in contrast to the P23H rat model, ER stress may not be the major cause of photoreceptor cell death. Nonetheless, it is likely that 17-DMAG would enhance proteasomal degradation of P23H rhodopsin in these models and thus ameliorate disease pathology.

Since 17-AAG was the first Hsp90 inhibitor to enter clinical trial in 1998, many small molecular weight compounds including GA derivatives (17-DMAG, IPI-504) and synthetic, non GA derivatives (i.e. AUY9222, STA-9090, Debio 0932, etc) have been developed and tested in up to 63 clinical trials (clinicaltrials.gov). However, complications such as liver toxicity associated with GA derivative compounds remain; whereas synthetic compounds (second generation of Hsp90 inhibitors) can cause ocular toxicity despite being more potent Hsp90 inhibitors compared to the first generation drugs. For example, the oral Pfizer compound SNX-5422 was terminated due to its excessive eye toxicity and potential for irreversible retinal damage (Rajan *et al.*, 2011) while AUY922 has been shown to cause retinal dysfunction (Hong *et al.*, 2013). So far, STA-9090 (MW = 364.39) which has been developed by Synta Pharmaceuticals Corp., USA has been shown to be a much more potent Hsp90 inhibitor compared to 17-AAG and not associated with visual side effects which on balance seem prevalent enough to be a potential class side effect of Hsp90 inhibitors (Shimamura *et al.*, 2012, Ying *et al.*, 2012, Hong *et al.*, 2013). Therefore, it would be of interest to investigate the efficacy of STA-9090 in preventing retinal degeneration in IMPDH1 and P23H models and to compare these results with those obtained in these studies for 17-DMAG.

To summarize, the studies in this PhD thesis provide proof of principle that transient, reversible and size selective modulation of iBRB via the CLDN5 AAV2/9 system facilitates delivery of low molecular weight molecules of up to 1 kDa into the retina via

systemic administration. Moreover, this therapeutic approach has recently been designated with orphan medicinal product status by the European Medicines Agency which should expedite translation to clinical use in the short term.

Appendix

>Sequence of the *IMP224* transgene (UPPERCASE) and of IMP224 pAAV (lowercase: vector genome)

(LITR)cctgcaggcagctgcgcgctcgctcgctcactgaggccgcccgggcaaagcccgggcgtcgggcgacctttggtcg
cccggcctcagtgagcgagcgagcgcgcagagagggagtggccaactccatcactaggggttcct
GCGGCCGCACGC

(NheI site) G

(Rhodopsin promoter)
CTAGCTGGGGATGGGGGCAGGGTAGATCTGGGGCTGACCACCAGGGTCAGAA
TCAGAACCTCCATCTTGACCTCATTAACGCTGGTCTTAATCACCAAGCCAAGCT
CCTTAAACTGCTAGTGGCCAACTCCCAGGCCCTGACACACATACCTGCCCTGT
GTTCCCAAACAAGACACCTGCATGGAAGGAAGGGGGTTGCTTTTCTAAGCAAA
CATCTAGGAATCCCGGGTGCAGTGTGAGGAGACTAGGCGAGGGAGTACTTTAA
GGGCCTCAAGGCTCAGAGAGGAATACTTCTTCCCTGGTTAGCCTCGTGCCTAG
GCTCCAGGGTCTTTGTCCTGCCTGGATACCTATGTGGCAAGGGGCATAGCATTT
CCCCCACCATCAGCTCTTAGCTCAACCTTATCTTCTCGGAAAGGCTGCGCAGTG
TAACAACACAGCAGAGACTTTTCTTTTGTCCCCTGTCTACCCCTGTAACTGCTA
CTCAGAAGCATCTTTCTCACAGGGTACTGGCTTCTTGCATCCAGAGTTTTTTGT
CTCCCTCGGGCCCCCAGAATCAAATTCTTCCTCTGGGACTCAGTGGATGTTTCA
CACACGTATCGGCCTGACAGTCATCCTGGAGCATCCTACACAGGGGCCATCAC
AGCTGCATGTCAGAGATGCTGGCCTCACATCCTCAGACACCAGGCCTAGTGCT
GGTCTTCCTCAGACTGGCGTCCCCAGCAGGCCAGTAGGATCATCTTTTAGCCTA
CAGAGTTCTGAAGCCTCAGAGCCCCAGGTCCCTGGTCATCTTCTCTGCCCCTGA
GATTTTTCCAAGTTGTATGCCTTCTAGGTAAGGCAAAACTTCTTACGCCCCTCC
TCGTGGCCTCCAGGCCCCACATGCTCACCTGAATAACCTGGCAGCCTGCTCCCT
CATGCAGGGACCACGTCCTGCTGCACCCAGCAGGCCATCCCGTCTCCATAGCC
CATGGTCATCCTTCCCTGGACAGGAATGTGTCTCCTCCCCTGGCTGAGTCTTGC
TCAAGCTAGAAGCACTCCGAACAGGGTTATGGGCGCCTCCTCCATCTCCCAAG
TGGCTGGCTTATGAATGTTTAATGTACATGTGAGTGAACAAATTCCAATTGAAC
GCAACAAATAGTTATCGAGCCGCTGAGCCGGGGGCGGGGGGTGTGAGACTGG
AGGCGATGGACGGAGCTGACGGCACACACAGCTCAGATCTGTCAAGTGAGCC
ATTGTCAGGGCTTGGGGACTGGATAAGTCAGGGGGTCTCCTGGGAAGAGATGG
GATAGGTGAGTTCAGGAGGAGACATTGTCAACTGGAGCCATGTGGAGAAGTG
AATTTAGGGCCCAAAGGTTCCAGTCGCAGCCTGAGGCCACCAGACTGACATGG
GGAGGAATTCCCAGAGGACTCTGGGGCAGACAAGATGAGACACCCTTTCCTTT
CTTTACCTAAGGGCCTCCACCCGATGTCACCTTGGCCCCTCTGCAAGCCAATTA
GGCCCCGGTGGCAGCAGTGGGATTAGCGTTAGTATGATATCTCGCGGATGCTG
AATCAGCCTCTGGCTTAGGGAGAGAAGGTCACTTTATAAGGGTCTGGGGGGGG
TCAGTGCCTGGAGTTGCGCTGTGGGAGCCGTCAGTGGCTGAGCTCGCCAAGCA
GCCTTGGTCTCTGTCTACGAAGAGCCCGTGGGGCAGC

(Beta globin intron)
AATCCCGGCCGGGAACGGTGCATTGGAACGCGGATTCCCCGTGCCAAGAGTGA
CGTAAGTACCGCCTATAGAGTCTATAGGCCCACAAAAAATGCTTTCTTCTTTTA
AT
ATACTTTTTTGTTTATCTTATTTCTAATACTTTCCCTAATCTCTTTCTTTCAGGGC
AATAATGATACAATGTATCATGCCTCTTTGCACCATTCTAAAGAATAACAGTG
ATAATTTCTGGGTTAAGGCAATAGCAATATTTCTGCATATAAATATTTCTGCAT
ATAAATTGTAACTGATGTAAGAGGTTTCATATTGCTAATAGCAGCTACAATCC
AGCTACCATTCTGCTTTTATTTTATGGTTGGGATAAGGCTGGATTATTCTGAGT
CCAAGCTAGGCCCTTTTGCTAATCATGTTCATACCTCTTATCTTCCTCCCACAGC
TCCTGGGCAACGTGCTGGTCTGTGTGCTGGCCCATCACTTTGGCAAAGAATTGG
GATTCGAACATCGATAATTAACCCTCACTAAAGGGAACAAAAGCTGGAGCTCC
ACCGCGGTG

(NotI site) GCGGCCGC
TCTAGCCCGGGCGGATCCGAATTCGCATGCGTCGA

(XhoI site) CTCGAG

(IMPDH1 containing mutant at aa 224, without exons 1, 2 and a few bases of exons 3 and 17)
ATGGCGGACTACCTGATCAGCGGCGGCACCGGCTACGTGCCCGAGGATGGGCT
CACCGCGCAGCAGCTCTTCGCCAGCGCCGACGGCCTCACCTACAACGACTTCC
TGATTCTCCCAGGATTCATAGACTTCATAGCTGATGAGGTGGACCTGACCTCAG
CCCTGACCCGGAAGATCACGCTGAAGACGCCACTGATCTCCTCCCCCATGGAC
ACTGTGACAGAGGCTGACATGGCCATTGCCATGGCTCTGATGGGAGGTATTGG
TTTCATTCACCACAACTGCACCCCAGAGTTCCAGGCCAACGAGGTGCGGAAGG
TCAAGAAGTTTGAACAGGGCTTCATCACGGACCCTGTGGTGCTGAGCCCCTCG
CACACTGTGGGCGATGTGCTGGAGGCCAAGATGCGGCATGGCTTCTCTGGCAT
CCCCATCACTGAGACGGGCACCATGGGCAGCAAGCTGGTGGGCATCGTCACCT
CCCGAGACATCGACTTTCTTGCTGAGAAGGACCACACCACCCTCCTCAGTGAG
GTGATGACGCCAAGGATTGAACTGGTGGTGGCTCCAGCAGGTGTGACGTTGAA
AGAGGCAAATGAGATCCTGCAGCGTAGCAAGAAAGGGAAGCTGCCTATCGTC
AATGATTGCGATGAGCTGGTGGCCATCATCGCCCCCACCGACCTGAAGAAGAA
CCGAGACTACCCTCTGGCCTCCAAGGATTCCCAGAAGCAGCTGCTCTGTGGGG
CAGCTGTGGGCACCCGTGAGGATGACAAATACCGTCTGGACCTGCTCACCCAG
GCGGGCGTCGACGTCATAGTCTTGGACTCGTCCCAAGGGAATTCGGTGTATCA
GATCGCCATGGTGCATTACATCAAACAGAAGTACCCCCACCTCCAGGTGATTG
GGGGGAACGTGGTGACAGCAGCCCAGGCCAAGAACCTGATTGATGCTGGTGT
GGACGGGCTGCGCGTGGGCATGGGCTGCGGCTCCATCTGCATCACCCAGGAAG
TGATGGCCTGTGGTCGGCCCCAGGGCACTGCTGTGTACAAGGTGGCTGAGTAT
GCCCGGCGCTTTGGTGTGCCCATCATAGCCGATGGCGGCATCCAGACCGTGGG
ACACGTGGTCAAGGCCCTGGCCCTTGGAGCCTCCACAGTGATGATGGGCTCCC
TGCTGGCCGCCACTACGGAGGCCCCTGGCGAGTACTTCTTCTCAGACGGGGTG
CGGCTCAAGAAGTACCGGGGCATGGGCTCACTGGATGCCATGGAGAAGAGCA
GCAGCAGCCAGAAACGATACTTCAGCGAGGGGGATAAAGTGAAGATCGCGCA

GGGTGTCTCGGGCTCCATCCAGGACAAAGGATCCATTCAGAAGTTCGTGCCCT
ACCTCATAGCAGGCATCCAACACGGCTGCCAGGATATCGGGGCCCGCAGCCTG
TCTGTCCTTCGGTCCATGATGTACTCAGGAGAGCTCAAGTTTGAGAAGCGGAC
CATGTCGGCCCAGATTGAGGGTGGTGTCCATGGCCTGCACTCTTACGAAAAGC
GGCTGTACTGA

(XhoI site) CTCGAG

(Multiple cloning site)
GACTACAAGGATGACGATGACAAGGATTACAAAGACGACGATGATAAGGACT
ATAAGGATGATGACGACAAATAATAGCAATTCCTCGACGACTGCATAGGGTTA
CCCCC

(IRES)
CTCTCCCTCCCCCCCCCCTAACGTTACTGGCCGAAGCCGCTTGGAATAAGGCCG
GTGTGCGTTTGTCTATATGTTATTTTCCACCATATTGCCGTCTTTTGGCAATGTG
AGGGCCCGGAAACCTGGCCCTGTCTTCTTGACGAGCATTCCTAGGGGTCTTTCC
CCTCTCGCCAAAGGAATGCAAGGTCTGTTGAATGTCGTGAAGGAAGCAGTTCC
TCTGGAAGCTTCTTGAAGACAAACAACGTCTGTAGCGACCCTTTGCAGGCAGC
GGAACCCCCCACCTGGCGACAGGTGCCTCTGCGGCCAAAAGCCACGTGTATAA
GATACACCTGCAAAGGCGGCACAACCCCAGTGCCACGTTGTGAGTTGGATAGT
TGTGGAAAGAGTCAAATGGCTCTCCTCAAGCGTATTCAACAAGGGGCTGAAGG
ATGCCCAGAAGGTACCCCATTGTATGGGATCTGATCTGGGGCCTCGGTGCACA
TGCTTTACATGTGTTTAGTCGAGGTTAAAAAACGTCTAGGCCCCCCGAACCAC
GGGGACGTGGTTTTCCTTTGAAAAACACGATGATAATGGCCACAACC

(hrGFP)
ATGGTGAGCAAGCAGATCCTGAAGAACACCGGCCTGCAGGAGATCATGAGCTT
CAAGGTGAACCTGGAGGGCGTGGTGAACAACCACGTGTTCACCATGGAGGGCT
GCGGCAAGGGCAACATCCTGTTCGGCAACCAGCTGGTGCAGATCCGCGTGACC
AAGGGCGCCCCCCTGCCCTTCGCCTTCGACATCCTGAGCCCCGCCTTCCAGTAC
GGCAACCGCACCTTCACCAAGTACCCCGAGGACATCAGCGACTTCTTCATCCA
GAGCTTCCCCGCCGGCTTCGTGTACGAGCGCACCCTGCGCTACGAGGACGGCG
GCCTGGTGGAGATCCGCAGCGACATCAACCTGATCGAGGAGATGTTCGTGTAC
CGCGTGGAGTACAAGGGCCGCAACTTCCCCAACGACGGCCCCGTGATGAAGA
AGACCATCACCGGCCTGCAGCCCAGCTTCGAGGTGGTGTACATGAACGACGGC
GTGCTGGTGGGCCAGGTGATCCTGGTGTACCGCCTGAACAGCGGCAAGTTCTA
CAGCTGCCACATGCGCACCCTGATGAAGAGCAAGGGCGTGGTGAAGGACTTCC
CCGAGTACCACTTCATCCAGCACCGCCTGGAGAAGACCTACGTGGAGGACGGC
GGCTTCGTGGAGCAGCACGAGACCGCCATCGCCCAGCTGACCAGCCTGGGCAA
GCCCCTGGGCAGCCTGCACGAGTGGGTGT

(hGHPA)
AATAGGGTACCAGGTAAGTGTACCCAATTCGCCCTATAGTGAGTCGTATTAGA
TCTACGGGTGGCATCCCTGTGACCCCTCCCCAGTGCCTCTCCTGGCCCTGGAAG
TTGCCACTCCAGTGCCCACCAGCCTTGTCCTAATAAAATTAAGTTGCATCATTT

TGTCTGACTAGGTGTCCTTCTATAATATTATGGGGTGGAGGGGGGTGGTATGG
AGCAAGGGGCAAGTTGGGAAGACAACCTGTAGGGCCTGCGGGGTCTATTGGG
AACCAAGCTGGAGTGCAGTGGCACAATCTTGGCTCACTGCAATCTCCGCCTCC
TGGGTTCAAGCGATTCTCCTGCCTCAGCCTCCCGAGTTGTTGGGATTCCAGGCA
TGCATGACCAGGCTCAGCTAATTTTTGTTTTTTTGGTAGAGACGGGGTTTCACC
ATATTGGCCAGGCTGGTCTCCAACTCCTAATCTCAGGTGATCTACCCACCTTGG
CCTCCCAAATTGCTGGGATTACAGGCGTGAACCACTGCTCCCTTCCCTGTCCTT
CTGATTTTGTAGGTAACCACGTG **(RsrII site)** CGGACCGA

(NotI site) GCGGCCGC

(RITR)
aggaacccctagtgatggagttggccactccctctctgcgcgctcgctcgctcactgaggccgggcgaccaaaggtcgcccgac
gcccgggctttgcccgggcggcctcagtgagcgagcgagcgcgcagctgcctgcagg
ggcgcctgatgcggtattttctccttacgcatctgtgcggtatttcacaccgcatacgtcaaagcaaccatagtacgcgccctgtagc
ggc

(f1ori)
gcattaagcgcggcgggtgtggtggttacgcgcagcgtgaccgctacacttgccagcgccctagcgcccgctcctttcgctttcttc
ccttcctttctcgccacgttcgccggctttccccgtcaagctctaaatcgggggctcccttagggttccgatttagtgctttacggcac
ctcgaccccaaaaaacttgatttgggtgatggttcacgtagtgggccatcgccctgatagacggtttttcgccctttgacgttggagtc
cacgttctttaatagtggactcttgttccaaactggaacaa
cactcaaccctatctcgggctattcttttgatttataagggattttgccgatttcggcctattggttaaaaaatgagctgatttaacaaaaa
tttaacgcgaattttaacaaaatattaacgtttacaattttatggtgcactctcagtacaatctgctctgatgccgcatagttaagccagc
cccgacacccgccaacacccgctgacgcgccctgacgggcttgtctgctcccggcatccgcttacagacaagctgtgaccgtctc
cgggagctgcatgtgtcagaggttttcaccgtcatcaccgaaacgcgcgagacgaaagggcctcgtgatacgcctatttttataggt
taatgtcatgataataatggtttcttagacgtcaggtggcacttttcggggaaatgtgcgcggaaccccctatttgtttatttttctaaatac
attcaaatatgtatccgctcatgagacaataaccctgataaatgcttcaataatattgaaaaaggaagagt

(ampicillin resistant gene)
atgagtattcaacatttccgtgtcgcccttattccctttttgcggcattttgccttcctgtttttgctcacccagaaacgctggtgaaagta
aaagatgctgaagatcagttgggtgcacgagtgggttacatcgaactggatctcaacagcggtaagatccttgagagttttcgcccc
gaagaacgttttccaatgatgagcacttttaaagttctgctatgtggcgcggtattatcccgtattgacgccgggcaagagcaactcg
gtcgccgcatacactattctcagaatgacttggttgagtactcaccagtcacagaaaagcatcttacggatggcatgacagtaagag
aattatgcagtgctgccataaccatgagtgataacactgcggccaacttacttctgacaacgatcggaggaccgaaggagctaacc
gcttttttgcacaacatgggggatcatgtaactcgccttgatcgttgggaaccggagctgaatgaagccataccaaacgacgagcg
tgacaccacgatgcctgtagcaatggcaacaacgttgcgcaaactattaactggcgaactacttactctagcttcccggcaacaatt
aatagactggatggaggcggataaagttgcaggaccacttctgcgctcggcccttccggctggctggtttattgctgataaatctgg
agccggtgagcgtgggtctcgcggtatcattgcagcactggggccagatggtaagccctcccgtatcgtagttatctacacgacgg
ggagtcaggcaactatggatgaacgaaatagacagatcgctgagataggtgcctcactgattaagcattgg
Taactgtcagaccaagtttactcatatatactttagattgatttaaaacttcatttttaatttaaaaggatctaggtgaagatccttttgata
atctcatgaccaaaatcccttaacgtgagttttcgttccactgagcgtcagacccc

(pUCori)
gtagaaaagatcaaaggatcttcttgagatcctttttttctgcgcgtaatctgctgcttgcaaacaaaaaaaccaccgctaccagcggt
ggtttgtttgccggatcaagagctaccaactctttttccgaaggtaactggcttcagcagagcgcagataccaaatactgtccttctag

tgtagccgtagttaggccaccacttcaagaactctgtagcaccgcctacatacctcgctctgctaatcctgttaccagtggctgctgc
cagtggcgataagtcgtgtcttaccgggttggactcaagacgatagttaccggataaggcgcagcggtcgggctgaacgggggg
ttcgtgcacacagcccagcttggagcgaacgacctacaccgaactgagatacctacagcgtgagctatgagaaagcgccacgctt
cccgaagggagaaaggcggacaggtatccggtaagcggcagggtcggaacaggagagcgcacgagggagcttccagggggg
aaacgcctggtatctttatagtcctgtcgggtttcgccacctctgacttgagcgtcgatttttgtgatgctcgtcaggggggcggagcc
tatggaaaaacgccagcaacgcggcctttttacggttcctggccttttgctggccttttgctcacatgt

Appendix Figure 1: IMP224 pAAV sequence

The IMP224 transgene inserted to founder mice is located between NheI and RsrII restriction sites (blue).

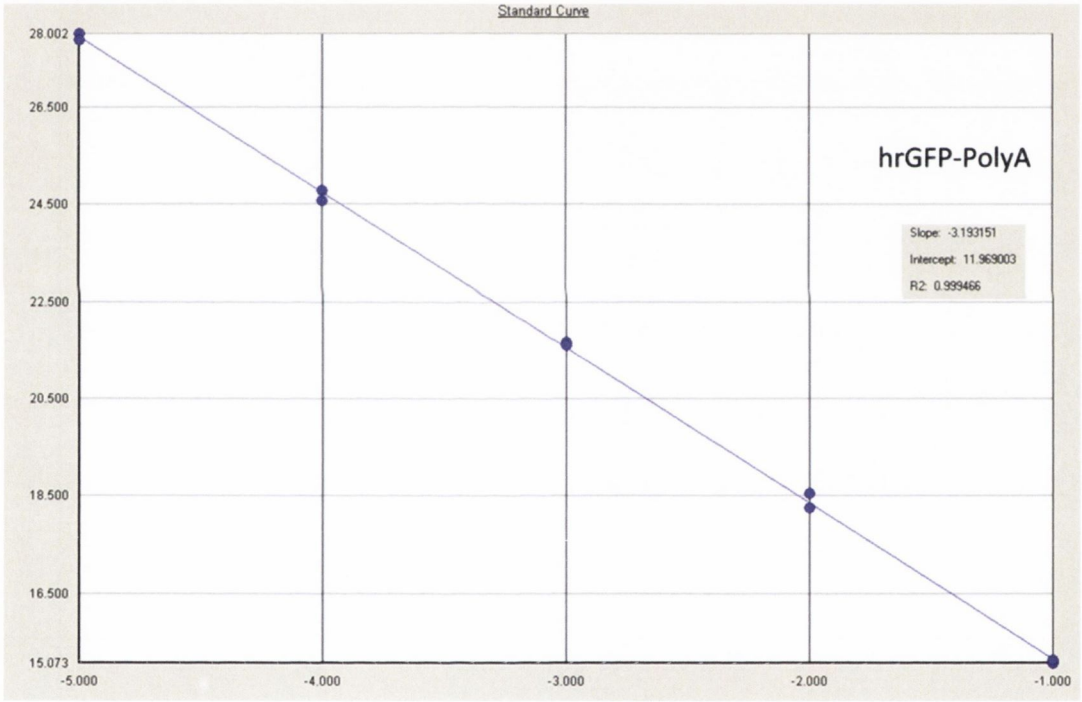

Appendix Figure 2: Standard curve of hrGFP-PolyA primers.

A representative result from a quantitative PCR shows that the slope of the standard curve is -3.19 which gives an efficiency of 105.6%.

Detector Name	Slope	Intercept	R2	Number of Standards					
hIMPDH1	**-3.221631**	15.22314	0.988942	10					
Sample Name	Detector	Task	Ct	StdDev Ct	Quantity	Mean Qty	StdDev Qt	Filtered	Tm
IMP224 pAAV	hIMPDH1	Standard	18.2785	4.83	0.1				84.7
IMP224 pAAV	hIMPDH1	Standard	17.9091	4.83	0.1				84.7
IMP224 pAAV	hIMPDH1	Standard	21.2377	4.83	0.01				84.7
IMP224 pAAV	hIMPDH1	Standard	22.9257	4.83	0.01				84.7
IMP224 pAAV	hIMPDH1	Standard	25	4.83	0.001				84.7
IMP224 pAAV	hIMPDH1	Standard	24.9652	4.83	0.001				84.7
IMP224 pAAV	hIMPDH1	Standard	28.3261	4.83	1.00E-04				84.7
IMP224 pAAV	hIMPDH1	Standard	27.8308	4.83	1.00E-04				84.7
IMP224 pAAV	hIMPDH1	Standard	31.0287	4.83	1.00E-05				84.7
IMP224 pAAV	hIMPDH1	Standard	31.3785	4.83	1.00E-05				84.4
h20	hIMPDH1	Unknown	Undetermined					Noisy BL	71.6
c572 12.5ng	hIMPDH1	Unknown	Undetermined					Noisy BL	
c572 12.5ng	hIMPDH1	Unknown	Undetermined					Noisy BL	

Detector Name	Slope	Intercept	R2	Number of Standards					
hrGFP-polyA	**-3.193151**	11.969	0.999466	10					
Sample Name	Detector	Task	Ct	StdDev Ct	Qty	Mean Qty	StdDev Qt	Filtered	Tm
IMP224 pAAV	hrGFP-polyA	Standard	15.0732	4.76	0.1				85.6
IMP224 pAAV	hrGFP-polyA	Standard	15.1439	4.76	0.1				85.6
IMP224 pAAV	hrGFP-polyA	Standard	18.55	4.76	0.01				85.6
IMP224 pAAV	hrGFP-polyA	Standard	18.2463	4.76	0.01				85.6
IMP224 pAAV	hrGFP-polyA	Standard	21.6569	4.76	0.001				85.6
IMP224 pAAV	hrGFP-polyA	Standard	21.5924	4.76	0.001				85.6
IMP224 pAAV	hrGFP-polyA	Standard	24.7739	4.76	1.00E-04				85.6
IMP224 pAAV	hrGFP-polyA	Standard	24.5764	4.76	1.00E-04				85.6
IMP224 pAAV	hrGFP-polyA	Standard	28.0023	4.76	1.00E-05				85.3
IMP224 pAAV	hrGFP-polyA	Standard	27.8693	4.76	1.00E-05				85.3
h20	hrGFP-polyA	Unknown	Undetermined					Noisy BL	81.7
c572 12.5ng	hrGFP-polyA	Unknown	Undetermined					Noisy BL	84.7
c572 12.5ng	hrGFP-polyA	Unknown	Undetermined					Noisy BL	84.4

Detector Name	Slope	Intercept	R2	Number of Standards					
C5AR	**-3.143084**	29.62753	0.997568	7					
Sample Name	Detector	Task	Ct	StdDev Ct	Qty	Mean Qty	StdDev Qt	Filtered	Tm
c57 2	C5AR	Standard	26.527	2.81	10				81.6
c57 2	C5AR	Standard	26.366	2.81	10				81.6
c57 2	C5AR	Standard	28.7414	2.82	2				81.6
c57 2	C5AR	Standard	30.8352	2.80.4	0.4				81.6
c57 2	C5AR	Standard	31.0288	2.80.4	0.4				81.3
c57 2	C5AR	Standard	33.2113	2.80.08	0.08				81.3
c57 2	C5AR	Standard	32.8475	2.80.08	0.08				81.3
h20	C5AR	Unknown	Undetermined						82.2

Detector Name	Slope	Intercept	R2	Number of Standards					
Mouse β-actin	**-3.019236**	29.65699	0.993373	10					
Sample Name	Detector	Task	Ct	StdDev Ct	Qty	Mean Qty	StdDev Qt	Filtered	Tm
F RLEP	beta actin	Standard	24.7066	3.16	50				83.4
F RLEP	beta actin	Standard	24.7304	3.16	50				83.4
F RLEP	beta actin	Standard	26.7135	3.16	10				83.4
F RLEP	beta actin	Standard	26.4476	3.16	10				83.4
F RLEP	beta actin	Standard	28.733	3.16	2				83.1
F RLEP	beta actin	Standard	28.3174	3.16	2				83.1
F RLEP	beta actin	Standard	30.4501	3.16	0.4				83.1
F RLEP	beta actin	Standard	30.9728	3.16	0.4				82.8
F RLEP	beta actin	Standard	33.1728	3.16	0.08				83.1
F RLEP	beta actin	Standard	33.2369	3.16	0.08				83.1
h20	beta actin	Unknown	36	1.79	0.007927	0.0313447	0.0331		74.2

Appendix Table 1: Quantitative PCR results of primers for the IMPDH1 transgene and house-keeping genes.

IMP224 pAAV DNA was used for the standard curves of humanIMPDH1 and hrGFP-polyA primers, whereas control DNA was used for the standard curves of C5AR and mouse β-actin genes. The slopes of all standard curves show that the efficiencies of these primers are within 104-114% which is acceptable for real time PCR reaction. In addition, DNA samples of C57BL/6J mice were not amplified in the reactions for the transgene, thus indicating the specificities of these primers. No primer dimer formations were detected in wells added with water.

References

Acland, G.M., G.D. Aguirre, J. Bennett, T.S. Aleman, A.V. Cideciyan, J. Bennicelli, N.S. Dejneka, S.E. Pearce-Kelling, A.M. Maguire, K. Palczewski, W.W. Hauswirth, and S.G. Jacobson. 2005. Long-term restoration of rod and cone vision by single dose rAAV-mediated gene transfer to the retina in a canine model of childhood blindness. *Molecular therapy : the journal of the American Society of Gene Therapy*. 12:1072-1082.

Aherne, A., A. Kennan, P.F. Kenna, N. McNally, D.G. Lloyd, I.L. Alberts, A.S. Kiang, M.M. Humphries, C. Ayuso, P.C. Engel, J.J. Gu, B.S. Mitchell, G.J. Farrar, and P. Humphries. 2004. On the molecular pathology of neurodegeneration in IMPDH1-based retinitis pigmentosa. *Hum Mol Genet*. 13:641-650.

Alcock, F., and E. Swanton. 2009. Mammalian OS-9 is upregulated in response to endoplasmic reticulum stress and facilitates ubiquitination of misfolded glycoproteins. *J Mol Biol*. 385:1032-1042.

Ali, R. R., Reichel, M. B., Thrasher, A. J., Levinsky, R. J., Kinnon, C., Kanuga, N., Hunt, D. M. & Bhattacharya, S. S. 1996. Gene transfer into the mouse retina mediated by an adeno-associated viral vector. *Hum Mol Genet,* 5**,** 591-4.

Allen, T. M. 2002. Ligand-targeted therapeutics in anticancer therapy. *Nat Rev Cancer,* 2**,** 750-63.

Aller, E., Najera, C., Millan, J. M., Oltra, J. S., Perez-Garrigues, H., Vilela, C., Navea, A. & Beneyto, M. 2004. Genetic analysis of 2299delG and C759F mutations (USH2A) in patients with visual and/or auditory impairments. *Eur J Hum Genet,* 12**,** 407-10.

Allocca, M., Tessitore, A., Cotugno, G. & Auricchio, A. 2006. AAV-mediated gene transfer for retinal diseases. *Expert Opin Biol Ther,* 6**,** 1279-94.

Ameri, K., and A.L. Harris. 2008. Activating transcription factor 4. *Int J Biochem Cell Biol*. 40:14-21.

Andres, A., P. Garriga, and J. Manyosa. 2003. Altered functionality in rhodopsin point mutants associated with retinitis pigmentosa. *Biochem Biophys Res Commun*. 303:294-301.

Anukanth, A., and H.G. Khorana. 1994. Structure and function in rhodopsin. Requirements of a specific structure for the intradiscal domain. *The Journal of biological chemistry*. 269:19738-19744.

Applebury, M.L., and P.A. Hargrave. 1986. Molecular biology of the visual pigments. *Vision Res*. 26:1881-1895.

Araujo Couto, L., Sampaio Narciso, M., Hokoc, J. N. & Blanco Martinez, A. M. 2004. Calpain inhibitor 2 prevents axonal degeneration of opossum optic nerve fibers. *J Neurosci Res,* 77**,** 410-9.

Arndt, V., Dick, N., Tawo, R., Dreiseidler, M., Wenzel, D., Hesse, M., Furst, D. O., Saftig, P., Saint, R., Fleischmann, B. K., Hoch, M. & Hohfeld, J. 2010. Chaperone-assisted selective autophagy is essential for muscle maintenance. *Curr Biol,* 20**,** 143-8.

Artus, C., Maquarre, E., Moubarak, R. S., Delettre, C., Jasmin, C., Susin, S. A. & Robert-Lezenes, J. 2006. CD44 ligation induces caspase-independent cell death via a novel calpain/AIF pathway in human erythroleukemia cells. *Oncogene,* 25**,** 5741-51.

Astuto, L. M., Bork, J. M., Weston, M. D., Askew, J. W., Fields, R. R., Orten, D. J., Ohliger, S. J., Riazuddin, S., Morell, R. J., Khan, S., Kremer, H., van Hauwe, P., Moller, C. G., Cremers, C. W., Ayuso, C., Heckenlively, J. R., Rohrschneider, K., Spandau, U., Greenberg, J., Ramesar, R., Reardon, W., Bitoun, P., Millan, J., Legge, R., Friedman, T. B. & Kimberling, W. J. 2002. CDH23 mutation and phenotype heterogeneity: a profile of 107 diverse families with Usher syndrome and nonsyndromic deafness. *Am J Hum Genet,* 71**,** 262-75.

Athanasiou, D., M. Kosmaoglou, N. Kanuga, S.S. Novoselov, A.W. Paton, J.C. Paton, J.P. Chapple, and M.E. Cheetham. 2012. BiP prevents rod opsin aggregation. *Molecular biology of the cell*. 23:3522-3531.

Aufsatz, W., Mette, M. F., van der Winden, J., Matzke, A. J. & Matzke, M. 2002. RNA-directed DNA methylation in Arabidopsis. *Proc Natl Acad Sci U S A,* 99 Suppl 4**,** 16499-506.

Auluck, P. K., Chan, H. Y., Trojanowski, J. Q., Lee, V. M. & Bonini, N. M. 2002. Chaperone suppression of alpha-synuclein toxicity in a Drosophila model for Parkinson's disease. *Science,* 295, 865-8.

Auricchio, A., Kobinger, G., Anand, V., Hildinger, M., O'Connor, E., Maguire, A. M., Wilson, J. M. & Bennett, J. 2001. Exchange of surface proteins impacts on viral vector cellular specificity and transduction characteristics: the retina as a model. *Hum Mol Genet,* 10, 3075-81.

Ausayakhun, S., Yuvaves, P., Ngamtiphakom, S. & Prasitsilp, J. 2005. Treatment of cytomegalovirus retinitis in AIDS patients with intravitreal ganciclovir. *J Med Assoc Thai,* 88 Suppl 9, S15-20.

Azarian, S. M., Schlamp, C. L. & Williams, D. S. 1993. Characterization of calpain II in the retina and photoreceptor outer segments. *J Cell Sci,* 105 (Pt 3), 787-98.

Azuma, M. & Shearer, T. R. 2008. The role of calcium-activated protease calpain in experimental retinal pathology. *Surv Ophthalmol,* 53, 150-63.

Azuma, M., Sakamoto-Mizutani, K., Nakajima, T., Kanaami-Daibo, S., Tamada, Y. & Shearer, T. R. 2004. Involvement of calpain isoforms in retinal degeneration in WBN/Kob rats. *Comp Med,* 54, 533-42.

Baffi, J., Byrnes, G., Chan, C. C. & Csaky, K. G. 2000. Choroidal neovascularization in the rat induced by adenovirus mediated expression of vascular endothelial growth factor. *Invest Ophthalmol Vis Sci,* 41, 3582-9.

Bainbridge, J. W., Smith, A. J., Barker, S. S., Robbie, S., Henderson, R., Balaggan, K., Viswanathan, A., Holder, G. E., Stockman, A., Tyler, N., Petersen-Jones, S., Bhattacharya, S. S., Thrasher, A. J., Fitzke, F. W., Carter, B. J., Rubin, G. S., Moore, A. T. & Ali, R. R. 2008. Effect of gene therapy on visual function in Leber's congenital amaurosis. *N Engl J Med,* 358, 2231-9.

Banin, E., Bandah-Rozenfeld, D., Obolensky, A., Cideciyan, A. V., Aleman, T. S., Marks-Ohana, D., Sela, M., Boye, S., Sumaroka, A., Roman, A. J., Schwartz, S. B., Hauswirth, W. W., Jacobson, S. G., Hemo, I. & Sharon, D. 2010. Molecular anthropology meets genetic medicine to treat blindness in the North African Jewish population: human gene therapy initiated in Israel. *Hum Gene Ther,* 21, 1749-57.

Barar, J., Javadzadeh, A. R. & Omidi, Y. 2008. Ocular novel drug delivery: impacts of membranes and barriers. *Expert Opin Drug Deliv,* 5, 567-81.

Bartel, D. P. & Chen, C. Z. 2004. Micromanagers of gene expression: the potentially widespread influence of metazoan microRNAs. *Nat Rev Genet,* 5, 396-400.

Bartel, D. P. 2004. MicroRNAs: genomics, biogenesis, mechanism, and function. *Cell,* 116, 281-97.

Bauer H-C, T. A., and Bauer H 2004. *Proteins of the tight junction in the blood-brain barrier, in Blood-Spinal Cord and Brain Barriers in Health and Disease,* San Diego, Elsevier.

Baumeister, P., S. Luo, W.C. Skarnes, G. Sui, E. Seto, Y. Shi, and A.S. Lee. 2005. Endoplasmic reticulum stress induction of the Grp78/BiP promoter: activating mechanisms mediated by YY1 and its interactive chromatin modifiers. *Mol Cell Biol.* 25:4529-4540.

Bazzoni, G. 2006. Endothelial tight junctions: permeable barriers of the vessel wall. *Thromb Haemost,* 95, 36-42.

Beales, P. L., Elcioglu, N., Woolf, A. S., Parker, D. & Flinter, F. A. 1999. New criteria for improved diagnosis of Bardet-Biedl syndrome: results of a population survey. *J Med Genet,* 36, 437-46.

Bellavance, M. A., Blanchette, M. & Fortin, D. 2008. Recent advances in blood-brain barrier disruption as a CNS delivery strategy. *AAPS J,* 10, 166-77.

Benali-Furet, N.L., M. Chami, L. Houel, F. De Giorgi, F. Vernejoul, D. Lagorce, L. Buscail, R. Bartenschlager, F. Ichas, R. Rizzuto, and P. Paterlini-Brechot. 2005. Hepatitis C virus core triggers apoptosis in liver cells by inducing ER stress and ER calcium depletion. *Oncogene.* 24:4921-4933.

Bernasconi, R., T. Pertel, J. Luban, and M. Molinari. 2008. A dual task for the Xbp1-responsive OS-9 variants in the mammalian endoplasmic reticulum: inhibiting secretion of misfolded protein conformers and enhancing their disposal. *J Biol Chem.* 283:16446-16454.

Bernstein, E., Caudy, A. A., Hammond, S. M. & Hannon, G. J. 2001. Role for a bidentate ribonuclease in the initiation step of RNA interference. *Nature,* 409, 363-6.

Bernstein, E., Kim, S. Y., Carmell, M. A., Murchison, E. P., Alcorn, H., Li, M. Z., Mills, A. A., Elledge, S. J., Anderson, K. V. & Hannon, G. J. 2003. Dicer is essential for mouse development. *Nat Genet,* 35, 215-7.

Berson, E. L., Sandberg, M. A., Rosner, B., Birch, D. G. & Hanson, A. H. 1985. Natural course of retinitis pigmentosa over a three-year interval. *Am J Ophthalmol,* 99, 240-51.

Berson, E.L., B. Rosner, M.A. Sandberg, C. Weigel-DiFranco, and T.P. Dryja. 1991. Ocular findings in patients with autosomal dominant retinitis pigmentosa and rhodopsin, proline-347-leucine. *American journal of ophthalmology.* 111:614-623.

Berson, E.L., B. Rosner, M.A. Sandberg, K.C. Hayes, B.W. Nicholson, C. Weigel-DiFranco, and W. Willett. 1993a. A randomized trial of vitamin A and vitamin E supplementation for retinitis pigmentosa. *Arch Ophthalmol.* 111:761-772.

Berson, E.L., B. Rosner, M.A. Sandberg, K.C. Hayes, B.W. Nicholson, C. Weigel-DiFrano, and W. Willett. 1993b. Vitamin A supplementation for retinitis pigmentosa. *Arch Ophthalmol.* 111:1456-1459.

Bidere, N., Lorenzo, H. K., Carmona, S., Laforge, M., Harper, F., Dumont, C. & Senik, A. 2003. Cathepsin D triggers Bax activation, resulting in selective apoptosis-inducing factor (AIF) relocation in T lymphocytes entering the early commitment phase to apoptosis. *J Biol Chem,* 278, 31401-11.

Bird, J., Kim, H. P. & Lee, H. J. 1986. Topical anti-inflammatory activity of esters of steroid 21-oic acids. *Steroids,* 47, 35-40.

Bito, L. Z. & Baroody, R. A. 1981. The penetration of exogenous prostaglandin and arachidonic acid into, and their distribution within, the mammalian eye. *Curr Eye Res,* 1, 659-69.

Bizat, N., Galas, M. C., Jacquard, C., Boyer, F., Hermel, J. M., Schiffmann, S. N., Hantraye, P., Blum, D. & Brouillet, E. 2005. Neuroprotective effect of zVAD against the neurotoxin 3-nitropropionic acid involves inhibition of calpain. *Neuropharmacology,* 49, 695-702.

Blennow, K., Wallin, A., Fredman, P., Karlsson, I., Gottfries, C. G. & Svennerholm, L. 1990. Blood-brain barrier disturbance in patients with Alzheimer's disease is related to vascular factors. *Acta Neurol Scand,* 81, 323-6.

Blomgren, K., Zhu, C., Wang, X., Karlsson, J. O., Leverin, A. L., Bahr, B. A., Mallard, C. & Hagberg, H. 2001. Synergistic activation of caspase-3 by m-calpain after neonatal hypoxia-ischemia: a mechanism of "pathological apoptosis"? *J Biol Chem,* 276, 10191-8.

Boden, D., Pusch, O., Silbermann, R., Lee, F., Tucker, L. & Ramratnam, B. 2004. Enhanced gene silencing of HIV-1 specific siRNA using microRNA designed hairpins. *Nucleic Acids Res,* 32, 1154-8.

Bowes, C., Li, T., Danciger, M., Baxter, L. C., Applebury, M. L. & Farber, D. B. 1990. Retinal degeneration in the rd mouse is caused by a defect in the beta subunit of rod cGMP-phosphodiesterase. *Nature,* 347, 677-80.

Bowne, S. J., Humphries, M. M., Sullivan, L. S., Kenna, P. F., Tam, L. C., Kiang, A. S., Campbell, M., Weinstock, G. M., Koboldt, D. C., Ding, L., Fulton, R. S., Sodergren, E. J., Allman, D., Millington-Ward, S., Palfi, A., McKee, A., Blanton, S. H., Slifer, S., Konidari, I., Farrar, G. J., Daiger, S. P. & Humphries, P. 2011. A dominant mutation in RPE65 identified by whole-exome sequencing causes retinitis pigmentosa with choroidal involvement. *Eur J Hum Genet,* 19, 1074-81.

Bowne, S. J., Liu, Q., Sullivan, L. S., Zhu, J., Spellicy, C. J., Rickman, C. B., Pierce, E. A. & Daiger, S. P. 2006a. Why do mutations in the ubiquitously expressed housekeeping gene IMPDH1 cause retina-specific photoreceptor degeneration? *Invest Ophthalmol Vis Sci,* 47, 3754-65.

Bowne, S. J., Sullivan, L. S., Blanton, S. H., Cepko, C. L., Blackshaw, S., Birch, D. G., Hughbanks-Wheaton, D., Heckenlively, J. R. & Daiger, S. P. 2002. Mutations in the inosine monophosphate dehydrogenase 1 gene (IMPDH1) cause the RP10 form of autosomal dominant retinitis pigmentosa. *Hum Mol Genet,* 11, 559-68.

Bowne, S. J., Sullivan, L. S., Mortimer, S. E., Hedstrom, L., Zhu, J., Spellicy, C. J., Gire, A. I., Hughbanks-Wheaton, D., Birch, D. G., Lewis, R. A., Heckenlively, J. R. & Daiger, S. P. 2006b. Spectrum and frequency of mutations in IMPDH1 associated with autosomal dominant retinitis pigmentosa and leber congenital amaurosis. *Invest Ophthalmol Vis Sci,* 47, 34-42.

Brightman, M. W. & Reese, T. S. 1969. JUNCTIONS BETWEEN INTIMATELY APPOSED CELL MEMBRANES IN VERTEBRATE BRAIN. *Journal of Cell Biology,* 40, 648-&.

Bucciantini, M., Giannoni, E., Chiti, F., Baroni, F., Formigli, L., Zurdo, J., Taddei, N., Ramponi, G., Dobson, C. M. & Stefani, M. 2002. Inherent toxicity of aggregates implies a common mechanism for protein misfolding diseases. *Nature,* 416, 507-11.

Bucciantini, M., Giannoni, E., Chiti, F., Baroni, F., Formigli, L., Zurdo, J., Taddei, N., Ramponi, G., Dobson, C. M. & Stefani, M. 2002. Inherent toxicity of aggregates implies a common mechanism for protein misfolding diseases. *Nature,* 416, 507-11.

Calin, G. A., Dumitru, C. D., Shimizu, M., Bichi, R., Zupo, S., Noch, E., Aldler, H., Rattan, S., Keating, M., Rai, K., Rassenti, L., Kipps, T., Negrini, M., Bullrich, F. & Croce, C. M. 2002. Frequent deletions and down-regulation of micro- RNA genes miR15 and miR16 at 13q14 in chronic lymphocytic leukemia. *Proc Natl Acad Sci U S A,* 99, 15524-9.

Campbell, M., Hanrahan, F., Gobbo, O. L., Kelly, M. E., Kiang, A. S., Humphries, M. M., Nguyen, A. T., Ozaki, E., Keaney, J., Blau, C. W., Kerskens, C. M., Cahalan, S. D., Callanan, J. J., Wallace, E., Grant, G. A., Doherty, C. P. & Humphries, P. 2012. Targeted suppression of claudin-5 decreases cerebral oedema and improves cognitive outcome following traumatic brain injury. *Nat Commun,* 3, 849.

Campbell, M., Humphries, M. M., Kiang, A. S., Nguyen, A. T., Gobbo, O. L., Tam, L. C., Suzuki, M., Hanrahan, F., Ozaki, E., Farrar, G. J., Kenna, P. F. & Humphries, P. 2011. Systemic low-molecular weight drug delivery to pre-selected neuronal regions. *EMBO Mol Med,* 3, 235-45.

Campbell, M., Kiang, A. S., Kenna, P. F., Kerskens, C., Blau, C., O'Dwyer, L., Tivnan, A., Kelly, J. A., Brankin, B., Farrar, G. J. & Humphries, P. 2008. RNAi-mediated reversible opening of the blood-brain barrier. *J Gene Med,* 10, 930-47.

Campbell, M., Nguyen, A. T., Kiang, A. S., Tam, L. C., Gobbo, O. L., Kerskens, C., Ni Dhubhghaill, S., Humphries, M. M., Farrar, G. J., Kenna, P. F. & Humphries, P. 2009. An experimental platform for systemic drug delivery to the retina. *Proc Natl Acad Sci U S A,* 106, 17817-22.

Campbell, M., Nguyen, A. T., Kiang, A. S., Tam, L., Kenna, P. F., Dhubhghaill, S. N., Humphries, M., Farrar, G. J. & Humphries, P. 2010. Reversible and size-selective opening of the inner Blood-Retina barrier: a novel therapeutic strategy. *Adv Exp Med Biol,* 664, 301-8.

Campbell, M., Ozaki, E. & Humphries, P. 2010b. Systemic delivery of therapeutics to neuronal tissues: a barrier modulation approach. *Expert Opin Drug Deliv,* 7, 859-69.

Caramelo, J.J., O.A. Castro, L.G. Alonso, G. De Prat-Gay, and A.J. Parodi. 2003. UDP-Glc:glycoprotein glucosyltransferase recognizes structured and solvent accessible hydrophobic patches in molten globule-like folding intermediates. *Proc Natl Acad Sci U S A.* 100:86-91.

Carr, S. F., Papp, E., Wu, J. C. & Natsumeda, Y. 1993. Characterization of human type I and type II IMP dehydrogenases. *J Biol Chem,* 268, 27286-90.

Cashman, S. M., Bowman, L., Christofferson, J. & Kumar-Singh, R. 2006. Inhibition of choroidal neovascularization by adenovirus-mediated delivery of short hairpin RNAs targeting VEGF as a potential therapy for AMD. *Invest Ophthalmol Vis Sci,* 47, 3496-504.

Cashman, S. M., Desai, A., Ramo, K. & Kumar-Singh, R. 2011. Expression of complement component 3 (C3) from an adenovirus leads to pathology in the murine retina. *Invest Ophthalmol Vis Sci,* 52, 3436-45.

Castanotto, D., Sakurai, K., Lingeman, R., Li, H., Shively, L., Aagaard, L., Soifer, H., Gatignol, A., Riggs, A. & Rossi, J. J. 2007. Combinatorial delivery of small interfering RNAs reduces RNAi efficacy by selective incorporation into RISC. *Nucleic Acids Res,* 35, 5154-64.

Cekaite, L., Furset, G., Hovig, E. & Sioud, M. 2007. Gene expression analysis in blood cells in response to unmodified and 2'-modified siRNAs reveals TLR-dependent and independent effects. *J Mol Biol,* 365, 90-108.

Chader, G. J. 2002. Animal models in research on retinal degenerations: past progress and future hope. *Vision Res,* 42, 393-9.

Chang, G. Q., Hao, Y. & Wong, F. 1993. Apoptosis: final common pathway of photoreceptor death in rd, rds, and rhodopsin mutant mice. *Neuron,* 11, 595-605.

Chapple, J.P., and M.E. Cheetham. 2003. The chaperone environment at the cytoplasmic face of the endoplasmic reticulum can modulate rhodopsin processing and inclusion formation. *J Biol Chem.* 278:19087-19094.

Chapple, J.P., C. Grayson, A.J. Hardcastle, R.S. Saliba, J. van der Spuy, and M.E. Cheetham. 2001. Unfolding retinal dystrophies: a role for molecular chaperones? *Trends Mol Med.* 7:414-421.

Chatterjee, S., Berger, S. J. & Berger, N. A. 1999. Poly(ADP-ribose) polymerase: a guardian of the genome that facilitates DNA repair by protecting against DNA recombination. *Mol Cell Biochem,* 193, 23-30.

Chavany, C., E. Mimnaugh, P. Miller, R. Bitton, P. Nguyen, J. Trepel, L. Whitesell, R. Schnur, J. Moyer, and L. Neckers. 1996. p185erbB2 binds to GRP94 *in vivo*. Dissociation of the p185erbB2/GRP94 heterocomplex by benzoquinone ansamycins precedes depletion of p185erbB2. *J Biol Chem.* 271:4974-4977.

Cheetham, M. E. & Caplan, A. J. 1998. Structure, function and evolution of DnaJ: conservation and adaptation of chaperone function. *Cell Stress Chaperones,* 3, 28-36.

Chen, X. 2004. A microRNA as a translational repressor of APETALA2 in Arabidopsis flower development. *Science,* 303, 2022-5.

Chevalier, M., H. Rhee, E.C. Elguindi, and S.Y. Blond. 2000. Interaction of murine BiP/GRP78 with the DnaJ homologue MTJ1. *J Biol Chem.* 275:19620-19627.

Chiu, K., Lam, T. T., Ying Li, W. W., Caprioli, J. & Kwong Kwong, J. M. 2005. Calpain and N-methyl-d-aspartate (NMDA)-induced excitotoxicity in rat retinas. *Brain Res,* 1046, 207-15.

Chrai, S. S., Makoid, M. C., Eriksen, S. P. & Robinson, J. R. 1974. Drop size and initial dosing frequency problems of topically applied ophthalmic drugs. *J Pharm Sci,* 63, 333-8.

Christianson, J.C., T.A. Shaler, R.E. Tyler, and R.R. Kopito. 2008. OS-9 and GRP94 deliver mutant alpha1-antitrypsin to the Hrd1-SEL1L ubiquitin ligase complex for ERAD. *Nat Cell Biol.* 10:272-282.

Christie, J. G. & Kompella, U. B. 2008. Ophthalmic light sensitive nanocarrier systems. *Drug Discov Today,* 13, 124-34.

Chrysostomou, V., J. Stone, and K. Valter. 2009. Life history of cones in the rhodopsin-mutant P23H-3 rat: evidence of long-term survival. *Investigative ophthalmology & visual science.* 50:2407-2416.

Chrysostomou, V., Stone, J. & Valter, K. 2009. Life history of cones in the rhodopsin-mutant P23H-3 rat: evidence of long-term survival. *Invest Ophthalmol Vis Sci,* 50, 2407-16.

Chua, B. T., Guo, K. & Li, P. 2000. Direct cleavage by the calcium-activated protease calpain can lead to inactivation of caspases. *J Biol Chem,* 275, 5131-5.

Chuang, J.Z., C. Vega, W. Jun, and C.H. Sung. 2004. Structural and functional impairment of endocytic pathways by retinitis pigmentosa mutant rhodopsin-arrestin complexes. *J Clin Invest.* 114:131-140.

Chung, K. H., Hart, C. C., Al-Bassam, S., Avery, A., Taylor, J., Patel, P. D., Vojtek, A. B. & Turner, D. L. 2006. Polycistronic RNA polymerase II expression vectors for RNA interference based on BIC/miR-155. *Nucleic Acids Res,* 34, e53.

Cideciyan, A. V., Aleman, T. S., Boye, S. L., Schwartz, S. B., Kaushal, S., Roman, A. J., Pang, J. J., Sumaroka, A., Windsor, E. A., Wilson, J. M., Flotte, T. R., Fishman, G. A., Heon, E., Stone, E. M., Byrne, B. J., Jacobson, S. G. & Hauswirth, W. W. 2008. Human gene therapy for RPE65 isomerase deficiency activates the retinoid cycle of vision but with slow rod kinetics. *Proc Natl Acad Sci U S A,* 105, 15112-7.

Cideciyan, A. V., Jacobson, S. G., Aleman, T. S., Gu, D., Pearce-Kelling, S. E., Sumaroka, A., Acland, G. M. & Aguirre, G. D. 2005. *In vivo* dynamics of retinal injury and repair in the rhodopsin mutant dog model of human retinitis pigmentosa. *Proc Natl Acad Sci U S A,* 102, 5233-8.

Citic, R. 1989. [The present surgical status in the diagnosis and treatment of acute traumatic intracranial hemorrhage]. *Neurologija,* 38, 223-30.

Colegio, O. R., Van Itallie, C. M., McCrea, H. J., Rahner, C. & Anderson, J. M. 2002. Claudins create charge-selective channels in the paracellular pathway between epithelial cells. *Am J Physiol Cell Physiol,* 283, C142-7.

Conchillo-Sole, O., N.S. de Groot, F.X. Aviles, J. Vendrell, X. Daura, and S. Ventura. 2007. AGGRESCAN: a server for the prediction and evaluation of "hot spots" of aggregation in polypeptides. *BMC Bioinformatics*. 8:65.

Conley, S. M., Stricker, H. M. & Naash, M. I. 2010. Biochemical analysis of phenotypic diversity associated with mutations in codon 244 of the retinal degeneration slow gene. *Biochemistry,* 49, 905-11.

Connell, G., Bascom, R., Molday, L., Reid, D., McInnes, R. R. & Molday, R. S. 1991. Photoreceptor peripherin is the normal product of the gene responsible for retinal degeneration in the rds mouse. *Proc Natl Acad Sci U S A,* 88, 723-6.

Cornuel, J. F., Moraillon, A. & Gueron, M. 2002. Participation of yeast inosine 5'-monophosphate dehydrogenase in an *in vitro* complex with a fragment of the C-rich telomeric strand. *Biochimie,* 84, 279-89.

Coura Rdos, S. & Nardi, N. B. 2007. The state of the art of adeno-associated virus-based vectors in gene therapy. *Virol J,* 4, 99.

Cullinan, S.B., and J.A. Diehl. 2004. PERK-dependent activation of Nrf2 contributes to redox homeostasis and cell survival following endoplasmic reticulum stress. *The Journal of biological chemistry*. 279:20108-20117.

Cunnea, P., McMahon, J., O'Connell, E., Mashayekhi, K., Fitzgerald, U. & McQuaid, S. 2010. Gene expression analysis of the microvascular compartment in multiple sclerosis using laser microdissected blood vessels. *Acta Neuropathol,* 119, 601-15.

Daiger, S. P., Bowne, S. J. & Sullivan, L. S. 2007. Perspective on genes and mutations causing retinitis pigmentosa. *Arch Ophthalmol,* 125, 151-8.

Daiger, S. P., Sullivan, L. S., Bowne, S. J., Kennan, A., Humphries, P., Birch, D. G. & Heckenlively, J. R. 2003. Identification of the RP1 and RP10 (IMPDH1) genes causing autosomal dominant RP. *Adv Exp Med Biol,* 533, 1-11.

Dalkara, D., Kolstad, K. D., Caporale, N., Visel, M., Klimczak, R. R., Schaffer, D. V. & Flannery, J. G. 2009. Inner limiting membrane barriers to AAV-mediated retinal transduction from the vitreous. *Mol Ther,* 17, 2096-102.

Daugas, E., Susin, S. A., Zamzami, N., Ferri, K. F., Irinopoulou, T., Larochette, N., Prevost, M. C., Leber, B., Andrews, D., Penninger, J. & Kroemer, G. 2000. Mitochondrio-nuclear translocation of AIF in apoptosis and necrosis. *FASEB J,* 14, 729-39.

Dehouck, Y., A. Grosfils, B. Folch, D. Gilis, P. Bogaerts, and M. Rooman. 2009. Fast and accurate predictions of protein stability changes upon mutations using statistical potentials and neural networks: PoPMuSiC-2.0. *Bioinformatics*. 25:2537-2543.

Dejneka, N. S., Auricchio, A., Maguire, A. M., Ye, X., Gao, G. P., Wilson, J. M. & Bennett, J. 2001. Pharmacologically regulated gene expression in the retina following transduction with viral vectors. *Gene Ther,* 8, 442-6.

Dejneka, N. S., Rex, T. S. & Bennett, J. 2003. Gene therapy and animal models for retinal disease. *Dev Ophthalmol,* 37, 188-98.

Delyfer, M. N., Leveillard, T., Mohand-Said, S., Hicks, D., Picaud, S. & Sahel, J. A. 2004. Inherited retinal degenerations: therapeutic prospects. *Biol Cell,* 96, 261-9.

Dhallan, R. S., Macke, J. P., Eddy, R. L., Shows, T. B., Reed, R. R., Yau, K. W. & Nathans, J. 1992. Human rod photoreceptor cGMP-gated channel: amino acid sequence, gene structure, and functional expression. *J Neurosci,* 12, 3248-56.

Dobson, C. M. 2004. Experimental investigation of protein folding and misfolding. *Methods,* 34, 4-14.

Doench, J. G., Petersen, C. P. & Sharp, P. A. 2003. siRNAs can function as miRNAs. *Genes Dev,* 17, 438-42.

Dong, M., J.P. Bridges, K. Apsley, Y. Xu, and T.E. Weaver. 2008. ERdj4 and ERdj5 are required for endoplasmic reticulum-associated protein degradation of misfolded surfactant protein C. *Mol Biol Cell*. 19:2620-2630.

Donovan, M. & Cotter, T. G. 2002. Caspase-independent photoreceptor apoptosis *in vivo* and differential expression of apoptotic protease activating factor-1 and caspase-3 during retinal development. *Cell Death Differ,* 9, 1220-31.

Donovan, M., Carmody, R. J. & Cotter, T. G. 2001. Light-induced photoreceptor apoptosis *in vivo* requires neuronal nitric-oxide synthase and guanylate cyclase activity and is caspase-3-independent. *J Biol Chem,* 276, 23000-8.

Doonan, F., Donovan, M. & Cotter, T. G. 2003. Caspase-independent photoreceptor apoptosis in mouse models of retinal degeneration. *J Neurosci,* 23, 5723-31.

Doonan, F., Donovan, M. & Cotter, T. G. 2005. Activation of multiple pathways during photoreceptor apoptosis in the rd mouse. *Invest Ophthalmol Vis Sci,* 46, 3530-8.

Drinnenberg, I. A., Weinberg, D. E., Xie, K. T., Mower, J. P., Wolfe, K. H., Fink, G. R. & Bartel, D. P. 2009. RNAi in budding yeast. *Science,* 326, 544-50.

Dryja, T. P., Hahn, L. B., Cowley, G. S., McGee, T. L. & Berson, E. L. 1991. Mutation spectrum of the rhodopsin gene among patients with autosomal dominant retinitis pigmentosa. *Proc Natl Acad Sci U S A,* 88, 9370-4.

Dryja, T. P., McEvoy, J. A., McGee, T. L. & Berson, E. L. 2000. Novel rhodopsin mutations Gly114Val and Gln184Pro in dominant retinitis pigmentosa. *Invest Ophthalmol Vis Sci,* 41, 3124-7.

Dryja, T. P., McGee, T. L., Reichel, E., Hahn, L. B., Cowley, G. S., Yandell, D. W., Sandberg, M. A. & Berson, E. L. 1990. A point mutation of the rhodopsin gene in one form of retinitis pigmentosa. *Nature,* 343, 364-6.

Dunaief, J. L., Dentchev, T., Ying, G. S. & Milam, A. H. 2002. The role of apoptosis in age-related macular degeneration. *Arch Ophthalmol,* 120, 1435-42.

Duvvuri, S., Majumdar, S. & Mitra, A. K. 2003. Drug delivery to the retina: challenges and opportunities. *Expert Opin Biol Ther,* 3, 45-56.

Egorin, M. J., Lagattuta, T. F., Hamburger, D. R., Covey, J. M., White, K. D., Musser, S. M. & Eiseman, J. L. 2002. Pharmacokinetics, tissue distribution, and metabolism of 17-(dimethylaminoethylamino)-17-demethoxygeldanamycin (NSC 707545) in CD2F1 mice and Fischer 344 rats. *Cancer Chemother Pharmacol,* 49, 7-19.

Egorin, M. J., Rosen, D. M., Wolff, J. H., Callery, P. S., Musser, S. M. & Eiseman, J. L. 1998. Metabolism of 17-(allylamino)-17-demethoxygeldanamycin (NSC 330507) by murine and human hepatic preparations. *Cancer Res,* 58, 2385-96.

Egorin, M. J., Zuhowski, E. G., Rosen, D. M., Sentz, D. L., Covey, J. M. & Eiseman, J. L. 2001. Plasma pharmacokinetics and tissue distribution of 17-(allylamino)-17-demethoxygeldanamycin (NSC 330507) in CD2F1 mice1. *Cancer Chemother Pharmacol,* 47, 291-302.

Ehrlich, P. 1885. *On the oxygen consumption of the body. A study using intravital dyes,* Berlin, Verlag von August Hirchwald.

Eichler, W., Kuhrt, H., Hoffmann, S., Wiedemann, P. & Reichenbach, A. 2000. VEGF release by retinal glia depends on both oxygen and glucose supply. *Neuroreport,* 11, 3533-7.

Eichler, W., Yafai, Y., Wiedemann, P. & Reichenbach, A. 2004. Angiogenesis-related factors derived from retinal glial (Muller) cells in hypoxia. *Neuroreport,* 15, 1633-7.

Elbashir, S. M., Harborth, J., Lendeckel, W., Yalcin, A., Weber, K. & Tuschl, T. 2001a. Duplexes of 21-nucleotide RNAs mediate RNA interference in cultured mammalian cells. *Nature,* 411, 494-8.

Elbashir, S. M., Harborth, J., Weber, K. & Tuschl, T. 2002. Analysis of gene function in somatic mammalian cells using small interfering RNAs. *Methods,* 26, 199-213.

Elbashir, S. M., Lendeckel, W. & Tuschl, T. 2001b. RNA interference is mediated by 21- and 22-nucleotide RNAs. *Genes Dev,* 15, 188-200.

Eletto, D., D. Dersh, and Y. Argon. 2010. GRP94 in ER quality control and stress responses. *Seminars in cell & developmental biology.* 21:479-485.

Ellis, R. J. & Hartl, F. U. 1999. Principles of protein folding in the cellular environment. *Curr Opin Struct Biol,* 9, 102-10.

Evans, M. J., von Hahn, T., Tscherne, D. M., Syder, A. J., Panis, M., Wolk, B., Hatziioannou, T., McKeating, J. A., Bieniasz, P. D. & Rice, C. M. 2007. Claudin-1 is a hepatitis C virus co-receptor required for a late step in entry. *Nature,* 446, 801-5.

Farinha, C.M., and M.D. Amaral. 2005. Most F508del-CFTR is targeted to degradation at an early folding checkpoint and independently of calnexin. *Mol Cell Biol.* 25:5242-5252.

Farrar, G. J., Kenna, P. F. & Humphries, P. 2002. On the genetics of retinitis pigmentosa and on mutation-independent approaches to therapeutic intervention. *EMBO J,* 21, 857-64.

Farrar, G. J., Kenna, P., Redmond, R., McWilliam, P., Bradley, D. G., Humphries, M. M., Sharp, E. M., Inglehearn, C. F., Bashir, R., Jay, M. & *et al.* 1990. Autosomal dominant retinitis

pigmentosa: absence of the rhodopsin proline----histidine substitution (codon 23) in pedigrees from Europe. *Am J Hum Genet,* 47, 941-5.

Favaloro, B., Allocati, N., Graziano, V., Di Ilio, C. & De Laurenzi, V. 2012. Role of apoptosis in disease. *Aging (Albany NY),* 4, 330-49.

Fernandez-Sanchez, L., P. Lax, G. Esquiva, J. Martin-Nieto, I. Pinilla, and N. Cuenca. 2012. Safranal, a saffron constituent, attenuates retinal degeneration in P23H rats. *PLoS One.* 7:e43074.

Fernandez-Sanchez, L., P. Lax, I. Pinilla, J. Martin-Nieto, and N. Cuenca. 2011. Tauroursodeoxycholic acid prevents retinal degeneration in transgenic P23H rats. *Invest Ophthalmol Vis Sci.* 52:4998-5008.

Fewell, S.W., K.J. Travers, J.S. Weissman, and J.L. Brodsky. 2001. The action of molecular chaperones in the early secretory pathway. *Annu Rev Genet.* 35:149-191.

Fire, A., Xu, S., Montgomery, M. K., Kostas, S. A., Driver, S. E. & Mello, C. C. 1998. Potent and specific genetic interference by double-stranded RNA in Caenorhabditis elegans. *Nature,* 391, 806-11.

Fischer, H., U. Koenig, L. Eckhart, and E. Tschachler. 2002. Human caspase 12 has acquired deleterious mutations. *Biochem Biophys Res Commun.* 293:722-726.

Fletcher, E. L., Jobling, A. I., Vessey, K. A., Luu, C., Guymer, R. H. & Baird, P. N. 2011. Animal models of retinal disease. *Prog Mol Biol Transl Sci,* 100, 211-86.

Foust, K. D., Nurre, E., Montgomery, C. L., Hernandez, A., Chan, C. M. & Kaspar, B. K. 2009. Intravascular AAV9 preferentially targets neonatal neurons and adult astrocytes. *Nat Biotechnol,* 27, 59-65.

Foust, K. D., Wang, X., McGovern, V. L., Braun, L., Bevan, A. K., Haidet, A. M., Le, T. T., Morales, P. R., Rich, M. M., Burghes, A. H. & Kaspar, B. K. 2010. Rescue of the spinal muscular atrophy phenotype in a mouse model by early postnatal delivery of SMN. *Nat Biotechnol,* 28, 271-4.

Fox, D. A., Poblenz, A. T. & He, L. 1999. Calcium overload triggers rod photoreceptor apoptotic cell death in chemical-induced and inherited retinal degenerations. *Ann N Y Acad Sci,* 893, 282-5.

Frank, J. A., Dwyer, A. J., Girton, M., Knop, R. H., Sank, V. J., Gansow, O. A., Magerstadt, M., Brechbiel, M. & Doppman, J. L. 1986. Opening of blood-ocular barrier demonstrated by contrast-enhanced MR imaging. *J Comput Assist Tomogr,* 10, 912-6.

Frederick, J. M., Krasnoperova, N. V., Hoffmann, K., Church-Kopish, J., Ruther, K., Howes, K., Lem, J. & Baehr, W. 2001. Mutant rhodopsin transgene expression on a null background. *Invest Ophthalmol Vis Sci,* 42, 826-33.

Freireich, E.J., E.A. Gehan, D.P. Rall, L.H. Schmidt, and H.E. Skipper. 1966. Quantitative comparison of toxicity of anticancer agents in mouse, rat, hamster, dog, monkey, and man. *Cancer chemotherapy reports. Part 1.* 50:219-244.

Frydman, J. 2001. Folding of newly translated proteins *in vivo*: the role of molecular chaperones. *Annu Rev Biochem,* 70, 603-47.

Fu, H.Y., T. Minamino, O. Tsukamoto, T. Sawada, M. Asai, H. Kato, Y. Asano, M. Fujita, S. Takashima, M. Hori, and M. Kitakaze. 2008. Overexpression of endoplasmic reticulum-resident chaperone attenuates cardiomyocyte death induced by proteasome inhibition. *Cardiovasc Res.* 79:600-610.

Fujikake, N., Nagai, Y., Popiel, H. A., Okamoto, Y., Yamaguchi, M. & Toda, T. 2008. Heat shock transcription factor 1-activating compounds suppress polyglutamine-induced neurodegeneration through induction of multiple molecular chaperones. *J Biol Chem,* 283, 26188-97.

Fujita, K., Katahira, J., Horiguchi, Y., Sonoda, N., Furuse, M. & Tsukita, S. 2000. Clostridium perfringens enterotoxin binds to the second extracellular loop of claudin-3, a tight junction integral membrane protein. *FEBS Lett,* 476, 258-61.

Fukuda, M.N., D.S. Papermaster, and P.A. Hargrave. 1979. Rhodopsin carbohydrate. Structure of small oligosaccharides attached at two sites near the NH2 terminus. *J Biol Chem.* 254:8201-8207.

Fukuyo, Y., Hunt, C. R. & Horikoshi, N. 2010. Geldanamycin and its anti-cancer activities. *Cancer Lett,* 290, 24-35.

Furuse, M. & Tsukita, S. 2006. Claudins in occluding junctions of humans and flies. *Trends in Cell Biology,* 16, 181-188.

Furuse, M., Sasaki, H. & Tsukita, S. 1999. Manner of interaction of heterogeneous claudin species within and between tight junction strands. *J Cell Biol,* 147, 891-903.

Gafni, J., Cong, X., Chen, S. F., Gibson, B. W. & Ellerby, L. M. 2009. Calpain-1 cleaves and activates caspase-7. *J Biol Chem,* 284, 25441-9.

Gaudana, R., Ananthula, H. K., Parenky, A. & Mitra, A. K. 2010. Ocular drug delivery. *AAPS J,* 12, 348-60.

Gavrilov, K. & Saltzman, W. M. 2012. Therapeutic siRNA: principles, challenges, and strategies. *Yale J Biol Med,* 85, 187-200.

George, J. M. 2002. The synucleins. *Genome Biol,* 3, REVIEWS3002.

Ghazizadeh, S., Carroll, J. M. & Taichman, L. B. 1997. Repression of retrovirus-mediated transgene expression by interferons: implications for gene therapy. *J Virol,* 71, 9163-9.

Giam, M., Huang, D. C. & Bouillet, P. 2008. BH3-only proteins and their roles in programmed cell death. *Oncogene,* 27 Suppl 1, S128-36.

Gillece, P., J.M. Luz, W.J. Lennarz, F.J. de La Cruz, and K. Romisch. 1999. Export of a cysteine-free misfolded secretory protein from the endoplasmic reticulum for degradation requires interaction with protein disulfide isomerase. *J Cell Biol.* 147:1443-1456.

Glaze, E. R., Lambert, A. L., Smith, A. C., Page, J. G., Johnson, W. D., McCormick, D. L., Brown, A. P., Levine, B. S., Covey, J. M., Egorin, M. J., Eiseman, J. L., Holleran, J. L., Sausville, E. A. & Tomaszewski, J. E. 2005. Preclinical toxicity of a geldanamycin analog, 17-(dimethylaminoethylamino)-17-demethoxygeldanamycin (17-DMAG), in rats and dogs: potential clinical relevance. *Cancer Chemother Pharmacol,* 56, 637-47.

Goldmann, E. 1913. Vitalfärbungen am Zentralnervensystem. Beitrag zur Physio-Pathologie des Plexus Choroideus und der Hirnhäute. [Intravital labelling of the central nervous system. A study on the pathophysiology of the choroid plexus and the meninges.] *Abhandlungen der königlich preußischen Akademie der Wissenschaften, Physikalisch-Mathematische Classe 1,* 1-64.

Goll, D. E., Thompson, V. F., Li, H., Wei, W. & Cong, J. 2003. The calpain system. *Physiol Rev,* 83, 731-801.

Gomez-Vicente, V., Donovan, M. & Cotter, T. G. 2005. Multiple death pathways in retina-derived 661W cells following growth factor deprivation: crosstalk between caspases and calpains. *Cell Death Differ,* 12, 796-804.

Gonzalez, S., Castanotto, D., Li, H., Olivares, S., Jensen, M. C., Forman, S. J., Rossi, J. J. & Cooper, L. J. 2005. Amplification of RNAi--targeting HLA mRNAs. *Mol Ther,* 11, 811-8.

Gonzalez-Mariscal, L., Betanzos, A. & Avila-Flores, A. 2000. MAGUK proteins: structure and role in the tight junction. *Semin Cell Dev Biol,* 11, 315-24.

Gorbatyuk, M. S., Knox, T., LaVail, M. M., Gorbatyuk, O. S., Noorwez, S. M., Hauswirth, W. W., Lin, J. H., Muzyczka, N. & Lewin, A. S. 2010. Restoration of visual function in P23H rhodopsin transgenic rats by gene delivery of BiP/Grp78. *Proc Natl Acad Sci U S A,* 107, 5961-6.

Goto, Y., Peachey, N. S., Ripps, H. & Naash, M. I. 1995. Functional abnormalities in transgenic mice expressing a mutant rhodopsin gene. *Invest Ophthalmol Vis Sci,* 36, 62-71.

Grewal, S. I. & Moazed, D. 2003. Heterochromatin and epigenetic control of gene expression. *Science,* 301, 798-802.

Griciuc, A., L. Aron, and M. Ueffing. 2011. ER stress in retinal degeneration: a target for rational therapy? *Trends in molecular medicine.* 17:442-451.

Grieger, J. C. & Samulski, R. J. 2005. Packaging capacity of adeno-associated virus serotypes: impact of larger genomes on infectivity and postentry steps. *J Virol,* 79, 9933-44.

Grimm, C. & Reme, C. E. 2013. Light damage as a model of retinal degeneration. *Methods Mol Biol,* 935, 87-97.

Grimm, D., Streetz, K. L., Jopling, C. L., Storm, T. A., Pandey, K., Davis, C. R., Marion, P., Salazar, F. & Kay, M. A. 2006. Fatality in mice due to oversaturation of cellular microRNA/short hairpin RNA pathways. *Nature,* 441, 537-41.

Gu, J. J., Spychala, J. & Mitchell, B. S. 1997. Regulation of the human inosine monophosphate dehydrogenase type I gene. Utilization of alternative promoters. *J Biol Chem,* 272, 4458-66.

Gu, J. J., Stegmann, S., Gathy, K., Murray, R., Laliberte, J., Ayscue, L. & Mitchell, B. S. 2000. Inhibition of T lymphocyte activation in mice heterozygous for loss of the IMPDH II gene. *J Clin Invest,* 106**,** 599-606.

Gu, J. J., Tolin, A. K., Jain, J., Huang, H., Santiago, L. & Mitchell, B. S. 2003. Targeted disruption of the inosine 5'-monophosphate dehydrogenase type I gene in mice. *Mol Cell Biol,* 23**,** 6702-12.

Gunther, M., Lipka, J., Malek, A., Gutsch, D., Kreyling, W. & Aigner, A. 2011. Polyethylenimines for RNAi-mediated gene targeting *in vivo* and siRNA delivery to the lung. *Eur J Pharm Biopharm,* 77**,** 438-49.

Guo, P., Coban, O., Snead, N. M., Trebley, J., Hoeprich, S., Guo, S. & Shu, Y. 2010. Engineering RNA for targeted siRNA delivery and medical application. *Adv Drug Deliv Rev,* 62**,** 650-66.

Guo, S. & Kemphues, K. J. 1995. par-1, a gene required for establishing polarity in C. elegans embryos, encodes a putative Ser/Thr kinase that is asymmetrically distributed. *Cell,* 81**,** 611-20.

Guth, S., C. Volzing, A. Muller, M. Jung, and R. Zimmermann. 2004. Protein transport into canine pancreatic microsomes: a quantitative approach. *European journal of biochemistry / FEBS.* 271:3200-3207.

Haas, I.G., and M. Wabl. 1983. Immunoglobulin heavy chain binding protein. *Nature.* 306:387-389.

Haeri, M., and B.E. Knox. 2012. Endoplasmic Reticulum Stress and Unfolded Protein Response Pathways: Potential for Treating Age-related Retinal Degeneration. *Journal of ophthalmic & vision research.* 7:45-59.

Hager, P. W., Collart, F. R., Huberman, E. & Mitchell, B. S. 1995. Recombinant human inosine monophosphate dehydrogenase type I and type II proteins. Purification and characterization of inhibitor binding. *Biochem Pharmacol,* 49**,** 1323-9.

Haim, M. 2002. Epidemiology of retinitis pigmentosa in Denmark. *Acta Ophthalmol Scand Suppl***,** 1-34.

Hammond, S. M., Bernstein, E., Beach, D. & Hannon, G. J. 2000. An RNA-directed nuclease mediates post-transcriptional gene silencing in Drosophila cells. *Nature,* 404**,** 293-6.

Hammond, S. M., Boettcher, S., Caudy, A. A., Kobayashi, R. & Hannon, G. J. 2001. Argonaute2, a link between genetic and biochemical analyses of RNAi. *Science,* 293**,** 1146-50.

Hannon, G. J. & Conklin, D. S. 2004. RNA interference by short hairpin RNAs expressed in vertebrate cells. *Methods Mol Biol,* 257**,** 255-66.

Hannon, G. J. 2002. RNA interference. *Nature,* 418**,** 244-51.

Harding, H.P., I. Novoa, Y. Zhang, H. Zeng, R. Wek, M. Schapira, and D. Ron. 2000. Regulated translation initiation controls stress-induced gene expression in mammalian cells. *Mol Cell.* 6:1099-1108.

Harding, H.P., Y. Zhang, and D. Ron. 1999. Protein translation and folding are coupled by an endoplasmic-reticulum-resident kinase. *Nature.* 397:271-274.

Hargrave, P.A. 2001. Rhodopsin structure, function, and topography the Friedenwald lecture. *Invest Ophthalmol Vis Sci.* 42:3-9.

Hartl, F. U. & Hayer-Hartl, M. 2002. Molecular chaperones in the cytosol: from nascent chain to folded protein. *Science,* 295**,** 1852-8.

Hartong, D. T., Berson, E. L. & Dryja, T. P. 2006. Retinitis pigmentosa. *Lancet,* 368**,** 1795-809.

Haurogne, K., Bach, J. M. & Lieubeau, B. 2007. Easy and rapid method of zygosity determination in transgenic mice by SYBR Green real-time quantitative PCR with a simple data analysis. *Transgenic Res,* 16**,** 127-31.

Hauswirth, W. W., Aleman, T. S., Kaushal, S., Cideciyan, A. V., Schwartz, S. B., Wang, L., Conlon, T. J., Boye, S. L., Flotte, T. R., Byrne, B. J. & Jacobson, S. G. 2008. Treatment of leber congenital amaurosis due to RPE65 mutations by ocular subretinal injection of adeno-associated virus gene vector: short-term results of a phase I trial. *Hum Gene Ther,* 19**,** 979-90.

Hawkins, B. T. & Davis, T. P. 2005. The blood-brain barrier/neurovascular unit in health and disease. *Pharmacol Rev,* 57**,** 173-85.

Hawkins, B. T., Abbruscato, T. J., Egleton, R. D., Brown, R. C., Huber, J. D., Campos, C. R. & Davis, T. P. 2004. Nicotine increases *in vivo* blood-brain barrier permeability and alters cerebral microvascular tight junction protein distribution. *Brain Res,* 1027**,** 48-58.

Haze, K., H. Yoshida, H. Yanagi, T. Yura, and K. Mori. 1999. Mammalian transcription factor ATF6 is synthesized as a transmembrane protein and activated by proteolysis in response to endoplasmic reticulum stress. *Mol Biol Cell.* 10:3787-3799.

Haze, K., T. Okada, H. Yoshida, H. Yanagi, T. Yura, M. Negishi, and K. Mori. 2001. Identification of the G13 (cAMP-response-element-binding protein-related protein) gene product related to activating transcription factor 6 as a transcriptional activator of the mammalian unfolded protein response. *Biochem J.* 355:19-28.

He, L. & Hannon, G. J. 2004. MicroRNAs: small RNAs with a big role in gene regulation. *Nat Rev Genet,* 5**,** 522-31.

Heasman, J. 2002. Morpholino oligos: making sense of antisense? *Dev Biol,* 243**,** 209-14.

Hebert, D.N., J.F. Simons, J.R. Peterson, and A. Helenius. 1995. Calnexin, calreticulin, and Bip/Kar2p in protein folding. *Cold Spring Harbor symposia on quantitative biology.* 60:405-415.

Heckenlively, J. R., Yoser, S. L., Friedman, L. H. & Oversier, J. J. 1988. Clinical findings and common symptoms in retinitis pigmentosa. *Am J Ophthalmol,* 105**,** 504-11.

Heidel, J. D., Yu, Z., Liu, J. Y., Rele, S. M., Liang, Y., Zeidan, R. K., Kornbrust, D. J. & Davis, M. E. 2007. Administration in non-human primates of escalating intravenous doses of targeted nanoparticles containing ribonucleotide reductase subunit M2 siRNA. *Proc Natl Acad Sci U S A,* 104**,** 5715-21.

Heiskala, M., Peterson, P. A. & Yang, Y. 2001. The roles of claudin superfamily proteins in paracellular transport. *Traffic,* 2**,** 93-8.

Hendershot, L., J. Wei, J. Gaut, J. Melnick, S. Aviel, and Y. Argon. 1996. Inhibition of immunoglobulin folding and secretion by dominant negative BiP ATPase mutants. *Proc Natl Acad Sci U S A.* 93:5269-5274.

Hendershot, L.M. 2004. The ER function BiP is a master regulator of ER function. *The Mount Sinai journal of medicine, New York.* 71:289-297.

High, S., F.J. Lecomte, S.J. Russell, B.M. Abell, and J.D. Oliver. 2000. Glycoprotein folding in the endoplasmic reticulum: a tale of three chaperones? *FEBS Lett.* 476:38-41.

Hirschi, K. K. & D'Amore, P. A. 1996. Pericytes in the microvasculature. *Cardiovasc Res,* 32**,** 687-98.

Hohfeld, J. & Jentsch, S. 1997. GrpE-like regulation of the hsc70 chaperone by the anti-apoptotic protein BAG-1. *EMBO J,* 16**,** 6209-16.

Hong, D. S., Banerji, U., Tavana, B., George, G. C., Aaron, J. & Kurzrock, R. 2013. Targeting the molecular chaperone heat shock protein 90 (HSP90): lessons learned and future directions. *Cancer Treat Rev,* 39**,** 375-87.

Hood, J. L., Brooks, W. H. & Roszman, T. L. 2004. Differential compartmentalization of the calpain/calpastatin network with the endoplasmic reticulum and Golgi apparatus. *J Biol Chem,* 279**,** 43126-35.

Hornung, V., Guenthner-Biller, M., Bourquin, C., Ablasser, A., Schlee, M., Uematsu, S., Noronha, A., Manoharan, M., Akira, S., de Fougerolles, A., Endres, S. & Hartmann, G. 2005. Sequence-specific potent induction of IFN-alpha by short interfering RNA in plasmacytoid dendritic cells through TLR7. *Nat Med,* 11**,** 263-70.

Hoshino, T., T. Nakaya, W. Araki, K. Suzuki, T. Suzuki, and T. Mizushima. 2007. Endoplasmic reticulum chaperones inhibit the production of amyloid-beta peptides. *Biochem J.* 402:581-589.

Hosoya, K. & Tachikawa, M. 2009. Inner blood-retinal barrier transporters: role of retinal drug delivery. *Pharm Res,* 26**,** 2055-65.

Hosoya, K., Tomi, M. & Tachikawa, M. 2011. Strategies for therapy of retinal diseases using systemic drug delivery: relevance of transporters at the blood-retinal barrier. *Expert Opin Drug Deliv,* 8**,** 1571-87.

Huang, W., Fileta, J., Rawe, I., Qu, J. & Grosskreutz, C. L. 2010. Calpain activation in experimental glaucoma. *Invest Ophthalmol Vis Sci,* 51**,** 3049-54.

Hughes, P. M., Olejnik, O., Chang-Lin, J. E. & Wilson, C. G. 2005. Topical and systemic drug delivery to the posterior segments. *Adv Drug Deliv Rev,* 57**,** 2010-32.

Hughes, S., Gardiner, T., Hu, P., Baxter, L., Rosinova, E. & Chan-Ling, T. 2006. Altered pericyte-endothelial relations in the rat retina during aging: implications for vessel stability. *Neurobiol Aging,* 27, 1838-47.

Humphries, M. M., Kiang, S., McNally, N., Donovan, M. A., Sieving, P. A., Bush, R. A., Machida, S., Cotter, T., Hobson, A., Farrar, J., Humphries, P. & Kenna, P. 2001. Comparative structural and functional analysis of photoreceptor neurons of Rho-/- mice reveal increased survival on C57BL/6J in comparison to 129Sv genetic background. *Vis Neurosci,* 18, 437-43.

Humphries, M. M., Rancourt, D., Farrar, G. J., Kenna, P., Hazel, M., Bush, R. A., Sieving, P. A., Sheils, D. M., McNally, N., Creighton, P., Erven, A., Boros, A., Gulya, K., Capecchi, M. R. & Humphries, P. 1997. Retinopathy induced in mice by targeted disruption of the rhodopsin gene. *Nat Genet,* 15, 216-9.

Hwa, J., J. Klein-Seetharaman, and H.G. Khorana. 2001. Structure and function in rhodopsin: Mass spectrometric identification of the abnormal intradiscal disulfide bond in misfolded retinitis pigmentosa mutants. *Proc Natl Acad Sci U S A.* 98:4872-4876.

Illing, M.E., R.S. Rajan, N.F. Bence, and R.R. Kopito. 2002. A rhodopsin mutant linked to autosomal dominant retinitis pigmentosa is prone to aggregate and interacts with the ubiquitin proteasome system. *J Biol Chem.* 277:34150-34160.

Jackson, A. L., Bartz, S. R., Schelter, J., Kobayashi, S. V., Burchard, J., Mao, M., Li, B., Cavet, G. & Linsley, P. S. 2003. Expression profiling reveals off-target gene regulation by RNAi. *Nat Biotechnol,* 21, 635-7.

Jackson, A. L., Burchard, J., Schelter, J., Chau, B. N., Cleary, M., Lim, L. & Linsley, P. S. 2006. Widespread siRNA "off-target" transcript silencing mediated by seed region sequence complementarity. *RNA,* 12, 1179-87.

Jacobson, S. G., Cideciyan, A. V., Ratnakaram, R., Heon, E., Schwartz, S. B., Roman, A. J., Peden, M. C., Aleman, T. S., Boye, S. L., Sumaroka, A., Conlon, T. J., Calcedo, R., Pang, J. J., Erger, K. E., Olivares, M. B., Mullins, C. L., Swider, M., Kaushal, S., Feuer, W. J., Iannaccone, A., Fishman, G. A., Stone, E. M., Byrne, B. J. & Hauswirth, W. W. 2012. Gene therapy for leber congenital amaurosis caused by RPE65 mutations: safety and efficacy in 15 children and adults followed up to 3 years. *Arch Ophthalmol,* 130, 9-24.

Jager, R. D., Aiello, L. P., Patel, S. C. & Cunningham, E. T., Jr. 2004. Risks of intravitreous injection: a comprehensive review. *Retina,* 24, 676-98.

Jana, N. R., Tanaka, M., Wang, G. & Nukina, N. 2000. Polyglutamine length-dependent interaction of Hsp40 and Hsp70 family chaperones with truncated N-terminal huntingtin: their role in suppression of aggregation and cellular toxicity. *Hum Mol Genet,* 9, 2009-18.

Janicke, R. U., Sprengart, M. L., Wati, M. R. & Porter, A. G. 1998. Caspase-3 is required for DNA fragmentation and morphological changes associated with apoptosis. *J Biol Chem,* 273, 9357-60.

Janoria, K. G., Gunda, S., Boddu, S. H. & Mitra, A. K. 2007. Novel approaches to retinal drug delivery. *Expert Opin Drug Deliv,* 4, 371-88.

Janz, J.M., J.F. Fay, and D.L. Farrens. 2003. Stability of dark state rhodopsin is mediated by a conserved ion pair in intradiscal loop E-2. *J Biol Chem.* 278:16982-16991.

Jastrzebska, B., A. Debinski, S. Filipek, and K. Palczewski. 2011. Role of membrane integrity on G protein-coupled receptors: Rhodopsin stability and function. *Prog Lipid Res.* 50:267-277.

Jayaram, H. N., Cooney, D. A., Grusch, M. & Krupitza, G. 1999. Consequences of IMP dehydrogenase inhibition, and its relationship to cancer and apoptosis. *Curr Med Chem,* 6, 561-74.

Jhaveri, K., Miller, K., Rosen, L., Schneider, B., Chap, L., Hannah, A., Zhong, Z., Ma, W., Hudis, C. & Modi, S. 2012. A phase I dose-escalation trial of trastuzumab and alvespimycin hydrochloride (KOS-1022; 17 DMAG) in the treatment of advanced solid tumors. *Clin Cancer Res,* 18, 5090-8.

Ji, J., Wernli, M., Klimkait, T. & Erb, P. 2003. Enhanced gene silencing by the application of multiple specific small interfering RNAs. *FEBS Lett,* 552, 247-52.

Jin, Y., M. Zhuang, and L.M. Hendershot. 2009. ERdj3, a luminal ER DnaJ homologue, binds directly to unfolded proteins in the mammalian ER: identification of critical residues. *Biochemistry*. 48:41-49.

Jin, Y., W. Awad, K. Petrova, and L.M. Hendershot. 2008. Regulated release of ERdj3 from unfolded proteins by BiP. *EMBO J.* 27:2873-2882.

Jordan, S. A., Farrar, G. J., Kenna, P., Humphries, M. M., Sheils, D. M., Kumar-Singh, R., Sharp, E. M., Soriano, N., Ayuso, C., Benitez, J. & *et al.* 1993. Localization of an autosomal dominant retinitis pigmentosa gene to chromosome 7q. *Nat Genet,* 4, 54-8.

Judge, A. D., Sood, V., Shaw, J. R., Fang, D., McClintock, K. & MacLachlan, I. 2005. Sequence-dependent stimulation of the mammalian innate immune response by synthetic siRNA. *Nat Biotechnol,* 23, 457-62.

Kabani, M., McLellan, C., Raynes, D. A., Guerriero, V. & Brodsky, J. L. 2002. HspBP1, a homologue of the yeast Fes1 and Sls1 proteins, is an Hsc70 nucleotide exchange factor. *FEBS Lett,* 531, 339-42.

Kajiwara, K., Berson, E. L. & Dryja, T. P. 1994. Digenic retinitis pigmentosa due to mutations at the unlinked peripherin/RDS and ROM1 loci. *Science,* 264, 1604-8.

Kajiwara, K., Hahn, L. B., Mukai, S., Travis, G. H., Berson, E. L. & Dryja, T. P. 1991. Mutations in the human retinal degeneration slow gene in autosomal dominant retinitis pigmentosa. *Nature,* 354, 480-3.

Kampinga, H. H. & Craig, E. A. 2010. The HSP70 chaperone machinery: J proteins as drivers of functional specificity. *Nat Rev Mol Cell Biol,* 11, 579-92.

Kapulkin, W.J., B.G. Hiester, and C.D. Link. 2005. Compensatory regulation among ER chaperones in C. elegans. *FEBS Lett*. 579:3063-3068.

Karan, G., Z. Yang, K. Howes, Y. Zhao, Y. Chen, D.J. Cameron, Y. Lin, E. Pearson, and K. Zhang. 2005. Loss of ER retention and sequestration of the wild-type ELOVL4 by Stargardt disease dominant negative mutants. *Molecular vision*. 11:657-664.

Kato, M., Nonaka, T., Maki, M., Kikuchi, H. & Imajoh-Ohmi, S. 2000. Caspases cleave the amino-terminal calpain inhibitory unit of calpastatin during apoptosis in human Jurkat T cells. *J Biochem,* 127, 297-305.

Katsanis, N. 2004. The oligogenic properties of Bardet-Biedl syndrome. *Hum Mol Genet,* 13 Spec No 1, R65-71.

Kaufmann, S. H., Kottke, T. J., Martins, L. M., Henzing, A. J. & Earnshaw, W. C. 2001. Analysis of caspase activation during apoptosis. *Curr Protoc Cell Biol,* Chapter 18, Unit 18 2.

Kaufmann, T., Strasser, A. & Jost, P. J. 2012. Fas death receptor signalling: roles of Bid and XIAP. *Cell Death Differ,* 19, 42-50.

Kaur, C., Foulds, W. S. & Ling, E. A. 2008. Blood-retinal barrier in hypoxic ischaemic conditions: basic concepts, clinical features and management. *Prog Retin Eye Res,* 27, 622-47.

Kaur, C., Sivakumar, V. & Foulds, W. S. 2006. Early response of neurons and glial cells to hypoxia in the retina. *Invest Ophthalmol Vis Sci,* 47, 1126-41.

Kaur, I. P., Smitha, R., Aggarwal, D. & Kapil, M. 2002. Acetazolamide: future perspective in topical glaucoma therapeutics. *Int J Pharm,* 248, 1-14.

Kaushal, S. 2006. Effect of rapamycin on the fate of P23H opsin associated with retinitis pigmentosa (an American Ophthalmological Society thesis). *Trans Am Ophthalmol Soc*. 104:517-529.

Kaushal, S., and H.G. Khorana. 1994. Structure and function in rhodopsin. 7. Point mutations associated with autosomal dominant retinitis pigmentosa. *Biochemistry*. 33:6121-6128.

Kaushal, S., K.D. Ridge, and H.G. Khorana. 1994. Structure and function in rhodopsin: the role of asparagine-linked glycosylation. *Proceedings of the National Academy of Sciences of the United States of America*. 91:4024-4028.

Keats, B. J. & Savas, S. 2004. Genetic heterogeneity in Usher syndrome. *Am J Med Genet A,* 130A, 13-6.

Kennan, A., Aherne, A., Palfi, A., Humphries, M., McKee, A., Stitt, A., Simpson, D. A., Demtroder, K., Orntoft, T., Ayuso, C., Kenna, P. F., Farrar, G. J. & Humphries, P. 2002. Identification of an IMPDH1 mutation in autosomal dominant retinitis pigmentosa (RP10) revealed following comparative microarray analysis of transcripts derived from retinas of wild-type and Rho(-/-) mice. *Hum Mol Genet,* 11, 547-57.

Kennerdell, J. R. & Carthew, R. W. 1998. Use of dsRNA-mediated genetic interference to demonstrate that frizzled and frizzled 2 act in the wingless pathway. *Cell,* 95, 1017-26.

Kerr, J. F., Wyllie, A. H. & Currie, A. R. 1972. Apoptosis: a basic biological phenomenon with wide-ranging implications in tissue kinetics. *Br J Cancer,* 26, 239-57.

Kiang, A. S., Palfi, A., Ader, M., Kenna, P. F., Millington-Ward, S., Clark, G., Kennan, A., O'Reilly, M., Tam, L. C., Aherne, A., McNally, N., Humphries, P. & Farrar, G. J. 2005. Toward a gene therapy for dominant disease: validation of an RNA interference-based mutation-independent approach. *Mol Ther,* 12, 555-61.

Kijas, J. W., Cideciyan, A. V., Aleman, T. S., Pianta, M. J., Pearce-Kelling, S. E., Miller, B. J., Jacobson, S. G., Aguirre, G. D. & Acland, G. M. 2002. Naturally occurring rhodopsin mutation in the dog causes retinal dysfunction and degeneration mimicking human dominant retinitis pigmentosa. *Proc Natl Acad Sci U S A,* 99, 6328-33.

Kim, S. H., Csaky, K. G., Wang, N. S. & Lutz, R. J. 2008. Drug elimination kinetics following subconjunctival injection using dynamic contrast-enhanced magnetic resonance imaging. *Pharm Res,* 25, 512-20.

Kim, T., Keum, G. & Pae, A. N. 2013. Discovery and development of heat shock protein 90 inhibitors as anticancer agents: a review of patented potent geldanamycin derivatives. *Expert Opin Ther Pat.*

Kimberling, W. J., Orten, D. & Pieke-Dahl, S. 2000. Genetic heterogeneity of Usher syndrome. *Adv Otorhinolaryngol,* 56, 11-8.

Kleinman, M. E., Yamada, K., Takeda, A., Chandrasekaran, V., Nozaki, M., Baffi, J. Z., Albuquerque, R. J., Yamasaki, S., Itaya, M., Pan, Y., Appukuttan, B., Gibbs, D., Yang, Z., Kariko, K., Ambati, B. K., Wilgus, T. A., DiPietro, L. A., Sakurai, E., Zhang, K., Smith, J. R., Taylor, E. W. & Ambati, J. 2008. Sequence- and target-independent angiogenesis suppression by siRNA via TLR3. *Nature,* 452, 591-7.

Klohs, J., Baeva, N., Steinbrink, J., Bourayou, R., Boettcher, C., Royl, G., Megow, D., Dirnagl, U., Priller, J. & Wunder, A. 2009. *In vivo* near-infrared fluorescence imaging of matrix metalloproteinase activity after cerebral ischemia. *J Cereb Blood Flow Metab,* 29, 1284-92.

Knoblach, S. M., Alroy, D. A., Nikolaeva, M., Cernak, I., Stoica, B. A. & Faden, A. I. 2004. Caspase inhibitor z-DEVD-fmk attenuates calpain and necrotic cell death *in vitro* and after traumatic brain injury. *J Cereb Blood Flow Metab,* 24, 1119-32.

Kobayashi, Y., Kume, A., Li, M., Doyu, M., Hata, M., Ohtsuka, K. & Sobue, G. 2000. Chaperones Hsp70 and Hsp40 suppress aggregate formation and apoptosis in cultured neuronal cells expressing truncated androgen receptor protein with expanded polyglutamine tract. *J Biol Chem,* 275, 8772-8.

Kornberg, A. & Baker, T. A. 1992. *DNA Replication,* New York

Korschen, H. G., Beyermann, M., Muller, F., Heck, M., Vantler, M., Koch, K. W., Kellner, R., Wolfrum, U., Bode, C., Hofmann, K. P. & Kaupp, U. B. 1999. Interaction of glutamic-acid-rich proteins with the cGMP signalling pathway in rod photoreceptors. *Nature,* 400, 761-6.

Kos, R., Tucker, R. P., Hall, R., Duong, T. D. & Erickson, C. A. 2003. Methods for introducing morpholinos into the chicken embryo. *Dev Dyn,* 226, 470-7.

Kosmaoglou, M., and M.E. Cheetham. 2008. Calnexin is not essential for mammalian rod opsin biogenesis. *Molecular vision*. 14:2466-2474.

Kosmaoglou, M., N. Kanuga, M. Aguila, P. Garriga, and M.E. Cheetham. 2009. A dual role for EDEM1 in the processing of rod opsin. *J Cell Sci.* 122:4465-4472.

Kosmaoglou, M., Schwarz, N., Bett, J. S. & Cheetham, M. E. 2008. Molecular chaperones and photoreceptor function. *Prog Retin Eye Res,* 27, 434-49.

Koto, T., Takubo, K., Ishida, S., Shinoda, H., Inoue, M., Tsubota, K., Okada, Y. & Ikeda, E. 2007. Hypoxia disrupts the barrier function of neural blood vessels through changes in the expression of claudin-5 in endothelial cells. *Am J Pathol,* 170, 1389-97.

Kozma, P., Hughbanks-Wheaton, D. K., Locke, K. G., Fish, G. E., Gire, A. I., Spellicy, C. J., Sullivan, L. S., Bowne, S. J., Daiger, S. P. & Birch, D. G. 2005. Phenotypic characterization of a large family with RP10 autosomal-dominant retinitis pigmentosa: an Asp226Asn mutation in the IMPDH1 gene. *Am J Ophthalmol,* 140, 858-867.

Krause, G., Winkler, L., Mueller, S. L., Haseloff, R. F., Piontek, J. & Blasig, I. E. 2008. Structure and function of claudins. *Biochim Biophys Acta,* 1778**,** 631-45.

Krebs, M.P., D.C. Holden, P. Joshi, C.L. Clark, 3rd, A.H. Lee, and S. Kaushal. 2010. Molecular mechanisms of rhodopsin retinitis pigmentosa and the efficacy of pharmacological rescue. *Journal of molecular biology.* 395:1063-1078.

Krebs, M.P., S.M. Noorwez, R. Malhotra, and S. Kaushal. 2004. Quality control of integral membrane proteins. *Trends in biochemical sciences.* 29:648-655.

Kubota, K., Furuse, M., Sasaki, H., Sonoda, N., Fujita, K., Nagafuchi, A. & Tsukita, S. 1999. Ca(2+)-independent cell-adhesion activity of claudins, a family of integral membrane proteins localized at tight junctions. *Curr Biol,* 9**,** 1035-8.

La Cour, M. 2002. *Adler's Physiology of the Eye,* St Louis, MO, Mosby.

Lai, E., G. Bikopoulos, M.B. Wheeler, M. Rozakis-Adcock, and A. Volchuk. 2008. Differential activation of ER stress and apoptosis in response to chronically elevated free fatty acids in pancreatic beta-cells. *American journal of physiology. Endocrinology and metabolism.* 294:E540-550.

Lancet, J.E., I. Gojo, M. Burton, M. Quinn, S.M. Tighe, K. Kersey, Z. Zhong, M.X. Albitar, K. Bhalla, A.L. Hannah, and M.R. Baer. 2010. Phase I study of the heat shock protein 90 inhibitor alvespimycin (KOS-1022, 17-DMAG) administered intravenously twice weekly to patients with acute myeloid leukemia. *Leukemia.* 24:699-705.

Lankiewicz, S., Marc Luetjens, C., Truc Bui, N., Krohn, A. J., Poppe, M., Cole, G. M., Saido, T. C. & Prehn, J. H. 2000. Activation of calpain I converts excitotoxic neuron death into a caspase-independent cell death. *J Biol Chem,* 275**,** 17064-71.

Lawson, B., J.W. Brewer, and L.M. Hendershot. 1998. Geldanamycin, an hsp90/GRP94-binding drug, induces increased transcription of endoplasmic reticulum (ER) chaperones via the ER stress pathway. *J Cell Physiol.* 174:170-178.

Lebherz, C., Maguire, A., Tang, W., Bennett, J. & Wilson, J. M. 2008. Novel AAV serotypes for improved ocular gene transfer. *J Gene Med,* 10**,** 375-82.

Lederkremer, G.Z., and M.H. Glickman. 2005. A window of opportunity: timing protein degradation by trimming of sugars and ubiquitins. *Trends Biochem Sci.* 30:297-303.

Lee, A.H., N.N. Iwakoshi, and L.H. Glimcher. 2003a. XBP-1 regulates a subset of endoplasmic reticulum resident chaperone genes in the unfolded protein response. *Mol Cell Biol.* 23:7448-7459.

Lee, J.M., M.J. Calkins, K. Chan, Y.W. Kan, and J.A. Johnson. 2003b. Identification of the NF-E2-related factor-2-dependent genes conferring protection against oxidative stress in primary cortical astrocytes using oligonucleotide microarray analysis. *J Biol Chem.* 278:12029-12038.

Lee, M. S., Kwon, Y. T., Li, M., Peng, J., Friedlander, R. M. & Tsai, L. H. 2000. Neurotoxicity induces cleavage of p35 to p25 by calpain. *Nature,* 405**,** 360-4.

Lee, R. C., Feinbaum, R. L. & Ambros, V. 1993. The C. elegans heterochronic gene lin-4 encodes small RNAs with antisense complementarity to lin-14. *Cell,* 75**,** 843-54.

Lee, Y. S., Nakahara, K., Pham, J. W., Kim, K., He, Z., Sontheimer, E. J. & Carthew, R. W. 2004. Distinct roles for Drosophila Dicer-1 and Dicer-2 in the siRNA/miRNA silencing pathways. *Cell,* 117**,** 69-81.

Lee, Y., Ahn, C., Han, J., Choi, H., Kim, J., Yim, J., Lee, J., Provost, P., Radmark, O., Kim, S. & Kim, V. N. 2003. The nuclear RNase III Drosha initiates microRNA processing. *Nature,* 425**,** 415-9.

Lee, Y., Jeon, K., Lee, J. T., Kim, S. & Kim, V. N. 2002. MicroRNA maturation: stepwise processing and subcellular localization. *EMBO J,* 21**,** 4663-70.

Lei, K., and R.J. Davis. 2003. JNK phosphorylation of Bim-related members of the Bcl2 family induces Bax-dependent apoptosis. *Proc Natl Acad Sci U S A.* 100:2432-2437.

Leist, M. & Jaattela, M. 2001. Four deaths and a funeral: from caspases to alternative mechanisms. *Nat Rev Mol Cell Biol,* 2**,** 589-98.

Lewandowski, M. 1990. Zur Lehre von der Cerebrospinalflüssigkeit. [On the cerebrospinal fluid.]. *Z. Klein Forsch***,** 480-494.

Li, H., Thompson, V. F. & Goll, D. E. 2004. Effects of autolysis on properties of mu- and m-calpain. *Biochim Biophys Acta,* 1691**,** 91-103.

Li, J., and A.S. Lee. 2006. Stress induction of GRP78/BiP and its role in cancer. *Current molecular medicine*. 6:45-54.

Li, L. Y., Luo, X. & Wang, X. 2001. Endonuclease G is an apoptotic DNase when released from mitochondria. *Nature,* 412, 95-9.

Li, W. & Cha, L. 2007. Predicting siRNA efficiency. *Cell Mol Life Sci,* 64, 1785-92.

Liang, C.J., K. Yamashita, C.G. Muellenberg, H. Shichi, and A. Kobata. 1979. Structure of the carbohydrate moieties of bovine rhodopsin. *J Biol Chem*. 254:6414-6418.

Liang, F. Q., Anand, V., Maguire, A. M. & Bennett, J. 2001. Intraocular delivery of recombinant virus. *Methods Mol Med,* 47, 125-39.

Liberek, K., J. Marszalek, D. Ang, C. Georgopoulos, and M. Zylicz. 1991. Escherichia coli DnaJ and GrpE heat shock proteins jointly stimulate ATPase activity of DnaK. *Proc Natl Acad Sci U S A*. 88:2874-2878.

Lievremont, J.P., R. Rizzuto, L. Hendershot, and J. Meldolesi. 1997. BiP, a major chaperone protein of the endoplasmic reticulum lumen, plays a direct and important role in the storage of the rapidly exchanging pool of Ca2+. *J Biol Chem*. 272:30873-30879.

Lin, J. H. & Lavail, M. M. 2010. Misfolded proteins and retinal dystrophies. *Adv Exp Med Biol,* 664, 115-21.

Lin, J.H., H. Li, D. Yasumura, H.R. Cohen, C. Zhang, B. Panning, K.M. Shokat, M.M. Lavail, and P. Walter. 2007. IRE1 signaling affects cell fate during the unfolded protein response. *Science*. 318:944-949.

Lin, J.H., H. Li, Y. Zhang, D. Ron, and P. Walter. 2009. Divergent effects of PERK and IRE1 signaling on cell viability. *PLoS One*. 4:e4170.

Liu, X., P. Garriga, and H.G. Khorana. 1996. Structure and function in rhodopsin: correct folding and misfolding in two point mutants in the intradiscal domain of rhodopsin identified in retinitis pigmentosa. *Proceedings of the National Academy of Sciences of the United States of America*. 93:4554-4559.

Llave, C., Xie, Z., Kasschau, K. D. & Carrington, J. C. 2002. Cleavage of Scarecrow-like mRNA targets directed by a class of Arabidopsis miRNA. *Science,* 297, 2053-6.

Lukason, M., DuFresne, E., Rubin, H., Pechan, P., Li, Q., Kim, I., Kiss, S., Flaxel, C., Collins, M., Miller, J., Hauswirth, W., Maclachlan, T., Wadsworth, S. & Scaria, A. 2011. Inhibition of choroidal neovascularization in a nonhuman primate model by intravitreal administration of an AAV2 vector expressing a novel anti-VEGF molecule. *Mol Ther,* 19, 260-5.

Luo, S., P. Baumeister, S. Yang, S.F. Abcouwer, and A.S. Lee. 2003. Induction of Grp78/BiP by translational block: activation of the Grp78 promoter by ATF4 through and upstream ATF/CRE site independent of the endoplasmic reticulum stress elements. *J Biol Chem*. 278:37375-37385.

Ma, Y., and L.M. Hendershot. 2004. ER chaperone functions during normal and stress conditions. *Journal of chemical neuroanatomy*. 28:51-65.

Maattanen, P., K. Gehring, J.J. Bergeron, and D.Y. Thomas. 2010. Protein quality control in the ER: the recognition of misfolded proteins. *Seminars in cell & developmental biology*. 21:500-511.

Macha, S. & Mitra, A. K. 2002. Ocular disposition of ganciclovir and its monoester prodrugs following intravitreal administration using microdialysis. *Drug Metab Dispos,* 30, 670-5.

Machida, S., Kondo, M., Jamison, J. A., Khan, N. W., Kononen, L. T., Sugawara, T., Bush, R. A. & Sieving, P. A. 2000. P23H rhodopsin transgenic rat: correlation of retinal function with histopathology. *Invest Ophthalmol Vis Sci,* 41, 3200-9.

Machida, S., M. Kondo, J.A. Jamison, N.W. Khan, L.T. Kononen, T. Sugawara, R.A. Bush, and P.A. Sieving. 2000. P23H rhodopsin transgenic rat: correlation of retinal function with histopathology. *Invest Ophthalmol Vis Sci*. 41:3200-3209.

MacKenzie, D., A. Arendt, P. Hargrave, J.H. McDowell, and R.S. Molday. 1984. Localization of binding sites for carboxyl terminal specific anti-rhodopsin monoclonal antibodies using synthetic peptides. *Biochemistry*. 23:6544-6549.

Maguire, A. M., Simonelli, F., Pierce, E. A., Pugh, E. N., Jr., Mingozzi, F., Bennicelli, J., Banfi, S., Marshall, K. A., Testa, F., Surace, E. M., Rossi, S., Lyubarsky, A., Arruda, V. R., Konkle, B., Stone, E., Sun, J., Jacobs, J., Dell'Osso, L., Hertle, R., Ma, J. X., Redmond, T. M., Zhu, X., Hauck, B., Zelenaia, O., Shindler, K. S., Maguire, M. G., Wright, J. F., Volpe, N. J.,

McDonnell, J. W., Auricchio, A., High, K. A. & Bennett, J. 2008. Safety and efficacy of gene transfer for Leber's congenital amaurosis. *N Engl J Med,* 358, 2240-8.

Maguire, A. M., Simonelli, F., Pierce, E. A., Pugh, E. N., Jr., Mingozzi, F., Bennicelli, J., Banfi, S., Marshall, K. A., Testa, F., Surace, E. M., Rossi, S., Lyubarsky, A., Arruda, V. R., Konkle, B., Stone, E., Sun, J., Jacobs, J., Dell'Osso, L., Hertle, R., Ma, J. X., Redmond, T. M., Zhu, X., Hauck, B., Zelenaia, O., Shindler, K. S., Maguire, M. G., Wright, J. F., Volpe, N. J., McDonnell, J. W., Auricchio, A., High, K. A. & Bennett, J. 2008. Safety and efficacy of gene transfer for Leber's congenital amaurosis. *N Engl J Med,* 358, 2240-8.

Maguire, A.M., K.A. High, A. Auricchio, J.F. Wright, E.A. Pierce, F. Testa, F. Mingozzi, J.L. Bennicelli, G.S. Ying, S. Rossi, A. Fulton, K.A. Marshall, S. Banfi, D.C. Chung, J.I. Morgan, B. Hauck, O. Zelenaia, X. Zhu, L. Raffini, F. Coppieters, E. De Baere, K.S. Shindler, N.J. Volpe, E.M. Surace, C. Acerra, A. Lyubarsky, T.M. Redmond, E. Stone, J. Sun, J.W. McDonnell, B.P. Leroy, F. Simonelli, and J. Bennett. 2009. Age-dependent effects of RPE65 gene therapy for Leber's congenital amaurosis: a phase 1 dose-escalation trial. *Lancet.* 374:1597-1605.

Makoid, M. C., Sieg, J. W. & Robinson, J. R. 1976. Corneal drug absorption: an illustration of parallel first-order absorption and rapid loss of drug from absorption depot. *J Pharm Sci,* 65, 150-3.

Mannermaa, E., Vellonen, K. S. & Urtti, A. 2006. Drug transport in corneal epithelium and blood-retina barrier: emerging role of transporters in ocular pharmacokinetics. *Adv Drug Deliv Rev,* 58, 1136-63.

Mansergh, F. C., Millington-Ward, S., Kennan, A., Kiang, A. S., Humphries, M., Farrar, G. J., Humphries, P. & Kenna, P. F. 1999. Retinitis pigmentosa and progressive sensorineural hearing loss caused by a C12258A mutation in the mitochondrial MTTS2 gene. *Am J Hum Genet,* 64, 971-85.

Mao, H., Gorbatyuk, M. S., Rossmiller, B., Hauswirth, W. W. & Lewin, A. S. 2012. Long-term rescue of retinal structure and function by rhodopsin RNA replacement with a single adeno-associated viral vector in P23H RHO transgenic mice. *Hum Gene Ther,* 23, 356-66.

Mao, H., James, T., Jr., Schwein, A., Shabashvili, A. E., Hauswirth, W. W., Gorbatyuk, M. S. & Lewin, A. S. 2011. AAV delivery of wild-type rhodopsin preserves retinal function in a mouse model of autosomal dominant retinitis pigmentosa. *Hum Gene Ther,* 22, 567-75.

Mao, H., James, T., Jr., Schwein, A., Shabashvili, A. E., Hauswirth, W. W., Gorbatyuk, M. S. & Lewin, A. S. 2011. AAV delivery of wild-type rhodopsin preserves retinal function in a mouse model of autosomal dominant retinitis pigmentosa. *Hum Gene Ther,* 22, 567-75.

Marmorstein, L. Y., Munier, F. L., Arsenijevic, Y., Schorderet, D. F., McLaughlin, P. J., Chung, D., Traboulsi, E. & Marmorstein, A. D. 2002. Aberrant accumulation of EFEMP1 underlies drusen formation in Malattia Leventinese and age-related macular degeneration. *Proc Natl Acad Sci U S A,* 99, 13067-72.

Martin, P. M., Dun, Y., Mysona, B., Ananth, S., Roon, P., Smith, S. B. & Ganapathy, V. 2007. Expression of the sodium-coupled monocarboxylate transporters SMCT1 (SLC5A8) and SMCT2 (SLC5A12) in retina. *Invest Ophthalmol Vis Sci,* 48, 3356-63.

Maruri-Avidal, L., S. Lopez, and C.F. Arias. 2008. Endoplasmic reticulum chaperones are involved in the morphogenesis of rotavirus infectious particles. *J Virol.* 82:5368-5380.

Marzec, M., D. Eletto, and Y. Argon. 2012. GRP94: An HSP90-like protein specialized for protein folding and quality control in the endoplasmic reticulum. *Biochim Biophys Acta.* 1823:774-787.

Matlack, K.E., B. Misselwitz, K. Plath, and T.A. Rapoport. 1999. BiP acts as a molecular ratchet during posttranslational transport of prepro-alpha factor across the ER membrane. *Cell.* 97:553-564.

Mattapallil, M. J., Wawrousek, E. F., Chan, C. C., Zhao, H., Roychoudhury, J., Ferguson, T. A. & Caspi, R. R. 2012. The Rd8 mutation of the Crb1 gene is present in vendor lines of C57BL/6N mice and embryonic stem cells, and confounds ocular induced mutant phenotypes. *Invest Ophthalmol Vis Sci,* 53, 2921-7.

Mattson, M. P. 2000. Apoptosis in neurodegenerative disorders. *Nat Rev Mol Cell Biol,* 1, 120-9.

Matus, S., L.H. Glimcher, and C. Hetz. 2011. Protein folding stress in neurodegenerative diseases: a glimpse into the ER. *Curr Opin Cell Biol.* 23:239-252.

Mayer, M. P. 2010. Gymnastics of molecular chaperones. *Mol Cell,* 39, 321-31.

McCarty, D. M., Young, S. M., Jr. & Samulski, R. J. 2004. Integration of adeno-associated virus (AAV) and recombinant AAV vectors. *Annu Rev Genet,* 38, 819-45.

McCullough, K.D., J.L. Martindale, L.O. Klotz, T.Y. Aw, and N.J. Holbrook. 2001. Gadd153 sensitizes cells to endoplasmic reticulum stress by down-regulating Bcl2 and perturbing the cellular redox state. *Mol Cell Biol.* 21:1249-1259.

McGinnis, K. M., Gnegy, M. E., Park, Y. H., Mukerjee, N. & Wang, K. K. 1999. Procaspase-3 and poly(ADP)ribose polymerase (PARP) are calpain substrates. *Biochem Biophys Res Commun,* 263, 94-9.

McGuire, R. E., Gannon, A. M., Sullivan, L. S., Rodriguez, J. A. & Daiger, S. P. 1995. Evidence for a major gene (RP10) for autosomal dominant retinitis pigmentosa on chromosome 7q: linkage mapping in a second, unrelated family. *Hum Genet,* 95, 71-4.

McKie, A. B., McHale, J. C., Keen, T. J., Tarttelin, E. E., Goliath, R., van Lith-Verhoeven, J. J., Greenberg, J., Ramesar, R. S., Hoyng, C. B., Cremers, F. P., Mackey, D. A., Bhattacharya, S. S., Bird, A. C., Markham, A. F. & Inglehearn, C. F. 2001. Mutations in the pre-mRNA splicing factor gene PRPC8 in autosomal dominant retinitis pigmentosa (RP13). *Hum Mol Genet,* 10, 1555-62.

McLaughlin, M., and K. Vandenbroeck. 2011. The endoplasmic reticulum protein folding factory and its chaperones: new targets for drug discovery? *Br J Pharmacol.* 162:328-345.

McLean, J. E., Hamaguchi, N., Belenky, P., Mortimer, S. E., Stanton, M. & Hedstrom, L. 2004. Inosine 5'-monophosphate dehydrogenase binds nucleic acids *in vitro* and *in vivo*. *Biochem J,* 379, 243-51.

McNally, N., Kenna, P., Humphries, M. M., Hobson, A. H., Khan, N. W., Bush, R. A., Sieving, P. A., Humphries, P. & Farrar, G. J. 1999. Structural and functional rescue of murine rod photoreceptors by human rhodopsin transgene. *Hum Mol Genet,* 8, 1309-12.

McWilliam, P., Farrar, G. J., Kenna, P., Bradley, D. G., Humphries, M. M., Sharp, E. M., McConnell, D. J., Lawler, M., Sheils, D., Ryan, C. & *et al.* 1989. Autosomal dominant retinitis pigmentosa (ADRP): localization of an ADRP gene to the long arm of chromosome 3. *Genomics,* 5, 619-22.

Mehalow, A. K., Kameya, S., Smith, R. S., Hawes, N. L., Denegre, J. M., Young, J. A., Bechtold, L., Haider, N. B., Tepass, U., Heckenlively, J. R., Chang, B., Naggert, J. K. & Nishina, P. M. 2003. CRB1 is essential for external limiting membrane integrity and photoreceptor morphogenesis in the mammalian retina. *Hum Mol Genet,* 12, 2179-89.

Melloni, E., Averna, M., Stifanese, R., De Tullio, R., Defranchi, E., Salamino, F. & Pontremoli, S. 2006. Association of calpastatin with inactive calpain: a novel mechanism to control the activation of the protease? *J Biol Chem,* 281, 24945-54.

Melnick, J., J.L. Dul, and Y. Argon. 1994. Sequential interaction of the chaperones BiP and GRP94 with immunoglobulin chains in the endoplasmic reticulum. *Nature.* 370:373-375.

Mendes, C.S., C. Levet, G. Chatelain, P. Dourlen, A. Fouillet, M.L. Dichtel-Danjoy, A. Gambis, H.D. Ryoo, H. Steller, and B. Mollereau. 2009. ER stress protects from retinal degeneration. *EMBO J.* 28:1296-1307.

Mendes, H. F. & Cheetham, M. E. 2008. Pharmacological manipulation of gain-of-function and dominant-negative mechanisms in rhodopsin retinitis pigmentosa. *Hum Mol Genet,* 17, 3043-54.

Mendes, H.F., J. van der Spuy, J.P. Chapple, and M.E. Cheetham. 2005. Mechanisms of cell death in rhodopsin retinitis pigmentosa: implications for therapy. *Trends Mol Med.* 11:177-185.

Messaoudi, S., Peyrat, J. F., Brion, J. D. & Alami, M. 2011. Heat-shock protein 90 inhibitors as antitumor agents: a survey of the literature from 2005 to 2010. *Expert Opin Ther Pat,* 21, 1501-42.

Metzler, M., Wilda, M., Busch, K., Viehmann, S. & Borkhardt, A. 2004. High expression of precursor microRNA-155/BIC RNA in children with Burkitt lymphoma. *Genes Chromosomes Cancer,* 39, 167-9.

Meunier, L., Y.K. Usherwood, K.T. Chung, and L.M. Hendershot. 2002. A subset of chaperones and folding enzymes form multiprotein complexes in endoplasmic reticulum to bind nascent proteins. *Mol Biol Cell.* 13:4456-4469.

Mihelec, M., R.A. Pearson, S.J. Robbie, P.K. Buch, S.A. Azam, J.W. Bainbridge, A.J. Smith, and R.R. Ali. 2011. Long-term preservation of cones and improvement in visual function following gene therapy in a mouse model of leber congenital amaurosis caused by guanylate cyclase-1 deficiency. *Hum Gene Ther.* 22:1179-1190.

Millay, R. H., Klein, M. L., Shults, W. T., Dahlborg, S. A. & Neuwelt, E. A. 1986. Maculopathy associated with combination chemotherapy and osmotic opening of the blood-brain barrier. *Am J Ophthalmol,* 102, 626-32.

Millington-Ward, S., Chadderton, N., O'Reilly, M., Palfi, A., Goldmann, T., Kilty, C., Humphries, M., Wolfrum, U., Bennett, J., Humphries, P., Kenna, P. F. & Farrar, G. J. 2011. Suppression and replacement gene therapy for autosomal dominant disease in a murine model of dominant retinitis pigmentosa. *Mol Ther,* 19, 642-9.

Millington-Ward, S., O'Neill, B., Tuohy, G., Al-Jandal, N., Kiang, A. S., Kenna, P. F., Palfi, A., Hayden, P., Mansergh, F., Kennan, A., Humphries, P. & Farrar, G. J. 1997. Strategems *in vitro* for gene therapies directed to dominant mutations. *Hum Mol Genet,* 6, 1415-26.

Moiseyev, G., Chen, Y., Takahashi, Y., Wu, B. X. & Ma, J. X. 2005. RPE65 is the isomerohydrolase in the retinoid visual cycle. *Proc Natl Acad Sci U S A,* 102, 12413-8.

Molday, R.S., and D. MacKenzie. 1983. Monoclonal antibodies to rhodopsin: characterization, cross-reactivity, and application as structural probes. *Biochemistry.* 22:653-660.

Molinari, M., V. Calanca, C. Galli, P. Lucca, and P. Paganetti. 2003. Role of EDEM in the release of misfolded glycoproteins from the calnexin cycle. *Science.* 299:1397-1400.

Momoi, T. 2004. Caspases involved in ER stress-mediated cell death. *Journal of chemical neuroanatomy.* 28:101-105.

Morimura, H., Fishman, G. A., Grover, S. A., Fulton, A. B., Berson, E. L. & Dryja, T. P. 1998. Mutations in the RPE65 gene in patients with autosomal recessive retinitis pigmentosa or leber congenital amaurosis. *Proc Natl Acad Sci U S A,* 95, 3088-93.

Morita, K., Sasaki, H., Furuse, M. & Tsukita, S. 1999. Endothelial claudin: claudin-5/TMVCF constitutes tight junction strands in endothelial cells. *J Cell Biol,* 147, 185-94.

Morris, J.A., A.J. Dorner, C.A. Edwards, L.M. Hendershot, and R.J. Kaufman. 1997. Immunoglobulin binding protein (BiP) function is required to protect cells from endoplasmic reticulum stress but is not required for the secretion of selective proteins. *J Biol Chem.* 272:4327-4334.

Morrissey, D. V., Lockridge, J. A., Shaw, L., Blanchard, K., Jensen, K., Breen, W., Hartsough, K., Machemer, L., Radka, S., Jadhav, V., Vaish, N., Zinnen, S., Vargeese, C., Bowman, K., Shaffer, C. S., Jeffs, L. B., Judge, A., MacLachlan, I. & Polisky, B. 2005. Potent and persistent *in vivo* anti-HBV activity of chemically modified siRNAs. *Nat Biotechnol,* 23, 1002-7.

Mortimer, S. E. & Hedstrom, L. 2005. Autosomal dominant retinitis pigmentosa mutations in inosine 5'-monophosphate dehydrogenase type I disrupt nucleic acid binding. *Biochem J,* 390, 41-7.

Moss, E. G., Lee, R. C. & Ambros, V. 1997. The cold shock domain protein LIN-28 controls developmental timing in C. elegans and is regulated by the lin-4 RNA. *Cell,* 88, 637-46.

Mourelatos, Z., Dostie, J., Paushkin, S., Sharma, A., Charroux, B., Abel, L., Rappsilber, J., Mann, M. & Dreyfuss, G. 2002. miRNPs: a novel class of ribonucleoproteins containing numerous microRNAs. *Genes Dev,* 16, 720-8.

Muresan, Z., and P. Arvan. 1997. Thyroglobulin transport along the secretory pathway. Investigation of the role of molecular chaperone, GRP94, in protein export from the endoplasmic reticulum. *J Biol Chem.* 272:26095-26102.

Naash, M. I., Hollyfield, J. G., al-Ubaidi, M. R. & Baehr, W. 1993. Simulation of human autosomal dominant retinitis pigmentosa in transgenic mice expressing a mutated murine opsin gene. *Proc Natl Acad Sci U S A,* 90, 5499-503.

Nagai, M., Natsumeda, Y., Konno, Y., Hoffman, R., Irino, S. & Weber, G. 1991. Selective up-regulation of type II inosine 5'-monophosphate dehydrogenase messenger RNA expression in human leukemias. *Cancer Res,* 51, 3886-90.

Nagase, K., Tomi, M., Tachikawa, M. & Hosoya, K. 2006. Functional and molecular characterization of adenosine transport at the rat inner blood-retinal barrier. *Biochim Biophys Acta,* 1758, 13-9.

Nakagawa, T., H. Zhu, N. Morishima, E. Li, J. Xu, B.A. Yankner, and J. Yuan. 2000. Caspase-12 mediates endoplasmic-reticulum-specific apoptosis and cytotoxicity by amyloid-beta. *Nature*. 403:98-103.

Nakanishi, K., T. Sudo, and N. Morishima. 2005. Endoplasmic reticulum stress signaling transmitted by ATF6 mediates apoptosis during muscle development. *J Cell Biol*. 169:555-560.

Nakashima, T., Tomi, M., Katayama, K., Tachikawa, M., Watanabe, M., Terasaki, T. & Hosoya, K. 2004. Blood-to-retina transport of creatine via creatine transporter (CRT) at the rat inner blood-retinal barrier. *J Neurochem,* 89**,** 1454-61.

Napoli, C., Lemieux, C. & Jorgensen, R. 1990. Introduction of a Chimeric Chalcone Synthase Gene into Petunia Results in Reversible Co-Suppression of Homologous Genes in trans. *Plant Cell,* 2**,** 279-289.

Narfstrom, K., Katz, M. L., Ford, M., Redmond, T. M., Rakoczy, E. & Bragadottir, R. 2003. *In vivo* gene therapy in young and adult RPE65-/- dogs produces long-term visual improvement. *J Hered,* 94**,** 31-7.

Nath, R., Raser, K. J., Stafford, D., Hajimohammadreza, I., Posner, A., Allen, H., Talanian, R. V., Yuen, P., Gilbertsen, R. B. & Wang, K. K. 1996. Non-erythroid alpha-spectrin breakdown by calpain and interleukin 1 beta-converting-enzyme-like protease(s) in apoptotic cells: contributory roles of both protease families in neuronal apoptosis. *Biochem J,* 319 (Pt 3)**,** 683-90.

Natsumeda, Y., Ohno, S., Kawasaki, H., Konno, Y., Weber, G. & Suzuki, K. 1990. Two distinct cDNAs for human IMP dehydrogenase. *J Biol Chem,* 265**,** 5292-5.

Nguyen, A. T., Campbell, M., Kenna, P. F., Kiang, A. S., Tam, L., Humphries, M. M. & Humphries, P. 2012. Calpain and photoreceptor apoptosis. *Adv Exp Med Biol,* 723**,** 547-52.

Ni, M., and A.S. Lee. 2007. ER chaperones in mammalian development and human diseases. *FEBS Lett*. 581:3641-3651.

Nishikawa, S., J.L. Brodsky, and K. Nakatsukasa. 2005. Roles of molecular chaperones in endoplasmic reticulum (ER) quality control and ER-associated degradation (ERAD). *Journal of biochemistry*. 137:551-555.

Nishitoh, H., A. Matsuzawa, K. Tobiume, K. Saegusa, K. Takeda, K. Inoue, S. Hori, A. Kakizuka, and H. Ichijo. 2002. ASK1 is essential for endoplasmic reticulum stress-induced neuronal cell death triggered by expanded polyglutamine repeats. *Genes Dev*. 16:1345-1355.

Nitta, T., Hata, M., Gotoh, S., Seo, Y., Sasaki, H., Hashimoto, N., Furuse, M. & Tsukita, S. 2003. Size-selective loosening of the blood-brain barrier in claudin-5-deficient mice. *J Cell Biol,* 161**,** 653-60.

Nixon, R. A. 2003. The calpains in aging and aging-related diseases. *Ageing Res Rev,* 2**,** 407-18.

Noell, W. K., Walker, V. S., Kang, B. S. & Berman, S. 1966. Retinal damage by light in rats. *Invest Ophthalmol,* 5**,** 450-73.

Nollen, E. A. & Morimoto, R. I. 2002. Chaperoning signaling pathways: molecular chaperones as stress-sensing 'heat shock' proteins. *J Cell Sci,* 115**,** 2809-16.

Noorwez, S.M., D.A. Ostrov, J.H. McDowell, M.P. Krebs, and S. Kaushal. 2008. A high-throughput screening method for small-molecule pharmacologic chaperones of misfolded rhodopsin. *Investigative ophthalmology & visual science*. 49:3224-3230.

Noorwez, S.M., R. Malhotra, J.H. McDowell, K.A. Smith, M.P. Krebs, and S. Kaushal. 2004. Retinoids assist the cellular folding of the autosomal dominant retinitis pigmentosa opsin mutant P23H. *The Journal of biological chemistry*. 279:16278-16284.

Noorwez, S.M., R.R. Sama, and S. Kaushal. 2009. Calnexin improves the folding efficiency of mutant rhodopsin in the presence of pharmacological chaperone 11-cis-retinal. *The Journal of biological chemistry*. 284:33333-33342.

Noorwez, S.M., V. Kuksa, Y. Imanishi, L. Zhu, S. Filipek, K. Palczewski, and S. Kaushal. 2003. Pharmacological chaperone-mediated *in vivo* folding and stabilization of the P23H-opsin mutant associated with autosomal dominant retinitis pigmentosa. *The Journal of biological chemistry*. 278:14442-14450.

Nykanen, A., Haley, B. & Zamore, P. D. 2001. ATP requirements and small interfering RNA structure in the RNA interference pathway. *Cell,* 107**,** 309-21.

Ohgane, K., K. Dodo, and Y. Hashimoto. 2010. Retinobenzaldehydes as proper-trafficking inducers of folding-defective P23H rhodopsin mutant responsible for retinitis pigmentosa. *Bioorg Med Chem.* 18:7022-7028.

Ohkura, Y., Akanuma, S., Tachikawa, M. & Hosoya, K. 2010. Blood-to-retina transport of biotin via Na+-dependent multivitamin transporter (SMVT) at the inner blood-retinal barrier. *Exp Eye Res,* 91, 387-92.

Ohoka, N., S. Yoshii, T. Hattori, K. Onozaki, and H. Hayashi. 2005. TRB3, a novel ER stress-inducible gene, is induced via ATF4-CHOP pathway and is involved in cell death. *EMBO J.* 24:1243-1255.

Olsson, J. E., Gordon, J. W., Pawlyk, B. S., Roof, D., Hayes, A., Molday, R. S., Mukai, S., Cowley, G. S., Berson, E. L. & Dryja, T. P. 1992. Transgenic mice with a rhodopsin mutation (Pro23His): a mouse model of autosomal dominant retinitis pigmentosa. *Neuron,* 9, 815-30.

O'Reilly, M., Millington-Ward, S., Palfi, A., Chadderton, N., Cronin, T., McNally, N., Humphries, M. M., Humphries, P., Kenna, P. F. & Farrar, G. J. 2008. A transgenic mouse model for gene therapy of rhodopsin-linked Retinitis Pigmentosa. *Vision Res,* 48, 386-91.

O'Reilly, M., Palfi, A., Chadderton, N., Millington-Ward, S., Ader, M., Cronin, T., Tuohy, T., Auricchio, A., Hildinger, M., Tivnan, A., McNally, N., Humphries, M. M., Kiang, A. S., Humphries, P., Kenna, P. F. & Farrar, G. J. 2007. RNA interference-mediated suppression and replacement of human rhodopsin *in vivo. Am J Hum Genet,* 81, 127-35.

O'Reilly, M., Palfi, A., Chadderton, N., Millington-Ward, S., Ader, M., Cronin, T., Tuohy, T., Auricchio, A., Hildinger, M., Tivnan, A., McNally, N., Humphries, M. M., Kiang, A. S., Humphries, P., Kenna, P. F. & Farrar, G. J. 2007. RNA interference-mediated suppression and replacement of human rhodopsin *in vivo. Am J Hum Genet,* 81, 127-35.

Ostrovsky, O., C.A. Makarewich, E.L. Snapp, and Y. Argon. 2009b. An essential role for ATP binding and hydrolysis in the chaperone activity of GRP94 in cells. *Proc Natl Acad Sci U S A.* 106:11600-11605.

Ostrovsky, O., N.T. Ahmed, and Y. Argon. 2009a. The chaperone activity of GRP94 toward insulin-like growth factor II is necessary for the stress response to serum deprivation. *Mol Biol Cell.* 20:1855-1864.

Otero, J.H., B. Lizak, and L.M. Hendershot. 2010. Life and death of a BiP substrate. *Seminars in cell & developmental biology.* 21:472-478.

Oyadomari, S., and M. Mori. 2004. Roles of CHOP/GADD153 in endoplasmic reticulum stress. *Cell Death Differ.* 11:381-389.

Pacey, S., Wilson, R. H., Walton, M., Eatock, M. M., Hardcastle, A., Zetterlund, A., Arkenau, H. T., Moreno-Farre, J., Banerji, U., Roels, B., Peachey, H., Aherne, W., de Bono, J. S., Raynaud, F., Workman, P. & Judson, I. 2011. A phase I study of the heat shock protein 90 inhibitor alvespimycin (17-DMAG) given intravenously to patients with advanced solid tumors. *Clin Cancer Res,* 17, 1561-70.

Paddison, P. J., Caudy, A. A., Sachidanandam, R. & Hannon, G. J. 2004. Short hairpin activated gene silencing in mammalian cells. *Methods Mol Biol,* 265, 85-100.

Palczewski, K., T. Kumasaka, T. Hori, C.A. Behnke, H. Motoshima, B.A. Fox, I. Le Trong, D.C. Teller, T. Okada, R.E. Stenkamp, M. Yamamoto, and M. Miyano. 2000. Crystal structure of rhodopsin: A G protein-coupled receptor. *Science.* 289:739-745.

Palfi, A., Ader, M., Kiang, A. S., Millington-Ward, S., Clark, G., O'Reilly, M., McMahon, H. P., Kenna, P. F., Humphries, P. & Farrar, G. J. 2006. RNAi-based suppression and replacement of rds-peripherin in retinal organotypic culture. *Hum Mutat,* 27, 260-8.

Palfi, A., Millington-Ward, S., Chadderton, N., O'Reilly, M., Goldmann, T., Humphries, M. M., Li, T., Wolfrum, U., Humphries, P., Kenna, P. F. & Farrar, G. J. 2010. Adeno-associated virus-mediated rhodopsin replacement provides therapeutic benefit in mice with a targeted disruption of the rhodopsin gene. *Hum Gene Ther,* 21, 311-23.

Palfi, A., S. Millington-Ward, N. Chadderton, M. O'Reilly, T. Goldmann, M.M. Humphries, T. Li, U. Wolfrum, P. Humphries, P.F. Kenna, and G.J. Farrar. 2010. Adeno-associated virus-mediated rhodopsin replacement provides therapeutic benefit in mice with a targeted disruption of the rhodopsin gene. *Human gene therapy.* 21:311-323.

Pang, J. J., Chang, B., Kumar, A., Nusinowitz, S., Noorwez, S. M., Li, J., Rani, A., Foster, T. C., Chiodo, V. A., Doyle, T., Li, H., Malhotra, R., Teusner, J. T., McDowell, J. H., Min, S. H.,

Li, Q., Kaushal, S. & Hauswirth, W. W. 2006. Gene therapy restores vision-dependent behavior as well as retinal structure and function in a mouse model of RPE65 Leber congenital amaurosis. *Mol Ther,* 13, 565-72.

Papadopoulos, M. C., Saadoun, S., Binder, D. K., Manley, G. T., Krishna, S. & Verkman, A. S. 2004. Molecular mechanisms of brain tumor edema. *Neuroscience,* 129, 1011-20.

Paquet-Durand, F., Azadi, S., Hauck, S. M., Ueffing, M., van Veen, T. & Ekstrom, P. 2006. Calpain is activated in degenerating photoreceptors in the rd1 mouse. *J Neurochem,* 96, 802-14.

Paquet-Durand, F., Johnson, L. & Ekstrom, P. 2007. Calpain activity in retinal degeneration. *J Neurosci Res,* 85, 693-702.

Paquet-Durand, F., Sanges, D., McCall, J., Silva, J., van Veen, T., Marigo, V. & Ekstrom, P. 2010. Photoreceptor rescue and toxicity induced by different calpain inhibitors. *J Neurochem,* 115, 930-40.

Pardridge, W. M. 2002. Why is the global CNS pharmaceutical market so under-penetrated? *Drug Discov Today,* 7, 5-7.

Pardridge, W. M. 2003. Blood-brain barrier drug targeting: the future of brain drug development. *Mol Interv,* 3, 90-105, 51.

Pardridge, W. M. 2007. Blood-brain barrier delivery. *Drug Discov Today,* 12, 54-61.

Parodi, A.J. 2000. Protein glucosylation and its role in protein folding. *Annual review of biochemistry.* 69:69-93.

Pennings, R. J., Fields, R. R., Huygen, P. L., Deutman, A. F., Kimberling, W. J. & Cremers, C. W. 2003. Usher syndrome type III can mimic other types of Usher syndrome. *Ann Otol Rhinol Laryngol,* 112, 525-30.

Perche, O., Doly, M. & Ranchon-Cole, I. 2007. Caspase-dependent apoptosis in light-induced retinal degeneration. *Invest Ophthalmol Vis Sci,* 48, 2753-9.

Perche, O., Doly, M. & Ranchon-Cole, I. 2009. Calpains are activated by light but their inhibition has no neuroprotective effect against light-damage. *Exp Eye Res,* 89, 989-94.

Persson, H., Kawashima, S. & Karlsson, J. O. 1993. Immunohistochemical localization of calpains and calpastatin in the rabbit eye. *Brain Res,* 611, 272-8.

Petrova, K., S. Oyadomari, L.M. Hendershot, and D. Ron. 2008. Regulated association of misfolded endoplasmic reticulum lumenal proteins with P58/DNAJc3. *EMBO J.* 27:2862-2872.

Petrs-Silva, H., Dinculescu, A., Li, Q., Deng, W. T., Pang, J. J., Min, S. H., Chiodo, V., Neeley, A. W., Govindasamy, L., Bennett, A., Agbandje-McKenna, M., Zhong, L., Li, B., Jayandharan, G. R., Srivastava, A., Lewin, A. S. & Hauswirth, W. W. 2011. Novel properties of tyrosine-mutant AAV2 vectors in the mouse retina. *Mol Ther,* 19, 293-301.

Petrs-Silva, H., Dinculescu, A., Li, Q., Min, S. H., Chiodo, V., Pang, J. J., Zhong, L., Zolotukhin, S., Srivastava, A., Lewin, A. S. & Hauswirth, W. W. 2009. High-efficiency transduction of the mouse retina by tyrosine-mutant AAV serotype vectors. *Mol Ther,* 17, 463-71.

Petty, M. A. & Lo, E. H. 2002. Junctional complexes of the blood-brain barrier: permeability changes in neuroinflammation. *Prog Neurobiol,* 68, 311-23.

Philp, N. J., Yoon, H. & Grollman, E. F. 1998. Monocarboxylate transporter MCT1 is located in the apical membrane and MCT3 in the basal membrane of rat RPE. *Am J Physiol,* 274, R1824-8.

Pieper, A. A., Verma, A., Zhang, J. & Snyder, S. H. 1999. Poly (ADP-ribose) polymerase, nitric oxide and cell death. *Trends Pharmacol Sci,* 20, 171-81.

Pittler, S. J. & Baehr, W. 1991. Identification of a nonsense mutation in the rod photoreceptor cGMP phosphodiesterase beta-subunit gene of the rd mouse. *Proc Natl Acad Sci U S A,* 88, 8322-6.

Poetsch, A., Molday, L. L. & Molday, R. S. 2001. The cGMP-gated channel and related glutamic acid-rich proteins interact with peripherin-2 at the rim region of rod photoreceptor disc membranes. *J Biol Chem,* 276, 48009-16.

Pollock, R., Issner, R., Zoller, K., Natesan, S., Rivera, V. M. & Clackson, T. 2000. Delivery of a stringent dimerizer-regulated gene expression system in a single retroviral vector. *Proc Natl Acad Sci U S A,* 97, 13221-6.

Polt, R., Porreca, F., Szabo, L. Z., Bilsky, E. J., Davis, P., Abbruscato, T. J., Davis, T. P., Harvath, R., Yamamura, H. I. & Hruby, V. J. 1994. Glycopeptide enkephalin analogues produce

analgesia in mice: evidence for penetration of the blood-brain barrier. *Proc Natl Acad Sci U S A,* 91, 7114-8.

Pratt, W. B. & Toft, D. O. 2003. Regulation of signaling protein function and trafficking by the hsp90/hsp70-based chaperone machinery. *Exp Biol Med (Maywood),* 228, 111-33.

Prawitt, D., Brixel, L., Spangenberg, C., Eshkind, L., Heck, R., Oesch, F., Zabel, B. & Bockamp, E. 2004. RNAi knock-down mice: an emerging technology for post-genomic functional genetics. *Cytogenet Genome Res,* 105, 412-21.

Price, B. A., Sandoval, I. M., Chan, F., Nichols, R., Roman-Sanchez, R., Wensel, T. G. & Wilson, J. H. 2012. Rhodopsin gene expression determines rod outer segment size and rod cell resistance to a dominant-negative neurodegeneration mutant. *PLoS One,* 7, e49889.

Price, B. A., Sandoval, I. M., Chan, F., Simons, D. L., Wu, S. M., Wensel, T. G. & Wilson, J. H. 2011. Mislocalization and degradation of human P23H-rhodopsin-GFP in a knockin mouse model of retinitis pigmentosa. *Invest Ophthalmol Vis Sci,* 52, 9728-36.

Puchowicz, M. A., Xu, K., Magness, D., Miller, C., Lust, W. D., Kern, T. S. & LaManna, J. C. 2004. Comparison of glucose influx and blood flow in retina and brain of diabetic rats. *J Cereb Blood Flow Metab,* 24, 449-57.

Putcha, G.V., S. Le, S. Frank, C.G. Besirli, K. Clark, B. Chu, S. Alix, R.J. Youle, A. LaMarche, A.C. Maroney, and E.M. Johnson, Jr. 2003. JNK-mediated BIM phosphorylation potentiates BAX-dependent apoptosis. *Neuron.* 38:899-914.

Puthalakath, H., L.A. O'Reilly, P. Gunn, L. Lee, P.N. Kelly, N.D. Huntington, P.D. Hughes, E.M. Michalak, J. McKimm-Breschkin, N. Motoyama, T. Gotoh, S. Akira, P. Bouillet, and A. Strasser. 2007. ER stress triggers apoptosis by activating BH3-only protein Bim. *Cell.* 129:1337-1349.

Rabinowitz, J. E. & Samulski, J. 1998. Adeno-associated virus expression systems for gene transfer. *Curr Opin Biotechnol,* 9, 470-5.

Rajan, A., Kelly, R. J., Trepel, J. B., Kim, Y. S., Alarcon, S. V., Kummar, S., Gutierrez, M., Crandon, S., Zein, W. M., Jain, L., Mannargudi, B., Figg, W. D., Houk, B. E., Shnaidman, M., Brega, N. & Giaccone, G. 2011. A phase I study of PF-04929113 (SNX-5422), an orally bioavailable heat shock protein 90 inhibitor, in patients with refractory solid tumor malignancies and lymphomas. *Clin Cancer Res,* 17, 6831-9.

Rajan, R.S., and R.R. Kopito. 2005. Suppression of wild-type rhodopsin maturation by mutants linked to autosomal dominant retinitis pigmentosa. *J Biol Chem.* 280:1284-1291.

Ramanathan, R.K., M.J. Egorin, C. Erlichman, S.C. Remick, S.S. Ramalingam, C. Naret, J.L. Holleran, C.J. TenEyck, S.P. Ivy, and C.P. Belani. 2010. Phase I pharmacokinetic and pharmacodynamic study of 17-dimethylaminoethylamino-17-demethoxygeldanamycin, an inhibitor of heat-shock protein 90, in patients with advanced solid tumors. *J Clin Oncol.* 28:1520-1526.

Rao, M. & Sockanathan, S. 2005. Molecular mechanisms of RNAi: implications for development and disease. *Birth Defects Res C Embryo Today,* 75, 28-42.

Rao, M., Baraban, J. H., Rajaii, F. & Sockanathan, S. 2004. *In vivo* comparative study of RNAi methodologies by in ovo electroporation in the chick embryo. *Dev Dyn,* 231, 592-600.

Rao, R.V., A. Peel, A. Logvinova, G. del Rio, E. Hermel, T. Yokota, P.C. Goldsmith, L.M. Ellerby, H.M. Ellerby, and D.E. Bredesen. 2002. Coupling endoplasmic reticulum stress to the cell death program: role of the ER chaperone GRP78. *FEBS Lett.* 514:122-128.

Rapoport, T. A. 2007. Protein translocation across the eukaryotic endoplasmic reticulum and bacterial plasma membranes. *Nature,* 450, 663-9.

Rattner, A., Sun, H. & Nathans, J. 1999. Molecular genetics of human retinal disease. *Annu Rev Genet,* 33, 89-131.

Ravid, T., Doolman, R., Avner, R., Harats, D. & Roitelman, J. 2000. The ubiquitin-proteasome pathway mediates the regulated degradation of mammalian 3-hydroxy-3-methylglutaryl-coenzyme A reductase. *J Biol Chem,* 275, 35840-7.

Ray, S. K., Karmakar, S., Nowak, M. W. & Banik, N. L. 2006. Inhibition of calpain and caspase-3 prevented apoptosis and preserved electrophysiological properties of voltage-gated and ligand-gated ion channels in rat primary cortical neurons exposed to glutamate. *Neuroscience,* 139, 577-95.

Reagan-Shaw, S., M. Nihal, and N. Ahmad. 2008. Dose translation from animal to human studies revisited. *FASEB J.* 22:659-661.

Reese, T. S. & Karnovsky, M. J. 1967. Fine structural localization of a blood–brain barrier to exogenous peroxidase, . *Journal of Cell Biology,* 34, 207-217.

Reichenbach, A., Wurm, A., Pannicke, T., Iandiev, I., Wiedemann, P. & Bringmann, A. 2007. Muller cells as players in retinal degeneration and edema. *Graefes Arch Clin Exp Ophthalmol,* 245, 627-36.

Reimold, A.M., N.N. Iwakoshi, J. Manis, P. Vallabhajosyula, E. Szomolanyi-Tsuda, E.M. Gravallese, D. Friend, M.J. Grusby, F. Alt, and L.H. Glimcher. 2001. Plasma cell differentiation requires the transcription factor XBP-1. *Nature*. 412:300-307.

Ritter, C., K. Quirin, M. Kowarik, and A. Helenius. 2005. Minor folding defects trigger local modification of glycoproteins by the ER folding sensor GT. *EMBO J.* 24:1730-1738.

Rivera, V. M., Clackson, T., Natesan, S., Pollock, R., Amara, J. F., Keenan, T., Magari, S. R., Phillips, T., Courage, N. L., Cerasoli, F., Jr., Holt, D. A. & Gilman, M. 1996. A humanized system for pharmacologic control of gene expression. *Nat Med,* 2, 1028-32.

Rivolta, C., Berson, E. L. & Dryja, T. P. 2002. Paternal uniparental heterodisomy with partial isodisomy of chromosome 1 in a patient with retinitis pigmentosa without hearing loss and a missense mutation in the Usher syndrome type II gene USH2A. *Arch Ophthalmol,* 120, 1566-71.

Rohr, U. P., Wulf, M. A., Stahn, S., Steidl, U., Haas, R. & Kronenwett, R. 2002. Fast and reliable titration of recombinant adeno-associated virus type-2 using quantitative real-time PCR. *J Virol Methods,* 106, 81-8.

Ron, D., and P. Walter. 2007. Signal integration in the endoplasmic reticulum unfolded protein response. *Nat Rev Mol Cell Biol.* 8:519-529.

Roof, D. J., Adamian, M. & Hayes, A. 1994. Rhodopsin accumulation at abnormal sites in retinas of mice with a human P23H rhodopsin transgene. *Invest Ophthalmol Vis Sci,* 35, 4049-62.

Ross, J. W., Fernandez de Castro, J. P., Zhao, J., Samuel, M., Walters, E., Rios, C., Bray-Ward, P., Jones, B. W., Marc, R. E., Wang, W., Zhou, L., Noel, J. M., McCall, M. A., DeMarco, P. J., Prather, R. S. & Kaplan, H. J. 2012. Generation of an inbred miniature pig model of retinitis pigmentosa. *Invest Ophthalmol Vis Sci,* 53, 501-7.

Rousseau, F., Serrano, L. & Schymkowitz, J. W. 2006. How evolutionary pressure against protein aggregation shaped chaperone specificity. *J Mol Biol,* 355, 1037-47.

Roy, B., and A.S. Lee. 1999. The mammalian endoplasmic reticulum stress response element consists of an evolutionarily conserved tripartite structure and interacts with a novel stress-inducible complex. *Nucleic Acids Res.* 27:1437-1443.

Rungger-Brandle, E., Dosso, A. A. & Leuenberger, P. M. 2000. Glial reactivity, an early feature of diabetic retinopathy. *Invest Ophthalmol Vis Sci,* 41, 1971-80.

Rutkowski, D.T., S.M. Arnold, C.N. Miller, J. Wu, J. Li, K.M. Gunnison, K. Mori, A.A. Sadighi Akha, D. Raden, and R.J. Kaufman. 2006. Adaptation to ER stress is mediated by differential stabilities of pro-survival and pro-apoptotic mRNAs and proteins. *PLoS Biol.* 4:e374.

Ryoo, H.D., and H. Steller. 2007. Unfolded protein response in Drosophila: why another model can make it fly. *Cell Cycle.* 6:830-835.

Ryoo, H.D., P.M. Domingos, M.J. Kang, and H. Steller. 2007. Unfolded protein response in a Drosophila model for retinal degeneration. *EMBO J.* 26:242-252.

Saari, J. C., Nawrot, M., Kennedy, B. N., Garwin, G. G., Hurley, J. B., Huang, J., Possin, D. E. & Crabb, J. W. 2001. Visual cycle impairment in cellular retinaldehyde binding protein (CRALBP) knockout mice results in delayed dark adaptation. *Neuron,* 29, 739-48.

Saitou, M., Furuse, M., Sasaki, H., Schulzke, J. D., Fromm, M., Takano, H., Noda, T. & Tsukita, S. 2000. Complex phenotype of mice lacking occludin, a component of tight junction strands. *Mol Biol Cell,* 11, 4131-42.

Sakami, S., Maeda, T., Bereta, G., Okano, K., Golczak, M., Sumaroka, A., Roman, A. J., Cideciyan, A. V., Jacobson, S. G. & Palczewski, K. 2011. Probing mechanisms of photoreceptor degeneration in a new mouse model of the common form of autosomal dominant retinitis pigmentosa due to P23H opsin mutations. *J Biol Chem,* 286, 10551-67.

Sakamoto, Y. R., Nakajima, T. R., Fukiage, C. R., Sakai, O. R., Yoshida, Y. R., Azuma, M. R. & Shearer, T. R. 2000. Involvement of calpain isoforms in ischemia-reperfusion injury in rat retina. *Curr Eye Res,* 21, 571-80.

Sakurai, E., Matsuda, Y., Ozeki, H., Kunou, N., Nakajima, K. & Ogura, Y. 2001. Scleral plug of biodegradable polymers containing ganciclovir for experimental cytomegalovirus retinitis. *Invest Ophthalmol Vis Sci,* 42, 2043-8.

Saliba, R. S., Munro, P. M., Luthert, P. J. & Cheetham, M. E. 2002. The cellular fate of mutant rhodopsin: quality control, degradation and aggresome formation. *J Cell Sci,* 115, 2907-18.

Sanges, D. & Marigo, V. 2006. Cross-talk between two apoptotic pathways activated by endoplasmic reticulum stress: differential contribution of caspase-12 and AIF. *Apoptosis,* 11, 1629-41.

Sanges, D., Comitato, A., Tammaro, R. & Marigo, V. 2006. Apoptosis in retinal degeneration involves cross-talk between apoptosis-inducing factor (AIF) and caspase-12 and is blocked by calpain inhibitors. *Proc Natl Acad Sci U S A,* 103, 17366-71.

Sanyal, S. & Bal, A. K. 1973. Comparative light and electron microscopic study of retinal histogenesis in normal and rd mutant mice. *Z Anat Entwicklungsgesch,* 142, 219-38.

Sasagawa, Y., K. Yamanaka, and T. Ogura. 2007. ER E3 ubiquitin ligase HRD-1 and its specific partner chaperone BiP play important roles in ERAD and developmental growth in Caenorhabditis elegans. *Genes Cells.* 12:1063-1073.

Sasaki, T., Kishi, M., Saito, M., Tanaka, T., Higuchi, N., Kominami, E., Katunuma, N. & Murachi, T. 1990. Inhibitory effect of di- and tripeptidyl aldehydes on calpains and cathepsins. *J Enzyme Inhib,* 3, 195-201.

Saxena, S., Jonsson, Z. O. & Dutta, A. 2003. Small RNAs with imperfect match to endogenous mRNA repress translation. Implications for off-target activity of small inhibitory RNA in mammalian cells. *J Biol Chem,* 278, 44312-9.

Schatz, P., Ponjavic, V., Andreasson, S., McGee, T. L., Dryja, T. P. & Abrahamson, M. 2005. Clinical phenotype in a Swedish family with a mutation in the IMPDH1 gene. *Ophthalmic Genet,* 26, 119-24.

Scheufler, C., Brinker, A., Bourenkov, G., Pegoraro, S., Moroder, L., Bartunik, H., Hartl, F. U. & Moarefi, I. 2000. Structure of TPR domain-peptide complexes: critical elements in the assembly of the Hsp70-Hsp90 multichaperone machine. *Cell,* 101, 199-210.

Schoenwald, R. D., Deshpande, G. S., Rethwisch, D. G. & Barfknecht, C. F. 1997. Penetration into the anterior chamber via the conjunctival/scleral pathway. *J Ocul Pharmacol Ther,* 13, 41-59.

Senda, M. & Natsumeda, Y. 1994. Tissue-differential expression of two distinct genes for human IMP dehydrogenase (E.C.1.1.1.205). *Life Sci,* 54, 1917-26.

Seydoux, G. & Fire, A. 1994. Soma-germline asymmetry in the distributions of embryonic RNAs in Caenorhabditis elegans. *Development,* 120, 2823-34.

Sharma, K., R.M. Vabulas, B. Macek, S. Pinkert, J. Cox, M. Mann, and F.U. Hartl. 2012. Quantitative proteomics reveals that Hsp90 inhibition preferentially targets kinases and the DNA damage response. *Mol Cell Proteomics.* 11:M111 014654.

Sharma, S. K., De los Rios, P., Christen, P., Lustig, A. & Goloubinoff, P. 2010. The kinetic parameters and energy cost of the Hsp70 chaperone as a polypeptide unfoldase. *Nat Chem Biol,* 6, 914-20.

Shen, J., X. Chen, L. Hendershot, and R. Prywes. 2002. ER stress regulation of ATF6 localization by dissociation of BiP/GRP78 binding and unmasking of Golgi localization signals. *Developmental cell.* 3:99-111.

Sherman, M. Y. & Goldberg, A. L. 2001. Cellular defenses against unfolded proteins: a cell biologist thinks about neurodegenerative diseases. *Neuron,* 29, 15-32.

Shimamura, T., Perera, S. A., Foley, K. P., Sang, J., Rodig, S. J., Inoue, T., Chen, L., Li, D., Carretero, J., Li, Y. C., Sinha, P., Carey, C. D., Borgman, C. L., Jimenez, J. P., Meyerson, M., Ying, W., Barsoum, J., Wong, K. K. & Shapiro, G. I. 2012. Ganetespib (STA-9090), a nongeldanamycin HSP90 inhibitor, has potent antitumor activity in *in vitro* and *in vivo* models of non-small cell lung cancer. *Clin Cancer Res,* 18, 4973-85.

Shimazawa, M., Suemori, S., Inokuchi, Y., Matsunaga, N., Nakajima, Y., Oka, T., Yamamoto, T. & Hara, H. 2010. A novel calpain inhibitor, ((1S)-1-((((1S)-1-Benzyl-3-cyclopropylamino-2,3-di-oxopropyl)amino)carbony l)-3-methylbutyl)carbamic acid 5-methoxy-3-oxapentyl ester (SNJ-1945), reduces murine retinal cell death *in vitro* and *in vivo*. *J Pharmacol Exp Ther,* 332, 380-7.

Shintani, K., D.L. Shechtman, and A.S. Gurwood. 2009. Review and update: current treatment trends for patients with retinitis pigmentosa. *Optometry*. 80:384-401.

Simo, R., Villarroel, M., Corraliza, L., Hernandez, C. & Garcia-Ramirez, M. 2010. The retinal pigment epithelium: something more than a constituent of the blood-retinal barrier--implications for the pathogenesis of diabetic retinopathy. *J Biomed Biotechnol,* 2010, 190724.

Sioud, M. 2005. Induction of inflammatory cytokines and interferon responses by double-stranded and single-stranded siRNAs is sequence-dependent and requires endosomal localization. *J Mol Biol,* 348, 1079-90.

Sioud, M. 2006. Single-stranded small interfering RNA are more immunostimulatory than their double-stranded counterparts: a central role for 2'-hydroxyl uridines in immune responses. *Eur J Immunol,* 36, 1222-30.

Sioud, M. 2010. Recent advances in small interfering RNA sensing by the immune system. *N Biotechnol,* 27, 236-42.

Smith, K. & Leyden, J. J. 2005. Safety of doxycycline and minocycline: a systematic review. *Clin Ther,* 27, 1329-42.

Smith, M. A. & Schnellmann, R. G. 2012. Calpains, mitochondria, and apoptosis. *Cardiovasc Res,* 96, 32-7.

Song, B., D. Scheuner, D. Ron, S. Pennathur, and R.J. Kaufman. 2008. Chop deletion reduces oxidative stress, improves beta cell function, and promotes cell survival in multiple mouse models of diabetes. *J Clin Invest*. 118:3378-3389.

Sousa, M., and A.J. Parodi. 1995. The molecular basis for the recognition of misfolded glycoproteins by the UDP-Glc:glycoprotein glucosyltransferase. *EMBO J*. 14:4196-4203.

Sousa, M.C., M.A. Ferrero-Garcia, and A.J. Parodi. 1992. Recognition of the oligosaccharide and protein moieties of glycoproteins by the UDP-Glc:glycoprotein glucosyltransferase. *Biochemistry*. 31:97-105.

Spellicy, C. J., Daiger, S. P., Sullivan, L. S., Zhu, J., Liu, Q., Pierce, E. A. & Bowne, S. J. 2007. Characterization of retinal inosine monophosphate dehydrogenase 1 in several mammalian species. *Mol Vis,* 13, 1866-72.

Srivastava, A. 1994. Parvovirus-based vectors for human gene therapy. *Blood Cells,* 20, 531-6; discussion 536-8.

Stark, G. R., Kerr, I. M., Williams, B. R., Silverman, R. H. & Schreiber, R. D. 1998. How cells respond to interferons. *Annu Rev Biochem,* 67, 227-64.

Stieger, K., Le Meur, G., Lasne, F., Weber, M., Deschamps, J. Y., Nivard, D., Mendes-Madeira, A., Provost, N., Martin, L., Moullier, P. & Rolling, F. 2006. Long-term doxycycline-regulated transgene expression in the retina of nonhuman primates following subretinal injection of recombinant AAV vectors. *Mol Ther,* 13, 967-75.

Stieger, K., Schroeder, J., Provost, N., Mendes-Madeira, A., Belbellaa, B., Le Meur, G., Weber, M., Deschamps, J. Y., Lorenz, B., Moullier, P. & Rolling, F. 2009. Detection of intact rAAV particles up to 6 years after successful gene transfer in the retina of dogs and primates. *Mol Ther,* 17, 516-23.

Stilwell, J. L. & Samulski, R. J. 2003. Adeno-associated virus vectors for therapeutic gene transfer. *Biotechniques,* 34, 148-50, 152, 154 passim.

Stoetzel, C., Laurier, V., Faivre, L., Megarbane, A., Perrin-Schmitt, F., Verloes, A., Bonneau, D., Mandel, J. L., Cossee, M. & Dollfus, H. 2006. BBS8 is rarely mutated in a cohort of 128 Bardet-Biedl syndrome families. *J Hum Genet,* 51, 81-4.

Sun, H., Y. Wang, I.H. Pang, J. Shen, X. Tang, Y. Li, C. Liu, and B. Li. 2011. Protective effect of a JNK inhibitor against retinal ganglion cell loss induced by acute moderate ocular hypertension. *Mol Vis*. 17:864-875.

Sung, C. H., Makino, C., Baylor, D. & Nathans, J. 1994. A rhodopsin gene mutation responsible for autosomal dominant retinitis pigmentosa results in a protein that is defective in localization to the photoreceptor outer segment. *J Neurosci,* 14, 5818-33.

Sung, C.H., B.G. Schneider, N. Agarwal, D.S. Papermaster, and J. Nathans. 1991. Functional heterogeneity of mutant rhodopsins responsible for autosomal dominant retinitis pigmentosa. *Proc Natl Acad Sci U S A*. 88:8840-8844.

Surace, E. M. & Auricchio, A. 2008. Versatility of AAV vectors for retinal gene transfer. *Vision Res,* 48, 353-9.

Surosky, R. T., Urabe, M., Godwin, S. G., McQuiston, S. A., Kurtzman, G. J., Ozawa, K. & Natsoulis, G. 1997. Adeno-associated virus Rep proteins target DNA sequences to a unique locus in the human genome. *J Virol,* 71, 7951-9.

Susin, S. A., Daugas, E., Ravagnan, L., Samejima, K., Zamzami, N., Loeffler, M., Costantini, P., Ferri, K. F., Irinopoulou, T., Prevost, M. C., Brothers, G., Mak, T. W., Penninger, J., Earnshaw, W. C. & Kroemer, G. 2000. Two distinct pathways leading to nuclear apoptosis. *J Exp Med,* 192, 571-80.

Susin, S. A., Lorenzo, H. K., Zamzami, N., Marzo, I., Snow, B. E., Brothers, G. M., Mangion, J., Jacotot, E., Costantini, P., Loeffler, M., Larochette, N., Goodlett, D. R., Aebersold, R., Siderovski, D. P., Penninger, J. M. & Kroemer, G. 1999. Molecular characterization of mitochondrial apoptosis-inducing factor. *Nature,* 397, 441-6.

Suzuki, K., Hata, S., Kawabata, Y. & Sorimachi, H. 2004. Structure, activation, and biology of calpain. *Diabetes,* 53 Suppl 1, S12-8.

Suzuki, K., Imajoh, S., Emori, Y., Kawasaki, H., Minami, Y. & Ohno, S. 1987. Calcium-activated neutral protease and its endogenous inhibitor. Activation at the cell membrane and biological function. *FEBS Lett,* 220, 271-7.

Syntichaki, P. & Tavernarakis, N. 2003. The biochemistry of neuronal necrosis: rogue biology? *Nat Rev Neurosci,* 4, 672-84.

Szathmary, R., R. Bielmann, M. Nita-Lazar, P. Burda, and C.A. Jakob. 2005. Yos9 protein is essential for degradation of misfolded glycoproteins and may function as lectin in ERAD. *Mol Cell.* 19:765-775.

Tabara, H., Sarkissian, M., Kelly, W. G., Fleenor, J., Grishok, A., Timmons, L., Fire, A. & Mello, C. C. 1999. The rde-1 gene, RNA interference, and transposon silencing in C. elegans. *Cell,* 99, 123-32.

Takata, K., Kasahara, T., Kasahara, M., Ezaki, O. & Hirano, H. 1992. Ultracytochemical localization of the erythrocyte/HepG2-type glucose transporter (GLUT1) in cells of the blood-retinal barrier in the rat. *Invest Ophthalmol Vis Sci,* 33, 377-83.

Takeuchi, H., Kobayashi, Y., Yoshihara, T., Niwa, J., Doyu, M., Ohtsuka, K. & Sobue, G. 2002. Hsp70 and Hsp40 improve neurite outgrowth and suppress intracytoplasmic aggregate formation in cultured neuronal cells expressing mutant SOD1. *Brain Res,* 949, 11-22.

Tam, B.M., and O.L. Moritz. 2006. Characterization of rhodopsin P23H-induced retinal degeneration in a Xenopus laevis model of retinitis pigmentosa. *Invest Ophthalmol Vis Sci.* 47:3234-3241.

Tam, B.M., O.L. Moritz, L.B. Hurd, and D.S. Papermaster. 2000. Identification of an outer segment targeting signal in the COOH terminus of rhodopsin using transgenic Xenopus laevis. *J Cell Biol.* 151:1369-1380.

Tam, L. C., Kiang, A. S., Campbell, M., Keaney, J., Farrar, G. J., Humphries, M. M., Kenna, P. F. & Humphries, P. 2010. Prevention of autosomal dominant retinitis pigmentosa by systemic drug therapy targeting heat shock protein 90 (Hsp90). *Hum Mol Genet,* 19, 4421-36.

Tam, L. C., Kiang, A. S., Kennan, A., Kenna, P. F., Chadderton, N., Ader, M., Palfi, A., Aherne, A., Ayuso, C., Campbell, M., Reynolds, A., McKee, A., Humphries, M. M., Farrar, G. J. & Humphries, P. 2008. Therapeutic benefit derived from RNAi-mediated ablation of IMPDH1 transcripts in a murine model of autosomal dominant retinitis pigmentosa (RP10). *Hum Mol Genet,* 17, 2084-100.

Tan, E., Wang, Q., Quiambao, A. B., Xu, X., Qtaishat, N. M., Peachey, N. S., Lem, J., Fliesler, S. J., Pepperberg, D. R., Naash, M. I. & Al-Ubaidi, M. R. 2001. The relationship between opsin overexpression and photoreceptor degeneration. *Invest Ophthalmol Vis Sci,* 42, 589-600.

Tan, M.H., A.J. Smith, B. Pawlyk, X. Xu, X. Liu, J.B. Bainbridge, M. Basche, J. McIntosh, H.V. Tran, A. Nathwani, T. Li, and R.R. Ali. 2009. Gene therapy for retinitis pigmentosa and Leber congenital amaurosis caused by defects in AIPL1: effective rescue of mouse models of partial and complete Aipl1 deficiency using AAV2/2 and AAV2/8 vectors. *Hum Mol Genet.* 18:2099-2114.

Tan, Y., Dourdin, N., Wu, C., De Veyra, T., Elce, J. S. & Greer, P. A. 2006. Ubiquitous calpains promote caspase-12 and JNK activation during endoplasmic reticulum stress-induced apoptosis. *J Biol Chem,* 281, 16016-24.

Taylor, S.C., A.D. Ferguson, J.J. Bergeron, and D.Y. Thomas. 2004. The ER protein folding sensor UDP-glucose glycoprotein-glucosyltransferase modifies substrates distant to local changes in glycoprotein conformation. *Nat Struct Mol Biol.* 11:128-134.

Thuerauf, D.J., L. Morrison, and C.C. Glembotski. 2004. Opposing roles for ATF6alpha and ATF6beta in endoplasmic reticulum stress response gene induction. *J Biol Chem.* 279:21078-21084.

Timmons, L. & Fire, A. 1998. Specific interference by ingested dsRNA. *Nature,* 395, 854.

Toda, K., Bush, R. A., Humphries, P. & Sieving, P. A. 1999. The electroretinogram of the rhodopsin knockout mouse. *Vis Neurosci,* 16, 391-8.

Tomi, M., Mori, M., Tachikawa, M., Katayama, K., Terasaki, T. & Hosoya, K. 2005. L-type amino acid transporter 1-mediated L-leucine transport at the inner blood-retinal barrier. *Invest Ophthalmol Vis Sci,* 46, 2522-30.

Travers, K.J., C.K. Patil, L. Wodicka, D.J. Lockhart, J.S. Weissman, and P. Walter. 2000. Functional and genomic analyses reveal an essential coordination between the unfolded protein response and ER-associated degradation. *Cell.* 101:249-258.

Travis, G. H., Sutcliffe, J. G. & Bok, D. 1991. The retinal degeneration slow (rds) gene product is a photoreceptor disc membrane-associated glycoprotein. *Neuron,* 6, 61-70.

Tretiach, M., Madigan, M. C., Wen, L. & Gillies, M. C. 2005. Effect of Muller cell co-culture on *in vitro* permeability of bovine retinal vascular endothelium in normoxic and hypoxic conditions. *Neurosci Lett,* 378, 160-5.

Unlu, N. & Robinson, J. R. 1998. Scleral permeability to hydrocortisone and mannitol in the albino rabbit eye. *J Ocul Pharmacol Ther,* 14, 273-81.

Urano, F., X. Wang, A. Bertolotti, Y. Zhang, P. Chung, H.P. Harding, and D. Ron. 2000. Coupling of stress in the ER to activation of JNK protein kinases by transmembrane protein kinase IRE1. *Science.* 287:664-666.

van der Krol, A. R., Mur, L. A., Beld, M., Mol, J. N. & Stuitje, A. R. 1990. Flavonoid genes in petunia: addition of a limited number of gene copies may lead to a suppression of gene expression. *Plant Cell,* 2, 291-9.

Van Itallie, C. M. & Anderson, J. M. 2006. Claudins and epithelial paracellular transport. *Annu Rev Physiol,* 68, 403-29.

Van Itallie, C. M., Colegio, O. R. & Anderson, J. M. 2004. The cytoplasmic tails of claudins can influence tight junction barrier properties through effects on protein stability. *J Membr Biol,* 199, 29-38.

van Soest, S., Westerveld, A., de Jong, P. T., Bleeker-Wagemakers, E. M. & Bergen, A. A. 1999. Retinitis pigmentosa: defined from a molecular point of view. *Surv Ophthalmol,* 43, 321-34.

Vanags, D. M., Porn-Ares, M. I., Coppola, S., Burgess, D. H. & Orrenius, S. 1996. Protease involvement in fodrin cleavage and phosphatidylserine exposure in apoptosis. *J Biol Chem,* 271, 31075-85.

Vandenberghe, L. H. & Auricchio, A. 2012. Novel adeno-associated viral vectors for retinal gene therapy. *Gene Ther,* 19, 162-8.

Vasireddy, V., C. Vijayasarathy, J. Huang, X.F. Wang, M.M. Jablonski, H.R. Petty, P.A. Sieving, and R. Ayyagari. 2005. Stargardt-like macular dystrophy protein ELOVL4 exerts a dominant negative effect by recruiting wild-type protein into aggresomes. *Molecular vision.* 11:665-676.

Vasireddy, V., V.R. Chavali, V.T. Joseph, R. Kadam, J.H. Lin, J.A. Jamison, U.B. Kompella, G.B. Reddy, and R. Ayyagari. 2011. Rescue of photoreceptor degeneration by curcumin in transgenic rats with P23H rhodopsin mutation. *PLoS One.* 6:e21193.

Vihtelic, T.S., C.J. Doro, and D.R. Hyde. 1999. Cloning and characterization of six zebrafish photoreceptor opsin cDNAs and immunolocalization of their corresponding proteins. *Vis Neurosci.* 16:571-585.

Vithana, E. N., Abu-Safieh, L., Allen, M. J., Carey, A., Papaioannou, M., Chakarova, C., Al-Maghtheh, M., Ebenezer, N. D., Willis, C., Moore, A. T., Bird, A. C., Hunt, D. M. & Bhattacharya, S. S. 2001. A human homolog of yeast pre-mRNA splicing gene, PRP31,

underlies autosomal dominant retinitis pigmentosa on chromosome 19q13.4 (RP11). *Mol Cell,* 8, 375-81.

Vogen, S., T. Gidalevitz, C. Biswas, B.B. Simen, E. Stein, F. Gulmen, and Y. Argon. 2002. Radicicol-sensitive peptide binding to the N-terminal portion of GRP94. *J Biol Chem.* 277:40742-40750.

Wada, Y., Abe, T., Takeshita, T., Sato, H., Yanashima, K. & Tamai, M. 2001. Mutation of human retinal fascin gene (FSCN2) causes autosomal dominant retinitis pigmentosa. *Invest Ophthalmol Vis Sci,* 42, 2395-400.

Wada, Y., Sandberg, M. A., McGee, T. L., Stillberger, M. A., Berson, E. L. & Dryja, T. P. 2005. Screen of the IMPDH1 gene among patients with dominant retinitis pigmentosa and clinical features associated with the most common mutation, Asp226Asn. *Invest Ophthalmol Vis Sci,* 46, 1735-41.

Walsh, N., D. van Driel, D. Lee, and J. Stone. 2004. Multiple vulnerability of photoreceptors to mesopic ambient light in the P23H transgenic rat. *Brain Res.* 1013:194-203.

Wang, F., Rendahl, K. G., Manning, W. C., Quiroz, D., Coyne, M. & Miller, S. S. 2003. AAV-mediated expression of vascular endothelial growth factor induces choroidal neovascularization in rat. *Invest Ophthalmol Vis Sci,* 44, 781-90.

Wang, X. T., Mion, B., Aherne, A. & Engel, P. C. 2011. Molecular recruitment as a basis for negative dominant inheritance? propagation of misfolding in oligomers of IMPDH1, the mutated enzyme in the RP10 form of retinitis pigmentosa. *Biochim Biophys Acta,* 1812, 1472-6.

Wang, K. K. 2000a. Calpain and caspase: can you tell the difference? *Trends Neurosci,* 23, 20-6.

Wang, K. K. 2000b. Calpain and caspase: can you tell the difference?, by kevin K.W. WangVol. 23, pp. 20-26. *Trends Neurosci,* 23, 59.

Wang, Y. L., Hui, Y. N., Guo, B. & Ma, J. X. 2007. Strengthening tight junctions of retinal microvascular endothelial cells by pericytes under normoxia and hypoxia involving angiopoietin-1 signal way. *Eye (Lond),* 21, 1501-10.

Wassenberg, J.J., R.C. Reed, and C.V. Nicchitta. 2000. Ligand interactions in the adenosine nucleotide-binding domain of the Hsp90 chaperone, GRP94. II. Ligand-mediated activation of GRP94 molecular chaperone and peptide binding activity. *J Biol Chem.* 275:22806-22814.

Watanabe, S., Sanuki, R., Ueno, S., Koyasu, T., Hasegawa, T. & Furukawa, T. 2013. Tropisms of AAV for subretinal delivery to the neonatal mouse retina and its application for *in vivo* rescue of developmental photoreceptor disorders. *PLoS One,* 8, e54146.

Waza, M., Adachi, H., Katsuno, M., Minamiyama, M., Sang, C., Tanaka, F., Inukai, A., Doyu, M. & Sobue, G. 2005. 17-AAG, an Hsp90 inhibitor, ameliorates polyglutamine-mediated motor neuron degeneration. *Nat Med,* 11, 1088-95.

Wenzel, A., Grimm, C., Samardzija, M. & Reme, C. E. 2005. Molecular mechanisms of light-induced photoreceptor apoptosis and neuroprotection for retinal degeneration. *Prog Retin Eye Res,* 24, 275-306.

Wightman, B., Ha, I. & Ruvkun, G. 1993. Posttranscriptional regulation of the heterochronic gene lin-14 by lin-4 mediates temporal pattern formation in C. elegans. *Cell,* 75, 855-62.

Willis, C. L., Leach, L., Clarke, G. J., Nolan, C. C. & Ray, D. E. 2004. Reversible disruption of tight junction complexes in the rat blood-brain barrier, following transitory focal astrocyte loss. *Glia,* 48, 1-13.

Wong, V. & Gumbiner, B. M. 1997. A synthetic peptide corresponding to the extracellular domain of occludin perturbs the tight junction permeability barrier. *J Cell Biol,* 136, 399-409.

Wood, D. E., Thomas, A., Devi, L. A., Berman, Y., Beavis, R. C., Reed, J. C. & Newcomb, E. W. 1998. Bax cleavage is mediated by calpain during drug-induced apoptosis. *Oncogene,* 17, 1069-78.

Workman, P. 2002. Challenges of PK/PD measurements in modern drug development. *Eur J Cancer,* 38, 2189-93.

Wu, J., Gorman, A., Zhou, X., Sandra, C. & Chen, E. 2002. Involvement of caspase-3 in photoreceptor cell apoptosis induced by *in vivo* blue light exposure. *Invest Ophthalmol Vis Sci,* 43, 3349-54.

Wu, T. H., Ting, T. D., Okajima, T. I., Pepperberg, D. R., Ho, Y. K., Ripps, H. & Naash, M. I. 1998. Opsin localization and rhodopsin photochemistry in a transgenic mouse model of retinitis pigmentosa. *Neuroscience,* 87, 709-17.

Xiao, M. & Hendrickson, A. 2000. Spatial and temporal expression of short, long/medium, or both opsins in human fetal cones. *J Comp Neurol,* 425, 545-59.

Xu, D., Cobb, G., Spellicy, C. J., Bowne, S. J., Daiger, S. P. & Hedstrom, L. 2008. Retinal isoforms of inosine 5'-monophosphate dehydrogenase type 1 are poor nucleic acid binding proteins. *Arch Biochem Biophys,* 472, 100-4.

Yamaguchi, H., and H.G. Wang. 2004. CHOP is involved in endoplasmic reticulum stress-induced apoptosis by enhancing DR5 expression in human carcinoma cells. *J Biol Chem.* 279:45495-45502.

Yamamoto, K., H. Ichijo, and S.J. Korsmeyer. 1999. BCL-2 is phosphorylated and inactivated by an ASK1/Jun N-terminal protein kinase pathway normally activated at G(2)/M. *Mol Cell Biol.* 19:8469-8478.

Yamashima, T. 2004. Ca2+-dependent proteases in ischemic neuronal death: a conserved 'calpain-cathepsin cascade' from nematodes to primates. *Cell Calcium,* 36, 285-93.

Yang, D., Buchholz, F., Huang, Z., Goga, A., Chen, C. Y., Brodsky, F. M. & Bishop, J. M. 2002a. Short RNA duplexes produced by hydrolysis with Escherichia coli RNase III mediate effective RNA interference in mammalian cells. *Proc Natl Acad Sci U S A,* 99, 9942-7.

Yang, G. S., Schmidt, M., Yan, Z., Lindbloom, J. D., Harding, T. C., Donahue, B. A., Engelhardt, J. F., Kotin, R. & Davidson, B. L. 2002b. Virus-mediated transduction of murine retina with adeno-associated virus: effects of viral capsid and genome size. *J Virol,* 76, 7651-60.

Yang, L.P., L.M. Wu, X.J. Guo, and M.O. Tso. 2007. Activation of endoplasmic reticulum stress in degenerating photoreceptors of the rd1 mouse. *Investigative ophthalmology & visual science.* 48:5191-5198.

Yang, Q., Y.S. Kim, Y. Lin, J. Lewis, L. Neckers, and Z.G. Liu. 2006. Tumour necrosis factor receptor 1 mediates endoplasmic reticulum stress-induced activation of the MAP kinase JNK. *EMBO reports.* 7:622-627.

Ye, H., Cande, C., Stephanou, N. C., Jiang, S., Gurbuxani, S., Larochette, N., Daugas, E., Garrido, C., Kroemer, G. & Wu, H. 2002. DNA binding is required for the apoptogenic action of apoptosis inducing factor. *Nat Struct Biol,* 9, 680-4.

Yi, R., Doehle, B. P., Qin, Y., Macara, I. G. & Cullen, B. R. 2005. Overexpression of exportin 5 enhances RNA interference mediated by short hairpin RNAs and microRNAs. *RNA,* 11, 220-6.

Ying, W., Du, Z., Sun, L., Foley, K. P., Proia, D. A., Blackman, R. K., Zhou, D., Inoue, T., Tatsuta, N., Sang, J., Ye, S., Acquaviva, J., Ogawa, L. S., Wada, Y., Barsoum, J. & Koya, K. 2012. Ganetespib, a unique triazolone-containing Hsp90 inhibitor, exhibits potent antitumor activity and a superior safety profile for cancer therapy. *Mol Cancer Ther,* 11, 475-84.

Yoneda, T., K. Imaizumi, K. Oono, D. Yui, F. Gomi, T. Katayama, and M. Tohyama. 2001. Activation of caspase-12, an endoplastic reticulum (ER) resident caspase, through tumor necrosis factor receptor-associated factor 2-dependent mechanism in response to the ER stress. *J Biol Chem.* 276:13935-13940.

Yoshida, H., K. Haze, H. Yanagi, T. Yura, and K. Mori. 1998. Identification of the cis-acting endoplasmic reticulum stress response element responsible for transcriptional induction of mammalian glucose-regulated proteins. Involvement of basic leucine zipper transcription factors. *J Biol Chem.* 273:33741-33749.

Yoshida, H., T. Matsui, A. Yamamoto, T. Okada, and K. Mori. 2001. Xbp1 mRNA is induced by ATF6 and spliced by IRE1 in response to ER stress to produce a highly active transcription factor. *Cell.* 107:881-891.

Yoshida, H., T. Matsui, N. Hosokawa, R.J. Kaufman, K. Nagata, and K. Mori. 2003. A time-dependent phase shift in the mammalian unfolded protein response. *Dev Cell.* 4:265-271.

Yoshida, M., Yamamoto, N., Nitta, T., Uehara, T., Terao, R., Hatano, E., Iimuro, Y. & Yamaoka, Y. 2002. Suppression of proliferative cholangitis by E2F decoy oligodeoxynucleotide. *J Surg Res,* 102, 95-101.

Yoshizawa, T., Hattori, Y., Hakoshima, M., Koga, K. & Maitani, Y. 2008. Folate-linked lipid-based nanoparticles for synthetic siRNA delivery in KB tumor xenografts. *Eur J Pharm Biopharm,* 70, 718-25.

Youle, R. J. & Strasser, A. 2008. The BCL-2 protein family: opposing activities that mediate cell death. *Nat Rev Mol Cell Biol,* 9, 47-59.

Young, J. C., Agashe, V. R., Siegers, K. & Hartl, F. U. 2004. Pathways of chaperone-mediated protein folding in the cytosol. *Nat Rev Mol Cell Biol,* 5, 781-91.

Yu, D.Y., S. Cringle, K. Valter, N. Walsh, D. Lee, and J. Stone. 2004. Photoreceptor death, trophic factor expression, retinal oxygen status, and photoreceptor function in the P23H rat. *Investigative ophthalmology & visual science*. 45:2013-2019.

Yu, S. W., Wang, H., Poitras, M. F., Coombs, C., Bowers, W. J., Federoff, H. J., Poirier, G. G., Dawson, T. M. & Dawson, V. L. 2002. Mediation of poly(ADP-ribose) polymerase-1-dependent cell death by apoptosis-inducing factor. *Science,* 297, 259-63.

Yuan, X., Naguib, S. & Wu, Z. 2011. Recent advances of siRNA delivery by nanoparticles. *Expert Opin Drug Deliv,* 8, 521-36.

Zamore, P. D., Tuschl, T., Sharp, P. A. & Bartel, D. P. 2000. RNAi: double-stranded RNA directs the ATP-dependent cleavage of mRNA at 21 to 23 nucleotide intervals. *Cell,* 101, 25-33.

Zeiss, C. J. 2003. The apoptosis-necrosis continuum: insights from genetically altered mice. *Vet Pathol,* 40, 481-95.

Zeiss, C. J., Neal, J. & Johnson, E. A. 2004. Caspase-3 in postnatal retinal development and degeneration. *Invest Ophthalmol Vis Sci,* 45, 964-70.

Zeviani, M., Moraes, C. T., DiMauro, S., Nakase, H., Bonilla, E., Schon, E. A. & Rowland, L. P. 1988. Deletions of mitochondrial DNA in Kearns-Sayre syndrome. *Neurology,* 38, 1339-46.

Zhang, H., Kolb, F. A., Brondani, V., Billy, E. & Filipowicz, W. 2002. Human Dicer preferentially cleaves dsRNAs at their termini without a requirement for ATP. *EMBO J,* 21, 5875-85.

Zhong, Y., Enomoto, K., Tobioka, H., Konishi, Y., Satoh, M. & Mori, M. 1994. Sequential decrease in tight junctions as revealed by 7H6 tight junction-associated protein during rat hepatocarcinogenesis. *Jpn J Cancer Res,* 85, 351-6.

Zhu, L., Jang, G. F., Jastrzebska, B., Filipek, S., Pearce-Kelling, S. E., Aguirre, G. D., Stenkamp, R. E., Acland, G. M. & Palczewski, K. 2004. A naturally occurring mutation of the opsin gene (T4R) in dogs affects glycosylation and stability of the G protein-coupled receptor. *J Biol Chem,* 279, 53828-39.

Zolotukhin, S. 2005. Production of recombinant adeno-associated virus vectors. *Hum Gene Ther,* 16, 551-7.

An experimental platform for systemic drug delivery to the retina

Matthew Campbell[a,1], Anh T. H. Nguyen[a], Anna-Sophia Kiang[a], Lawrence C. S. Tam[a], Oliviero L. Gobbo[b], Christian Kerskens[c], Sorcha Ni Dhubhghaill[a], Marian M. Humphries[a], G.-Jane Farrar[a], Paul F. Kenna[a], and Peter Humphries[a]

[a]Ocular Genetics Unit, Department of Genetics, [b]School of Pharmacy and Pharmaceutical Sciences, and [c]Trinity College Institute of Neuroscience, Trinity College Dublin, Dublin 2, Ireland

Edited by John E. Dowling, Harvard University, Cambridge, MA, and approved September 2, 2009 (received for review July 29, 2009)

Degenerative retinopathies, including age-related macular degeneration, diabetic retinopathy, and hereditary retinal disorders—major causes of world blindness—are potentially treatable by using low-molecular weight neuroprotective, antiapoptotic, or antineovascular drugs. These agents are, however, not in current systemic use owing to, among other factors, their inability to passively diffuse across the microvasculature of the retina because of the presence of the inner blood–retina barrier (iBRB). Moreover, preclinical assessment of the efficacies of new formulations in the treatment of such conditions is similarly compromised. We describe here an experimental process for RNAi-mediated, size-selective, transient, and reversible modulation of the iBRB in mice to molecules up to 800 Da by suppression of transcripts encoding claudin-5, a protein component of the tight junctions of the inner retinal vasculature. MRI produced no evidence indicative of brain or retinal edema, and the process resulted in minimal disturbance of global transcriptional patterns analyzed in neuronal tissue. We show that visual function can be improved in IMPDH1$^{-/-}$ mice, a model of autosomal recessive retinitis pigmentosa, and that the rate of photoreceptor cell death can be reduced in a model of light-induced retinal degeneration by systemic drug delivery after reversible barrier opening. These findings provide a platform for high-throughput drug screening in models of retinal degeneration, and they ultimately could result in the development of a novel "humanized" approach to therapy for conditions with little or no current forms of treatment.

blood–retina barrier | retinitis pigmentosa | RNAi | tight junctions | claudin-5

In transducing photons into electrical energy, the retina has the highest oxygen consumption per weight of any tissue in the human body (1). This, combined with a delicacy characteristic of all neuronal tissues, underlines a requirement for a unique and abundant blood supply capable of sustaining the retina's energy demands while at the same time possessing efficient barriers, excluding potentially harmful bloodborne agents such as pathogens, antibodies, immune cells, and anaphylatoxins (2). There are two sources of blood supply to the retina: the central retinal artery, entering the retina at the optic disc, the arterioles of which terminate in both the inner plexiform layer and outer plexiform layer (OPL) and are readily visualized in images of the retinal surface, and the underlying choroidal circulation, providing nutriment primarily to the outermost layer of the retina, the photoreceptors (3). This outer layer of the retina remains avascular. The retina has two highly evolved and efficient barriers that maintain retinal homeostasis: the inner and outer blood–retina barriers (iBRB and oBRB, respectively). The iBRB comprises retinal endothelial cells, which line retinal microvessels, allowing for the maintenance of blood vessel integrity, preserving vessel homeostasis and mediating highly selective transport of molecules to the surrounding neural tissue (4). The oBRB is made up of a single layer of retinal pigment epithelial (RPE) cells situated at the back of the eye that act as a selective filter to restrict the passage of macromolecules to the outer segments of the retina (5). It is now widely accepted that up to 98% of low-molecular weight drugs cannot passively diffuse across these barriers (6), in part because of the highly evolved "tight junctions" (TJs) formed between adjacent endothelial cells or RPE cells.

TJs are formed at the apical periphery of endothelial cells of the iBRB and RPE of the oBRB, and they perform the dual role of creating a primary barrier to the diffusion of solutes through the paracellular pathway while also maintaining cell polarity (7). TJs are complex and dynamic structures, composed of a series of integral and peripheral membrane proteins. The transmembrane proteins of the tight junction include occludin, junctional adhesion molecule, and claudins 1–24, proteins which extend into the paracellular space, creating the seal characteristic of the TJ (8). There are differences, however, in the molecular components of TJs of oBRBs and iBRBs, and in the context of the current study it is of note that claudin-5 is absent from the TJs of the oBRB in adult mice (9). Claudins have been shown previously to interact homotypically with proteins on adjacent endothelial cells (10) and, in particular, claudin-5 knockout mice have altered blood–brain barrier (BBB) integrity (11). Although removal of claudin-5 compromised BBB function by allowing it to become permeable to molecules of up to ≈800 Da, the barrier could still form, remaining intact and impervious to larger molecules, with fully formed TJs. These mice did, however, die within 10 h of birth, most likely because of the importance of claudin-5 in developmental processes. We have reported recently that levels of claudin-5 can be suppressed in adult mice by using an RNAi approach. Transient suppression of claudin-5 in the microvasculature of the brain causes a size-selective increase in passive diffusion of low-molecular weight molecules from the blood to the brain without any outward adverse detriment to such mice. Indeed, potentially pathological molecules far exceed the size-selectivity of barrier opening when claudin-5 is suppressed (12). Moreover, endogenous bloodborne molecules below 800 Da will be excluded from the brain and retina because of the presence of efflux transporters and specific receptors on the luminal surface of endothelial cells lining the microvasculature of the brain and retina (13).

Here, we report a preclinical and experimental platform technology allowing delivery of low-molecular weight therapeutics to the outer layers of the retina while excluding molecules greater than ≈1 kDa. RNAi-mediated suppression of claudin-5 in the retinas of adult mice causes a transient and size-selective increase in paracellular permeability of microvessels without the development of retinal edema or changes in retinal function as assayed by electrophysiology. Moreover, we demonstrate the therapeutic potential of this technique by enhancing the delivery of two distinct low-molecular weight molecules to the neural retina of two rodent models of retinopathy: IMPDH1$^{-/-}$ mice (14), a model of auto-

Author contributions: M.C., G.-J.F., and P.H. designed research; M.C., A.T.H.N., A.-S.K., O.L.G., S.N.D., M.M.H., and P.F.K. performed research; M.C., A.T.H.N., A.-S.K., L.C.S.T., O.L.G., C.K., M.M.H., P.F.K., and P.H. analyzed data; and M.C. and P.H. wrote the paper.

The authors declare no conflict of interest.

This article is a PNAS Direct Submission.

Freely available online through the PNAS open access option.

[1]To whom correspondence should be addressed. E-mail: matthew.campbell@tcd.ie.

This article contains supporting information online at www.pnas.org/cgi/content/full/0908561106/DCSupplemental.

GENETICS

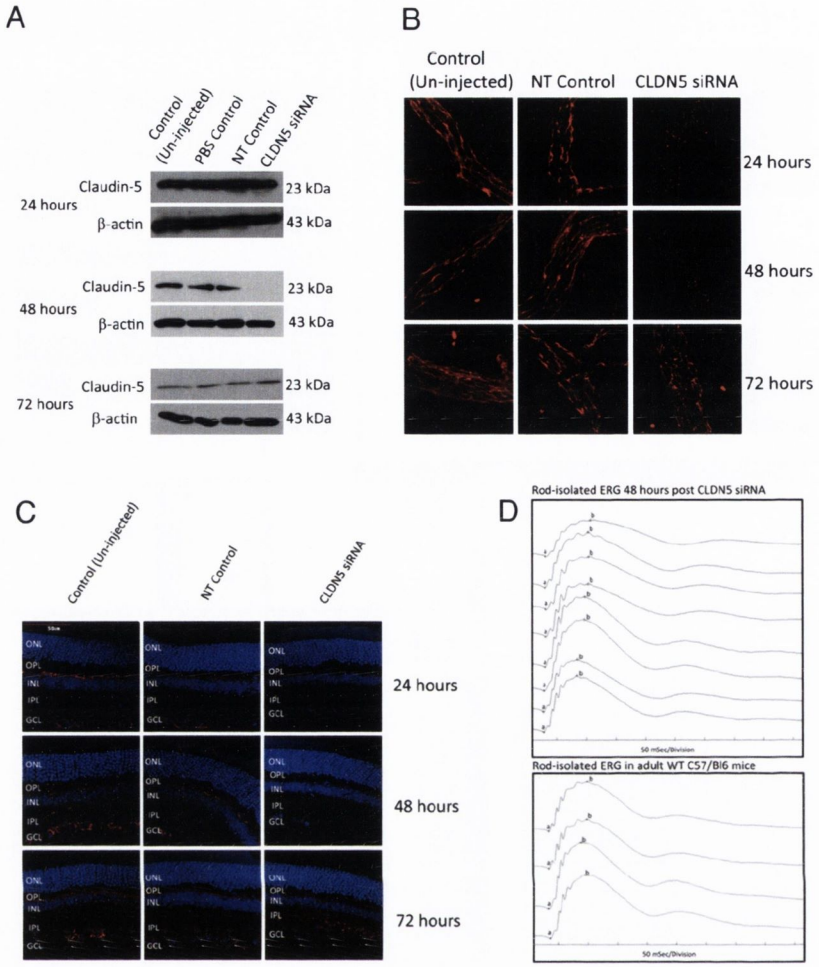

Fig. 1. Suppression of claudin-5 in retinal vasculature. (A) Western blot analysis of claudin-5 levels in the neural retinas of mice at 24, 48, and 72 h after injection of siRNA showed a significant decrease in levels 48 h after siRNA injection. **, P = 0.0011. Western blots are representative of three independent experiments. (B) Flatmount analysis of claudin-5 levels in the microvasculature of the neural retina showed decreased levels of expression and aberrant localization of claudin-5. At 24 and 48 h after injection of siRNA, the pattern of claudin-5 staining appeared diffuse and fragmented compared with the control groups. (40× objective.) (C) Claudin-5 expression was isolated to the retinal microvessels, processing as far as the OPL of the retina. At 24 and 48 h after injection of claudin-5 siRNA, levels of claudin-5 appeared mislocalized and fragmented. (40× objective.) (D) ERG analysis of adult C57/Bl6 mice revealed no distinct changes in ERG tracings 48 h after injection of claudin-5 siRNA, with mean ERG readings of 841 □V in each eye from four mice (Upper). This finding was in comparison to standard mean ERG readings of between 800 □V an 1 mV in uninjected mice (Lower).

somal recessive retinitis pigmentosa (RP) that lacks the key enzyme involved in the de novo synthesis of GTP (15), and a mouse model of light-induced retinal degeneration (16). These results highlight the safety and efficacy of selective iBRB modulation as an experimental tool for the systemic screening of a wide range of potentially therapeutic molecules in rodent models of retinopathies. Ultimately, a humanized approach involving localized inducible barrier opening could offer the potential to treat conditions where no therapeutic interventions are available, representing a unique example of combining gene therapy with a pharmacological approach to disease treatment.

Results

Suppression of Claudin-5 in the Retina. Levels of expression of claudin-5 were significantly decreased 48 h after injection of siRNA targeting claudin-5 compared with the uninjected control, PBS control, and nontargeting (NT) control siRNA-injected mice. Suppression was transient, with levels returning to those observed in the control groups after 72 h (Fig. 1*A* and Figs. S1–S3). After retinal flatmount analysis of claudin-5 levels after delivery of siRNA, claudin-5 localization in retinal microvessels was manifested as a discontinuous pattern of staining 24 and 48 h after injection of claudin-5 siRNA compared with the control groups (Fig. 1*B*). These findings were in contrast to the continuous and intense pattern of staining of claudin-5 in the control groups and, indeed, at the 72 h time point after injection of siRNA, levels of claudin-5 in the retina appeared similar to the control groups, highlighting the transient nature of suppression. Although by Western blot analysis, levels of expression of claudin-5 appeared unchanged 24 h after siRNA injection, the pattern of staining in retinal flatmounts was not evident. Therefore, protein expression by Western blot at 24 h after claudin-5 siRNA injection more than likely represents immunoreactive yet non-TJ-associated claudin-5. Immunohistochemical analysis of retinal cryosections showed claudin-5 expression in vessels up to and including the OPL, with levels decreased and mislocalized 24 and 48 h after injection of claudin-5 siRNA (Fig. 1*C*). Discontinuous and decreased expression of claudin-5 was not evident 72 h after injection. After suppression of claudin-5, electroretinographic (ERG) analysis of retinal function in mice 48 h after siRNA injection showed normal electrophysiological readouts in rod-isolated responses, with average readings of 841 □V in each eye for four mice compared with typical ERG readouts from adult C57/Bl6 mice that had not been exposed to experimental conditions (Fig. 1*D*).

Transient and Size-Selective iBRB Modulation. To assess the integrity of the iBRB after suppression of claudin-5, we used two distinct molecules that do not normally passively diffuse across the iBRB. Initially, by using MRI analysis, we observed no distinct changes in T2-weighted images (Fig. 2*A*), which would readily allow for imaging of ocular edema. T2-weighted imaging revealed no aberrancies in the ocular regions of mice from any experimental group. Moreover, when the contrasting agent gadolinium-diethylene triamine *N*,*N*,*N*′,*N*′,*N*′-pentaacetic acid (Gd-DTPA; 742 Da) was injected in mice, we observed large amounts of extravasation from microvessels in the retina. T1-weighted imaging after Gd-DTPA injection showed distinct contrasting in both eyes of mice 24 and 48 h after injection of claudin-5 siRNA (Fig. 2*B*). Such contrasting

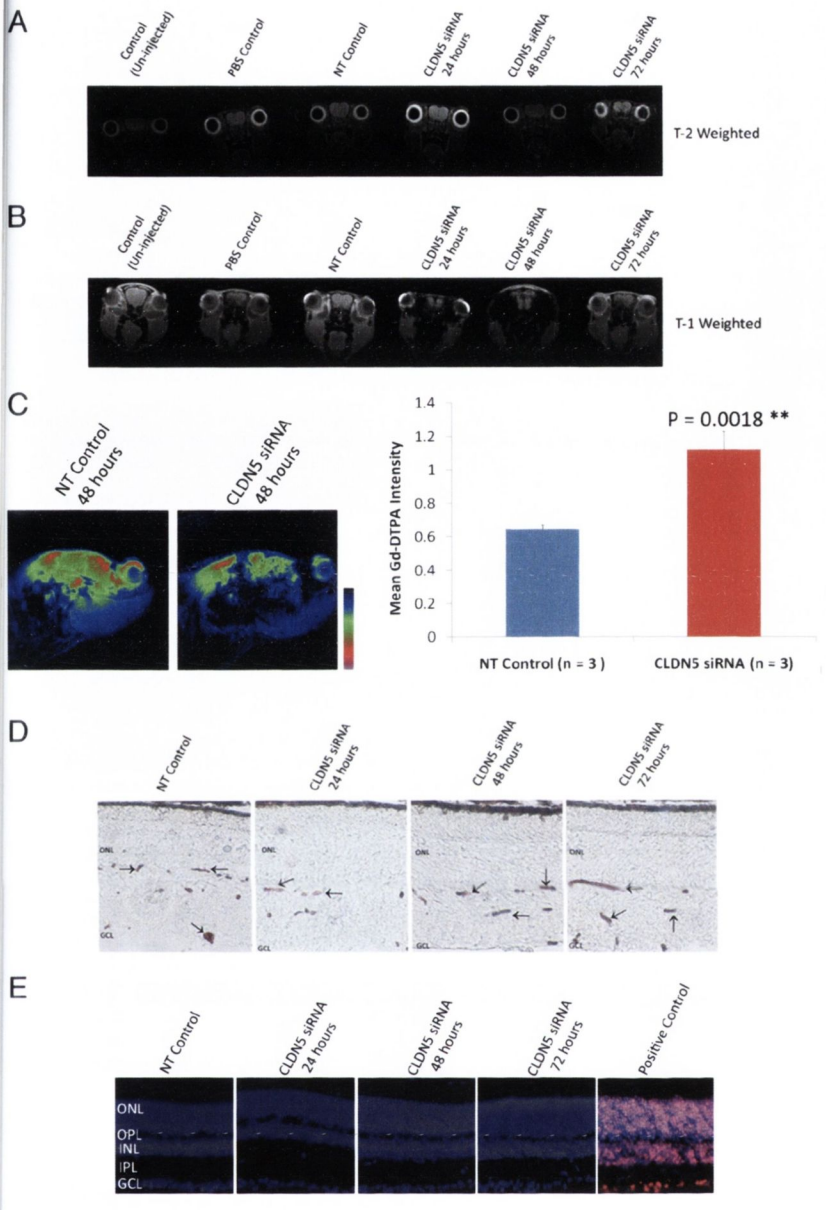

Fig. 2. Transient and size-selective modulation of iBRB function. (A) MRI with T2-weighted sequence (resolution, 0.141 × 0.141 × 5 □m^3; repetition and echo times (TR/TE, 4179.3/36 ms; alpha = 9°), which will allow for edema visualization, showed no signs of ocular edema in any experimental group of mice analyzed (three to five mice per group). All images are in a coronal orientation. (B) After injection of the contrast agent Gd-DTPA (742 Da), however, intense contrasting was observed both 24 and 48 h after injection of claudin-5 siRNA when observed with T1-weighted imaging (resolution, 0.156 × 0.156 × 5 mm^3; field of view, 20 × 20 × 17.9 mm^3; matrix = 128 × 128 × 30; TR/TE, 500/2.7 ms; flip angle, 30°; number of averages, 3; acquisition time, 2 min 24 sec; repetitions, 10). This contrasting manifested as intense dark contrasting in the ocular region of the mouse. All images are in a coronal orientation. (C) After analysis of mice in a sagittal orientation, it was clear that extravasation of Gd-DTPA was occurring in large quantities. Enhanced signals, pseudocolored in red and green, showed highly significant levels of Gd-DTPA in mice 48 h after injection of claudin-5 siRNA compared with NT control mice. **, P = 0.0018. (D) Postexperimental treatments. Mice were perfused at 24, 48, and 72 h after injection with 5 □L/g body weight of 25 mg/mL microperoxidase. Microperoxidase was subsequently visualized (dark brown/red staining indicated by arrows) in retinal cryosections to be localized within the microvessels of all experimental groups (n = 5 mice per group). GCL indicates ganglion cell layer. (40× objective.) (E) Levels of retinal cell death were assayed by TUNEL staining (red staining in positive control). None of the experimental groups showed signs of retinal cell death at any time point after injection of siRNA. Nuclei were counterstained with DAPI. INL indicates inner nuclear layer; IPL, inner plexiform layer. (40× objective.)

was not observed in the control groups of mice, nor was it observed at the 72-h time point after injection of claudin-5 siRNA. Gd-DTPA has a molecular mass of 742 Da and will not freely passively diffuse across microvessels into the retina in homeostatic circumstances. In a sagittal perspective, levels of Gd-DTPA were observed to infiltrate the retina in large quantities at the 48-h time point after siRNA injection compared with NT siRNA control mouse, with densitometric analysis of mice showing significantly increased levels of contrasting agent in the eyes of mice 48 h after injection of claudin-5 siRNA (P = 0.0018; Fig. 2*C*, double asterisk).

The size-selective nature of transient modulation of the iBRB was readily observable when a molecule of ≈1,900 Da was perfused in mice after clauidn-5 siRNA injection. Microperoxidase (molecular mass, 1,881 Da) was detected in the microvessels of the retinas of all mice after all experimental treatments. In conditions where the iBRB or BBB is damaged, microperoxidase will extravasate in vast quantities, yet this was not the case when claudin-5 was suppressed (Fig. 2*D*). Size-selective barrier opening observed, as well as being a transient process, did not appear to cause any neuronal cell death in any layer of the retina of mice after analysis of DNA fragmentation in retinal layers after siRNA delivery (Fig. 2*E*).

Enhanced Delivery of GTP to the Retinas of IMPDH1$^{-/-}$ Mice. Given our observations of maximum suppression of claudin-5 levels 48 h after injection of siRNA, this was chosen as the optimum time point at which to assess efficacy of therapeutic systemic delivery of compounds to the retina. IMPDH1$^{-/-}$ mice lack the rate-limiting enzyme for the de novo synthesis of GTP, a central mediator of visual phototransduction. With increasing age, these mice develop a mild retinopathy, as evidenced by decreases in electrophysiological readout from the retina in tandem with a thinning of the photoreceptor outer nuclear layer (ONL) in animals older than 10 months (14). GTP has a molecular mass of 523 Da and will not freely passively diffuse across the iBRB if injected systemically. Indeed, we have previously attempted to inject GTP intraocularly to induce increases in ERG in IMPDH1$^{-/-}$ mice (= 4), but without success (Fig. 3*A*). At 48 h after injection of siRNA, levels of claudin-5 were significantly decreased in IMPDH1$^{-/-}$ mice (Fig. 3*B*). Suppression was manifested by a distinct change in the pattern of staining observed in retinal cryosections compared with mice receiving NT siRNA (Fig. 3*C*). Before experimentation, retinal function of all IMPDH1$^{-/-}$ mice was assessed by ERG, and 48 h

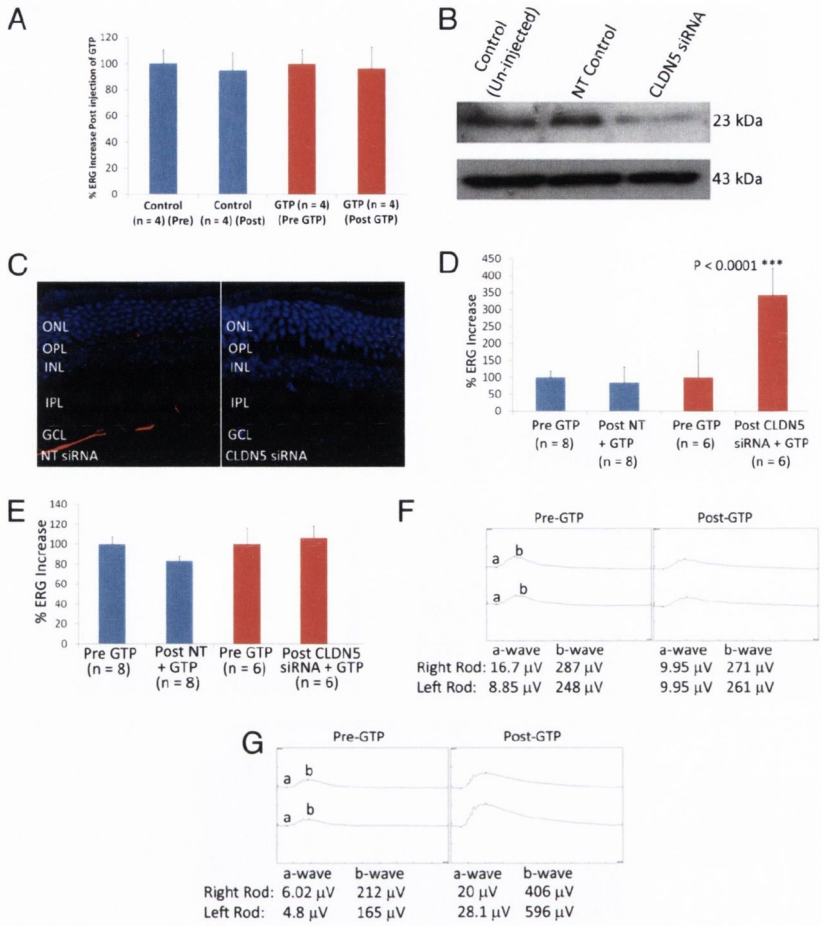

Fig. 3. Enhanced delivery of GTP to retinas of IMPDH1$^{-/-}$ mice. (A) After analysis of ERG readout in IMPDH1$^{-/-}$ mice, animals were injected with a 3- L solution containing 0.6 mg of GTP. Mice were again analyzed by ERG, and the percentage change in electrical readout from the retina was plotted. There was no significant difference in ERG readouts in IMPDH1$^{-/-}$ mice after intraocular injection of GTP (n = 4 mice per group). (B) Levels of expression of claudin-5 in the retinas of IMPDH1$^{-/-}$ mice were assessed by Western blotting, with levels decreased 48 h after injection of claudin-5 siRNA. (C) From immunohistochemical analysis of claudin-5 levels (red staining) in retinal cryosections, it was clear that levels were decreased in all retinal layers. Sections were counterstained with DAPI (blue staining). (40× objective.) (D) IMPDH1$^{-/-}$ mice were subjected to ERG analysis of rod function, and 48 h after injection of either an NT or claudin-5 siRNA, mice were administered an injection of GTP, and ERG readout was assessed again. Electrical readout of rod photoreceptors was expressed as percentage changes, and a significant increase (***, $P < 0.0001$) in rod-isolated ERG was observed in mice receiving claudin-5 siRNA and 3.3 mg of GTP compared with mice receiving NT siRNA and 3.3 mg of GTP. (E) No change in retinal cone function was observed after injection of GTP in either experimental group. (F) Rod-isolated ERG tracings in IMPDH1$^{-/-}$ mice before and after injection of GTP with NT siRNA showed no distinct changes in waveform; however, upon analysis of ERG tracings before and after GTP injection with claudin-5 siRNA, well-formed a and b waves were observed in the retinas of mice.

before injection of GTP, mice were injected with either an NT or claudin-5-targeting siRNA. Subsequently, after injection of GTP i.p., retinal function was assessed immediately by ERG, and a highly significant increase in rod-isolated b-wave amplitude was observed in those mice that had received claudin-5 siRNA (= 6) compared with the NT control (= 8) group (Fig. 3*D*). Analysis of cone-isolated ERG after enhanced delivery of GTP did not show any significant differences between the experimental groups (Fig. 3*E*). ERG tracings revealed well-formed a and b waves in mice after enhanced systemic delivery of GTP to the retina (Fig. 3*G*), in contrast to mice receiving no iBRB modulation (Fig. 3*F*), where no change in ERG output was observed.

Enhanced Delivery of ALLM to the Retinas of Light-Exposed BalB/c Mice. Light-induced retinopathy in albino BalB/c mice has been used previously to induce photoreceptor cell apoptosis. Indeed, many antiapoptotic agents have been screened in vivo by using this technique but by direct intraocular injection of these agents before light ablation (17). Ca^{2+} activated calpains have been shown to be associated with neuronal cell death in different neuropathological diseases, including retinopathy (18). Calpains are often associated with necrotic cell death; however, they are also found to be activated during apoptosis (19). We chose to assay the effects of enhanced systemic delivery of a known calpain inhibitor, *N*-acetyl-Leu-Leu-Met-CHO (ALLM). This molecule has a molecular mass of 401 Da and is a potent inhibitor of both calpain I (K_i = 120 nM), calpain II (K_i = 230 nM), cathepsin-L (K_i = 0.6 nM), cathepsin-B (K_i = 100 nM), and the proteasome (20). It does not readily passively diffuse across the iBRB and has been used previously to demonstrate efficacy in preventing photoreceptor apoptosis when intraocularly injected (17). Forty-eight hours before injection of ALLM (20 mg/kg), mice received an injection of either an NT siRNA or a claudin-5 siRNA. Mice were dark-adapted for a further 24 h after injection of ALLM, after which time they were exposed to 6,000-lux white light for 2 h. Mice were returned to the dark room, and 12, 24, and 48 h after light ablation, photoreceptor nuclei were analyzed for TUNEL for identification of end-stage dying cells. With enhanced systemic delivery of ALLM, at 12 h (P = 0.0011; Fig. 4*A*, **) and 24 h (P = 0.0252; Fig. 4*B*, *) after light exposure, the retinas of BalB/c mice showed significantly fewer TUNEL-positive cells in the ONL of the retina, directly implying less photoreceptor cell death. ALLM slows the rate of cell death, because 48 h after light exposure (Fig. 4*C*), the number of TUNEL-positive cells increased in the group of mice receiving ALLM subsequent to claudin-5 siRNA (*, P = 0.0191). Mice analyzed at 4 days and 7 days after light ablation showed no differences in TUNEL-positive cells in the ONL (Fig. S4).

Discussion

Although degenerative retinopathies, including age-related macular degeneration (AMD), diabetic retinopathy, and RP represent major causes of world blindness, treatment options are currently exceedingly limited (15, 21–24). No form of prevention is available for the nonexudative (dry) form of AMD, apart from dietary intervention. With regard to the exudative (wet) form of AMD, intraocular injection of the monoclonal antibody Lucentis (Genentech Inc), targeting VEGF, is being used in a growing number of cases; however, severe endophthalmitis, resulting in blindness, has been reported to occur in up to 2% of treated patients (25). Proliferative diabetic retinopathy is treatable by scatter and focal laser surgery, but the procedure itself induces significant retinal damage and can involve in excess of 1,000 laser burns to the retinas of diseased

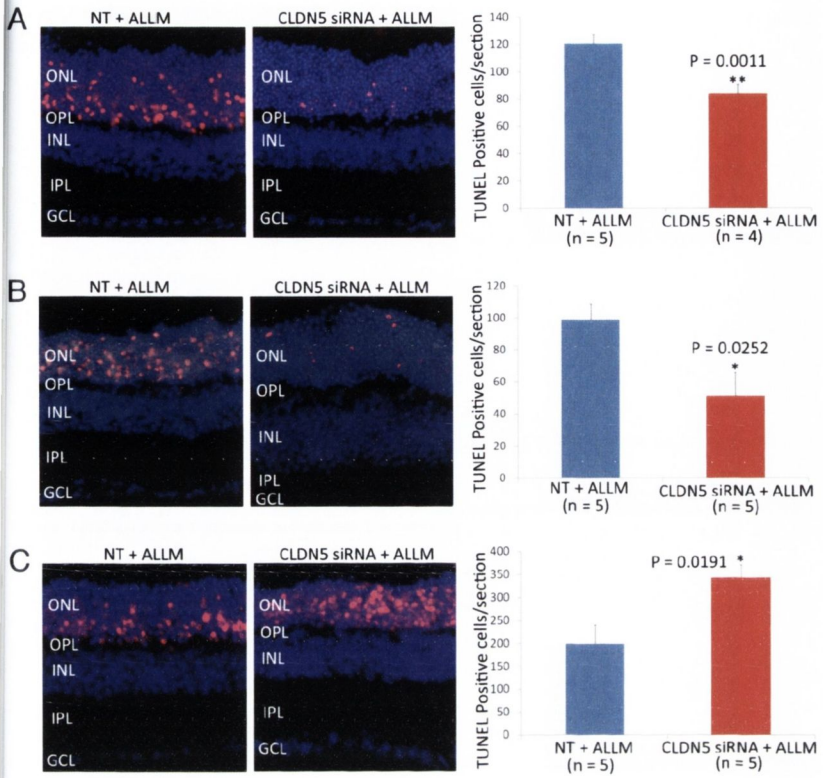

Fig. 4. Enhanced delivery of a calpain inhibitor to retinas of light-exposed BalB/c mice. Effects of either an NT or claudin-5 siRNA together with a potent calpain inhibitor, ALLM, on light-induced retinal degeneration were assessed in BalB/c mice. Claudin-5 or NT siRNA was administered to BALB/c mice 48 h before injection of 20 mg/kg ALLM. Mice were dark-adapted for 24 h before being exposed to white fluorescent light of 7,900 lux for 2 h. (A) At 12 h after light ablation, TUNEL-positive nuclei present in the ONL of retinal sections of mice injected with claudin-5 siRNA and ALLM were significantly fewer than those injected with NT siRNA. **, P = 0.0011. (B) At 24 h after light ablation, the number of TUNEL-positive cells in mice that received claudin-5 siRNA and ALLM was significantly decreased compared with mice receiving NT siRNA and ALLM. *, P = 0.0252. (C) There were significantly more TUNEL-positive nuclei in retinas of claudin-5 siRNA- and ALLM-injected mice compared with NT siRNA- and ALLM-injected mice at 48 h after light exposure. *, P = 0.0191. (40× objective.)

patients (26). No form of preventive therapy is yet available for RP, and the immense genetic heterogeneity encountered in this condition is clearly a substantial impediment to the development of gene-based methods of disease prevention (27). On the other hand, many low-molecular weight, potentially therapeutic compounds, including VEGF (28), GPR91 (29), and C3a/C5a anaphylatoxin receptor antagonists (30), as well as many neuroprotective and antiapoptotic drugs, could potentially preserve retinal function or slow photoreceptor cell death in such conditions, yet regular intraocular injection of such compounds is not a feasible strategy for the reasons outlined above. Moreover, systemic administration of such drugs is restricted in view of the very low rates of passive diffusion of these compounds into the retina across the iBRB (31).

We report an experimental, RNAi-mediated approach for transient modulation of iBRB function by targeting the TJ component claudin-5. Claudin-5 plays a role in the formation of paracellular pores or channels that function in mediating selective ion permeability (11, 32). However, the function of claudin-5 in the retina appears to be more dynamic than simply structural. It has recently been reported that mice exposed to hypoxic conditions exhibit down-regulation of claudin-5, which size-selectively disrupts the iBRB, allowing passage of small molecules into the retina, similar to the phenotype seen in claudin-5-deficient mice (33). Moreover, levels of claudin-5 in the brain appear to fluctuate depending on environmental stimuli, such as exposure to alcohol, traumatic brain injury, and stroke (34–36).

To explore the therapeutic potential of transient compromise in barrier integrity, we sought to deliver therapeutic molecules to the retinas of two mouse models of retinopathy. First, we chose a model of autosomal recessive RP, the IMPDH1$^{-/-}$ mouse (14). These animals lack one of the two rate-limiting enzymes of de novo synthesis of GTP, a central mediator of visual phototransduction (15). With increasing age, these mice develop a mild retinopathy, as evidenced by decreases in electrophysiological readout from the retina in tandem with a thinning of the photoreceptor ONL in animals older than 10 months. GTP has a molecular mass of 523 Da, and direct intraocular injection (Fig. 3*A*) did not have an impact on ERG function in these mice because of a low rate of diffusion of the compound across the iBRB and limited diffusion across intact cell layers of the inner retina. However, when levels of claudin-5 were suppressed, enhanced systemic delivery of GTP to the outer layers of the retina resulted in a significant increase in the rod-isolated ERG response from IMPDH1$^{-/-}$ mice in comparison with those receiving NT siRNA compared with a pre-GTP ERG. ERG readings of up to 600 μV were observed (Fig. 3*G*). Taking into consideration that a standard ERG readout is between 800 and 1,000 μV, these findings represent significant advances in visual enhancement in these mice. GTP is likely being actively transported into photoreceptors after enhanced systemic delivery; however, it is also feasible to postulate that GTP may passively diffuse across the plasma membranes of photoreceptors, and enhanced delivery will simply allow for increased quantities of GTP to access the neural retina before being rapidly hydrolyzed.

Second, we explored the efficacy of enhanced delivery of an antiapoptotic agent to the retinas of mice before light-induced ablation of photoreceptors. Albino BalB/c mice exposed to varying degrees of intense white light are very susceptible to photoreceptor cell death, due in part to activation of calpains in photoreceptors of the retina (37). To study the effects of increased delivery of ALLM on photoreceptor cell survival, we injected 20 mg/kg of the inhibitor intraperitoneal 24 h before light exposure with and without iBRB modulation. TUNEL staining became apparent 12 h after the initial exposure to light; however, significantly less cell death was observed in the group of mice that received ALLM when the iBRB was modulated with claudin-5 siRNA compared with NT siRNA. ALLM has a molecular mass of 401 Da and will have a low rate of diffusion across the iBRB. Indeed, photoreceptor cell death did not manifest in the claudin-5 siRNA-injected mice until 48 h after light exposure. These findings display enhanced delivery of ALLM to the retina and also highlight the influence increased delivery of this calpain inhibitor has on the rate of photoreceptor cell death.

As a method of enhanced delivery of low-molecular weight therapeutics to the retina, RNAi-mediated suppression of claudin-5

can now be used in animal models of retinopathy to screen a wide range of potentially therapeutic molecules ranging from antiapoptotic agents to antiangiogenic compounds. Not only does suppression of claudin-5 have little impact on neuronal homeostasis, we have also shown minimal disturbance of global transcriptional patterns in neuronal tissue when the BBB is transiently modulated (Tables S1 and S2). This indicates that rather than "breaking" the BBB and iBRB, targeted suppression of claudin-5 selectively modulates barrier function while not causing neuroinflammatory activation, edema, or cell death. Indeed, coupled with commercially available reagents, such as

-jetPEI (Polyplus-transfection), regular barrier opening in experimental rodents could be used for longer-term studies pertaining to drug delivery. This, however, would not be the case in "humanizing" this delivery system, and for the purposes of systemic delivery of drugs targeting degenerative retinal conditions in humans, localized barrier opening could, in principle, be limited to retinal tissues by incorporating barrier-opening machinery into an inducible viral delivery system. In this regard, it is of note that adeno-associated virus (AAV) delivery systems have now been approved for use in a growing number of gene therapy trials, including those recently initiated for the congenital retinopathy Leber's congenital amaurosis (38–40), and recent studies have indicated that AAV9 is capable of targeting vascular endothelial cells, rendering the concept of an inducible AAV9 system for barrier opening potentially feasible (41).

Materials and Methods

Animal Experiments and Experimental Groups. All studies carried out in the Ocular Genetics Unit at Trinity College Dublin (TCD) adhere to the Association for Research in Vision and Ophthalmology statement for the use of Animals in Ophthalmic and Vision Research. Mice were sourced from Jackson Laboratories and bred on site at the Ocular Genetics Unit in TCD. Extensive Materials and Methods are outlined in SI Text.

In Vivo Delivery of siRNA to Retinal Capillary Endothelial Cells. Rapid high-pressure, high-volume tail vein injections were carried out essentially as successfully used previously at this laboratory (12, 42, 43).

Antibodies for Western blots were as follows: polyclonal rabbit anti-claudin-5 (1:500; Zymed Laboratories) and polyclonal rabbit anti- -actin (1:1,000; Abcam). Membranes were washed with Tris buffered saline (0.05 M Tris, 150 mM NaCl, pH 7.5) and incubated with a secondary anti-rabbit (IgG) antibody with HRP conjugates (1:2,500; Sigma–Aldrich), or with anti-mouse (IgG; 1:1,000; Sigma–Aldrich), for 3 h at room temperature. Immune complexes were detected by using ECL. All Western blot analyses were repeated a minimum of three times (n = 3 mice per treatment).

ERG Analysis of C57/Bl6 and IMPDH1$^{-/-}$ Mice. Extensive details are outlined in SI Text.

Assessment of iBRB Integrity by Perfusion of Tracer Molecules. After RNAi-mediated ablation of transcripts encoding claudin-5, microperoxidase [5 L/g body weight of 25 mg/mL microperoxidase (MP-11; 1,862 Da; Sigma–Aldrich] was perfused at 37 °C through the left ventricle of the beating heart of anesthetized mice 24, 48, and 72 h after hydrodynamic delivery of claudin-5 siRNA.

MRI. After injection of siRNA and by using appropriate controls, iBRB integrity to a molecule of 742 Da (Gd-DTPA) was assessed via MRI using a dedicated small rodent Bruker BioSpec 70/30 magnet system (i.e., 7-T field strength, 30-cm bore diameter) with an actively shielded USR magnet.

TUNEL Analysis. Data after TUNEL staining were expressed as mean TUNEL-positive cells per section ± SEM, as determined by an individual blinded to the treatment. Results were analyzed by using a two-tailed Student's t test, with $P < 0.05$ considered significant.

ACKNOWLEDGMENTS. We thank Caroline Woods, David Flynn, and Rebecca Robertson for animal husbandry. IMPDH1$^{-/-}$ mice were kindly donated by Dr. Beverly Mitchell. The Ocular Genetics Unit at TCD is supported by Science Foundation Ireland, The Wellcome Trust, European Vision Institute, EVI-Genoret Grant LSHG-CT-2005-512036, Fighting Blindness Ireland, and Enterprise Ireland.

1. Masland RH (2001) The fundamental plan of the retina. Nat Neurosci 4:877–886.
2. Gardiner TA, Archer DB, Curtis TM, Stitt AW (2007) Arteriolar involvement in the microvascular lesions of diabetic retinopathy: Implications for pathogenesis. Microcirculation 14:25–38.
3. Antonetti DA, Lieth E, Barber AJ, Gardner TW (1999) Molecular mechanisms of vascular permeability in diabetic retinopathy. Semin Ophthalmol 14:240–248.
4. Antonetti DA, et al. (1998) Vascular permeability in experimental diabetes is associated with reduced endothelial occludin content: Vascular endothelial growth factor decreases occludin in retinal endothelial cells. Diabetes 47:1953–1959.
5. Rizzolo LJ, Chen X, Weitzman M, Sun R, Zhang H (2007) Analysis of the RPE transcriptome reveals dynamic changes during the development of the outer blood-retinal barrier. Mol Vis 23:1259–1273.
6. Pardridge WM (2005) Molecular biology of the blood-brain barrier. Mol Biotechnol 30:57–70.
7. Campbell M, et al. (2006) Involvement of MAPKs in endostatin-mediated regulation of blood-retinal barrier function. Curr Eye Res31:1033–1045.
8. Fanning AS, Anderson JM (1998) PDZ domains and the formation of protein networks at the plasma membrane. Curr Top Microbiol Immunol 228:209–233.
9. Kojima S, Rahner C, Peng S, Rizzolo LJ (2002) Claudin 5 is transiently expressed during the development of the retinal pigment epithelium. J Membr Biol 186:81–88.
10. Piontek J, et al. (2008) Formation of tight junction: Determinants of homophilic interaction between classic claudins. FASEB J22:146–158.
11. Nitta T, et al. (2003) Size-selective loosening of the blood-brain barrier in claudin-5-deficient mice. J Cell Biol 161:653–660.
12. Campbell M, et al. (2008) RNAi-mediated reversible opening of the blood-brain barrier. J Gene Med 10:930–947.
13. Pardridge WM (2006) Molecular Trojan horses for blood-brain barrier drug delivery. Curr Opin Pharmacol 6:494–500.
14. Aherne A, et al. (2004) On the molecular pathology of neurodegeneration in IMPDH1-based retinitis pigmentosa. Hum Mol Genet 13:641–650.
15. Tam LC, et al. (2008) Therapeutic benefit derived from RNAi-mediated ablation of IMPDH1 transcripts in a murine model of autosomal dominant retinitis pigmentosa (RP10). Hum Mol Genet 17:2084–2100.
16. Joly S, Samardzija M, Wenzel A, Thiersch M, Grimm C (2009) Nonessential role of beta3 and beta5 integrin subunits for efficient clearance of cellular debris after light-induced photoreceptor degeneration. Invest Ophthalmol Vis Sci 50:1423–1432.
17. Sanges D, Comitato A, Tammaro R, Marigo V (2006) Apoptosis in retinal degeneration involves cross-talk between apoptosis-inducing factor (AIF) and caspase-12 and is blocked by calpain inhibitors. Proc Natl Acad Sci USA 103:17366–17371.
18. Perche O, Doly M, Ranchon-Cole I (2007) Caspase-dependent apoptosis in light-induced retinal degeneration. Invest Ophthalmol Vis Sci 48:2753–2759.
19. Paquet-Durand F, Johnson L, Ekström P (2007) Calpain activity in retinal degeneration. J Neurosci Res85:693–702.
20. Sasaki T, et al. (1990) Inhibitory effect of di-and tripeptidyl aldehydes on calpains and cathepsins. J Enzyme Inhib 3:195–201.
21. Nussenblatt RB, Ferris F, III (2007) Age-related macular degeneration and the immune response: Implications for therapy. Am J Ophthalmol 144:618–626.
22. Bhatwadekar AD, et al. (2008) Advanced glycation of fibronectin impairs vascular repair by endothelial progenitor cells: Implications for vasodegeneration in diabetic retinopathy. Invest Ophthalmol Vis Sci 49:1232–1241.
23. Chadderton N, et al. (2009) Improved retinal function in a mouse model of dominant retinitis pigmentosa following AAV-delivered gene therapy. Mol Ther 17:593–599.
24. O'Reilly M, et al. (2007) RNA interference-mediated suppression and replacement of human rhodopsin in vivo. Am J Hum Genet 81:127–135.
25. Montezuma SR, Sobrin L, Seddon JM (2007) Review of genetics in age related macular degeneration. Semin Ophthalmol 22:229–240.
26. Fong DS, Girach A, Boney A (2007) Visual side effects of successful scatter laser photocoagulation surgery for proliferative diabetic retinopathy: A literature review. Retina 27:816–824.
27. Humphries P, Kenna P, Farrar GJ (1992) On the molecular genetics of retinitis pigmentosa. Science256:804–808.
28. De Boüard S, et al. (2007) Antiangiogenic and anti-invasive effects of sunitinib on experimental human glioblastoma. Neuro Oncol 9:412–423.
29. Sapieha P, et al. (2008) The succinate receptor GPR91 in neurons has a major role in retinal angiogenesis. Nat Med 14:1067–1076.
30. Edwards AO, Malek G (2007) Molecular genetics of AMD and current animal models. Angiogenesis 10:119–132.
31. Brankin B, Campbell M, Canning P, Gardiner TA, Stitt AW (2005) Endostatin modulates VEGF-mediated barrier dysfunction in the retinal microvascular endothelium. Exp Eye Res 81:22–31.
32. Matter K, Balda MS (2003) Holey barrier: Claudins and the regulation of brain endothelial permeability. J Cell Biol 161:459–460.
33. Koto T, et al. (2007) Hypoxia disrupts the barrier function of neural blood vessels through changes in the expression of claudin-5 in endothelial cells. Am J Pathol 170:1389–1397.
34. Haorah J, et al. (2005) Ethanol-induced activation of myosin light chain kinase leads to dysfunction of tight junctions and blood-brain barrier compromise. Alcohol Clin Exp Res 29:999–1009.
35. Nag S, Venugopalan R, Stewart DJ (2007) Increased caveolin-1 expression precedes decreased expression of occludin and claudin-5 during blood-brain barrier breakdown Acta Neuropathol 114:459–469.
36. McColl BW, Rothwell NJ, Allan SM (2008) Systemic inflammation alters the kinetics of cerebrovascular tight junction disruption after experimental stroke in mice J Neurosci 28:9451–9462.
37. Donovan M, Cotter TG (2002) Caspase-independent photoreceptor apoptosis in vivo and differential expression of apoptotic protease activating factor-1 and caspase-3 during retinal development. Cell Death Differ 9:1220–1231.
38. Maguire AM, et al. (2008) Safety and efficacy of gene transfer for Leber's congenital amaurosis. N Engl J Med 358:2240–2248.
39. Bainbridge JW, et al. (2008) Effect of gene therapy on visual function in Leber's congenital amaurosis. N Engl J Med 358:2231–2239.
40. Hauswirth WW, et al. (2008) Treatment of leber congenital amaurosis due to RPE65 mutations by ocular subretinal injection of adeno-associated virus gene vector: Short-term results of a phase I trial. Hum Gene Ther 19:979–990.
41. Foust KD, et al. (2009) Intravascular AAV9 preferentially targets neonatal neurons and adult astrocytes. Nat Biotechnol 27:59–65.
42. Reynolds A, et al. (2004) Rational siRNA design for RNA interference. Nat Biotechnol 22:326–330.
43. Kiang AS, et al. (2005) Toward a gene therapy for dominant disease: Validation of an RNA interference-based mutation-independent approach. Mol Ther 12:555–561.

EMBO Molecular Medicine

Systemic low-molecular weight drug delivery to pre-selected neuronal regions

Matthew Campbell[1], Marian M. Humphries[1], Anna-Sophia Kiang[1], Anh T. H. Nguyen[1], Oliviero L. Gobbo[2], Lawrence C. S. Tam[1], Mayu Suzuki[1], Finnian Hanrahan[1], Ema Ozaki[1], G.-Jane Farrar[1], Paul F. Kenna[1], Peter Humphries[1]*

Keywords: age-related macular degeneration; blood–brain barrier; blood–retina barrier; drug delivery; RNAi/claudin-5

DOI 10.1002/emmm.201100126

Received October 11, 2010
Revised February 04, 2011
Accepted February 07, 2011

→See accompanying Closeup by John J. Rossi
DOI: http://dx.doi.org/10.1002/emmm.201100132

We describe a procedure for controlled, periodic, reversible modulation of selected regions of the blood–brain barrier (BBB) or the inner-blood–retina barrier (iBRB) based on incorporation into an AAV-2/9 vector of a doxycycline-inducible gene encoding shRNA targeting claudin-5, one of 30 or so proteins constituting the BBB and iBRB. The vector may be introduced stereotaxically into pre-selected regions of the brain or into the retina, rendering these regions permeable to low-molecular weight compounds up to approximately 1 kDa for the period of time during which the inducing agent, doxycycline, is administered in drinking water, but excluding potentially toxic higher molecular weight materials. We report on the use of barrier modulation in tandem with systemic drug therapy to prevent retinal degeneration and to suppress laser-induced choroidal neovascularization (CNV), the latter being the hallmark pathology associated with the exudative, or wet, form of age-related macular degeneration (AMD). These observations constitute the basis of a minimally invasive systemic therapeutic modality for retinal diseases, including retinitis pigmentosa and AMD, where, in early stage disease, the iBRB is intact and impervious to systemically administered drugs.

INTRODUCTION

The tight junctions associated with the blood–brain and inner blood–retina barriers (BBB/iBRB) are comprised of a series of up to 30 proteins, interacting to provide a tight seal between adjacent endothelial cells lining the neuronal and inner retinal microvasculatures. They have evolved for the specific purpose of protecting neuronal tissues from potentially damaging blood-borne agents and, hence, breakage of such barriers, for the purposes of systemic drug delivery or for other purposes, would have serious adverse effects (Campbell et al, 2009). However, remodelling of the BBB/iBRB by selectively modulating levels of tight junction proteins, such as to render these barriers controllably and reversibly permeable to low-molecular weight compounds, could have substantial therapeutic potential given that the vast majority of low-molecular weight drugs (an estimated 98%) cannot gain access to neuronal tissues from the peripheral circulation. Moreover, those drugs that can gain access and are in clinical use (*e.g.* lipophilic antipsychotic drugs) may require dosages sufficiently high as to cause serious adverse clinical reactions—Clozapine, for example (MW 327 Da), can require daily dosages of up to 1 g (Kane et al, 1988). We have previously shown in mice that systemic administration (tail vein injection) of siRNA targeting transcripts derived from the claudin-5 gene, encoding one of the protein components of the tight junctions of the neuronal and retinal microvasculatures, renders the BBB and iBRB reversibly permeable to compounds up to approximately 1 kDa for periods of up to 36 h, starting 24 h post-siRNA delivery (Campbell et al, 2008, 2009). Importantly, however, molecules greater than approximately 1 kDa do not passively diffuse from the blood to the brain or retina when claudin-5 is suppressed, an observation made more significant by the fact that many low-molecular weight drugs lie within this size range, with larger substances, such as antibodies, blood-borne soluble enzymes, anaphylatoxins and pathogens being excluded.

Here, we describe an adeno-associated virus (AAV-2/9 serotype; Foust et al, 2009, 2010) expressing a doxycycline-

(1) Ocular Genetics Unit, Department of Genetics, Trinity College Dublin, Dublin 2, Ireland.
(2) School of Pharmacy and Pharmaceutical Sciences, Trinity College Dublin, Dublin 2, Ireland.
***Corresponding author:** Tel: +353 1 8962484; Fax: +353 1 8963848; E-mail: matthew.campbell@tcd.ie

 © 2011 EMBO Molecular Medicine

inducible shRNA targeting transcripts encoding claudin-5. The process allows for localized and inducible modulation of the BBB or iBRB independently of each other and provides a means of delivery to pre-selected neuronal regions of low-molecular weight compounds up to approximately 1 kDa in molecular weight for the period of time during which the inducing agent is administered. The process has no negative impact on neuronal function, nor does it induce neuronal oedema. Using the retina as a model system for assessment of neuronal function, we have validated the barrier modulation approach to systemic drug delivery by demonstrating protection of photoreceptors against light-induced damage by treatment with the calpain inhibitor ALLM. We have also shown that laser-induced choroidal neovascularization (CNV), the latter being the hallmark of vision threatening disease pathology in age-related macular degeneration (AMD), can be suppressed by systemic drug therapy using the low-molecular weight compounds, Sunitinib malate (Sutent®, Pfizer) and 17-AAG (Bristol-Myers Squibb) following induced barrier modulation. These observations form the basis of a novel and minimally invasive means of drug delivery to neuronal tissues while also representing a valuable experimental tool for the evaluation and screening of low-molecular weight drug efficacy for neurodegenerative conditions. The translational potential of this technology is potentially large and could be applied to a range of neurodegenerative and neuromalignant conditions.

RESULTS

Assessment of the efficacy of CLDN5 AAV-2/9

The system described here allows for reversible modulation of the iBRB with the exclusion of the BBB, and *vice versa*. To achieve this, we incorporated shRNA targeting claudin-5 into a doxycycline-inducible plasmid system. Subsequently, this was incorporated into the genome of an AAV-2/9 vector (these viruses have recently been shown to transduce endothelial cells of the neuronal microvasculature with high efficiency; Fig 1A and B; Foust et al, 2009, 2010). Viral purity was assessed using SDS–PAGE (Supplementary Fig 1).

An experimental group of C57/Bl6 mice received a sub-retinal inoculation of 3 μl of 5×10^{11} viral particles/ml of CLDN5 AAV-2/9 in the right eye. Mice received a non-targeting (NT) AAV-2/9 in their left eye. These animals were then supplemented in their drinking water with 2 mg/ml doxycycline and 5% sucrose for 3 weeks prior to analysis. Western blot analysis showed significant decreases ($^{***}p = 0.0005$) in the levels of expression of claudin-5 in retinas of mice injected with the CLDN5 AAV-2/9 compared to the NT AAV-2/9 injected retinas (Fig 1C and D). This suppression was also manifested by significant decreases ($^{*}p = 0.0218$) in claudin-5 transcript levels in retinal RNA samples (Fig 1E). Qualitative retinal flatmount analysis of claudin-5 expression showed a distinct and continuous pattern of expression in the NT AAV-2/9-injected retinas compared to the CLDN5 AAV-2/9-injected retinas (Fig 1F and G), and this was also observed in retinal cryosections, where decreased levels of expression and a discontinuous, fragmented pattern of staining was observed in the vascularized retinal layers as far as the outer plexiform layer (OPL; up to five mice analysed/group; Fig 1H).

Phenotype assessment of CLDN5 AAV-2/9

Although in use both experimentally and clinically, AAV serotypes will have differing transduction patterns when injected sub-retinally (Bainbridge et al, 2008; Hauswirth et al, 2008; Maguire et al, 2008). In this regard, we wished to assess the pattern of transduction of AAV-2/9 using an eGFP reporter gene. Mice sub-retinally injected with this AAV showed widespread transduction when a retinal whole-mount was prepared (Fig 2A). Indeed, transduction was widespread throughout the entire retinal pigment epithelium (RPE), which as a point of interest does not express claudin-5 (Rizzolo et al, 2007). Efficient transduction of the neural retina was, however, localized to the site of injection (arrow in Fig 2B and inset image) and following retinal cryosectioning and staining with an endothelial cell-specific isolectin (Griffonia-simplicifolia isolectin-Alexa 568), we observed co-labelling of eGFP and endothelial cells in the ganglion cell layer (GCL), inner plexiform layer (IPL), and OPL. While not all microvessels were transduced by AAV-2/9, the degree of transduction was sufficient enough to allow for significant modulation of claudin-5 expression (Fig 2B and C). Importantly, and unlike other AAV serotypes, for instance AAV-2/8 (Stieger et al, 2008), there was no transduction of AAV-2/9 along the optic nerve, which highlights an initial safety profile of this serotype. Transduction appeared to be retained solely to retinal tissue (Supplementary Fig 2).

Following confirmation of the efficiency of suppression of the inducible CLDN5 AAV-2/9, we undertook a series of magnetic resonance imaging (MRI) experiments to allow a phenotypic assessment of the system. In mice receiving CLDN5 AAV-2/9 sub-retinally in the right eye and a NT AAV-2/9 in the left eye, contrast-enhanced MRI showed significant quantities of Gd-DTPA (742 Da) extravasation specifically in the CLDN5 AAV-2/9-injected eye (Fig 2D). The pattern of extravasation appeared greatest in the region of sub-retinal injection, and this pattern was similar in horizontal and sagittal orientations ($^{***}p = 0.0001$; Fig 2E and F; Supplementary Fig 3). Each quantitative bar represents the enhanced contrasting observed in the CLDN5 AAV-2/9-injected eye when the background from the contra-lateral NT-AAV-2/9-injected eye was subtracted. As Gd-DTPA has a molecular weight of 742 Da, we wished to determine the size-selectivity of iBRB modulation, so we perfused mice with a solution of microperoxidase (1881 Da). Following retinal cryosectioning, microperoxidase was observed to be confined in the retinal microvasculature with suppression of claudin-5 (Fig 2G). Therefore, while the iBRB was modulated to a molecule of 742 Da, the iBRB remains impermeable to a molecule of 1881 Da. This phenotype produced no adverse effects on the rod or cone isolated electroretinogram (ERG) readouts of mice and importantly, (Fig 2H) barrier modulation using CLDN5 AAV-2/9 produced no signs of retinal oedema as assessed by high-resolution T-2-weighted MRI analyses (Fig 2I).

 © 2011 EMBO Molecular Medicine

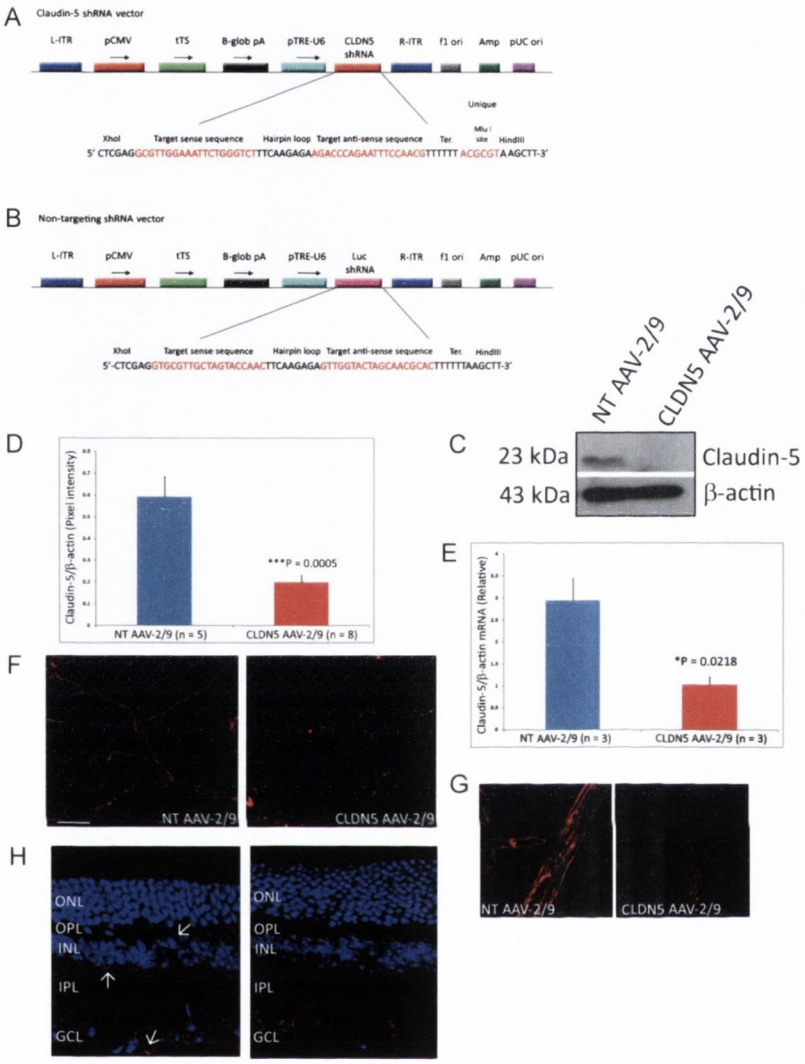

Figure 1. Assessment of the efficacy of CLDN5 AAV-2/9.

A,B. The plasmid incorporating the inducible system with claudin-5 shRNA (A) or a NT luciferase shRNA (B) was cloned into the plasmid pAAV-MCS, such as to incorporate L-ITR and R-ITR. Abbreviations: tTS, tetracycline-inducible transcriptional suppressor; β-globpA, beta-globin promoter; pTRE-U6, Tet-responsive U6 promoter; f1 ori, f1 origin of replication; Amp, ampicillin selection; pUC, pUC origin of replication. AAV-2/9 was then generated using a triple transfection system in a stably transfected HEK-293 cell line for the generation of high-titre viruses. tTS is a fusion of the Tet repressor and the Kid-1 KRAB-AB silencing domain. In the absence of doxycycline, tTS repressor binds to Tet operator (TetO) elements in a modified polIII promoter (pTRE-U6), inhibiting expression of claudin-5 (or NT luciferase) shRNAs. In the presence of doxycycline, tTS no longer binds to the promoter, allowing expression of shRNA.

C. 3 weeks post-sub-retinal inoculation of 3 μl of 5×10^{11} viral particles/ml of the NT AAV-2/9 or CLDN5 AAV-2/9 and subsequent supplementation in the drinking water of mice of 2 mg/ml doxycycline with 5% sucrose.

D,E. Strong and significant suppression of claudin-5 was observed at both the protein ($^{***}p = 0.0005$) and transcript level ($^{*}p = 0.0218$).

F,G. Qualitative assessment of claudin-5 expression in retinal flatmounts showed a continuous and strong pattern of staining at the endothelial cell margins in the microvasculature of the retinas of mice injected with the NT AAV-2/9. However, following sub-retinal inoculation of the CLDN5 AAV-2/9, this pattern of staining, while not completely ablated, was discontinuous and fragmented, with large immunoreactive precipitates of claudin-5 manifesting in the microvasculature.

H. Analysis of claudin-5 expression in retinal cryosections of mice injected with the NT AAV showed claudin-5 expression associated with the microvessels of the retina, permeating as far as the OPL (Arrows). Mice injected with the CLDN5 AAV-2/9 showed a significant decrease in expression and localization of claudin-5 in each layer permeated by microvessels. Outer nuclear layer (ONL), inner nuclear layer (INL), IPL and GCL.

Systemic and stereotaxic injection of CLDN5 AAV-2/9

Systemic administration of CLDN5 AAV caused a phenotype similar to that observed at the iBRB, and as expected also manifested in increased permeability of Gd-DTPA across the BBB correlated with suppression of brain capillary claudin-5 (Supplementary Fig 4). Moreover, a stereotaxic inoculation of 2 μl of the CLDN5 AAV-2/9 (5×10^{11} vp/ml) in the region of the right hippocampus showed a localized and inducible BBB modulation site-specifically when mice were supplemented with doxycycline (2 mg/ml) in their drinking water. This localized modulation of the BBB caused enhanced passive diffusion of Gd-DTPA from the blood to the brain while causing no signs of oedema formation. Specifically, dark contrasting observed in the right hippocampus of Fig 3E was manifested as intensely high-contrast blue in the pseudo-coloured image of Fig 3F. Each of nine individual mice injected had significantly higher Gd-DTPA contrasting in their right hippocampus compared to the left (Supplementary Fig 5). Importantly, the inducibility of the barrier modulating system was highlighted when doxycycline was removed from the drinking water and no barrier permeability was observed (Supplementary Fig 6).

Prevention of retinal degeneration using barrier modulation

We chose initially to use a mouse model of retinal degeneration in order to assess the efficacy of neuronal barrier modulation using CLDN5 AAV-2/9 to enhance delivery of an anti-apoptotic agent to the retina. Light-induced retinal degeneration is a

 © 2011 EMBO Molecular Medicine

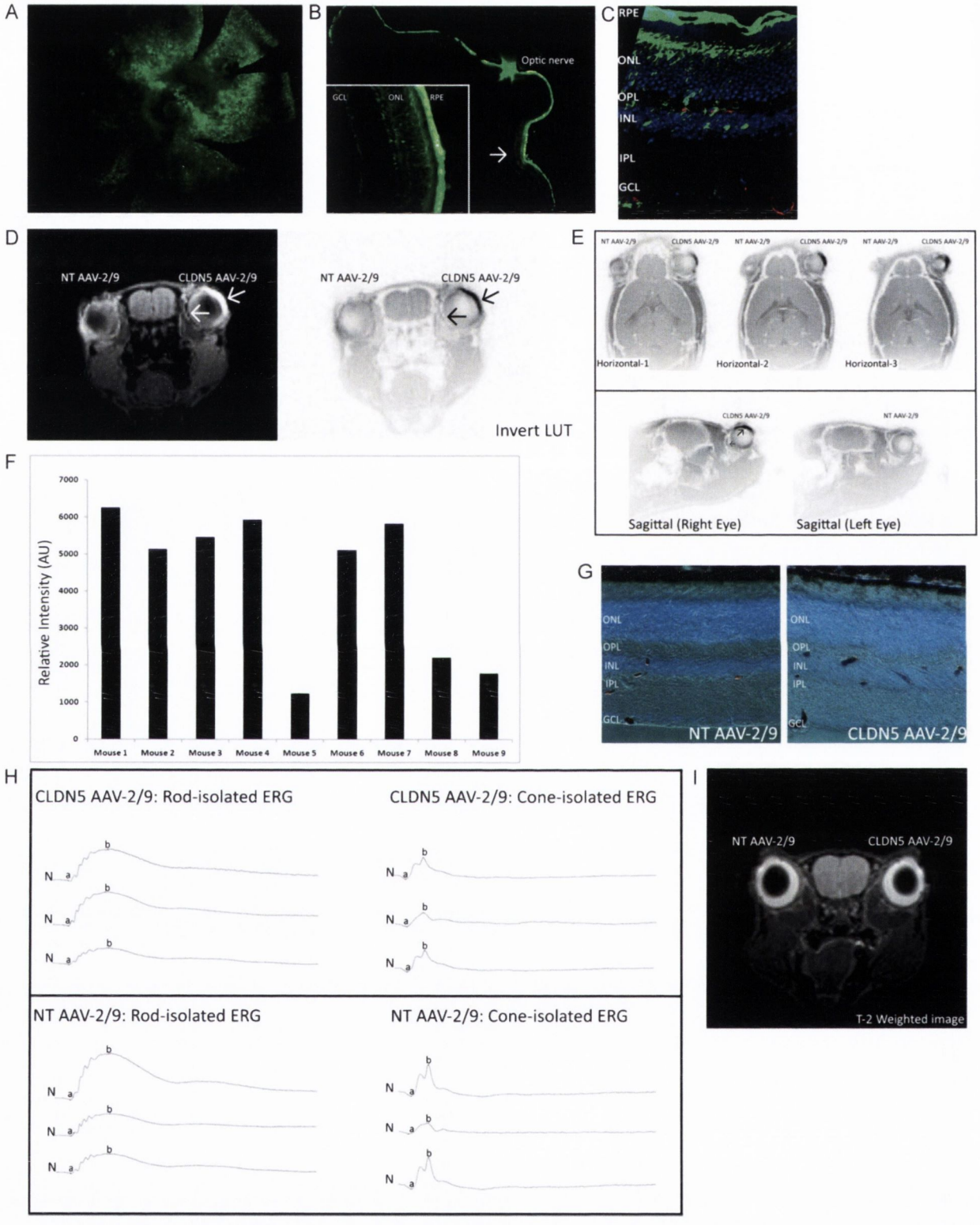

 © 2011 EMBO Molecular Medicine

Figure 2. Phenotype assessment of CLDN5 AAV-2/9.

A. An AAV-2/9 with an eGFP reporter gene was injected sub-retinally in an adult C57/Bl6 mouse and 3 weeks post-injection, a retinal whole-mount showed the pattern of transduction to be widespread (green).

B. Although transduction was observed throughout the retina, it was apparent that this transduction was heavily localized just to the neural retina (30–50% transduction) at the site of injection (arrow and high magnification inset), with the entire RPE being transduced. There was no transduction of AAV-2/9 observed along the optic nerve.

C. High-magnification microscopy of retinal cryosections injected sub-retinally with the eGFP AAV-2/9 (green) in the region of neural retina transduction and subsequent staining with a griffonia-simplicifolia isolectin-Alexa-568 (endothelial cell staining—red), showed the transduction efficiency of the AAV-2/9 serotype for endothelial cells.

D. Contrast-enhanced MRI showed extravasation of the MRI contrasting agent Gd-DTPA (MW 742 Da) in mice injected in the right eye with CLDN5 AAV-2/9, but not in the left eye, injected with NT AAV-2/9, when animals were supplemented with the inducing agent doxycycline (2 mg/ml with 5% sucrose in their drinking water) for 3 weeks post-injection. The inverted (LUT) image highlights the localized extravasation of Gd-DTPA in the right eye compared to the contra-lateral control (arrows).

E. Both horizontal and sagittal MRI show the pattern of extravasation of Gd-DTPA localized to the site of sub-retinal inoculation but that Gd-DTPA permeates the entire retina of the CLDN5 AAV-2/9-injected eye.

F. This extravasation was a consistent observation ($^{***}p = 0.0001$) in all mice analysed ($n = 9$), with the background pixel intensity from the NT AAV-2/9-injected eye being subtracted from the CLDN5 AAV-2/9-injected eye.

G. Retinal cryosections of CLDN5 AAV-2/9-injected mice perfused with microperoxidase (1881 Da) showed this tracer molecule to be confined within the retinal microvasculature, without signs of extravasation ($n = 4$).

H. Rod and cone isolated ERGs showed typical ERG tracings expected 3 weeks post-sub-retinal injection and no differences between the NT AAV-2/9-injected eyes and the CLDN5 AAV-2/9-injected eyes.

I. T-2-weighted coronal MRI analysis revealed no signs of retinal oedema in either NT AAV-2/9 or CLDN5 AAV-2/9 injected eyes ($n = 9$).

commonly used model to induce rapid photoreceptor cell death and we have previously shown that siRNA-mediated suppression of claudin-5 allows for enhanced delivery of the potent calpain inhibitor ALLM to the neural retina (Campbell et al, 2009). Calpain activity has been described as being central to light-induced photoreceptor cell degeneration and to this end, we injected albino BalB/c mice in their right eye with CLDN5 AAV-2/9 or in their left eye with a NT AAV-2/9. Again, mice were supplemented with the inducing agent doxycycline (2 mg/ml) in their drinking water and 24 h prior to light ablation all mice received an intraperitoneal (i.p.) injection of 20 mg/kg ALLM prior to dark adaptation. ALLM has a molecular weight of 401 Da and is a potent inhibitor of calpain I ($K_i = 120$ nM), calpain II ($K_i = 230$ nM), cathepsin-L ($K_i = 0.6$ nM), cathepsin-B ($K_i = 100$ nM), and the proteasome. Following dilation of their pupils, mice were then exposed to 7900 lux light for 2 h and 24 h

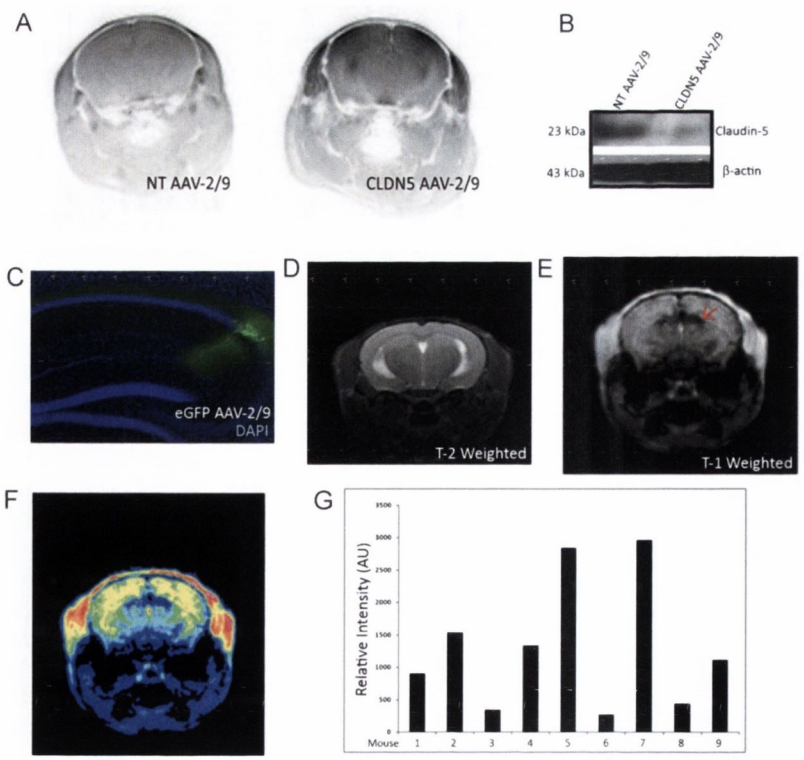

Figure 3. Systemic and stereotaxic injection of CLDN5 AAV-2/9.

A. BBB modulation to Gd-DTPA was observed throughout the brain and in the region of the hippocampus, extravasation of Gd-DTPA was manifested by dark contrasting in inverted LUT MR images following systemic injection of AAV.

B. Western blot analysis in a capillary isolated fraction of brain tissue showed suppression of claudin-5 in CLDN5 AAV-2/9-injected mice compared to NT AAV-2/9-injected mice.

C. An eGFP expressing AAV-2/9 was also injected to identify the transduced region and showed efficient transduction of cells within the hippocampus (green), with retrograde transport observed in neuronal cells.

D. High-resolution T-2-weighted MRI showed no signs of neuronal oedema at the site of injection.

E. Post-Gd-DTPA injection, enhanced contrasting was observed within the hippocampus specifically at the site of injection.

F. Extravasation of Gd-DTPA at the side of injection was highlighted in the pseudo-coloured image (arrows).

G. Quantitative analysis of regions of interest in the right hippocampus of individual mice were assessed and compared to the contra-lateral hippocampus. In each mouse analysed, there was a significant enhancement of Gd-DTPA in the region of the hippocampus injected with CLDN5 AAV-2/9.

 © 2011 EMBO Molecular Medicine

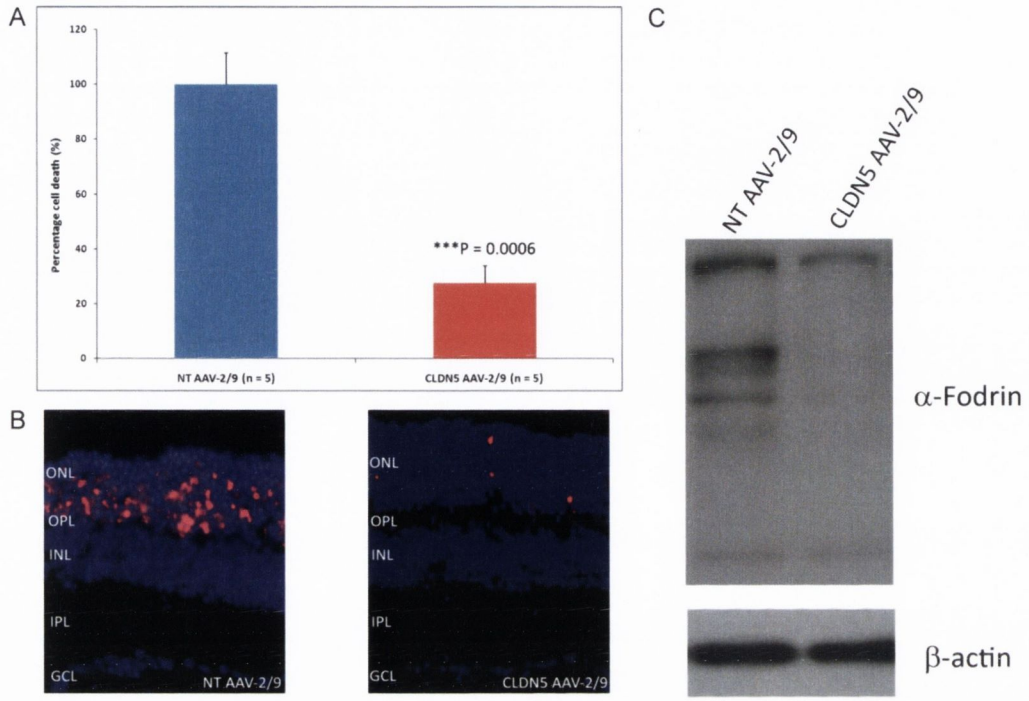

Figure 4. Systemic drug delivery to the retina and inhibition of retinal degeneration.

A. Albino BalB/c mice were inoculated sub-retinally with either the NT AAV-2/9 in their left eye or the CLDN5 AAV-2/9 in their right eye. Mice were administered 2 mg/ml doxycycline in their drinking water for 3 weeks and 24 h prior to light ablation, they received an i.p. injection of 20 mg/kg ALLM. Mice were subsequently exposed to 7900 lux light for 2 h and 24 h post-light exposure, retinal cryosections were analysed for end stage apoptotic/necrotic photoreceptors by counting of TUNEL positive cells. Cell counts from the CLDN5 AAV-2/9-injected eyes and the corresponding NT AAV-2/9-injected eye were expressed as a percentage of each other as each individual animal received identical light ablation in each eye. Significant protection of photoreceptor cells was observed in the right eyes (CLDN5 AAV-2/9) of mice compared to the left eyes (NT AAV-2/9; $^{***}p = 0.0006$).

B. TUNEL positive cells were shown to be consistently localized in large numbers to the ONL of NT AAV-2/9-injected retinas compared to CLDN5 AAV-2/9-injected retinas.

C. Extensive cleavage of the calpain substrate α-fodrin was observed in mice receiving the NT AAV compared to mice receiving the CLDN5 AAV with ALLM prior to light ablation.

later, eyes were harvested and stained for DNA fragmentation (TUNEL staining) for the identification of end stage dying photoreceptor cells and in effect the assessment of retinal degeneration. We observed up to 70% protection in the retinas of mice injected with CLDN5 AAV-2/9 compared to the NT AAV-2/9-injected retinas with i.p. injection of ALLM (Fig 4A and B). This degree of retinal protection has been shown previously, however, it was with intra-ocular injection of ALLM, in contrast to the systemic mode of delivery used here (Sanges et al, 2006). Systemic administration of anti-apoptotic agents in conjunction with CLDN5 AAV-2/9 appears to be highly efficient in preventing retinal degeneration. Moreover, decreases in cell death was concomitant with a distinct decrease in the amount of α-fodrin cleavage, a key substrate of calpain activity (Fig 4C).

Prevention of choroidal neovascularization using neuronal barrier modulation

In order to assess the effects of enhanced delivery of therapeutics for the treatment of CNV using CLDN5 AAV-2/9, we chose to use a laser-induced model of CNV. This model involves the use of a targeted and intense laser burn to the back of the eye to cause a localized disruption of the RPE and Bruch's membrane. Localized increases in VEGF at the site of the laser burn have previously been reported to cause a CNV-like lesion and represent the best available animal model of the central pathology associated with wet AMD (Sakurai et al, 2003). Moreover, these lesions are extremely poorly perfused as outlined in Fig 5A, with green fluroescence representing perfused fluorescein isothiocyanate (FITC)-conjugated dextran (FITC-dextran), while red staining represents the actual endothelial cells of the CNV. To this end, we wished to determine the effects of barrier modulation in tandem with systemic treatment of two well characterized and clinically relevant VEGF inhibitors, 17-AAG (MW: 585 Da; Sausville et al, 2003) and Sunitinib malate (Sutent®) (MW: 532 Da; Motzer et al, 2007). Mice were administered a sub-retinal injection of either CLDN5 AAV-2/9 in the right eye and a NT AAV-2/9 in the left eye. Mice were subsequently treated with 2 mg/ml doxycycline in their drinking water for 3 weeks prior to the administration of targeted laser burns (three/eye) in each eye.

 © 2011 EMBO Molecular Medicine

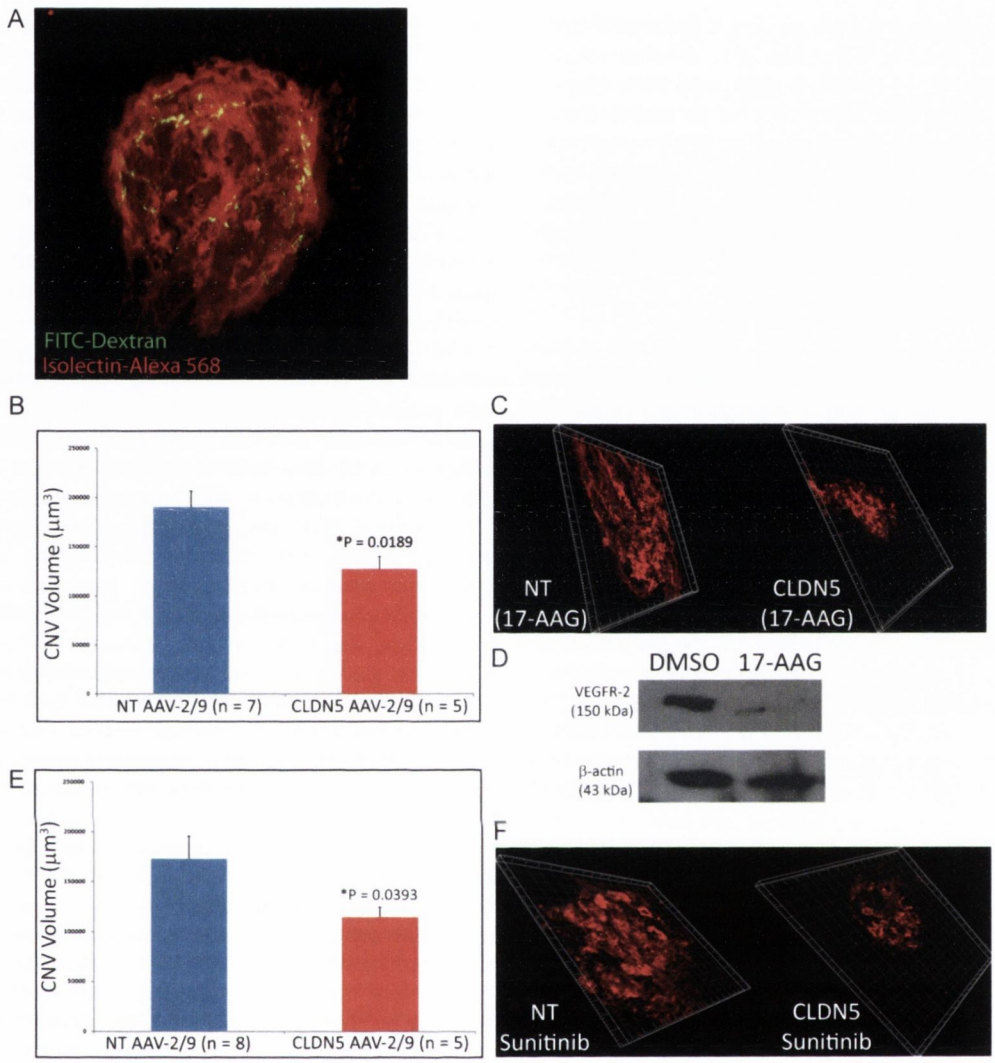

Figure 5. Inhibition of CNV using barrier modulation.

A. Mice perfused with FITC-dextran-200 (FD-200) prior to preparation of choroidal flatmounts, displayed poorly perfused lesions (green) at the site of the laser burn when compared to the density of endothelial cells in the region stained with isolectin-Alex 568 (red).

B. C57/Bl6 mice were administered NT AAV-2/9 in their left eye and CLDN5 AAV-2/9 in their right eye with doxycycline supplementation (2 mg/ml) in their drinking water for 3 weeks. CNV was induced with a targeted laser burn (140 mW, 100 mS, 50 μm spot size) in either the NT AAV-2/9 or CLDN5 AAV-2/9 injected eye and 4 days post-laser burn, mice were injected with 31.25 mg/kg 17-AAG i.p. Mice were injected again 4 days later. CNV volumes in the eyes of mice receiving the CLND5 AAV-2/9 were significantly reduced when compared to the NT AAV-2/9 injected eyes ($^*p = 0.0189$).

C. CNV formation in mice inoculated sub-retinally with CLDN5 AAV-2/9 were shown to be consistently reduced when compared to the NT AAV-injected eyes ($n = 5$–7 mice per experimental group).

D. 17-AAG is a potent inhibitor of VEGFR-2 expression via the inhibition of hsp-90.

E. In the same manner as described above, mice were injected with 20 mg/kg Sunitinib malate (Sutent®) i.p. on days 4 and 8 post-laser burn and CNV volumes were shown to be significantly reduced in CLDN5 AAV-2/9-injected mice compared to NT AAV-2/9 controls ($^*p = 0.0393$).

F. Again, confocal Z-stack images showed consistently decreased CNV volumes in the CLDN5 AAV-2/9-injected eyes compared to the NT AAV-2/9-injected eyes.

All animals were assessed for CNV formation 14 days post-burn and in the intervening period, animals received two i.p. injections of either 17-AAG (31.25 mg/kg) or Sunitinib malate (20 mg/kg). CNV volumes were assessed following removal of the neural retina and staining of eyecups with a Griffonia-simplicifolia isolectin-Alexa-568 molecule in order to stain endothelial cells. Confocal scanning laser microscopy (CSLM) was used to create Z-stacks of each CNV by assessing the fluorescence in each layer of the CNV. These CNV's were then compiled into a 3D image and subsequently assessed using dedicated Imaris® software which will allow for the determination of both CNV area and, importantly, depth. We observed

 © 2011 EMBO Molecular Medicine

significant decreases in CNV volumes in CLDN5 AAV-2/9-injected eyes with 17-AAG (Fig 5A and B) or Sunitinib malate (Sutent®; Fig 5D and E) when these drugs were administered systemically. Animals injected with 17-AAG also showed significant decrease in expression of VEGFR-2 (Fig 5C). Importantly, each CLDN5 AAV-2/9-injected eye was compared to a contra-lateral NT AAV-2/9-injected eye so each eye was exposed to identical quantities of active compound ($n = 5$–7 mice/group).

DISCUSSION

In terms of the safety profile of using barrier-modulating technology, we have seen very few differentially regulated genes in neuronal tissues when claudin-5 is suppressed (Campbell et al, 2009). It must also be considered that a relatively small number of drugs can cause ocular complications when administered systemically and, therefore, modulation of the barriers could exacerbate such complications (Abdollahi et al, 2004). However, it must be stressed that these agents are relatively few in number, are extremely well documented and could easily be avoided by individuals receiving a sub-retinal or stereotaxic inoculation of CLDN5 AAV-2/9.

CNV's are very badly perfused and similar to the blood–tumour barrier (Giannini et al, 2005), systemic drug treatment is limited as active compound needs to be exposed to a large area of tissue to be efficacious. Tet elements have also been used previously in a long-term safety study in the retinas of macaques and have shown to be an efficient and safe means to regulate gene expression. Repeated induction of gene expression was also observed for 2.5 years after initial injection (Stieger et al, 2006). Therapeutically, claudin-5 shRNA would be expressed for very short periods of time and given that the half-life of claudin-5 is approximated to be 30 h, the barrier would reform once shRNA expression is prevented upon removal of doxycycline. Given the lack of impact on retinal electrophysiology and retinal histology, it is highly unlikely that shRNA is expressed in sufficient quantities to interfere with the endogenous miRNA pathways. Indeed, miRNA are involved in the control of expression of up to 30% of genes and from a previous microarray study (Campbell et al, 2009), we have observed very few differentially regulated genes when claudin-5 is suppressed using siRNA. Moreover, we have observed no up-regulation of IL12 or RANTES expression in the neural retinas of mice administered NT AAV-2/9 or CLDN5 AAV-2/9, demonstrating that innate immune system activation is not an issue with this method of delivery (Supplementary Fig 6).

Although doxycycline has previously been reported to cause up-regulation in systemic PEDF levels and subsequent decreases in CNV volumes (Samtani et al, 2009), we have controlled for this using the NT AAV-2/9-injected contra-lateral eye. Moreover, the levels of doxycycline used in this study (2 mg/ml with 5% sucrose in drinking water) to induce claudin-5 shRNA expression are well below that used to prevent CNV formation alone. All evidence to date indicates that AAV infection of neuronal tissues is long lasting or may even be permanent and, hence, repeated injections of this inducible barrier-modulating agent should not be required (Bainbridge et al, 2008; Hauswirth et al, 2008; Maguire et al, 2008). Indeed, endothelial cells of the iBRB and BBB, while possessing high-turnover rates and replication potential do not in fact undergo nuclear division, and AAV transduction should persist long-term following one injection. In this regard, CLDN5 AAV-2/9 used in conjunction with known anti-neovascular agents such as 17-AAG or Sunitinib malate could form the basis of a novel and pre-emptive therapeutic strategy for wet AMD. Indeed, the levels of active compound that would be needed would be far less than that currently used for these drugs and this would apply to other molecules with proven efficacies in treating molecular pathologies associated with other neurodegenerative conditions. The method described here has distinct advantages over BBB disruption using ultrasound or mannitol in that it is size-selective to low-molecular weight molecules (Muldoon et al, 1995; Yang et al, 2010). The two methods outlined above are not size-selective and will allow for extravasation of plasma constituents such as albumin or IgG. Moreover, the use of intra-carotid administered mannitol, which is used clinically to break down the BBB for drug delivery in Glioblastoma multiforme (GBM) treatment, can induce severe seizures in patients and is neither size-selective nor short-term, with effects being manifested for days after the infusion (Neuwelt et al, 1986). A direct comparison of mannitol infusion and AAV-mediated barrier modulation was not performed during the course of this study given the disparity between the two approaches. Mannitol infusion causes global BBB disruption, for short periods of time, and this is neither size-selective, nor is it localized to distinct neuronal regions. Our AAV approach allows for periodic and localized barrier modulation specifically at the site of injection of the virus and has been designed in such a way that barriers only become reversibly permeable to low-molecular weight material. While the use of mannitol has been described in relation to attempts to improve access of cytotoxic drugs to the brain for treatment of GBM, its administration must be performed under highly specialized surgical conditions and it cannot be used for chronic conditions such as those described here in view of the fact that repeated administration may produce abnormal neurological and renal side-effects (Helmy et al, 2007).

While further GLP/GMP grade safety/toxicology studies mandated for experimental systems such as that described here are currently on-going, to date, the AAV-2/9 barrier modulating system for systemic drug delivery of therapeutics appears safe, tolerable and represents a novel form of chronic preventative therapy. Indeed, this system may now have a very broad range of applications for other neurodegenerative conditions that could be amenable to small molecule therapeutics. We have established that enhanced delivery of anti-neovascular and anti-apoptotic compounds following reversible modulation of the iBRB provides a direct proof of principle of an AAV-mediated system for inducible neuronal barrier modulation in human subjects. The short periods of time during which shRNAs are sequentially expressed will reduce any negative effects that could be induced by their permanent expression

 © 2011 EMBO Molecular Medicine

within the retina. We have also demonstrated that the system can be readily adapted to the brain microvasculature, allowing in principle, localized and inducible modulation of any distinct region of the brain inoculated with the virus. We anticipate that inducible suppression of claudin-5 in humans will represent an attractive avenue for controlled delivery of low-molecular weight therapeutics currently deemed unusable as they do not cross the neuronal or retinal blood barriers. In the case of AMD, the initial target here (AMD is the most prevalent cause of blindness in the developed world) (deJong, 2006; Seddon et al, 2006; Tan et al, 2008; The Eye Disease Prevalence Group, 2004), it is envisioned that a human therapeutic regime would involve delivery to the endothelial cells of the inner retina of an AAV vector expressing an inducible claudin-5 transcript inhibitory system. More generally, this technology represents a fundamental platform for drug delivery protocols in a wide range of neurodegenerative conditions where the BBB can be similarly modulated.

MATERIALS AND METHODS

Animal and experimental groups

All studies carried out in the Ocular Genetics Unit in TCD adhere to the ARVO statement for the use of Animals in Ophthalmic and Vision Research. Mice were originally sourced from Jackson Laboratories and bred on-site at the Ocular Genetics Unit in TCD.

AAV production

shRNAs designed to target transcripts derived from mouse claudin-5 were incorporated into AAV-2/9 vectors. shRNA was cloned into the pSingle-tTS-shRNA (Clontech) vector. The plasmid incorporating the inducible system with claudin-5 shRNA was digested with BsrBI and BsrGI and ligated into the Not1 site of the plasmid pAAV-MCS, such as to incorporate left and right AAV inverted terminal repeats. (L-ITR and R-ITR). AAV-2/9 was then generated using a triple transfection system in a stably transfected HEK-293 cell line for the generation of high-titre viruses (Vector BioLabs; Tam et al, 2008 and 2010; Chadderton et al, 2009; O'Reilly et al, 2007).

Sub-retinal AAV injection

Sub-retinal injections were carried out in compliance with the ARVO statement for the use of animals in ophthalmic and vision research.

Stereotaxic injection of AAV in mice

Using stereotaxic co-ordinates of the mouse brain, high-titre inducible AAV particles containing claudin-5 shRNA were injected into the hippocampus of the mouse brain (2.5 mm posterior and 1.0 mm lateral to bregma and 2.2 mm depth) using a hamilton syringe at a rate of 0.1 μl/min over a 10 min period.

Murine models of choroidal neovascularization

CNV, in which the vascular bed proliferates into the retina, mimicking neovascular AMD, was induced in mice using a green 532 nm Iridex Iris laser (532 nm, 140 mW, 100 mS, 50 μm spot size, three spots/eye) incorporating a microscopic delivery system as described previously. Following administration of laser burns, mice were returned to their cages and each injected i.p. on days 4 and 8 post-laser burn with either 20 mg/kg Sunitinib malate (Sutent®) or 31.25 mg/kg 17-AAG. Mice were sacrificed 14 days post-experiment and the neural retina was removed. Eye-cups were cut radially and fixed for 2 h at room temperature with 4% PFA (pH 7.4). Eye-cups were then incubated with a Griffonia-simplicifolia-isolectin-Aleax-568 molecule (1:300) overnight at 4°C. Eye-cups were washed three times with PBS and flatmounted on a glass slide using aqua-polymount. CNV's were assessed by confocal microscopy and Imaris® 7.0 (Bitplane Scientific Software).

Western blot analyses

Protein was isolated from total retinal tissue by homogenizing in lysis buffer containing 62.5 mM Tris, 2% SDS, 10 mM dithiothreitol, 10 μl protease inhibitor cocktail/100 ml (Sigma–Aldrich, Ireland). The homogenate was centrifuged at 10,000 × *g* for 20 min at 4°C, and the supernatant was removed for claudin-5 analysis (Campbell et al, 2009). Antibodies for Western blots were as follows: polyclonal rabbit anti-claudin-5 (Zymed Laboratories, San Francisco, CA) (1:500) and polyclonal rabbit anti-β-actin (Abcam, Cambridge, UK) (1:1000), mouse monoclonal anti-α-fodrin (Enzo Life Sciences) and VEGFR-2 (Abcam). Membranes were washed with TBS and incubated with a secondary anti-rabbit (IgG) antibody with horseradish peroxidase (HRP) conjugates (1:2500; Sigma–Aldrich), or anti-mouse (IgG) (1:1000; Sigma–Aldrich), for 3 h at room temperature. Immune complexes were detected using enhanced chemiluminescence (ECL). All Western blots were repeated a minimum of three times.

Real-time RT-PCR analysis

RNA was analysed by real-time RT-PCR using a Quantitect Sybr Green Kit as outlined by the manufacturer (Qiagen–Xeragon) under the following conditions: 50°C for 20 min; 95°C for 15 min; 38 cycles of 94°C for 15 s, 57°C for 20 s, 72°C for 10 s. Primers (Sigma–Genosys, Cambridge, UK) for the sequences amplified were as follows CLDN5 (Forward 5′-TTTCTTCTATGCGCAGTTGG-3′, Reverse 5′-GCAGTTTGGTGCCTACTTCA-3′), β-actin (Forward 5′-TCACCCA-CACTGTGCCCATCTA-3′, Reverse 5′ CAGCGGAACCGCTCATTGCCA-3′). IL12p40 (Forward 5′-CCACTTGGCCTTATGCTGTT-3′, Reverse 5′-TTGCA-TAATAGGGCCTGGTC-3′).

MRI analyses

Following AAV-mediated inducible RNAi of claudin-5, mice were analysed using a dedicated small rodent 7 T MRI system located at the Trinity College Institute of Neuroscience (TCIN), Dublin, Ireland (www.neuroscience.tcd.ie/technologies/mri.php). Mice were anesthetized with 3% isofluorane and maintained under sedation using 1%. For full MRI method, see SI text.

Indirect immunostaining of retinal flatmounts and retinal cryosections

Following fixation of eyes with 4% Paraformaldehyde (pH 7.4) for 4 h at room temperature and three subsequent washes with PBS, retinal cryosections were blocked with 5% normal goat serum (NGS) in PBS for 20 min at room temperature. Rabbit anti-Claudin-5 (Zymed), was incubated on sections overnight at 4°C. Secondary rabbit IgG-Cy3, (Jackson-Immuno-research, Europe) antibodies were incubated with the sections at 37°C for 2 h followed by three washes with PBS. All

 © 2011 EMBO Molecular Medicine

The paper explained

PROBLEM:

Up to 98% of systemically deliverable low-molecular weight drugs, many of which could be used in treatment and prevention of the world's most common neurodegenerative and vision-threatening disorders, are not in current clinical use because they cannot cross the so-called BBB and iBRB.

RESULTS:

We have developed an AAV-2/9 vector, expressing an inducible shRNA designed to downregulate transcripts encoding claudin-5, a tight junction protein expressed in the brain and retinal microvasculatures. The AAV-2/9 vector was sub-retinally inoculated into the retinas of mice or stereotaxically injected into distinct regions of the brain. Subsequent treatment of inoculated mice with the inducing agent doxycycline turns on the genetic machinery that down-regulates claudin-5. Stopping doxycycline treatment shuts off the system. In this way, the iBRB and the BBB can be exclusively modulated—temporarily and reversibly—to allow passive diffusion of small molecules from the blood into the neural retina or brain.

IMPACT:

This form of therapy, using the inducible AAV-2/9 system, has the potential to be developed for use in humans, using one or more of a wide range of EMEA/FDA-approved anti-neovascular drugs in the case of wet AMD and a range of neuroprotective and anti-apoptotic agents for numerous other conditions with little or no current forms of therapy.

sections were counterstained with DAPI for 30 s at a dilution of 1:5000 of a stock 1 mg/ml solution. Analysis of stained sections was performed at room temperature with an epifluorescence microscope (Zeiss Axioplan 2, Oberkochen, Germany) or confocal laser scanning microscopy (Olympus FluoView TM FV1000).

ERG analysis of mice

C57/Bl6 mice injected with wither a NT AAV-2/9 or a CLDN5 AAV-2/9 were dark-adapted overnight and prepared for electroretinography under dim red light. Pupillary dilation was carried out by instillation of 1% cyclopentalate and 2.5% phenylephrine. Animals were anesthetized by i.p. injection of ketamine (2.08 mg/15 g body weight) and xylazine (0.21 mg/15 g body weight). Standardized flashes of light were presented to the mouse in a Ganzfeld bowl to ensure uniform retinal illumination. The ERG responses were recorded simultaneously from both eyes by means of gold wire electrodes (Roland Consulting Gmbh) using Vidisic (Dr Mann Pharma, Germany) as a conducting agent and to maintain corneal hydration.

Light ablation of albino BalB/c mice

Mice were injected in their left eye with a NT AAV-2/9 or in their right eye with a CLDN5 AAV-2/9 virus. During the 3 weeks period when mice were supplemented in their drinking water with 2 mg/ml doxycycline/5% sucrose, animals were kept in cyclic light (12 h light and 12 h dark; 60 lux) prior to all experimentation. 24 h prior to light ablation, mice received ALLM i.p. (20 mg/kg) (Calbiochem, Germany) and were subsequently dark adapted for 24 h before being exposed to constant light.

TUNEL analysis

Eyes from mice injected with either the NT AAV-2/9 or the CLDN5 AAV-2/9 were fixed in 3.5% formaldehyde for 4 h followed by three washes in PBS. Eyes were cryoprotected using a sucrose gradient (10–30% sucrose in PBS), and subsequently 12 μm sections were cut using a cryostat. To detect cell death, sections were then incubated with staining mix (*in situ* cell death detection kit, TMR red, Roche) according to manufacturer's instructions.

Author Contributions

MC designed and undertook experiments; MH generated AAV constructs; ATHN performed TUNEL assays and light ablation; OG performed MRI analysis; LCST performed experimental design and cloning; MS performed RT-PCR analyses; FH and EO analysed cell culture and RT-PCR; GJF and ASK performed experimental design cell culture and RT-PCR; PFK performed sub-retinal injections and ERG analyses. PH performed experimental design and data analysis.

Acknowledgements

The Ocular Genetics Unit at TCD is supported by Science Foundation Ireland (SFI), The Wellcome Trust, Irish Research Council for Science Engineering and Technology (IRCSET) and Fighting Blindness Ireland (FB-Ireland). Health Research Board of Ireland (HRB), Enterprise Ireland (EI) and the US Department of Defense-Telemedicine and Advanced Technology Research Center (TATRC). We would like to thank Caroline Woods, Charles Murray, David Flynn and Rebecca Robertson for animal breeding and husbandry. The authors would also like to thank Dr Christian Kerskens for his advice with MRI experiments and the Research Foundation at the Royal Victoria Eye and Ear Hospital for assistance in the acquisition of the Iridex laser system.

Supporting information is available at EMBO Molecular Medicine online.

The authors declare that they have no conflict of interest.

 © 2011 EMBO Molecular Medicine

For more information

Smurfit Institute of Genetics
www.tcd.ie/genetics

Fighting Blindness
www.fightingblindness.ie

References

Abdollahi M, Shafiee A, Bathaiee FS, Sharifzadeh M, Nikfar S (2004) Drug-induced toxic reactions in the eye: an overview. J Infus Nurs 27: 386-398

Bainbridge JW, Smith AJ, Barker SS, Robbie S, Henderson R, Balaggan K, Viswanathan A, Holder GE, Stockman A, Tyler N, *et al* (2008) Effect of gene therapy on visual function in Leber's congenital amaurosis. N Engl J Med 358: 2231-2239

Campbell M, Kiang AS, Kenna PF, Kerskens C, Blau C, O'Dwyer L, Tivnan A, Kelly JA, Brankin B, Farrar GJ, *et al* (2008) RNAi-mediated reversible opening of the blood–brain barrier. J Gene Med 10: 930-947

Campbell M, Nguyen AT, Kiang AS, Tam LC, Gobbo OL, Kerskens C, Ni Dhubhghaill S, Humphries MM, Farrar GJ, Kenna PF, *et al* (2009) An experimental platform for systemic drug delivery to the retina. Proc Natl Acad Sci USA 106: 17817-17822

Chadderton N, Millington-Ward S, Palfi A, O'Reilly M, Tuohy G, Humphries MM, Li T, Humphries P, Kenna PF, Farrar GJ (2009) Improved retinal function in a mouse model of dominant retinitis pigmentosa following AAV-delivered gene therapy. Mol Ther 17: 593-599

deJong PTVM (2006) Age-related macular degeneration. N Engl J Med 355: 1474-1485

Foust KD, Nurre E, Montgomery CL, Hernandez A, Chan CM, Kaspar BK (2009) Intravascular AAV9 preferentially targets neonatal neurons and adult astrocytes. Nat Biotechnol 27: 59-65

Foust KD, Wang X, McGovern VL, Braun L, Bevan AK, Haidet AM, Le TT, Morales PR, Rich MM, Burghes AH (2010) Rescue of the spinal muscular atrophy phenotype in a mouse model by early postnatal delivery of SMN. Nat Biotechnol 28: 271-274

Giannini C, Sarkaria JN, Saito A, Uhm JH, Galanis E, Carlson BL, Schroeder MA, James CD (2005) Patient tumor EGFR and PDGFRA gene amplifications retained in an invasive intracranial xenograft model of glioblastoma multiforme. Neuro Oncol 7: 164-176

Hauswirth WW, Aleman TS, Kaushal S, Cideciyan AV, Schwartz SB, Wang L, Conlon TJ, Boye SL, Flotte TR, Byrne BJ, *et al* (2008) Treatment of leber congenital amaurosis due to RPE65 mutations by ocular subretinal injection of adeno-associated virus gene vector: short-term results of a phase I trial. Hum Gene Ther 19: 979-990

Helmy A, Vizcaychipi M, Gupta AK (2007) Traumatic brain injury: intensive care management. Br J Anaesth 99: 32-42

Kane J, Honigfeld G, Singer J, Meltzer H (1988) Clozapine for the treatment-resistant schizophrenic. A double-blind comparison with chlorpromazine. Arch Gen Psychiatry 45: 789-796

Maguire AM, Simonelli F, Pierce EA, Pugh EN, Jr, Mingozzi F, Bennicelli J, Banfi S, Marshall KA, Testa F, Surace EM, *et al* (2008) Safety and efficacy of gene transfer for Leber's congenital amaurosis. N Engl J Med 358: 2240-2248

Motzer RJ, Hutson TE, Tomczak P, Michaelson MD, Bukowski RM, Rixe O, Oudard S, Negrier S, Szczylik C, Kim ST, *et al* (2007) Sunitinib *versus* interferon alfa in metastatic renal-cell carcinoma. N Engl J Med 356: 115-124

Muldoon LL, Nilaver G, Kroll RA, Pagel MA, Breakefield XO, Chiocca EA, Davidson BL, Weissleder R, Neuwelt EA (1995) Comparison of intracerebral inoculation and osmotic blood–brain barrier disruption for delivery of adenovirus, herpesvirus, and iron oxide particles to normal rat brain. Am J Pathol 147: 1840-1851

Neuwelt EA, Howieson J, Frenkel EP, Specht HD, Weigel R, Buchan CG, Hill SA (1986) Therapeutic efficacy of multiagent chemotherapy with drug delivery enhancement by blood–brain barrier modification in glioblastoma. Neurosurgery 19: 573-582

O'Reilly M, Palfi A, Chadderton N, Millington-Ward S, Ader M, Cronin T, Tuohy T, Auricchio A, Hildinger M, Tivnan A *et al* (2007) RNA interference-mediated suppression and replacement of human rhodopsin *in vivo*. Am J Hum Genet 81: 127-135

Owen CG, Fletcher AE, Donoghue M, Rudnicka AR (2003) How big is the burden of visual loss caused by age related macular degeneration in the United Kingdom. Br J Ophthalmol 87: 312-317

Rizzolo LJ, Chen X, Weitzman M, Sun R, Zhang H (2007) Analysis of the RPE transcriptome reveals dynamic changes during the development of the outer blood–retinal barrier. Mol Vis 23: 1259-1273

Sakurai E, Anand A, Ambati BK, van Rooijen N, Ambati J (2003) Macrophage depletion inhibits experimental choroidal neovascularization. Invest Ophthalmol Vis Sci 44: 3578-3585

Samtani S, Amaral J, Campos MM, Fariss RN, Becerra SP (2009) Doxycycline-mediated inhibition of choroidal neovascularization. Invest Ophthalmol Vis Sci 50: 5098-5106

Sanges D, Comitato A, Tammaro R, Marigo V (2006) Apoptosis in retinal degeneration involves cross-talk between apoptosis-inducing factor (AIF) and caspase-12 and is blocked by calpain inhibitors. Proc Natl Acad Sci USA 103: 17366-17371

Sausville EA, Tomaszewski JE, Ivy P (2003) Clinical development of 17-allylamino, 17-demethoxygeldanamycin. Curr Cancer Drug Targets 3: 377-383

Seddon JM, George S, Rosner B (2006) Cigarette smoking, fish consumption, omega-3 fatty acid intake, and associations with age-related macular degeneration: the US Twin Study of age-related macular degeneration. Arch Ophthalmol 124: 995-1001

Stieger K, Le Meur G, Lasne F, Weber M, Deschamps JY, Nivard D, Mendes-Madeira A, Provost N, Martin L, Moullier P, *et al* (2006) Long-term doxycycline-regulated transgene expression in the retina of nonhuman primates following subretinal injection of recombinant AAV vectors. Mol Ther 13: 967-975

Stieger K, Colle MA, Dubreil L, Mendes-Madeira A, Weber M, Le Meur G, Deschamps JY, Provost N, Nivard D, Cherel Y, *et al* (2008) Subretinal delivery of recombinant AAV serotype 8 vector in dogs results in gene transfer to neurons in the brain. Mol Ther 16: 916-923

Tam LC, Kiang AS, Kennan A, Kenna PF, Chadderton N, Ader M, Palfi A, Aherne A, Ayuso C, Campbell M, *et al* (2008) Therapeutic benefit derived from RNAi-mediated ablation of IMPDH1 transcripts in a murine model of autosomal dominant retinitis pigmentosa (RP10). Hum Mol Genet 17: 2084-2100

Tam LC, Kiang AS, Campbell M, Keaney J, Farrar GJ, Humphries MM, Kenna PF, Humphries P (2010) Prevention of autosomal dominant retinitis pigmentosa by systemic drug therapy targeting heat shock protein 90 (Hsp90). Hum Mol Genet 19: 4421-4436

Tan JS, Wang JJ, Flood V, Rochtchina E, Smith W, Mitchell P (2008) Dietary antioxidants and the long-term incidence of age-related macular degeneration: the Blue Mountains Eye Study. Ophthalmology 115: 334-341

The Eye Disease Prevalence Group (2004) Prevalence of age-related macular degeneration in United States. Arch Ophthalmol 122: 564-572

Yang FY, Lin YS, Kang KH, Chao TK (2010) Reversible blood–brain barrier disruption by repeated transcranial focused ultrasound allows enhanced extravasation. J Control Release [Epub a head of print]

 © 2011 EMBO Molecular Medicine